Perspectives
in Medical Virology
Volume 3

animal virus structure

M.V. NERMUT and A.C. STEVEN
Editors

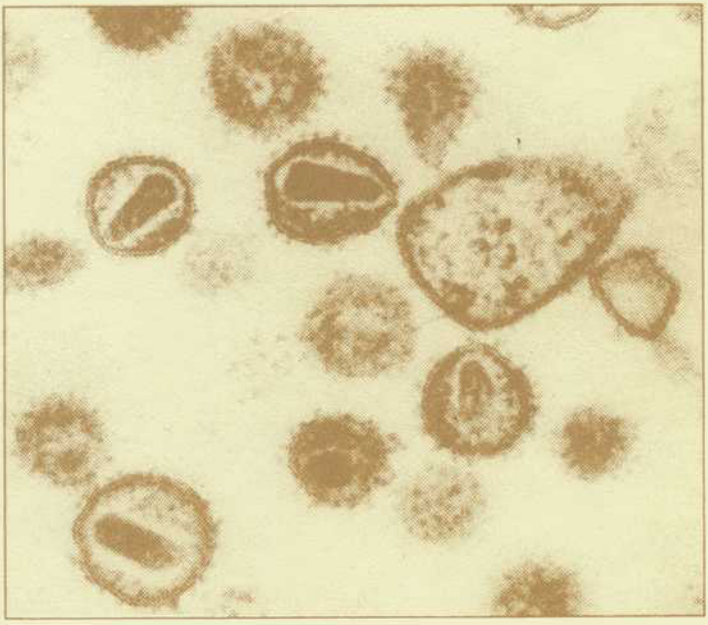

Elsevier

Animal Virus Structure

Perspectives in Medical Virology

Volume 3

General Editor

A.J. Zuckerman

Professor of Microbiology
Department of Microbiology
London School of Hygiene and Tropical Medicine

ELSEVIER
AMSTERDAM · NEW YORK · OXFORD

Animal Virus Structure

Editors

M.V. Nermut

National Institute for Medical Research,
The Ridgeway, Mill Hill, London, U.K.

and

A.C. Steven

National Institute of Arthritis, Musculoskeletal and Skin Diseases,
NIH, Bethesda, MD, U.S.A.

1987

ELSEVIER

AMSTERDAM · NEW YORK · OXFORD

ISBN 0-444-80879-5/ISSN 0168-7069

Published by:

Elsevier Science Publishers B.V. (Biomedical Division
P.O. Box 211
1000 AE Amsterdam
The Netherlands

Sole distributors for the USA and Canada

Elsevier Science Publishing Company, Inc.
52 Vanderbilt Avenue
New York, NY 10017
USA

Library of Congress Cataloging-in-Publication Data

Animal virus structure.

(Perspectives in medical virology, ISSN 0168-7069 ;
v. 3)
Includes bibliographies and index.
1. Viruses--Morphology. I. Nermut, M.V. II. Steven,
A.C. [DNLM: 1. Virus Diseases--veterinary. 2. Viruses
--ultrastructure. W1 PE871AV v.3 / QW 160 A5985]
QR450.A55 1987 576'.6484 87-13593
ISBN 0-444-80879-5 (U.S.)

Printed in The Netherlands

Editors' foreword

The past 10–15 years have witnessed enormous progress in our understanding of virus structure and it has been the confluence of information from diverse biophysical and biochemical methodologies which has stimulated these advances. In consequence, structural virology has developed beyond the stage of 'descriptive morphology' to a new era of 'structural analysis' encompassing both morphological and chemical characterization of virus particles. Viruses are, above all, assemblies of macromolecules, and a deep understanding of their architecture will come only by appreciating the mutual interactions of their structural elements at the molecular level.

It is the purpose of this book to provide a concise summary of what is now known about the structure of each of the presently recognized families of animal viruses. These accounts are preceded by introductory chapters on taxonomy and on the basic principles of structural organization, as well as brief overviews of what have emerged as the three major experimental approaches to the determination of viral structure: electron microscopy, X-ray diffraction, and neutron diffraction. Different virus families vary widely with regard to structural complexity and experimental tractability, and these factors underlie an unevenness of progress in structural studies among the various families that is at times substantial, and which precludes strictly parallel coverage of all viruses. Nevertheless, the information in each chapter has been arranged as far as possible in a uniform pattern to allow for correlation between different virus families.

The original literature has been cited rather sparsely as a matter of editorial policy, but in the reference lists recent full-scale reviews and monographs have been included with the intention that these should serve as entry-points to the original literature. We have aimed at compiling a summary that is succinct and reasonably up-to-date, and may serve a broad spectrum of readers that includes postgraduate and advanced undergraduate students in the biological and medical sciences, as well as teachers and researchers in virology.

And what, after all, is a virus? It is inevitable and essential that any account of virus structure must, implicitly or explicitly, take into consideration both the physical-chemical properties and the biological functions that these structures fulfil. Since knowledge of the chemical composition and of the mutual interactions

between macromolecular complexes is vital to an understanding of viral architecture, an effort has been made to cover these topics wherever possible.

The operative principle underlying viral infection can be described as maximization of the number of copies of the viral genome. In these terms the rationale of virus structure relates to the design of 'smart' delivery systems capable of surviving in the extra-cellular milieu, identifying and infiltrating susceptible cells, and initiating further replication. Accordingly, the structural characteristics of each virus embody a set of molecular mechanisms capable of accomplishing these goals. In this idiom, the extreme diversity exhibited by the structures of different viruses ultimately reflects the range of viable strategies for such replication cycles in and between animal cells.

To comprehend the properties of virions in terms of the stereo-chemistry of their molecular consituents will ultimately require, as with other nucleo-protein assemblies, visualization of individual amino-acids and nucleotides, i.e. a spatial resolution of 0.3 nm or better. In the past several years, analyses at this level of detail have been accomplished in single-crystal X-ray diffraction studies of several relatively small and uncomplicated plant viruses. Very recently, comparable results have been obtained for the first animal viruses, both picornaviridae. However, such small and regularly organized virions consitute only a small minority of the animal viruses, and the proposition of virion crystallography may well prove impracticable for many of the larger and more complex viruses. In such cases, single-crystal diffraction studies of individual molecular constituents of subviral particles provide the most likely source of structural information at appropriately high resolution, as has already been achieved for the adenovirus hexon and the influenza virus haemagglutinin and neuraminidase glycoproteins.

However, for present purposes and for most virus families, the structural issues of current concern still relate to the mapping of macromolecules rather than individual amino-acids, and many basic questions persist at this lower level of resolution. In order to summarize current concepts, many contributors to this volume have prepared 'three-dimensional' drawings, collating dimensions, shapes, spatial relationships, and the locations of specific molecules and antigens. Other authors have applied the powerful emerging technology of computer graphics to convey similar information. In all cases, the experimental rigour of the various pieces of information integrated in the model varies considerably, and inevitably many of the specific details, and perhaps also some basic features, will be revised as more definitive experiments are performed. Thus these models amount to visual representations of working hypotheses, hopefully the most reasonable hypotheses that can be framed on the basis of current data.

Many people have contributed in various ways to this book, and they deserve our grateful thanks. Each of the chapters has been evaluated by peer review, and we thank our colleagues who performed this task: W. Bohn (Hamburg, F.R.G.),

F. Brown (Beckenham, U.K.), D. Buxby (Liverpool, U.K.), J. Calafat (Amsterdam, The Netherlands), J. Carrascosa (Madrid, Spain), Monique Dubois-Dalcq (Bethesda, U.S.A.), J.T. Finch (Cambridge, U.K.), M. Ferguson (London, U.K.), H. Frank (Tübingen, F.R.G.), D.J. Garwes (Compton, U.K.), H. Gelderblom (Berlin, F.R.G.), Kathryn V. Holmes (Bethesda, U.S.A.), R.W. Horne (Norwich, U.K.), M. Horzinek (Utrecht, The Netherlands), B. Jacrot (Grenoble, France), F. Lehman-Grube (Hamburg, F.R.G.), B. Mahy (Pirbright, U.K.), R. Michalides (Amsterdam, The Netherlands), S. Patterson (Harrow, U.K.), C. Pringle (Warwick, U.K.), K. Quade (London, U.K.), R. Ruigrok (London, U.K.), W.C. Russell (St. Andrews. U.K.), N.H. Sarkar (New York, U.S.A.), G. Siegel (Berne, Switzerland), C.H. Smale (Pirbright, U.K.), S. Straus (Bethesda, U.S.A.), B.L. Trus (Bethesda, U.S.A.). We also much appreciate the generally constructive responses of the authors to this input. Valuable contributions have also been made by many scientists who provided figures from their work, often of as yet unpublished results.

In conclusion, it has become increasingly apparent to us that the progress of the last 10–15 years, dramatic though it has been, has not yet realized a comprehensive understanding of how viruses are put together. Although the field is now established on a generally quantitative and analytical basis, structural virology is still pitched largely at the phenomenological level. It is our hope that in the next decade a more comprehensive understanding of the structure of all viruses will be obtained which will be of benefit to both general and medical virology.

M.V. Nermut
A.C. Steven

This Page Intentionally Left Blank

List of contributors

T.S. Baker	Department of Biology, Purdue University, West Lafayette, IN 47907, U.S.A.
C.-H. von Bonsdorff	Department of Virology, University of Helsinki, 00290 Helsinki 29, Finland.
J.C. Brown	Department of Microbiology, University of Virginia Medical School, Charlottesville, VA 22908, U.S.A.
B.J. Carter	Laboratory of Molecular and Cellular Biology, National Institute of Arthritis, Diabetes, and Digestive and Kidney Diseases, Bldg. 8, Room 304, National Institutes of Health, Bethesda, MD 20892, U.S.A.
M.J. Carter	Department of Virology, University of Newcastle-upon-Tyne, Royal Victoria Infirmary, Newcastle-upon-Tyne NE1 4LD, U.K.
F. Darcy	Centre d'Immunologie et de Biologie Parasitaire, Institut Pasteur, 15 rue Camille Guerin, 59019-Lille, Cedex, France.
H.A. Davies	Section of Electron Microscopy, Clinical Research Centre, Harrow, Mddx., U.K.
G. Devauchelle	Laboratoire de Microbiologie. LA 203 du CRNS 706130-Mont-Saint-Aignan, France.
D.S. Ellis	Laboratory of Electron Microscopy, London School of Hygiene and Tropical Medicine, Keppel Street, London WC1E 7HT, U.K.

J.T. Finch — MRC Laboratory for Molecular Biology, Hills Road, Cambridge, U.K.

H. Frank — Max-Planck Institut fur Entwicklungsbiologie, Spemanstrasse 35, 7400-Tubingen, F.R.G.

H. Gelderblom — Robert-Koch-Institut, Nordufer 20, 1000-Berlin 65.

J. Hay — Department of Microbiology, Uniformed Services University of the Health Sciences, 4301 Jones Bridge Road, Bethesda, MD 20014, U.S.A.

D.J. Hockley — National Institute for Biological Standards and Control, Blanche Lane, South Mimms, Potters Bar, Herts EN6 3QG, U.K.

B. Jacrot — Laboratoire Européen de Biologie Moleculaire, 156X Avenue des Martyres, 38042 Grenoble, France.

D.C. Kelly — Institute of Virology, Mansfield Road, Oxford, OX1 3SR, U.K.

M.R. Macnaughton — Boots-Celltech Diagnostics Limited, 240, Bath Road, Slough, SL1 4ET, U.K.

C.R. Madeley — Department of Virology, University of Newcastle-upon-Tyne, Royal Victoria Infirmary, Newcastle, NE1 4LD, U.K.

P. Metcalf — European Molecular Biology Laboratory Outstation, 156, Avenue des Martyres, 38042 Grenoble, France.

P. Minor — National Institute for Biological Standards and Control, Blanche Lane, South Mimms, Potters Bar, Herts EN6 3QG, U.K.

G. Müller — Bernhard-Nocht-Institut, Bernhard-Nocht-Str. 74, 2000 - Hamburg 4, F.R.G.

F.A. Murphy — Division of Viral Diseases, Centers for Disease Control, Atlanta, GA 30333, U.S.A.

M.V. Nermut — Laboratory of Cell Surface Interactions, National Institute for Medical Research, Mill Hill, London NW7 1AA, U.K.

W.W. Newcomb — Department of Microbiology, University of Virginia, Charlottesville, VA 22908, U.S.A.

J.S. Oxford — National Institute for Biological Standards and Control, Blanche Lane, South Mimms, Potters Bar, Herts EN6 3QG, U.K.

R.F. Pettersson — Ludwig Institute for Cancer Research, Box 60202, S-10401 Stockholm, Sweden.

I. Rayment — Department of Biochemistry, University of Arizona, Tucson, AZ 85721, U.S.A.

C.R. Roberts — Department of Microbiology, Uniformed Services University of the Health Sciences, 4301 Jones Bridge Road, Bethesda, MD 20014, U.S.A.

W.T. Ruyechan — Department of Microbiology, Uniformed Services University of the Health Sciences, 4301 Jones Bridge Road, Bethesda, MD 20014, U.S.A.

N.H. Sarkar — Laboratory of Molecular Virology, Department of Cell and Molecular Biology, Medical College of Georgia, Augusta, GA 30912, U.S.A.

A. Scheid — Institut für Medizinische Mikrobiologie und Virologie, Universitätstrasse 1, 4000 Düsseldorf, F.R.G.

K. Simons — European Molecular Biology Laboratory, Postfach 10.2209, Meyerhofstrasse 1, 6900 Heidelberg, F.R.G.

L.M. Stannard — Department of Microbiology, Medical School, Observatory C.P., 7925, Republic of South Africa.

A.C. Steven — Laboratory of Physical Biology, National Institute of Arthritis, Musculoskeletal and Skin Diseases, NIH, Bldg. 6, Rm. 114, Bethesda, MD 20892, U.S.A.

P.J. Tattersall — Department of Human Genetics, Yale University School of Medicine, 333 Cedar Street, New Haven, CT 06510, U.S.A.

J.D. Williamson — Department of Medical Microbiology (Virology), St. Mary's Hospital Medical School, Praed Street, London W2 1PG, U.K.

P.R. Young — Department of Medical Microbiology, London School of Hygiene and Tropical Medicine, Keppel Street, London, WC1E 7HT, U.K.

Contents

CHAPTER 2B

Electron microscopy: methods for study of virus/cell interactions

M.V. Nermut, D.J. Hockley and H. Gelderblom

CHAPTER 2C

Electron microscopy: image processing and quantitative electron microscopy

A.C. Steven

CHAPTER 3

X-ray diffraction from viruses

J.T. Finch

CHAPTER 11

Togaviridae

C.-H. von Bonsdorff and K. Simons

CHAPTER 12

Coronaviridae

M.R. Macnaughton and H.A. Davies

CHAPTER 13

Arenaviridae

P.R. Young

CHAPTER 14

Rhabdoviridae

J.C. Brown and W.W. Newcomb

CHAPTER 15

Orthomyxoviridae

J.S. Oxford and D.J. Hockley

CHAPTER 16

Paramyxoviridae

A. Scheid

CHAPTER 17A

Retroviridae

H. Frank

CHAPTER 17B(i)

Oncovirinae: type B oncovirus

N.H. Sarkar

CHAPTER 17B(ii)

Oncovirinae: type C oncovirus

H. Frank

CHAPTER 17B(iii)

Oncovirinae: type D oncovirus

H. Gelderblom

CHAPTER 17C

Lentivirinae

H. Frank

CHAPTER 17D

Spumavirinae

H. Gelderblom and H. Frank

CHAPTER 18

The filoviridae

D.S. Ellis

Part V. DNA-containing virus families

CHAPTER 19

Parvoviridae

B.J. Carter and P.J. Tattersall

CHAPTER 20

Papovaviridae

T.S. Baker and I. Rayment

CHAPTER 21

Baculoviridae

D.C. Kelly

CHAPTER 22

Hepadnaviridae

L.M. Stannard

CHAPTER 23

Adenoviridae

M.V. Nermut

CHAPTER 24

Herpesviridae

J. Hay, C.R. Roberts, W.T. Ruyechan and A.C. Steven

CHAPTER 25

Iridoviridae

F. Darcy and G. Devauchelle

CHAPTER 26

Poxviridae

G. Müller and J.D. Williamson

PART I

General principles of virus architecture

This Page Intentionally Left Blank

Nermut/Steven (eds) Animal Virus Structure

CHAPTER 1

General principles of virus architecture

M.V. NERMUT

National Institute for Medical Research, London NW7, U.K.

1.1. Introduction

A comprehensive definition of viruses should take into account not only their physical and chemical properties, but also their biological and pathological aspects. In this chapter on the structure of viruses we shall refrain from an attempt at a comprehensive definition and will restrict ourselves to the statement that 'viruses are organized associations of macromolecules'. This physical-chemical concept of viruses provides a basis for understanding the principles of virus architecture and the mechanisms of virus assembly. However, we should make it clear that there is no unique morphological entity – the virion – but a great variety of architectural solutions to the fundamental principle of viral pathogenesis: the transfer of viral genome from cell to cell. Nevertheless, there are certain common features and general principles in virus architecture and these will be discussed in this chapter.

The architecture of a virus is specified primarily by the properties of its constituent macromolecules. They form the 'basic structural elements' of the virion, i.e. the morphological entities, that are often observable in the electron microscope (e.g. capsomers, spikes). These usually associate into 'structural complexes' formed by two or more different types of 'basic structural elements', e.g. an envelope is formed by a lipid bilayer and the glycoprotein spikes, a virus core consists of a core shell and a nucleoprotein complex, more complex viruses comprise a nucleocapsid, core shell and envelope or capsid, etc. These terms will be explained below. The shapes and sizes of viruses are influenced in large part by the size, number and surface properties of their protein elements, and their mutual af-

finities, i.e. the types of interactions that take place during virus assembly. A whole series of stabilizing interactions participate in maintaining the structural integrity of the virion: hydrophobic bonds, hydrogen bonds, salt linkages and long- or short-range electrostatic interactions (Kaper, 1975).

The most important element of an infectious virus particle is the nucleic acid (RNA or DNA). It is always associated with one or more viral polypeptides which either form a protective case (closed shell) or interact tightly with the nucleic acid (NA) to form a helical nucleoprotein complex, thereby fulfilling a protective and/or a compacting role. The NA/protein and protein/protein interactions play major roles in the morphogenesis of viruses. They determine whether the nucleoprotein complex will be a helix or a nucleosome-like bead or an icosahedral shell. In simple viruses the protein(s) usually protect nucleic acid against nucleases, which is not always the case in complex viruses where the NA-associated protein rather helps to organize the NA within the virion during assembly (for example by neutralizing negatively charged phosphates and bending the relatively stiff 'rod' of dsDNA into a helix); viral protein might also be needed for transportation of the virus genome into the cell nucleus or for transcription or replication of the genome.

Certain groups of viruses contain lipid envelopes derived from various types of cellular membranes during virus assembly. All virus envelopes also contain virus-specific transmembrane proteins; some of them interact with specific cell surface receptors during the first stages of viral infection.

The most important principle in the formation of the virion is that of self-assembly. This has been amply demonstrated by in vitro assembly of plant viruses, but examples from animal viruses are also available. The best known is the self-assembly of icosahedral capsids (adenoviruses) or core shells (e.g. M-protein in Sendai virus) or helical nucleocapsids (rhabdovirus). Similarly, in vitro reconstitution of virus envelopes and incorporation of virus spikes into liposomes (= virosomes) have been reported for togaviruses, myxo- and paramyxoviruses, to quote but a few examples.

The virion-assembly process differs among the virus families and in many cases takes advantage of the cellular mechanisms for transportation and exocytosis. For more information see Dalton and Haguenau (1974), Simons and Garoff (1980) and Dubois-Dalcq et al. (1984).

1.2. Brief survey of virus anatomy

Before dealing with the various forms of viruses it will be useful to define the individual structural components of the virion.

1.2.1. Terminology and definitions

The virion = intact, fully assembled, infective virus particle.
Subviral particles = breakdown products from in vitro treatment of virions resulting in loss of some structural elements or complexes (e.g. spikeless particles of myxoviruses or adenovirus cores).
The capsid = outermost protein shell enclosing either nucleic acid only, or a nucleoprotein complex, or a core. Capsids have cubic (mostly icosahedral) symmetry, but cylindrical (usually aberrant) forms are also known. Morphological units forming the capsid are called capsomers; those with six neighbours are six-coordinated or hexavalent; capsomers at vertices of the icosahedron have five neighbours, are therefore five-coordinated or pentavalent. Capsomers consist of polypeptide protomers called structure units. This follows the original definition by Caspar et al. (1962) that 'structure units are the smallest functionally equivalent building units of a capsid'.
The nucleocapsid (NC) = nucleic acid within an icosahedral protein shell (capsid) or within a helical protein complex. More than one virus protein is often associated with NA. Though 'capsid' means a closed shell (box) it has been commonly used to designate both icosahedral and linear nucleic acid/protein(s) complexes. Linear nucleocapsids form either flexible helices (nucleohelix) or in a few cases small nucleosome-like bodies (beads on string). Most enveloped viruses (Myxo-, Paramyxoviridae) possess 'nucleohelices'; the nucleosome-like organization has been best shown in members of Papovaviridae. However, in many families the structure of the NA/protein complex is not known and many linear nucleocapsids are only assumed to be helical.
The envelope or virus membrane = lipid bilayer with glycoprotein projections (spikes, knobs, etc.) called peplomers. Some envelopes contain additional protein apposed to their inner surface or even inserted into the lipid bilayer (e.g. Coronaviridae).
The core = internal body containing nucleoprotein complex within a protein shell (core-shell). The core can be icosahedral (e.g. adenovirus, type C oncovirus), spherical or cylindrical (e.g. myxovirus) and enclosed in a capsid or in an envelope.

Viruses vary widely in their shapes, sizes and architecture. They can be relatively simple and small (tobacco mosaic virus = TMV, picornavirus, parvovirus) or rather complex and so large as to be visible in the light microscope (pox virus). Thus far, over 20 animal virus families have been distinguished and these can be categorized into several architectural classes.

Naked nucleocapsids are the simplest forms of animal virus structure. They consist of NA enclosed in an icosahedral capsid (Table 1.1, Fig. 1.1a). There is little specificity in the interaction between NA and the capsid. The function of the protein capsid is mainly protective. Naked helical NCs are common among plant viruses (e.g. TMV) and can be rigid or flexuous. However, no naked 'nucleohelices' are known among animal viruses.

TABLE 1.1.
Basic structural properties of animal viruses arranged from the simplest to the most complex virions

Viruses with icosahedral nucleocapsids

	Refer to Fig. 1.	Family	Genome (sense)	Symmetry of NC (T=)	OC or envelope
Naked nucleocapsid	a	Picornaviridae	ssRNA (negative)	Icosahedral, T=1	-
		Caliciviridae	ssRNA (negative)	Cubic	-
		Birnaviridae	dsRNA	Icosahedral, T=13 l,d	-
		Parvoviridae	ssDNA	Icosahedral, T=1	-
Encapsidated nucleocapsid	b	Reoviridae	dsRNA	Icosahedral, T=13 l	Icosahedral, T=13 l
		Hepadnaviridae	dsDNA	Icosahedral (?)	Icosahedral (?)
Enveloped nucleocapsid	c	Togaviridae	ssRNA (positive)	Icosahedral, T=3	T=4[a]
		Baculoviridae	dsDNA	11-start helix	-

Viruses with helical or complex nucleocapsids

	Refer to Fig. 1.	Family	Genome (sense)	Symmetry of NC	Capsid or envelope
Encapsidated NC	d	Papovaviridae	dsDNA	Nucleosomes(helical)	Icosahedral, T=7 d or l
Enveloped NC (nucleohelix)	e	Bunyaviridae	ssRNA (negative)	Helical(?)	T=12[b]
	f	Arenaviridae	ssRNA (negative)	Helical(?)	Spherical
	f	Coronaviridae	ssRNA (positive)	Helical	Spherical
	h	Rhabdoviridae	ssRNA (negative)	Helical	Cylindrical
Encapsidated core	g	Adenoviridae	dsDNA	Nucleosome-like(?)	Icosahedral, T=25
Enveloped core	h	Orthomyxoviridae	ssRNA (negative)	Helical	Spherical or cylindrical
	h	Paramyxoviridae	ssRNA (negative)	Helical	Spherical or cylindrical
	i	Retroviridae	ssRNA (positive)	Helical(?)	Icosahedral core[d]
	j	Herpesviridae[c]	dsDNA	?	T=16
Complex virions	j	Iridoviridae	dsDNA	Helical(?)	Icosahedral capsid
	k	Poxviridae	dsDNA	?	

Abbreviations: NC = nucleocapsid; OC = outer capsid; T = triangulation number.
[a]Spike trimers form icosahedral lattice with T = 4.
[b]Spikes cluster into an icosahedral lattice with T = 12.
[c]The assignment of Herpesviridae to 'enveloped cores' is provisional because of the uncertainty about the organization of the virus interior.
[d]Only in Oncovirus C particles.

Encapsidated nucleocapsids are icosahedral protein shells (capsids) with icosahedral or helical NC enclosed. In reoviruses the surface shell is called the outer capsid (Fig. 1.1b), in papovaviruses the enclosed NC is organized as nucleosomes (Fig. 1.1d).

Alternatively, virus nucleocapsids, either icosahedral or helical, can be *enveloped* by a lipid bilayer with spiky projections, (Fig. 1.1c,e,f). The envelope

has a protective role but also represents a permeability barrier. The glycoprotein projections may be essential for entry of the virion into a cell.

Glycosylated spiky projections have been found in all enveloped viruses, but some viruses have additional non-glycosylated proteins apposed to the internal

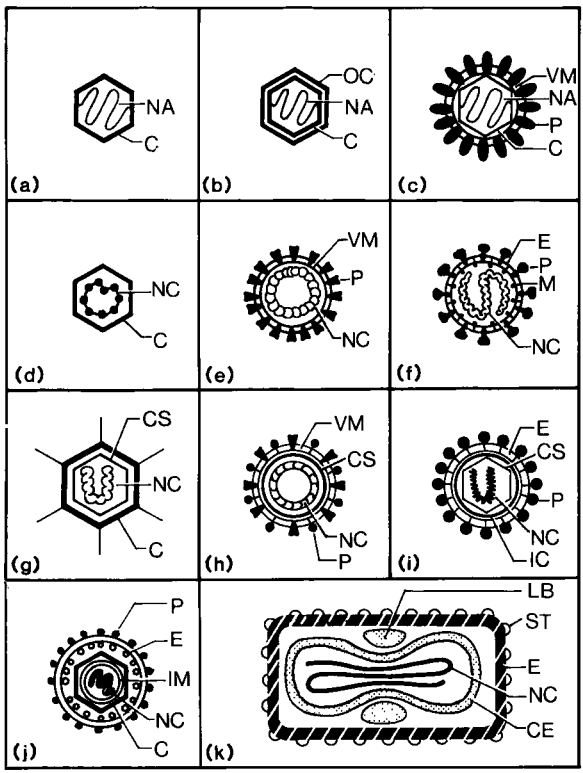

Fig. 1.1. Diagrammatic representation of the architecture of animal viruses. See Table 1.1 for representatives of individual categories. (a) Naked icosahedral nucleocapsid (NA = nucleic acid, C = capsid); (b) encapsidated icosahedral nucleocapsid (OC = outer capcid); (c) enveloped icosahedral nucleocapsid (VM = virus membrane, P = peplomers); (d) encapsidated 'nucleosomes'; (e) enveloped 'helical' nucleocapsid. Virus projections can cluster into a regular pattern, (f) enveloped 'helical' nucleocapsid. Envelope (E) contains another protein (M) in addition to typical surface projections. (g) Encapsidated core consisting of 'helical' nucleocapsid, plus core shell (CS) and capsid; (h) enveloped core. Membrane apposed protein (M) forms continuous spherical shell (CS) enclosing helical nucleocapsid (nucleohelix). Virus membrane contains two types of surface projections; (i) enveloped icosahedral core. Envelope contains knob-like surface projections (P) and 'inner coat' protein (IC) in close association with lipid bilayer. Nucleocapsid is probably helical. (j) Complex virion with envelope, inner lipid membrane (IM), icosahedral capsid and probably linear nucleocapsid inside. (k) Enveloped core of high degree of complexity. Linear nucleocapsid is surrounded by a 'core envelope' (CE), and two lateral bodies (LB) are present underneath the virus envelope covered with proteinaceous 'surface tubules' (ST).

surface of the membrane. This type of protein (usually called M) can form a continuous shell separating the NC from the viral membrane (Fig. 1.1h). In some families the M-protein is partly or fully inserted into the lipid bilayer and does not form a continuous layer (e.g. Coronaviridae; Fig. 1.1f). In myxoviruses an internal body (the virus core) comprising both the helical NC (nucleohelix) and the M-protein can be separated from its envelope. Some retroviruses contain icosahedral cores which can be readily isolated. These viruses can be designated *enveloped cores* (Fig. 1.1h,i). Cores of enveloped viruses are probably responsible for the shape of the virion (spherical, cylindrical or icosahedral). However, cores have also been described in icosahedral viruses such as Adenoviridae. We call them *encapsidated cores* (Fig. 1.1g). Adenovirus cores can be readily isolated after breaking up the capsid, whereas cores of enveloped viruses (e.g. myxoviridae) are rather fragile and their preparation is difficult.

Herpesviridae and Iridoviridae represent a further degree of complexity in virus architecture. Herpes simplex virus consists of an icosahedral capsid containing DNA and several viral proteins. It is in fact equivalent to a core as defined above, but is traditionally named nucleocapsid. It is enveloped by a membrane with a loosely apposed protein layer called the tegument. In principle its anatomy is similar to that of retroviruses (Fig. 1.1i) though its chemical composition is different. A very similar arrangement pertains in frog virus 3 (Iridoviridae), but this virus has an additional layer of lipids (the inner membrane) below the icosahedral capsid (Fig. 1.1j).

Finally, the most complex and largest viruses (Poxviridae) consist of a complex core, two lateral bodies, and an envelope covered with tubular proteinaceous structures (Fig. 1.1k).

The structural variety of viruses is far from being fully comprehensible in the present state of our knowledge, especially if one takes into account the limited number of functions that the structural complexes of the virion fulfil; attachment to the host cell, protection of virus nucleic acid before and after replication in the intracellular environment, and survival outside the cell. In this overview we followed the path of complexity in virus architecture from naked nucleocapsids to large and complex virions of Poxviridae.

This attempt at anatomical classification of viruses might prove useful in comparative studies of viral families and also in clinical diagnosis of viruses by means of electron microscopy. For example, shapes of envelope projections or nucleoprotein complexes and the presence or absence of virus cores can prove useful and in some cases decisive for correct identification of the observed virus particles.

1.3. Symmetries associated with viruses

Crick and Watson (1956) suggested that coats of small viruses are built up of identical protein molecules packed together in a regular way. Both theoretical considerations and experimental studies which followed showed that there are only a limited number of possible designs for a biological 'container' to be constructed from identical building blocks (Caspar and Klug, 1962, 1963; Caspar, 1980). Indeed, virus nucleoproteins (as we now know them) are organized either as helical structures or as isometric bodies with one of the cubic symmetries, the most frequent one being the icosahedral.

(A) HELICAL SYMMETRY

In 1950, Crane pointed out that linear structures made of identical asymmetrical subunits interacting in an identical way are organized as helices. Most viral 'nucleohelices' have a low pitch ($P = u \times p$, where u is the number of units per turn and p is the axial rise per unit) and are of single-start type, i.e. made of one strand. However, two or more start helices have been described in some virus shells (Baculoviridae, tubes of polyoma virus). The principle of helical symmetry is well illustrated in the structure of tobacco mosaic virus (TMV) (Fig. 1.2), which is a rigid rod of about 18 nm in diameter and 300 nm long. The length of TMV (and of any other viral helical nucleocapsid) is determined by the length of NA. In a strict helical symmetry such as TMV (whose helical axis is straight) the protein subunits are in equivalent environments; however, this cannot be true when the

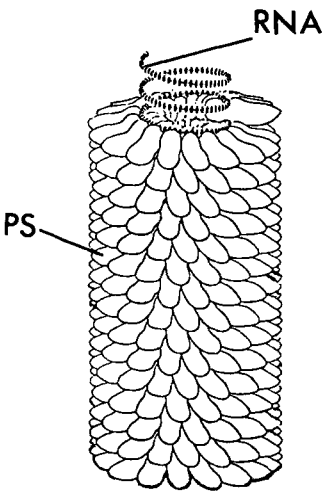

Fig. 1.2. Helical organization of tobacco mosaic virus. PS = protein subunits. Adapted from Caspar and Klug (1962).

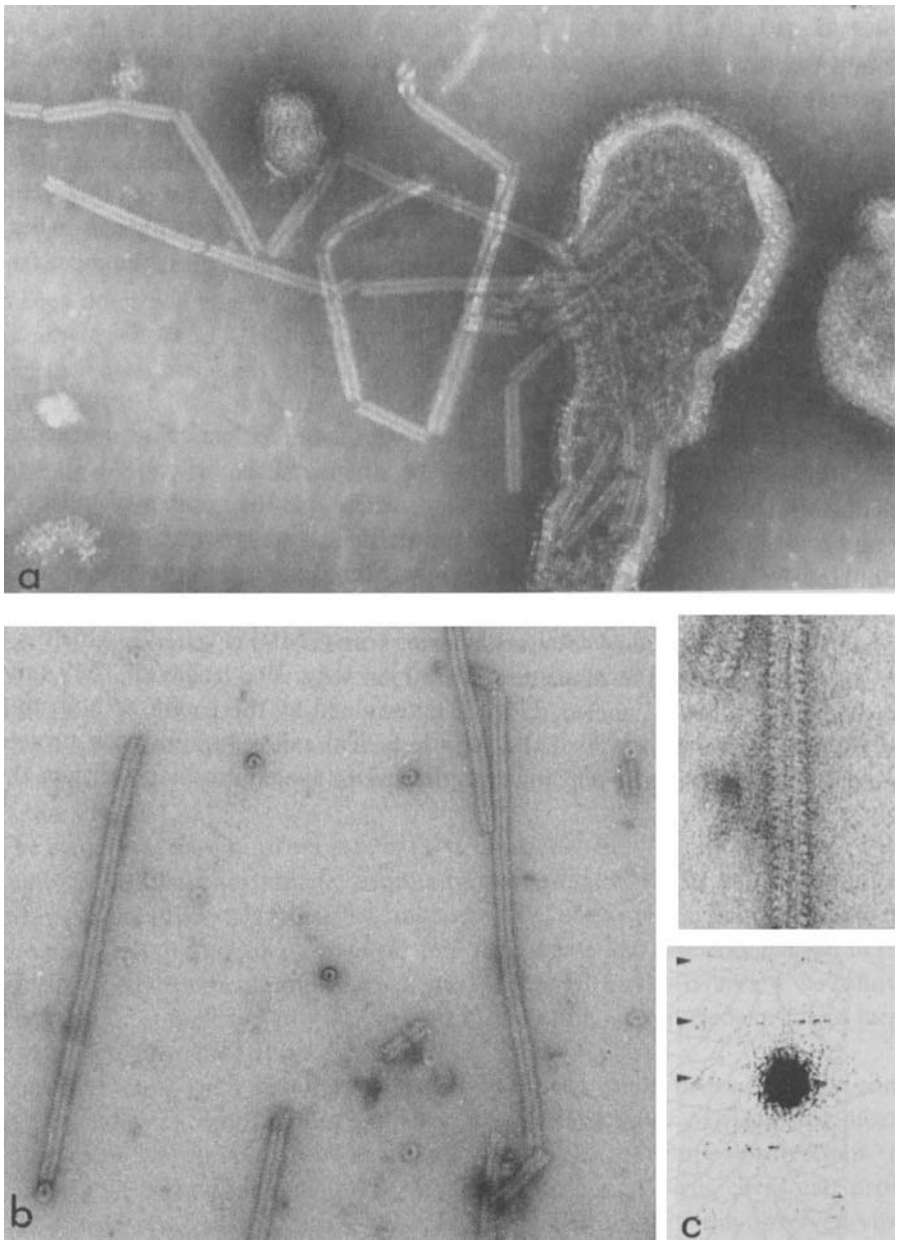

Fig. 1.3. (a) Sendai virus particle with released nucleocapsids. Negative staining. × 100 000. Courtesy of Dr. D. Hockley. (b) Isolated nucleocapsids of Sendai virus negatively stained with uranyl acetate. Note the herring-bone appearance and the rings – probably one turn of the helix. × 120 000. (c) A nucleohelix at higher magnification with optical diffraction pattern typical of helix. Courtesy of Dr. Y. Hosaka.

helix is curved or flexed as when packaged inside spherical viruses such as myxo- or paramyxoviruses. However, even here stretches of straight 'nucleohelices' exist which display a high order of helical symmetry (Fig. 1.3).

(B) CUBIC (ICOSAHEDRAL, 5.3.2.) SYMMETRY

As shown in Fig. 1.1, animal viruses – with the exception of rhabdoviruses and poxviruses – are spherical or icosahedral, though aberrant cylindrical or filamentous variants have been observed in a few cases (e.g. Myxoviridae, Iridoviridae). The icosahedron is one of the five platonic solids shown in Fig. 1.4. The symmetry of these solids is generally referred to as cubic, but since most viruses possess an icosahedral symmetry the latter term will be used throughout this volume. The term deltahedron designates solids with equilateral triangular faces such as the tetrahedron, octahedron and icosahedron. The regular icosahedron has 20 equilateral triangular facets, 30 edges and 12 vertices. It exhibits 2-fold, 3-fold and 5-fold rotational symmetries as shown in Fig. 1.5. Caspar and Klug (1962, 1963) showed that icosahedral symmetry is optimal for making a closed shell from identical (protein) subunits, because it fulfils the requirement of maximum bonding between subunits and so of minimum free energy.

The minimum number of morphological units to form an icosahedron is 12, but such viruses are very small (e.g. parvovirus). Strictly speaking such a capsid would consist of a maximum of 60 identical subunits ($=12 \times 5$ subunits). However, chemical and structural studies showed that many virus capsids are made from more than 12 morphological units (or 60 structure units). How then can the capsid

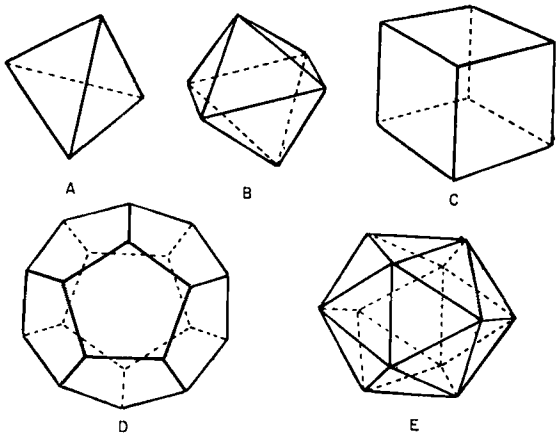

Fig. 1.4. The five platonic solids: (A) tetrahedron, (B) octahedron, (C) cube, (D) dodecahedron, (E) icosahedron. They can be inscribed in a sphere and their symmetries are generally designated cubic. Solids (A), (B) and (E) are also referred to as deltahedra because their surfaces are composed of equilateral triangles.

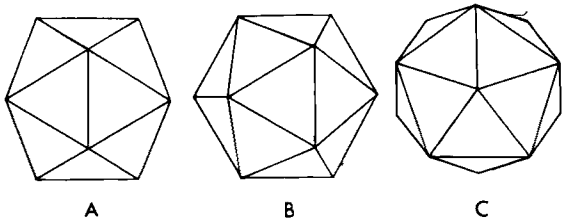

Fig. 1.5. The icosahedron in 5-fold (A), 3-fold (B) and 2-fold (C) symmetry orientations.

be constructed by a regular bonding of a multiple of 60 units? The solution was found in the principle of triangulation, i.e. subdivisions of the triangular facet of the icosahedron into a number of identical equilateral triangles (Fig. 1.6). The number of triangles is given by the so-called triangulation number (T) which can be deduced from the Goldberg diagram or calculated using a formula: $T = H^2 + HK + K^2$, where H and K are indices of the lattice points in the diagram (Fig. 1.7).

The triangulation number can also be defined as $T = f^2P$, where f is the number of subdivisions of each side of the triangular facet and f^2 then is the number of subtriangles (e.g. for $T = 4$ $f = 2$ and $f^2 = 4$). P represents a category or class of triangulation numbers based on the following equation: $P = h^2 + hk + k^2$, where h and k are non-negative integers with no common factor. Since $f \cdot h = H$ ($f \cdot k = K$) P equals 1 for all icosahedra with indices $H = 1,2,3 \ldots$ and $K = 0$, and $P = 3$ for icosahedra with indices $H = 1,2,3 \ldots$ and $K = 1,2,3 \ldots$ Generally for $h = 1$, $k = 0$, $P = 1$; for $h = 1$, $k = 1$, $P = 3$. All other triangulation numbers belong to the skew class (e.g. $T = 7$ for $h = 2$, $k = 1$). For the $P = 1$ class the lattice lines of the icosahedron run parallel to the edges (cf. Figs. 1.7 and 1.8), in

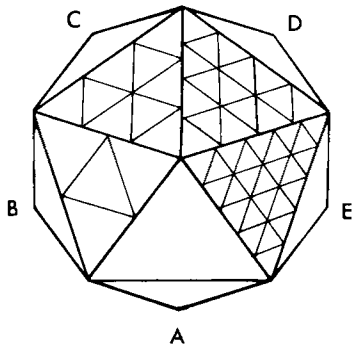

Fig. 1.6. Principle of triangulation. The basic triangular facet of the icosahedron (A) is subdivided into 4 triangles (B), or 9 (C) or 16 (D) or 25 (E). The triangulation numbers are consequently 1, 4, 9, 16 and 25 and the numbers of subdivisions on an edge f equal 1, 2, 3, 4 and 5. There is no direct relationship between the triangulation number and the size of the virion, but viruses with higher T numbers tend to be larger.

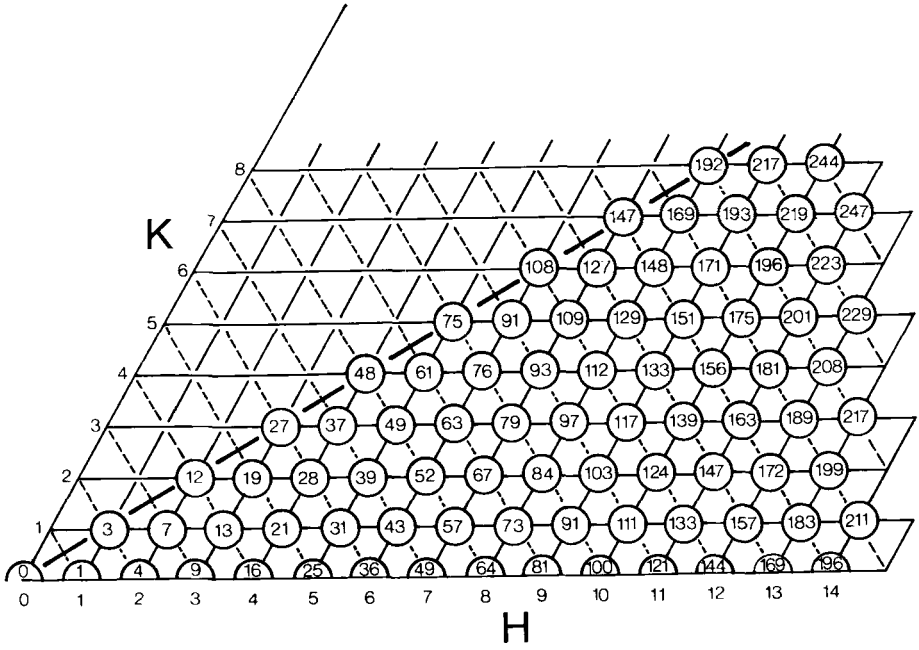

Fig. 1.7. Triangulation numbers (in circles) ($T = H^2 + HK + K^2$) represented on an equilateral triangular net (Goldberg triangle). An icosahedron with a 5-fold vertex at the origin of this net and a neighbouring 5-fold vertex at the lattice points of index H and K will have $10T+2$ vertices (12 of them five-coordinated) and $20T$ triangular facets. For example, viruses in $P=1$ class will have T equal to 1, 4, 9, 16, 25, etc., those in $P=3$ will have T = 3, 12, 27, etc. and those in a skew class of symmetry will have T = 7, 13, 19, 21, etc.

the $P=3$ class they bisect the angles between connecting edges. In a skew class the lattice lines are not symmetrically disposed with respect to the facet-edges. The deltahedra of the class $P=1$ can be considered as higher orders of the basic icosahedron (for H = 2,3 ... Fig. 1.8), and those of class $P=3$ as constructed from a pentagonal dodecahedron (Fig. 1.9). All deltahedra of the skew class occur in two enantiomorphs, left-handed (*laevo*) and right-handed (*dextro*, Figs. 1.9 and 1.10). The number of morphological units (N) equals $10T+2$. The number of structure units (polypeptides) within one morphological unit can be 2, 3, 5 or 6. The present state of our knowledge indicates that capsomers of animal viruses are either homooligomers, i.e. trimers (adenovirus, iridovirus), pentamers (papovavirus) or hexamers (herpesvirus) of one polypeptide, or heterooligomers consisting of two or more polypeptide chains (picornaviruses, possibly also parvoviruses and outer capsid of reovirus). In large viruses (e.g. adenovirus) the pentavalent capsomers are formed by a type of viral polypeptide other than the hexavalent capsomers. The clustering of structure units can be based on rather weak surface bonding between polypeptide chains or can be brought about by

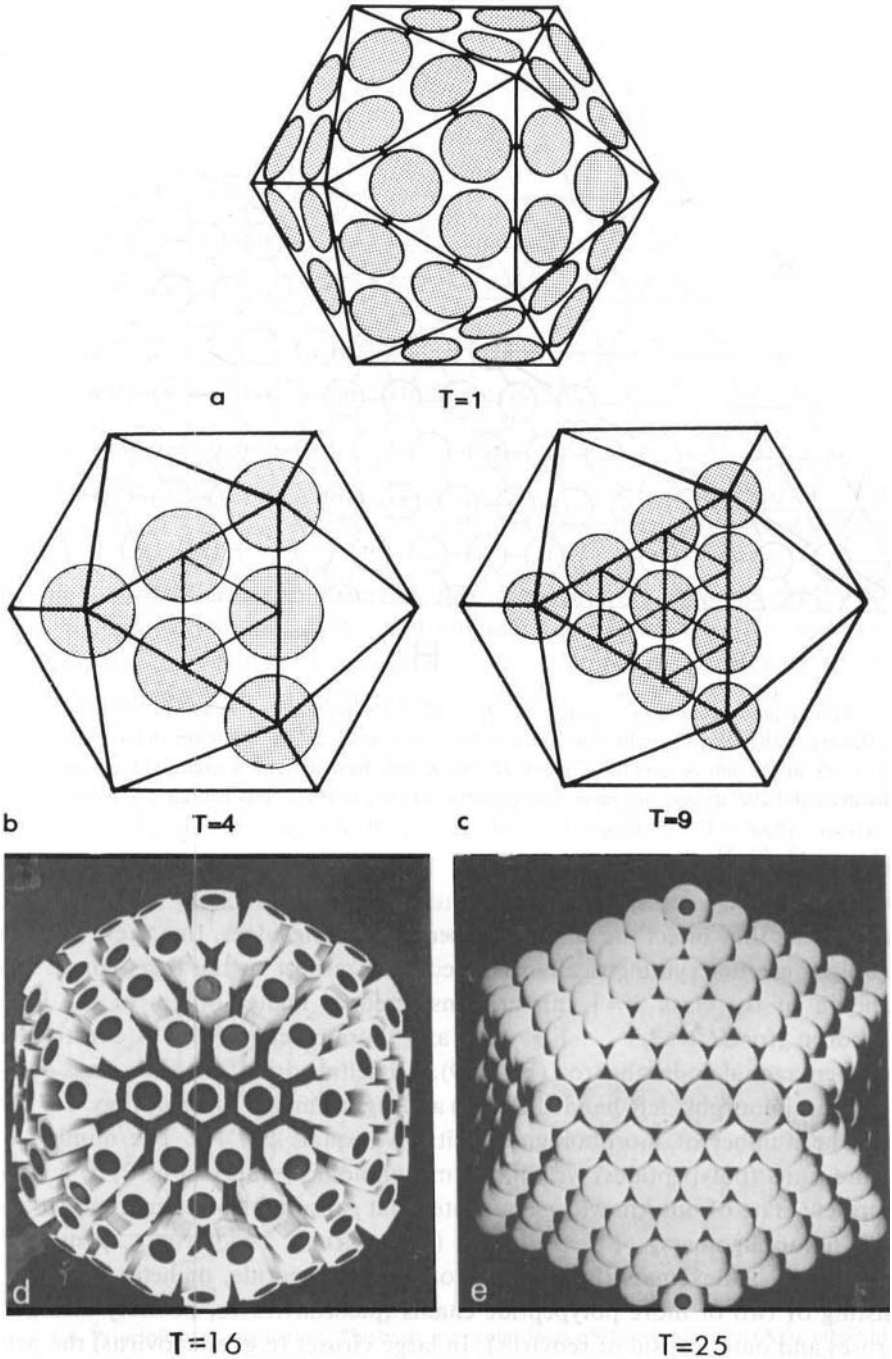

Fig. 1.8. Diagrams of the first five icosahedral capsids of $P=1$ class. (a) Simplest possible capsid from 60 structure units clustered into 12 pentamers, $T=1$. (b) $T=4$, (c) $T=9$, (d) $T=16$ (herpes virus), (e) $T=25$ (adenovirus; pentons are labelled with black dots). Pictures d and e kindly supplied by Dr. R.W. Horne.

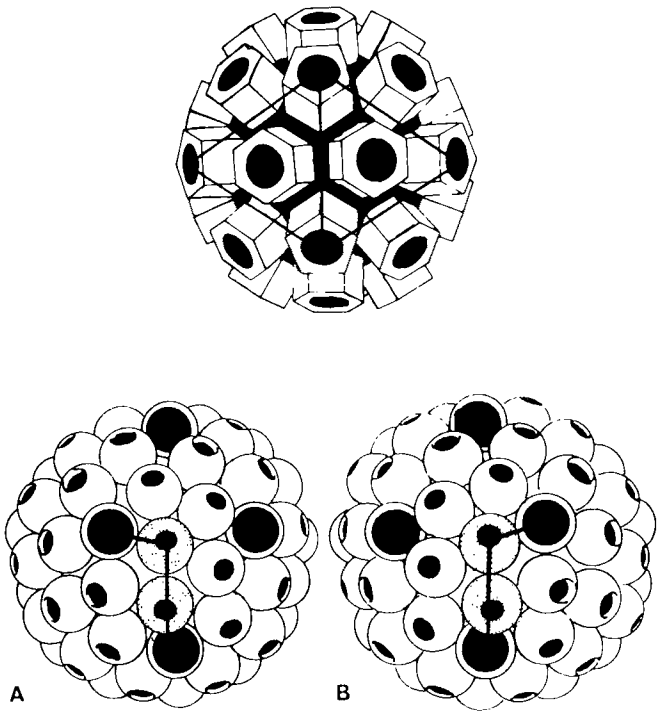

Fig. 1.9. Top. Model of a capsid of the $P=3$ class with $T=3$ in a two-fold symmetry orientation. Bottom. Model of a skew capsid with $T=7$. A = left-handed (*laevo*, l), B = right-handed (*dextro*, d) enantiomorph.

stronger protein/protein interactions, making the capsomer rather stable and difficult to dissociate. In most cases the capsomers are located at the lattice points of the triangular net of the icosahedron (e.g. in adenovirus), but sometimes they are centered on the lattice points of the icosahedral capsid (e.g. in Reoviridae). Theoretically both versions are possible, but only one of them is usually found in a particular virus genus.

Electron microscopy is usually the first applied and most practical tool for the determination of the triangulation number provided the capsomers are easily recognized. In the $P=1$ class it is sufficient to identify two neighbouring pentavalent capsomers and determine the number of capsomers (n) on the edge, including both pentavalent ones. Then $T=(n-1)^2$. However, this formula does not apply to the $P=3$ and skew classes, though their triangulation numbers can be determined from one-sided images produced by negative staining or shadowing.

Icosahedral symmetry in enveloped viruses

Some enveloped viruses possess icosahedral cores (oncovirus C) or capsids (Toga-, Herpes- and Iridoviridae). However, regular patterns strongly indicative of

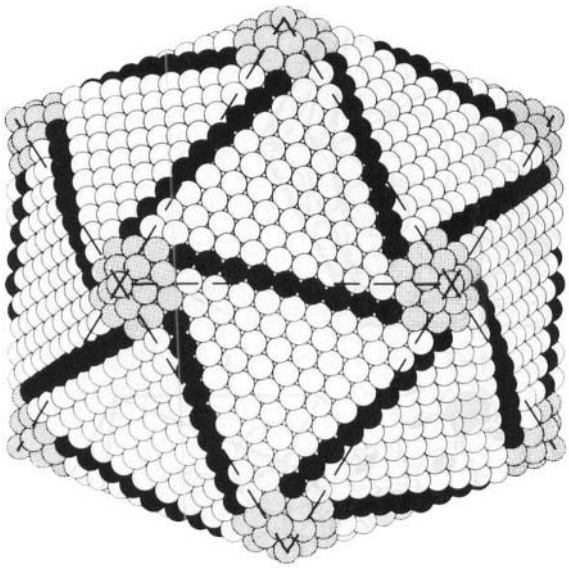

Fig. 1.10. Complex design of Iridovirus capsid with $T = 156$, as proposed by Wrigley (J.Gen. Virol. 5 (1969) 123). Black spheres represent so-called disymmetrons, groups of grey spheres at vertices are pentasymmetrons. Kindly supplied by Dr. N.G. Wrigley.

icosahedral symmetry have also been described in virus envelopes of some togaviruses, bunyaviruses and B-type retroviruses. A regular hexagonal arrangement of spikes has been observed in C-type influenza virus. In several cases the interaction of glycoprotein spikes with an underlying icosahedral capsid (togaviruses) or core shell (influenza virus?) could account for this phenomenon. However, in virus families where no core seems to be present (e.g. Bunyaviridae) the clustering of spikes into a regular icosahedral pattern is not well understood.

Finally, it should be noted that both types of symmetries are present in some viruses; for example, some retroviruses have an icosahedral 'core shell' and a helical RNP-complex; Papoviridae have an icosahedral capsid, but the DNA forms two helical turns in nucleosomes. Other possible examples of double symmetry are Iridoviridae and Herpesviridae.

1.4. The meaning of quasi-equivalence and deviations from the doctrine

Caspar and Klug (1962) pointed out that it is impossible to put more than 60 identical units on the sphere in such a way that all are identically situated. This is only possible with 12, 24 or 60 subunits. In addition an isometric shell built with $60n$ subunits in equivalent bonding positions should exhibit a circular contour (which

is the case with some small viruses). However, medium-size viruses such as adenovirus show angular contours and planar facets. To solve these problems Caspar and Klug introduced the concept of quasi-equivalence - nearly identical bonding positions of the capsomers - based on flexibility of bonds between two protein subunits permitting bending by up to 5° in any direction.

However, during the past decade, X-ray crystallography, chemical analyses and high-resolution electron microscopy brought new data on the organization of viral capsids, often contradicting the proposals outlined above. Recently X-ray crystallography of small plant viruses (Harrison, 1984, 1985) showed that it is not possible to deform protein domains to the extent required by Caspar and Klug (1962) though a certain flexibility can be achieved by quaternary structural changes in protein oligomers (Rossman, 1984).

However, the most striking findings concern the number of structure units in the hexavalent or pentavalent capsomers. For example, the adenovirus hexavalent capsomer, the hexon, is a trimer and, similarly, the six-coordinated capsomers of some iridoviruses are trimers.

Another striking example of a structural unorthodoxy was reported by Rayment et al. (1982): all 72 capsomers of polyoma virus, i.e. both the pentavalent and hexavalent ones, are pentamers. More about this and the above examples can be found in the appropriate chapters. These new data called for certain reassessments of the theory of quasiequivalence. Klug (1983) analysed the new situation and concluded that 'the icosahedral surface lattice is the optimal way of arranging units in a closed packed array on a closed surface'. Klug also stressed that we must distinguish between the geometrical design of a shell (economy of covering) and its structural realization (property of quasiequivalence).

Acknowledgements

The author wishes to thank Professor R.W. Horne and Dr. R. Ruigrok for helpful comments on the manuscript and in particular Dr. A.C. Steven for helpful criticisms and long-lasting discussions of the fundamental problems in this chapter.

Suggested reading

Burnett, R.M. (1984) Structural investigation of hexon, the major coat protein of adenovirus. In Biological Macromolecules and Assemblies, Eds. F.A. Jurnak and A. McPherson; Vol. 1: Virus Structures, pp. 337-385. J. Wiley & Sons, New York.

Caspar, D.L.D. and Klug, A. (1962) Physical principles in the construction of regular viruses. Cold Spring Harbor Symp. Quant. Biol. 27, 1-24.

Caspar, D.L.D., Dulbecco, R., Klug, A., Lwoff, A., Stoker, M.G.P., Tournier, P. and Wildy, P. (1962) Proposals. Cold Spring Harbor Symp. Quant. Biol. 27, 49.

Caspar, D.L.D. and Klug, A. (1963) Structure and assembly of regular virus particles. In Viruses, Nucleic Acids, and Cancer, pp. 27-39. Williams and Wilkins, Baltimore.

Caspar, D.L.D. (1980) Movement and self-control in protein assemblies. Quasi-equivalence revisited. Biophys. J. 32, 103-108.

Crane, H.R. (1950) Principles and problems of biological growth. Sci. Mon. 70, 376-389.

Crick, F.H.C. and Watson, J.D. (1956) The structure of small viruses. Nature (London) 177, 473-475.

Dalton, A.J. and Haguenau, F. (1973) Ultrastructure of animal viruses and bacteriophages. An Atlas. Academic Press, New York and London.

Dubois-Dalcq, M., Holmes, K.V. and Rentier, B. (1984) Assembly of enveloped RNA viruses. Springer Verlag, Vienna, New York.

Harrison, S.C. (1984) Virus structure: high resolution perspectives. Adv. Virus Res. 28, 175-240.

Harrison, S. (1985) Principles of Virus Structure. In Virology, Ed. B.N. Fields, pp. 27-45. Raven Press, New York.

Horne, R.W. and Wildy, P. (1961) Symmetry in virus architecture. Virology 15, 348-373.

Horne, R.W. (1979) The formation of virus crystalline and paracrystalline arrays for electron microscopy and image analysis. Adv. Virus Res. 24, 173-221.

Hosaka, Y. and Hosoi, J. (1983) Study of negatively stained images of Sendai virus nucleocapsids using minimum-dose system. J. Ultrastruct. Res. 84, 140-150.

Joklik, W.K., Willett, H.P. and Amos, D.B. (1984) Zinsser Microbiology, 18th edn., Appleton-Century-Crofts, Norwalk, CT.

Kaper, J. (1975) The chemical basis of virus structure, dissociation and reassembly. North Holland, Amsterdam.

Liljas, L. (1986) The structure of spherical viruses. Prog. Biophys. Mol. Biol. 48, 1-36.

Klug, A. (1983) Architectural design of spherical viruses. Nature 303, 378-379.

Lwoff, A., Horne, R. and Tournier, P. (1962) A system of viruses. Cold Spring Harbor Symp. Quant. Biol. 27, 51-60.

Nermut, M.V. (1984) The architecture of adenoviruses. In The Adenoviridae, Ed. H.S. Ginsberg, pp. 5-34. Plenum Press, New York and London.

Palmer, E.L. and Martin, M.L. (1982) An atlas of mammalian viruses. CRC Press, Boca Raton, FL.

Rayment, I., Baker, T.S., Caspar, D.L.D. and Murakami, W.T. (1982) Polyoma virus capsid structure at 22.5 A resolution. Nature 295, 11-115.

Rossman, M. (1984) Constraints on the assembly of spherical virus particles. Virology 134, 1-11.

Simons, K. and Garoff, H. (1980) The budding mechanisms of enveloped viruses. J.Gen.Virol. 50, 1-21.

Watson, D.H. (1978) Form and Function - II. Viruses. In Essays in Microbiology, Eds. J.R. Norris and M.H. Richmond, pp. 4111-4132.

Wildy, P. (1971) Classification and nomenclature of viruses. In Monographs in Virology, Ed. J.L. Melnick, Vol. 5. S. Karger, Basel.

Wiley, D.C. (1985) Viral Membranes. In Virology, Ed. B.N. Fields, pp. 45-67. Raven Press, New York.

PART II

Methods for the study of virus structure

This Page Intentionally Left Blank

Nermut/Steven (eds) Animal Virus Structure

CHAPTER 2A

Electron microscopy: methods for studies of virus particles and virus-infected cells

Methods for 'structural analysis' of the virion

M.V. NERMUT[1], D.J. HOCKLEY[2] and H. GELDERBLOM[3]

[1]National Institute for Medical Research, London NW7, [2]National Institute for Biological Standards and Control, South Mimms, Potters Bar, Herts EN6 3QG, U.K., and [3]Robert Koch Institut, Nordufer 20, 1000 Berlin 65, Germany

2A.1. Negative staining

Negative staining is one of the most useful methods for the visualization of virus particles and is therefore frequently used in both research and clinical diagnosis (Horne and Wildy, 1979). Its principle is simple. Virus particles are mixed with a heavy metal salt solution and thus after drying become 'embedded' in high-contrast material, which dominates the scattering of electrons so that virus particles look bright within a dark background. The most useful 'negative stains' are those solutions which do not tend to bind with biological structures or interact to cause disruption. The most commonly used stains are salts of tungstic acid or uranium (Table 2.1).

2A.1.1. Supporting films for negative staining

Carbon-coated plastic films are recommended for routine work, e.g. parlodion, formvar, butvar, pioloform etc., usually mounted on 400-mesh grids. For high-

TABLE 2A.1.

Negative stains suitable for use in virus research

Name (abbreviated formula)	Usual concn.	pH range (optimum)
Phosphotungstate (Na, K) $H_3PO_4 \cdot 12WO_3$	1.0–2.0%	5.0–8.0 (6.8)
Silicotungstate (Na) $SiO_2 \cdot 12WO_3$	3.0–4.0%	5.0–8.0 (6.8)
Methylamine tungstate $CH_3NH_2 \cdot WO_3$ (approx.)	1.0–2.0%	6.5–8.0
Ammonium molybdate $(NH_4)_6Mo_7O_{24}$	3%	5.2–8.0 (6.5)
Uranyl acetate $UO_2(CH_3 \cdot COO)_2$	0.5–2.0%	4.2–4.5
Uranyl formate $UO_2(H \cdot COO)_2$	1.0–2.0%	4.4
Uranyl nitrate $UO_2(NO_3)_2$	0.5–1.0%	4.4
Uranyl oxalate $UO_2(COO)_2$	0.5–1.0%	5.0–7.0
Uranyl sulphate UO_2SO_4	2%	4.2

resolution work plain carbon films (5–10 nm thick) can also be used routinely, but thinner carbon films must be supported by holey supporting film (micronets - see Pease, 1975, and Nermut, 1982a, for more information). For even negative staining carbon films must be made hydrophilic. This is most easily achieved by subjecting the grids with supporting film to a glow discharge in air, nitrogen or amylamine using a vacuum coating apparatus. Alternatively grids can be exposed to UV for about 30 min or treated with 1% Alcian blue for 5 min. Addition of bacitracin to negative stain supports even spreading of stain on the film (Gregory and Pirie, 1972). Carbon films freshly floated off mica (see Valentine et al., 1968) are hydrophilic on their 'inner' side and do not require any further treatment.

2A.1.2. One-step and two-step procedures

Two different procedures have been developed since the introduction of the negative staining technique in virology. (i) One-step (or simultaneous) procedures: a fairly concentrated virus suspension (e.g. 10^6–10^{12} particles/ml) is mixed with the staining solution (e.g. 2% PTA) and applied to EM grids by spraying, pipetting or depositing with a bacteriological loop or by floating on a drop of the virus/stain mixture. The advantage of the spraying technique is that it is quantitative. This is not always so with the drop method, because of different rates of adsorption of particles of different size (e.g. spikes and whole virus particles). (ii) Two-step (or sequential) procedures: virus particles are first adsorbed onto the grids and then the stain is applied. This is usually achieved by placing grids onto a drop of virus suspension (for 1–20 min, depending on virus concentration), washing by transferring the grids to one or more drops of distilled water, and finally by floating them on a drop of negative stain for about 20 s or longer if required. Excess stain is usually removed by touching the grid to the blotting paper. Transferring grids from drop to drop with forceps can break thin supporting films;

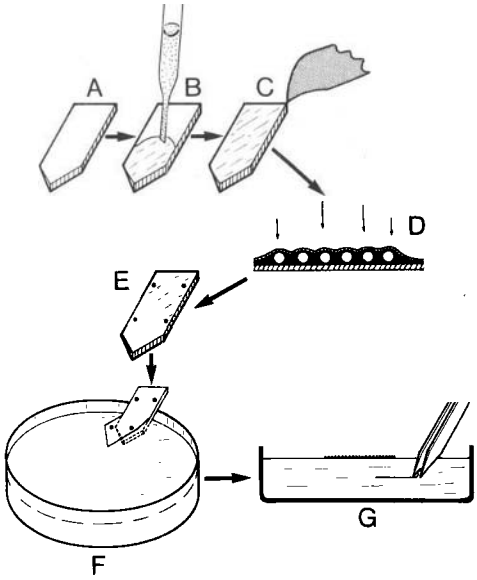

Fig. 2A.1. Diagram of the negative staining-carbon film technique. A: freshly cleaved mica 2 × 1 cm pointed. B: mixture of virus (1–2 mg/ml) suspension and 3% ammonium molybdate spread onto surface. C: excess liquid drained with filter paper. Specimen air-dried. D: very thin film of carbon evaporated onto specimen. E: mark placed on carbon to identify specimen. F: specimen released by slow immersion of mica into second negative stain solution (e.g. 0.5% uranyl acetate). G: specimen picked up from below on copper grid with holey carbon film.

when plain carbon films are used the grids are transferred by means of a platinum wire loop. For the final drying stage, the wire loop with a grid is placed onto a piece of filter paper with specimen uppermost and the loop is removed 2–3 s later after the stain has drained away. When only a small volume of virus suspension is available, 2–5 μl can be deposited onto a grid held in a forceps or a special 'needle holder'. Other useful modifications of negative staining are the Valentine method (see above) and the 'sandwich technique' introduced by Lake (1978) and recently modified by Smith and Seegan (1984). For additional technical information see reviews by Haschemeyer and de Harven (1974) and Nermut (1982a) (Fig. 2A.1).

One of the advantages of negative staining is its suitability for image analysis and processing. However, the image-processing techniques are dependent on being able to 'average' information from areas recorded in electron micrographs containing relatively large areas of repeating features.

The method of crystallizing viruses by mixing solutions of highly concentrated virus suspensions with ammonium molybdate adjusted to a suitable pH, followed by spreading onto a freshly cleaved mica surface, was described by Horne and Pasquali-Ronchetti (1974) as the 'negative staining carbon film technique'. Under the conditions they described, the virus suspensions rapidly form large areas of

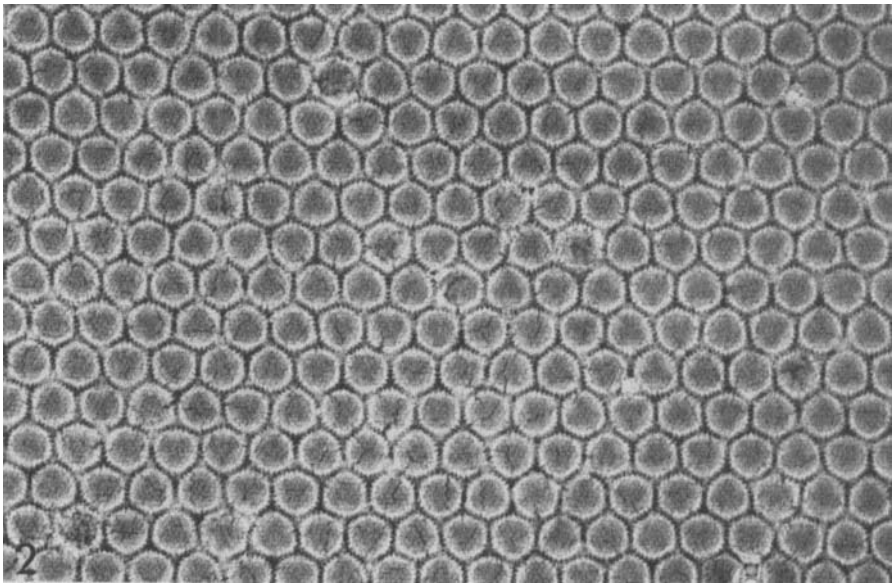

Fig. 2A.2. Two-dimensional array of adenovirus prepared using the negative staining–carbon film technique with ammonium molybdate as the first and uranyl acetate as the second stain. × 100 000. Courtesy of Dr. R.W. Horne.

two-dimensional or three-dimensional crystalline or paracrystalline arrays. The liquid suspensions of virus and negative stain are allowed to dry at room temperature and a thin film of carbon is evaporated onto it. This is released from the mica surface by slow immersion into a second negative stain (usually 2% uranyl acetate). The thin carbon films are then collected at the liquid/air interface of the second stain using copper support grids as shown in the diagram (Fig. 2A.1). The results of this method (Fig. 2A.2) and of other techniques of the negative staining principle when analysed by image processing have been extensively reviewed by Horne (1979).

2A.1.3. Interpretation of negative staining and practical hints

The procedures described stain virus particles in most cases from both sides (top and bottom, Fig. 2A.3) although one-sided images are occasionally observed, especially with the two-step procedure. It is recommended to use stereo electron microscopy to see whether the viruses were stained from below or from both sides. One can also use a procedure for 'one-sided negative staining' (see Nermut 1982a for details). Obviously, only one-sided images can provide correct information about the organization of virus projections or capsomers in icosahedral capsids (class of symmetry, triangulation number). Interestingly, macromolecules or virus

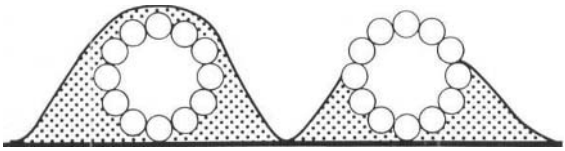

Fig. 2A.3. Diagram of a virus particle stained from both sides (left) and from below (right). From Nermut (1982a) with permission.

fragments are usually stained from below. This is important to note when studying cylindrical structures such as capsomers (see e.g. adenovirus hexon).

Collapse of virus particles due to air-drying is not completely eliminated by embedding in negative stain. Thus the size of negatively stained particles usually exceeds that of freezed-dried ones. Also particles are less collapsed when penetrated by the stain. This is illustrated in Fig. 2A.4 of MuLV negatively stained

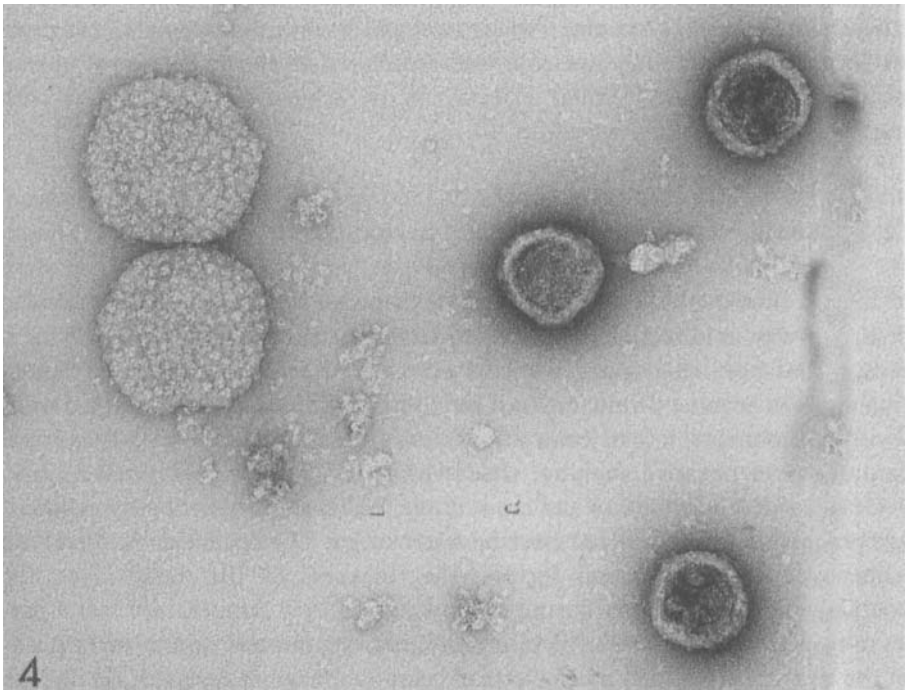

Fig. 2A.4. Murine leukaemia virus (MuLV) particles negatively stained with uranyl acetate. Particles on the left are not penetrated by stain; they appear collapsed and surface knobs are well visualized. The remaining three particles penetrated by uranyl acetate are less collapsed and reveal internal structure. × 130 000. Courtesy of Dr. H. Frank.

with uranyl acetate. Stain-penetrated particles are much smaller than those which are only stained on the surface and therefore displaying their surface projections.

Surface properties of the supporting films can infuence the final image. The meniscus of the negative stain around the virus particle or macromolecule depends on the surface properties of both the protein structure and the supporting film (hydrophilic or hydrophobic; see diagram in Nermut 1982a). Hydrophobic patches can develop within several days on glow-discharged films. In such places MuLV particles look distorted and no surface structures are visible (Fig. 2A.5).

Specific effects and pH of negative stains should also be taken into consideration. For example, uranyl acetate has a stabilizing effect on viral membranes and gives higher contrast than phosphotungstates. It penetrates deeper into protein crystals, but binds to phosphates and carboxyl groups and the staining often turns positive. It may cause aggregation of virus components such as nucleoprotein complexes etc., probably due to its low pH. Salts of phosphotungstic acid (PTA, STA) can have deleterious effects on enveloped viruses and are often responsible for the pleomorphic appearance of influenza virus or the tailed particles of MuLV. Generally, staining at low pH (e.g. 5 to 6) results in better preservation of the virus particles and in surface staining, whereas at pH 8 phosphotungstates penetrate virus particles and stain their nucleoprotein structures (as shown e.g. in paramyxoviruses and poxviruses). Similar effects can be achieved by prefixation with glutaraldehyde or osmium tetroxide.

2A.2. Shadowing techniques

One of the first methods used to increase contrast of viruses in the electron microscope was unidirectional shadow-casting with chromium. Neglected for a decade, it has been resurrected with the advent of freeze-fracturing and freeze-drying and has become a valuable tool for the visualization of virus nucleic acids and viral components, in particular after freeze-fracturing. Shadowing has several advantages over negative staining: shadowed specimens are radiation-resistant, provide one-sided information and are suitable for 3D reconstruction by means of image processing or using stereo electron microscopy. The resolution in shadowed specimens depends on several factors: the thickness of the metal layer; the temperature of the specimen during shadowing - at low temperature metal particles remain attached to sites of first impact; high vacuum also improves the quality of the image, particularly when electron beam evaporators are used; finally, the angle of shadowing can influence the visualization of fine structural details (e.g. 35°–40° is right for icosahedral viruses, but 30° is better for isolated macromolecules). Unidirectional shadowing provides information about the height of virus particles; rotary shadowing is more suitable for contour length

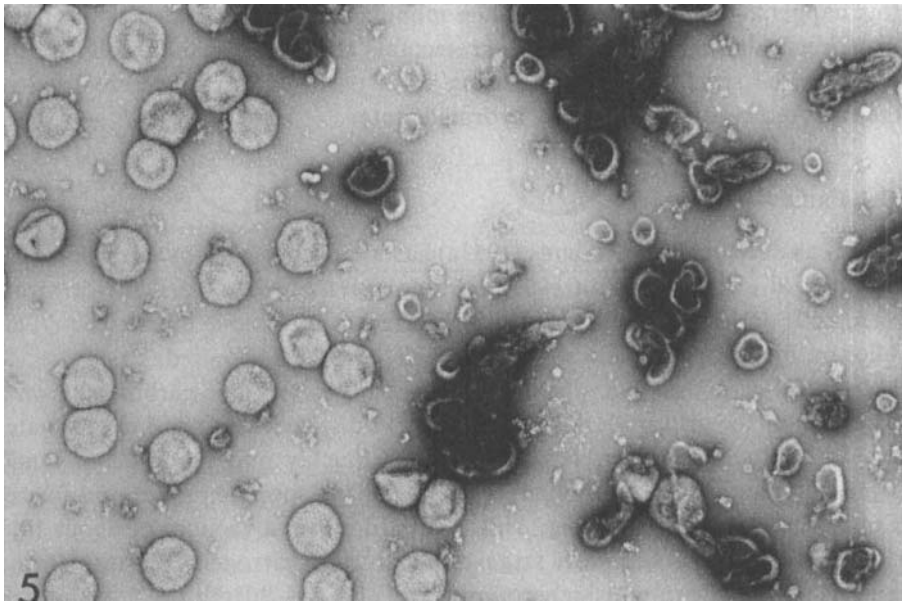

Fig. 2A.5. MuLV particles negatively stained with uranyl acetate for 5 s only. Note even staining and good preservation of virus particles on the left (hydrophilic area) and distortion of virus particles on the right (hydrophobic area). Carbon films were glow-discharged about a week before use and hydrophobic patches developed. × 90 000. Courtesy of Dr. H. Frank.

measurements (e.g. nucleic acids) or for periodic structures such as 2D regular arrays of virus particles. The improved resolution of heavy metal shadowing (2 nm or less) has been achieved thanks to the introduction of electron beam evaporators allowing the use of metals with very high melting points such as Pt, W or Ta/W. Fig. 25.15 in the chapter on Iridoviridae shows the surface structure of Frog virus 3 after freeze-etching and shadowing with Pt/C. Image analysis of such pictures revealed the trimeric nature of the virus capsomers with a resolution of about 2.5 nm. Very good results have also been obtained with adenoviruses (Fig. 23.1b and 23.3b in the chapter on Adenoviridae).

Rotary shadowing is most frequently used for the visualization of viral nucleic acids (for technical details see review by Evenson, 1977).

2A.3. Low-temperature techniques in virus research

The merit of all 'cryotechniques' is physical fixation due to rapid freezing of virus or cell suspensions. However, unless the freezing is extremely rapid (e.g. cooling rate over 10 000 K/s) cryoprotectants (glycerol, DMSO) must be used to prevent ice crystal formation and damage to, or dislocations in, the specimens. The risk

of this happening is much reduced when monolayers of virus particles are used, e.g. for freeze-drying, so that no cryoprotectants are necessary on account of the thinness of the specimen. After freezing virus particles can be freeze-dried or freeze-factured or observed in the hydrated state.

2A.3.1 Freeze-drying (FD)

Spray-FD as developed by Williams (1953a) has been superseded by adsorption FD (Nermut et al., 1972; Nermut, 1977). Monolayers of virus particles or virus-infected cells are rapidly frozen and dried in vacuo to remove external ice. This is followed by shadowing and replication with carbon if required.

In a typical case virus particles are applied to a hydrophilic carbon film on a 400-mesh grid, the grid is washed three times in distilled water and excess water is removed with filter paper; it is then dipped quickly into Freon 22 or liquid nitrogen and then placed onto a precooled ($-150°C$) specimen stage of a freeze-etch unit (e.g. Balzers) for drying. This is carried out in a vacuum of about 10^{-6} torr at $-80°C$ at the specimen stage using a liquid nitrogen cold-trap in the vacuum chamber. Drying at higher temperature (e.g. $-30°C$ or $-50°C$) is not recommended because of possible artefacts caused by complete dehydration and strong thermal collapse. After 20–30 min the specimen is shadowed (best with Pt using an electron beam evaporator) and then warmed to room temperature before being taken out of the vacuum chamber. Large viruses or virus-infected cells are better applied onto a glass coverslip of freshly cleaved mica and, after freeze-drying and shadowing, are replicated with carbon. The replica is floated off onto bleach for cleaning followed by 70% sulphuric acid if necessary, washed on distilled water and picked up on a 400-mesh grid. For more technical details see Nermut (1977, 1982a) and Robards and Sleytr (1985).

2A.3.2. Freeze-fracture (-etching)

The classical procedure of cutting a glycerinated pellet of virus particles in a freeze-etch unit has been practically abandoned, since it requires too much purified virus suspension and does not allow deep-etching.

Freeze-fracturing by means of a hinged double replica device is more economical and also more rewarding. A small volume (1–5 μl) of virus pellet is usually sandwiched between two copper plates or mica and copper. A gold or copper grid (spacer) can be placed between the plates to increase the cooling rate. No cryoprotectants are needed if the metal sandwich is plunged rapidly into liquid propane or flushed with propane in a propane jet device (e.g. Cryojet from Balzers). However, it is advisable to use 20% glycerol, 10% dimethyl sulphoxide or 30% polyvinylpyrrolidone when a mica/copper sandwich is frozen by manual dipping into liquid Freon.

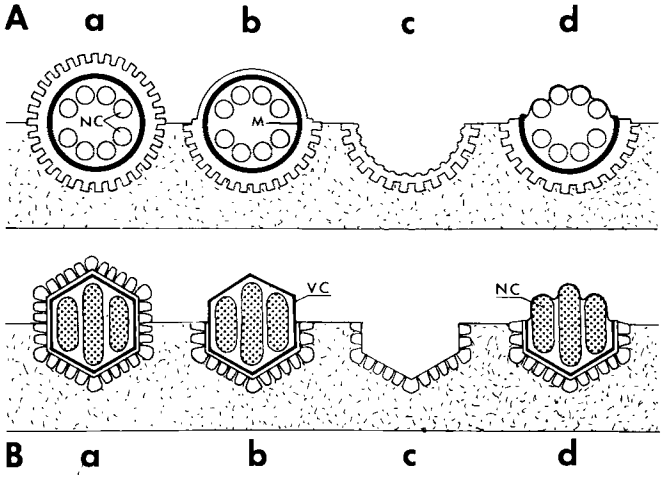

Fig. 2A.6. Diagram of fracture faces in enveloped viruses (A) and icosahedral viruses (B). Aa, virus surface revealed by etching, b, convex fracture face of virus membrane; c, concave fracture face of virus membrane; d, cross-fractured virion after fixation with formaldehyde. Virus nucleocapsid exposed (NC). M = M-protein or 'core shell'. Ba, virus surface revealed by freeze-fracturing (-etching) in buffer or water; b, virus core (VC) exposed by freeze-fracture in glycerol (or within cells); c, inner face of virus capsid after the core has been fractured away; d, cross-fractured virus particle with nucleocapsid (NC) 'rods'.

The sandwich is separated by means of a double replica device (Nermut and Williams, 1977) and the fracture faces (or etch faces) are shadowed and replicated. Carbon replicas can be easily floated off the mica, but problems can arise with the copper plates. Here it appears practical to reinforce the carbon replica with a drop of 0.1% parlodion, remove excess and dry. The plate is then cut into 2–4 small pieces, which are placed on 25% nitric acid until the copper is dissolved. This is followed by cleaning on 30–70% sulphuric acid, washing on distilled water (2×) and mounting on a grid from below. Parlodion is then dissolved in amyl acetate (about 1 h).

Interpretation of freeze-fracture images

Different viruses fracture in different ways depending on their chemical composition and to some extent on their size and architecture. In enveloped viruses the cleavage occurs preferentially through the viral membrane (lipid bilayer) whereas in naked viruses the fracture plane is random (Fig. 2A.6). It follows that under normal conditions enveloped viruses are not cross-fractured so that their interior cannot be visualized by the freeze-fracture technique. However, cross-fractured particles have been observed in large viruses (vaccinia virus, Sendai virus, Frog

virus 3) and with influenza virus prefixed with formaldehyde (which cross-links the viral membrane; Nermut, 1982a). Naked viruses cross-fracture more frequently when infiltrated with glycerol or caesium chloride.

2A.3.3. Ultrathin frozen sections

See Section 2B.4 on immunoelectron microscopy for details.

2A.3.4. Electron microscopy of frozen hydrated viruses

Most preparatory techniques for electron microscopy dehydrate virus particles and this can change both the gross morphology and the fine structural features of the virion (distortion, disruption, shrinkage, aggregation, etc.). Freeze-drying or freeze-etching both minimize dehydration, but provide only a shadowed surface replica of limited resolution. The observation of thin layers of ice containing virus particles allows one to assess the real size and shape of virus particles in solution (Adrian et al., 1984).

Briefly, highly concentrated virus suspension is deposited onto a plain copper grid or a grid with a holey carbon film and the excess of suspension is drained away by touching lightly with blotting paper. The grid is then plunged into liquid propane or ethane to vitrify the thin layer of water and kept at $-150°C$ or lower in order to prevent the phase transition from vitreous ice into crystalline ice which takes place at $T_d \approx -133$ to $-140°C$ before observation in the electron microscope. A special low-temperature specimen stage is required and suitably cooled specimen holders are now commercially available for use with several models of electron microscopes. Usually the contrast of the unstained virus particles is low, but increases with underfocussing (phase contrast). The radiation damage is about one-third that at room temperature.

The first results thus obtained have, for example, confirmed that influenza virus is not pleomorphic, but spherical as demonstrated by Williams (1953b) and Nermut and Frank (1971) using freeze-drying. However, they have already provided new information on the size of viruses and the organization of the virus surface in a few cases (Adrian et al., 1984; Booy et al., 1985; and the chapters on Myxo-, Papova- and Togaviridae in this volume).

2A.4. Tactics of structural analysis of viruses

The aim of structural analysis of viruses is to determine the shape, size, surface structure and internal organization of the virion. Obviously a number of different preparatory methods have to be applied for this purpose. Only a general outline of recommendations can be given here because of the diversity in size, structure

and chemical composition of viruses, and the reader is referred to a more detailed account in a review by Nermut (1982a). A summary of the procedures recommended is given in Table 2.2.

What follows is a brief account of procedures which have to be applied with respect to the specific features of individual virus families and to the amount and nature of the specimen available.

(i) Negative staining with salts of tungstic acid at different pH values and with uranyl acetate using both unfixed and fixed viruses. This will first provide information on the shape and size of virus particles, surface projections and possibly the virus interior.

(ii) Ultrathin sections of virus suspensions or even better of cells with budding or intracellular viruses will reveal more about the presence of membranes or internal bodies than about tiny surface projections usually difficult to visualize with routine staining procedures.

(iii) Freeze-drying is indispensable for studies of the native shape of virions and of their surface pattern. It can be combined with negative staining or followed by shadowing.

(iv) Freeze-etching in the absence of cryoprotectants is equivalent to freeze-drying, but has the benefit of a low degree of shrinkage and is therefore recommended for size determinations. Freeze-fracturing can also dissect virus particles under suitable conditions and provide useful information about virus membranes and virus cores. Frozen-hydrated virus suspensions are probably superior to any other method for determining the size and shape of viruses.

(v) Gentle dissociation of virus particles on the grid (e.g. by detergent treatment) followed by negative staining is useful for studies of virus capsids or capsomers, spikes or some internal components.

TABLE 2A.2.

To obtain best information about:	Use the following procedures (in order of preference)
Shape of virion	Freeze-dry or freeze-etch shadowing; frozen-hydrated specimens; ultrathin sectioning; critical-point-drying; negative staining of fixed preparations or with uranyl acetate.
Size	Frozen-hydrated specimens; freeze-etching; freeze-dry negative staining; negative staining (in case of small viruses); thin sectioning.
Surface structure	Negative staining at acidic pH (4.2–6.0); freeze-dry negative staining; freeze-etch or freeze-dry shadowing (possibly followed by image processing).
Internal organization	Negative staining at alkaline pH (8.0) or after fixation, or after mild dissociation of the virion; ultrathin sectioning.

(vi) Finally, high-resolution electron microscopy of purified structural components (negative staining, rotary shadowing, image processing, etc.) completes the list of the procedures which should be employed, in particular in studies of newly isolated viruses.

References

Adrian, M., Dubochet, J., Lepault, J. and McDowell, A.W. (1984) Cryo-electron microscopy of viruses. Nature 308, 32–36.

Booy, F.P., Ruigrok, R.W.H. and van Bruggen, E.F.J. (1985) Electron microscopy of influenza virus. A comparison of negatively stained and ice-embedded particles. J. Mol. Biol. 184, 667–676.

Evenson, D.P. (1977) Electron Microscopy of Viral Nucleic Acids. In Methods in Virology, Eds. K. Maramorosch and H. Korowski, pp. 219–264, Academic Press, New York.

Gregory, D.W. and Pirie, B.J.S. (1972) Wetting agents for electron microscopy of biological specimens. Proc. 5th Eur. Congr. Electron Microsc. Manchester, pp. 234–235.

Haschemeyer, R.H. and De Harven, E. (1974) Electron microscopy of enzymes. Annu. Rev. Biochem. 43, 279–301.

Horne, R.W. (1979) The formation of virus crystalline and paracrystalline arrays for electron microscopy and image analysis. Adv. Virus Res. 24, 173–221.

Horne, R.W. and Pasquali-Ronchetti, I. (1974) A negative staining-carbon film technique for studying viruses in the electron microscope: I. Preparative procedures for examining icosahedral and filamentous viruses. J. Ultrastruct. Res. 47, 361–383.

Horne, R.W. and Wildy P. (1979) An historical account of the development and applications of the negative staining technique to the electron microscopy of viruses. J. Microsc. 117, 103–122.

Lake, J.A. (1978) Electron microscopy of specific proteins: three-dimensional mapping of ribosomal proteins using antibody labels. In Advanced Techniques in Biological Electron Microscopy II, Ed. J.K. Koehler, pp. 173–211. Springer-Verlag, Berlin.

Nermut, M.V. (1977) Freeze-drying for electron microscopy. In Principles and Techniques of Electron Microscopy, Ed. M.A. Hayat, Vol. VII, pp. 79–117, Van Nostrand Rheinhold Co., New York.

Nermut, M.V. (1982a) Advanced methods in electron microscopy of viruses. In New Developments in Practical Virology, Ed. C. Howard, pp. 1–58. A. Liss, New York.

Nermut, M.V. (1982b) The cell monolayer technique in membrane research: A review. Eur. J. Cell Biol. 2, 160–172.

Nermut, M.V. and Frank, H. (1971) Fine structure of influenza A2 (Singapore) as revealed by negative staining, freeze-drying and freeze-etching. J. Gen. Virol. 10, 37–51.

Nermut, M.V., Frank, H. and Schäfer, W. (1972) Properties of mouse leukemia viruses. III. Electron microscopic appearance as revealed after conventional preparation techniques as well as freeze-drying and freeze-etching. Virology 49, 345–358.

Nermut, M.V. and Williams, L.D. (1977) Freeze-fracturing of monolayers (capillary layers) of cell membranes and viruses: some technical considerations. J. Microsc. 110, 121–132.

Pease, D.C. (1975) Micronets for electron microscopy. Micron 6, 85–92.

Plattner, H. and Bachmann, L. (1982) Cryofixation. A tool in biological research. Int. Rev. Cytol. 79, 237–304.

Robards. A.W. and Sleytr, U.B. (1985) Low-temperature methods in biological electron microscopy. In Practical Methods in Electron Microscopy, Ed. A.M. Glauert, Vol. 10. Elsevier Biomedical, Amsterdam.

Smith, C.A. and Seegan, G.W. (1984) The pleated sheet: an unusual negative-staining method for transmission electron microscopy of biological macromolecules. J. Ultrastruct. Res. 89, 111–122.

Valentine, R.C., Shapiro, B.M. and Stadtman, E.R. (1968) Regulation of glutamine synthetase. XII. Electron microscopy of the enzyme from *Escherichia coli*. Biochemistry 7, 2143–2152.

Williams, R.C. (1953a) A method of freeze-drying for electron microscopy. Exp. Cell Res. 4, 188–201.

Williams, R.C. (1953b) The shapes and sizes of purified viruses as determined by electron microscopy. Cold Spring Harbor Symp. Quant. Biol. 18, 185–196.

This Page Intentionally Left Blank

Nermut/Steven (eds) Animal Virus Structure

CHAPTER 2B

Electron microscopy: methods for studies of virus particles and virus-infected cells

Methods for study of virus/cell interactions

M.V. NERMUT[1], D.J. HOCKLEY[2] and H. GELDERBLOM[3]

[1]National Institute for Medical Research, London NW7, [2]National Institute for Biological Standards and Control, South Mimms, Potters Bar, Herts EN6 3QG, U.K., and [3]Robert Koch Institut, Nordufer 20, 1000 Berlin 65, Germany

Interactions of viruses with the host cell comprise their adsorption to the cell surface (in most cases via specific receptors), uptake and transport in the cytoplasm, followed by uncoating and release of the genome, nucleic acid replication, and finally synthesis of virus proteins leading to the assembly of new virus progeny. All these stages in the virus/cell interaction can be monitored and studied with the electron microscope, but a range of different preparatory methods are required. These include ultrathin sectioning, scanning electron microscopy, replicas of cell surfaces or cell interior, and a series of more sophisticated procedures such as autoradiography, low-temperature electron microscopy of frozen sections, cytochemistry and immunolabelling.

2B.1. Ultra-thin sectioning

Fixation, embedding and sectioning of virus-infected cells for transmission elec-

tron microscopy (TEM) can provide much information about the structure of viruses and the processes of cell infection. In addition to straightforward morphological studies, sectioning techniques can also be combined with immunocytochemical and autoradiographic labelling methods for further localization of viral components in cells. These methods may require modifications of the standard thin-sectioning procedures but for all the techniques it is in vitro cultured monolayers of infected cells that have provided the most valuable results rather than pathological specimens derived from infected animals. The standard techniques for preparation of ultrathin sections can be found in many other publications (e.g. Glauert, 1975) and the following comments are addressed mainly to the specialized requirements of preparing cell cultures for sectioning. Monolayers of cultured cells demand particularly gentle treatment during fixation and embedding and whenever possible it is desirable to use in situ methods.

Fixation in situ of cells which grow attached to a substrate (i.e. the base of the culture vessel or a coverslip in the dish) can be achieved by slowly adding to the culture medium an equal volume of double-strength glutaraldehyde (2.5%) in the same buffer as used for the medium or in an isotonic buffer (300 mosmols) such as the following: 1.6 g sodium cacodylate, 0.4 g sodium chloride, 0.2 ml 1 M calcium chloride, 0.2 ml 1 M magnesium chloride, 80 ml distilled water; adjust to pH 7.2 with 1 N hydrochloric acid; make up to a final volume of 100 ml. Fixation should commence at 37°C but after 5 min processing can proceed at room temperature or at 4°C if storage is necessary. Isotonic buffer is recommended for the osmium tetroxide fixative and for all washes until after osmium fixation.

Good fixation of cultured cells is also obtained with a mixture of glutaraldehyde and osmium tetroxide followed by fixation or 'en-bloc staining' with uranyl acetate (Hirsch and Fedorko, 1968). The glutaraldehyde and osmium mixture cannot be used at 37°C but it can be used at room temperature if the components are mixed immediately before use and if fixation continues in the dark. Combined glutaraldehyde and osmium fixation followed by treatment with uranyl acetate is recommended for examination of enveloped viruses budding at the cell surface, since the fixative not only preserves membrane lipids but is also particularly successful for demonstrating the spikes and M-protein of influenza virus. The glycoprotein spikes on the envelope of mouse leukaemia virus are better visualized if propylene oxide is also omitted from the embedding schedule (Fig. 2B.1). Good preservation of membranes and associated proteins (e.g. surface spikes) is achieved by addition of either tannic acid to glutaraldehyde (Fig. 2B.2) or potassium ferricyanide to osmium tetroxide (La Fountain et al., 1977; Maupin and Pollard, 1983; McDonald, 1984).

Despite the above remarks concerning in situ fixation, cells that grow in suspension either must be allowed to settle in a small tube or should be centrifuged gently for about 2 min in a bench centrifuge at low speed (200 $\times$ *g* maximum) before the medium is removed and replaced with glutaraldehyde fixative. Five ml of a

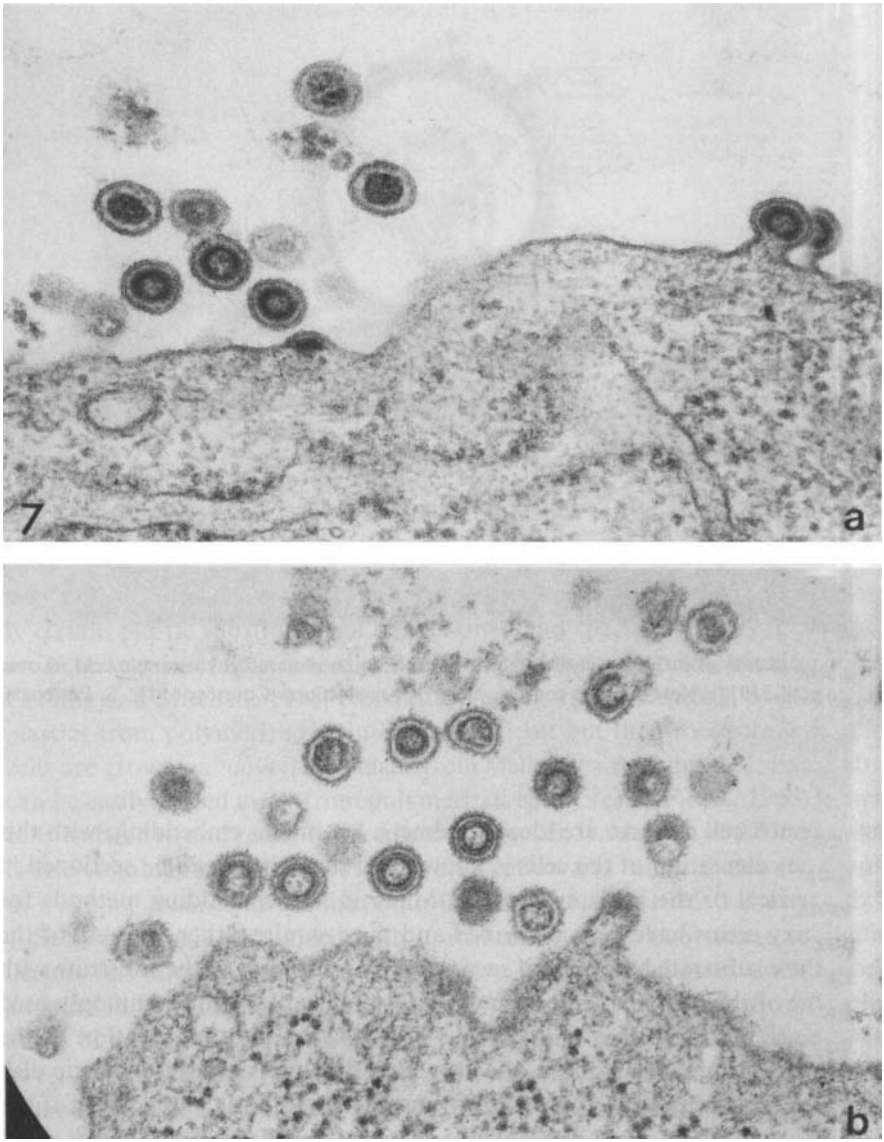

Fig. 2B.1. Ultrathin section of MuLV with (a) and without (b) propylene oxide used in the embedding procedure. Note better visualization of surface projections in (b). × 35 000. Courtesy of Dr. H. Frank.

suspension culture will usually provide an optimum size of pellet and if the cells are undisturbed while the fixative is added then the pellet is stabilized and can be treated subsequently like a small piece of tissue. This method obviates the need for repeated centrifugation during subsequent processing which usually leads to some loss of cells and addition of other debris to the specimen.

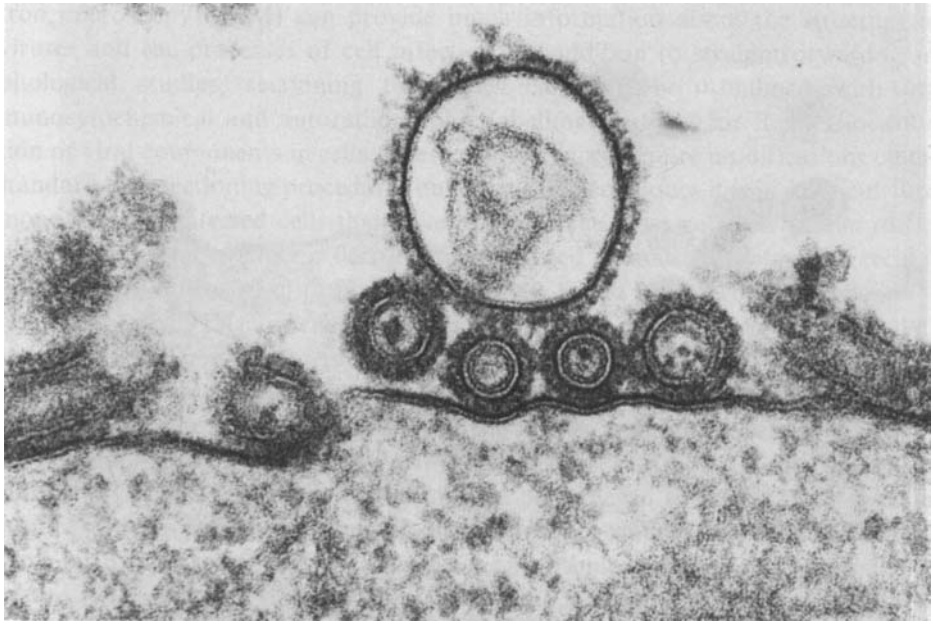

Fig. 2B.2. Thin section of influenza-virus-infected cell fixed with glutaraldehyde tannic acid mixture (LaFountain et al., 1977). Note the high contrast of surface projections. Courtesy of Dr. S. Patterson. × 160 000.

Virus-infected cell cultures are ideal specimens for in situ embedding; with this technique the orientation of the cells is known and the culture can be sectioned in either the vertical or the horizontal plane. Many in situ embedding methods for use with epoxy resins have been described and they require either removal of the cells from their substrate before final sectioning or sectioning of the substrate with the cells. One of the simplest removal methods is applicable to the commonly used polystyrene cell culture dishes and flasks. After fixation and dehydration of the cells in the dish, propylene oxide is added, which slowly dissolves the plastic dish so that the cell monolayer lifts off its substrate (Steinman and Cohn, 1972). If the monolayer is scored into 3–4-mm squares during dehydration then these small pieces of the culture will remain as a flat monolayer and can be oriented in the final embedding medium (Kuhn, 1981). Even if the detached cells are simply pelleted in the embedding medium the basal surface of the cells can always be recognized by the adjacent layer of electron-dense material which is derived from the surface of the culture dish. The propylene oxide removal method is also applicable to cells cultured on polystyrene beads (Sargeant et al., 1981).

More precise orientation of cultures and, indeed, selection of single cells can be obtained either by removal of the supporting dish or coverslip after final

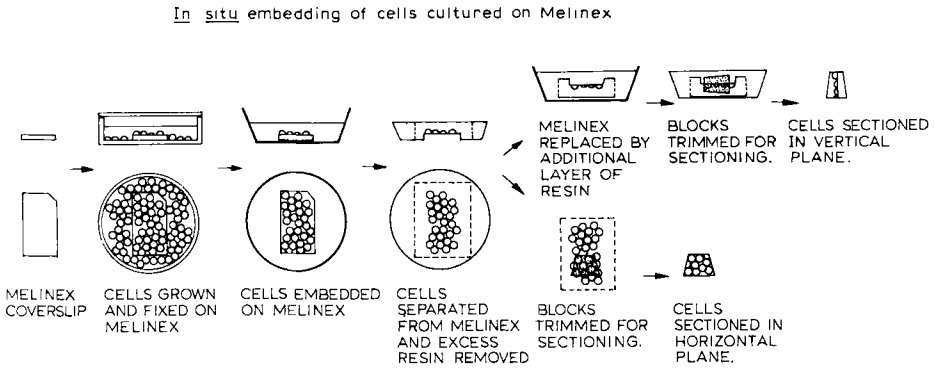

Fig. 2B.3. Procedure for embedding cell monolayers on Melinex coverslips. After removal of Melinex from polymerized resin the cells are immediately available for sectioning in the horizontal plane. If only this plane of sectioning is required then small pieces of Melinex with cells can be embedded in the lid of an inverted BEEM capsule. Re-embedding is necessary for vertical-plane sectioning; these specimens should be trimmed carefully in order not to cause separation of the two layers of resin.

polymerization of the embedding resin or by sectioning cells on their substate. Only certain plastic substrates can be sectioned and special methods for dehydration are necessary in order not to dissolve or distort the substrate (Brinkley et al, 1967; Codling and Mitchell, 1976; Nopanitaya et al., 1977). Removal of glass and most plastics from polymerized resin can be difficult but the procedure is simplified if cells are grown on 'coverslips' made from Melinex (= Agralon, ICI, England), which can be easily peeled away from polymerized epoxy resin (Firket, 1966), leaving the cells embedded and ready for sectioning (Fig. 2B.3). Melinex of 0.075 mm thickness is also suitable for light microscopy, and Teflon and cellulose acetate can be used in a similar manner to Melinex (van Ewijk and Hosli, 1975; Lahav et al., 1982).

Sections should be stained with uranyl acetate and lead citrate even if uranyl acetate has already been used as a fixative. This method gives the best available staining at present and is particularly important for demonstration of the DNA cores of some viruses. It should be remembered when making comparisons between sectioned and negative-stained specimens that fixation, dehydration and embedding cause considerable shrinkage and that the resolution available in sections is rarely better than 2 nm. Nevertheless, there is much information to be gained from thin sections and the amount can be increased by the use of autoradiographic and immunocytochemical labelling procedures (Williams, 1977).

2B.2. Scanning electron microscopy (SEM)

Large viruses can be visualized on the surface of cells by SEM using a medium-resolution (7 nm) conventional instrument. SEM is particularly useful for ex-

amination of enveloped viruses budding from the surface of cells, but may also be applicable to other large viruses. For example, adenovirus (80 nm diameter) can be recognized even when adsorbed to cells because of its icosahedral shape. Cultured cell monolayers are again the cells of choice for such experiments and 'coverslip' cultures are also excellent specimens, in many respects, for SEM. There have been many studies of cell cultures using the 'standard' SEM methods of glutaraldehyde and osmium tetroxide fixation followed by dehydration and critical-point drying (CPD) and full accounts of these methods have recently been given by Wolosewick and Porter (1979) and Brunk et al. (1981) among others.

The main requirement in preparation of cell cultures for SEM is to minimize shrinkage and prevent distortion of cell surface features. Thus these specimens require not only in situ fixation but also in situ drying procedures, which means that the cells must remain on their coverslip and under a fluid until they finally emerge from the critical-point drying apparatus. This can be achieved by the use of a continuous-flow or fluid-exchange apparatus for fixatives, washing and dehydrating fluids, and several such machines have been described (van Ewijk and Hosli, 1975; Baigent et al., 1978; Peters, 1980; Rostgaard and Tranum-Jensen, 1980). The simplest of these devices is Baigent's apparatus, which is briefly described again here (Fig. 2B.4). The fluid-exchange method allows the specimens to remain under a fluid at all times and therefore they experience no major surface tension forces during their preparation. Furthermore the fluid changes can be made slowly and gently and processing of multiple specimens is simplified. Cell cultures prepared by fluid exchange exhibit erect and uniform surface protrusions and microvilli (not collapsed and tangled) and less shrinkage than is seen in sequentially processed specimens (Fig. 2B.5).

The Baigent apparatus requires that cells are grown on 22 × 7 mm glass coverslips in Petri dishes or tubes and are fixed in situ with glutaraldehyde. Cells cultured in suspension can be attached to coverslips with poly-L-lysine. Attachment may alter cellular morphology and therefore the cells must be fixed in suspension, but thorough washing with isotonic buffer after glutaraldehyde fixation and a 14 h sedimentation period will result in attachment of all cells to the coverslip (Sanders et al., 1975). The coverslips are transferred under buffer into the specimen chamber of the Baigent apparatus (Fig. 2B.4) and processing of the specimens then follows the schedule described by Katsumoto et al. (1981), which gives good preservation of cultured cells. The specimens are fixed in 1% osmium tetroxide in isotonic buffer followed by extensive washing with buffer and then treatment for 60 min with 1% tannic acid (Mallinckrodt, Cat. No. 1764, MW 322) in isotonic buffer, which is again followed by extensive washing in water and further treatment with 1% osmium tetroxide in water for 30 min. The cells are dehydrated rapidly in absolute ethanol and then introduced into the CPD apparatus in a manner which ensures that the specimens remain covered by alcohol until the CPD apparatus is filled with liquid carbon dioxide. This can be achieved

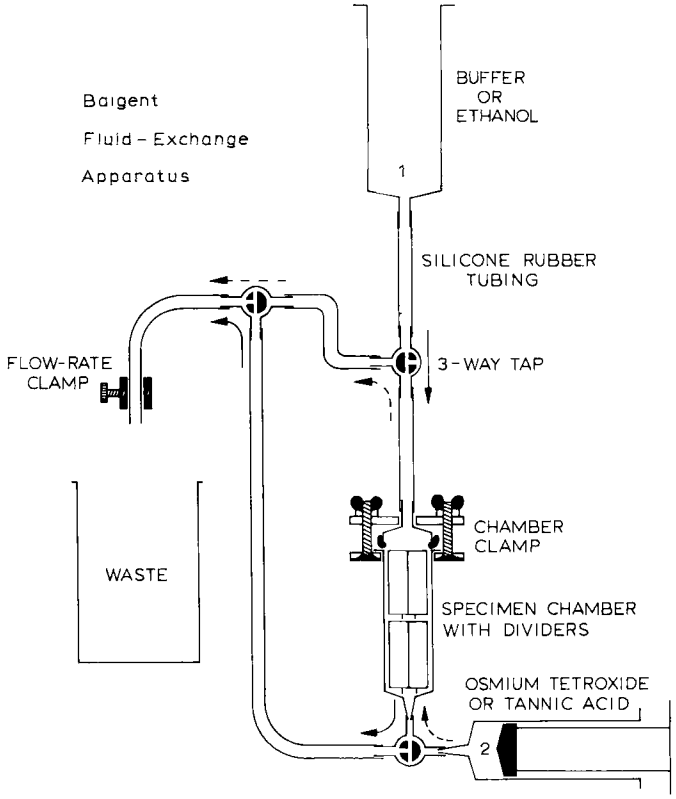

Fig. 2B.4. Baigent apparatus for processing cell cultures for SEM. Two containers (1 and 2) consisting of 10- or 20-ml disposable syringes are connected to top and bottom of specimen chamber, which is constructed from 5-ml syringe. Eight coverslips can be accommodated in the chamber by constructing dividers from the syringe plunger. Three-way taps (AHS International, Herstal, Belgium) allow descending flow (➞) from reservoir 1 and ascending flow (— — ►) from reservoir 2. The whole apparatus with the exception of the chamber clamp, which must be manufactured from brass, consists of disposable laboratory items; it is mounted on a vertical board with Terry clips. All fluid changes in the specimen chamber are made on the principle of one fluid displacing another from either above or below according to their specific gravity. The heavier fluids, osmium tetroxide and tannic acid, are slowly introduced into the specimen chamber from below. Lower-density ethanol and buffer washes enter the chamber from above by gravity and the rate of flow is kept low by a clamp on the silicone tubing at the exit from the specimen chamber. The specimen chamber, with syringe outlet plugged, is removed from the apparatus for loading or CPD.

by placing the Baigent specimen chamber vertically inside the Polaron critical-point drier. Further important aspects of the CPD process have been reviewed by Bartlett and Burstyn (1975).

The above processing schedule is designed to prevent the formation of holes and cracks in the plasma membrane of the cells and to minimize cell shrinkage. All

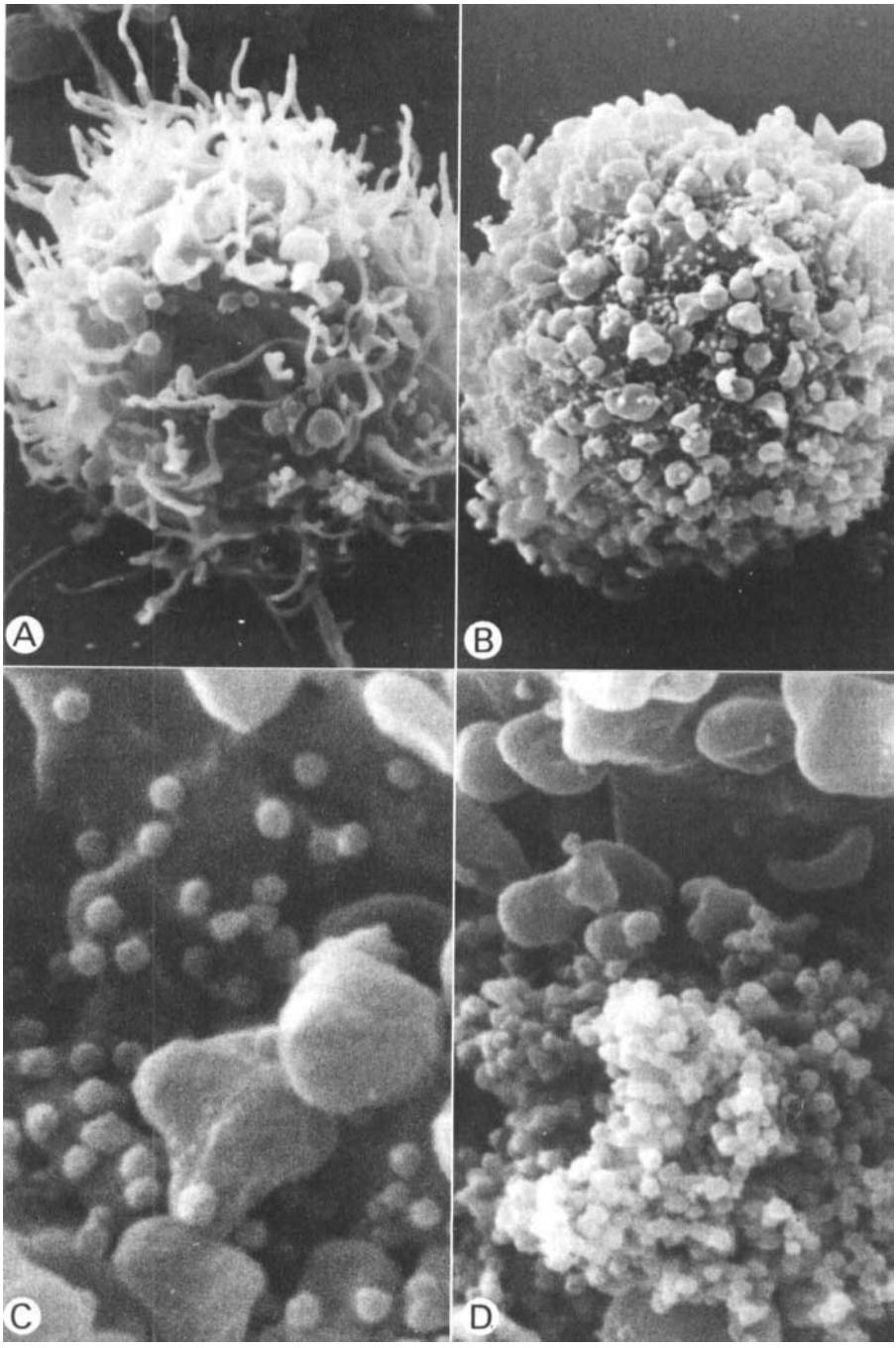
A
B
C
D

preparation methods for SEM in current use cause shrinkage; simple glutaraldehyde and osmium fixation followed by CPD typically gives a 70% volume shrinkage in red blood cells (Eskelinen and Saukko, 1983) and a 40% reduction in the diameter of lymphocytes (Schneider, 1976). In cell cultures this often means that gaps are created between cells although some cell lines such as MDCK have well-developed intercellular junctions which prevent the formation of gaps between at least some of the cells. Clearly shrinkage is a problem still waiting for a solution and meanwhile scanning electron microscopists must be able to recognize such artefacts in their specimens.

SEM is a more recently developed technique than TEM and the use of labelling techniques with SEM is not so far advanced as with TEM. A variety of markers have been proposed, including viruses themselves. Gonda, Gilden and Hsu (1979) have used antibodies labelled with haemocyanin to distinguish different retroviruses budding on the surface of cells. However, the most potentially useful label appears to be colloidal gold particles (Horisberger, 1981). Further developments can also be expected in the use of the microscope itself, since the interaction of the scanning beam of electrons with the specimen results not only in secondary electrons but also in several other signals. Back-scattered electrons appear to be particularly useful for detecting heavy elements such as gold (Soligo and de Harven, 1981).

2B.3. Replica techniques

Carbon replicas of cells, either intact or freeze-fractured, represent an alternative choice for studies of the different stages in virus cell/interaction, at least in the case of enveloped viruses. They provide a high-resolution view of relatively large areas of cell surface or cell interior (after freeze-fracturing or lysis). Replicas, in combination with gold-immunolabelling, are also well suited to studies of virus-specific receptors or virus-coded transmembrane proteins (glycoprotein projections).

Fig. 2B.5. Scanning electron microscopy of H 9 cultured lymphocytes infected with human or simian T-lymphotropic virus type III (HTLV-III or STLV-III). Changes in cell morphology due to the cytopathic effect of the virus can be recognized and it is also possible to see the individual budding virus particles and their distribution on the cell surface. Fixed and processed for SEM using the Baigent apparatus. A. Normal, uninfected H 9 lymphocyte with long microvilli and some blebs on its surface. ×6500. B. H 9 cell infected with HTLV-III; microvilli are absent and the cell is covered with numerous blebs. ×6500. C. Budding virus particles of HTLV-III on the surface of H 9 lymphocyte; they are mostly located between the surface blebs. ×40 000. D. Aggregation of budding particles of STLV-III on the surface of an infected H 9 cell. ×27 000.

2B.3.1. Replicas of outer surface of virus-infected cells

Cells grown in suspension must be washed three times in a fresh medium or isotonic buffer and attached to positively charged mica or glass coverslips (by settling or centrifugation). Monolayers of cells grown on coverslips are washed similarly in situ. Next, the cells are fixed with 1–2% glutaraldehyde, followed by 1% osmium tetroxide and/or 1% uranyl acetate as described above, before being washed in distilled water and finally dried. There are three options here: air-drying from alcohol (structures are reasonably preserved but flattened); critical-point drying (see paragraph on SEM above; membranes may show signs of damage, but 3D preservation of cellular projections is very good); and freeze-drying (best preservation of fine structure, but prone to collapse of microvilli if not prefixed with osmium or uranyl acetate). For more details and references see Nermut (1982a). After drying, cells are shadowed with Pt/C (unidirectionally or rotary) and replicated with carbon from 50° to 70° using a rotary stage (Fig. 2B.6).

Monolayers of virus-infected cells grown on coverslips can be freeze-dried as follows. Cells washed with serum-free medium or suitable buffer are fixed with glutaraldehyde followed by osmium tetroxide or uranyl acetate in the usual way. Repeated washing in distilled water precedes freezing in Freon 22 or liquid nitrogen followed by drying at $-80°C$ for about 30 min, shadowing and rotary replication with carbon from 50° to 70°, which helps to obtain large pieces of contiguous replicas even when cells possess microvilli.

2B.3.2. Freeze-fracture (-etching) of virus-infected cells

Virus-infected cells can be sedimented and prepared for freeze-fracture in the same way as virus pellets. Cells can be fractured with a blade or sandwiched between two copper plates as described for virus pellets. Again, cryoprotectants might be necessary if Freon is used as the cryogen. Good results were obtained in particular using polyvinylpyrrolidone in studies of adenovirus-infected HeLa cells. Polyvinylpyrrolidone does not penetrate through the plasma membrane so that limited etching is possible and well-defined structural details of cross-fractured virus particles can be obtained (Nermut, 1978).

Alternatively, cell monolayers can be prepared on positively charged supports (mica or glass; Nermut, 1982b), sandwiched with a copper plate and fractured as described above. In this case, because of the positive charge, the fracture plane follows the mica surface and splits the plasma membrane attached to the mica. However, deviations across the cell are frequent if the monolayer is not dense.

Cells growing in monolayers (on plastic coverslips) can also be fractured (in situ) if the coverslip is cut to a suitable size and cells are sandwiched, etc., as above. For technical details see for example Plattner and Bachmann (1982).

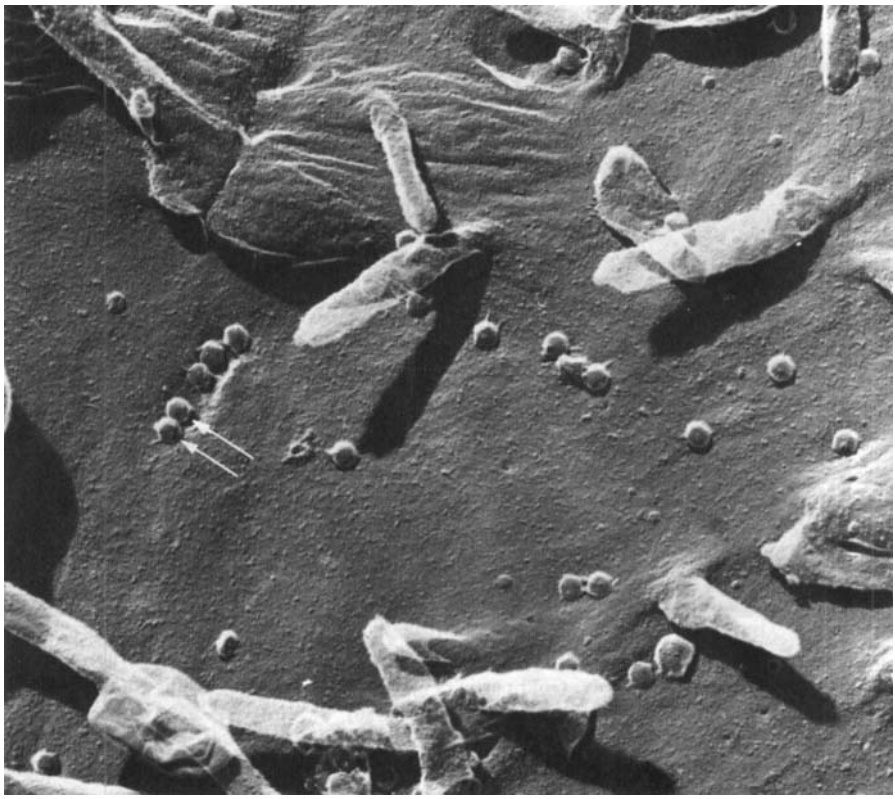

Fig. 2B.6. Replica of a HeLa cell 4 min after infection with adenovirus, showing good three-dimensional-preservation of microvilli and presence of virus paritcles (arrows). Critical-point-dried, shadowed vith Pt/C and rotary carbon coated from 45°. ×40 000.

2B.3.3. Observation of the protoplasmic surface of virus-infected cells

This is a useful procedure for studies of virus assembly at the plasma membrane. Briefly, cells attached to positively charged supports or grown in monolayers are lysed and broken open by means of squirting from a syringe; they are then fixed, freeze-dried and replicated with heavy metal and carbon. Immunolabelling of virus-specific proteins can be carried out before freeze-drying. Fig. 2B.7 shows the protoplasmic surface of BHK cell infected with vesicular stomatitis virus and gold-immunolabelled with anti-M-protein antibody. More technical data can be found in Nermut (1982a,b) and examples of application in Büechi and Bächi (1979), Rutter et al. (1985) and Dubois-Dalcq et al. (1984).

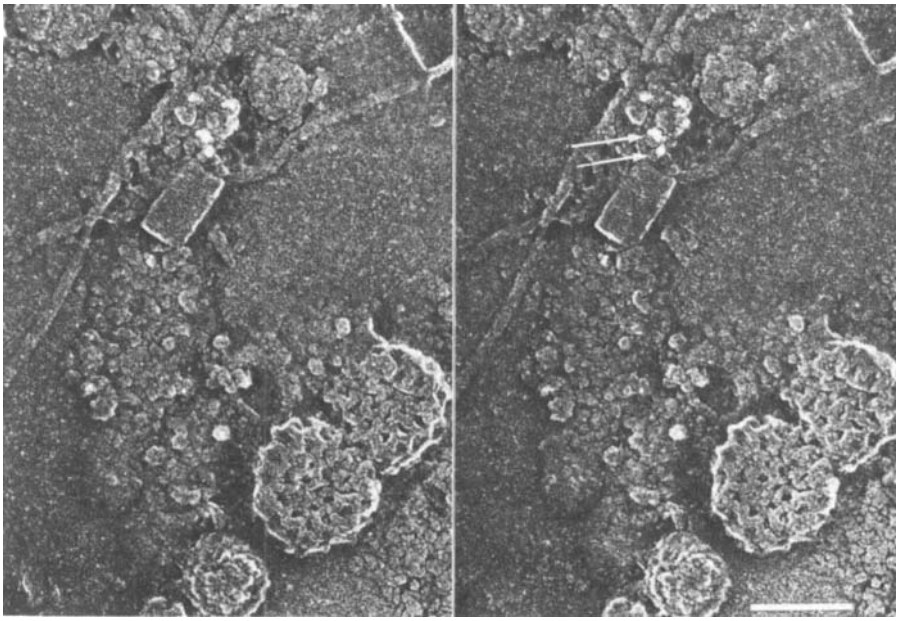

Fig. 2B.7. Protoplasmic surface of BHK cell infected with vesicular stomatitis virus and gold-immunolabelled with anti-M-antibody. Gold particles appear white (arrows) in this rotary-shadowed replica. Stereo-pair, ×131 500. From Odenwald et al. (1986). J. Virol. 57, 922, with permission. Courtesy of Dr. M. Dubois-Dalcq.

2B.4. Immuno-electron microscopy in virology

Immuno-electron microscopy (IEM) combines antibody specificity in detecting antigenic determinants and the high spatial resolution of electron microscopy in a most favourable way. In virology, IEM can either be applied to search for virus constituents in infected cells, i.e. immunocytochemistry, or the method can be used directly as 'dispersive' IEM for diagnostic purposes as well as for the mapping of antigenic determinants on the surface of isolated virus particles.

2B.4.1. Antibodies; definitions and properties

Antibodies are formed as part of the natural defence mechanism in vertebrates during an immune response against determinants on foreign biomacromolecules. The three-dimensional arrangement of the antigenic determinant (epitope) and its chemical nature will specify the reactivity of the antibody raised. Viral antigens consist of sterically prominent domains consisting of some five or six amino acid residues, or less frequently of sugar residues. The humoral immune response is polyclonal, i.e. against a single epitope on a macromolecule a series of monospe-

cific antibodies with different affinities are produced by the corresponding B-cell clones. A complex antigenic (immunogenic) structure such as a complete virion with its many different determinants elicits polyspecific, polyclonal antibodies in an animal. Polyclonal antibodies show a wide spectrum of binding affinities. Antigen-antibody binding can involve a variety of protein/protein interactions such as ionic, hydrogen, and van der Waals bonding as well as hydrophobic interaction; it is reversible and can be characterized by a binding constant (intrinsic affinity of one antibody binding region for a single determinant). The avidity of an antibody is defined as the total binding strength of the complete antibody molecule with a multi-determinant antigen.

Polyclonal antibodies are collected from the gammaglobulin fraction of natural or hyperimmune sera; this fraction represents approximately 15% of serum proteins. There are five classes of gammaglobulins and the predominant class in hyperimmune serum is the IgG molecule with an M_r of 150 000 (Fig. 2B.8). Even in highly immunized animals the amount of specific antibodies rarely exceeds 10% of the total IgG content. The majority is directed against determinants to which the animal was exposed before immunization. Consequently these unwanted, 'non-specific' immunoglobulins may lead to 'non-specific' binding, if corresponding determinants are present in the sample. This unwanted reactivity can be removed from serum by absorption with acetone-extracted normal cells. Antiviral antibodies as contained in a hyperimmune serum will interact with the variety of viral determinants with different avidities. These polyspecific, polyclonal antibodies, however, usually produce a reliable, dence immunolabelling because of the presence of some high-avidity antibodies and because of synergistic reactions between the different antibodies.

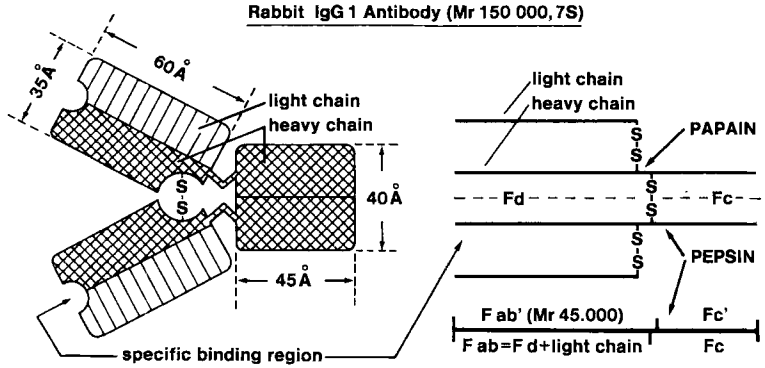

Fig. 2B.8. Morphological and biochemical properties of a rabbit IgG molecule (from Gelderblom, 1975, with permission). It consists of two heavy and two light chains, exhibiting two identical binding sites in the Fab parts. These subunits are linked together by intramolecular disulfide bonds.

Monoclonal antibodies (MABs), in contrast to the polyclonals contained in hyperimmune sera, each recognize a single determinant. MABs are usually raised in mouse-mouse hybridoma cells and many are now commercially available. It has to be kept in mind, however, that for IEM only MABs of high avidity are useful, since only a strong antigen-antibody binding will withstand the incubation and washing procedures. It should also be remembered that a MAB reacts with only a single determinant and that a 'cocktail' of MABs may provide a more reliable immunolabel.

2B.4.2. Tactics of immunolabelling for electron microscopy

Since the IgG molecule has a low electron density it must be coupled to electron-dense markers such as ferritin or colloidal gold or to enzymes, whose reaction products may be detected with heavy metal stains. The conjugation procedure can considerably reduce the binding capacity of the antibody to the antigen and it is also laborious, since each antibody to be used has to be coupled individually (see Fig. 2B.9).

Indirect, two-step labelling techniques partly circumvent these difficulties: antigen is reacted with unconjugated antibody, and the bound antibody is subsequently visualized by reaction with a second anti-immunoglobulin antibody coupled to a suitable marker molecule. The advantages of the indirect method are that (1) anti-IgG antibodies are of very high avidity; (2) more than one labelled anti-IgG molecule can bind to each unconjugated antibody, thus increasing the sensitivity of detection (Figs. 2B.9 and 2B.10), and (3) it is economical in the sense that one anti-rabbit IgG-marker conjugate can be used with all rabbit immune sera. Similarly an anti-mouse IgG-marker conjugate can be used with all mouse MABs. Finally, if the signal in two-step IEM labelling is weak, which often occurs when MABs are used in the first step, an intermediate incubation with unlabelled affinity-purified anti-mouse IgG antibody is performed, which in turn is detected by a third layer of a gold- or ferritin-labelled reagent (Fig. 2B.9e).

A further possibility for indirect labelling is the use of protein A, a cell wall protein from *Staphylococcus aureus*, which consists of a single polypeptide chain with an M_r of 42 000 and which has the ability to bind to the Fc portions of IgG molecules of most mammalian species. Protein A binds well to human and mouse IgG at neutral pH, but increasingly poorly to goat, rat, guinea pig, rabbit and sheep IgG molecules and very poorly to all IgM molecules (Lindmark et al., 1983). Protein A can be adsorbed to colloidal gold by simple mixing of the two solutions under the appropriate conditions (see Roth in Bullock and Petrusz, 1982, 1983; Slot and Geuze, 1985). Thus a versatile label is produced which can be used with antibodies of different species and which reacts in a 1:1 ratio with the primary antibody.

The high affinity of avidin/streptavidin to biotin can also be utilized for the formation of multi-step labelling in that biotinylated immunoglobulins, bound

already to the specimen, are detected through avidin-gold or -peroxidase complexes (Boorsma, 1983). Biotinylated immunoglobulins are especially useful for intracellular labelling, since the small size of biotin (M_r 248) does not significantly increase the size of the antibody or reduce its binding capacity. Biotinylated IgG is detected in the specimen by using either peroxidase-conjugated avidin or avidin followed by biotinylated peroxidase. Streptavidin has the advantage over egg-avidin of an isoelectric point (p*I*) near neutrality, i.e. p*I* 6 versus 9. Streptavidin conjugates can therefore be applied under more physiological conditions, which usually results in lower background labelling.

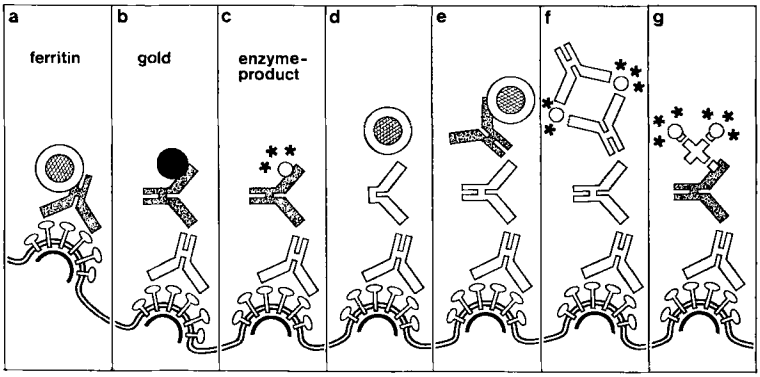

Fig. 2B.9. Diagrammatic synopsis of several immunolabelling techniques for electron microscopy. Antibodies covalently linked to markers are shaded.
(a) Direct immuno-ferritin labelling with antibody-ferritin conjugate as a one-step detection system.
(b) Indirect immuno-gold labelling. The specifically bound first antibody is revealed by an anti-IgG antibody coupled to colloidal, i.e. metallic, gold. This marker is more electron-dense than ferritin.
(c) Indirect immuno-enzyme technique. The detecting second antibody is labelled with an enzyme and is thus detectable by an enzyme substrate reaction, in which an insoluble, electron-dense dye (stars) is produced.
(d) Indirect immuno-ferritin hybrid-antibody (HY AB) technique. The anti-IgG portion of the HY AB binds the first antibody, the anti-ferritin portion binds to ferritin.
(e) Indirect immuno-ferritin technique; triple-layer using unlabelled affinity-purified anti-IgG as an intermediate (enhancing) antibody. Antigen is localized by sequential application of: antiserum produced in species 'A'; unlabelled antibody to IgG of species 'A' produced in species 'B'; and anti-B-antibodies from species 'A' labelled with ferritin.
(f) Indirect immuno-enzyme technique. The reaction sequence is similar to (e), but the third antibody, prepared in species 'A', is directed against an enzyme. Several application modes are possible: in this case a preformed peroxidase (open circles) anti-peroxidase (PAP) complex is used to increase the reaction product (stars).
(g) Indirect biotin-avidin immuno-labelling. Biotin (open square) is covalently coupled to the second antibody. Binding of this antibody is revealed sequentially by avidin/streptavidin (cross), biotinylated enzyme (open rings) and enzyme-substrate reaction (stars).
The techniques (d) and (f) completely avoid the use of covalent immuno-conjugates by employing exclusively immunological binding for bridging to the marker.

Covalently bound ferritin-IgG conjugates and IgG-gold complexes exhibit decreased binding capacity compared with an unlabelled antibody mainly because of steric hindrance of the specific binding sites by the marker molecule. Usually less than 10% of the initial activity of the native antibody is available in the conjugate. This problem led Hämmerling et al. (1968) to use hybrid antibodies (HY AB) for the binding of an electron-dense marker to the antigen-antibody complex. HY AB are bispecific $F(ab')_2$ fragments, i.e. they show two binding regions of different specificities. These heterodimers bind the antigen to one recognition site with one Fab' arm, the (ferritin) marker with the second arm, thus functioning as an immunological bridge. HY AB do not occur in vivo. They can

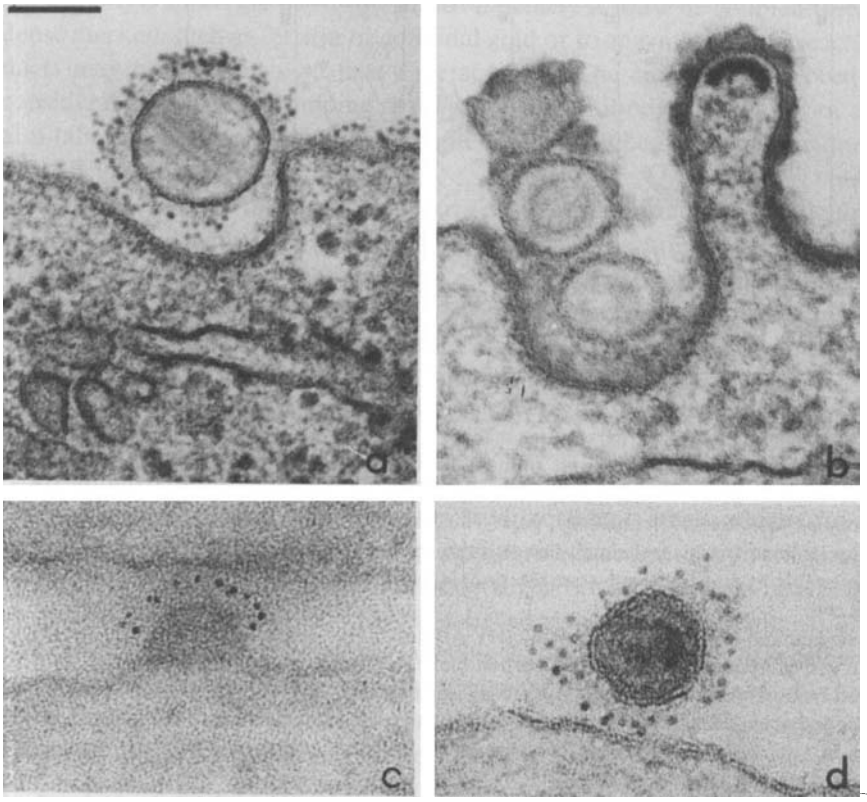

Fig. 2B.10. (a) Pre-embedding IEM: indirect labelling of Mason-Pfizer monkey virus, a type D retrovirus, using homologous antiserum and covalent anti-IgG ferritin conjugates. The marker forms a heavy corona well above the viral envelope. Bar = 100 nm. × 120 000. (b) Indirect labelling of simian sarcoma virus, a type C retrovirus, using homologous antibody and anti-IgG peroxidase. An electron-dense precipitate coats the viral bud as well as three cell-released particles. (c,d) Indirect labelling of avian C type leucosis viruses using homologous, neutralizing antibody, HY AB and ferritin for generating an immunological bridge. (c) Budding virus particle; (d) released virus particle with a dense corona of ferritin (from Gelderblom, 1975, with permission). Bar = 100 nm. × 120 000.

be prepared routinely from appropriate pairs of immunoglobulins of rabbit or guinea pig hyperimmune sera but not of other species (Hämmerling et al., 1968; Gelderblom, 1975). Compared to the more commonly used covalent conjugates HY AB show a very low nonspecific background labelling in direct and indirect IEM. This technique allows a discrete, spatially more defined labelling due to the constant dimensions and strict immunobinding involved (Fig. 2B.9b,d and 2B.10c,d). For the preparation of bispecific antibodies of species other than rabbit or guinea pig another elegant technique based on controlled recombination of multiple interchain disulfide bonds has been devised recently. Due to its applicability also to mouse monoclonal IgG 1 it seems to merit further attention in IEM (Brennan et al., 1985).

In indirect, and especially in multi-step, labelling techniques it is advisable to work with affinity-purified antibodies (see Polak and Van Noorden, 1983, for reference). A further tactic in antibody application is pepsin digestion of IgG, which removes the Fc portion of the antibody without changing the specific binding properties of the resulting $F(ab')_2$. Removal of the Fc portion, which has a high affinity for the respective Fc receptors expressed on, for example, lymphocytes, helps in reducing non-specific antibody binding. Reduction of the bivalent $F(ab')_2$ results in monovalent Fab' fragments; the small size of these fragments may be an advantage in intracellular pre-embedding IEM. IEM must be performed with proper controls, which ideally should include a positive control and negative controls by omission of the specific antibody or use of an unrelated antibody in addition to specificity controls of the antibody-conjugate.

2B.4.3. Electron-dense markers

Immuno-ferritin conjugates

Ferritin is an iron storage protein with a diameter of 11 nm and an iron-containing core of only 7 nm. Horse spleen ferritin is coupled to purified immunoglobulin by glutaraldehyde or other bifunctional reagents, preferentially using a two-step method (Takamiya et al., 1974, 1975). Such conjugates are well-suited for pre-embedding IEM of virus and viral antigens on cell surfaces (Morgan et al., 1961; Gelderblom, 1975; Gelderblom et al., 1985b; Fig. 10a). To detect intracellular determinants by pre-embedding immuno-ferritin labelling, cells must first be permeabilized (see later).

Immuno-enzyme techniques

Enzyme-IgG conjugates are considerably smaller than ferritin-IgG conjugates and therefore more diffusible in intracellular compartments. IgG-peroxidase conjugates are most widely used in direct or indirect IEM. The catalytic action of the coupled enzyme with H_2O_2 is used to bring about the reduction and cyclization of the chromogen diaminobenzidine. The resulting precipitate is osmiophilic and thus

may be seen not only with the electron microscope but also by light microscopy. Since this precipitate may be enlarged, i.e. the signal can be amplified depending on incubation time, temperature, and concentration of the substrate, immuno-enzyme techniques appear superior in sensitivity to ferritin labelling. To improve intracellular penetration, these reagents have been miniaturized by coupling a small, haem-octapeptide of cytochrome *c*, showing catalysing activity, to a Fab' fragment of the IgG molecule (Kraehenbuhl and Jamieson, 1972). The use of peroxidase-antiperoxidase complexes in the so-called PAP technique (for details see Sternberger, 1979) reinforces the sensitivity of the immuno-enzyme technique (Fig. 2B.9f). The main disadvantages of immuno-enzyme techniques are low spatial resolution and contrast compared to ferritin or gold conjugates; thus enzyme conjugates are more appropriate for low-resolution work (Fig. 2B.10b).

Colloidal gold

Metallic, colloidal gold represents a marker system showing several advantages over ferritin. The high mass density of 19.3 g/cm^3 renders the gold marker easily detectable even if 3–5-nm gold particles are applied. Colloidal gold is prepared from tetrachloroauric acid by reduction with different chemical agents, routinely producing a wide range of defined size classes (for references see Bullock and Petrusz, 1982, 1983; Slot and Geuze, 1985). Being highly negatively charged, gold particles will form complexes with many biologically interesting ligands, e.g. immunoglobulins, lectins, protein A, avidin/streptavidin, toxins etc. Gold particles with different diameters and complexed to different ligands allow double-labelling IEM, and the gold complexes, showing an intense red color, can also be used for the localization of antigens by light microsopy. Owing to its high contrast the gold marker is especially suitable for post-embedding IEM and immunocryoultramicrotomy; however, gold conjugates are inferior to ferritin reagents in labelling density (Gelderblom et al., 1985b).

2B.4.4. Fixation

As a general rule, a balance between preservation of structural detail and antigenicity of the specimen has to be worked out before performing IEM. The effect of different fixatives and concentrations can be tested by immunofluorescence techniques using semithin 0.5 μm cryosections. Fixation leads to the crosslinking of cellular constituents and reduces lateral diffusion of membrane proteins, which would lead to an artifactual redistribution of antigens (e.g. surface receptors) during incubation with the antibody. Prefixation is indispensable for cells suffering from severe virus-induced cytopathic changes and is essential in immunocryoultramicrotomy; otherwise the thawed ultrathin section would lose most of its structural detail during immunolabelling. Prefixation will also exclude any possible biohazard when working with live virus. Fixation is most efficiently achieved by

glutaraldehyde (GA). However, because many antigens are sensitive to cross-linking by GA, it is recommended to use concentrations of 0.1% or less for short periods of time. The addition of 2–8% formaldehyde (FA, freshly prepared from paraformaldehyde) to low concentrations of GA has proved helpful in preserving antigenicity together with morphology. However, fixation in FA only (e.g. 3% for 10 min) is often necessary when using MABs which bind only to a single determinant. It is always necessary to block free aldehyde groups in FA/GA-fixed specimens to prevent non-specific binding of antibodies. For immunolabelling protocols see Bullock and Petrusz (1982, 1983, 1985), Gelderblom et al. (1985b), Griffith et al. (1984), Polack and Van Norden (1983), and Polak and Varndell (1984).

2B.4.5. Pre-embedding IEM

Pre-embedding immunolabelling of viral antigens on cell surfaces can be performed either with a suspension of cells in a small centrifuge tube or in situ with monolayer cultures grown in microtest plates (for details see Gelderblom et al., 1985b). The advantage of microtest plates is that only 10 μl of reagent are needed for each well. Cells growing in suspension can be attached to the bottom of the microtest well by poly-L-lysine or Alcian-blue prior to immunolabelling. Immune incubations are followed by in situ embedding; individual wells are removed from the microtest plate and after re-embedding the cell layer is covered from both sides with Epon. This technique offers several advantages, e.g. extracellular antigens may be localized very efficiently by indirect immuno-ferritin techniques, resulting in a pronounced, dense label. In addition to antigen localization, in situ IEM permits observation of undisturbed virus–cell and cell–cell interactions.

Cells immunolabelled for the presence of surface antigens can be evaluated not only in sections, but also by SEM or in freeze-dry or critical-point-dry replicas as described in Section 2B.3. Colloidal gold appears to be a very successful marker in replica studies of budding viruses (Mannweiler et al., 1982).

Intracellular antigens are accessible only after permeabilization of the cells prior to immunolabelling (Bohn, 1978; Willingham et al., 1978), but these techniques have certain disadvantages. Permeabilization causes deterioration of fine structure and, in spite of the loss of cellular components, the immunoreagents still meet difficulties in diffusing into the cytoplasmic or nuclear environment. To further the penetration of the immunoreagents within the intracellular compartments the following alternative has been developed. Immunoperoxidase labelling of cryostat section of tissues prefixed by formaldehyde or periodate-lysine-paraformaldehyde combined with DMSO cryoprotection allows high-resolution indirect labelling of intracellular receptors together with excellent tissue preservation. Prefixation with glutaraldehyde, in contrast, due to its pronounced cross-linking properties, prevents penetration of the immunoreagents throughout the 15–20 μm cryostat

section (Brown and Farquhar, 1984). Biotinylated antibodies are well suited for intracellular labelling, since the small size of biotin (M_r 248) does not significantly increase the size of the antibody or reduce antigen binding.

2B.4.6. POST-EMBEDDING IEM

The modern hydrophilic resins Lowicryl K4M (Carlemalm et al., 1982) and L-R White (Newman et al., 1983) offer advantages which make them widely used for post-embedding immunolabelling (for more information see Causton in Polak and Varndell, 1984). Embedding of specimens and polymerization of the methacrylate Lowicryl can be performed at temperatures of $-40°C$ or below, due to the low viscosity of this resin. This results in minimal denaturation and extraction of antigens. The acrylic L-R White allows infiltration of specimens still containing 30% water. This resin is polymerized at 50°C. Its hydrophilic nature together with its low cross-linking density permits diffusion of IgG molecules even within the plastic of the ultrathin section. Thus, antigens within the depth of the L-R White section might be labelled when using the immuno-enzyme techniques. In general, post-embedding IEM allows the detection of determinants exposed on the surface of ultrathin sections, but in this way the antibody still has access to every cellular compartment. If both sides of the section are incubated sequentially with two different sera and IgG-gold conjugates differing in size, it is even possible to achieve double labelling of structures (Bendayan, 1982). In the future, a combination of fast freezing rather than chemical fixation with freeze substitution techniques, and finally using low-temperature embedding resins will possibly result in still better preservation of antigenicity and fine structure.

Immunolabelling of ultrathin cryosections after thawing (immunocryoultramicrotomy) based on the pioneering work of W. Bernhard in the early 1970s was developed by Tokuyasu, to become the most sensitive post-embedding IEM technique availble today (Tokuyasu, 1983). Apart from the possible denaturation of antigenic determinants by the initial fixation, no further steps which might abolish the antigenicity of the specimen are involved (for a review see Gelderblom et al., 1985b; Griffith et al., 1984). After a mild prefixation the specimens are infused with 2.1–2.3 M sucrose, frozen by immersion into liquid nitrogen and finally cut at $-110°C$ using 'dry' glass knives. The sucrose serves as a cryoprotectant and also makes cutting easier. Sections 50–120 nm in thickness may be obtained; after thawing they are immunolabelled preferentially using indirect techniques and gold markers (Fig. 2B.11a,b). Because of the high degree of contrast introduced by the final staining steps, immuno-ferritin labelling is less advantageous than immunogold labelling. The higher sensitivity of immunocryoultramicrotomy as compared to post-embedding IEM using the new resins is explained by the fact that antibodies can penetrate the sections after thawing. In cases of uncertainty about the localization of the marker stereomicrographs can help.

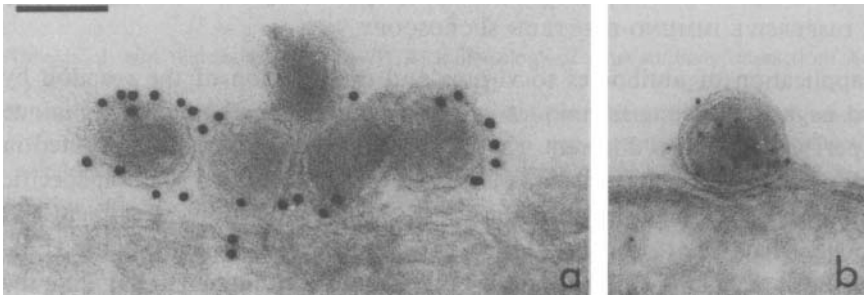

Fig. 2B.11. Post-embedding IEM: indirect technique using ultrathin cryosections of human T-cell lymphotropic virus type III (HTLV-III). After thawing the cryosections were incubated with human ARC (= AIDS related complex) sera followed by anti-human IgG-gold complexes. In (a), using a 10 nm gold probe, the serum detects virus envelope determinants, while in (b) serum from another patient shows reactivity mainly against virus core components. Bar = 100 nm. × 120 000.

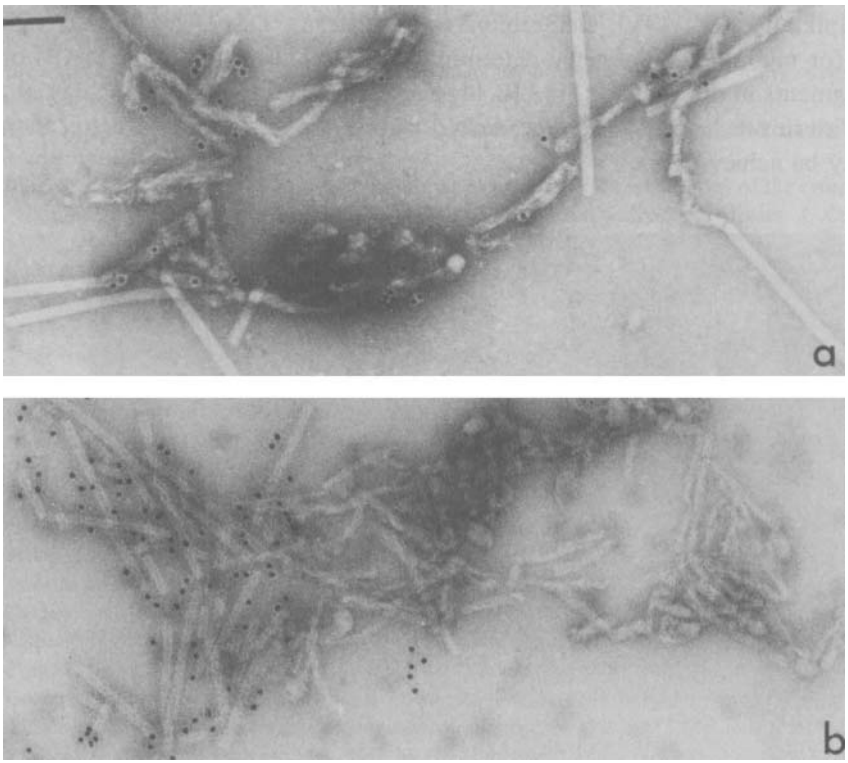

Fig. 2B.12. Indirect solid phase IEM of a mixture of scrapie-associated fibrils (SAF) and tobacco mosaic virus (TMV) using hyperimmune sera and appropriate anti-IgG-gold complexes. (a) After incubation with anti-SAF serum, the label is confined to this protein, while TMV, serving as a control, remains unlabelled. (b) After incubation of the preadsorbed virus mixture with anti-TMV, the virus is heavily labelled, but the SAF is devoid of any marker. Bar = 100 nm. × 120 000.

2B.4.7. DISPERSIVE IMMUNO-ELECTRON MICROSCOPY

Direct application of antibodies to viruses and examination of the reaction by standard negative staining techniques is a valuable IEM method. The technique can be performed in two different ways: 1, virus and antibody are incubated in suspension, or 2, one of the reactants is bound to the grid either via non-specific adhesion or using poly-L-lysine, protein A, etc., as a 'conditioning' treatment and the partner is incubated on this solid phase (pre-absorption or solid-phase IEM, SPIEM). Both techniques will show a fringe of bound antibodies surrounding the virion if antibody binding occurs. In addition, antibody-mediated aggregation of the isolated, scattered particles may also be observed, which is a help in diagnostic detection, especially of small viruses. Dispersive IEM can also be performed using the indirect technique, and IgG- or protein A-gold conjugates may be applied, thus making the attached antibodies more easily detectable, resulting often in very clear-cut results (Fig. 2B.12; for detailed information see Almeida and Waterson, 1969; Kapikian et al., 1980; Gelderblom et al., 1985a). Dispersive IEM is well adapted for mapping of antigenic determinants, especially when using MABs or Fab′ fragments in direct IEM (Fig. 2B.13; Schwarz et al., 1983; Taniguchi et al., 1983). With this technique an unprecedented high spatial resolution of better than 20 Å may be achieved.

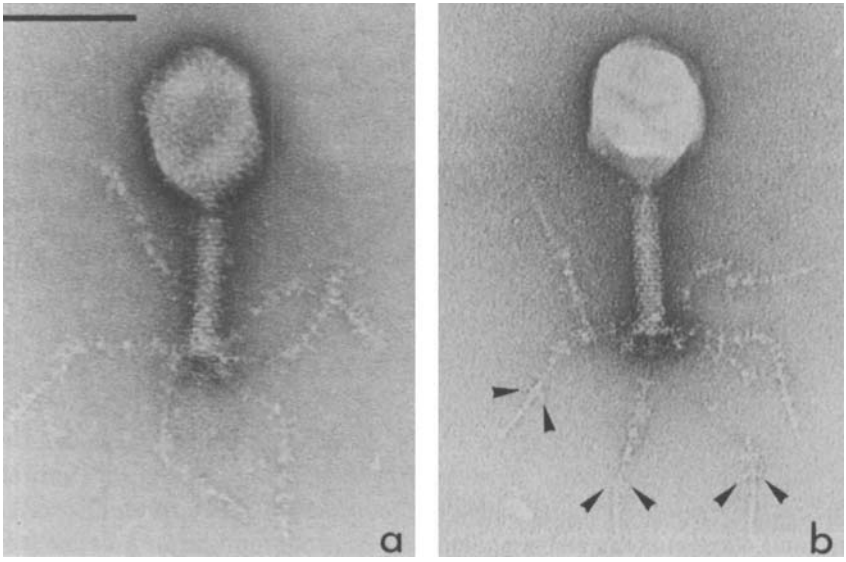

Fig. 2B.13. Direct high-resolution dispersive IEM: demonstration of cross-reactivity between two T-even type phages. Note total labelling with Fab molecules in the homologous reaction (a) and selective binding at distinct sites of the tail fibres (b) after incubation with Fab from a heterologous, but related antiserum (from Schwarz et al., 1983, with permission). Bar = 100 nm. × 180 000.

References

Almeida, J. and Waterson, A.P. (1969) The morphology of virus-antibody interaction. Adv. Virus Res. 15, 307–338.

Baigent, C.L., Mannweiler, K., Andersen, I., Rutter, G.A. and Neumayer, U. (1978) Verbessertes und vereinfachtes 'Austauschverfahren' zur Präparation von infektiösen Deckglaszellkulturen für vergleichende REM-und TEM-studien. Beitr. elektronenmikroskop. Direktabb.-Oberfl. 11, 251–263.

Bartlett, A.A. and Burtstyn, H.P. (1975) A review of the physics of critical-point-drying. In: Scanning Electron Microscopy/1975/1, pp. 305–316. ITT Research Institute, Chicago.

Bendayan, M. (1982) Double immunocytochemical labelling applying the protein A-gold technique. J. Histochem. Cytochem. 30, 81–85.

Bohn, W. (1978) A fixation method for improved antibody penetration in electron microscopical immuno-peroxidase studies. J. Histochem. Cytochem. 26, 293–297.

Boorsma, D.M. (1983) Conjugation methods and biotin-avidin systems. In Techniques in Immunocytochemistry, Eds. G.R. Bullock and P. Petrusz, Vol. 2, pp. 155–174. Academic Press, London, New York.

Brennan, M., Davison, P.F. and Paulus, H. (1985) Preparation of bispecific antibodies by chemical recombination of monoclonal immunoglobulin G_1 fragments. Science 229, 81–83.

Brinkley, B.R., Murphy, P. and Richardson, L.C. (1967) Procedure for embedding in situ selected cells cultured in vitro. J. Cell Biol. 35, 227–283.

Brown, W.J. and Farquhar, M.G. (1984) The mannose-6-phosphate receptor for lysosomal enzymes is concentrated in cis Golgi cisternae. Cell 36, 295–307.

Brunk, U., Collins, P. and Arro, E. (1981) The fixation, dehydration, drying and coating of cultured cells for SEM. J. Microsc. 123, 121–131.

Büechi, M. and Bächi, T. (1979) Immunofluorescence and electron microscopy of the cytoplasmic surface of the human erythrocyte membrane and its interaction with Sendai viruses. J. Cell Biol. 83, 338–347.

Bullock, G.R. and Petrusz, P. (Eds.) (1982, 1983, 1985) Techniques in Immuno-cytochemistry, Vols. 1–3, Academic Press, London.

Codling, B.W. and Mitchell, J.C. (1976) A method of embedding tissue culture preparations in situ for transmission electron microscopy. J. Microsc. 106, 103–106.

Carlemalm, E., Garavito, R.M. and Villiger, W. (1982) Resin development for electron microscopy and an analysis of embedding at low temperature. J. Microsc. 126, 123–143.

Dubois-Dalcq, M., Holmes, K.V. and Rentier, B. (1984) Assembly of enveloped viruses. Springer-Verlag, Vienna, New York.

Eskelinen, S. and Saukko, P. (1983) Effects of glutaraldehyde and critical-point drying on the shape and size of erythrocytes in isotonic and hypotonic media. J. Microsc. 130, 63–71.

Firket, H. (1966) Polyester sheeting (Melinex 0), a tissue-culture support easily separable from epoxy resins after flat-face embedding. Stain Technol. 41, 189–191.

Gelderblom, H. (1975) The preparation and application of hybrid antibody for the detection of tumor-specific cell surface antigens. In Applied Tumor Immunology, Eds. H. Götz and E.S. Bücherl, pp. 131–153. Walter de Gruyter, Berlin, New York.

Gelderblom, H., Beutin, L., Hajiyiannis, D. and Reupke, H. (1985a) Rapid typing of pili of pathogenic *Escherichia coli* by dispersive immunoelectron microscopy. In Rapid Methods and Automation in Microbiology and Immunology, Ed. K.-O. Habermehl, pp. 390–400. Springer-Verlag, Berlin, Heidelberg, New York, Tokyo.

Gelderblom, H., Kocks, C., L'Age-Stehr, J. and Reupke, H. (1985b) Comparative immunoelectron microscopy with monoclonal antibodies on yellow fever virus-infected cells: pre-embedding labelling versus immunocryoultramicrotomy. J. Virol. Methods 10, 225–239.

Glauert, A.M. (1975) Fixation, dehydration and embedding of biological specimens. In Practical Methods in Electron Microscopy, Ed. A.M. Glauert, Vol. 3(1). North-Holland, Amsterdam.

Gonda, M.A., Gilden, R.V. and Hsu, K.C. (1979) An unlabelled antibody macromolecule technique using hemocyanin for the identification of type B and type C retrovirus envelope and cell surface antigens by correlative fluorescence, transmission electron, and scanning electron microscopy. J. Histochem. Cytochem. 27, 1445-1454.

Griffiths, G., McDowall, A., Back, R. and Dubochet, J. (1984) On the preparation of cryosections for immunocytochemistry. J. Ultrastruct. Res. 89, 65-78.

Hämmerling, U., Aoki, T., de Harven, E., Boyse, E.A. and Old, L.J. (1968) Use of hybrid antibody with anti-γ G and anti-ferritin specificities in locating cell surface antigens by electron microscopy. J. Exp. Med. 128, 1461-1473.

Hirsch, J.G. and Fedorko, M.E. (1968) Ultrastructure of human leukocytes after simultaneous fixation with glutaraldehyde and osmium tetroxide and 'post-fixation' in uranyl acetate. J. Cell Biol. 38, 615-627.

Horisberger, M. (1981) Colloidal gold: a cytochemical marker for light and fluorescent microscopy and for transmission and scanning electron microscopy. In Scanning Electron Microscopy/1981/II, pp. 9-31. SEM Inc. AMF O'Hare, Chicago.

Kapikian, A.Z., Dienstag, J.L. and Purcell, R.H. (1980) Immune electron microscopy as a method for the detection, identification, and characterization of agents not cultivable in an in vitro system. Manual of Clinical Immunology, 2nd Edn., Eds. N.E. Rose and H. Friedmann, American Society for Microbiology, Washington.

Katsumoto, T., Naguro, T., Iino, A. and Takagi, A. (1981) The effect of tannic acid on the preservation of tissue culture cells for scanning electron microscopy. J. Electron Microsc. 30, 177-182.

Kraehenbuhl, J.P. and Jamieson, J.D. (1972) Solid-phase conjugation of ferritin to Fab-fragments of immunoglobulin G for use in antigen localization on thin sections. Proc. Natl. Acad. Sci. USA 69, 1771-1775.

Kuhn, H. (1981) A simple method for the preparation of cell cultures for ultrastructural investigation. J. Histochem. Cytochem. 29, 84-86.

LaFountain, J.R., Zobel, C.R., Thomas, H.R. and Talbreath, C. (1977) Fixation and staining of F-actin and microfilaments using tannic acid. J. Ultrastruct. Res. 58, 78-86.

Lahav, M., Ishii, Y., Craft, J. and Tauber, J. (1982) Versatile method for evaluating a cell culture by various morphological methods. Stain Technol. 57, 341-347.

Lindmark, R., Thorén-Tolling, K. and Sjöquist, J. (1983) Binding of immunoglobulins to protein A and immunoglobulin levels in mammalian sera. J. Immunol. Methods 62, 1-13.

Mannweiler, K., Hohenberg, H., Bohn, W. and Rutter, G. (1982) Protein-A gold particles as markers in replica immunocytochemistry: high resolution electron microscope investigations of plasma membrane surfaces. J. Microsc. 126, 145-149.

Maupin, P. and Pollard, T.D. (1983) Improved preservation and staining of HeLa cell actin filaments, clathrin-coated membranes and other cytoplasmic structures by tannic acid-glutaraldehyde-saponin fixation. J. Cell Biol. 96, 51-62.

McDonald, K. (1984) Osmium ferricyanide fixation improves microfilament preservation and membrane visualization in a variety of animal cell types. J. Ultrastruct. Res. 86, 107-118.

Morgan, C., Rifkind, R.A., Hsu, K.C., Holden, M., Seegal, B.C. and Rose, H.M. (1961) Electron microscopic localization of intracellular viral antigen by the use of ferritin-conjugated antibody. Virology 14, 292-296.

Nermut, M.V. (1978) Structural elements in adenovirus cores. Studies by means of freeze-fracturing and ultrathin sectioning. Arch. Virol. 57, 323-337.

Nermut, M.V. (1982a) Advanced methods in electron microscopy of viruses. In New Developments in Practical Virology, Ed. C. Howard, pp. 1-58. A.R. Liss, New York.

Nermut, M.V. (1982b) The cell monolayer technique in membrane research: a review. Eur. J. Cell Biol. 2, 160-172.

Newman, G.R., Jasani, B. and Williams, E.D. (1983) A simple postembedding system for the rapid detection of tissue antigens under the electron microscope. Histochem. J. 15, 543-555.

Nopanitaya, W., Charlton, R.K., Turchin, R.L. and Grisham, J.W. (1977) Ultrastructure of cell cultures on polycarbonate membranes. Stain Technol. 52, 143–148.

Peters, K.R. (1980) Improved handling of structural fragile cell biological specimens during electron microscopic preparation by the exchange method. J. Microsc. 118, 429–441.

Plattner, H. and Bachmann, L. (1982) Cryofixation. A tool in biological research. Int. Rev. Cytol. 79, 237–304.

Polak, J.M. and Van Noorden, S. (Eds.) (1983) Immunocytochemistry. Wright PSG, Bristol, London, Boston.

Polak, J.M. and Varndell, I.M. (Eds.) (1984) Immunolabelling for Electron Microscopy. Elsevier, Amsterdam.

Rostgaard, J. and Tranum-Jensen, J. (1980) A procedure for minimizing cellular shrinkage in electron microscope preparation: a quantitative study on frog gall bladder. J. Microsc. 119, 213–232.

Rutter, G., Bohn, W., Hohenberg, H. and Mannweiler, K. (1985) Preparation of apical plasma membranes from cells grown on coverslips. Electron microscopic investigations of the protoplasmic surface. Eur. J. Cell Biol. 394, 443–448.

Sanders, S.K., Alexander, E.L. and Braylan, R.C. (1975) A high-yield technique for preparing cells fixed in suspension for scanning electron microscopy. J. Cell Biol. 67, 476–480.

Sargent, G.F., Sims, T.A. and McNeish, A.S. (1981) The use of polystyrene microcarriers to prepare cell monolayers for transmission electron microscopy. J. Microsc. 122, 209–212.

Schneider, G.B. (1976) The effects of preparative procedures for scanning electron microscopy on the size of isolated lymphocytes (1). Am. J. Anat. 146, 93–100.

Schwarz, H., Riede, I. and Henning, U. (1983) Degrees of relatedness of T-even type *E.coli* phages using different or the same receptors and topology of serologically cross-reacting sites. EMBO J. 2, 375–380.

Slot, J.W. and Gueze, H.J. (1985) A new method of preparing gold probes for multiple labelling cytochemistry. Eur. J. Cell Biol. 38, 87–93.

Soligo, D. and de Harven, E. (1981) Ultrastructural cytochemical localizations by back-scattered electron imaging of white blood cells. J. Histochem. Cytochem. 29, 1071–1079.

Steinman, R.M. and Cohn, Z.A. (1972) The interaction of soluble horseradish peroxidase with mouse peritoneal macrophages in vitro. J. Cell Biol. 55, 186–204.

Sternberger, L.A. (1979) Immunocytochemistry, 2nd Edn., John Wiley and Sons, New York.

Takamiya, H., Shimizu, F. and Vogt, A. (1974) A two-stage method for cross-linking antibody globulin to ferritin by glutaraldehyde. II. Antigen binding and agglutinating capacity. J. Immunol. Methods 4, 381–386.

Takamiya, H., Shimizu, F. and Vogt, A. (1975) A two stage method for cross-linking antibody globulin to ferritin by glutaraldehyde. III. Size and antibody activity of the conjugates. J. Immunol. Methods 8, 301–306.

Taniguchi, K., Urasawa, S. and Urasawa, T. (1983) Monoclonal antibodies reactive with different sites of N and H antigenic particles of poliovirus. J. Gen. Virol. 64, 2803–2808.

Tokuyasu, K.T. (1983) Present state of immunocryoultramicrotomy. J. Histochem. Cytochem. 31, 164–167.

Van Ewijk, W. and Hosli, P. (1975) A new method for comparative light and electron microsopic studies of individual cells, selected in the living state. J. Microsc. 105, 19–31.

Williams, M.A. (1977) Autoradiography and immunocytochemistry. In Practical Methods in Electron Microscopy, Ed. A.M. Glauert. Vol. 6(1). North-Holland, Amsterdam.

Willingham, M.C., Yamada, S.S. and Pastan, I. (1978) Ultrastructural antibody localization of α_2-macroglobulin in membrane-limited vesicles in cultured cells. Proc. Natl. Acad. Sci. USA 75, 4359–4363.

Wolosewick, J.J. and Porter, K.R. (1979) Preparation of cultured cells for electron microscopy. In Practical Tissue Culture Applications, Eds. K. Maramorosch and H. Hirumi, pp. 59–85. Academic Press, New York.

This Page Intentionally Left Blank

Nermut/Steven (eds) Animal Virus Structure

CHAPTER 2C

Electron microscopy: image processing and quantitative electron microscopy

ALASDAIR C. STEVEN

Laboratory of Physical Biology, National Institute of Arthritis, Musculoskeletal and Skin Diseases, National Institutes of Health, Bethesda, MD 20892, U.S.A.

2C.1. Image analysis and image processing

Even with optimized preparations, electron microscope images are frequently difficult to interpret, particularly at the finest level of detail accessible with stained or shadowed specimens, viz. 2.5–2.0 nm, exceptionally approaching 1.5 nm resolution. This limitation is imposed by several factors, any of which may be limiting in a given instance: radiation damage, grain size in the stain layer or shadow deposit, optical aberrations (e.g. excessive de-focus, astigmatism, or specimen drift), or ambiguities of interpretation posed by the various levels of co-projected structure viewed in a transmission electron micrograph. In many such circumstances, it has proved rewarding to subject the data to quantitative analysis by the methods of optical diffraction and computer image processing (Misell, 1978). Over the twenty years or so during which these techniques have been under development, the range of problems to which they may be applied has diversified greatly. As explained below, this type of analysis is most effective with specimens that possess regular or periodic structural features. Many virological specimens have such features (e.g. icosahedral capsids, helical nucleocapsids, arrays of capsomers, and crystals of virus particles or of their components): accordingly, applications of image processing to problems in structural virology are steadily expanding (Steven, 1981; Baker, 1981).

2C.1.1. Optical diffraction

In optical diffraction analysis, an area of interest of the micrograph negative is illuminated with a beam of coherent monochromatic light (helium-neon lasers are now used almost exclusively for this purpose). An objective lens is used to form the diffraction pattern of the transmitted light (Fig. 2C.1; see Goodman, 1968), which is then inspected visually or recorded photographically. From the diffraction pattern, one may ascertain certain properties of the image more readily and more quantitatively than by direct scrutiny of the original image. The diffraction pattern of a typical bright-field transmission electron micrograph has the form of a system of concentric bright and dark rings. By measuring their positions relative to the centre of the pattern, the resolution of the image may be assessed, as well as the amount of de-focus at which it was recorded. Astigmatism and drift are expressed in the pattern as departures from circular symmetry (see Misell, 1978).

However, optical diffraction is particularly useful when applied to images of regular objects, such as helices, two-dimensional arrays, or other crystalline or para-crystalline assemblies. The regularly organized structure generates discrete, symmetrically disposed reflections in the diffraction pattern that are often relatively intense, and hence easily recognized; cf. Fig. 2C.1. By measuring the positions of these periodic reflections, it is possible to make a precise determination of the spacings. Furthermore, from their relative positions in the pattern, it is frequently possible to work out the geometrical arrangement of repeating units in the specimen. In addition, the furthest spacing from the center of the pattern to which these discrete reflections extend gives a precise measure of the 'useful' resolution of the image. This value of resolution is distinct from, and usually considerably less than, the instrumental resolution given by the outermost limit of detectable intensity in the diffraction pattern.

2C.1.2. Computer image processing

In computer image processing, a digital representation of the image is first encoded by scanning the negative with a microdensitometer (except with those microscopes, still rather rare, which are equipped for digital recording of images). This procedure yields a two-dimensional matrix of numbers that represent the optical densities at the sampled set of points. In this form, the image is analysed by a sequence of mathematical operations implemented as computer programs or subroutines. Numerical output may be obtained and assessed at any stage of the analysis, and an extensive range of hardware devices which permit visual display of the imagery are now commercially available. These include various kinds of plotters, television monitors, and cameras or film-writers which convert digital images into photographic format.

The nature and complexity of appropriate image-processing operations vary

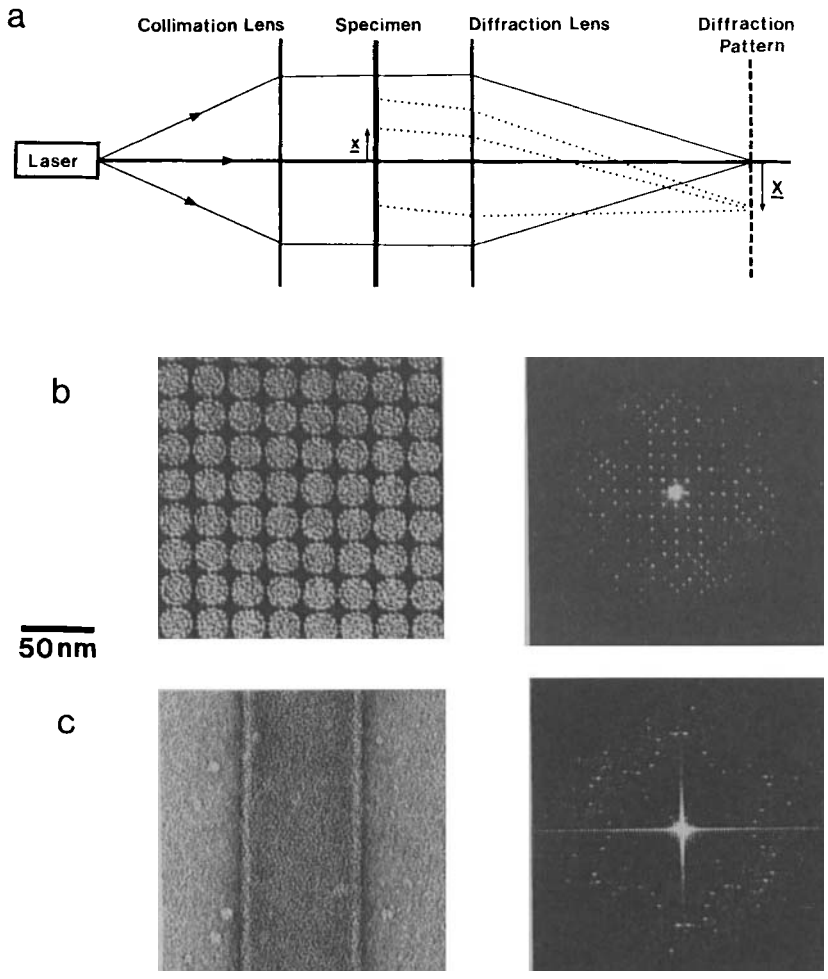

Fig. 2C.1. (a) Schematic diagram (simplified) of the layout of an optical diffractometer. The specimen, usually a micrograph negative, is illuminated uniformly with coherent, monochromatic light. The dotted lines shown as emanating from several points of the specimen (e.g. x) and converging at point X in the diffraction plane indicate how each point of the diffractogram receives a contribution transmitted from each point of the specimen. Shown below are two bright-field CTEM micrographs and their diffraction patterns: (b) a two-dimensional crystal of negatively stained icosahedral virus particles (cowpea chlorotic mottle virus); (c) a tubular protein polymer related to the capsid of bacteriophage T4. Its organization is as a cylindrical folding of a hexagonal surface lattice of capsid proteins. The particle has flattened on the grid so that its diffraction pattern shows two superimposed hexagonal lattices, rather than a helical pattern. Note that, although conspicuous in the diffractogram, the hexagonal symmetry of the surface lattice is not evident in the micrograph itself.

widely according to the goals of particular projects. However, the digital Fourier transform (which gives the computational counterpart of the optical diffraction pattern) provides a powerful tool that is useful in many contexts. Fourier analysis of images has been greatly facilitated by the devising, originally by Cooley and Tukey in the mid 1960s, of efficient algorithms to perform these otherwise dauntingly time-consuming computations (Brigham, 1974). Two other major factors have contributed to the recent proliferation of image-processing activity in biological electron microscopy. These are (i) the advent of small, powerful, and financially non-prohibitive laboratory computers, and (ii) the development of integrated systems of computer programs capable of performing wide ranges of processing operations (e.g. Smith, 1978; Frank et al., 1981; Trus and Steven, 1981; Van Heel and Keegstra, 1981).

In practice, optical diffraction is generally used to screen a set of negatives for the images with the highest resolution (cf. Fig. 2C.2). Thereafter, although analysis may vary widely, two general types of processing are most commonly used in problems of structural virology: (i) image filtering to improve the signal-to-noise ratio, there by making the information content of the image more evident, and (ii) three-dimensional reconstruction, to retrieve the full structure from a set of two-dimensional projections.

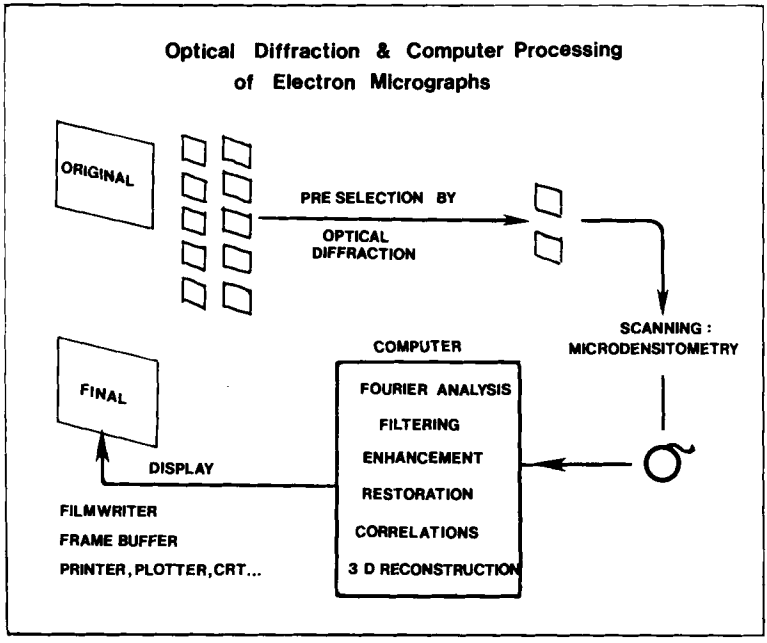

Fig. 2C.2. Flow chart depicting the overall sequence of operations in an image-processing project.

2C.1.3. Image filtering and image averaging

Over the past twenty years, increasingly sophisticated and powerful methods have evolved for reducing the noise level of electron images. These techniques are all based on the precept that each representation of a structure of interest (e.g. a capsomer, a virion, etc.) may be considered as an 'ideal' image, overlaid by random noise. With different images of ostensibly identical specimens, the underlying ideal image is held to be common to each, whereas the noise content varies randomly from image to image. Accordingly, if a set of such images are averaged in some way, their (mutually consistent) signals are reinforced, while the noise contributions tend to cancel out. The greater the degree of averaging, the more effectively the noise is suppressed, at least (for practical purposes) up to the point where it is reduced to an insignificant level. Clearly, the effectiveness of any such procedure depends critically on the precision with which the averaging is done. Imprecise registration of images will result in the smearing out of finer features, and gross misalignment can generate artifactual structures. The technique is most readily applied to two-dimensionally periodic specimens whose repeating units are viewed in the same orientation.

(a) Photographic image averaging

In the early 1960s, Markham and co-workers introduced photographic averaging to enhance repetitive features in images of specimens with translational or rotational symmetries. According to this approach, a series of superimposed exposures is made with the negative being translated or rotated between successive exposures. Alternatively, lightly exposed transparencies (of the identical field) may be superimposed at appropriate relative offsets: the composite image is then printed. The main advantages of this methodology are its simplicity and the absence of requirement for specialized equipment. Its limitations lie in the small amount of averaging that can (easily) be done, and in its non-quantitative nature. Also, photographic averaging depends on a visual determination of the repeat distance, and relatively subtle repeats (such as pseudo-symmetries) are likely to be missed. For these reasons, this method has been largely superseded by the more quantitative procedures described below.

(b) Optical filtering

Essentially the same type of noise suppression may be accomplished, with certain practical advantages, by using coherent optics. For this purpose, the optical path outlined in Fig. 2C. 1 is extended to include a reconstruction lens. This forms a telescopic image of the micrograph under analysis. In the intervening diffraction plane, however, the 'ideal' image is spatially separated from the noise. In effect, it is concentrated into the discrete periodic reflections, whereas the noise is distributed all over the diffraction plane. Accordingly, by introducing, in the dif-

fraction plane, a mask with holes which transmit the periodic reflections while most of the noise is blocked off, one can obtain a 'filtered' image of the original. For images of two-dimensional lattices, this technique is formally equivalent to translational averaging of the lattice motif, with the amount of averaging depending on the size of the mask-holes used (Fraser and Millward, 1970).

The advantages of optical filtering over photographic averaging are the large amount of averaging that may be achieved, and that the optical diffraction pattern may be used to determine the basic symmetry of the object, and to serve as a template in making the filtration mask. Furthermore, if several lattices are superimposed, their combined projection image presents a complex moiré pattern. Providing that the lattices are not in angular alignment, their separate images may be extracted from the moiré by means of optical filtering (Klug and DeRosier, 1966). For micrographs of extended, well-ordered, lattices of conventionally prepared (i.e. negatively stained or shadowed) specimens, optical filtering yields results equivalent to those obtained by computer filtering (Aebi et al., 1973), and this is the method of choice for laboratories not equipped for computer analysis.

(c) Computer filtering

The analagous operations may also be carried out by computer processing, whereby the digital Fourier transform replaces the optical transform, and a numerical matrix applied multiplicatively to the transform substitutes for the physical mask. The major advantages of the computational method are: (i) the analysis is absolutely quantitative at each step, which is particularly useful in tailoring the filter mask to the set of periodic reflections, and in manipulating the contrast of the final image; (ii) unlike optical processing, the phase information of the Fourier transform is explicitly available, which is useful for such purposes as determining orders of symmetry; (iii) computer analysis may be more easily applied to small areas of lattice, whose diffractograms have only diffuse and relatively faint reflections.

(d) Correlation averaging

The quality of a diffractogram may also be impaired by disordering effects. Individual motifs may be displaced from their ideal lattice positions, either by random local offsets and/or rotational shifts, or by a long-range meandering of the lattice lines. If these disordering effects are sufficiently great, the resolution estimated from the crystalline diffraction pattern may underestimate the intrinsic resolution. Similarly, a filtered image obtained on the assumption that the motifs do indeed occuppy their ideal lattice positions will be degraded by smearing caused by the disordering. A recent refinement in computer averaging technique is designed to compensate for such disordering effects. The principle of the method (correlation averaging - see e.g. Frank et al., 1978) is to identify the true location and orientation of each repeating unit, by maximizing its cross-correlation func-

tion as calculated with a reference object, whose location is known with certainty. Once the locations have been identified, the image of each motif may be appropriately aligned for averaging by means of interpolation. The cross-correlation method is capable of localizing objects precisely even in the presence of substantial noise. The reference object is usually taken to be a low-resolution filtered image, so that the cycle of correlation averaging is intended to improve the resolution of this representation. With well-ordered lattices, there is little to be gained from correlation averaging as opposed to the other techniques. However, its advantage is that it is applicable to a broader class of specimens, as it relaxes the requirement for very exact crystallinity. Using this technique, one may also scavenge an adequately large set of repeating units by combining input from several relatively small, loosely ordered patches, or even individual free-standing particles.

2C.1.4. Three-dimensional reconstruction

In order to resolve the full three-dimensional structure of an object, it is necessary to combine the information content of different views of the object. With objects that possess internal symmetries, such as icosahedra or helices, a single projection image may suffice for reconstruction, because the symmetries generate corresponding numbers of 'different' views. More generally, different views can be obtained by tilting the specimen on a goniometer stage. This procedure has the drawback that micrographs recorded late in the series visualize a specimen that has sustained considerably more radiation damage, and that in practice it is possible to cover only a limited range of tilt-angles (up to $\pm 60°$). Nevertheless, the resulting data enable a reconstruction to be made, although to a resolution that may be somewhat lower than for a single projection image recorded at low electron dose, and lower still in the dimension perpendicular to the specimen grid, on account of the incomplete angular range covered.

The objective of reconstruction from projections arises in several other contexts, including diagnostic tomography. Consequently, much effort, both theoretical and applied, has been invested in devising and evaluating reconstruction algorithms. Broadly, these may be distinguished into algorithms that operate in 'real space', to give three-dimensional density distribution that best accounts for the projections, and 'Fourier space' methods. The latter have been mainly used in biological electron microscopy. Generally, they proceed by building up as fully as possible the 3-D Fourier transform of the specimen's density distribution, uniting the various 2-D projection images by exploiting the fundamental property that each, when Fourier transformed, affords a planar slice of the full 3-D transform, passing through its origin. Finally, an inverse Fourier transformation yields the 3-D structure of the specimen. A treatment of this kind, particularly designed to exploit the internal symmetry of icosahedra, has been developed and applied to several icosahedral viruses (Crowther and Amos, 1972). Helical structures may be reconstructed by an analagous procedure (DeRosier and Moore, 1970).

2C.2. Scanning transmission electron microscopy (STEM)

The STEM was initially developed during the 1960s by the group of Crewe at the University of Chicago, but such microscopes are now commercially available, both in the form of dedicated STEMs and as an adaptive imaging mode of several models of conventional TEM (Ruigrok et al., 1984). Certain aspects of STEM image formation and recording are particularly well suited for visualization of unstained biological specimens with adequate contrast (Fig. 2C.3), at low-to-moderate electron doses. Accordingly, this approach appears to have great potential for structural studies in virology, as well as in molecular and cellular biology at large. The STEM applications published thus far, although relatively few in number, appear to bear out these positive expectations.

In contrast to the CTEM, which illuminates a substantial area of specimen with a spread beam, image formation in the STEM involves scanning the specimen with a finely focussed electron probe, and separately recording the electrons scattered from each point of the raster scanned. Unlike the conventional scanning electron microscope (CSEM), it is the transmitted electrons rather than the back-scattered

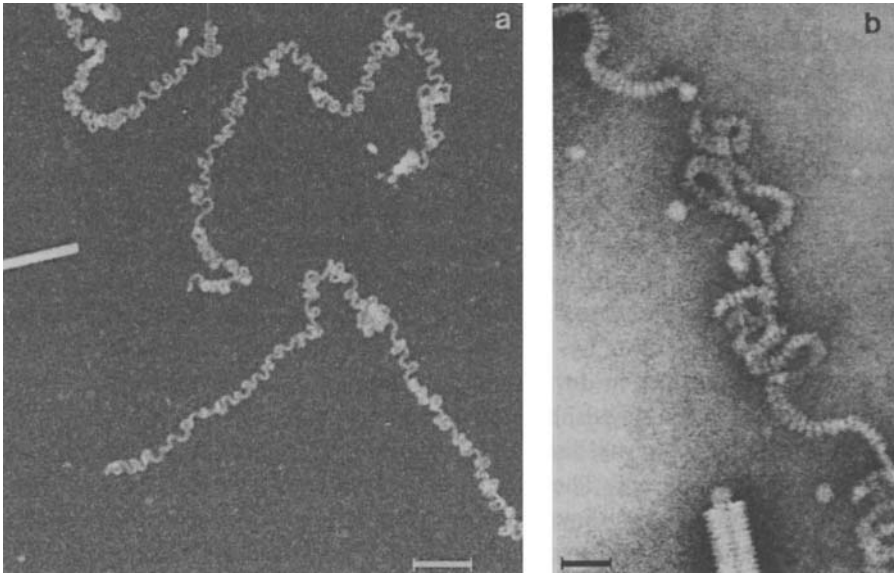

Fig. 2C.3. STEM micrographs of purified nucleocapsids of vesicular stomatitis virus (see Brown and Newcomb, Chapter 14 of this volume). (a) Unstained, frozen-dried specimen visualized in STEM annular dark-field mode; (b) negatively stained with 2% phosphotungstic acid. The wider straight particles also present in both fields are reference particles of tobacco mosaic virus. These micrographs were recorded with the Brookhaven National Laboratory STEM (Wall, 1979); A.C. Steven and J.S. Wall, unpublished results.

secondary electrons that are detected in STEM imaging. Because scattering events which generate transmitted electrons occur much more frequently than back-scattering for a given electron dose, STEM requires much lower exposures than CSEM to produce statistically defined images of radiation-sensitive specimens. This property facilitates the preservation of structural detail to relatively high resolution.

Instrumentally, atomic resolution (of heavy atoms) has been achieved by STEMs (Crewe et al., 1970) with optimized objective lenses capable of focussing the beam into a sufficiently fine probe, and using field emission guns to provide an adequately bright source of illumination. Moreover, direct digital image acquisition is readily implemented in STEM by electronic recording of the signal(s) via electron detector(s). Parallel detection of several images may be achieved by deploying a configuration of different detectors for simultaneous recording of classes of electrons that are scattered into distinct angular zones relative to the optical axis. Because the quantum detection efficiency of modern detectors approaches 100%, utilization of information is extremely efficient. In particular, a simple and efficent dark-field mode is achieved by the use of annular detectors. The unscattered as well as most of the inelastically scattered electrons pass through the central hole of the detector, and therefore do not reduce the contrast of the image generated by the elastic electrons scattered into the annular detection zone. Depending on the collection angle covered, such a detector may pick up $\approx$ 40–50% of all elastically scattered electrons, thus forming an image that is particularly useful for visualizing unstained biological macromolecules with high contrast, at moderate electron doses (e.g. $\approx 10^2$–10^3 e^-/nm^2). Moreover, since there is an essentially linear relationship between this dark-field signal and the mass sampled by the beam, this image is ideally suited for various kinds of quantitative image analysis.

2C.2.1. Mass determination of individual macromolecules and complexes

The concept of determining a particle's mass from its cumulative electron scattering power preceded the advent of the STEM (Brakenhoff et al., 1972; Bahr et al., 1976). However, the optical attributes of STEM – particularly its dark-field mode – are ideally suited for this purpose, since particles must be unstained for direct mass measurements to be possible (Wall, 1979; Engel, 1982). For such analyses, specimens are best prepared by freeze-drying after adsorption to a very thin and uniform carbon film and extensive washing to minimize the residue of non-volatile salts. Computational methods are applied to the resulting data to integrate the total projected density in areas of the image field occupied by individual particles, with a background subtraction made to compensate for the contribution of the carbon film substrate. It is thus possible to measure masses directly from the absolute electron scattering, but it is more common practice to calibrate experimental specimens against an internal standard of known mass (e.g. tobacco mosaic virus).

In priniple, the major sources of random error in such measurements are statistical fluctuations in the carbon film thickness and in the number of electrons applied per pixel. Under ideal experimental conditions, these should cause only a very slight error for particles in the size range of viruses (e.g. $\approx$ 0.1–1.0%). In practice, however, observed standard deviations tend to be somewhat higher, reflecting the influence of particle heterogeneity, variable amounts of salt residues, and non-ideality of the support film structure, among other factors. Nevertheless, it appears that standard deviations of 5% or better may be generally expected, and figures of $\lesssim$ 1% have been achieved in some cases. As experience with the technique accumulates, there is every reason to expect further improvement in precision. Furthermore, comparisons of STEM mass values obtained for such test specimens as oligomeric enzymes and ribosomal subunits with the results given by conventional methods show good agreement (Wall and Hainfeld, 1984). This concurrence indicates that, for these model systems at least, the STEM data are accurate and the method is not compromised by some unforeseen systematic error.

This approach possesses several major advantages over conventional biophysical methods for mass determination, e.g. those based on hydrodynamic or light-scattering techniques. Only miniscule quantities of experimental material are required, although it is desirable that the specimen be available in sufficient quantity to allow complementary biochemical analysis. It is not essential that the specimen be homogeneous or monodisperse, merely that it be morphologically recognizable. This property makes the technique uniquely appropriate for characterization of populations of particles that are intrinsically polymorphic (e.g. coated vesicles – Steven et al., 1983). Thus, because it makes possible a quantitative analysis of the extent of structural variation, the STEM method should be particularly useful for characterization of pleomorphic viruses. A further advantage is that particles that are evidently damaged or otherwise incomplete may be recognized as such and omitted from the determination. This procedure may also be extended to characterize and establish relationships among various types of subviral particle, either as isolated from infected cells or obtained as controlled degradation products from preparations of purified virions (Thomas et al., 1985). Furthermore, STEM mass determination can be used to calculate the absolute molecular composition of the virion in viral systems where the relative abundances of the constituents have been ascertained by biochemical quantitation.

2C.2.3. Mass-mapping (determination of spatial density distributions)

In addition to evaluation of the total masses of individual particles, the spatial information implicit in electron microscope images means that mass-mapping is also possible. In the simplest instances, this may involve calculating average mass-per-unit-length values for filamentous speciemens (Lamvik, 1977), which is immediately germane to the study of filamentous viruses or to extended nucleocap-

sids. Alternatively, the separate masses of distinctive structural domains, such as nodules, protrusions, etc., may be determined and correlated with molecular content, as in the analysis of the domains of the fibrinogen molecule by Mosesson et al. (1979).

Proceeding to successively finer levels of structural detail brings the requirement of increasingly sophisticated computational image analysis which involves averaging over many different images of the same structure in order to overcome the statistical noise implicit in any single image. Several types of algorithm to achieve this end have already been implemented and this field is evolving rapidly. For instance, averaged maps of projected density have been calculated for specimens that are periodic in two dimension (Engel et al., 1982), and average radial density distributions may be obtained for cylindrical, filamentous or spheroidal specimens (Steven et al., 1984). Ultimately, it seems likely that most of the analytical procedures developed for images of negatively stained specimens will prove applicable or adaptable to STEM images of unstained specimens. Density maps so obtained should afford valuable structural information complementary to that obtained by other techniques. In particular, edge detection in images of unstained specimens does not depend on assumptions about (the absence of) coincident positive staining of peripheral structural features. Accordingly, particle dimensions should be more reliably determined by this method. Furthermore, visualization of internal features of low density (cavities, etc.) should not be compromised by uncertainty about the extent to which negative stain may have infiltrated.

2C.3. Conclusions

Image processing, in its many forms, serves as an essential adjunct to high-resolution electron microscopic studies of biological specimens. These techniques have already been applied fruitfully in several animal virus systems and have the potential to contribute incisively to many others. To attain higher resolution than the present limit of $\approx$ 2 nm will depend on advances in specimen preparation and low-dose imaging methods, but it is unlikely to be achieved without image processing, because it seems improbable that higher resolution will be obtained from single micrographs. Rather, it will entail analyses combining the input of many micrographs, both on account of the high statistical noise level of images recorded at electron doses that are low enough for high-resolution structure to survive radiation damage, and because 3-D reconstruction becomes increasingly important for unambiguous interpretation of images at progressively higher resolutions.

Scanning transmission electron microscopy is a relatively novel imaging method which combines several major advantages for the observation of biological specimens with adequate contrast, without staining or shadowing with heavy metals. Among other potentialities of this kind of microscope, STEM dark-field

images have already been found to be particularly useful for direct mass measurements of individual macromolecular complexes, and for mass-mapping within such complexes. These capabilities should find many applications in structural virology.

References

Aebi, U., Smith, P.R., Dubochet, J., Henry, C. and Kellenberger, E. (1973) A study of the structure of the T-layer of *Bacillus brevis*. J. Supramol. Struct. 1, 498–522.

Bahr, G.F., Engler, W.F. and Mazzone, H.M. (1976) Determination of the mass of viruses by quantitative electron microscopy. Q. Rev. Biophys. 9, 459–489.

Baker, T.S. (1981) Image processing of biological specimens: a bibliography. In Electron Microscopy in Biology, Ed. J.D. Griffith, Vol. 1, pp. 189–290. Wiley, New York.

Brakenhoff, G.J., Nanninga, N. and Pieters, J. (1972) Relative mass determination from dark-field electron micrographs with an application to ribosomes. J. Ultrastruct. Res.. 41, 238–257.

Brigham, E.O. (1974) The Fast Fourier Transform. Prentice Hall, Englewood Cliffs, NJ.

Crewe, A.V., Wall, J.S. and Langmore, J. (1970) The visibility of single atoms. Science 168, 1338–1339.

Crowther, R.A. and Amos, L.A. (1972) Three-dimensional reconstruction of some small spherical viruses. Cold Spring Harbour Symp. Quant. Biol. 36, 489–494.

DeRosier, D.J. and Moore, P.B. (1970) Reconstruction of three-dimensional images from electron micrographs of structures with helical symmetry. J. Mol. Biol. 52, 355–369.

Engel, A. (1982) Mass determination by electron scattering. Micron 13, 425–436.

Engel, A., Baumeister, W, and Saxton, W.O. (1982) Mass mapping of a protein complex with the scanning transmission electron microscope. Proc. Natl. Acad. Sci. USA 79, 4050–4054.

Frank, J., Shimkin, B. and Dowse, H. (1981) SPIDER – a modular software system for electron image processing. Ultramicroscopy 6, 343–358.

Frank, J., Goldfarb, W., Eisenberg, D. and Baker, T.S. (1978) Reconstruction of glutamine synthetase using computer averaging. Ultramicroscopy 3, 283–290.

Fraser, R.D.B. and Millward, G.R. (1970) Image averaging by optical filtering. J. Ultrastruct. Res. 31, 203–211.

Goodman, J.W. (1968) Introduction to Fourier Optics. McGraw-Hill, San Francisco.

Klug, A. and DeRosier, D.J. (1966) Optical filtering of electron micrographs: reconstruction of one-sided images. Nature (London) 212, 435–440.

Lamvik, M.K. (1978) Muscle thick filament mass measured by electron scattering. J. Mol. Biol. 122, 55–68.

Markham, R., Frey, S. and Hills, G.J. (1963) Methods for the enhancement of image detail and accentuation of structure in electron microscopy. Virology 20, 88–102.

Misell, D.L. (1978) Image Analysis, Enhancement and Interpretation. North-Holland, Amsterdam.

Mosesson, M.W., Hainfeld, J., Haschemeyer, R.H. and Wall, J. (1981) Identification and mass analysis of human fibrinogen molecules and their domains by scanning transmission electron microscopy. J. Mol. Biol. 153, 695–718.

Ruigrok, R.W.H., Andree, P.J., Hooft Van Huysduynen, R.A.M. and Mellema, J.E. (1984) Characterization of three highly purified influenza virus strains by electron microscopy. J. Gen. Virol. 65, 799–802.

Smith, P.R. (1978) An integrated set of computer programs for processing electron micrographs of biological structures. Ultramicroscopy 3, 153–160.

Steven, A.C. (1981) Visualization of virus structure in three dimensions. In Three-dimensional Ultrastructure in Biology, Ed. J.N. Turner; Methods in Cell Biology, Vol. 22, pp. 298–324. Academic Press, New York.

Steven, A.C., Hainfeld, J.F., Wall, J.S. and Steer, C.J. (1983) Mass distributions of coated vesicles isolated from liver and brain: analysis by scanning transmission electron microscopy. J. Cell Biol. 97, 1714–1723.

Steven, A.C., Hainfeld, J.F., Trus, B.L., Steinert, P.M. and Wall, J.S. (1984) Radial distribution of density within macromolecular complexes determined from dark-field electron micrographs. Proc. Natl. Acad. Sci. USA 81, 6363–6367.

Thomas, D., Newcomb, W.W., Brown, J.C., Wall, J.S., Hainfeld, J.F., Trus, B.L. and Steven, A.C. (1985) Mass and molecular composition of vesicular stomatitis virus. J. Virol. 54, 598–607.

Trus, B.L. and Steven, A.C. (1981) Digital image processing of electron micrographs – the PIC system. Ultramicroscopy 6, 383–386.

Van Heel, M. and Keegstra, W. (1981) IMAGIC: a fast, flexible and friendly image analysis software system. Ultramicroscopy 7, 113–130.

Wall, J.S. (1979) Biological scanning transmission electron microscopy. Introduction to Analytical Electron Microscopy, Eds. J.J. Hren, J.I. Goldstein and D.C. Joy. pp. 333–342. Plenum, New York.

Wall, J.S. and Hainfeld, J.F. (1984) Towards the biochemistry of individual molecules. Proc. 42nd Annu. Meet. EMSA, pp. 154–157. San Francisco Press.

This Page Intentionally Left Blank

Nermut/Steven (eds) Animal Virus Structure

CHAPTER 3

X-ray diffraction from viruses

J.T. FINCH

MRC Laboratory for Molecular Biology, Hills Road, Cambridge, U.K.

3.1. Introduction

The pioneering work on tomato bushy stunt virus followed by that on other plant viruses has shown that X-ray diffraction studies on particles of such size can now be pursued to atomic detail. The aim of this section is to outline the procedures involved and to give an idea of judging the feasibility of such a study. More details of many of the methods are given in the books by Blundell and Johnson (1976) and McPherson (1982) and many of the results to date are described by Harrison (1983) and Jurnak and McPherson (1984).

X-ray diffraction from single crystals provides the most straightforward technique for investigating the structure of viruses at high resolution (i.e. to atomic detail). While it is indirect, in that the apparatus does not yield an instant structure, the basic methods of collecting the diffraction data and of processing these to yield an electron-density map have been well developed for protein crystallography and are by now fairly routine.

The main extra problems with X-ray diffraction from virus crystals arise from the considerably larger size of the virus particles: for a given resolution limit, the amount of data to be collected is increased and the average diffracted intensity weakened by factors proportional to the volumes of the particles. The earlier difficulties have all been considerably eased with the introduction of modern high-power X-ray sources and new detector systems, and by computer programmes that make use of the high symmetry of virus particles.

Provided reasonable crystals can be grown, it is feasible to aim for a high-resolution map of a virus which will give the required structural information. The

procedure can be divided into the three main areas of crystallization, data collection and data processing. In addition to three-dimensional crystallography, the methods of X-ray fibre diffraction have been applied to long helical plant and bacterial viruses and could well be applied to the helical components of animal viruses.

3.2. Crystallization

3.2.1. Crystallizability

The first question is what is likely to crystallize, and the answer is anything that is uniform in structure. Provided that the conditions appreciably favour a particular type of association, this will occur repetitively and, as long as it is compatible with one of the 65 possible crystallographic symmetries, crystals will grow. (There are 230 possible three-dimensional crystallographic symmetries (space groups: see International Tables for X-ray Crystallography) but only 65 do not involve mirror or centre relationships, which cannot occur for proteins (or viruses)). So, the virus must be one with a uniform and therefore fairly rigid structure: floppy structures are likely to allow some leeway in the structure and lower the uniformity. The ideal candidates are the small isometric viruses, and it is not surprising that it was viruses of this type that were the first to yield true crystals. But there is no reason why elongated particles such as those associated with alfalfa mosaic virus should not crystallize, provided they are of one class of uniform size and structure.

While slightly elongated particles may provide suitable crystals, considerable elongation brings us to the question of dimensions which can limit the feasibility of an X-ray diffraction study. Size in itself does not limit the ability to form crystals, but too large an object could yield a crystal with an unresolvable X-ray diffraction pattern. The X-ray data depend on the size in two ways. Firstly, the larger the unit cell (the translational repeat unit in the crystal, which for simple crystals would have dimensions somewhere about those of the virus particles) the more data are required for a given resolution, i.e. there are more X-ray reflections out to a given angle of diffraction, and so finer X-ray beams must be used to resolve them. Secondly, since the X-ray scattering is distributed between more reflections they are, on the average, proportionately weaker. The viruses which have been studied in detail so far are about 200–400 Å in diameter. Although larger viruses and larger unit cells of complex arrangements of smaller virus particles are being studied, the data collection problems become much greater and at present the possible results would have to be of considerable interest to warrant such an investigation.

If the complete virus is too large or non-uniform for X-ray crystallography to

be feasible, there remains the possibility of crystallizing part of the virus. This has been extremely successful with the haemagglutinin and neuraminidase of influenza virus, the hexon surface unit of adenovirus, and the two-turn disc aggregate of tobacco mosaic virus protein. Although these yield unit cells rather larger than the average proteins, they are relatively small by virus standards.

Having made the decision to try to grow crystals, one needs a pure specimen. Contaminants may affect or over-promote crystallization in a variable way and are better avoided so that reproducible conditions can be established. The aim is crystals of about 0.3–0.5 mm in diameter. Crystals larger than this will create resolution problems with the large number of diffracted rays. Crystals considerably smaller will diffract weakly. The basic methods for growing true three-dimensional crystals of viruses or their components will be described first and later the more specialized ways of preparing aligned specimens of rod viruses.

3.2.2. Precipitating agents and procedures

The aim of a crystallization procedure is to approach closely the equilibrium boundary between solid and liquid so that virus particles are sufficiently mobile to enable them to come together in a regular way. The first virus to be crystallized was the plant virus tomato bushy stunt (Bawden and Pirie, 1938); ammonium sulphate was added to precipitation point at room temperature and the result was stored at 4°C. The negative temperature coefficient of solubility pushed the conditions back towards solution, enabling larger crystals to grow at the expense of small precipitated aggregates. More often, the boundary is crossed slowly from the solution side so that the number of nuclei is small and time is available for them to grow into large crystals.

The two most frequently used precipitating agents are ammonium sulphate and polyethylene glycol, but a variety of other salts and organic solvents have been used (see Tables 4.1, 4.2 of MacPherson, 1982). In the absence of other information there is not much to choose between these; the salting-out concentration of ammonium sulphate may be rather high and polyethylene glycol might be regarded as a milder precipitant, but both can produce well-ordered crystals for X-ray work. If satisfactory crystals are not obtained with these (see below), or no crystals at all are produced, then other precipitants or combinations of precipitants can be tried.

Viruses vary considerably in their availability. With plentiful supplies one can experiment on a large scale, in a test tube or flask, to find precipitation conditions. It is less easy with poorer supplies but methods have been developed to scan conditions on a smaller scale. Unless one is sure of being close to satisfactory crystallization conditions, it is better not to try mixing in a closed tube set-up, but to have some method of varying conditions by vapour diffusion or dialysis – the choice is usually a personal one or biased by the experience of the laboratory. Thus, for

example, a simple crude survey could be made using vapour diffusion in the hanging-drop method. In this method, a drop of the virus solution, say 20 μl at about 10–25 mg/ml, in appropriate buffer and precipitant concentration is deposited on a siliconized cover slip which is then inverted over one of the 24 wells of a perspex tissue-culture tray, the well containing precipitant of higher concentration and the seal being made with soft grease or mineral oil. The aim is for the precipitant to be slightly below the critical concentration in the drop and slightly above it in the well so that, as vapour transfers between the two, the precipitation point in the drop is slowly reached and crystals nucleate and grow. If the concentration of precipitant is too low then the virus remains in solution, and if too high the virus is finely precipitated. It is likely that one knows the rough precipitation point, but if not, a crude survey can be implemented – say with wells at 20%, 40% and 60% saturated ammonium sulphate (5% lower in each drop) or say 10%, 18%, 25% PEG (3 or 4% lower in each drop). After a few days it will be evident where to concentrate the next finer grid of conditions and so on until the optimum conditions are found and crystals grow.

While it is useful for scanning conditions, the hanging drop is not the most suitable for growing crystals for the actual X-ray diffraction work. However, some indications can be seen in drops as to suitability for diffraction, mainly based on morphology.

3.2.3. Crystal assessment

The optimum crystal shape is fairly isometric: long fine needles or very thin plates are not welcomed – apart from being difficult to handle, the useable areas defined by the size of the collimated X-ray beam contain little volume and hence the crystals effectively diffract weakly. Ideally the crystals should grow in a clear polyhedral shape well separated from each other. Fans or groups of crystals growing from one nucleation point can sometimes be broken up to give individual crystals of useable size, but intimate intergrowing crystals of usually less regular shape cannot be used.

A polycrystalline character can often be easily detected with a polarizing microscope. Provided they are not of cubic symmetry, crystals will in general appear coloured between crossed polars, the colour extinguishing every 90° as the crystal is rotated about the axis of the microscope. A polycrystalline aggregate will show itself by the extinction of its members occurring at different orientations.

If the crystal shape or growth with a particular precipitant is unsatisfactory, one can of course start again with another precipitant. But it is sometimes possible to alter the crystal shape by modifying the crystallization solution slightly. For example, if the first unsatisfactory precipitant is ammonium sulphate then one might add a few percent of hexane-1,6-diol or 2-methylpentan-2,4-diol (not more or the ammonium sulphate may be precipitated). A two-dimensional hanging drop

survey varying the concentration of additive and main precipitant may well show a combination producing crystals more suitably shaped for X-ray work.

Having located the optimum conditions, a collection of small tubes containing say 50–100 μl of solution spanning these conditions can be set up from which the crystals are more easily mounted for X-ray diffraction. Alternatively, small dialysis tubes or cells can be set up to equilibrate in this range of conditions. It is important that glassware and solutions are clean since, in the relatively long times of crystallization and of waiting for X-raying, bacterial and fungal growth can create havoc. Silicone treatment of glassware to make it hydrophobic seems to help by reducing the number of nucleation points, leading to fewer, larger crystals.

Crystals are usually grown at either room temperature or at 4°C, since these are commonly available. In the former case, an air-conditioned room at constant temperature is the best choice, since this eliminates a variable in trying to reproduce conditions. Sharp temperature changes may also induce too many crystals to nucleate. To avoid this, it is a good idea to keep the crystallization experiments in a a cupboard to buffer short-term temperature fluctuations, and tubes can be stored submerged in rubber or expanded polystyrene racks to avoid temperature-gradient effects. Most virus crystals have been grown at 4°C to minimize breakdown before crystallization, but crystals themselves are usually fairly stable once formed.

The time taken for crystals to grow can vary from a few days to some weeks, although it is usually clear after a week or two what the final outcome will be. A few crystals are a good sign and hopefully they will continue to grow, but many small crystals suggest too rapid a precipitation and are unlikely to result in final crystals of a useable size.

3.2.4. Preliminary X-ray work

The final test of a crystal's suitability is by X-ray diffraction itself. It is a common practice to raise the concentration of the precipitant in the crystallization solution (mother liquor) at this point to stabilize the crystals against possible small changes in conditions during mounting and while being X-rayed. The crystal is sucked into a thin-wall glass capillary tube – a flexible tubing connection to a small syringe is useful for this – and the crystal is either manipulated or gently sucked free of mother liquor with a fine sliver of filter paper. A short column of mother liquor is often included in the tube a few mm from the crystal as a buffer of conditions, and this section of the tube, about 30 mm in length, is sealed with wax.

Preliminary X-ray work is usually done on a precession camera, although the first photograph is taken with the crystal still. The crystal is mounted on a goniometer head on which it can be adjusted so that some morphologically prominent direction is parallel to the X-ray beam (normally one would choose the direc-

tion of highest symmetry or a prominent crystal edge), and exposed for a time depending on the size of crystal and type of X-ray tube, but typically about 15 min.

The still photograph obtained (Fig. 3.1) shows a pattern of spots – the positions of the diffracted rays or reflections – and the angular extent of these reflections indicates the degree of order in the crystal, which can be calculated from the Bragg equation $\lambda = 2d \sin \theta$. λ is the wavelength of the X-rays used, almost always CuKα with $\lambda = 1.54$ Å. 2θ is the angular extent of the reflections from the incident direction of the X-ray beam. Inserting these values into the Bragg equation gives the limiting value for d – the shortest spacing that can be resolved in the crystals. For a high-resolution structure determination this should be at least 2.5 Å. If, instead of a photograph like Fig. 3.1, just a few spots occur close to the direct beam, then the crystal is very disordered. A few widely spaced spots over the film are characteristic of an inorganic crystal derived from the salts in the crystallization

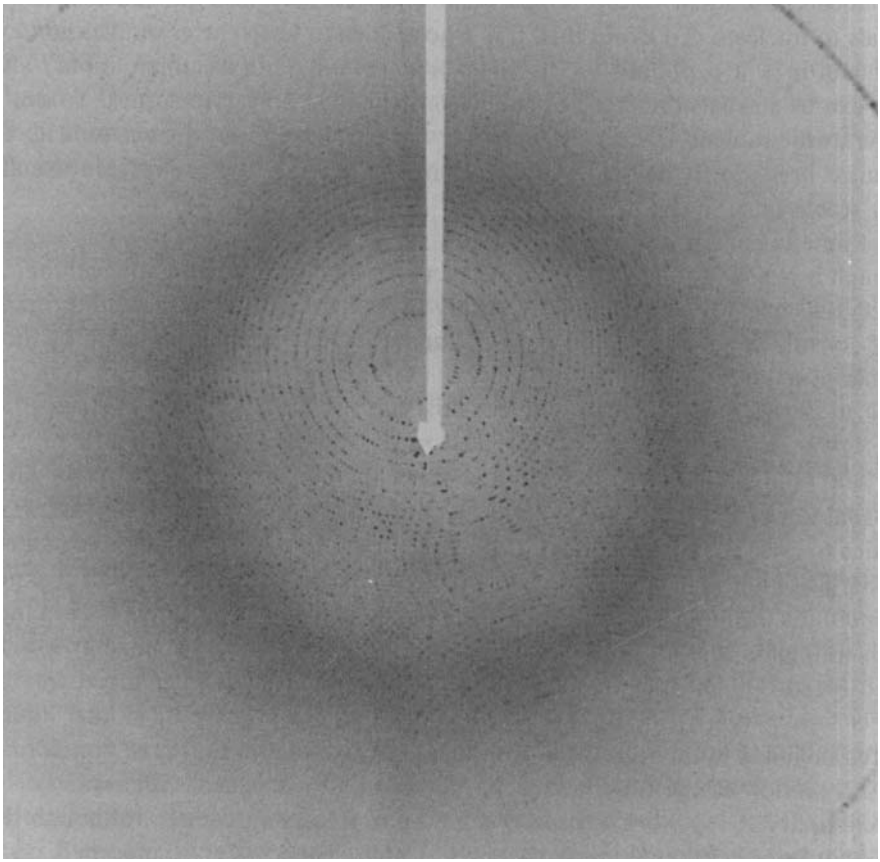

Fig. 3.1. X-ray diffraction 'still' photograph of a crystal of poliomyelitis virus. The extent of the pattern from the centre shows that the crystal is ordered to a resolution of about 2 Å.

solution: phosphate buffers are one of the worse offenders in this respect, producing crystals with cations from the precipitant.

Still photographs are the first stages in setting crystals to take precession photographs (the crystal and film are precessed about the line of the X-ray beam) from which the most important information is obtained, the space group symmetry of the crystal and the dimensions of the unit cell. The space group is deduced from the symmetry of the X-ray pattern and the reflections that occur (or rather that do not occur, since particular symmetries and lattices produce systematic absences of reflections). The symmetry elements of the space group act on an 'asymmetric' unit and produce the total contents of the unit cell, which is then repeated throughout the whole crystal by translation through vectors parallel to the sides of the unit cell.

The asymmetric unit of the crystal can be one of the molecules crystallized, or more than one, or, if the molecule itself possesses symmetry, part of the molecule. Since the isometric viruses have icosahedral symmetry, they can fall into the latter class; thus, for example, in crystals of tomato bushy stunt virus (TBSV), the asymmetric unit is 1/12 of a virus particle which the space group symmetry builds up into two virus particles per unit cell. This is the ideal situation for a virus crystal – a larger asymmetric unit would lead either to more virus particles per cell and hence to a larger cell with correspondingly greater difficulties in measuring more data for a given resolution, or to a space group with lower symmetry, thus again requiring more data to be collected. (There is a correlation between the symmetry of the three-dimensional diffraction effects and that of the crystal giving rise to them; for a given unit cell size, the higher the symmetry the more are the diffraction effects repeated and the smaller the sample that needs to be collected.) The most important point here is that the number of virus particles per unit cell is low – an estimate can be made from the volumes of the unit cell and of the virus particles, assuming that the volume occupied by solution will be somewhere about 50%. A check on the latter can be obtained by measuring the crystal density in a density gradient made with varying proportions of xylene and bromobenzene. If a large number of particles per cell is indicated it is worth searching for alternative crystallization conditions and possibly a better unit cell.

3.3. Data collection

If the crystal is satisfactory the next step towards structure determination is data collection. At present, the arrangement most frequently used is probably the rotation camera designed by Arndt and Wonacott (1977) with either a rotating anode X-ray set or one of the very high-powered synchrotron or storage-ring X-ray sources. The crystals are rotated about a known axis through a sufficiently small angle that reflections do not overlap. With TBSV, a 25° total rotation was re-

quired to record all of the symmetrically independent reflections, and this was made up of ½° steps. The crystals were sufficiently large, however, that by moving the crystal after one exposure a fresh piece could be brought into the X-ray beam, yielding two photographs per crystal. Thus 25 crystals were required for a data set. The next step is to scan the films in a microdensitometer and extract the intensities of the recorded spots corrected for background and geometrical effects to yield the amplitude of the reflections.

Each of the reflections corresponds to a Fourier component of the electron density in a unit cell, i.e. to a sinusoidal density variation through the unit cell of amplitude proportional to the amplitude of the reflection. The orientation and angle of diffraction of each ray give the direction and wavelength of the corresponding density variation. To determine the contents of the unit cell thus requires adding all these density components but in their correct relative phases, which have yet to be determined. The standard method for this in protein crystallography is to use heavy atom markers on the protein, sufficient to change appreciably the density in the unit cell and hence the intensities of the reflection, but insufficient to change the unit cell or the disposition of the protein within it (the native and derivative crystals are isomorphous). The same method has been used for viruses. If some relevant chemistry is known about the makeup of the specimen, particular heavy atom compounds can be reacted in a controlled way at a particular site (e.g. methyl mercury nitrate or parachloromercuribenzoate at SH groups); besides giving phase information, these can indicate the positions of the reacting sites in the unit cell. Much more often, however, crystals are soaked in any available solution of a heavy atom at a few mM concentration and precession photographs are taken to test whether the cell is still ordered, and is isomorphous with the native but with intensity changes. A list of some of the compounds used is given by Blundell and Johnson (1976, Chapter 8).

3.4. Data processing

With a minimum of heavy atom derivatives, provided one can locate the heavy atoms in the unit cell, the phases of most of the reflections can be calculated. In the case of viruses with many equivalent subunits, and hence sites of the atoms, a knowledge of the virus symmetry and the orientation of the symmetry axes is a help in this location. The procedure is to collect sets of data from each heavy atom derivative. Using the differences in the intensities between the native data set and each derivative, a Patterson map can be calculated – a map of the vectors between heavy atoms in which (one hopes) the locations of the atoms are indicated – and their coordinates can be refined against the original sets of data. This is relatively easy if there is only one site per subunit, but much less so for a multi-site derivative – the Patterson map may be uninterpretable. Having found the heavy atom sites,

the contributions of each of the heavy atom collections to the diffraction by the crystal can be calculated and, from the measured intensity modification, the phases of the native reflections can be obtained. In practice, the confidence in the phases so obtained varies, depending on the quality of the crystals and the derivatives - whether the heavy atoms are precisely located in a few positions or spread out over many sites with relatively low occupancy and maybe somewhat variable in position or perhaps perturbing the arrangement in the crystal.

In the case of TBSV, mercury and uranyl derivatives were used. The fact that the virus had icosahedral symmetry was used to refine the phases (Bricogne, 1976). These phases were then used with the native amplitudes to calculate an electron-density map of the crystal and detail in this was sharpened by again using the icosahedral symmetry to average over a virus particle. The fact that this averaging procedure has given an interpretable map justifies its use for TBSV, but for a less rigid virus the interparticle contacts in the crystal could well make the particle symmetry less well preserved and, in that case, symmetry averaging would smear out the structural details and the phase refinement procedure would not converge.

The structure of TBSV (Harrison et al., 1978) is illustrated in Fig. 3.2. It is based on the $T=3$ icosahedral surface lattice and it follows that there are 180 protein

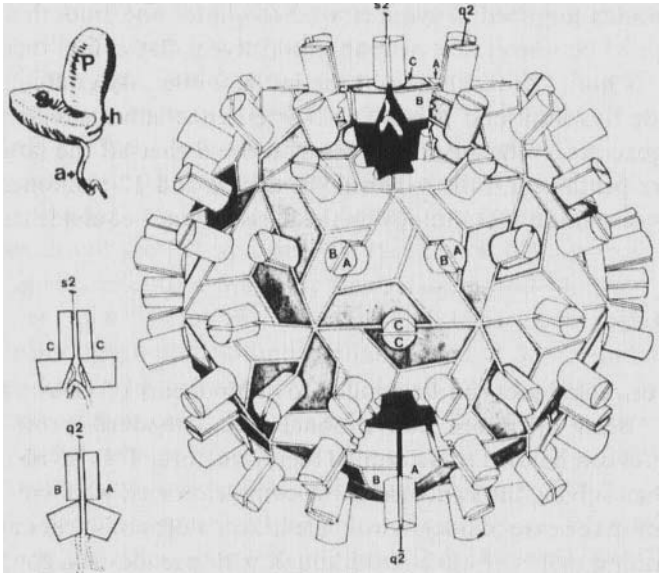

Fig. 3.2. The packing of the protein subunits in TBSV. Each subunit consists of two domains (P and S) connected by a hinge region (h) and an inner arm (a). The arrangement is based on the $T = 3$ icosahedral surface lattice and the subunits occur in quasi-equivalent locations, A, B and C. The outer P domains are clustered in A/B and C/C pairs about the local and strict 2-fold axes respectively, and these pairs show different settings of the hinge between the P and S domains as indicated on the left (Harrison et al., 1978).

subunits in three quasi-equivalent environments marked A, B and C. They form a compact shell about 30 Å thick and each subunit consists of two distinct globular domains connected by a hinge. The outer (P) domains cluster in AB and CC pairs to form 90 projections about the local and strict two-fold axes, and the inner (S) domains make up the more uniform density of the inner part of the shell. Although the domains are essentially the same for all subunits, the hinge between the P and S domains adopts two different settings in the A/B subunits and in the C subunits. Inward-projecting N-terminal arms from the C subunits interact with each other about the particle 3-fold axes but for the A and B subunits they were not visible in the map, indicating that for these the N-terminal arms are not in a fixed conformation. All of the ordered regions of the polypeptide chain have been traced in the map without ambiguity.

The structure of polyoma virus, rather larger than the above, has been determined to about 22.5 Å resolution without using the isomorphous replacement method to determine phases (Rayment et al., 1982). The starting point was a low-resolution model obtained from electron microscopy (large morphological units forming the hexamer-pentamer-type clustering pattern on a $T=7d$ icosahedral surface lattice). Phases were first calculated by putting this model into the crystal structure, and these phases together with measured amplitudes yielded a refined model structure. By imposing icosahedral symmetry on the latter and smoothing out any detail that appeared between the virus particles (solvent flattening) these phases were refined out to 30 Å, the resolution of the initial model. By gradually adding reflections outside this limit and preserving the flattened solvent region, phases to 22.5 Å were generated. The surprising result showed that all the large morphological units were pentamers, rather than 60 hexamers and 12 pentamers as expected from the low-resolution morphology on the basis of quasi-equivalence.

3.5. Components of viruses

The same crystallization techniques can be applied to components of viruses if these can be isolated. Being of more conventional size, standard protein crystallographic techniques can be used to determine their structure. This involves considerably less work than solving the structure of the complete virus, which may not even be crystallizable. In the case of adenovirus, the hexon morphological unit has been studied, confirming that it is a trimer although with pseudo-hexagonal features (Burnett, 1984). The structures of the neuraminidase (Varghese et al., 1983) and haemagglutinin (Wilson et al., 1981) of influenza virus have been determined. Apart from the intrinsic structural interest, it has been possible to map biologically important sites such as the receptor site in the haemagglutinin involved in binding to a target cell for infection and the main sites for the virus-neutralizing antibodies (Wiley et al., 1984).

3.6. Filamentous specimens

Although not in a three-dimensional crystalline form, the helical structures of the rod-shaped tobacco mosaic virus (TMV) and the longer flexible plant viruses and bacteriophage have also been studied by X-ray diffraction, using samples in which the particles were aligned as closely as possible. Since the same techniques could be applied to the linear components of more complex animal viruses, such as the nucleoproteins of the myxoviruses, a brief mention is made here of the methods used.

After purification, the first stage is to obtain an aligned specimen. In the case of TMV, which is a fairly rigid rod of length about 3000 Å and diameter 180 Å, concentrated samples can spontaneously form regions of alignment (tactoids) as a result of the particles' mutual mild repulsion causing them to space apart from each other as uniformly as possible. The art of making specimens for X-ray work is to induce a column of concentrated solution in a thin-wall glass capillary tube to form into one domain of uniform alignment parallel to the axis of the tube and recognized by uniform colouring and extinction as it is rotated between crossed polars in a polarizing microscope. Provided the virus concentration and buffer and salt conditions are satisfactory this can happen spontaneously or smaller domains can sometimes be induced to coalesce by pushing the solution up and down the capillary tube (Gregory and Holmes, 1965).

The longer flexible viruses are less cooperative than TMV, and some extra force is required to achieve good orientation. The plant viruses potato X (Wilson and Tollin, 1969) and narcissus mosaic (Wilson et al., 1973) were dried against a meniscus at the edge of a cover slip, a method introduced for TMV by Bernal and Fankuchen (1941). Much better orientation has been achieved for the bacteriophage Pfl by using the fact that it is built from parallel α-helices which align parallel to a magnetic field (Torbet and Monet, 1979): concentrated solutions, about 50 mg/ml, showing small birefringent inclusions were mounted in a strong magnetic field and partially dried to 98% relative humidity.

Ideally, then, the perfect sample has all the particles exactly aligned but in random orientation about their long axes. The X-ray pattern is confined to layer lines perpendicular to the axes of the particles, but is continuous along these lines (i.e. the intensity varies continuously through maxima and minima and does not occur in discrete sharp reflections unless there is some crystallographic relationship between the orientations of the particles). By analogy with the diffraction from crystals, where each diffracted ray can be thought of as a reflection from a set of planes and allotted an index accordingly, the intensity on each layer line of the diffraction pattern of a helical arrangement can be associated with a family of parallel helices through the subunits and is again allotted indices n,l where n is the number of parallel helices in the family and l depends on the helical pitch and is also the layer line number from the equator of the X-ray pattern. And, again as

in the case of crystals, the diffracted amplitudes correspond to sinusoidal density waves through the particle parallel to the appropriate helical family, and, if one knows the phases associated with each of these density waves, one can add up all the various density contributions and obtain the helical structure. The phases can be obtained again by using heavy atom derivatives (Holmes, 1984).

There are, however, various complications. First one has to know the helical parameters of the structure (i.e. the correct values of n), which may not be easy to determine, and secondly the different n contributions on a layer line may overlap and be difficult to untangle (Stubbs and Makowski, 1982).

The structural work on TMV has relied exclusively so far on heavy atom phasing. Other methods have been used to solve the structure of the bacteriophage Pfl (Makowski, 1984).

3.7. Solution scattering

In this case, all orientation is lost in the specimens and the diffraction pattern is effectively the spherically averaged diffraction from a particle. There is therefore no information on the relative orientation of the periodicities in the particle which give rise to the intensities in the diffraction pattern. However, some information about the particle as a whole can be derived from the low-angle scattering (Porod, 1982). The radius of gyration can be obtained from the shape of the low-angle pattern and the molecular weight from the absolute magnitude of the zero-angle scattering (extrapolated from low angles).

If the particles are spherically symmetric, then one can allot signs to the various peaks in the X-ray pattern and from these calculate the radial density distribution (Porod, 1982; Zipper, 1982). This procedure is also valid for the isometric viruses using data extending to spacings where the morphological substructure begins to be resolved. This limit will vary with the scale of the substructure and in itself can therefore indicate this scale as a pointer of the type of clustering of subunits on the particle surface (Jack and Harrison, 1978). Further information can be obtained by comparing the solution scattering of a virus with that of viral components: such data together with the effects of staining have associated a 29 Å spacing with the DNA in adenovirus 2 (Devaux, Timmins and Berthet-Colominas, 1983).

Although it is difficult or impossible to derive a structure directly from a spherically averaged diffraction pattern, it is possible to test model structures by calculating their diffraction patterns. However, it is not certain that a unique model will give the measured pattern. For complex viruses with several components this method is better applied to neutron scattering data, where the relative scattering of the components can be changed by altering the H_2O:D_2O ratio (see Jacrot, Chapter 4 of this volume). A fit to the scattering data at a variety of contrasts gives one much greater confidence in a proposed model structure.

While solution scattering may be the only diffraction method applicable to large or not precisely uniform viruses, it is confined to low resolution. Within this limit, the method can give useful information, but for high-resolution data there is no substitute for a single-crystal study and, if the complete virus is not amenable, then, as with influenza, it may be worth thinking of studying the separate components.

References

Arndt, U.W. and Wonacott, A.J. (1977) The rotation method in crystallography. North-Holland, Amsterdam.

Bawden, F.C. and Pirie, N.W. (1938) Crystalline preparations of tomato bushy stunt virus. Br. J. Exp. Pathol. 19, 251–263.

Bernal, J.D. and Fankuchen, I. (1941) X-ray and crystallographic studies of plant virus preparations. J. Gen. Physiol. 25, 111–165.

Blundell, T.L. and Johnson, L.N. (1976) Protein crystallography. Academic Press, London.

Bricogne, G. (1976) Methods and programs for direct-space exploitation of geometric redundancies. Acta Crystallogr. A32, 832–847.

Burnett, A.M. (1984) Structural investigations of Hexon, the major coat protein of adenovirus. In Biological Macromolecules and Assemblies, Vol. 1: Virus Structures; Ed. F.A. Jurnak and A. McPherson, pp. 337–385. John Wiley, New York.

Devaux, C., Timmins, P.A. and Berthet-Colominas, C. (1983) Structural studies of adenovirus type 2 by neutron and X-ray scattering. J. Mol. Biol. 167, 119–132.

Gregory, J. and Holmes, K.C. (1965) Methods of preparing oriented tobacco mosaic virus sols for X-ray diffraction. J. Mol. Biol. 13, 796–801.

Harrison, S.C. (1983) Virus structure: high resolution perspectives. Adv. Virus Res. 28, 175–240.

Harrison, S.C., Olson, A., Schutt, C.E., Winkler, F.K. and Bricogne, G. (1978) Tomato bushy stunt virus at 2.9 Å resolution. Nature 276, 368–373.

Holmes, K.C. (1984) The structure determination of tobacco mosaic virus. In Biological Macromolecules and Assemblies, Vol. 1: Virus Structures; Eds. F.A. Jurnak and A. McPherson, pp. 121–148. John Wiley, New York.

International tables for X-ray crystallography (1952) Kynoch Press, Birmingham, U.K.

Jack, A. and Harrison, S.C. (1975) On the interpretation of small angle X-ray solution scattering from spherical viruses. J. Mol. Biol. 99, 15–25.

Jurnak, F.A. and McPherson, A. (1984) Biological macromolecules and assemblies. John Wiley, New York.

Makowski, L. (1984) Structural diversity in filamentous Bacteriophages. In Biological Macromolecules and Assemblies, Vol. 1: Virus Structures; Eds. F.A. Jurnak and A. McPherson, pp. 203–253. John Wiley, New York.

McPherson, A. (1982) Preparation and analysis of protein crystals. John Wiley, New York.

Porod, G. (1982) In Small Angle X-ray Scattering, Eds. O. Glatter and O. Kratky. Academic Press, London.

Rayment, I., Baker, T.S., Caspar, D.L.D. and Marakami, W.T. (1982) Polyoma virus capsid structure at 22.5 Å resolution. Nature 295, 110–115.

Stubbs, G. and Makowski, L. (1982) Coordinated use of isomorphous replacement and layer line splitting in phasing of fibre diffraction data. Acta Crystallogr. A38, 417–425.

Torbet, J. and Monet, G. (1979) Fibres of highly oriented Pfl bacteriophage produced in a strong magnetic field. J. Mol. Biol. 134, 843–845.

Varghese, J.N., Laver, W.G. and Colman, P.M. (1983) Structure of the influenza virus glycoprotein antigen neuraminidase at 2.9 Å resolution. Nature 303, 35–40.

Wilson, I.A., Skehel, J.J. and Wiley, D.C. (1981) Structure of the haemagglutinin membrane glycoprotein of influenza virus at 3 Å resolution. Nature 289, 366–373.

Wiley, D.C., Wilson, I.A. and Skehel, J.J. (1984) The hemagglutinin membrane glycoprotein of influenza virus. In: Biological Macromolecules and Assemblies, Vol. 1: Virus Structure; Eds. F.A. Jurnak and A. McPherson, pp. 299–336. John Wiley, New York.

Wilson, H.R. and Tollin, P. (1969) Some observations on the structure of potato virus X. J. Gen. Virol. 5, 151–153.

Wilson, H.R., Tollin, P. and Rahman, A. (1973) The structure of narcissus mosaic virus. J. Gen. Virol. 18, 181–187.

Zipper, P. (1982) In Small Angle X-ray Scattering, Eds. O. Glatter and O. Kratky. Academic Press, London.

Nermut/Steven (eds) Animal Virus Structure

CHAPTER 4

Neutron scattering

B. JACROT

Laboratoire Européen de Biologie Moleculaire, 156 Avenue des Martyres, 38042 Grenoble, France

4.1. Introduction

The basic principles of neutron diffraction are identical to those of X-ray diffraction. But whereas X-ray diffraction is mainly used to elucidate virus structure at atomic resolution from single crystals, the main application of neutron diffraction is to determine low-resolution structures from viral suspensions. The difference between X-rays and neutron diffraction arises from the fact that the diffraction pattern obtained with X-rays is the result of their interaction with atomic electrons, whereas that obtained with neutrons has its origin in their interaction with the atomic nucleus. An important consequence is that hydrogen and deuterium (which are chemically similar but have different nuclei) are easily distinguished by neutrons, and this fact is the main basis for the complementarity of neutron diffraction to X-ray diffraction. Otherwise all that is done with X-ray diffraction could also be done with neutron diffraction. But the scarcity of neutron sources would make it unwise to use neutrons except when they bring information unavailable from experiments using X-rays.

4.2. Theory

When a photon (X-ray) or a neutron hits an atom it gives rise to a scattered wave. The interferences between these waves give rise to the diffraction pattern. The scattered wave is characterized by an amplitude. In Table 4.1 are listed amplitudes for the various atoms which are found in a virus or in its solvent. The difference

TABLE 4.1.
Scattering amplitudes of various atoms. They are given in units of 10^{-12}cm. For X-rays the amplitudes are those of forward scattering.

Atom	Neutrons	X-rays
Hydrogen	−0.3742	0.28
Deuterium	0.6671	0.28
Carbon	0.6551	1.67
Nitrogen	0.940	1.97
Oxygen	0.5804	2.25
Sodium	0.36	3.10
Magnesium	0.52	3.38
Phosphorus	0.52	4.23
Sulphur	0.28	4.51
Chlorine	0.96	4.79
Potassium	0.37	5.36
Calcium	0.47	5.64

between H and D is indeed very large, as the wave scattered by an H nucleus contributes with a negative sign. The numbers in this table are those which are directly used to calculate the diffraction pattern at very high resolution (atomic resolution) in which the position of each individual atom is relevant. So far, although high-resolution crystallography using neutrons is applied to proteins, it has not been done with viruses (and very likely will never be done). At lower resolution, the relevant figures are the average scattering densities, obtained by summing the scattering amplitude b of each atom over a volume V and dividing by that volume. Table 4.2 gives those densities for the main constituents of a virus and for water. The exact figure will vary slightly from protein to protein depending on its amino-acid composition. For all molecules the density is also dependent on the specific

TABLE 4.2.
Scattering densities of various compounds. These densities are expressed in units of 10^{-14}cm/Å^3.

	Neutron	X-rays
H_2O	−0.562	9.40
D_2O	6.404	9.40
Protein in H_2O	1.8	12
Protein in D_2O	3.1	12
RNA in H_2O	3.54	15.7
RNA in D_2O	4.55	15.7
DNA in H_2O	3.54	15
DNA in D_2O	4.30	15
Carbohydrate in H_2O	1.9	
Carbohydrate in D_2O	4.8	
Lipids in H_2O	0	

volume. However, the values given in the table are always correct to within a few percent accuracy and the following general conclusions can be drawn:

- Protein, nucleic acids and lipids have very different scattering densities.
- The scattering density of a H_2O-D_2O mixture can have any value between -0.56 and $6.40\text{-}10^{-14}$ cm/Å^3 depending on the amount of D_2O.
- It is always possible to find a mixture of H_2O and D_2O which will have a scattering density equal to that of a given macromolecule. The D_2O content of that solution is called the matching point of the molecule. With such a solution the *contrast* between the macromolecules and the solvent is zero. This matching point is around 40% D_2O for a protein, 65% for DNA, 70% for RNA, 10% for lipids and between 50 and 60% for carbohydrates. The exact value of the matching point varies from protein to protein, from sugar to sugar and from lipid to lipid; for all molecules it is dependent upon their specific volume and the percentage of labile protons which are effectively exchanged for deuterons. On the other hand, for all solvents used with viruses, the presence of salts does not in practice affect their scattering density and can usually be ignored in the analysis.

4.3. Experimental conditions

Scattering is measured with samples of viruses in solutions made with different percentages of D_2O. The most useful range of concentration is between 1 and 10 mg/ml, although samples of 0.1 mg/ml are useful for molecular weight determination. Sample thickness is 0.1–0.2 cm, corresponding to volumes of 100–200 μl (in standard quartz cells). Typical experiments will require about 5 different contrasts, so 1–10 mg of a virus are required for a neutron experiment. There is no damage to the specimen by neutron beams and samples can be used afterwards for other physical or biochemical analyses.

Neutron beams are produced by a medium- or high-flux reactor. There is at least one such reactor in each industrialized country. The beam must be made roughly monochromatic (e.g. $\Delta\lambda/\lambda \leqslant 10\%$) and the neutrons scattered by the sample are analysed with a small-angle scattering instrument which measures the scattered intensity in an angular range around 10^{-2}–10^{-1} radians with for instance neutrons of wavelength 10 Å. The data collection is done more quickly if one has a two-dimensional position-sensitive detector which allows simultaneous measurement of intensity over a large angular range. With such a detector and a high-flux reactor one scattering curve can be measured in about 10 min for high contrasts and 1 hour for low contrasts. Measurements can be done on a medium-flux reactor and, for instance, a linear detector, and the scattering curve will then be obtained in a few hours.

Fig. 4.1 shows a typical set of data collected from solutions of Semliki Forest virus. Each curve is obtained after subtraction of the solvent scattering, which

must also be measured. Those data correpond to spacings between 150 and 1000 Å. By modifying the experimental conditions (e.g. the wavelength or the angular range), the scattering curve can extend out to 20 Å or in to 10000 Å. In any particular case, the range of the curve is selected according to the size of the virus. In the range 40–20 Å and beyond, scattering from solution becomes inadequate and should be replaced by diffraction (X-rays or neutrons) from single crystals, which can reveal the structural details, such as the shape of each capsid protein, which strongly affects the scattering in this range.

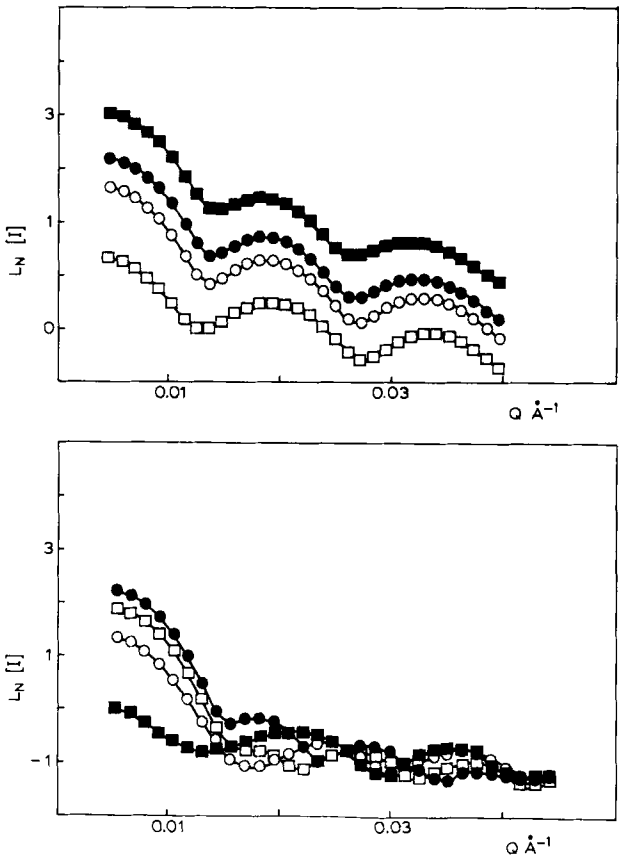

Fig. 4.1. Small-angle neutron scattering curves of solutions of Semliki Forest virus. The buffers have different D_2O content, as indicated. Upper set: ■, 100%; ●, 70%; ○, 55%; □, 40%. Lower set: ●, 0%; □, 10%; ○, 20%; ■, 28.5%. Scattering from the buffer has been subtracted. Concentrations were around 5 mg/ml. All data have been reduced to the same concentration, to show clearly the variations of intensities with the D_2O content. Intensity would vanish for 31.5% D_2O. The abscissa is in $Q = 2\pi\theta/\lambda$, where θ is the scattering angle and λ the neutron wavelength (here 10 Å).

4.4. The determination of the virus molecular weight and of its radius of gyration

In the lowest range of Q ($Q = 2\,\pi\theta/\lambda$ where θ is the scattering angle) the intensity can be represented by the expression

$$I(Q) = I(0)(1 - \tfrac{1}{3}\, R_G^2 Q^2)$$

R_G is the radius of gyration. The intensity $I(0)$ at zero scattering angle can be deduced from the data using this relationship. Both $I(0)$ and R_G vary with contrast; this is a consequence of the variation of the contribution of each chemical constituent of the virus with the D_2O content of the solvent.

Molecular weight. In H_2O the intensity $I(0)$ is given by

$$I(0) = N(\Sigma b - bsV)^2 A.$$

Σb is the sum of coherent scattering lengths over all nuclei in each particle, V is the volume of the particle, bs is the scattering density of the solvent and A is a factor which includes the incident beam intensity, the size of the sample, its transmission, and, more generally, all geometrical parameters of the experiment. For each component Σb and V are to a good approximation proportional to its molecular weight. The factor A is easily determined by a reference sample or simply by the scattering from a water sample. If N, the number of particles in the solution, is known, the measurement of $I(0)$ will give the molecular weight of the virus (for details, see Jacrot and Zaccai (1981)). The accuracy of the method is about 5%, the main limiting factor being the determination of the concentration. That determination requires methods giving absolute values, such as dry weight, phosphorus content or amino-acid analysis with an internal reference. The main experimental requirement is the availability of 50–100 μg of a pure and monodisperse sample. The method has been checked with many plant viruses. With adenovirus 2 it gives a mass of 157×10^6 (from its DNA length and chemical analysis, the mass is expected to be 164×10^6). With Semliki Forest virus one finds a mass of 45×10^6.

Radius of gyration. This gives an idea of the disposition of the components in the virion, but the information is better obtained from a complete analysis of the data with a model of the virus structure. It can be obtained by fitting the low-angle data with the expression given above.

4.5. The determination of a model of the virus

The simplest case is that of isometric viruses, which can to a good approximation be considered as made up of series of concentric spherical shells. Each shell is

characterized by its inner and outer radii and its scattering density. The scattering by that object can be calculated and the radii of the shells and their scattering densities can be adjusted to give the best possible fit to the data at all contrasts (Schneider et al., 1978; Chauvin et al., 1978; Cusack, 1984). The densities in each shell and their variation with contrast (which must be linear) give a direct determination of the chemical composition. This can be illustrated by the results of the analysis of the data for Semliki Forest virus shown in Fig. 4.1. These results are given in Table 4.3. Four shells were necessary to fit all the data: an internal shell very rich in RNA with a matching point at 66% D_2O, followed by a pure protein shell (matching point 45%); then one finds the lipid bilayer (matching point 12%) and the outer protein shell. This reveals a clear separation of the nucleocapsid into a core very rich in RNA and a shell with no (or very little) RNA penetration.

This analysis is valid so long as one can really approximate the virus as a spherical object. Viral components that are not distributed with spherical symmetry, such as small phage tails or the fibres in the adenovirus, do not contribute appreciably to neutron scattering (in contrast to the situation with hydrodynamical methods), provided that they do not account for a significant fraction of the total mass. Furthermore, it can be shown that for a virus having the shape of an icosahedron (e.g. the adenovirus) the scattering is to a very good approximation that of a sphere of equal volume. This is valid so long as one analyses only data collected in an angular range such that $Qd << 1$, where d is the distance between subunits in the protein shell. At larger scattering angles, the organization of the proteins to form the icosahedral shell modifies the scattering, and changes in that organization can sometimes be detected. For example, Cusack has interpreted changes in scattering from influenza virus B as due to an irreversible modification of the arrangement of the hemagglutinin when decreasing pH from 7 to 5.

TABLE 4.3.
Structural model of Semliki Forest virus deduced from the analysis of the data in Fig. 4.1.

Shell radius (Å)	Description	Mass (in 10^6)	Volume (10^6 Å^3)	Composition in volume (10^6 Å^3)			Experimental matching point
0–180	RNA 'core'	5.5	24.4	RNA	3.44	(14%)	66%
				Protein	1.9	(8%)	
				Water		(78%)	
180–210	Capsid	3.8	14.3	Protein	4.64	(30%)	45%
				Water		(70%)	
210–250	Lipid bilayer	14.9	26.6	Lipid	21	(80%)	12%
				Protein	3	(11%)	
				Water		(<10%)	
250–332	Spike layer	21.6	87.8	Protein	26	(30%)	45%
				Carbohydrate	2.6	(3%)	
				Water		(67%)	

4.6. Conclusion

Neutron scattering is a very useful method for obtaining structural information which is complementary to that obtained by electron microscopy. In favourable cases, it can show how proteins, lipids and nucleic acids are distributed inside viruses. As with all physical methods, a monodisperse sample is necessary to produce useful information, and it is always better to combine that method with others: electron microscopy, X-ray diffraction at large angle, and above all good biochemical characterization. Examples of this combination of methods are the work of Devaux et al. (1983) on adenovirus and that of Mellema et al. (1981) on influenza virus.

References

Chauvin, C., Witz, J. and Jacrot, B. (1978) Structure of the tomato bushy stunt virus: a model for protein RNA interaction. J. Mol. Biol. 124, 641–651.

Cusack, S. (1984) Neutron scattering studies of virus structures. In Neutrons in Biology, Ed. B.P. Schoenborn, pp. 173–188. Plenum, New York.

Devaux, C., Timmins, P.A., Berthet-Colominas, C. (1983) Structural studies of adenovirus type 2 by neutron and X-ray scattering. J. Mol. Biol. 167, 119–132.

Jacrot, B. and Zaccai, G. (1981) Determination of molecular weight by neutron scattering. Biopolymers 20, 2413–2426.

Mellema, J.E., Andree, P.J., Krijgsman, P.C.J., Kroon, C., Ruigrok, R.W.H., Cusack, S., Miller, A. and Zulauf, M. (1981) Structural investigations of influenza B virus. J. Mol. Biol. 151, 329–336.

Schneider, D., Zulauf, M., Schafer, R. and Franklin, R.M. (1978) Structure and synthesis of a lipid-containing bacteriophage. XXVI. Neutron small angle scattering on bacteriophage PM2. J. Mol. Biol. 124, 97–122.

This Page Intentionally Left Blank

Part III

Taxonomy of animal viruses

This Page Intentionally Left Blank

Nermut/Steven (eds) Animal Virus Structure

CHAPTER 5

Taxonomy of animal viruses

FREDERICK A. MURPHY

Division of Viral Diseases, Centers for Disease Control, Atlanta, GA 30333, U.S.A.

5.1. Introduction

In the experiments that led to the discovery of viruses by Beijerinck and Ivanovski (tobacco mosaic virus), Loeffler and Frosch (foot-and-mouth disease virus), and Reed and Carroll (yellow fever virus) at the turn of the century, the single physicochemical characteristic measured was filterability (Waterson and Wilkins, 1978). No other physicochemical measurements of viruses were possible at that time, and most studies of viruses were centered on infection processes and host responses. Thus, the earliest classifications of viruses were based on common pathogenic properties (e.g., 'hepatitis viruses', to include agents now known as hepatitis A virus, hepatitis B virus, yellow fever virus), common organ tropisms (e.g., 'respiratory viruses', to include agents now known as influenza viruses, rhinoviruses, adenoviruses), and common ecological charachteristics (e.g., 'arboviruses', to include agents now known as togaviruses, bunyaviruses, rhabdoviruses). In the early 1950s, the first groupings of viruses classified on the basis of common physicochemical properties emerged – the myxovirus group (Andrewes et al., 1955), the poxvirus group (Fenner and Barnet, 1957) and the herpesvirus group (Andrewes, 1954). From the same time, the early 1950s, there was also an explosion in the discovery of new viruses of humans and animals. Several individuals and committees, prompted by this rapidly growing mass of data, advanced their own classification schemes. The resulting confusion was only resolved when, in 1966, the International Committee on Nomenclature of Viruses (ICNV)*

*The International Committee on Nomenclature of Viruses (ICNV) became the International Committee on Taxonomy of Viruses (ICTV) in 1973.

was established (Matthews, 1983). At that time there was already a sense among virologists that a single, universal taxonomic scheme should be constructed. Lwoff, Horne and Tournier (1962) developed a system of virus taxonomy based on hierarchical divisions of nucleic acid type, strategy of replication, capsid symmetry, presence or absence of an envelope, and additional capsid structural details. This scheme became the basis of the universal system which has been built upon ever since (Wildy, 1971). In this system, as many virion characteristics as possible are considered and weighed as criteria for making divisions. The relative order and weight of each characteristic is in fact set arbitrarily, and is influenced by prejudgement of relationships that 'we would like to believe but are unable to prove' (Fenner, 1974). The system does not involve any hierarchical levels higher than families and does not imply any phylogenetic relationships beond those proven experimentally (e.g., by nucleic acid hybridization, nucleotide sequencing, gene reassortment, and recombination experiments). The system is pragmatic – it is useful and is being used, and it has replaced all competing schemes for all viruses. It removes ambiguity for student, teacher and researcher alike, and it brings precision to the virus research literature (Wildy, 1971).

5.2. The ICTV universal system of virus taxonomy

The present universal system for virus taxonomy is set arbitrarily at the hierarchical levels of family, genus and species. Lower hierarchical levels, such as subspecies or strain or variant, etc., are established and used by international specialty groups and by culture collections, but at present are not regulated by ICTV.

The most important criteria for classification of viruses are: morphology (shape, size, ultrastructure), and physical and chemical nature of viral components (type of nucleic acid, structure of genome, mode of replication, spectrum of structural proteins, presence of lipids). Such stable properties delineate first of all virus families; certain deviations then form the basis of genera.

A. Virus families are designated by terms ending in *-viridae*. Despite the arbitrariness of early criteria for creating families, this level in the hierarchy of taxa now seems soundly based and stable. Families represent clusters of genera of viruses with apparently common evolutionary origin; for example, it seems unlikely that the very many similar structural and replicative characteristics of all the many diverse poxviruses could stem from more than one common ancestor. Where new data disprove the sense of common ancestry of viruses now placed in the same family, there will probably be further divisions into more families.

B. Virus genera are designated by terms ending in *-virus*. This level in the hierarchy of taxa also seems soundly based, useful, and even more clearly descended from a common evolutionary origin. The criteria used to designate genera differ between families, and as more viruses are discovered there will be continuing

pressures to use more specific physicochemical or serological differences to create new genera in many families.

C. Virus species have not yet been designated formally (the experimental usage in the family *Adenoviridae* has now been abandoned by the ICTV decision in 1984). It is clear that this level in the hierarchy of taxa will come to be regarded as equivalent to the present vernacular usage of the term *virus*. That is, Sindbis virus, mumps virus and polio 1 virus meet all the definitions of the term *virus* and will most likely be designated as *species*. Problems come in properly defining the term *species* so that it can be used unambiguously and pragmatically in all virus families. Likewise, there are major problems in deciding on a nomenclature for species (Matthews, 1983, 1985). These problems should be overcome in the next few years, but, in the meantime, ICTV lists species under the heading 'English Vernacular Name' and leaves blank the heading 'International Name' (Matthews, 1982). Therefore the usage of 'species' throughout this book is to be regarded as provisional exept in cases of type species.

D. Unambiguous virus identification is one derivative value of the universal taxonomy system. For example, the system has had a major influence on the reduction of synonyms, even in vernacular usage. Despite the incompleteness of the system, it will soon be expected by journal editors (and others who are in a position to require unambiguous virus identification) that, somewhere in each publication, each virus be identified by family, genus, species terms – perhaps in combination with precise strain designation terms as developed by international specialty groups and by organizations with culture collections (e.g., *Picornaviridae, Enterovirus polio 1 [Strain: Brunhilde. ATCC VR 58.]* (Matthews, 1983). The key reference for virus taxonomy and nomenclature will continue to be the most current *Report of the International Committee on Taxonomy of Viruses – The Classification and Nomenclature of Viruses* (Matthews, 1982).

E. Virus characteristics used for building taxa vary from simple to complex, from rational to historical. Characteristics relating to nucleic acid, protein composition and strategy of replication may eventually predominate as classification criteria, but in practice today there is more dependence on easily discernible characteristics. For example, the methods for characterizing nucleic acids include base ratio determination, oligonucleotide mapping, restriction enzyme mapping, hybridization, determination of repeated and inverted sequences, heteroduplex mapping, base sequence analysis. These methods have not lent themselves to characterization of very large numbers of viruses, and where taxonomic divisions have been built on some of these criteria (e.g., in the family *Herpesviridae*) progress has been slow. To date, properties used most often in classification derive from electron microscopic examination of virions and infected cells (virion morphology, structure and dimensions, mode and site of morphogenesis, presence or absence of an envelope, etc.). Thus, in most cases viruses may be placed in their appropriate family and genus after being visualized and measured by negative-contrast and/or

TABLE 5.1.
Families containing human and animal viruses

Dividing characteristics	Virus families
ds DNA, enveloped	Poxviridae
	Iridoviridae
	Herpesviridae
ds DNA, nonenveloped	Adenoviridae
	Papovaviridae
	Hepadnaviridae
ss DNA, nonenveloped	Parvoviridae
ds RNA, nonenveloped	Reoviridae
	Birnaviridae
ss RNA, enveloped	
No DNA step in replication	
positive-sense genome	Togaviridae
	Flaviviridae
	Coronaviridae
negative-sense genome	
nonsegmented genome	Paramyxoviridae
	Rhabdoviridae
	[Filoviridae][a]
segmented genome	Orthomyxoviridae
	Bunyaviridae
	Arenaviridae
DNA step in replication	Retroviridae
ss RNA, nonenveloped	Picornaviridae
	Caliciviridae

[a]Brackets are used throughout this chapter to identify taxa and names that have not yet been approved by ICTV. Names included in brackets may or may not become official names.

Abbreviations and terms: ds = double-stranded; ss = single-stranded; enveloped = possessing an outer lipid-containing bilayer partly derived from host cell membrane; positive-sense genome = for RNA viruses, genomes that are composed of nucleotide sequences that are directly translated on ribosomes, = for DNA viruses, genomes that are composed of nucleotide sequences that are the same as the mRNA; negative-sense genome = genomes that are composed of nucleotide sequences complementary to the positive-sense strand.

thin-section electron microscopy (Murphy, 1973, 1983). In conventional classification efforts, electron microscopy is complemented by serology and measurements of virion stability (varying pH, lipid solvents, varying temperature, etc.). Such are the methods available in most virus laboratories throughout the world. Identification and taxonomic placement of a virus by these conventional means represents

more a repeat of historical steps in virus identification than a rational sequential identification protocol. The conventional scheme works because, after large numbers of virion characteristics have been used to develop taxa, few characteristics are generally necessary to allocate additional viruses to their proper niche. The exception comes when a virus does not fit and becomes a candidate for a new genus or a new family. In such a case, a comprehensive characterization, including nucleic acid and protein composition studies, replication strategy studies and structural studies, is called for.

F. Families containing the viruses of humans and animals. Of the more than 60 families of viruses recognized by the ICTV, 20 contain viruses of humans and animals. In addition, one more family has been proposed, but not yet approved. The listing of the families containing human and animal viruses in Table 5.1 is in the order now used by the ICTV. The order is set by nucleic acid type, presence or absence of envelope, genome replication strategy, positive or negative sense genome, and genome segmentation.

References

Andrewes, C.H. (1954) Nomenclature of viruses. Nature (London) 173, 260–261.

Andrewes, C.H., Bang, F.B. and Burnet, F.M. (1955) A short description of the Myxovirus group (influenza and related viruses). Virology 1, 176–180.

Fenner, F. (1974) The classification of viruses; why, when and how. Aust. J. Exp. Biol. Med. Sci. 52, 223–231.

Fenner, F. and Burnet, F.M. (1957) A short description of the Poxvirus group (vaccinia and related viruses). Virology 4, 305–310.

Lwoff, A., Horne, R. and Tournier, P. (1962) A system of viruses. Cold Spring Harbour Symp. Quant. Biol. 27, 51–55.

Matthews, R.E.F. (1982) Classification and nomenclature of viruses (Fourth Report of the ICTV). Intervirology 17, 1–199.

Matthews, R.E.F. editor (1983) A Critical Appraisal of Viral Taxonomy. CRC Press Inc., Boca Raton, FL.

Matthews, R.E.F. (1985) Viral taxonomy for the non virologist. Annu. Rev. Microbiol. 39, 451–474.

Melnick, J.L., Allison, A.C., Butel, J.S., Eckhart, E., Eddy, B.E., Kit, S., Levine, A.J., Miles, J.A.R., Pagano, J.S., Sachs, L. and Vonka, V. (1974) Papovaviridae. Intervirology 3, 106–120.

Murphy, F.A. (1973) Taxonomy of vertebrate viruses. In Handbook of Microbiology, 2nd Edn; Eds. A.I. Laskin and H.A. Lechevalier, pp. 623–637. CRC Press Inc., West Palm Beach, FL.

Murphy, F.A. (1983) Current problems in vertebrate virus taxonomy. In A Critical Appraisal of Viral Taxonomy, Ed. R.E.F. Matthews, Ch. 2. CRC Press Inc., Boca Raton, FL.

Waterson, A.P. and Wilkinson, L. (1978) An Introduction to the History of Virology. Cambridge University Press, London.

Wildy, P. (1971) Classification and nomenclature of viruses (First Report of the ICTV). Monogr. Virol. 5, 181.

This Page Intentionally Left Blank

PART IV

RNA-containing virus families

This Page Intentionally Left Blank

Nermut/Steven (eds) Animal Virus Structure

CHAPTER 6

Picornaviridae

P.MINOR

National Institute for Biological Standards and Control, Blanche Lane, South Mimms, Potters Bar, Herts EN6 3QG, U.K.

Family: Picornaviridae
Genera: enterovirus, cardiovirus, rhinovirus, aphthovirus

6.1. General characteristics

Picornaviruses are small non-enveloped viruses with an icosahedral shell enclosing an RNA genome. They replicate in the cytoplasm of infected cells, and cause a variety of diseases of man and animals, involving a range of specific target organs and tissues depending on the particular virus. No vectors are known.

Picornaviruses can be broadly classified into four categories: the enteroviruses (encompassing polioviruses, coxsackie viruses, echoviruses, numbered enteroviruses and possibly hepatitis A virus), the aphthoviruses of foot-and-mouth disease viruses, the rhinoviruses and the cardioviruses (including mengovirus and encephalomyocarditis virus).

The biophysical and molecular biological properties of all picornaviruses are broadly similar, but the categories differ in details such as the stability of the virion to various treatments, and certain features of the molecular organization of the genomes.

Recently the X-ray crystallographic structure of a rhinovirus has been reported, as has that of a poliovirus, and it is likely that by the time of going to press the structure of a cardiovirus (mengovirus) will also have been resolved and that of foot-and-mouth disease virus will be the subject of study. Detailed structural information is thus rapidly becoming available on the picornaviridae.

6.2. Enteroviruses: species poliovirus

6.2.1. Chemical and physical characteristics

The virus particle has a mass of approximately 8×10^6 daltons, of which the RNA genome contributes 2.6×10^6 daltons (32%). The virion contains no lipid or carbohydrate. The capsid is composed of sixty copies each of four non-glycosylated proteins of approximate molecular masses 30 000, 27 000, 24 000 and 7000 daltons designated VP1, VP2, VP3 and VP4 respectively. VP2 and VP4 are formed as the virus matures by cleavage of precursor protein VP0 and it is possible that the virus also contains one to two copies of uncleaved VP0 per virion, although this has been difficult to demonstrate or disprove.

The single-stranded RNA is of messenger sense with a sedimentation coefficient of 35 S and like many eukaryotic messenger RNAs terminates at the 3′ end in a sequence of 40 to 100 adenosine residues. A small virus-coded protein designated VPg (M_r 2500 daltons) is covalently linked to the 5′ terminus via a tyrosine-uridine linkage. Excluding the polyadenylate tract, the genome of poliovirus contains approximately 7430 bases. Complete or partial genome sequences are now known for several polioviruses and enteroviruses, including enterovirus 70 and coxsackie B3 virus. The organization of the genome is shown in Fig. 6.1 for poliovirus.

The sedimentation coefficient of the intact infectious virus is 155–160 S and the buoyant density of the enteroviruses in caesium chloride is 1.34 g/cm^3. In contrast to rhinoviruses and aphthoviruses, the enteroviruses are acid-stable. This formed the basis of earlier classifications of the picornaviridae.

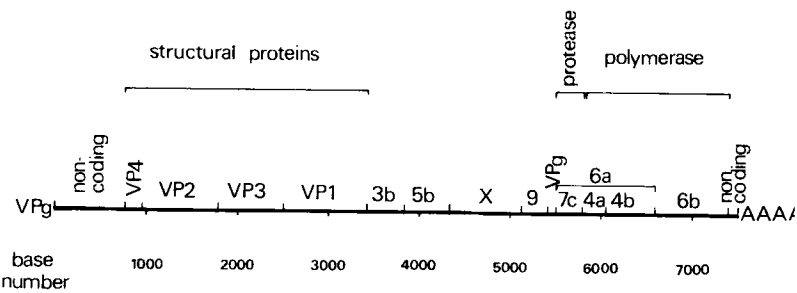

Fig. 6.1. Organization of the genome of a typical picornavirus (poliovirus) showing the 5′ genome-linked protein VPG, the 3′ polyadenylate and the positions of the various known virus-coded proteins. Note that the structural proteins are coded by the 5′ portion of the genome, and the polymerase, proteins and VPg non-structural proteins by the 3′ portion of the genome. The central portion codes for viral proteins of unknown function.

6.2.2. Structural characteristics

The virions of poliovirus and picornaviruses in general are 25–30 nm in diameter and appear approximately spherical (Fig. 6.2A), but high concentrations of virus can form hexagonal arrays (Fig. 6.2B) and individual particles can also appear hexagonal (Fig. 6.2C). Shadowing techniques produce shadows which are either blunt-ended (Fig. 6.2D) or pointed (Fig. 6.2E), consistent with an icosahedral particle. The particle is believed to be composed of capsomers 60–64 Å in diameter and to have a triangulation number $T=1$.

The outer shell or capsid of the virus can be seen when the viral RNA is positively stained with uranyl acetate after drying of the virus from ethanol; the capsid remains negatively stained in these specimens and is approximately 2.5 nm in thickness (Fig. 6.2F). Empty capsids, which, in contrast to the mature infectious virus, are penetrated by negative stains, also demonstrate a similar thickness of the capsid (Fig. 6.2G). The empty capsids often show incomplete contents in the form of small areas which are not penetrated by negative stain (Fig. 6.2H). The fully formed particles also show further details of the capsid when they become enlarged during drying and begin to allow entry of negative stain (Fig. 6.2I). The capsid becomes broken into portions (Fig. 6.2J) which usually appear circular or crescent-like (Fig. 6.2K and L). Destruction of the infectious virus by heating also results in aggregates of approximately twelve crescent-like (Fig. 6.2M and N) or circular (Fig. 6.2O) structures which presumably correspond to pentamers at each of the twelve vertices of the icosahedral capsid.

Architecture of the virion

The virus consists of a shell of 60 capsomers consisting of one copy each of VP1, VP2, VP3 and VP4. The shell surrounds the genomic RNA, and there is no evidence for a core structure. The term 'nucleocapsid' therefore applies to the whole virion. The small size of the essentially featureless virion has made examination by electron microscopy relatively uninformative (Fig. 6.2).

Surface labelling studies

Surface labelling of virions by various biochemical methods implies that VP1 is the most prominently exposed of the capsid proteins, followed by VP3 and VP2, while VP4 is completely inaccessible. In contrast, all proteins of empty capsids are equally exposed.

6.2.3. Antigenic properties of the virus

The antigenic characteristics of the virion, empty capsids, subcomponents and isolated capsid proteins differ. Thus poliovirus virions express a major antigen (D antigen) not found on empty capsids, and conversely empty capsids express a

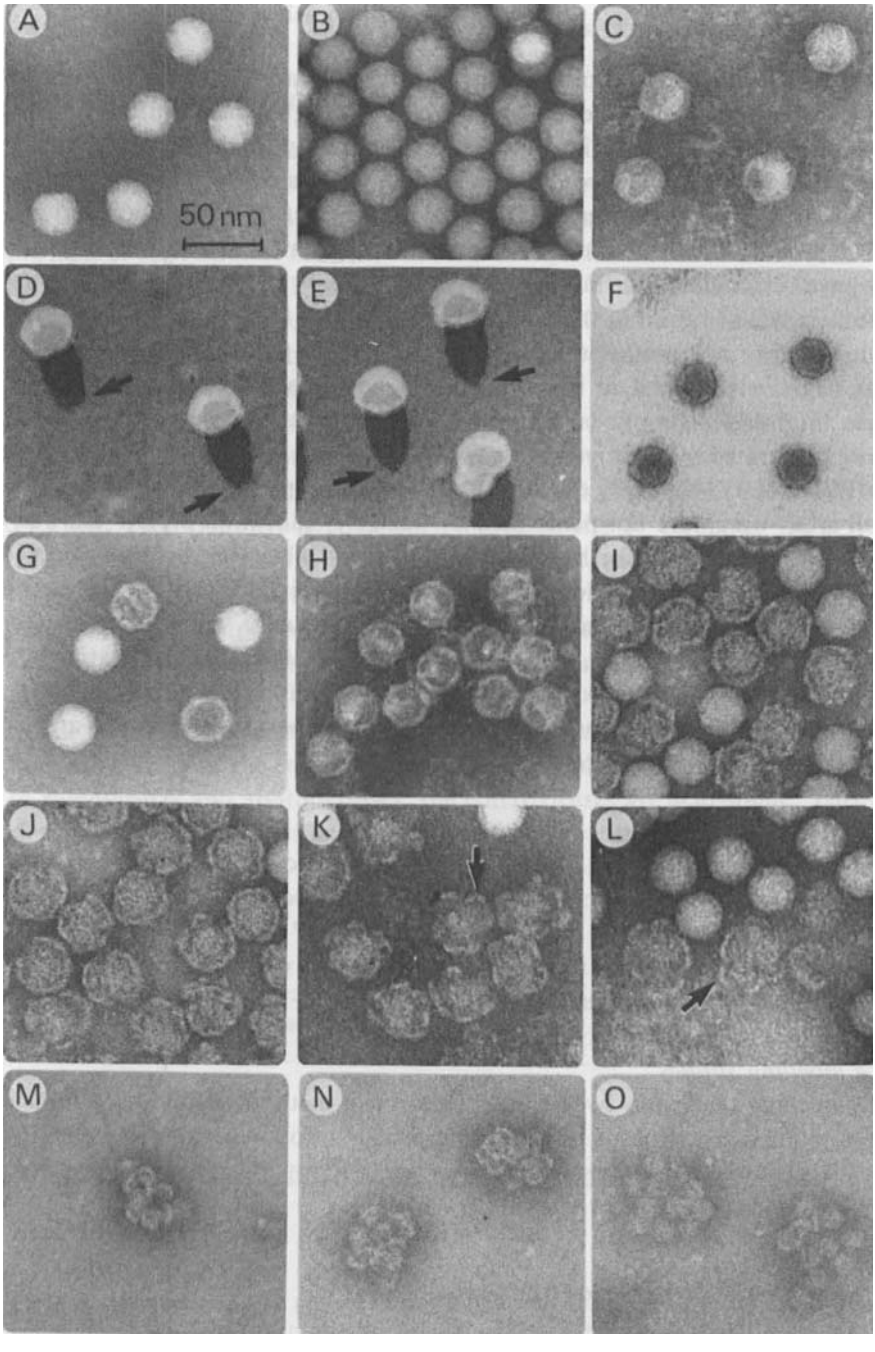
A
50 nm
B
C
D
E
F
G
H
I
J
K
L
M
N
O

major antigen (C antigen) not found on the virion. There is also evidence for common antigens between virions and empty capsids, in that some monoclonal antibodies will react with both.

Heating virions at 56°C converts the D antigen to C antigen with the concomitant loss of VP4. However, as VP4 is an internal protein of the virion it is likely that the antigenic differences between the particles are due to major conformational differences in proteins found in both types of particle. It has proved difficult to raise antisera which are exclusively C-specific or D-specific by immunizing animals with highly purified preparations of particles expressing C or D antigen.

Significant levels of neutralizing antibody are far more difficult to raise with isolated capsid proteins than with intact virions. It is generally held that VP1 is the most effective in this respect, although neutralizing antibody responses to both VP2 and VP3 have been reported.

Three serotypes of poliovirus are known and monoclonal antibodies have been raised to representative strains of each type. Mutants which are resistant to neutralization by such antibodies have been isolated and characterized from type 1 and type 3. For type 1 there is evidence for concentrations of mutations affecting neutralization in VP3 (which is 238 amino acids in length) in amino acids 58–60 and 71 and 73, and in VP1 (303 amino acids) at positions 220–222, amino acids being numbered from the N terminus of the protein. For type 3 the mutations are strongly concentrated in a region of VP1 89–100 amino acids from the N-terminus, or in a region 285–287 amino acids from the N-terminus of VP1, which consists of a total of 300 amino acids. The difference between the two serotypes is striking in view of the great similarity between them in other respects. It has been established by X-ray crystallographic methods that the sequences in which mutations are concentrated represent the sites to which antibodies bind rather than regions of the virus distant from the antibody attachment site, having a crucial importance in capsid structure. Synthetic peptides representing segments of the capsid proteins have been used in attempts to raise neutralizing antibodies with varying degrees of success.

Fig. 6.2. Electron micrographs of poliovirus. All specimens, except D, E and F, negatively stained with 4% sodium silicotungstate, × 200 000. A, Whole virus particles (D antigen), approximately 30 nm in diameter. B, High concentrations of virus in hexagonal array. C, Virus particles displaying hexagonal profiles. D and E, Shadowed virus (prints reversed to give black shadows) produces blunt-ended (D) or pointed (E) shadows consistent with an icosahedral particle. F, Viruses stained with uranyl acetate, after drying from ethanol; the central RNA is positively stained but the capsid remains negatively stained. G, Negative staining of full particles and empty particles which are penetrated by stain and show the capsid. H, Empty particles (C antigen) showing small central unstained portions consistent with incomplete contents. I and J, Particles which have flattened and begun to disintegrate during drying and are thus penetrated by stain. K and L, The capsid separates into angular or crecent-like portions as the particles disintegrate. M, N and O, Virus heated at 56°C for 2 min, producing aggregates of approximately 12 crescent-like or circular structures.

6.2.4. Summary of structure

The X-ray crystallographic structure of poliovirus type 1, strain Mahoney, is presented in Fig. 6.3 as a stereo pair of a sectioned (Fig. 6.3a) or intact (Fig. 6.3b) particle. The protomers are arranged with icosahedreal symmetry as a capsid about the naked RNA.

The location and tertiary structure of VP4 suggest that it is best regarded as an N-terminal extension of VP2. The other capsid proteins, VP1, VP2 and VP3, have tertiary structures which are very similar to each other and to the protein subunits

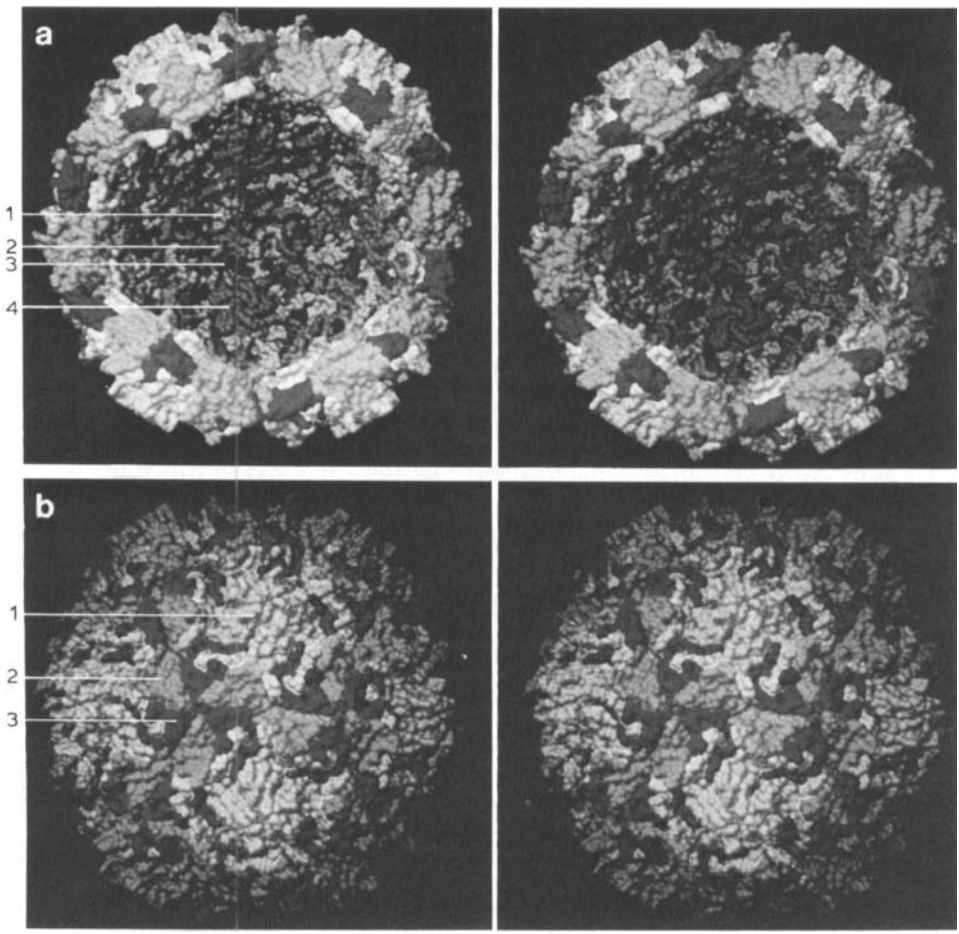

Fig. 6.3. Stereopair of poliovirus type 1 strain Mahoney. Sequences of VP1 (1), VP2 (2), VP3 (3) and VP4 (4) are shown. (a) Shell after removal of four pentamers to show the interior surface; (b) exterior surface. Reprinted from Hogle, J., Chow, M. and Filman, D.J. (1985) Science 229, 1358–1365. Copyright 1985 by the AAS.

of the spherical viruses of plants, consisting of a wedge-shaped core structure composed of eight strands arranged in an antiparallel beta array which forms a barrel (the beta barrel). This basic structure contains internal and C- and N-terminal elaborations depending on the protein, and these elaborations contain the major neutralizing antigenic sites, among other features. The N termini of VP1 and VP2 are not detectable, but lie within the virion.

The pointed end of the beta barrel of VP1 is located near the icosahedral apex close to the five-fold axis of symmetry, while the corresponding portions of VP2 and VP3 alternate about the trianglular icosahedral face and the three-fold axis of symmetry. The N-terminal portion of VP3 interacts strongly with the VP1 barrel on the inner surface of the virion, while the N-terminal portion of VP1 interacts with the VP3 barrel.

The protein shell is approximately 3 nm thick, extending from 11 to 14 nm from the particle centre; however, there is a peak extending to 16.5 nm at the five-fold axis of symmetry formed by residues from VP1, and a plateau rising to 15.0 nm on the icosahedral face about the three-fold axis of symmetry. These two elevated features are separated by a cleft (or canyon) which, it has been suggested, may include the site on the virus which attaches to the cell. The N termini of VP1, VP2, VP3 and VP4 form an extensive network linking adjacent capsomers into pentamers, so that the basic unit of construction of the capsid appears to be a pentamer of VP1, VP2, VP3 and VP4.

6.3. Enterovirus: species hepatitis A virus

Hepatitis A virus is responsible for infectious hepatitis of man, and can be isolated from stools of infected individuals. The virus is a small isometric particle 27–28 nm in diameter, not penetrated by electron microscopic stains, with a buoyant density of 1.32–1.33 g/cm^3 in caesium chloride. Virions sediment at 154–158 S and contain a single-stranded RNA molecule with a sedimentation coefficient of 33 S, and a molecular mass of 2.8×10^6 daltons (8000 nucleotides = 2.72 μm long). The virion capsid is known to contain proteins with molecular weights of 31 000, 26 000 and 21 000, approximately corresponding in size to VP1, VP2 and VP3 poliovirus. A fourth protein corresponding in size to VP4 (M_r = 8000–14 000) has been reported, but recent sequencing studies of the genomic RNA of the virus raise the possibility that this is not virus-coded, and that no virion polypeptide equivalent to VP4 type has been reported.

Hepatitis A virus is a picornavirus in all other properties reviewed above. So far only a single antigenic serotype has been identified.

6.4. Aphthoviruses: species foot-and-mouth disease virus

The aphthoviruses have many of the properties of the enteroviruses as well as certain distinct features of their own. The sequence of the RNA genome of foot-and-mouth disease virus is known in part. The total genome consists of approximately 8300 nucleotides and a 3′ sequence of 40–100 adenylate residues. In contrast to the enteroviruses, the genome has an internal tract of 50–150 cytidylate residues, the precise length of which depends on the strain, and there is a leader sequence of some 1200 bases including an open reading frame before the major open reading frame. The genome also codes for multiple copies of the small genome linked protein VPg.

The virion has a sedimentation coefficient of 146 S and a buoyant density in caesium chloride of 1.43 g/cm^3. A particle with the protein:RNA composition of picornavirus would be expected to have a buoyant density in caesium chloride of 1.47 g/cm^3 if freely permeable to caesium ions. The densities of the enteroviruses and cardioviruses (see below) therefore imply a capsid impermeable to caesium ions, while the capsid of foot and mouth virus is almost freely permeable. Rhinoviruses have an intermediate buoyant density (see below). These findings indicate significant differences in the capsid structures of the different picornaviruses.

Empty capsids sediment at 70 S, and the virions dissociate below pH 7 into units with a sedimentation coefficient of 12 S, which are believed to be trimers consisting of three copies each of VP1, VP2 and VP3. The 12 S, 70 S and 146 S species have different antigenic characteristics.

Trypsinization of the virion cleaves VP1, and simultaneously greatly reduces both infectivity and the ability to induce neutralizing antibody. Isolated VP1 of foot-and-mouth disease virus is a far more effective inducer of neutralizing antibody in animals than isolated VP1 of poliovirus, and synthetic peptides corresponding to amino acids 141–160 and 200–213 from the N terminus of VP1 have been shown to be highly effective in inducing neutralizing antibody. For the strain studied (O. Kaufbeuren) VP1 consists of 213 amino acids. There are seven recognized serotypes of foot-and-mouth disease virus, but different strains within a serotype do not necessarily confer cross-immunity, so that the distinction between type and subtype is sometimes rather artificial.

6.5. Rhinovirus: species HRV 14, HRV 2

There are currently 115 immunologically distinct known human rhinovirus serotypes. The complete sequence of the rhinovirus 14 RNA genome has been published; it consists of 7208 nucleotides, including a 5′ non-coding region of 624 nucleotides and a 3′ non-coding region of 47 nucleotides followed by a se-

quence of adenylate residues. The predicted amino acid sequence of the open reading frame is strikingly homologous to that of poliovirus. A partial sequence of rhinovirus 2 has also been obtained.

At the amino acid level the sequences of the two rhinovirus polymerase genes are only 55% homologous (compared to 97% for the three serotypes of poliovirus), but the homology of the 3′ non-coding region is high. The virions are acid-labile, dissociating below pH 5. They sediment at 160 S, and have a buoyant density of 1.40 g/cm^3 in caesium gradients, due to permeation of the virions (see above).

The structure of rhinovirus 14 was resolved before that of the type 1 poliovirus Mahoney, which has been reviewed above. The structures are very similar, and the details of the rhinovirus structure will therefore not be given here.

6.6. Cardioviruses: species Encephalomyocarditis virus, Mengovirus

The partial sequence of the genomic RNA of encephalomyocarditis virus has been published. The genome is over 7200 nucleotides in length, and like that of the aphthoviruses it contains a leader sequence and an internal polycytidilate tract of 50–150 cytidine residues. The buoyant density of the virion is 1.34 g/cm^3 and it

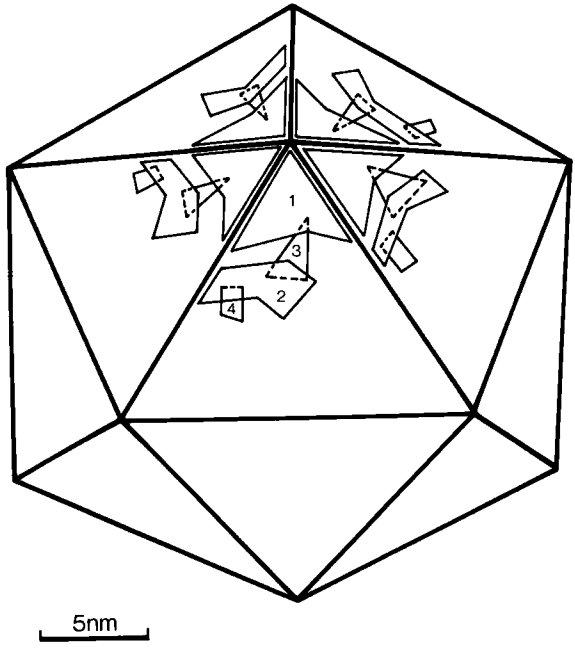

Fig. 6.4. Possible arrangement of the four virion capsid proteins within the capsid, based on studies with Mengovirus.

has a sedimentation coefficient of 160 S. The virion proteins are designated α, β, γ, and ϑ, corresponding to VP1, VP2, VP3 and VP4 of poliovirus respectively.

Chemical cross-linking studies of mengovirus virions led to the conclusion that α and β were closest together within the capsomer, and that the exposed portions of adjacent capsomers made contact chiefly via α. This suggests that the pentameric apices of the icosahedral virion are composed of α molecules. This model is summarized in Fig. 6.4 and is consistent with the structures of both rhinovirus and poliovirus. The resolution of the mengovirus structure is expected soon.

6.7. Virus–cell interactions

Picornaviruses attach to cells via receptors of still unknown structure. Studies of competitive binding between different picornaviruses and the recent derivation of anti-cellular monoclonal antibodies suggest that various distinct specific receptors exist. Thus all three serotypes of poliovirus share a common receptor distinct from other enteroviruses, and rhinoviruses as a group appear to attach to one of two distinct receptor sites on cells, depending on the serotype. The biochemical nature of these receptor sites remains to be established.

Adsorbed virus most probably enters the cell by receptor-mediated endocytosis. After adsorption the virus loses VP4 and undergoes an antigenic change (from D to C for poliovirus). A proportion of the virus is eluted as non-infectious particles (A particles) at this stage in the course of infection of cells in vitro. Similar particles, which consist of a protein shell of VP1, VP2 and VP3 surrounding the intact genomic RNA, may be isolated from cells, and the loss of VP4 and concomitant capsid rearrangement are believed to be the first step in virus uncoating, which can be induced by plasma membrane fractions in vitro. The final uncoating probably occurs in the cytosol after the virus has left the endosome. Synthesis of the viral proteins involves the translation of the genome-sense RNA into a precursor protein which is cleaved as it is synthesized by cellular and viral-coded proteases to give the various functional viral proteins. The coat proteins exist in the cell as a pentameric 14 S structure of the formula $(VP0,VP1,VP3)_5$ and 12 of these pentamers are then assembled by a cell-dependent process to form a procapsid. While assembly can occur in vitro in the absence of cellular components, the structure

---

Fig. 6.5. Electron micrographs of sectioned Vero cells which were infected with the Saukett strain of poliovirus for 6 h. A, Areas of vesicles (arrows) are present in the cytoplasm of infected cells, × 18 000. B, A few virus particles (or precursors) are found between the vesicles (arrows), and in other regions of the cell cytoplasm there are aggregates (a) of particles, × 55 000. C, Aggregated particles are regularly arranged in association with cellular intermediate filaments. A transversely sectioned aggregate (ts) shows hexagonal arrangement of filaments and particles, × 83 000.

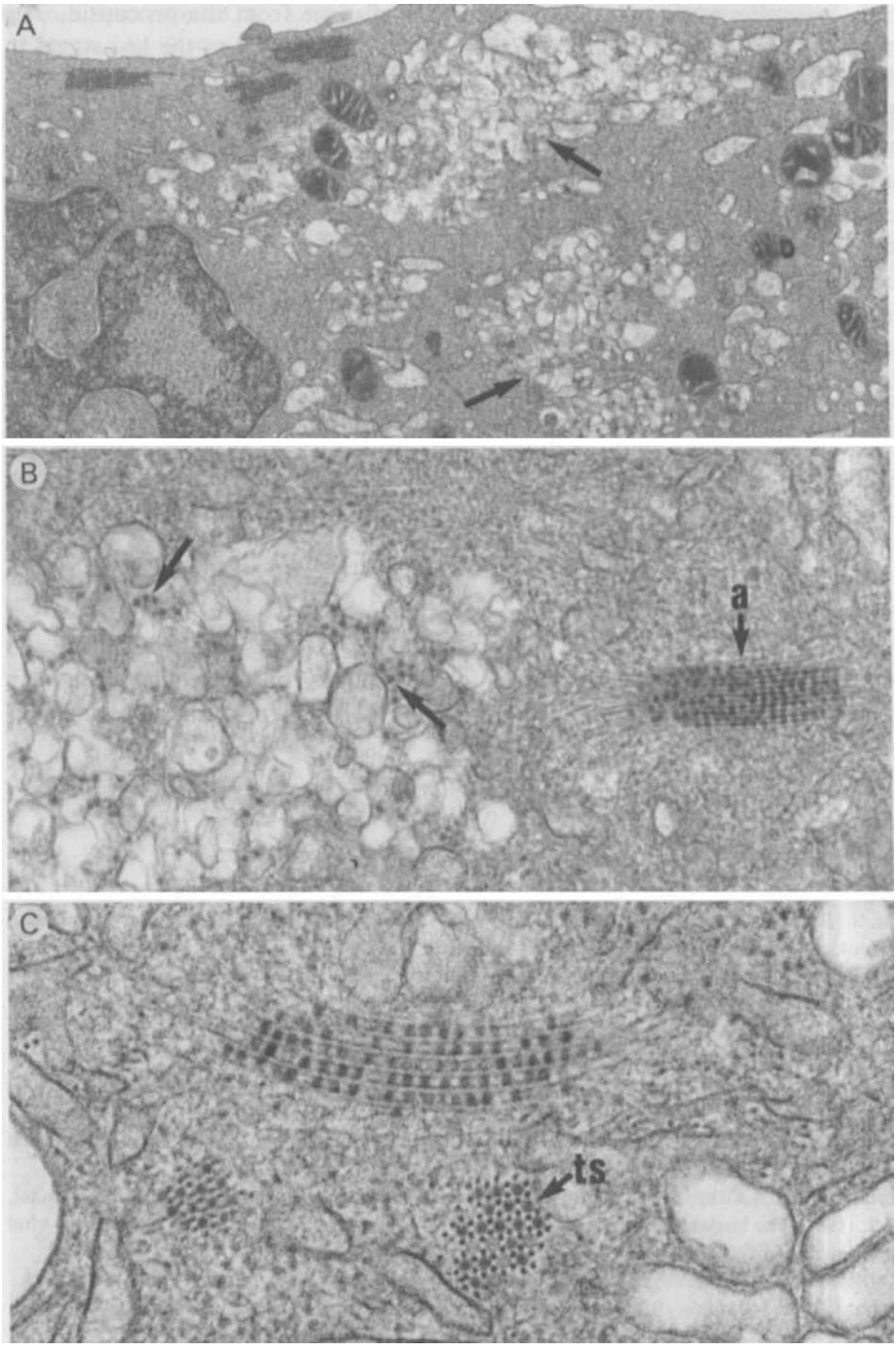
A
B
a
C
ts

formed is conformationally and antigenically distinct from the procapsid. The genomic RNA is inserted and VP0 cleaved to VP2 and VP4 as the last stages in virus maturation.

Electron microscopy of infected cells has shown that the most characteristic feature of the cytopathic effect caused by the virus is the production of membraneous vacuoles in the cytoplasm (Fig. 6.5A and B). Large numbers of vacuoles accumulate in the centre of the cell so that the nucleus typically becomes indented and displaced and the cell becomes swollen and rounded. A few virus particles can usually be found either inside the vacuoles or on their outer surface (Fig. 6.5B) but it has also been observed that the formation of vacuoles correlates temporally with viral RNA synthesis. Poliovirus infection can induce a rearrangement of the cell cytoskeleton, and in Vero and Hep-2 cells dense particles are associated with cellular intermediate filaments (Fig. 6.5C); these particles may be partly or fully formed virus. In HeLa cells the fully formed virus is found as large crystalline aggregates free in the cell cytoplasm. Virus is generally but not always released by cell lysis; there is no evidence for release by budding of the lipid-free virions.

Acknowledgements

I am grateful to Dr. L.M. Stannard for a summary of the available data on hepatitis A virus and to Drs. D.J. Hockley and M.V. Nermut for supplying electron micrographs.

Further reading

Forss, S., Strebel, K., Beck, E. and Schaller, H. (1984) Nucleotide sequence and genome organization of foot and mouth disease virus. Nucleic Acids Res. 12, 6587–6601.

Hogle, J.M., Chow, M. and Filman, D.J. (1985) The three-dimensional structure of poliovirus at 2.9 Å resolution. Science 229, 1358–1365.

Lewintow, L. (1974) The reproduction of picornaviruses. In Comprehensive Virology, Eds. H. Fraenkel-Conrat and R.R. Wagner; pp. Vol. 2, 109–169. Plenum, New York.

Linemeyer, D.L., Menke, J.G., Martin-Gallardo, A., Hughes, J.V., Young, A. and Mitra, S. (1985) Molecular cloning and partial sequencing of hepatitis A viral cDNA. J. Virol. 54, 247–255.

Macnaughton, M.R. (1982) The structure and replication of rhinoviruses. Current Topics Microbial Immunology 97, 1–26.

Palmenberg, A.C., Kirby, E.M., Janda, M.R., Drake, N.L., Duke, G.M., Potratz, K.F. and Collet, M.S. (1984) The nucleotide and deduced amino acid sequences of the encephalomyocarditis viral polyprotein coding region. Nucleic Acids Res. 12, 2969–2985.

Perez Bercoff, R. (Ed.) (1978) The molecular biology of picornaviruses. Plenum Press, New York.

Putnak, J.R. and Phillips, B.A. (1981) Picornaviral structure and assembly. Microbiol. Rev. 45, 287–315.

Rossman, M.G., Arnold, E., Erickson, J.W., Frankenberger, E.A., Griffith, J.P., Hecht, H.J., Johnson, J.E., Kramer, G., Luo, M., Mosser, A.G., Rueckert, R.R., Sherry, G. and Vriend, G. (1985) Structure of a human common cold virus and functional relationship to other picornaviruses. Nature 317, 145–153.

Rueckert, R. (1971) Picornaviral architecture. In Comparative Virology, Eds. K. Maramosch and E. Kurstak, pp. 225–306. Academic Press, New York.

Rueckert, R.R. and Wimmer, E. (1984) Systematic nomenclature of picornavirus proteins. J. Virol. 50, 957–959.

Skern, T., Sommergruber, W., Blaas, D., Gruendler, P., Fraundorfer, F., Pieler, C., Fogy, I. and Kuechler, E. (1985) Human rhinovirus 2: complete nucleotide sequence and proteolytic processing signals on the capsid protein region. Nucleic Acids Res. 13, 2111–2126.

Stanway, G., Hughes, P.J., Mountford, R.C., Minor, P.D. and Almond, J.W. (1984) The complete nucleotide sequence of a common cold virus: human rhinovirus 14. Nucleic Acids Res. 12, 7859–7875.

Toyoda, H., Kotard, M., Kataoka, Y., Suganuma, T., Omata, T., Imuta, N. and Nomoto, A. (1984) Complete nucleotide sequence of all three poliovirus serotype genomes: implementation for genetic relationships, gene function and antigenic determinants. J. Mol. Biol. 174, 561–585.

This Page Intentionally Left Blank

Nermut/Steven (eds) Animal Virus Structure

CHAPTER 7

Caliciviridae

M.J. CARTER and C.R. MADELEY

Department of Virology, University of Newcastle upon Tyne, Newcastle, U.K.

Family: Caliciviridae
Genus: Calicivirus
Species: San Miguel sea lion virus (SMSV), vesicular exanthema of swine virus (VESV), feline calicivirus (FCV)
Other members: human calicivirus (HCV), canine calicivirus, avian calicivirus

7.1. General characteristics

Caliciviruses are non-enveloped, isometric particles 30–40 nm in diameter. They contain an RNA genome of positive sense and replicate in the cytoplasm, causing cell lysis. Host cell requirements may be exacting; for example, human calicivirus (HCV) has been grown only in primary human embryonic kidney cell cultures. Other species are less demanding: SMSV and VESV are probably the same virus which can infect either host and multiply well in different cell lines in vitro. Virus has been spread experimentally by contact, faecal-orally and through contaminated foodstuffs. Lungworms may act as vectors in a fish–marine mammal transmission cycle. Pathogenesis is varied; HCV is associated with gastrointestinal illness, whilst the feline virus causes an oropharyngitis and SMSV/VESV gives rise to skin lesions. The particles have no haemagglutinating activity.

7.2. Chemical and physical characteristics

Calicivirus particles have a mass which has been estimated as $(10\text{–}20) \times 10^6$ daltons, of which 18% is RNA. No lipids or carbohydrates have been detected.

The virion contains only one major structural polypeptide (molecular weight $(60–70) \times 10^3$), but small amounts (less than 2% of the virion mass) of a smaller protein (molecular weight 15×10^3) have been observed. The location in the virion and role of this protein are not known. In addition, caliciviruses contain a protein VpG (molecular weight 10×10^3) one molecule of which is covalently attached to each RNA, which is vital for infectivity.

The RNA is a linear single-stranded molecule of positive sense and 2.8×10^6 in molecular weight. Naked RNA has a sedimentation coefficient of 30–40 S, and intact virions sediment at 160–207 S in sucrose gradients. Buoyant densities are in the range 1.36–1.4 g/cm^3, although this varies in different centrifugation media. Biophysical data for a number of strains are given in Table 7.1.

7.3. Structural characteristics

Shape and size: the appearance of the calicivirus particle is generally highly characteristic. Virions are 30–40 nm in diameter, with an ill-defined edge. Consequently sizes quoted for these viruses are less precise than those for other small cubic viruses.

The surface of the virus particles shows cup-shaped depressions similar to those found on a golf-ball but fewer in number and probably deeper because, in the electron microscope, substantial amounts of stain accummulate in them to give dark patches when seen by negative contrast (Fig. 7.1a). These hollows, from which the family takes its name (Latin, *calyx*, a cup), are located at the apices and faces of an icosahedron with five and six neighbours respectively. On the complete virion there will be 32 hollows but only a minority will be visible on the presenting surface, with the peripheral ones merging with the collar of stain which surrounds the particle.

TABLE 7.1.
Physico-chemical characteristics of caliciviruses

Virus	Diameter (nm)	Sedimentation coefficient of virion (S)	Buoyant density (CsCl)[a]	Capsid protein molecular weight ($\times 10^{-3}$)	RNA	
					Molecular weight ($\times 10^{-6}$)	Sedimentation coefficient (S)
VESV	35–40	160–170[b]	1.36–1.38	71	2.8	37
FCV	30–40	154–170	1.39	68	?	30–32
SMSV	32	180–183	1.37	71	2.8	38

[a]Buoyant density may be altered by centrifugation through different media.
[b]One estimate higher, at 207.

Data compiled from Schaffer et al. (1980) Intervirology 14, 1–6.

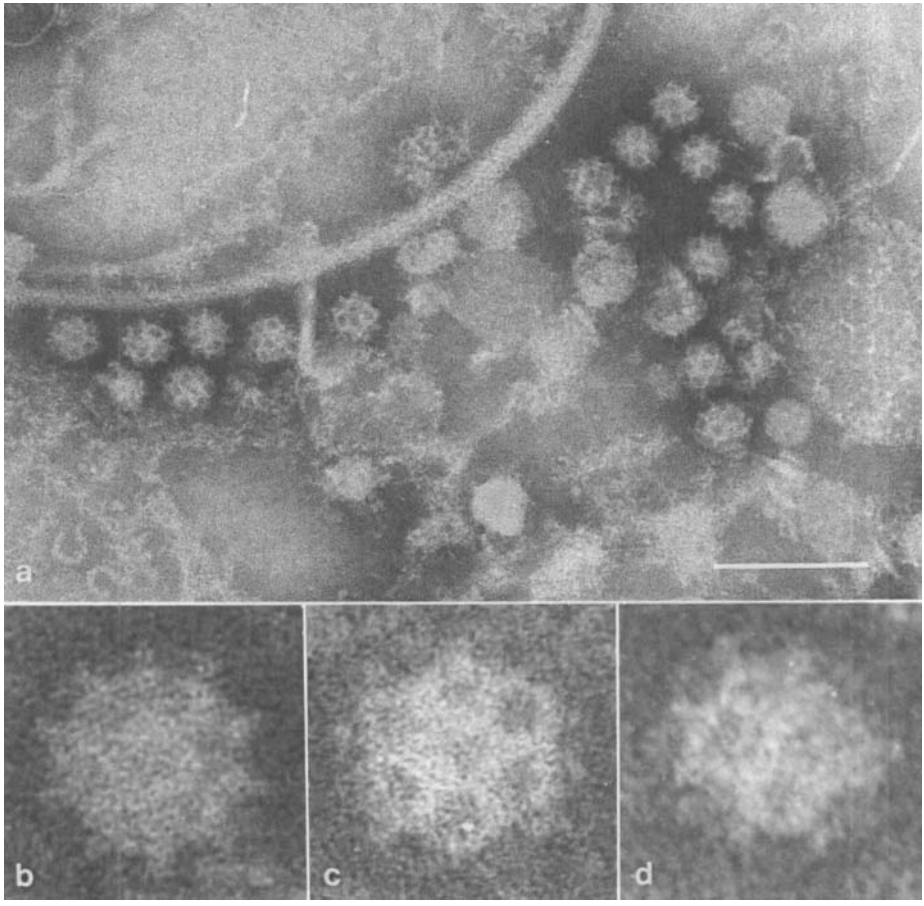

Fig. 7.1. (a) Particles of human calicivirus (HCV) visualized in a stool extract by negative staining (3% potassium phosphotungstate, pH 7), × 200 000. Scale bar = 100 nm. (b–d) Particles at higher magnification (approx. ×900 000) to illustrate the three axes of symmetry: (b) five-fold, (c) three-fold, (d) two-fold.

Nevertheless the patterns of the hollows which can be seen when viewed along the 5-, 3- and 2-fold axes of symmetry are characteristic and allow unequivocal recognition as a calicivirus. They are illustrated in Fig. 7.1b–d and show the following features:

(1) 5-fold axis, a central dark patch surrounded by a lighter ring of virion material which seems to bear a fringe of ten evenly-spaced 'spikes' formed by the tips of the cups seen in profile.
(2) 3-fold axis, a central dark patch surrounded by 6 others. This 'star of David' pattern is unique to this group of viruses.
(3) 2-fold axis, 4 patches in a rhomboid or diamond shape, often separated by a

prominent light area in the shape of an 'H'. These features are well illustrated by both human calicivirus (Fig. 7.1) and VESV (Fig. 7.2).

Markham rotation, applied to the VESV particles and illustrated in Fig. 7.2, reveals the 5 dark patches surrounding the central hollow, although these are not seen in unrotated particles. Rotation, however, confirms that the 'spikes' visible

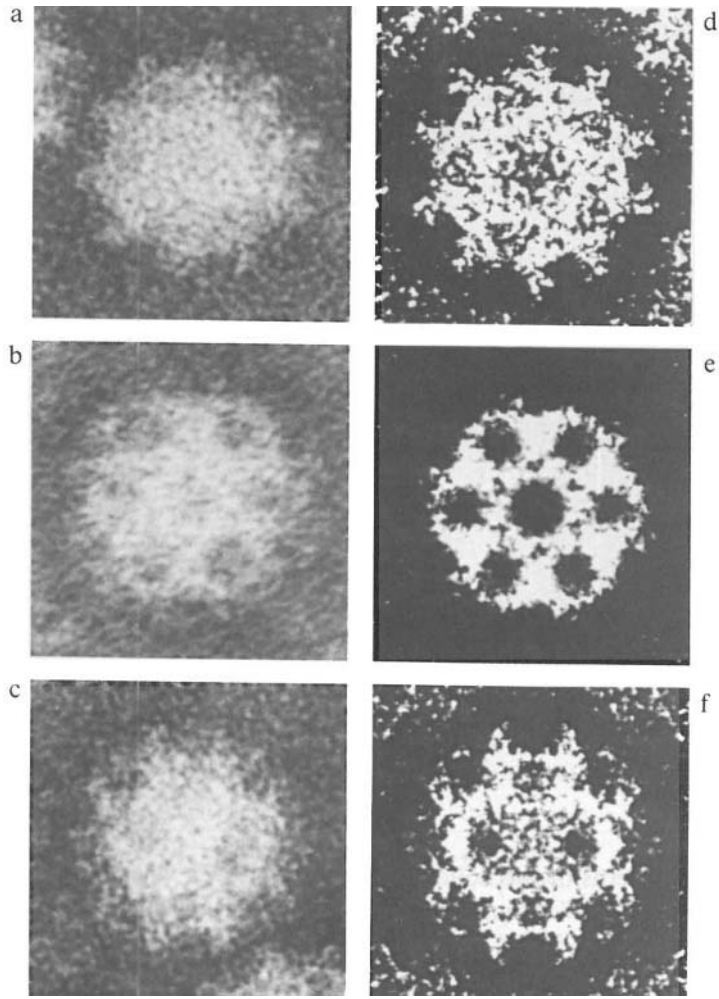

Fig. 7.2. VESV particles grown in Vero cells and demonstrated by negative staining. The particles exhibit morphology very similar to that of the HCV and show an identical pattern when viewed along the three axes of symmetry: (a) five-fold axis, (b) three-fold axis, (c) two-fold axis. These features are accentuated using Markham rotation techniques. (d) Five-fold rotation of the particle illustrated in (a); (e) three-fold rotation of the particle illustrated in (b); (f) two-fold rotation of the particle illustrated in (c). Reproduced with kind permission from Burroughs et al. (1978).

in these samples correspond to the rims of the stain-filled depressions around the periphery of the particle. The outer limit of the virus is thus provided by the ridges between the surface hollows. These are narrow and will not be clearly visible except in profile in negative contrast, and make it difficult to estimate size accurately.

7.4. Architecture of the virus

The fine details of the virus architecture are largely unknown but both VESV and FCV dissociate partially on storage or under acid conditions into small subunits. In the case of VESV these are trimers which sediment at 15 S. Sedimentation of the FCV subunits is similar and there is no reason to suppose that they are not also trimers of the capsid protein.

Models of virus structure

With the evidence (Burroughs et al., 1978) that 180 copies of the capsid protein are incorporated into the structure as 60 trimers, models based on other numbers are likely to be wrong. However, three models assuming 60 subunits have been proposed by Almeida et al. (1968), Peterson and Studdert (1970) and Burroughs et al. (1978). Of these, Almeida and her colleagues offered only a concept of how hollows might be made from 5 or 6 subunits instead of the (then) more expected surface knob or capsomer. They did not propose a complete detailed assembly but the other two papers went further in suggesting spatial arrangements of the 60 subunits. These are not incompatible but obviously are not literally correct as the subunits are not seen individually on the virion. There is, in any case, no reason to expect that the trimer would form something similar in shape to the table-tennis balls used by Burroughs and his colleagues to make their model.

The closest representation of the structure of the virus particle at the electron microscopic level was provided by the foam-rubber model of Almeida et al. and recreated in Fig. 7.3a–f. This model, when coated with barium and X-rayed, gives transmission images which are very similar to those obtained by negative contrast in the electron microscope. This close resemblance confirms the icosahedral symmetry of the virion and rules out other geometric figures.

Burroughs et al. (1978) used 60 table-tennis balls to assemble a model in which each trimeric structural unit was represented. This model (Fig. 7.4) does not produce a close resemblance to electron micrographs when focussed sharply (a–c), but blurring of the image (d–f) by defocussing enhances the similarity, suggesting that the actual shape of each unit is probably wrong but their location is probably right.

Hence both models help our understanding. The table-tennis ball model in-

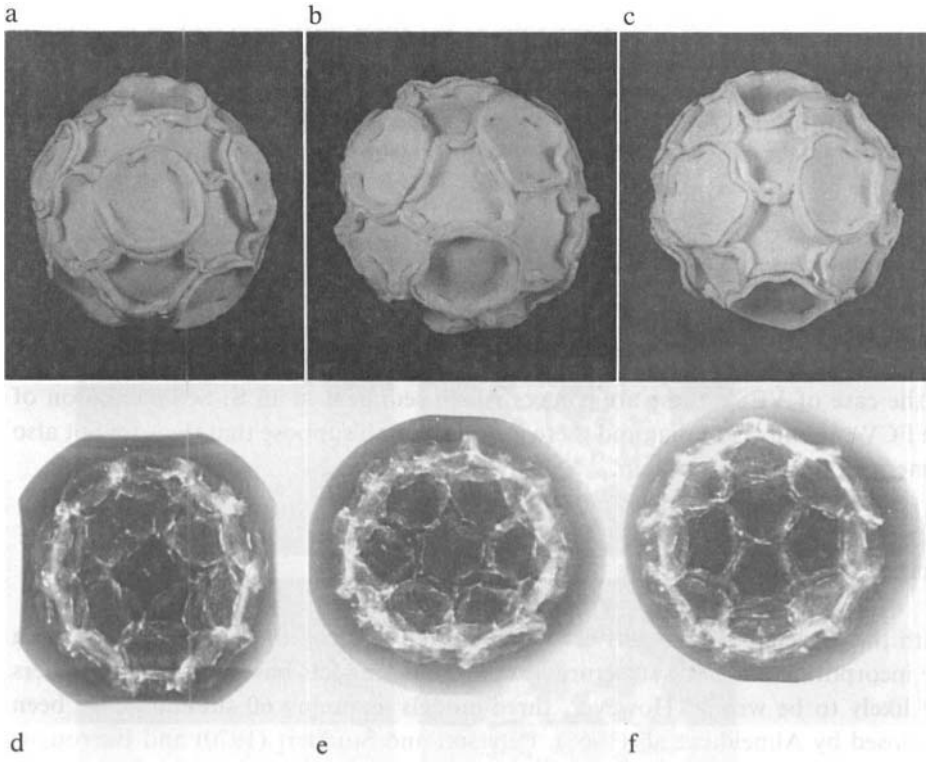

Fig. 7.3. Model of a calicivirus particle composed of 32 units (after Almeida et al., 1968). The model was made by stapling together 32 identical foam-rubber discs. Twelve (darker colour) each had five lighter-coloured discs stapled to them. Each light-coloured one had six neighbours (3 light and 3 dark discs). This gave an envelope of icosahedral symmetry with some distortion of the discs into cup-shaped depressions. The model was then inflated with a balloon, covered in barium sulphate and photographed and X-rayed along the 5-, 3- and 2-fold axes of symmetry. The X-picture was recorded by computer-enhanced transmission radiography. (a–c) Photographs on 5-, 3- and 2-fold axes; (d–f) X-rays along the same axes.

dicates how 60 essentially identical subunits could be arranged on the surface, while the foam rubber one provides a possible outline for their collective envelope. However, neither indicates their trimeric nature nor how and where they make contact with each other. Because each of the table-tennis balls is in contact with three others it would be possible to replace them with another structure of similar dimensions but having three-fold symmetry, such as a triangular prism. Some internal deformation will be required to make a 5-subunit ring but this does not present major difficulties. Computer modelling of the polypeptide chain when it has been sequenced will make it possible to compare theory and reality.

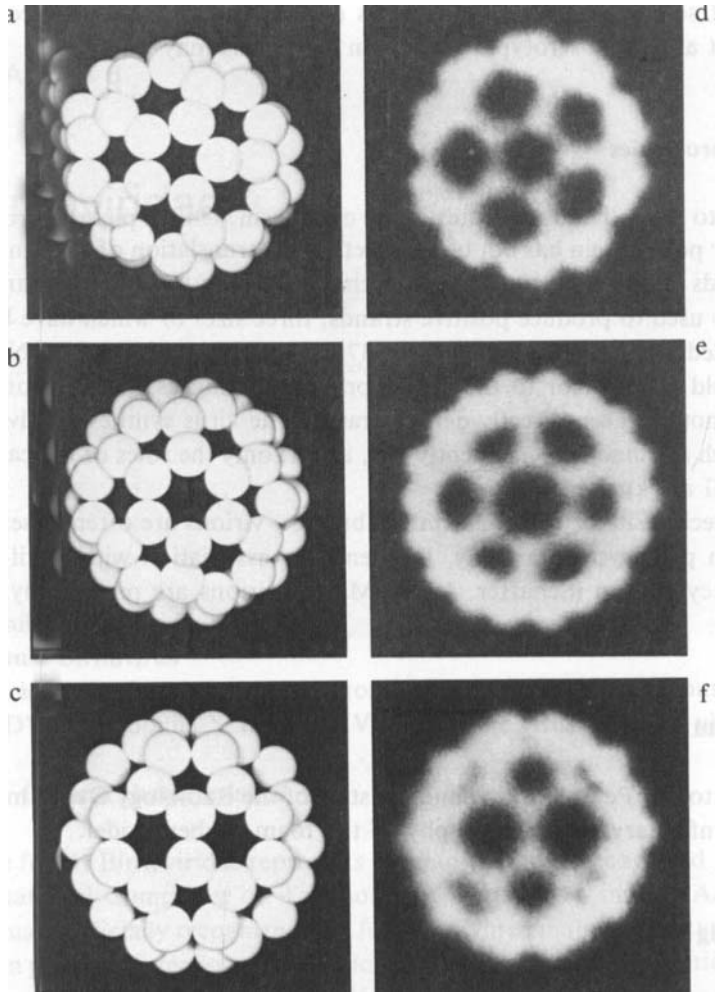

Fig. 7.4. Model of a calicivirus particle constructed from 60 table-tennis balls. The model is viewed along the axes of symmetry: (a) 5-fold, (b) 3-fold, (c) 2-fold: the images produced by defocussing are illustrated in panels (d–f). Reproduced with kind permission from Burroughs et al. (1978).

7.6. Antigenic properties

There are possibly 13 serotypes of VESV, and at least 12 of SMSV. There are probably two epitopes on the VESV capsid protein, of which one is involved in virus neutralization. No monoclonal antibodies have yet been used to dissect the structure further. All strains of feline calicivirus belong to one serotype, although there is some evidence for the existence of subtypes. Other viruses, human, canine and avian, are as yet insufficiently characterized to permit the unambiguous identifica-

tion of different serotypes. However, there is evidence, from immune electron microscopy, that at least 3 serotypes of human calicivirus may exist.

7.7. Biological properties

Virus is taken into the cell and replicates in the cytoplasm. Unlike picornaviruses, a giant precursor polyprotein has not been detected, but translation of the genome presumably yields an RNA polymerase which synthesizes a negative-stranded template. This is used to produce positive strands, three sizes of which have been identified with sedimentation coefficients of 37, 22 and 18 S. The 22 S RNA is translated to yield a precursor to the capsid protein; coding assignments of the other two have not yet been directly demonstrated. The virus synthesizes five or six proteins which are made independently but, as yet, only the roles of the capsid protein and VpG are known.

There is no specific site of virion assembly, but new virions are often observed inside the cell in paracrystalline array, frequently in association with fibril-like elements of the cytoplasm (Schaffer, 1979). Mature virions are released by cell lysis.

Acknowledgement

We are indebted to Dr. Peter Hacking and the staff of the Radiology Department, Royal Victoria Infirmary, for radiography of the foam-rubber model.

Suggested reading

Almeida, J.D., Waterson, A.P., Prydie, J. and Fletcher, E.W.L. (1968) The structure of a feline picornavirus and its relevance to cubic viruses in general. Arch. Ges. Virusforsch. 25, 105–114.

Burroughs, J.N., Doel, T.R., Smale, C.J. and Brown, F. (1978) A model for vesicular exanthema virus, the prototype of the calicivirus group. J. Gen. Virol. 40, 161–174.

Peterson, J.E. and Studdert, M. (1970) Feline picornavirus, structure of the virion and electron microscopic observations on infected cell cultures. Arch. Ges. Virusforsch. 32, 249–260.

Schaffer, F.L. (1979) Caliciviruses. In Comprehensive Virology, Eds. H. Fraenkel-Conrat and R.R. Wagner; Vol. 14, pp. 249–284. Plenum, New York.

Schaffer, F.L., Bachrach, H.L., Brown, F., Gillespie, J.H., Burroughs, J.N., Madin, S.H., Madeley, C.R., Povey, R.C., Scott, F., Smith, A.W. and Studdert, M.J. (1980) Caliciviridae. Intervirology 14, 1–6.

Nermut/Steven (eds) Animal Virus Structure

CHAPTER 8

Birnaviridae

D.C. KELLY

Institute of Virology, Mansfield Road, Oxford OX1 3SR, U.K.

Family: Birnaviridae
Genus: Birnavirus
Species: infectious pancreatic necrosis virus (IPNV), infectious bursitis disease virus (IBDV), Drosophila X virus (DXV), Thirlmere virus (TV), eel virus (Berlin) (EV)

8.1. General characteristics

The family Birnaviridae represents a group of viruses recognized in 1984 by the International Committee on Taxonomy of Viruses as a family. Although only one genus is officially recognized, the following three major virus 'types' are established in practice: infectious pancreatic necrosis virus (IPNV), infectious bursal disease virus (IBDV) and Drosophila X virus (DXV). IPNV infects fish, especially salmonids, and molluscs. IBDV (or Gumboro disease virus) is an important disease of poultry worldwide. Drosophila X virus and Thirlmere virus cause diseases in invertebrates.

Birnaviruses are non-enveloped isometric particles with an icosahedral surface shell (Figs. 8.1 and 8.2) and an RNA-containing 'core'. They replicate and assemble in the cytoplasm.

8.2. Chemical and physical characteristics

Birnaviruses contain a bi-segmented double-stranded RNA genome (hence the name birna) which accounts for 8.7% of the particle weight. There is no report

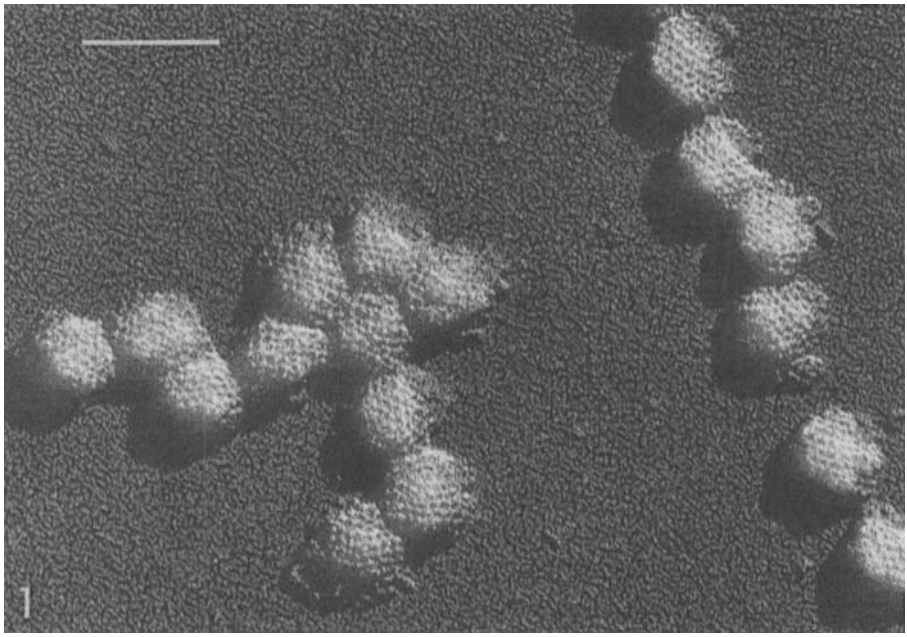

Fig. 8.1. IBDV after freeze-dry shadowing. × 180 000.

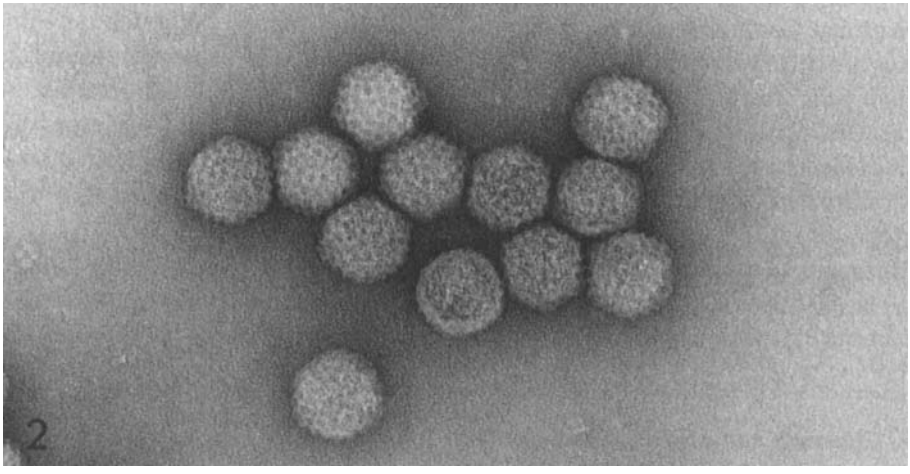

Fig. 8.2. IBDV after negative staining with uranyl acetate. Surface structure is similar to that seen after shadowing. × 180 000. (Figs. 8.2 and 8.3 were kindly supplied by Dr. H. Gelderblom.)

of the presence of glycoproteins, lipids or polyamines in mature virus particles. The total mass of the virus particle is about 55×10^6 daltons. The structural polypeptides are designated VP with an index of their molecular weight and four are recognized - VP 105, VP 54, VP 31 and VP 29.

The genome comprises two linear pieces of double-stranded RNA of molecular weight 2.5×10^6 and 2.3×10^6. Estimates of the sizes differ consistently with different isolates. Preliminary studies suggest that circular molecules may exist with the termini held together by a protein.

The virus contains a dsRNA-dependent RNA polymerase which functions in a dual role as a transcriptase and a replicase.

The virus has a buoyant density of 1.33 g/cm^3 in CsCl and a sedimentation coefficient of 435 S. It is stable between pH 3 and 9, and is insensitive to lipid solvents.

8.3. Structural characteristics

The virion is 60–65 nm in diameter. Tubular and incomplete forms of the virus are often observed (Figs. 8.3 and 8.4).

8.4. Architecture of the virus particle

The single-layered capsid is thought to show icosahedral symmetry with $T = 9$ (92 capsomers) or with a skew class triangulation number $T = 13$ (*dextro* in the

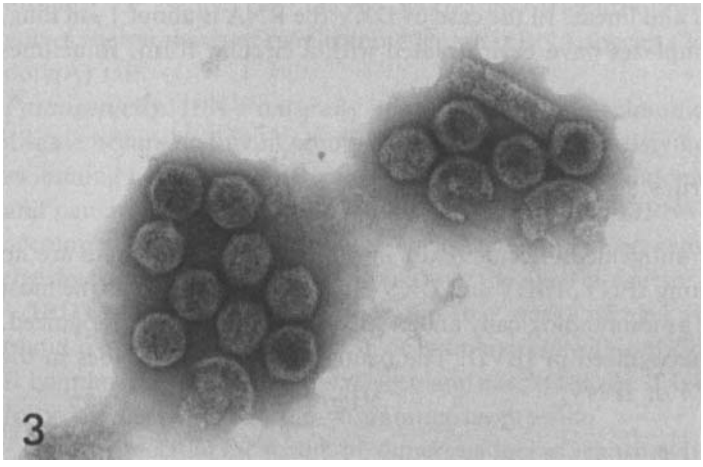

Fig. 8.3. Thirlmere virus particles negatively stained with ammonium molybdate showing the fine structure of the virus particles (Magnification × 100 000).

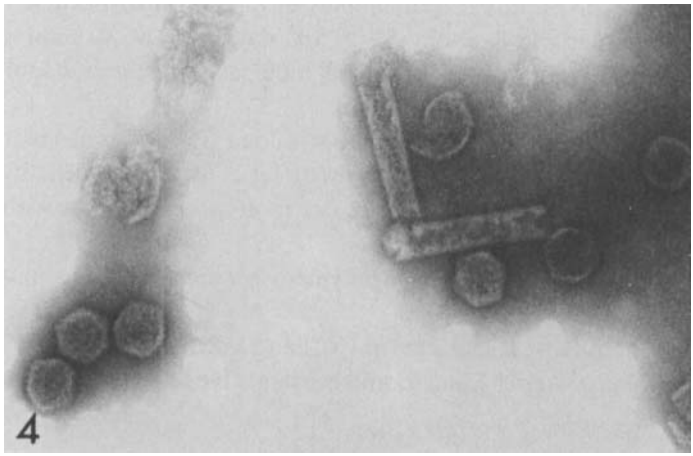

Fig. 8.4. Thirlmere virus particles negatively stained with ammonium molybdate showing tubular structures associated with virus preparations. (Magnification × 100 000).

case of IBDV and EV, *laevo* for IPNV), as recently suggested by Özel and Gelderblom (1985).

No morphologically distinct core has been derived from the virus particle, although in thin section a distinct structure is observed. The virus has a classic icosahedral 5:3:2: symmetry. The single-layered capsid is built up from 180 subunits shared between 92 capsomers in icosahedral forms of the virus. The final detail of the virus structure has yet to be elucidated.

Purified RNA isolated from virus particles is shown in Fig. 8.5 and can be seen to be double-stranded and linear. In the case of DXV the RNA is about 1 μm long, and RNA protein complexes have been isolated with a circular form, sometimes in a rosette form.

8.5. Antigenic properties

A number of distinct antigenic molecules exist in the virus particle. There are no common antigens among IPNV, IBDV and DXV virus particles. IPNV is the most extensively studied virus immunologically and at least 7 serogroups are recognized. Two serogroups are recognized in IBVD. The neutralizing antigen resides in the M_r 54 000 polypeptide of IPNV.

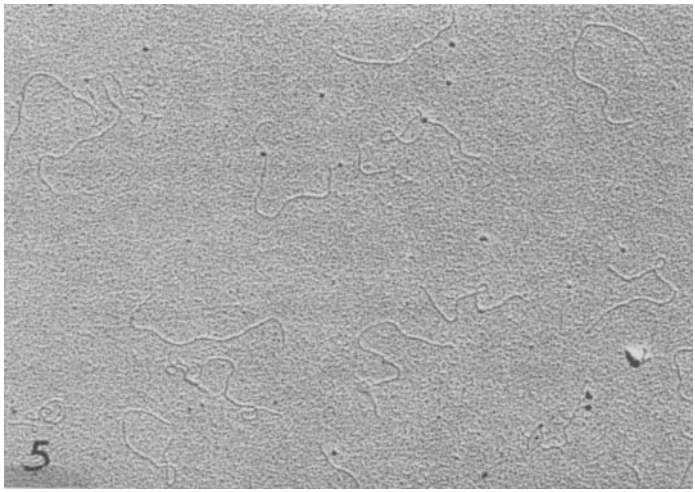

Fig. 8.5. Double-stranded RNA extracted from Thirlmere virus examined by the Kleinschmidt technique and rotary shadowing (magnification × 30 000).

8.6. Biological properties

Virus-cell interactions. The mode of uptake is unknown. Replication occurs within 8 h, and occurs in the cytoplasm. Two non-structural proteins are synthesized in cells - M_r 63 000 (a precursor of the structural VP 54) and M_r 29 000. RNA-dependent RNA polymerase and protease activities are induced in cells. The protease(s) cleave the 63-kDa precursor to VP 54, and cleave some of the 31-kDa to produce VP 29, and degrade the 29-kDa nonstructural protein. Transcription involves the synthesis of two genome-length mRNA species (24 S) that lack a 3′ end poly(A) tail.

Pathogenicity. IPNV naturally infects fish (mainly salmonids) and molluscs. The disease occurs mainly in young fish, which appear grossly normal but show spiral swimming interspersed with sluggish behaviour. The abdomens become distended and pancreatic necrosis occurs. Molluscs infected with IPNV suffer high mortality accompanied by thin and chalky shells, consequent on gross necrotic changes in the digestive gland which manufactures the shell precursor material.

IBDV also affects young stock (up to 5 weeks of age). The virus infects lymphoid tissue, causing destruction of lymphocytes within the bursa of Fabricius and B lymphocytes in the thymus, spleen and caecal tonsils. T lymphocytes appear not to be affected. This results in immunosuppression.

DXV infects larval forms of dipterous larvae, causing systemic infection.

Suggested reading

Cohen, J. and Scherrer, R. (1974) Le virus de la necrose pancreatique infectieuse. Ann. Rech. Vet. 5, 87–100.

Dobos, P., Hill, B.J., Hallett, R., Kells, D.T.C., Becht, H. and Teninges, D. (1979) Biophysical and biochemical characterisation of five animal viruses with bisegmented double stranded RNA genomes. J. Virol. 32, 593–605.

Kelly, D.C., Ayres, M.D., Howard, S.C., Lescott, T., Arnold, M.K., Seeley, N.D. and Primrose, S.B. (1982) Isolation of a bisegmented double stranded RNA virus from Thirlmere reservoir. J. Gen. Virol. 62, 313–322.

Nick, H., Cursiefen, D. and Becht, H. (1978) Structural and growth characteristics of infectious bursal disease virus. J. Gen. Virol. 18, 227–234.

Özel, M. and Gelderblom, H. (1985) Capsid symmetry of viruses of the proposed Birnavirus group. Arch. Virol. 84, 149–161.

Revet, B. and Delain, E. (1982) The Drosophila X virus contains a 1 μm double stranded RNA circularised by a 67 kd terminal protein: high resolution denaturation mapping of its genome. Virology 123, 29–44.

Nermut/Steven (eds) Animal Virus Structure

CHAPTER 9

Reoviridae

P. METCALF

Biochemistry Department, Harvard University, 7 Divinity Avenue, Cambridge, MA 02138, U.S.A.

Family:	Reoviridae	
Genera:	Orthoreovirus	(vertebrates)
	Rotavirus	(mammals)
	Orbivirus	(vertebrates, insects)
	Cypovirus	(insects)
	Phytoreovirus	(plants, insects)
	Fijivirus	(plants, insects)

9.1. General characteristics

The members of the virus family Reoviridae are non-lipid-containing spherical particles 70–80 nm in diameter consisting generally of two concentric protein shells (capsids) containing typically 10 to 12 1–4 kb dsRNA molecules. The capsids have icosahedral symmetry and in some cases have projections at the 5-fold symmetry axes. Virus particles within the cytoplasm of infected cells transcribe their internal dsRNA gene segments, producing mRNA molecules which then serve as templates for both viral protein translation and for progeny dsRNA synthesis. Members of the Reoviridae have an unusually large host range, including vertebrates, insects and plants, and many cause significant agricultural losses. Rotaviruses infect the intestinal lining and cause diarrhea in many animal species. Rotavirus-associated diarrhea causes widespread mortality in developing countries.

9.2. Orthoreovirus: species Reovirus type 3 (Dearing strain)

Chemical and physical characteristics

The composition of the virus is 85% protein and 12% dsRNA. The remainder consists primarily of short (3–20 bases) ssRNA molecules with sequences corresponding to the 5′ ends of the dsRNA segment plus strands. The outer capsid of the reovirus particle can be removed by chymotrypsin digestion to produce single-capsid particles* which enclose the dsRNA genome and contain active mRNA polymerase and capping enzymes. The physical characteristics of the single-capsid particles and of the double-capsid virus are given in Table 9.1. Properties of the proteins and RNA are listed in Table 9.2. The total dsRNA fraction of reovirus corresponds to approximately 23 kb per particle.

Structural characteristics

The dimensions of reovirus particles are given in Table 9.3. The locations of the structural proteins are indicated in Table 9.2.

Architecture of the virion

The outer capsid of reovirus consists of 200 triangular capsomers and 12 larger 'pentamer crater' capsomers. The capsomers have an edge length of approximately 12 nm and are arranged on the surface of the particle with $T = 13$ *laevo* symmetry. The triangle and pentamer capsomers are difficult to distinguish on negative-stain images of intact virions (Fig. 9.1a) but can be clearly seen in images of reovirus capsid fragments (Fig. 9.2a). The $T = 13$ *laevo* symmetry of the capsid is evident in freeze-etch images of intact particles, which also reveal a surface topography showing large pentamer craters and smaller hexamer rings (Fig. 9.1b). The 60 complete rings are each comprised of the extended portions of six adjacent triangular capsomers. Incomplete rings surround the pentamer craters. A model of the outer capsid showing the rings, triangles and pentamers is shown in Fig. 9.3. A three-dimensional model is shown in Fig. 9.4.

The icosahedral symmetry of the reovirus single-capsid particle is unknown, although it is likely to be $T = 13$ *laevo* by analogy with the case of rotavirus, where the symmetry of the inner capsid has been determined. There are 12 projections ('spikes') on its surface which have lateral dimensions similar to the pentamer

* The term 'reovirus core' is used in the literature to denote the single-capsid particle of this virus. However, for consistency in this chapter with the rotavirus 'core', which is a smaller isometric particle contained within the rotavirus inner-capsid, the latter term (single-capsid particle) will be used here.

TABLE 9.1.

Reovirus physical properties

	Virus particle	Single-capsid particle
Molecular mass (Daltons)	126.5×10^6	52.3×10^6
Sedimentation coefficient (S)	734	442
Density in CsCl (g/cm^3)	1.37	1.43
Density in H_2O (g/cm^3)	1.43	-
Diffusion constant (m^2/s)	4.45×10^{-12}	6.11×10^{-12}

TABLE 9.2.

Reovirus proteins and RNA

Protein	M_r ($\times 10^{-3}$)	Number/particle	Location	RNA	Length
λ1	155	100	Inner-capsid	L3	
λ2	140	100	Inner-capsid spike	L2	
λ3	135	12	Inner-capsid	L1	
μ2	70	12	Inner-capsid	M1	
μ1c[a]	72	550	Outer-capsid	M2	
σ1	42	24	Outer-capsid	S1	1416 bp
σ2	38	200	Inner-capsid	S2	1329 bp
σ3	34	900	Outer-capsid	S4	1196 bp
Non-structural proteins:					
μNS	75		NS	M3	
σNS	36		NS	S3	1198 bp

[a]μ1c is a cleavage product of μ1, a putative minor inner-capsid component.
Protein molecular weights are as determined by gel electrophoresis; the length of sequenced RNA molecules is given in base-pairs.

TABLE 9.3.

Reovirus dimensions (nm)

Diameter	Virus	Single-capsid particles
EM negative-stain	76.4	52
EM freeze-etch	80	60
X-ray scattering	83	60
Light scattering	96.4	52
Diameter of cavity inside inner capsid		49
Outer-capsid triangular capsomer length of edge		12
Outer-capsid pentamer crater-depth		3
Height of spike		6

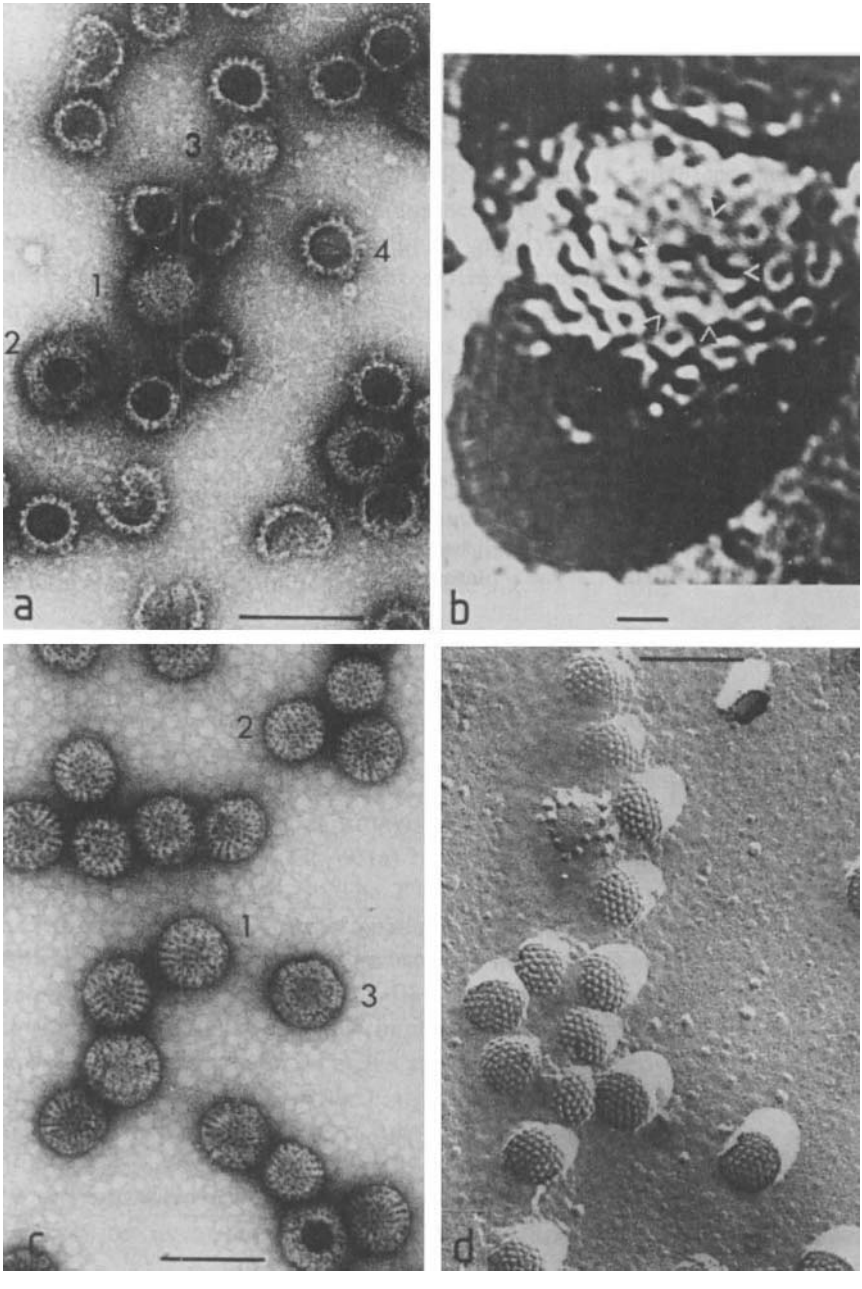
3
4
1
2
a
b
2
1
3
c
d

crater of the outer capsid. They occur at the icosahedral 5-fold axes and it is likely that these spikes are located directly under the pentamer craters of the outer capsid in the intact virus particle. A small linear array of single-capsid particles is shown in Fig. 9.2b.

Antigenic properties

The neutralizing type-specific antigen of reovirus is protein $\sigma 1$, which is an outer-capsid component probably located in the pentamer crater in conjunction with the spike protein $\lambda 2$. Protein $\sigma 1$ is also the viral hemagglutinin and the primary determinant of virus–cell interactions.

Biological properties

Reovirus can be easily grown in cultured mouse L-fibroplasts, producing yields of up to 3×10^4 particles per cell after 12 hours. Virus particles are thought to enter cells by receptor-mediated endocytosis. Virus assembly takes place within the cytoplasm. Subviral particles morphologically similar to single-capsid particles synthesize all 10 mRNAs, which are then translated or used as a template for dsRNA polymerization to produce the components of progeny virus. Recombinant virus particles containing dsRNA molecules originating from differing parental strains in mixed infections have been used to associate pathogenic and immunological phenotypes with individual virus proteins (Sharpe and Fields, 1985).

Pathogenicity

The term 'reo' is an acronym for '*r*espiratory *e*nteric *o*rphan'. The last term refers to the fact that reovirus causes no obvious symptoms in man. The virus is thought to be mainly enteric and is presumably widely distributed, since a large proportion of the general population carry reovirus antibodies. The virus occurs in many mammalian species, where there are three serotypes. Intracerebral innoculation of type 3 reovirus causes an acute, fatal encephalitis in newborn mice.

Fig. 9.1. (a) Negatively stained reovirus preparation showing: (1) intact (double-capsid) reovirus particle, (2) top component particle (i.e. virus without RNA), (3) reovirus single-capsid particle, (4) top component (= empty) single-capsid particle. Magnification bar = 100 nm. (b) Freeze-etched reovirus particle. Note the large pentamer-crater capsomer in the centre of the image (arrows). From Metcalf (1982) with permission. Magnification bar = 10 nm. (c) Negatively stained preparation containing: (1) rotavirus SA-11 double-capsid particle, (2) rotavirus SA-11 single-capsid particle, (3) reovirus particle. Magnification bar = 100 nm. (d) Freeze-etched SA-11 rotavirus single-capsid particles. Magnification bar = 100 nm.

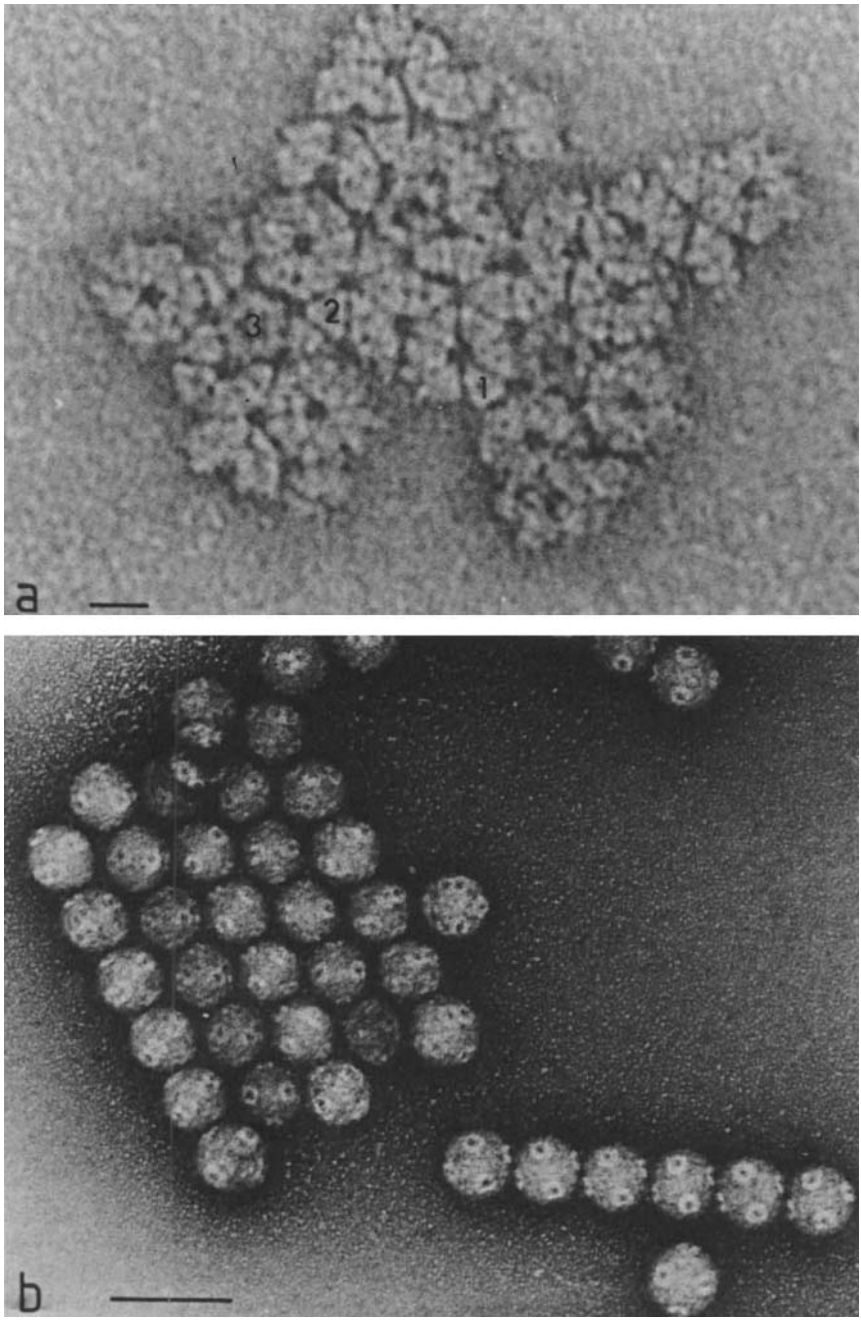
3
2
1
a
b

9.3. Rotavirus: species Simian rotavirus SA-11

General characteristics

Rotavirus has a genome consisting of 11 dsRNA segments contained within an inner capsid which, unlike that of reovirus, has no spikes. The inner capsid has $T = 13$ *laevo* symmetry and contains active transcriptase enzymes. The comparatively smooth outer capsid is likely also to have $T = 13$ *laevo* symmetry (the term 'rota', meaning wheel, refers to the appearance of the double-capsid particle in negatively stained preparations). Single and double-capsid particles are shown in Fig. 9.1c,d. A smaller isometric particle, 40 nm in diameter, the rotavirus core, is contained within the inner capsid. Cores are released when preparations of single-capsid particles are exposed to a high concentration (1.5 M) of $CaCl_2$ as shown for bovine rotavirus (Bican et al., 1982) and porcine rotavirus (Gorziglia et al., 1985; Ludert et al., 1986). The physical characteristics of SA-11 single and double-capsid particles and cores are listed in Table 9.4. The proteins and RNA molecules are listed in Table 9.5.

Biological properties

Like reovirus, human rotavirus appears to be ubiquitous, since a large proportion of the population carry rotavirus antibodies. The virus causes acute gastroenteritis occurring mainly in children up to two years old and can be readily isolated from patients' feces. Electrophoretic analysis of the RNA from such samples indicates the existence of multiple strains of the virus.

Until recently human rotaviruses have proved difficult to grow in cultured cells and most work has been carried out with a few animal strains, including the monkey virus SA-11 described here. The primary neutralizing antigen of SA-11 is the major capsid protein VP7, which is glycosylated in most isolates. The VP7-containing outer capsid of rotavirus appears to be added to the completed single-capsid particle as the latter buds through the endoplasmic reticulum membrane in the final stages of virus assembly.

Fig. 9.2. (a) Reovirus outer capsid fragment containing triangular (1, 2) and pentagonal (3) capsomers. Negative staining. Magnification bar = 10 nm. (b) Negative-stain image of reovirus single-capsid aggregates showing clearly defined spikes. The linear array consists of particles joined along their threefold axes. Magnification bar = 100 nm.

TABLE 9.4.

Simian rotavirus SA-11 physical characteristics

	Double-capsid particle	Single-capsid particle	Core[a]
Diameter (nm)	70	60	40
Sedimentation coefficient (S)	520–530	380–400	280
Density in CsCl (g/cm^3)	1.36	1.38	1.44

[a] Core data for bovine rotavirus.

TABLE 9.5.

Rotavirus SA-11 proteins and RNA

Protein	M_r ($\times 10^{-3}$)	Location	RNA	Length	Comments
VP1	125	Inner-capsid	S1		
VP2	94	Inner-capsid	S2		Major component
VP3	88	Outer-capsid	S4		
VP6	41	Inner-capsid	S6	1356 bp	Major component
VP7	38	Outer-capsid	S9	1062 bp	Glycosylated
VP9	27	Outer-capsid	S11		Very minor component
Non-structural proteins:					
	53		S5		
	34		S7	1104 bp	
	35		S8	1059 bp	
	20		S10	710 bp	Glycosylated

Double capsid particles exposed to trypsin during cultivation or in vitro contain the following cleavage products:
VP2 is cleaved to VP3* (88 kDa) and VP4* (84 kDa)
VP3 is cleaved to VP5* (60 kDa) and VP8* (28 kDa)

Protein molecular weights are as determined by gel electrophoresis; the length of sequenced RNA molecules is given in base-pairs.

9.4. Orbivirus: species Bluetongue virus (BTV)

BTV is spread by flying insects and affects sheep and other livestock in many parts of the world. The virus contains 10 dsRNA segments and the particles in negative-stain preparations appear to have a morphology similar to that of single-capsid rotavirus. A related virus causes the human disease Colorado tick fever.

9.5. Cypovirus: species Cytoplasmic polyhedrosis virus (CPV-1)

Members of the cypovirus genus occur widely and with a broad host range, isolates having been recorded in some 200 insect species. The silk-worm virus causes significant losses in the Japanese silk industry and has been extensively studied.

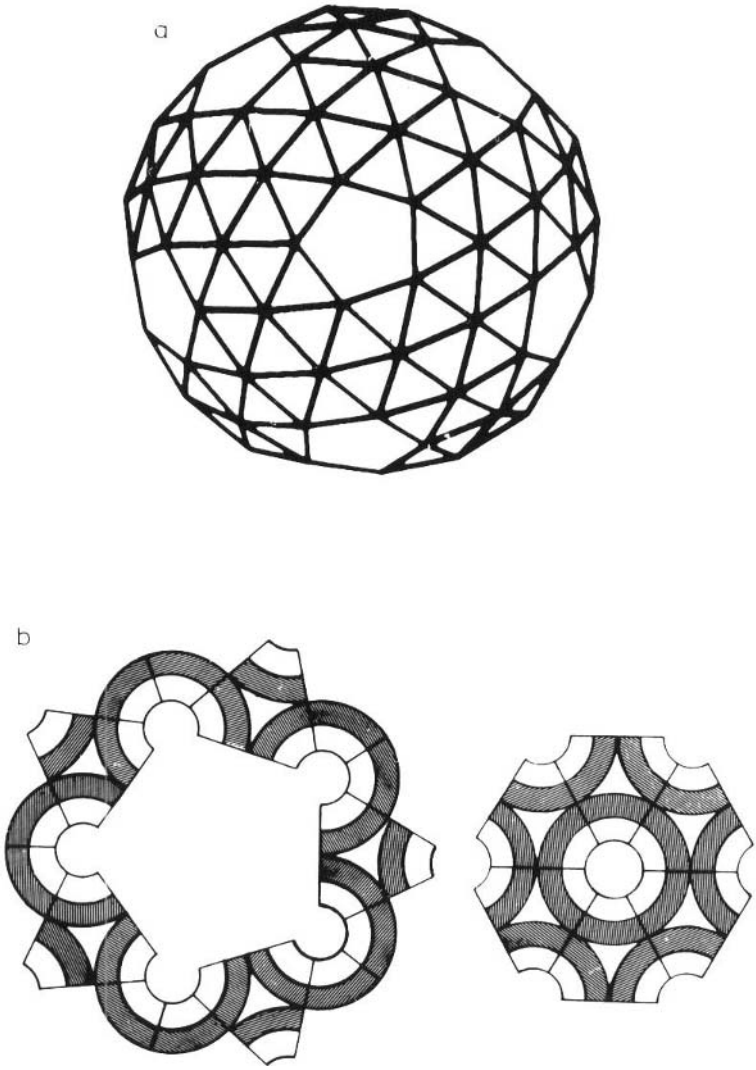

Fig. 9.3. (a) The $T = 13$ *laevo* model for the reovirus outer capsid. The model consists of pentagonal and triangular capsomers. (b) Detail of the reovirus outer capsid model showing the arrangement of the triangular capsomers around the pentamer-crater (left) and hexamer-ring (right) features of the surface topography seen in freeze-etch electron micrographs. The shaded parts represent elevated parts of the capsid surface.

The virus can be obtained in large quantities from infected larvae and has also recently been grown in cultured cell lines. CPV consists of particles similar to reovirus single-capsid particles which form numerous occlusions within large (≥ 3 μm) protein crystals. The crystals consist of polyhedrin, a 30 kDa protein coded by the smallest of the 10 dsRNA segments. Polyhedrin crystals appear to exclude particles other than CPV particles. The proteins of CPV particles have similar molecular weights and occur in approximately equivalent proportions to those of reovirus single-capsid particles and, like them, CPV particles produce capped, methylated mRNA in vitro.

9.6. Phytoreovirus: species Wound tumor virus (WTV)

WTV is an insect-transmitted virus causing root tumors in many dicotyledons. The virus can be grown in cultured vector cell lines. WTV contains 12 dsRNA segments and the particles appear similar to rotavirus in negative-stained preparations. Infected plant cells contain large inclusions ('viroplasms') visible by light microscopy.

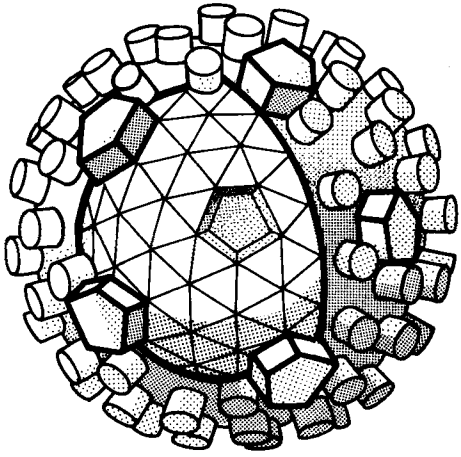

Fig. 9.4. Three-dimensional double-shelled model of the reovirus particle. The inner capsid is shown as a *T*-13 *laevo* network of triangles. This symmetry has been established for the rotavirus inner capsid and is assumed here to apply to reovirus also. The outer capsid, with the same symmetry, consists of cylindrical capsomers positioned over the vertices of the iner capsid lattice. These 'cylindrical capsomers' represent the 'hexamer rings' visualized in freeze-etch images (see Figs. 9.1b and 9.3b). Pentagonal structures representing the core 'spikes' connect the two capsids.

9.7. Fijivirus: species Fiji disease virus (FDV)

FDV and other members of its genus infect monocotyledons, specifically the Graminae. FDV causes serious losses in sugar cane production. The double-capsid particle has small protrusions at the 5-fold symmetry positions but otherwise appears similar to reovirus in negative-stain images. The single-capsid particle is similar to the reovirus single-capsid particle but has more clearly defined pentameric spikes. The orientation of individual spikes is clearly visible in shadowed preparations (Hatta and Francki, 1977) and is consistent with a $T = 13$ outer capsid lattice.

Suggested reading, References

Bican, P., Cohen, J., Charpilienne, A. and Scherrer, R. (1982) Purification and characterization of bovine rotavirus cores. J. Virol. 43, 1113–1117.

Compans, R.W. and Bishop, D.H. (Eds.) (1983) Double-stranded RNA viruses. Elsevier Biomedical, Amsterdam.

Estes, M., Palmer, E. and Obijeski, J. (1983) Rotaviruses: A Review. Curr. Top. Microbiol. Immunol. 105, 123–184.

Gorziglia, M., Larrera, C., Liprandi, F. and Esparza, J. (1985) Biochemical evidence for the oligomeric (possibly trimeric) structure of the major inner capsid polypeptide (45K) of rotaviruses. J. Gen. Virol. 66, 1889–1900.

Hatta, T. and Francki, R. (1977) Morphology of Fiji disease virus. Virology 76, 797.

Joklik, W.K. (Ed.) (1983) The Reoviridae. Plenum Press, New York, London.

Ludert, J.E., Gil, F., Liprandi, F. and Esparza, J. (1986) The structure of the rotavirus inner capsid studied by electron microscopy of chemically disrupted particles. J. Gen. Virol. 67, 1721–1725.

Metcalf, P. (1982) The symmetry of the reovirus outer shell. J. Ultrastruct. Res. 78, 292–301.

Roseto, A., Escaig, J., Delain, E., Cohen, J. and Scherrer, R. (1979) Structure of rotaviruses as studied by the freeze-drying technique. Virology 98, 471–474.

Sharpe, A. and Fields, B. (1985) Pathogenesis of viral infections: basic concepts derived from the reovirus model. N. Engl. J. Med. 312, 486–497.

This Page Intentionally Left Blank

Nermut/Steven (eds) Animal Virus Structure

CHAPTER 10

Bunyaviridae

RALF F. PETTERSSON[1] and CARL-HENRIK VON BONSDORFF[2]

[1]Recombinant DNA Laboratory, University of Helsinki, Valimotie 7, SF-00380 Helsinki, Finland, and [2]Department of Virology, University of Helsinki, Haartmaninkatu 3, SF-00290 Helsinki, Finland

Family: Bunyaviridae

Genera:	**(type species):**
Bunyavirus	(Bunyamwera virus) (> 150 viruses)
Phlebovirus	(Sandfly fever Sicilian virus) (37)
Nairovirus	(Crimean-Congo hemorrhagic fever virus) (28)
Uukuvirus	(Uukuniemi virus) (8)
Hantavirus	(Hantaan virus) (4)
Ungrouped viruses	at least 4 serogroups (about 10 viruses) and 11 unassigned viruses

10.1. General characteristics

Bunyaviruses are spherical enveloped viruses comprising three coiled, possibly helical, circular nucleoproteins. The genome consists of three single-stranded RNA segments of negative sense. In the case of Punta Toro virus (genus Phlebovirus), the smallest RNA segment has an 'ambisense' polarity. All bunyaviruses have four structural proteins: two envelope glycoproteins, one nucleocapsid protein and one minor RNP-associated polypeptide, but they lack an internal membrane (matrix) protein. Bunyaviruses replicate in the cytoplasm of infected cells and new particles are formed by budding into vesicles of the Golgi complex (Fig. 10.1).

The bunyaviruses are spread by arthropod vectors (e.g. mosquitoes, ticks, sandflies). At least some bunyaviruses are able to form recombinant viruses as a result

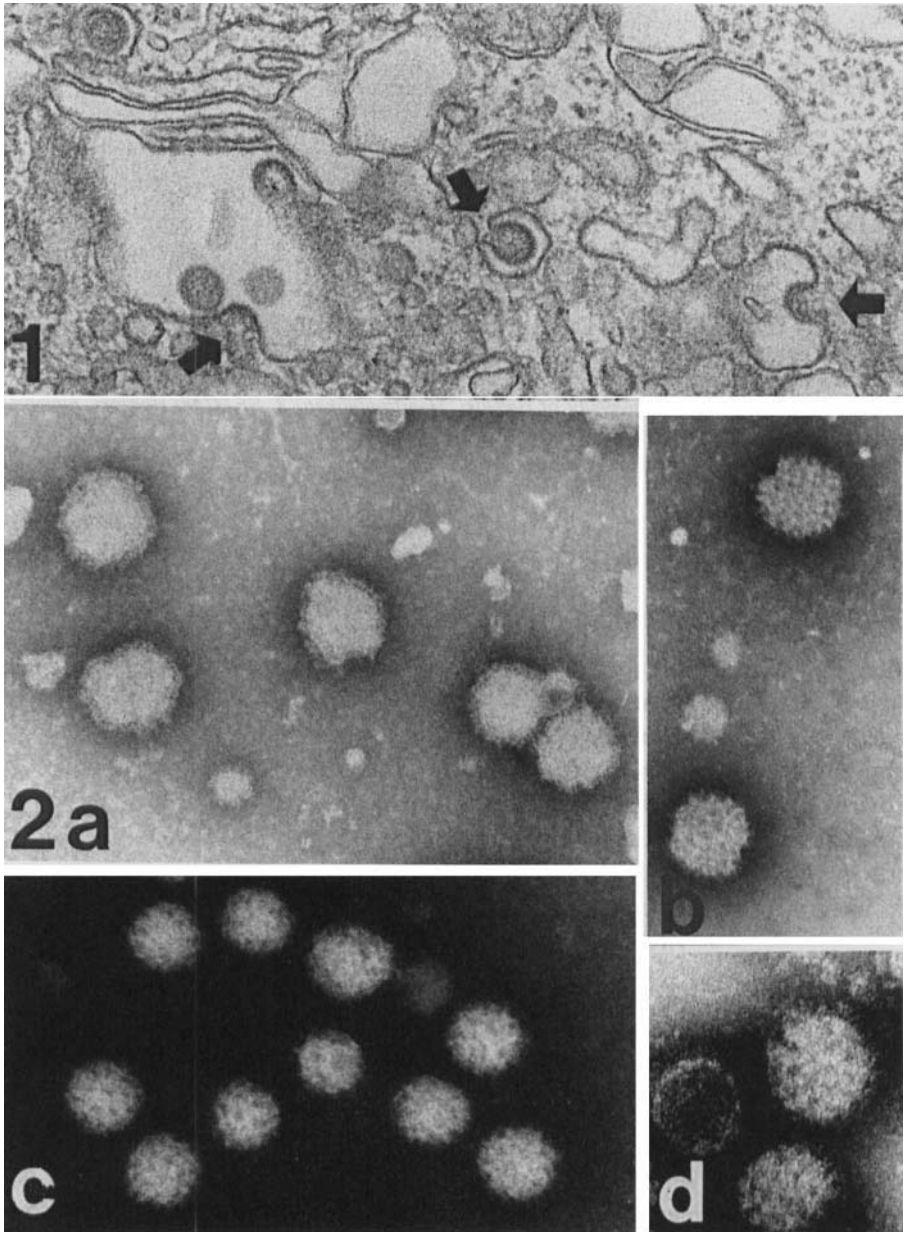

Fig. 10.1. Maturation of Bunyaviruses. The Golgi region of a chick fibroblast 9 h after Uukuniemi virus infection. Particles at different stages of budding can be seen (arrows).

Fig. 10.2. Different negative-staining conditions of snowshoe hare virus. (a) Potassium phosphotungstate (KPT), pH 7.2, unfixed virus; (b) KPT, pH 5.5, unfixed virus; (c and d) KPT, pH 5.5, glutaraldehyde fixed virus. In b, c and d, a regular arrangement of the glycoprotein spikes is visible. Magnifications: a and b, ×120 000; c, ×160 000; d, ×200 000.

of reassortment of RNA segments during dual infections. Transovarial, venereal and/or transstadial transmission in arthropods has been demonstrated. Many bunyaviruses cause diseases in man or animals (encephalitides, haemorrhagic fevers, sandfly fevers, etc.).

10.2. Chemical and physical characteristics

The chemical composition has been determined only for Uukuniemi virus and found to be about 2% RNA, 58% protein, 33% lipid and 7% carbohydrate. No reliable determinations of the molecular weight of virions have been carried out. The sedimentation coefficients of virus particles have been reported to be 350–470 S (Bunyavirus), 400 S (Phlebovirus), 400–450 S (Nairovirus) and 450 S (Uukuvirus). The density of bunyaviruses is about 1.17–1.19 g/cm^3 in sucrose and about 1.20 g/cm^3 in CsCl or potassium tartrate. The nucleoproteins band as one peak at a density of 1.31 g/cm^3.

The structural proteins of the virion are summarized in Table 10.1, and the size and coding strategy of the three RNA segments in Table 10.2. In La Crosse virus (Bunyavirus), G1 appears to be the haemagglutinin, and antibodies against G1 possess neutralizing activity. The L protein is probably the virion-associated RNA polymerase. The N protein is the structural protein of the nucleocapsid.

10.3. Structural characteristics

Shape and size. Bunyaviruses are spherical particles measuring 95–100 nm in diameter in both negatively stained and thin-sectioned preparations. In contrast with, for example, orthomyxo- and paramyxoviruses, the size of bunyavirus particles in thin-sectioned preparations appears rather homogeneous. Infrequently, tubular particles with a regular diameter of 85 nm but variable length have been described.

TABLE 10.1.
Structural proteins of bunyaviruses[a]

Protein	Genus					
	Bunyavirus	Phlebovirus	Nairovirus	Uukuvirus	Hantavirus	Location
L	180–200	180–200	180–200	180–200	200	Nucleocapsid
G1[b]	108–120	55–70	72–84	70	65–72	Envelope
G2[b]	29–41	50–60	30–40	65	55	Envelope
N	26.5[c]	27[c]	48–54	25	47[c]	Nucleocapsid

[a]Molecular weights $\times 10^{-3}$
[b]The numbering of the glycoproteins in each genus is based solely on size and not on their function.
[c]Deduced from the nucleotide sequence.

TABLE 10.2.

Bunyavirus RNAs[a]

Genus	RNA segment		
	L	M	S
Bunyavirus	2.8	1.5 (4458, 4527)	0.28–0.33 (880-981)
Phlebovirus	2.5–3.0	1.8–2.2 (3884, 4330)	0.7–0.8 (1904)
Nairovirus	4.1–4.9	1.5–1.9	0.6–0.7
Uukuvirus	2.3	1.1 (3231)	0.4
Hantavirus	2.7	1.2 (3616)	0.6 (1696)
Protein encoded	L	G1, G2[b] (NS_M)[d]	N, NS_S[c]

[a] Molecular weights $\times 10^{-6}$. In some cases the exact number of nucleotides as determined from the cloned gene is given in parentheses.

[b] Synthesized as a precursor, which in the case of Uukuniemi virus is cotranslationally cleaved.

[c] Coding strategy varies: Overlapping genes with different reading frames (Bunyavirus genus) and two non-overlapping genes in an ambisense genomic RNA (Phlebovirus genus). NS = nonstructural protein.

[d] NS_M demonstrated in vivo for Bunyavirus members and deduced from nucleotide sequence for Phlebovirus members.

10.4. Structural complexes – chemistry and organization

Envelope

The envelope of bunyaviruses consists of a lipid membrane with which two glycosylated polypeptides (G1 and G2) are associated (Table 10.1). There are very few data on the lipid composition. In Uukuniemi virus, a phospholipid composition resembling that of the host cell plasma membrane has been reported. The glycoproteins appear to be located on the external side of the lipid membrane, as evidenced by their sensitivity to protease digestion. A small peptide fragment remaining associated with the particle after protease treatment suggests that at least one of the polypeptides penetrates the lipid bilayer.

In thin-section electron microscopy the particle is characterized by a rather fuzzy 10–14-nm-thick layer outside a clearly resolved double-track structure typical of a lipid membrane. This is located at a diameter of about 60–70 nm (Figs. 10.1 and 10.7).

Negatively stained specimens of members of the Bunyavirus genus show a fuzzy surface layer with roughly radially oriented surface projections (Fig. 10.2A). Brief negative staining, especially with slightly acidic stain (pH 4.4–5.5), of unfixed (Fig. 10.2b) or prefixed viruses (Fig. 10.2c and d) reveals considerably more structural details on the particle surface, suggestive of a higher order of glycoprotein organization.

Regular arrays of apparently clustered glycoprotein spikes have been observed among members of the other genera. The clustered Uukuniemi virus glycoproteins appear as cylindrical subunits, 10–12 nm in diameter with a central cavity of about 5 nm (Fig. 10.3a). In freeze-etched preparations the units are seen as knobs (Fig. 10.3b). Both negative staining and freeze-etching suggest that these units are arranged in a $T=12$, $P=3$ icosahedral surface lattice (Fig. 10.3c–f). According to the classical Caspar and Klug model, this would imply that the surface is formed by 110 hexamers and 12 pentamers, i.e. 720 structure units. The composition of the structure unit is not known. G1 and G2 are present in nearly equimolar amounts in purified Uukuniemi virus. It is thus possible that a structure unit is composed of a G1-G2 dimer, hence a hexameric unit of 6 dimers and a pentameric unit of 5 dimers. Thus, each particle would contain 720 molecules each of G1 and G2, i.e. 1440 glycoproteins in total.

A surface structure resembling that of Uukuniemi virus has been observed in Phleboviruses, e.g. Punta Toro virus (Fig. 10.4a and b) and especially in Rift Valley Fever (RVF) virus, in which hollow cylindrical glycoprotein subunits are also apparent. However, no definite icosahedral arrangement has been proposed for any of these bunyaviruses. Regular glycoprotein arrays have also been observed in Nairo- and Hantaviruses.

Nucleocapsid (nucleoprotein complex)

Ribonucleic acids. As shown for Uukuniemi virus (Uukuvirus) and Lumbo virus (Bunyavirus), the single-stranded RNA segments, L (large), M (medium) and S (small), are present in circular forms under moderately denaturing conditions (Fig. 10.5A–C). Fully denatured linear molecules can be recircularized, when the level of denaturation is reduced. These results, together with direct sequence analyses of the 3′ and 5′ ends of the RNA segments, have shown that the circularization is due to inverted complementary sequences (10–15 nucleotides in length) at both ends of the molecules. The terminal sequences are conserved in the three RNA segments and also within members of each genus. The RNA species measured from electron micrographs fall into three distinct size classes corresponding to the L, M and S RNA species. Length determinations show variations in different reports.

Ribonucleoproteins (RNP). The three RNA segments each contain multiple copies of the N protein and a few copies of the L protein. The RNA in the RNPs is only partially protected from degradation by ribonuclease. All three RNPs have the same density in CsCl (1.31 g/cm^3), suggesting identical protein-to-RNA ratios. Thus, the amount of RNA species present in virions directly reflects the number of N protein molecules. For many bunyaviruses, the molar amount of L, M and S RNA species generally varies from one virus preparation to another, making any estimations of the amounts of N protein relative to the glycoproteins meaningless.

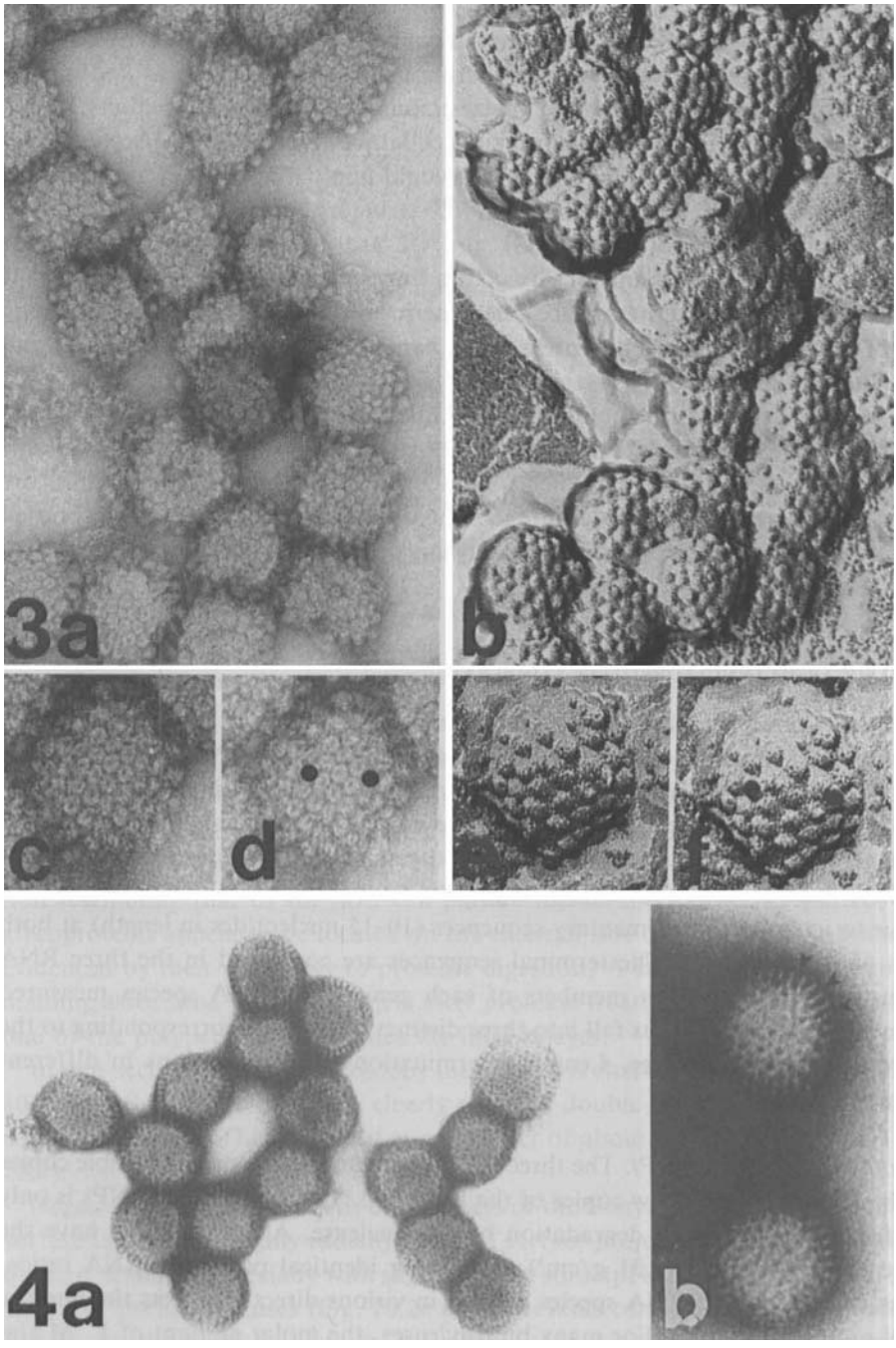
3a
b
c
d
4a
b

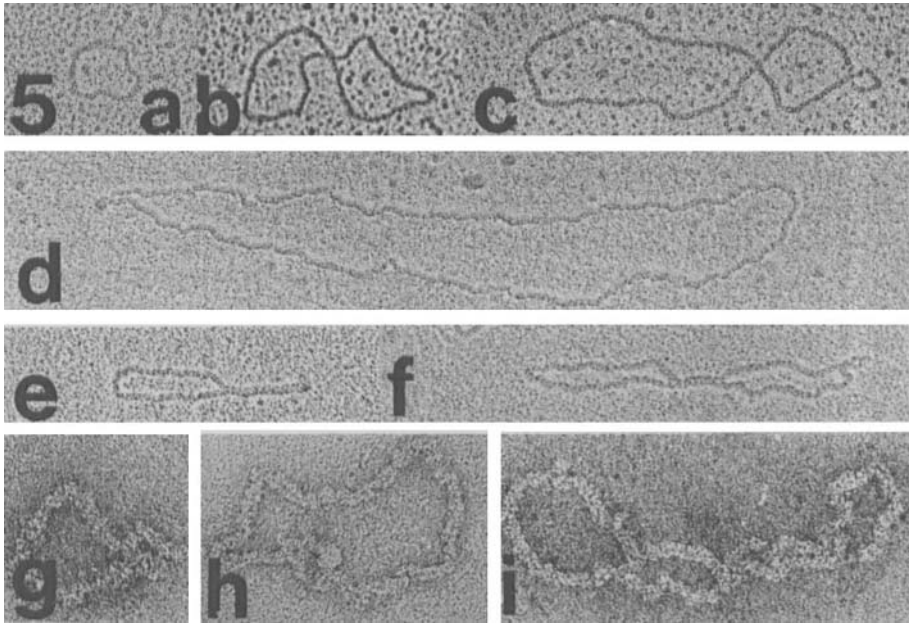

Fig. 10.5. The internal components of bunyaviruses. Rotary shadowing of: (a–c) isolated Lumbo virus RNA molecules representing the three size-classes S, M and L; (d–f) isolated extended Uukuniemi virus ribonucleoprotein (RNP) strands; (g–i) isolated Lumbo virus RNP strands in a coiled configuration. Magnifications: a–c, ×80 000; d–f, ×75 000; g–i, ×160 000. (a–c and g–i by courtesy of Dr. M. Bouloy and Dr. A. Samso, and with the permission of Imprimerie Gauthier-Villars.)

Each virus particle contains the three species of circular RNPs (S, M, L). The Uukuniemi virus RNPs have been described in stretched-out circular forms and are 2–3 nm thick (negative staining) and 2.8, 1.4 and 0.7 μm long, respectively (Fig. 10.5d–f). The nucleocapsid arrangement in the virion is not known. In principle, a circular molecule could be arranged as either a twisted helix (with two strands running in opposite directions as in a panhandle) or a single-stranded helix. The nucleoprotein strands released from damaged particles often show regular undula-

Fig. 10.3. Surface structure of Uukuniemi virus in negative staining (a, c, d) and freeze-etch replicas (b, e, f). In the selected particles the pentamer locations according to a $T = 12$ icosahedral surface lattice have been marked on the parallel picture. Magnifications: a and b, ×120 000; c–f, ×250 000.

Fig. 10.4. Surface structure of the Phlebovirus Punta Toro. The projections appear to form a regular array of hollow cylinders. Arrowheads point to well-resolved lateral views of projections. Magnifications: a, ×120 000; b, ×200 000. (By courtesy of Dr. J.F. Smith and Dr. D.Y. Pifat, and with the permission of Academic Press, Inc.).

tions suggestive of a helical structure (Fig. 10.8) and images of isolated nucleoproteins of Bunyavirus members (Fig. 10.5g–i) are highly suggestive of a one-stranded helix structure. Apart from a diameter of 8–10–12 nm (range in various reports) and apparent lengths of 700, 510 and 200–300 nm, respectively, no other helix parameters have been discernable.

In thin-sectioned virus particles the nucleocapsid appears to be located close to the membrane (Fig. 10.7). There is, however, no indication of a close or regular packing underneath the bilayer. In rare instances, a distinct layer of nucleoprotein has been observed in negatively stained Lumbo virus (Fig. 10.6) and Bunyamwera virus (not shown) particles.

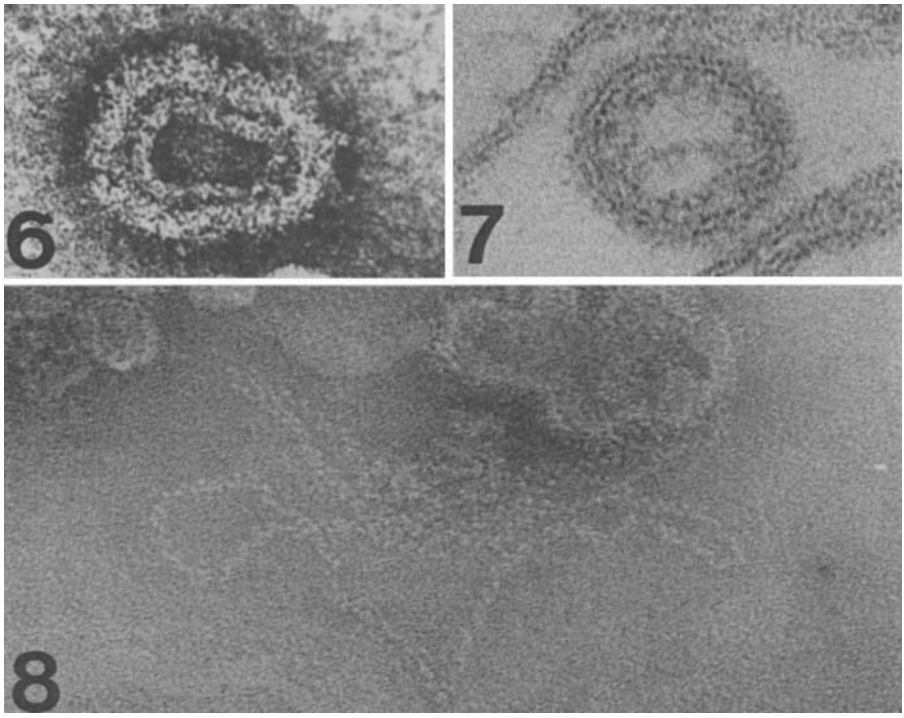

Fig. 10.6. A negatively stained Lumbo virus particle revealing a distinct nucleoprotein structure underneath the envelope. Magnification: ×350 000. (By courtesy of Dr. M. Bouloy.)

Fig. 10.7. Thin section of a Uukuniemi virus particle. The nucleoprotein appears to be rather irregularly arranged underneath the envelope. Magnification ×320 000.

Fig. 10.8. A Uukuniemi virus ghost from which loops of the coiled nucleoprotein strands have been released. Magnification: ×200 000.

10.5. The structural model

Based on existing data, only a highly tentative model can be constructed for the bunyaviruses (Fig. 10.9). One of the major postulations for the model is that the envelope glycoproteins form clusters which have icosahedral symmetry. This would mean that the glycoprotein–glycoprotein interactions may be very strong and important for the virus architecture. Although evidence is lacking, one has to postulate a direct interaction between the glycoproteins and the nucleocapsid in order to understand virus assembly. Note that bunyaviruses do not contain an internal membrane (matrix) protein which would contribute to structural stability and mediate contact between the glycoproteins and the nucleocapsid. It appears unlikely that the nucleocapsid would form a regular (icosahedral or spherical) structure on which the envelope would assemble. It is possible that the RNP only nucleates virus budding and that the assembly then proceeds by lateral glycoprotein–glycoprotein interaction. In the virion, all three RNP species must be present. The mechanism by which this is achieved is not understood, which is a problem common to all viruses with segmented genomes.

10.6. Biological properties

Virus–cell interactions and replication. The mode of entry of bunyaviruses has not been studied. La Crosse virus possesses fusion activity when the pH is lowered to 6.3 or below. This suggests that bunyaviruses enter the cell by adsorptive endocytosis via the coated pit–endosome pathway, as described for alphaviruses. Bunyaviruses replicate in the cytoplasm. No direct evidence for a nuclear involvement in virus replication has been obtained. Viral antigens have been observed in nuclei, but virus replication also takes place in enucleated cells, and in the presence of actinomycin D and α-aminitin. Primary transcription is carried out by the virion-associated RNA polymerase. The 5′ ends of capped host mRNAs appear to donate short (10–14 bases) oligonucleotide stretches to the 5′ end of complementary RNAs derived from the S RNA segment of La Crosse virus and snowshoe hare virus (Bunyavirus). These oligonucleotides apparently serve as primers for mRNA synthesis much in the same way as has been described for influenza virus.

Genetic and molecular analyses indicate that bunyavirus S RNA encodes a non-structural protein (NS_S) in addition to the N protein. The M segment of members of the Bunyavirus genus also appears to encode a non-structural protein NS_M, in addition to the two glycoproteins. The function of the NS proteins is not known.

In the case of Bunyaviruses, the N and NS_S proteins are synthesized from overlapping genes translated from two different open reading frames. For Punta Toro virus (Phlebovirus) these proteins are translated from non-overlapping genes present in opposite RNA strands (ambisense genomic RNA).

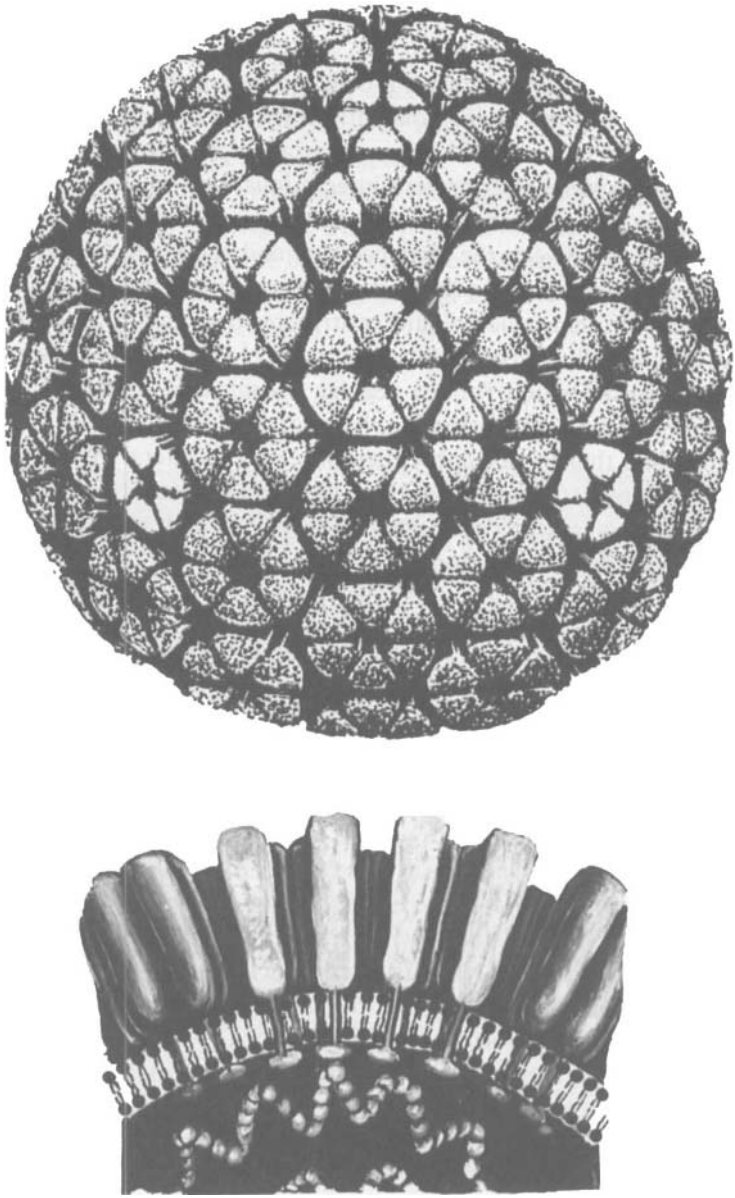

Fig. 10.9. Structure model. In the model, clustered glycoproteins have been arranged according to the $T=12$ icosahedral surface lattice found in Uukuniemi virus. The three pentameric positions are not shaded. The penetration of the glycoprotein through the lipid bilayer is seen in the cross-sectioned envelope (below). Note the absence of an internal membrane protein (M protein). The nucleocapsid is presented as a loosely coiled structure making, at least at some points, contact with the cytoplasmic portion of the glycoprotein(s). Approximately in scale.

Virus maturation occurs in the Golgi complex (Fig. 10.1). The glycoproteins of Uukuniemi virus have been shown to accumulate in the Golgi complex. Concomitantly with the expansion and vacuolization of the Golgi region, nucleocapsids also accumulate there. Electron microscopy reveals budding profiles at smooth-surface vesicles in the area where glycoproteins and nucleocapsids have accumulated (Fig. 10.1). The virus is probably transported to the cell surface in vacuoles that fuse with the plasma membrane. The site of maturation in the Golgi is characteristic of all bunyaviruses studied. No budding of bunyaviruses at the plasma membrane has been reported.

Suggested reading

Bishop, D.H.L., et al. (1980) Bunyaviridae. Intervirology 14, 125–143.

Bishop, D.H.L. (1985) Replication of arenaviruses and bunyaviruses. In Virology. Eds. B.N. Fields et al.; pp. 1083–1110. Raven Press, New York.

Bishop, D.H.L. and Shope, R.E. (1979) Bunyaviridae. In Comprehensive Virology. Eds. H. Fraenkel-Conrat and R.R. Wagner; Vol. 14, pp. 1–156. Plenum, New York, London.

Murphy, F.A., Harrison, A.K. and Whitfield, S.G. (1973) Bunyaviridae: Morphologic and morphogenic similarities on Bunyamwera serologic supergroup viruses and several other arthropod-borne viruses. Intervirology 1, 297–316.

Von Bonsdorff, C.-H. and Pettersson, R. (1975) Surface structure of Uukuniemi virus. J. Virol. 16, 1296–1307.

This Page Intentionally Left Blank

Nermut/Steven (eds) Animal Virus Structure

CHAPTER 11

Togaviridae

CARL-HENRIK VON BONSDORFF[1] and KAI SIMONS[2]

[1]Department of Virology, University of Helsinki, Haartmaninkatu 3, SF-00290 Helsinki, Finland, and [2]European Molecular Biology Laboratory, Meyerhofstrasse 1, 6900 Heidelberg 1, F.R.G.

Family:	Togaviridae
Genera:	**Prototype virus (number of species):**
Alphavirus	Sindbis virus (25)
Flavivirus*	Yellow fever virus (56)
Rubivirus	Rubella virus (1)
Pestivirus	Hog cholera virus (3)
Ungrouped viruses	Equine arteritis virus*
	Lactic dehydrogenase virus
	Cell-fusing agent of Aedes cell cultures
	Simian Hemorrhagic Fever virus

11.1. General characteristics

Togaviruses comprise a large rather arbitrarily defined family of small, 50–70 nm in diameter, enveloped RNA-viruses whose nucleocapsids are assumed to be icosahedral. Togaviruses replicate in the cytoplasm of infected cells and mature by

* The International Committee on Taxonomy of Viruses (ICTV) will remove the Flavivirus genus from the Togaviridae to form a new family, Flaviviridae. Also, the equine arteritis virus will become the prototype virus of an Arterivirus genus of Togaviridae.

budding through host cell membranes. All alpha- and most flaviviruses are spread by arthropod vectors. For some flaviviruses, the rubi- and pestiviruses, vectors are not known.

Togaviruses cause a number of different diseases of human and veterinary importance. Virulent alphaviruses are known to cause either infection of the central nervous system or a rubella-like disease characterized by rash and arthritis.

Antigenically Togaviridae also comprise a heterogeneous group. No immunological cross-reactivity exists between the genera. The degree of antigenic relatedness within each genus varies and appears to depend on the number of strains and their geographic distribution, i.e. for how long the strains have been isolated from each other. There is a high degree of cross-reactivity between species.

11.2. Physical and chemical characteristics

Comparative physicochemical properties of the Togavirus genera are given in Table 11.1. The alphaviruses have been most thoroughly characterized and this chapter will mainly concentrate on these viruses, with occasional reference to the other genera.

The alphaviruses contain close to 6% RNA, 57–60% protein, 27–30% lipid and 6% carbohydrate. They have a buoyant density of about 1.25 g/cm^3 in CsCl and about 1.20 g/cm^3 in sucrose. The viral RNA consists of a linear single-stranded RNA of positive polarity. The size of the RNA was estimated to be 4.0–4.5 $\times$ 10^6 daltons but the recently obtained complete nucleotide sequence gives the value of 4.06 (Sindbis) or 3.72 (SFV) $\times$ 10^6 daltons. There are 3 or 4 species of polypeptides in the virion (Table 11.1). In Semliki Forest virus (SFV) there appear to be about equal numbers of all four polypeptides as determined by labelling with radioactive amino acid mixtures. The copy number has been estimated to be in the range 180–240. The lipids of alphaviruses have been characterized in detail. About 50% of the lipid is cholesterol and the phospholipid composition appears to reflect that of the host cell plasma membrane. Virus grown in mosquito cells shows a very different lipid composition as compared to virus grown in mammalian cells in that phosphatidylethanolamine comprises about 2/3 of the total viral lipids and appears to replace the cholesterol. More than 90% of the viral carbohydrates are associated with the envelope proteins. They are *N*-glycosidic and of high mannose or of complex type.

Total mass of SFV as calculated from neutron diffraction is 45.8 $\times$ 10^6 daltons (see Jacrot, Chapter 4 of this volume).

TABLE 11.1

Physicochemical properties of togaviruses

Genus	Virion		Nucleocapsid diameter (nm)	RNA[a] size	Virion polypeptides	
	Diameter (nm)	Sedimentation constant (S)			$M_r \times 10^{-3}$	Location
Alphavirus (SFV)	65	240	40	3.7×10^6	50 (G)[b] E1	Envelope
					50 (G) E2	Envelope
					10 (G) E3	Envelope
					30	Capsid
Flavivirus (Dengue)	50	200	26	3.9×10^6	59 (G)	Envelope
					7–8	Envelope
					13	Capsid
Pestivirus (hog cholera)	53	N.D.	27	4×10^6	55 (G)	Envelope
					45 (G)	Envelope
					36	Capsid
Rubivirus (rubella)	58	240	33	3.8×10^6	58 (G)	Envelope
					47, 42 (G)[c]	Envelope
					33	Capsid

[a] The SFV RNA size is determined from the known sequence and it is smaller than the Sindbis virus RNA (4.06×10^6) due to a deletion in the region coding for non-structural proteins (K. Takkinen, personal communication). The values reported for flavi-, pesti- and rubiviruses are likely to be too high, since these RNA species sediment slightly faster than the alphavirus RNA.

[b] G = glycoprotein.

[c] These two species differ only in their glycosylation.

11.3. Structural characteristics

The envelope

The envelope consists of a lipid membrane containing two (Sindbis virus) or three (Semliki Forest virus) glycopeptides. Less than 0.5% of the host cell protein is associated with the virus particle. The lipids are of host cell origin and their composition resembles qualitatively and quantitatively that of the host cell plasma membrane, the budding site of togaviruses. The envelope polypeptides have been well characterized. The bulks of E1 and E2 (and the whole of E3) with their carbohydrate side-chains are on the surface of the virion. Both E1 and E2 envelope polypeptides contain a stretch of hydrophobic amino acids, which spans the lipid bilayer. The C-terminus of E2 has about 30 amino acids on the inner surface of

the viral envelope, whereas the terminal inner tail of E1 is only three amino acids long. All three envelope polypeptides are glycosylated and the carbohydrate side-chains are similar in structure to those of the host cell glycoproteins. The spikes seen on the virion surface are formed by one copy of each of the three (SFV) or two (Sindbis) polypeptides.

The viral glycoprotein spikes can, after detergent treatment of virus, be isolated by sucrose density gradient centrifugation. Relatively stable, soluble, star-shaped 29 S complexes of spike octamers are recovered. The detergent-solubilized glycoproteins can easily be reconstituted to lipid vesicles, whereby they regain their configuration of radially oriented spikes with the hydrophobic anchors extending into the lipid bilayer.

E1 glycoprotein has haemagglutinating activity and is probably responsible for low-pH-induced fusion activity, whereas E2 induces type-specific neutralizing antibody. Its C-terminal interacts with the capsid proteins.

The nucleocapsid

The nucleocapsid consists of one polypeptide species (M_r 30 000) which has a prominent cluster of basic amino acids in the amino terminal part of the sequence. The genomic RNA has been completely sequenced, and the gene order is known (Fig. 11.1). Portions of the (Sindbis virus) genome coding for nonstructural proteins show sequence homology to respective areas in certain plant viruses (tobacco

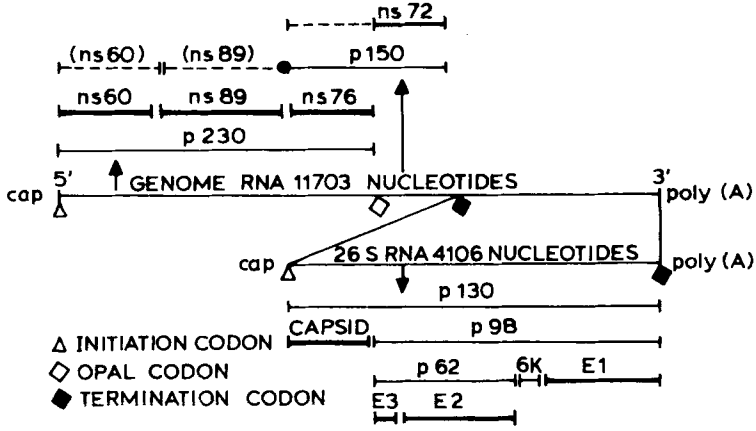

Fig. 11.1. Translation scheme of Sindbis virus. The intermediate polyproteins are presented in thin lines, the final cleaved polypeptides in thick lines. The nonstructural proteins are presented above the RNA. The fourth nonstructural protein (ns72) arises through a readthrough translation. The structural proteins are shown underneath the expanded 3′ end of the genome, which corresponds to the 26 S subgenomic mRNA in the infected cell. (Modified from Strauss and Strauss, 1983.)

mosaic virus, brome mosaic virus and alfalfa mosaic virus), suggesting an evolutionary relationship between those viruses.

11.4. Architecture of the virion

Low-angle X-ray diffraction data have shown that Sindbis and SFV nucleocapsids have a radius of about 20 nm. The nucleocapsid is enveloped by a lipid bilayer which is about 5 nm thick. The glycoprotein spikes extend to a radial distance of 32–34 nm.

In negative staining alphavirus particles display a 7–8 nm 'fuzzy' layer of spikes. However, when virus particles are stained very briefly to obtain one-sided staining, a regular pattern of clustered glycoproteins can be resolved. In Sindbis virus (Fig. 11.2A) the glycoproteins appear to be arranged in a trimer clustering, forming a $T = 4$ icosahedral surface lattice. The surface of the particle is formed by a lattice of equilateral triangles delineated by stain-filled grooves. In SFV only 5- or 6-coordinated pits in a $T = 4$ lattice are seen in negative staining (Fig. 11.2B). The Sindbis virus glycoprotein arrangement is also clearly resolved in freeze-etched specimens (Fig. 11.2C). The lateral interactions between the glycoprotein spikes appear to be considerable, since the trimer clustering is retained in the hexagonal lattices of glycoproteins found in virus envelopes from which the nucleocapsids have been released by mild detergent treatment. Thus the alphavirus glycoprotein layer bears a resemblance to icosahedral capsids. In fact, the alphaviruses crystallize rather easily (Fig. 11.3A,B) but the crystals obtained thus far do not diffract X-rays to high resolution. In flaviviruses only for dengue-2 have micrographs suggestive of a higher order of the glycoprotein arrangement been presented.

By detergent treatment of alphaviruses (Fig. 11.4A) followed by sucrose gradient centrifugation, a homogeneous population of nucleocapsids can easily be obtained (Fig. 11.4B). The 'spherical' nucleocapsid measures 38–40 nm in diameter in negative staining. Two features are characteristic of the alphavirus nucleocapsid. Firstly, the capsid does not seem to protect the RNA from RNase. Secondly, mild RNase treatment or exposure of the nucleocapsid to slightly acidic pH (less than 6.2) will contract the particle to a diameter of 30–32 nm. 'Empty' capsids devoid of RNA have never been found in alphaviruses. Together these findings suggest that RNA–protein interactions play an important role in the construction of the alphavirus capsid. In this respect the nucleocapsid resembles some of the small icosahedral plant viruses, e.g. cucumber mosaic virus.

The capsid architecture has been difficult to establish. The generally proposed icosahedral structure has been based on tentative evidence; a regular subunit clustering has occasionally been observed in negatively or positively stained nucleocapsids. Based on intersubunit distances, both $T = 3$ and $T = 4$ icosahedral surface lattices have been proposed for the capsid.

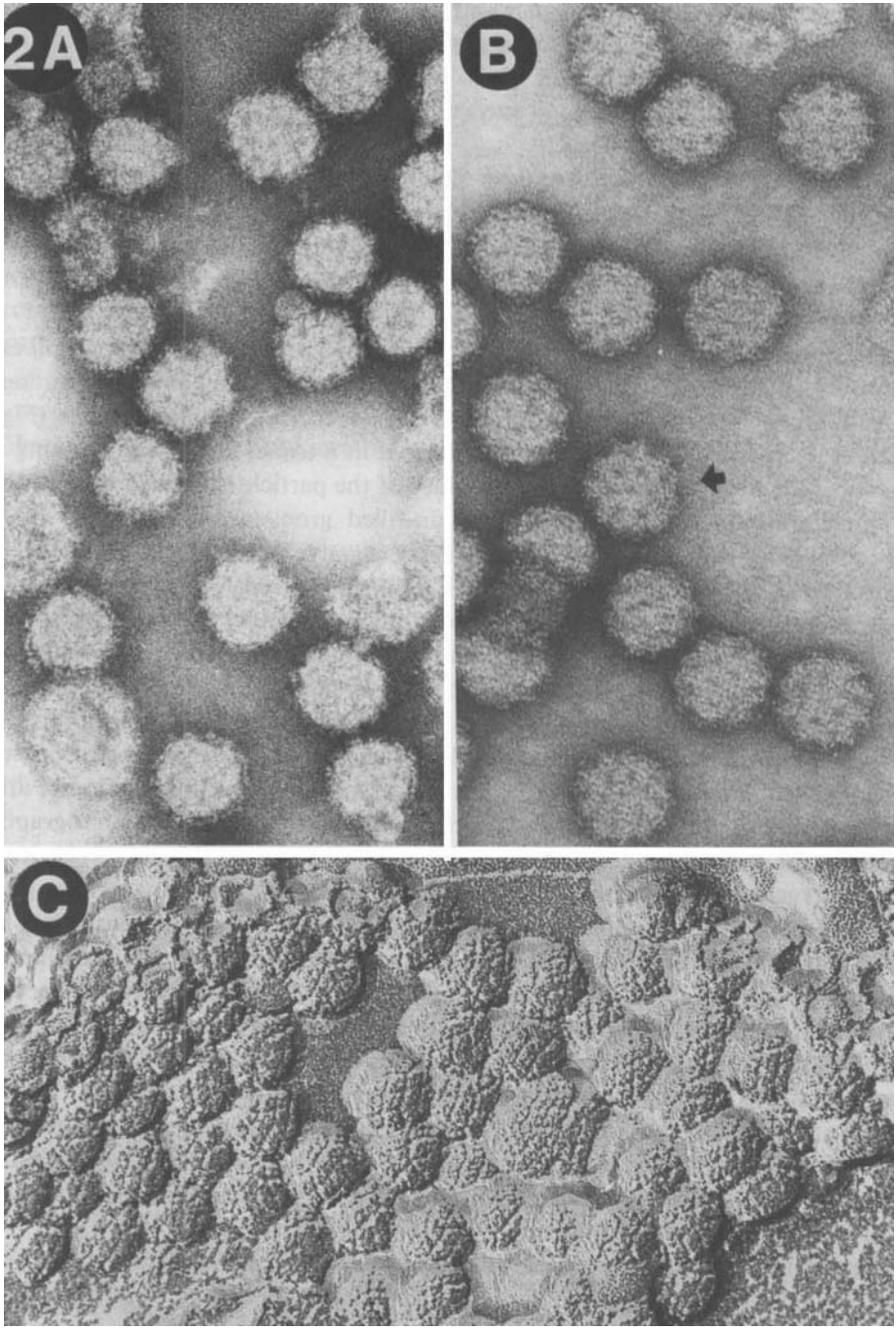
2A
B
C

The recently developed technique of cryo-electron microscopy allows the observation of virions frozen into thin films of buffer solution without staining. Thus, this technique eliminates most of the artefact-producing steps connected with air-dry negative staining. Fig. 11.6A shows a frozen hydrated suspension of SFV. By selecting favorably oriented particles an image reconstruction of the virion has been performed, and the result clearly shows that the surface of SFV is formed by spike trimers arranged on an icosahedral $T = 4$ surface lattice (Fig. 11.6B).

Further studies on Sindbis virus by cryo-electronmicroscopy have led to a refined image reconstruction which reveals an icosahedral nucleocapsid with a $T = 3$ symmetry. The capsid appears as a smooth-surfaced, fenestrated particle. The five-fold axes of the capsid and the envelope coincide in the virion. The centers of the spike trimers are located directly over holes in the capsid forming a complementary structure. The image reconstruction also reveals that the lipid bilayer is not spherical, but rather polyhedral between the capsid and the external parts of the spike trimers.

The $T = 4$ and $T = 3$ match between the envelope and the capsid proteins agrees well with the molecular weight determinations obtained by neutron diffraction. The virion is thus composed of 80 spike trimers and 180 capsid proteins in the icosahedral nucleocapsid. Comparisons of alpha virus capsid proteins and the capsid proteins of non-enveloped viruses forming $T = 3$ or $T = 3$-like nucleocapsids show striking similarities both in sequence and in structure.

11.5. Replication of the togaviruses

Alphaviruses were the first viruses shown to use the route of receptor-mediated en-

---

Fig. 11.2. The surface structure of alphaviruses. A. One-sided negative staining image of Sindbis virus particles revealing a network of equilateral triangles on the surface compatible with a $T = 4$ icosahedral lattice. Negative staining with 2% potassium phosphotungstate (KPT), pH 7.4. Magnification × 170000. B. A $T = 4$ surface lattice is also seen in SFV. The lattice is formed by 5- and 6-coordinated stain-filled pits (see Fig. 11.6B). Arrow points to a particle where two 5-coordinated pits cen be seen separated by a 6-coordinated pit; a prerequisite for a $T = 4$ lattice. Negative staining with 1% uranyl acetate. Magnification × 170000. C. Freeze-etch replica of purified Sindbis virus showing a regular pattern of grooves compatible with that seen in panel A on the virus surface. The 5-coordinated pits are identified by an angle difference between the radiating grooves as compared to the 5-coordinated ones. Shadowcasting with Pt/C from the right side below. Magnification × 170000.

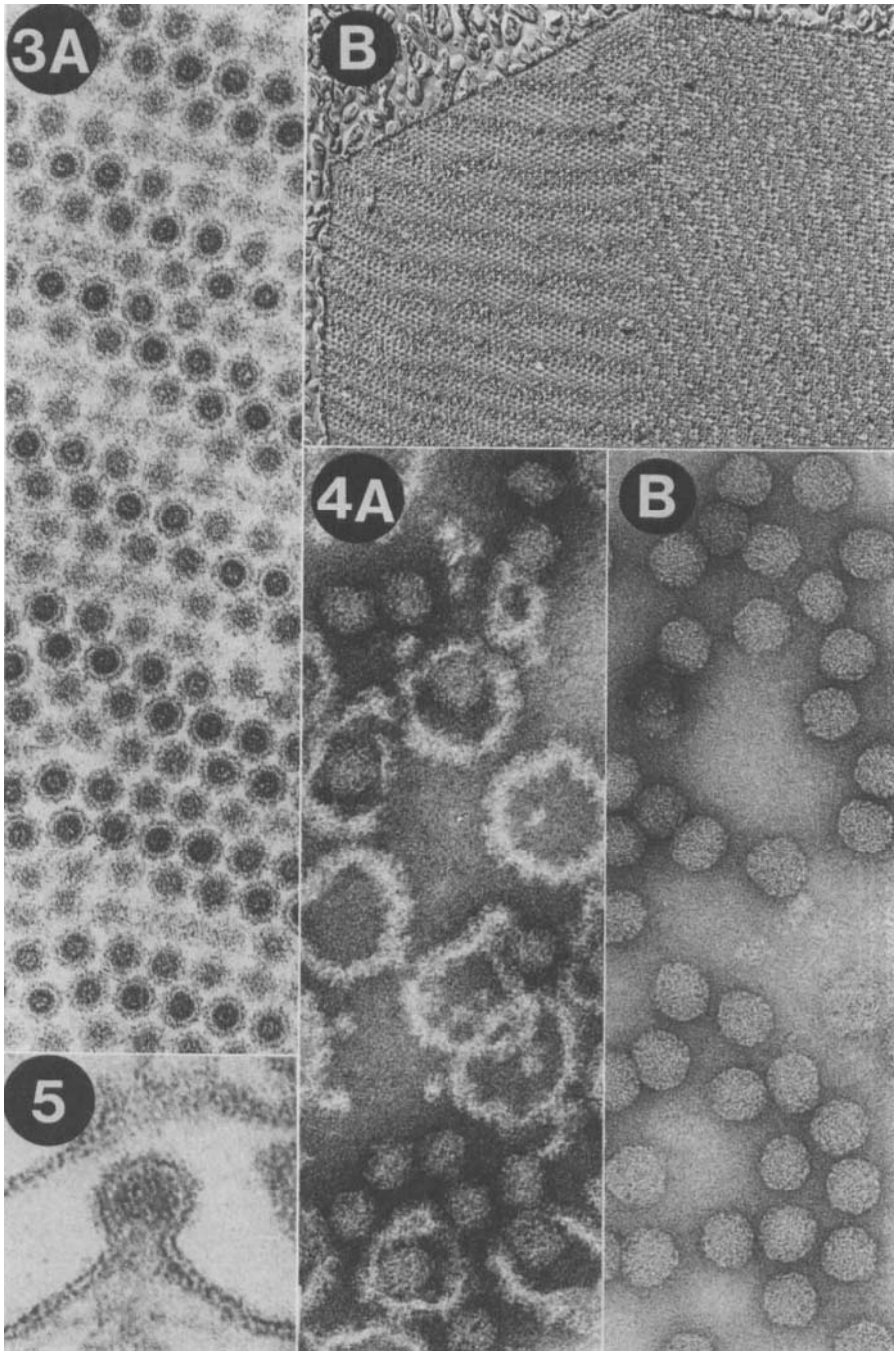
3A
B
4A
B
5

docytosis to infect their host cells. After adsorption to cellular receptors at the plasma membrane, the virus is rapidly internalized via coated pits into coated vesicles which carry the virus to the endosomes. The low endosomal pH triggers a fusion reaction between the viral envelope and the endosome membrane leading to the delivery of the nucleocapsid into the cytoplasm. The mode of translation of alphaviruses is presented in Fig. 11.1. In the cytoplasm the genomic RNA, which has a methylated cap at the 5′ end and a 50–60 nucleotide poly(A) 3′ end serves as an mRNA coding for a single polyprotein which is then cleaved to four nonstructural polypeptides. These are then responsible for the viral replication during which the 3′ third of the RNA is amplified as an mRNA for another polyprotein containing the virion structural polypeptides. A similar subgenomic mRNA for the structural proteins has also been described for rubella virus, whereas in flaviviruses the whole genome appears to serve as mRNA. The structural proteins of alphaviruses are made in the gene order C - E3 - E2 - E1. The capsid protein is synthesized in the cytoplasm and becomes bound to newly synthesized genomic RNA to form nucleocapsids. The glycoproteins are assembled into the membrane of the rough endoplasmic reticulum, and from there newly synthesized glycoproteins are transported through the Golgi apparatus to the plasma membrane. One of the glycoproteins is made as a precursor (p62) which at a late stage of the transport is cleaved into E2 and E3. In SFV E3 becomes incorporated into the virion, in Sindbis virus it is released from the cell. The nucleocapsid has been proposed to function as a template for the budding process at the cell surface (Fig. 11.5), which is envisaged to proceed by a self-assembly process. The budding site may be determined by two factors: (i) a critical concentration of spike proteins to initiate the budding; (ii) a conformational change of the spike protein,

---

Fig. 11.3. Crystal formation by SFV. A. Thin section through a pellet of SFV, which under these conditions forms small crystals. Magnification × 120 000. B. Freeze-fracture replica of an SFV crystal grown in ammonium sulphate. Magnification × 14 000. (Courtesy of F. Winkler and J. Lepault.)

Fig. 11.4. Effect of detergent (Triton X-100) on alphaviruses. A. At a low concentration (0.05%) of TX-100 the envelope of SFV swells and detaches from the nucleocapsid, which in many instances is released from the envelope. Negative staining with KPT, pH 7.0. Magnification × 200 000. B. At higher detergent concentration the nucleocapsids of Sindbus virus are released from the envelope and can be purified by gradient centrifugation. Negative staining with uranyl acetate. Magnification × 200 000.

Fig. 11.5. Thin section of a SFV particle budding from the plasma membrane of the host cell (baby hamster kidney cell, BHK-21). Magnification × 300 000.

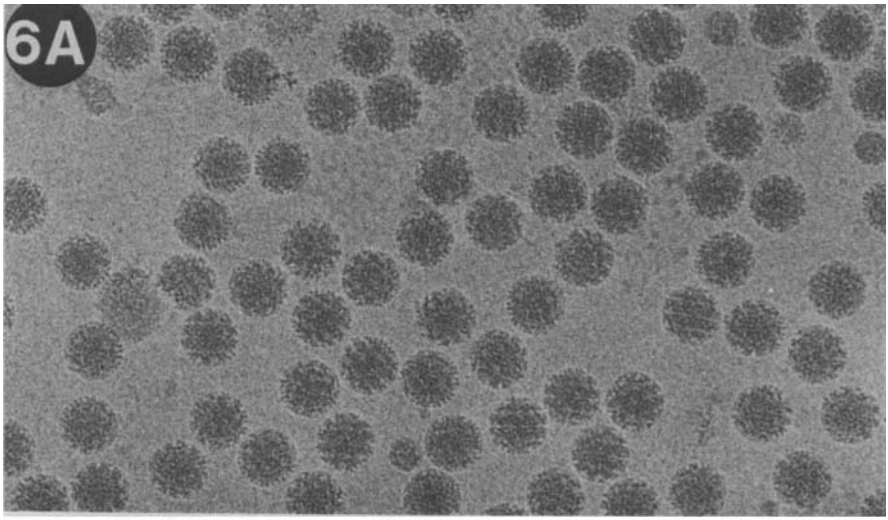
6A

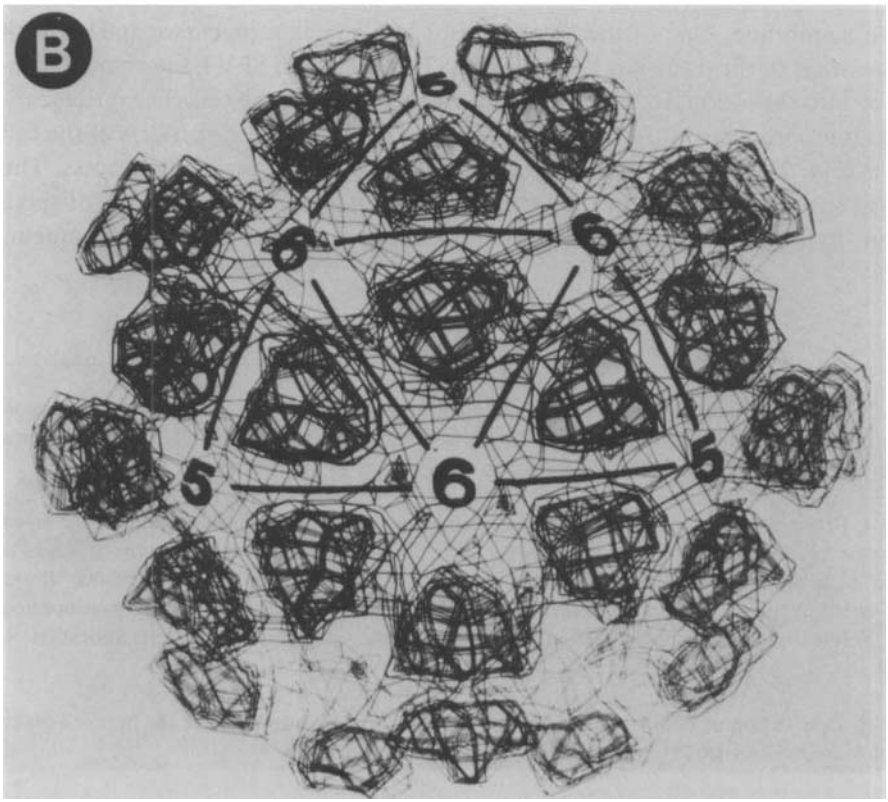
B
5
6
6
5
6
5

possibly induced by the cleavage of p62 and the ionic conditions of the extracellular environment. This conformational change would allow lateral interactions between the spike trimers to form the $T = 4$ surface lattice. The transmembrane interactions between the spike protein and the capsid which drive the budding process have not yet been studied in any detail, and they will probably not be understood before the structure of the virus particle has been further elucidated.

Not all togaviruses bud at the cell surface. Flaviviruses mature intracellularly from the membranes of the rough endoplasmic reticulum, where the capsid appears to assemble at the budding site. Rubella virus, on the other hand, has been described as budding in the Golgi area and at the plasma membrane. Also the rubella virus nucleocapsid is assembled at the budding site. Since budding occurs at the cellular site where the virus spike glycoproteins accumulate, the flavi virus and the rubella virus glycoproteins deserve further study as models for intracellular transport.

Fig. 11.6. A. Cryo-electron microscopy of unstained, unsupported Semliki Forest virus in a thin layer of vitreous ice. Magnification × 120000. (Courtesy of M. Adrian and J. Dubochet.) B. A three-dimensional reconstruction showing a section of SFV obtained by the 'optimized series expansion' method (Provencher, S.W. and Vogel, R.H. (1983) in Progress in Scientific Computing, Eds. P. Deuflhard and E. Hairer; Vol. 2, pp. 304–319, Birkhäuser, Boston) using selected particles from panel A. A $T = 4$ icosahedral surface lattice is superposed for clarity. The morphological unit is identified as a trimer. (Courtesy of R.H. Vogel and S.W. Provencher.)

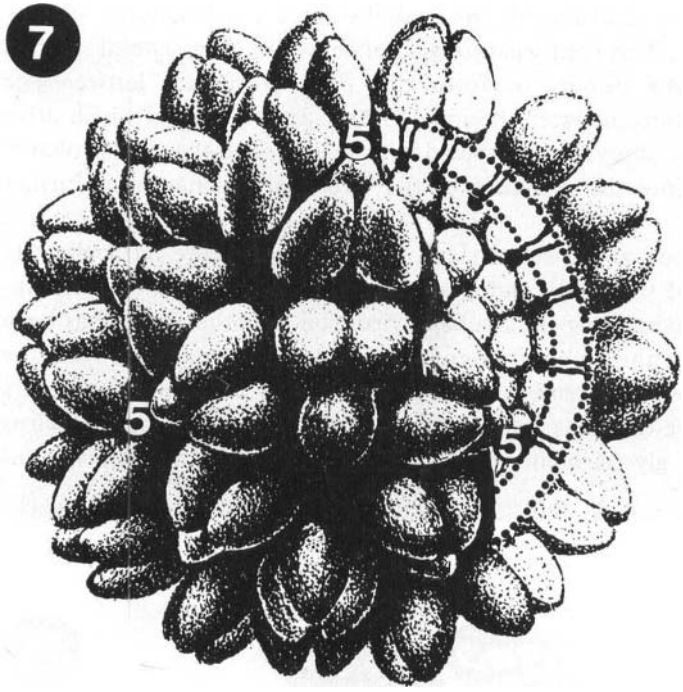

Fig. 11.7. Model of an alphavirion. The model is at the three-fold axis orientation. One icosahedral face is delineated by the 5-coordinated pits marked (5) and contains 4 trimer clusters of the spikes (each consisting of E1, E2 and E3 polypeptides). The sectioned part reveals the glycoprotein tails penetrating the lipid bilayer and making contact with the capsid, which is organized with the $T = 3$ symmetry (not shown).

Suggested reading

Adrian, M., Dubochet, J., Lepault, J. and McDowall, A.W. (1984) Cryo-electron microscopy of viruses. Nature (London) 308, 32–36.

Ahlquist, P., Strauss, E.G., Rice, V.M., Strauss, J.H., Haseloff, I. and Zimmern, D. (1985) Sindbis virus proteins nsP1 and nsP2 contain homology to nonstructural proteins from several RNA plant viruses. J. Virol. 53, 536–542.

Fuller, S.D. (1987) The $T=4$ envelope of Sindbis virus is organised by interactions with a complementary $T=3$ capsid. Cell 48, 923–934.

Harrison, S.C. (1984) Structure of Viruses. In The Microbe 1984, Eds. B.W.J. Mahy and J.R. Pattison; pp. 29–73. 36 Symp. Soc. Gen. Microb., Cambridge University Press, Cambridge, U.K.

Helenius, A., Kartenbeck, J., Simons, K. and Fries, E. (1980) On the entry of Semliki Forest virus into BHK-21 cells. J. Cell Biol. 84, 404–420.

Horzinek, M.C. (1981) Non-arthropod-borne Togaviruses. Academic Press, New York.

Kääriäinen, L. and Pesonen, M. (1982) Virus glycoproteins and glycolipids: structure, biosynthesis, biological function and interaction with host. Glycoconjugates 4, 191–242.

Schlesinger, R.W. (ed.) (1980) The Togaviruses. Biology, Structure and Replication, pp. 1–687. American Press, New York.

Schlesinger, S. and Schlesinger, M.J. (1972) Formation of Sindbus virus proteins: identification of a precursor for one of the envelope proteins. J. Virol. 10, 925–932.

Simons, K. and Warren, G. (1984) Semliki Forest virus: a probe for membrane traffic in the animal cell. Adv. Protein Chem. 36, 79–132.

Strauss, E.G. and Strauss, J.H. (1983) Replication strategies of single stranded RNA viruses of eukaryotes. Curr. Top. Microbiol. Immunol. 105, 1–98.

Vogel, R.H., Provencher, S.W., von Bonsdorff, C.-H., Adrian, M. and Dubochet, J. (1986) Envelope structure of Semliki Forest virus reconstructed from cryo-electron micrographs. Nature 320, 533–535.

von Bonsdorff, C.-H. and Harrison, S.C. (1975) Sindbis virus glycoproteins form regular icosahedral surface lattice. J. Virol. 16, 141–145.

This Page Intentionally Left Blank

Nermut/Steven (eds) Animal Virus Structure

CHAPTER 12

Coronaviridae

MALCOLM R. MACNAUGHTON[1] and HEATHER A. DAVIES[2]

[1] Boots Celltech Diagnostics Limited, 240 Bath Road, Slough, Berkshire, U.K., and [2] Clinical Research Centre, Watford Road, Harrow, Middlesex, U.K.

Family: Coronaviridae
Genus: Coronavirus
Species: Avian infectious bronchitis virus (IBV), bovine coronavirus (BCV), canine coronavirus (CCV), feline infectious peritonitis virus (FIPV), haemagglutinating encephalomyelitis virus (HEV), human coronavirus (HCV), mouse hepatitis virus (MHV), rat coronavirus (RCV), sialodacryoadenitis virus (SDAV), porcine transmissible gastroenteritis virus (TGEV).

12.1. General characteristics

Coronaviruses are spherical, lipid-containing, enveloped particles with tear-drop-shaped surface projections or peplomers. The genome is one molecule of ssRNA and the virions characteristically contain three major structural protein classes. The antigenic relationships of coronaviruses present a complex pattern. The geographic distribution of many coronaviruses is worldwide. Biological vectors of coronaviruses have not been reported, and the natural hosts form the major reservoirs for further infection.

12.2. Chemical and physical characteristics

Coronavirus particles contain three major protein classes, within which the polypeptides vary in number and molecular weight between species. The nucleocapsid protein is phosphorylated and is of molecular weight 50 000 to 60 000. The surface projection protein consists of one or two glycosylated polypeptides of molecular weight between 90 000 and 180 000. Finally, the transmembrane or 'matrix' protein is a single protein, which is glycosylated to different degrees, and has a molecular weight between 20 000 and 35 000.

The genome is a single-stranded linear molecule of RNA of positive sense, of molecular weight 5.4 to 6.9×10^6. It is polyadenylated at the 3′ terminal and capped at the 5′ terminal. The average density of coronavirus particles is 1.18 g/cm^3 in sucrose and 1.23–1.24 g/cm^3 in CsCl.

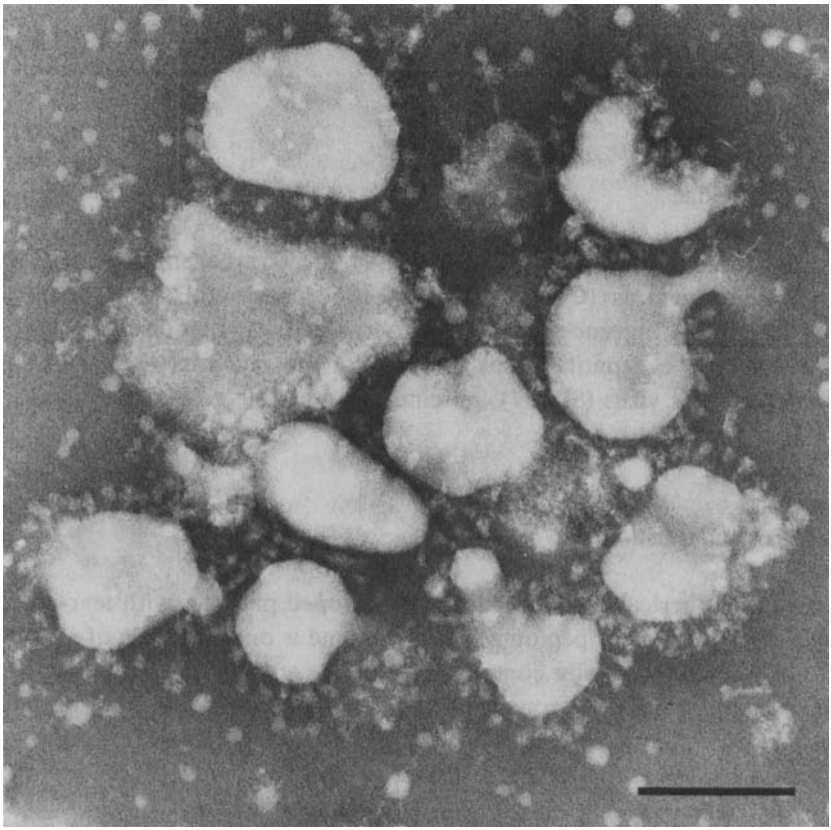

Fig. 12.1. A group of HCV 229E particles. The particles are enveloped, pleomorphic and are surrounded by a corona of surface projections. Some of the particles do not have a complete corona of surface projections. Negatively stained with 2% potassium phosphotungstate, pH 6.5. Magnification × 205 200. Bar represents 100 nm.

12.3. Structural characteristics

The apparent size and shapes of coronaviruses can vary considerably. Coronavirus particles are basically spherical, although negatively stained air-dried particles are often pleomorphic. They usually have a diameter, excluding projections, of between 80 and 120 nm, although in extreme cases the diameter can vary between 60 and 220 nm. The particles possess distinctive, tear-drop-shaped projections about 20 nm in length. Fig. 12.1 shows a preparation of typical coronavirus particles by negative staining. Particles are often seen with incomplete coronas of surface projections, which may be an artefact of preparation.

Two populations of IBV particles can be separated on equilibrium sucrose gradients. Particles with an average density of 1.18 g/cm^3 have typical coronavirus morphology and contain all the structural polypeptides and a complete genome, while less dense particles of average density 1.13 g/cm^3 have typical coronavirus morphology on negative staining but lack the nucleocapsid polypeptide and genome. These particle types can be differentiated on shadowing with carbon/platinum (Fig. 12.2). The lighter particles (Fig. 12.2a) are more flattened, producing shorter shadows than the particles with typical density of 1.18 g/cm^3 (Fig. 12.2b).

Virion architecture

The virion consists of two structural complexes: the envelope (= lipid bilayer plus two glycosylated transmembrane proteins) and the ribonucleoprotein complex. The possible arrangement of structural components within the virion is presented in Fig. 12.3. It is a tentative three-dimensional model based on our present knowledge, both morphological and biochemical.

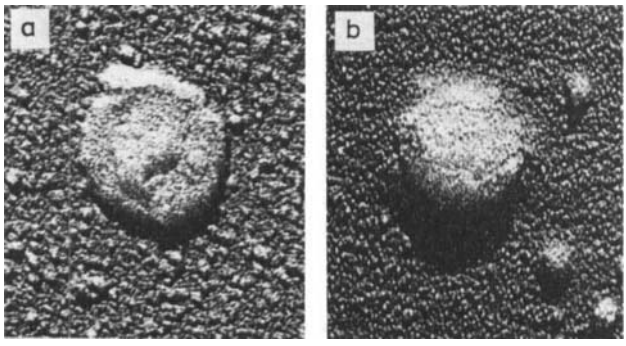

Fig. 12.2. IBV Beaudette particles from sucrose density gradients shadowed at 12° with platinum/carbon. (a) Collapsed particle from 1.13 g/cm^3 density band, showing a short shadow. (b) Particle of typical density 1.18 g/cm^3, showing a longer shadow. Magnification × 120 000. Bar represents 50 nm.

In ultrathin sections coronavirus particles display a triple-track membrane, but the surface projections are usually not visualized. Underneath the membrane is an electron-dense layer 10–20 nm wide. The centre appears usually less dense (Fig. 12.4a). However, in some species (e.g. IBV, FIPV, TGEV, BCV and MHV) the virus interior is rather electron-dense and closely apposed to the membrane (Fig. 12.4b). Finally, virus particles with a narrow electron-dense band directly beneath the membrane have also been described (Fig. 12.4c).

The different types described may be due to variation in the arrangement of 'matrix' protein and/or nucleocapsid protein and possibly the association of these two with each other in the virus particle, which may be dependent upon the virus strain and the cell type in which the virus replicates.

The morphology of coronavirus *surface projections* can vary considerably between different strains. The conventional structure on negative staining consists of tear-drop-shaped projections (Fig. 12.5a), although cone-shaped projections (Fig. 12.5b) are also observed. In all these cases the projections have the same length of about 20 nm. Other coronaviruses have short (5–10 nm) as well as 20-nm projections (Fig. 12.6). Projections with blebs on thin stalks have been reported for other coronaviruses.

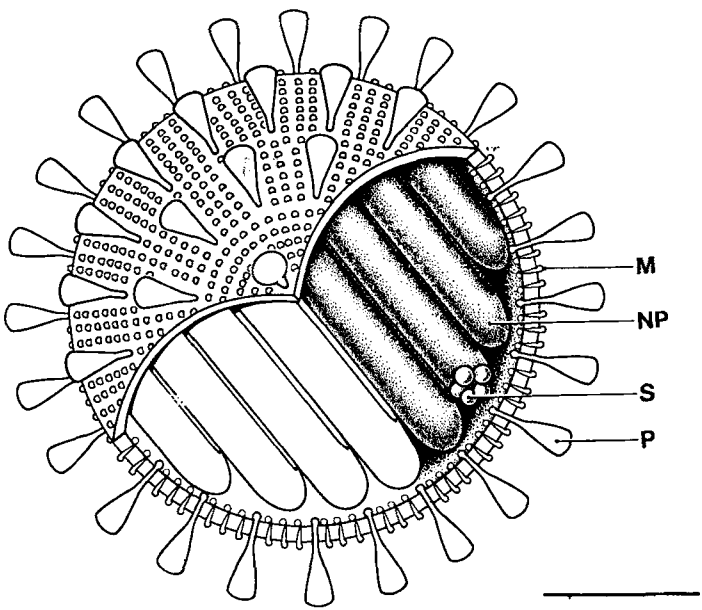

Fig. 12.3. Three-dimensional model of a coronavirus, drawn to scale. M, transmembrane protein; P, surface projection protein; NP, nucleocapsid protein; S, subunit of nucleocapsid protein. The shape of the transmembrane protein is not known. Bar represents 50 nm.

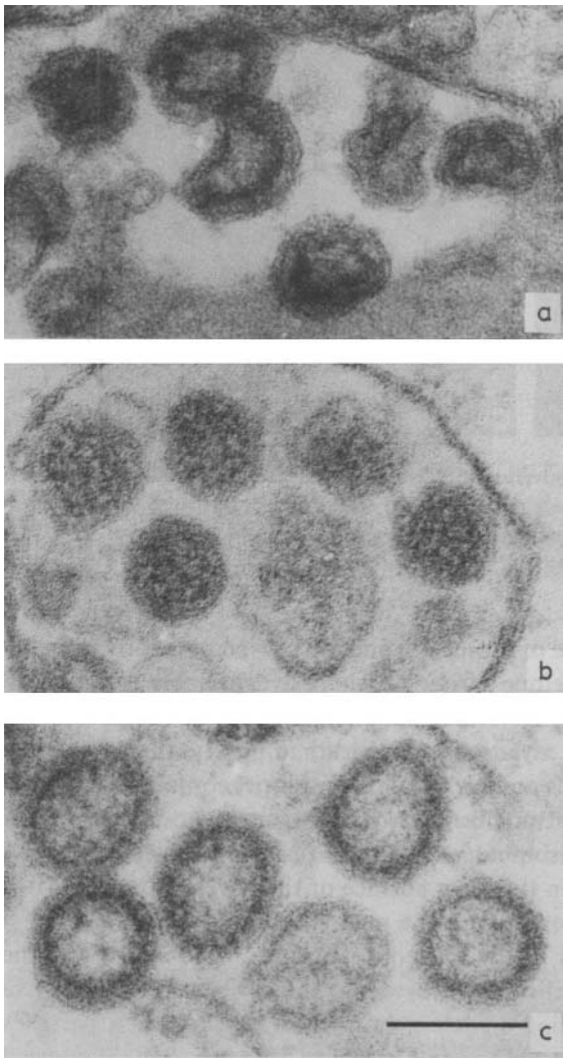

Fig. 12.4. Thin sections of purified pelleted coronaviruses grown in vitro. (a) HCV 229E grown in human macrophages, 24 hours post-infection. (b) MHV3 grown in human macrophages, 20 hours post-infection. (c) IBV Beaudette grown in the chorioallantoic membrane of a 10-day-old fertile chicken egg, 18 hours post-infection. Magnification × 185 000. Bar represents 100 nm.

Most authors suggest that the surface glycoprotein projection polypeptide is a high molecular weight glycoprotein of about 180 000 which may be an association of two non-identical subunits of about 90 000 or which can readily be cleaved into two molecules of about 90 000. IBV may be an exception to this in that the higher molecular weight form has not been observed. The surface projections can be

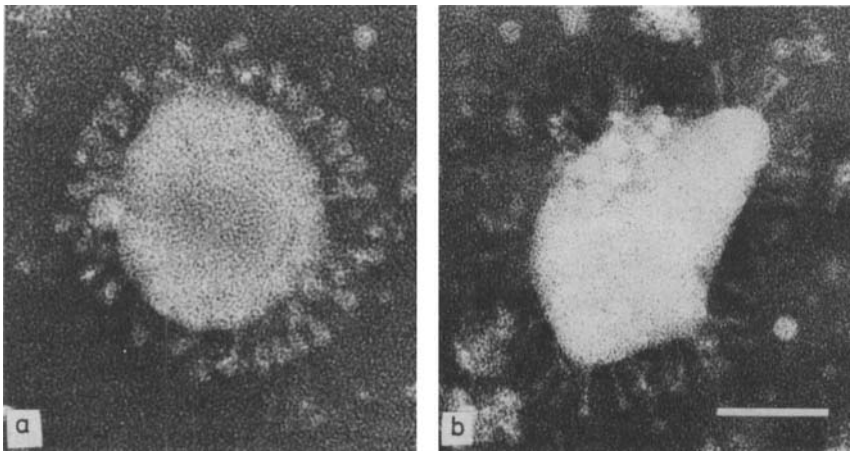

Fig. 12.5. Single coronavirus particles negatively stained with 2% potassium phosphotungstate, pH 6.5. (a) HCV 229E with tear-drop-shaped surface projections. (b) MHV3 with cone-shaped surface projections. Magnification × 307 800. Bar represents 50 nm. (Panel (a) is from Arch. Virol. 70 (1981) 301–313; panel (b) is from Arch. Virol. 59 (1979) 25–33 with permission.)

quantitatively removed by pronase or bromelain and the polypeptides are probably anchored to, or in, the viral envelope through a short hydrophobic region.

The *'matrix'* glycoprotein has a molecular weight of between 20 000 and 35 000 depending upon its degree of glycosylation and appears to possess three domains. A small hydrophilic region extends outside the viral envelope, contains all the carbohydrate of the molecule and can be removed by pronase or bromelain. A hydrophobic domain contains disulphide bonds and resides within the lipid bilayer. The third domain resides on the inner surface of the envelope, and in vitro evidence suggests that it may interact with the nucleocapsid.

The *nucleocapsid* is a complex of the nucleoprotein (M_r 50–60 × 10^3) and the RNA genome. Single-stranded helical structures have been observed by negative staining in spontaneously disrupting or detergent-disrupted coronavirus particles (Fig. 12.7). Diameters of the helices up to 14–16 nm have been reported. Shadowed nucleocapsids that have been released from disrupting virus particles reveal filaments (Fig. 12.8) similar to those observed on negative staining (Fig. 12.7).

It has been suggested that the coronavirus nucleocapsid consists of the linear genome of molecular weight 5.4–6.9 × 10^6 associated with phosphorylated nucleocapsid protein of molecular weight 50 000–60 000. The globular subunits of the nucleocapsid are 5–7 nm in the long axis and it is thought they are helically arranged and that five subunits, as shown in Fig. 12.3, represent one turn of the helix. In the virus particle, the nucleocapsid is coiled into a single-stranded helix which has been visualized inside virus particles, but is more readily observed when released from disrupted particles (Figs. 12.7 and 12.8).

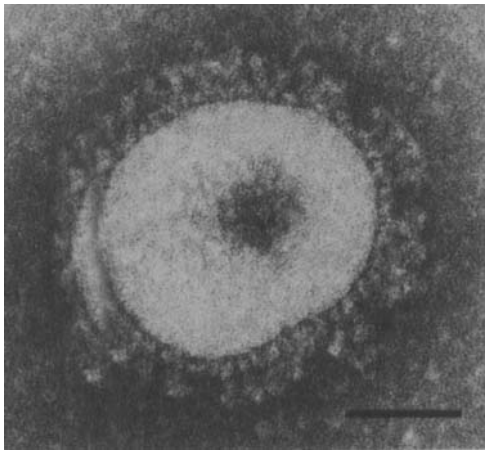

Fig. 12.6. A single particle of BCV, negatively stained with 2% potassium phosphotungstate, showing surface projections of 20 nm and the shorter ones of 5–10 nm. Magnification × 300 000. Bar represents 50 nm. (From Arch. Virol. 70 (1981) 301–313 with permission.)

12.4. Antigenic properties

Three distinct antigenic molecules are found in the virion, corresponding to each class of virion protein, i.e., surface projections, matrix and nucleocapsid protein. The surface projection antigen is involved in neutralization, virus attachment, cell-to-cell fusion activity and, where appropriate, haemagglutination. The nucleocap-

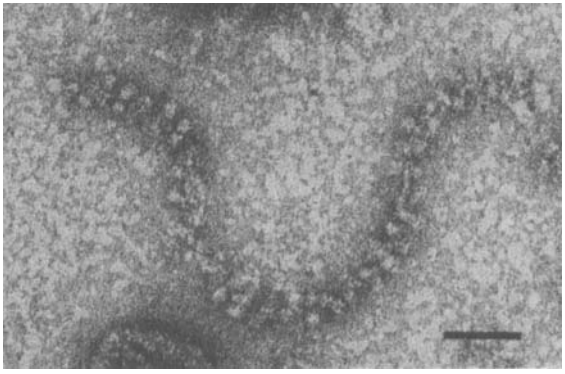

Fig. 12.7. Nucleocapsid of HCV 229E negatively stained with 1% uranyl acetate, pH 4.5. Magnification × 312 000. Bar represents 30 nm. (From J. Gen. Virol. 39 (1978) 545–550 with permission.)

Fig. 12.8. Nucleocapsids from spontaneously disrupted IBV Beaudette particles shadowed at 12° with platinum/carbon. Large arrows indicate the direction of shadowing. Magnification × 82 080. Bar represents 200 nm. (From J. Gen. Virol. 53 (1981) 67–74 with permission.)

sid protein antigens appear common to all coronaviruses. The main antigenic determinants reside in the surface projections and this antigen is used for serological grouping of coronaviruses. One avian and two mammalian serological groups have been identified (Table 12.1). HCVs are found in both mammalian serological groups, and all HCV strains belong to either the HCV 229E or the HCV OC43 serological groups.

TABLE 12.1.

Coronavirus serological groups

Group No:	1	2	3
Virus serotype	CCV	BCV	IBV
	FIPV	HCV OC43	
	HCV 229E	HEV	
	TGEV	MHV	
		RCV	
		SDAV	

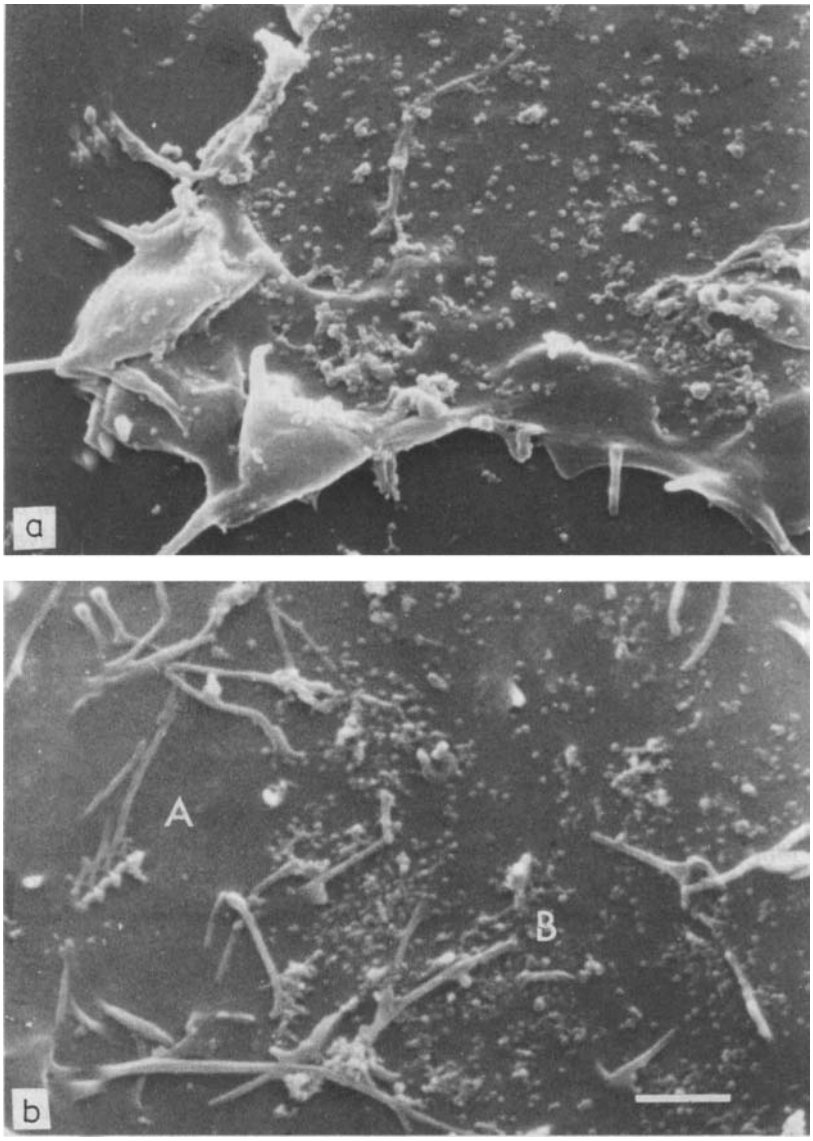

Fig. 12.9. Scanning electron micrographs of HCV 229E particles distributed on the surface of MRC continuous cells grown as a monolayer. (a) Cell prefixed with paraformaldehyde to immobilize membrane receptors and then absorbed with virus. The virus particles are randomly distributed. (b) After absorption at 0°C and then warming to 33°C for 20 min, virus particles redistribute. Region A is a peripheral area of the cell and has fewer particles than region B. Magnification × 125 000. Bar represents 1 μm. (From J. Gen. Virol. 53 (1981) 267–273 with permission.)

12.5. Biological properties

Coronaviruses bind to specific cell surface receptors via the surface projection glycoproteins (Fig. 12.9a) and redistribute to specific areas of cells (Fig. 12.9b). The marked host and tissue tropisms exhibited by coronaviruses are thought to be due to possible host cell receptor specificities. The entire replicative cycle occurs in the cytoplasm. Indeed, replication proceeds normally in enucleated cells.

Uptake of virus particles occurs by endocytosis. After 1–2 hours infection small endocytic vesicles with one or two virus particles are seen in ultrathin sections. Release of nucleocapsid probably occurs after fusion of the viral membrane with that of the endocytic vesicle. RNA is copied to produce mRNAs and subsequently protein products.

Complete virions are assembled in the rough endoplasmic reticulum (RER) or Golgi apparatus. Nucleocapsid is deposited beneath a length of membrane of the RER or Golgi vesicle in which surface projections are inserted. The vesicle then invaginates and is finally pinched off. Virus particles are released from the cell by 'reverse endocytosis' i.e. fusion of smooth-walled vesicles (Fig. 12.10, derived from the Golgi apparatus or RER) with plasma membrane, although a few reports suggest that cell lysis might occur (Fig. 12.11). Late in the infection period, virus particles may line the plasma membrane of a heavily infected cell.

Pathogenicity

Coronaviruses cause a wide range of disease in animals, including bronchitis in chickens, enteritis in calves, rats, mice and pigs, hepatitis in mice, peritonitis in cats, and encephalomyelitis in pigs. In man, disease is restricted to respiratory tract infections. These infections are generally mild and confined to the upper respiratory tract, although more serious lower respiratory tract infections can occur in children.

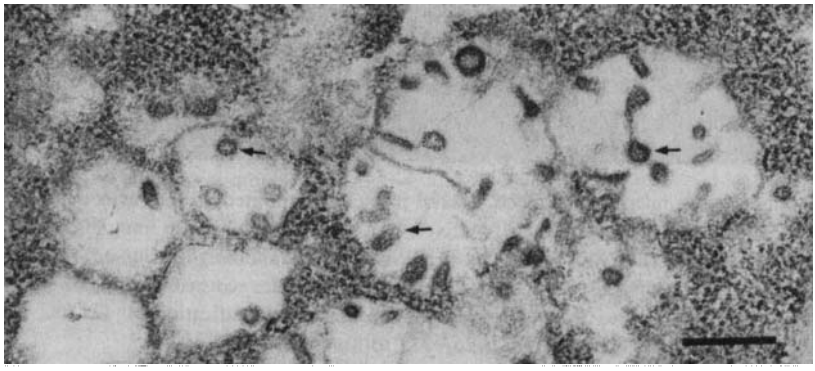

Fig. 12.10. HCV 229E particles (arrowed) in vesicles of an infected MRC continuous cell (MRCc cell line). Magnification × 41 040. Bar represents 300 nm.

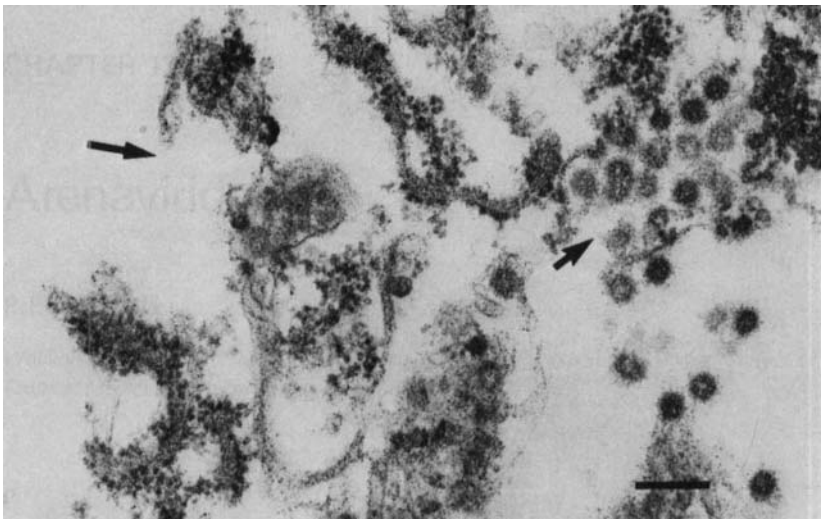

Fig. 12.11. Release of the coronavirus CV Paris from a lysed epithelial cell of calf colon. Note the absence of a limiting membrane at the edge of the cell (long arrow) and the virus-containing vesicle that has broken open (short arrow). Magnification × 47 880. Bar represents 200 nm.

Acknowledgements

We wish to express our thanks to our two typists, Deborah Ryan and Janet Gilbert, to the artist at the Clinical Research Centre, Keith Bullock, for the schematic model and to Steven Patterson for his useful comments.

Suggested reading

Davies, H.A. and Macnaughton, M.R. (1979) Comparison of the morphology of three coronaviruses. Arch. Virol. 59, 25–33.

Dubis-Dalcq, M., Holmes, K.V. and Rentier, B. (1984) Assembly of Enveloped RNA Viruses, pp. 100–119. Springer Verlag, Vienna, New York.

Siddell, S.G., Anderson, R., Cavanagh, D., Fujiwara, K., Klenk, H.D., Macnaughton, M.R., Pensaert, M., Stohlman, S.A., Sturman, L. and van der Zeijst, B.A.M. (1983) Coronaviridae. Intervirology 20, 181–189.

Siddell, S.G., Wege, H. and ter Meulen, V. (1982) The structure and replication of coronaviruses. Curr. Top. Microbiol. Immunol. 99, 131–163.

Sturman, L.S. and Holmes, K.V. (1983) The molecular biology of coronaviruses. Adv. Virus Res. 28, 35–112.

Wege, H., Siddell, S.G. and ter Meulen, V. (1982) The biology and pathogenesis of coronaviruses. Curr. Top. Microbiol. Immunol. 99, 165–200.

This Page Intentionally Left Blank

Nermut/Steven (eds) Animal Virus Structure

CHAPTER 13

Arenaviridae

P.R. YOUNG

Wolfson Unit of Molecular Medical Microbiology and Parasitology, London School of Hygiene and Tropical Medicine, Keppel Street, London WC1E 7HT, U.K.

Family: Arenaviridae
Genus: Arenavirus
Species: Lymphocytic choriomeningitis (LCM) virus, Lassa virus, Mopeia virus, Mobala virus, Junin virus, Machupo virus, Tacaribe virus, Pichinde virus, Amapari virus, Latino virus, Parana virus, Tamiami virus, Flexal virus.

13.1. General properties

The arenaviruses are a group of enveloped RNA viruses, consisting of 13 distinct members (see Table 13.1). All except one have a natural rodent host in which they cause persistent infections. The family is divided into two serologically distinguishable groups referred to as the Old World (including LCM virus - the prototype member of the group) and New World arenaviruses (comprising the Tacaribe complex of viruses).

The family name is derived from the characteristic presence within virions of fine granules ('arena' - Latin for sand) which are assumed to be host-cell ribosomes. The viruses replicate in the cytoplasm of infected cells and mature by budding through the cell plasma membrane. They have been shown to require a functional cell nucleus for replication and readily establish persistent infections in a wide range of host cells

Four members of the arenaviridae have been implicated in zoonotic infections

TABLE 13.1.

Members of the Arenaviridae

Virus	Natural host[b]	Location
Old World arenaviruses		
LCM[a]	*Mus musculus*	Worldwide
Lassa[a]	*Mastomys natalensis*	West Africa
Mopeia	*Mastomys natalensis*	Southern Africa
Mobala	*Praomys* spp.	Central African Republic
New World arenaviruses		
Junin[a]	*Calomys musculinus, Calomys laucha*	Argentina
Machupo[a]	*Akodon azarae, Calomys callosus*	Bolivia
Tacaribe	*Artibeus literatus, Artibeus jamaicensis*	Trinidad
Pichinde	*Oryzomys albigularis, Thomasomys fuscatus*	Colombia
Amapari	*Oryzomys goeldii, Neacomys guianae*	Brazil
Latino	*Calomys callosus*	Bolivia, Brazil
Parana	*Oryzomys buccinatus*	Paraguay
Tamiami	*Sigmodon hispidus*	Florida, USA; Brazil
Flexal	*Oryzomys oecomys*	Brazil

[a] Human pathogens.

[b] All arenaviruses have been isolated from rodent hosts except Tacaribe virus, isolated from fruit bats (*Artibeus* spp.).

in man leading to severe and sometimes fatal disease. These include Lassa, Junin and Machupo viruses, which are the aetiological agents respectively of Lassa fever, Argentinian haemorrhagic fever and Bolivian haemorrhagic fever. The fourth member, LCM virus, may cause inapparent infections or influenza-like symptoms and in some cases CNS involvement may follow.

13.2. Physical and chemical properties

As expected for enveloped viruses, the arenaviruses are sensitive to lipid solvents such as chloroform and ether. They rapidly lose infectivity below pH 5.5 and above pH 8.5 and are thermolabile.

The buoyant density of virus particles varies from 1.16–1.18 g/cm^3 in sucrose, 1.19–1.22 g/cm^3 in CsCl to 1.12–1.14 g/cm^3 in amido-trizoate. The viral nucleoprotein complex has a density of 1.31–1.34 g/cm^3 in CsCl and 1.24–1.25 g/cm^3 in amido-trizoate. The reported sedimentation coefficient for arenaviruses ranges from 220 to 500 S and reflects the inherent size heterogeneity of the group (see below).

The genome consists of segmented, single-stranded RNA. Five separate segments have been variably isolated from purified virus, three of which (28 S, 18

S and 4–5 S) are of host cell origin and are associated with the ribosomes incorporated into viral particles. The viral genome consists of the two remaining RNA species, 31–33 S and 22–25 S, referred to as L and S respectively. The molecular weights of these segments are $2.5–2.8 \times 10^6$ and $1.1–1.3 \times 10^6$, which correspond to approximately 7500 and 3500 bases respectively. When viewed by electron microscopy under non-denaturing conditions 'pan-handle' and closed circular structures are observed. The presence of complementary sequences at the 3′ and 5′ ends of the S RNA of Pichinde virus suggests that these circular forms arise through end-sequence base-pairing.

Three primary gene products have been identified. The nucleoprotein (N) and a glycoprotein precursor (GPC), from which the structural glycoproteins are derived by proteolytic cleavage, are coded for by the S RNA and a large molecular weight (L) protein by the L RNA. A novel coding strategy for the Pichinde virus S RNA has recently been identified. While the N polypeptide is coded in a subgenomic virus-complementary mRNA corresponding to the 3′ end of the S RNA, GPC is coded in a subgenomic, virus-sense mRNA corresponding to the 5′ end. The term ambisense RNA has been proposed to describe this arrangement.

Other structural polypeptides have been described and are summarized in Table 13.2; however, no definitive protein profile for arenaviruses has yet been establish-

TABLE 13.2.

Arenavirus proteins

Designation	M_r	Abundance (%)[a]	Location	Remarks
L	200 000	5	Internal	Possible RNA polymerase, nucleoprotein-associated
GPC	80 000	na	Cell-associated	Glycosylated precursor of structural glycoproteins
p72	72 000	2	Internal	Nucleoprotein-associated
N	62 000	60–70	Internal	Major nucleoprotein complex polypeptide phosphorylated by endogenous protein kinase
G1	54 000	10–15	Surface	Glycosylated
p47	47 000	v	Internal	Cleavage fragment of N
p36	36 000	v	Internal	Cleavage fragment of N
G2(G)[b]	34 000	10–15	Surface	Glycosylated, interacts with nucleoprotein
p25	25 000	v	Internal	Possible cleavage fragment of N
p15	15 000	2–4	Internal	Cleavage fragment of N

Information compiled from various sources: based primarily on Pichinde and LCM viruses.

[a] Based on labelled amino acid incorporation into virion structural polypeptides – average cpm values as percentage of total cpm.

[b] Some arenaviruses (Tacaribe and Tamiami viruses) contain only one structural glycoprotein (G); G1 is apparently lost or degraded.

v, present in variable amounts (<5%).

na, not applicable.

ed. Differences in the host cell, growth conditions and purification procedures employed have probably contributed to much of the observed variation.

Five separate enzyme activities have been detected in arenavirus particles. RNA-dependent RNA polymerase, protein kinase and ribonuclease activities are all found to be associated with isolated nucleoprotein complexes. Two host-derived enzymes, a poly(U) and a poly(A) polymerase, are found in association with the ribosomes incorporated into viral particles.

13.3. Structural characteristics

Shape and size: When viewed by electron microscopy arenavirus particles are spherical or pleomorphic in shape and range in size from 60 to over 300 nm in diameter (Fig. 13.1). The size distribution is generally skewed, with a mode diameter of around 110–130 nm (Fig. 13.2).

13.4. Architecture of the virion

The arenavirion is composed of a lipid envelope that is covered with surface projections surrounding an interior containing circular nucleoprotein complexes.

The viral envelope

The club-shaped surface projections that are embedded in the viral envelope are approximately 7 nm long (Fig. 13.3b). When viewed end-on, the clubbed head is shown to be approximately 5 nm wide and appears as a ring or a triangle (Fig. 13.3a). These projections are variably spaced over the viral surface in many preparations, which suggests limited lateral interactions.

Spikeless particles that are obtained following protease treatment are devoid of the virion glycoproteins (see Table 13.2), thereby implicating them as the structural components of the surface projections. However, the way in which they interact to form discrete spikes is still unclear. Chemical cross-linking studies have revealed a close association between the two glycoproteins in intact virions, suggesting that they may be components of a single projection. In addition, surface-specific radiolabelling techniques and monoclonal antibody studies have shown G1 to be the more externally disposed of the two species. These observations must be viewed, however, in the context of two members of the group (Tacaribe and Tamiami viruses) for which only a single structural glycoprotein (G) has been identified. Presumably the equivalent G1 component of these viruses is either degraded or released following cleavage of GPC. The site of cleavage of the GPC of LCM virus has been recently determined. Cleavage at the double basic amino-acid sequence Arg–Arg at residues 262–263 generates G1, comprising the amino-terminal half of GPC, and G2, which comprises the carboxyl half.

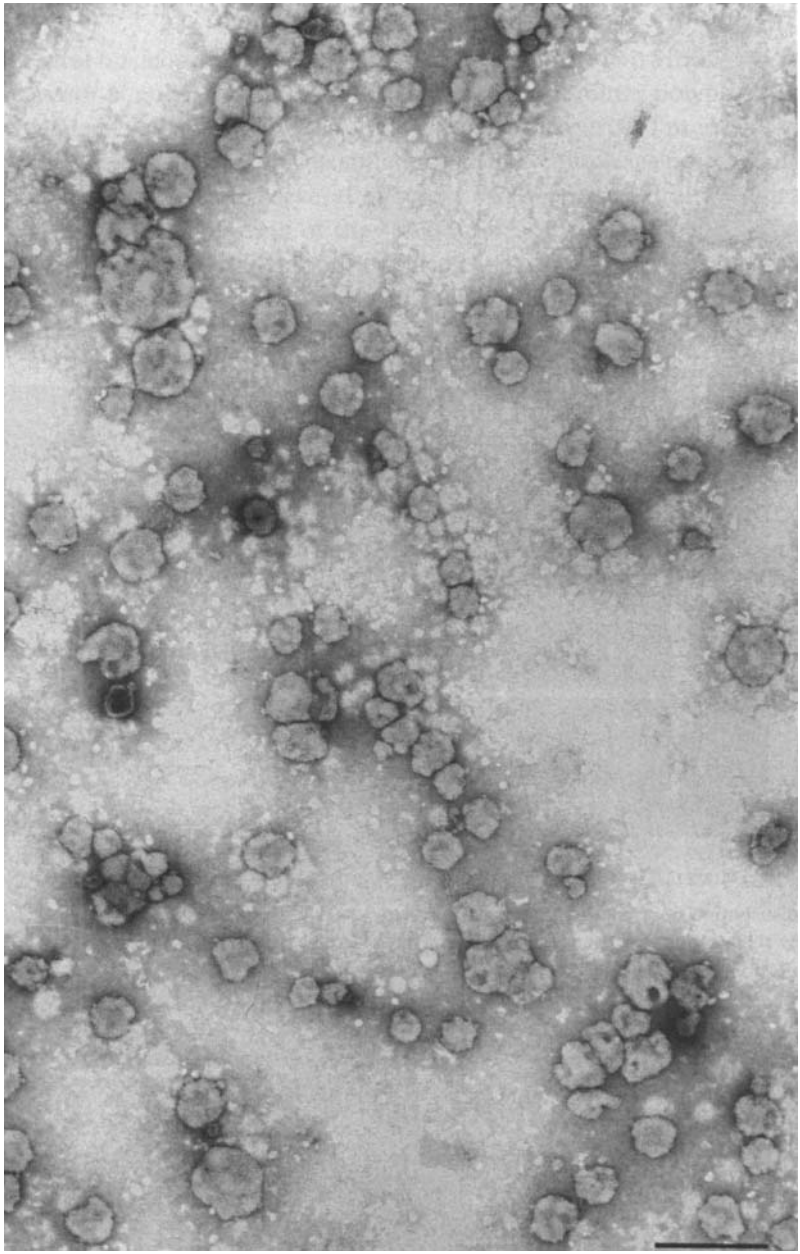

Fig. 13.1. Purified Tacaribe virus. Particle size can vary from 50 to over 300 nm in diameter after negative staining. Bar represents 200 nm.

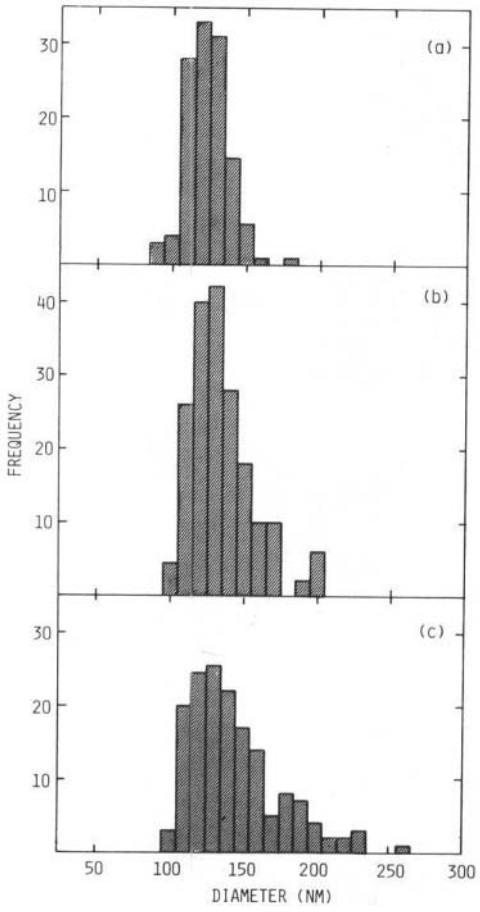

Fig. 13.2. Size distribution of extracellular particles harvested from Pichinde virus-infected Vero cells and examined by thin-section electron microscopy. Cultures were harvested at (a) 24 h, (b) 48 h and (c) 72 h post-infection.

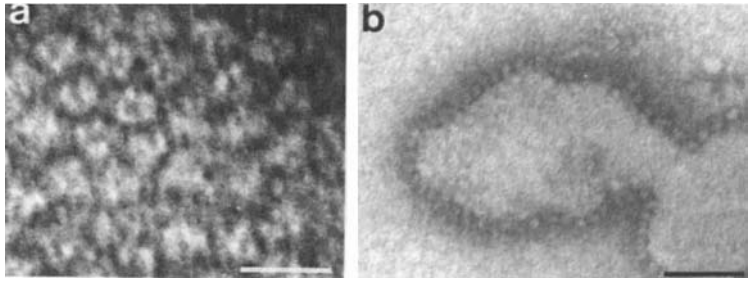

Fig. 13.3. Surface spikes of Pichinde virus. (a) Viewed head-on they are approximately 5 nm wide and appear as rings or triangles. (b) The spike is club-shaped and approximately 7–9 nm long. Bar markers represent (a) 10 nm, (b) 50 nm.

The viral nucleoprotein complex

The viral nucleoprotein (NP) complex consists of the two viral RNA segments and the major N polypeptide. In addition, a number of minor polypeptides and several associated enzyme activities have been detected in purified preparations (see Table 13.2). Electron microscopic examination of NP complexes prepared under varying conditions has revealed several different levels of structural organization.

The basic configuration of the NP is a linear array of globular units 4–5 nm in diameter with a centre-to-centre spacing of approximately 6 nm (Fig. 13.4a,b). Estimates of the molecular weight of each subunit based on size comparisons with

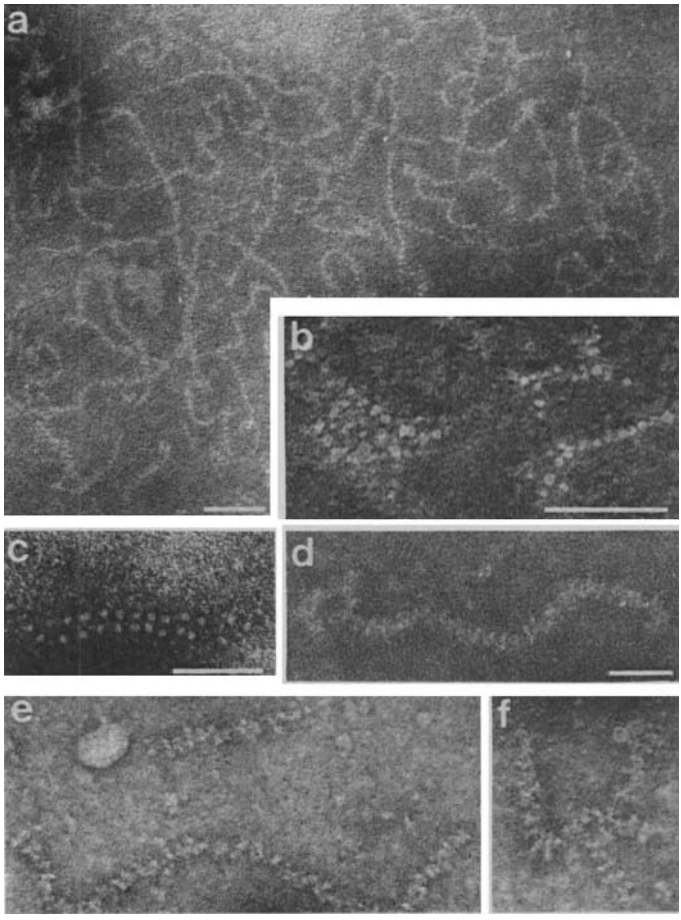

Fig. 13.4. Negative-stain electron micrographs of (a) linear array of globular subunits released from purified virus; (b) purified nucleoprotein complexes at low ionic strength; (c–f) linear structures with indication of helical organization. Bar markers represent 50 nm.

known standards suggest that they represent individual molecules of the N polypeptide. This filament appears to progressively fold through a number of intermediate helical structures which show an increasing number of subunits associated with each turn (Fig. 13.4c–f). The most stable configuration appears to be the 12–15-nm fibre forms which are regularly seen in spontaneously disrupted virus preparations (Fig. 13.5a–c). Globular condensations of approximately 15 nm in diameter are sometimes observed and are thought to arise from an association between neighbouring turns of the underlying helix (Fig. 13.6a,b).

Examination of purified NP complexes reveals closed circles (Fig. 13.7a,b) for which two predominant size classes of approximately 600 and 1300 nm have been described. However, these length distributions do not show a direct relationship with the size of the virus-specific L and S RNA species. In addition to the formation of pan-handle structures, these circular forms may also arise through interstrand base-pairing between the inverted repeat sequences at the 3′ terminus of

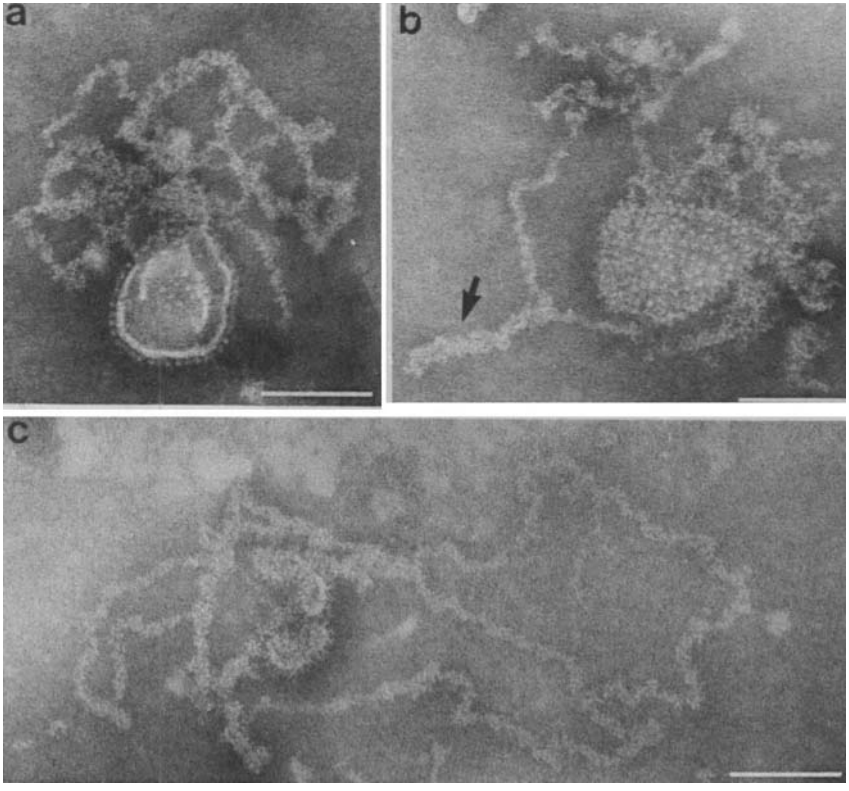

Fig. 13.5. Disrupted Pichinde virus. Twisting of the nucleoprotein fibres is frequently seen (arrowed in b). Bar markers represent 100 nm.

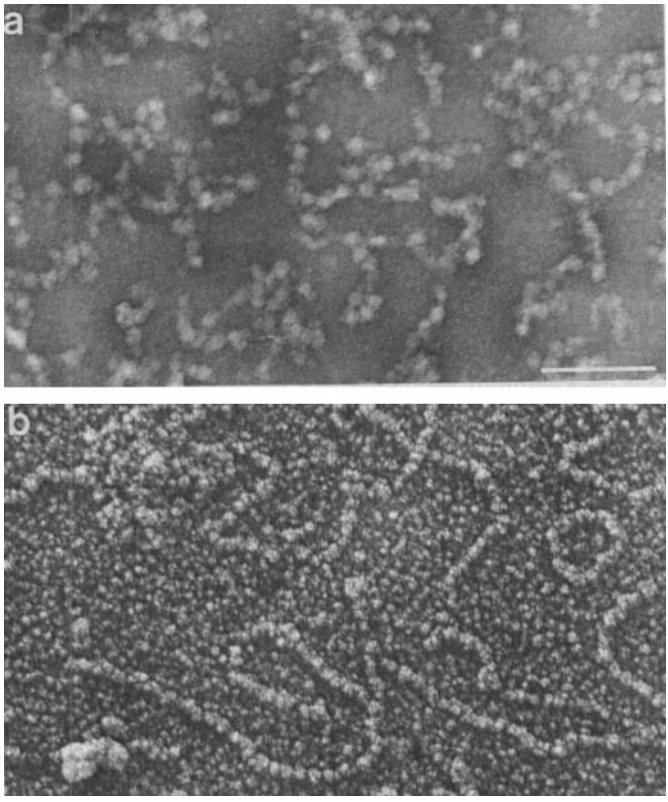

Fig. 13.6. Purified nucleoprotein complexes showing globular condensations along the strand; (a) negatively stained and (b) rotary-shadowed with platinum/carbon. Bar markers represent 100 nm.

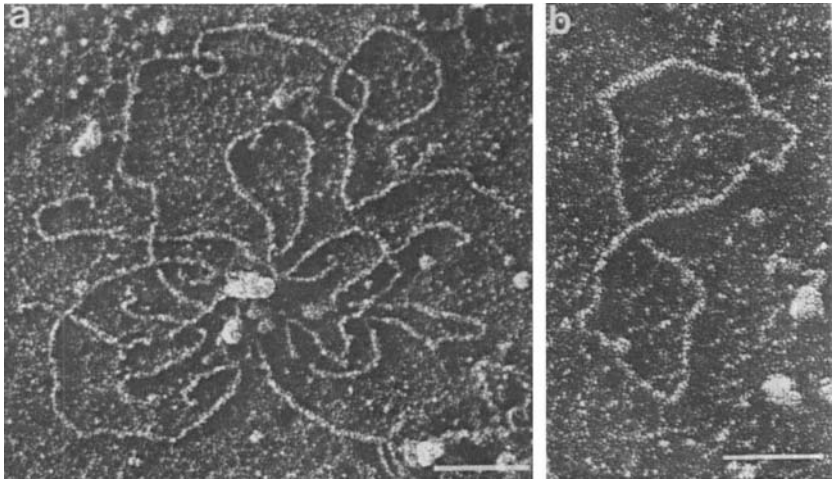

Fig. 13.7. Purified nucleoprotein complexes rotary-shadowed with gold/palladium. Both linear (a) and circular (b) forms are seen. Bar markers represent 100 nm.

both the L and the S RNA strands. Indeed, given the homology between the 3′-terminal nucleotide sequences of the two RNA species, circularization would not be restricted to specific strand interactions. The variable lengths of the NP complexes observed by electron microscopy do suggest that they may be composed of multiple copies of either one or both RNA species.

The supercoiling of many of the circular forms visualized by rotary shadowing results in the formation of filaments approximately 20 nm in diameter (see Fig. 13.5b) which are also seen in isolated viral core-like structures (Fig. 13.8a,b). These structures appear to be organized as an extensive convolution of the supercoiled filaments. However, the mechanisms involved in determining the degree of association and subsequent packaging of individual NP complexes are unknown.

Analysis of the architecture of the LCM virion by chemical cross-linking has revealed an association between the internal N protein and the G2 glycoprotein (Bruns and Lehmann-Grube, 1983). A similar interaction between this envelope glycoprotein and the NP complex of Pichinde virus has also been shown and was found to be electrostatic in nature following their effective dissociation only after detergent solubilization in high salt concentrations (in excess of 0.5 M NaCl). Whether this complex reflects an association between the glycoprotein and the N polypeptide or viral RNA is unknown. Given the apparent absence of a matrix

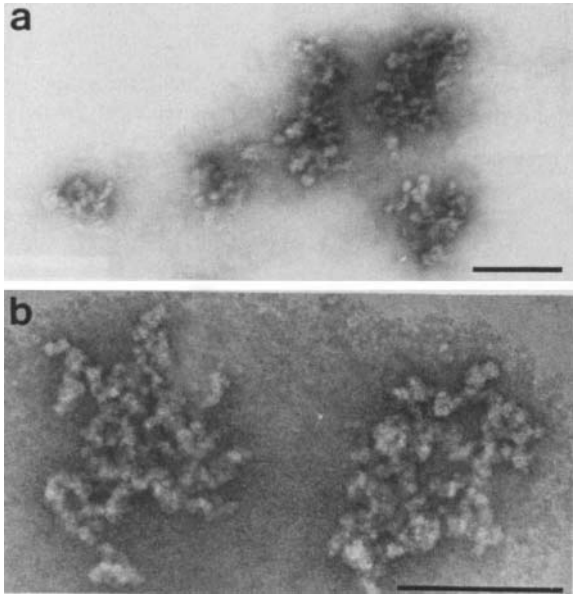

Fig. 13.8. Pichinde virus core-like structures (a) prepared by sonication of purified virus and (b) isolated from infected Vero cells. Both were separated by isopycnic urografin gradient centrifugation. Bar markers represent 200 nm.

protein for arenaviruses, its formation is likely to play an important role in the initiation of virion assembly.

Both the ribosomal material incorporated into viral particles and the L protein co-purify with NP complexes following detergent solubilization in low salt concentrations. However, ribosomes are not associated with NP complexes isolated in high salt. Additional minor polypeptides have also been identified in association with the NP (outlined in Table 13.2).

A schematic model of the structure of the arenavirion is shown in Fig. 13.9. The surface spike is presented as a simple complex of the glycoproteins G1 and G2, which are derived by proteolytic cleavage of a common precursor (GPC). The conformation and number of polypeptides within individual projections are unknown. G1 is the more externally disposed of the two species and transmembrane domains of G2 are thought to interact with the underlying NP. For Tacaribe and Tamiami viruses an equivalent G1 has not been found. The nucleoprotein (NP) is shown to be composed of a linear array of N molecules in association with viral RNA (vRNA); however, the details of this structural interaction are unknown. The NP appears to progressively fold through a number of intermediate helical structures which form closed circles that supercoil. Ribosomes and the L protein are shown in association with the NP complexes but the way in which these structures interact is not clear.

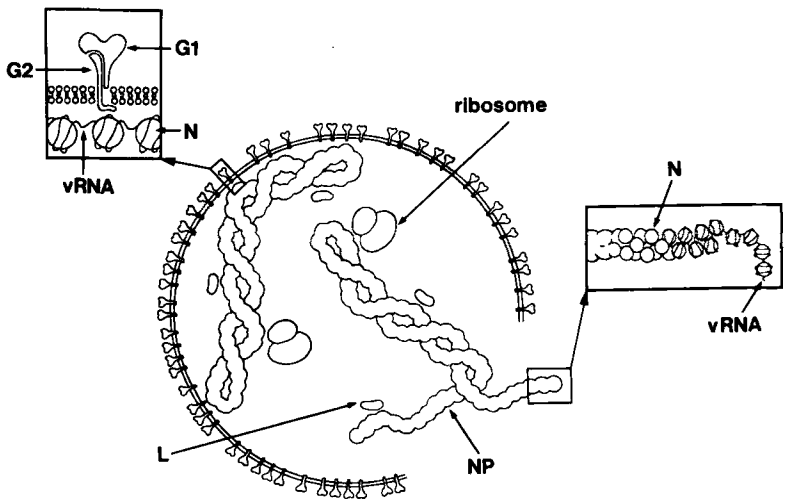

Fig. 13.9. Model of arenavirus. NP is nucleoprotein complex, vRNA is viral RNA. The way in which these species are shown to interact is schematic only; details are unknown. G1 and G2 are the surface glycoproteins derived by cleavage from a common precursor. Some arenaviruses contain only one spike glycoprotein. L is the putative polymerase. See text for details. Approximately $\times 200\,000$.

13.5. Antigenic properties

Type-specific antigenic determinants reside in the surface glycoproteins, and monoclonal antibody studies with LCM virus have shown type-specific neutralization primarily with anti-G1 antibodies. The group-specific antigens are associated with the internal nucleocapsid protein, and the broadest relationships within the group are demonstrated by complement fixation (CF). The soluble CF antigen is produced during infection and is probably composed of proteolytic degradation products of the N protein.

13.6. Virus–cell interactions

Maximal adsorption of arenaviruses to different cell lines varies from 30 to 60 min, with viropexis being complete after a further 20–45 min. RNA replication and viral protein synthesis occur in the cytoplasm and assembly proceeds by budding of NP complexes through the virally modified host cell plasma membrane (Fig. 13.10a,b). Occasional intracytoplasmic membrane involvement may lead to the accumulation of some virus particles within vacuoles. The membrane changes observed at the site of viral maturation are characteristic. Viral proteins are first inserted into the host plasma membrane and accumulate in patches, resulting in an increase in the apparent density of the membrane (Fig. 13.10a). In early harvests this modified membrane, in association with distinct surface projections, denotes the discrete boundary of nascent viral buds (Fig. 13.10b). As the virus is extruded, ribosome-like particles appear to migrate from the cytoplasm to align beneath the budding membrane and are subsequently incorporated into mature virions (Fig. 13.10c). Later in infection, more extensive and often continuous areas of modified membrane are observed (Fig. 13.10e). The extrusion of these larger sections of envelope yields a more heterogeneously sized population containing a high proportion of larger virus particles. However, the modal distribution of virion size remains essentially the same (Fig. 13.2).

During the infection, distinctive intracytoplasmic inclusion bodies are formed which consist of a complex of ribosomal particles and the viral N protein in a matrix of varying density. The degree of packing is clearly related to the course of infection, as they become progressively denser and assume smoother margins in later harvests. A functional role for these inclusions in the replication strategy of arenaviruses has not been identified.

Persistent infections are readily established in a wide range of different cell lines and in vivo in their natural hosts. Their establishment has been shown to be dependent on a number of factors, including the generation of defective interfering (DI) particles and virus variants.

Cytopathic changes in infected cells primarily involve modifications in

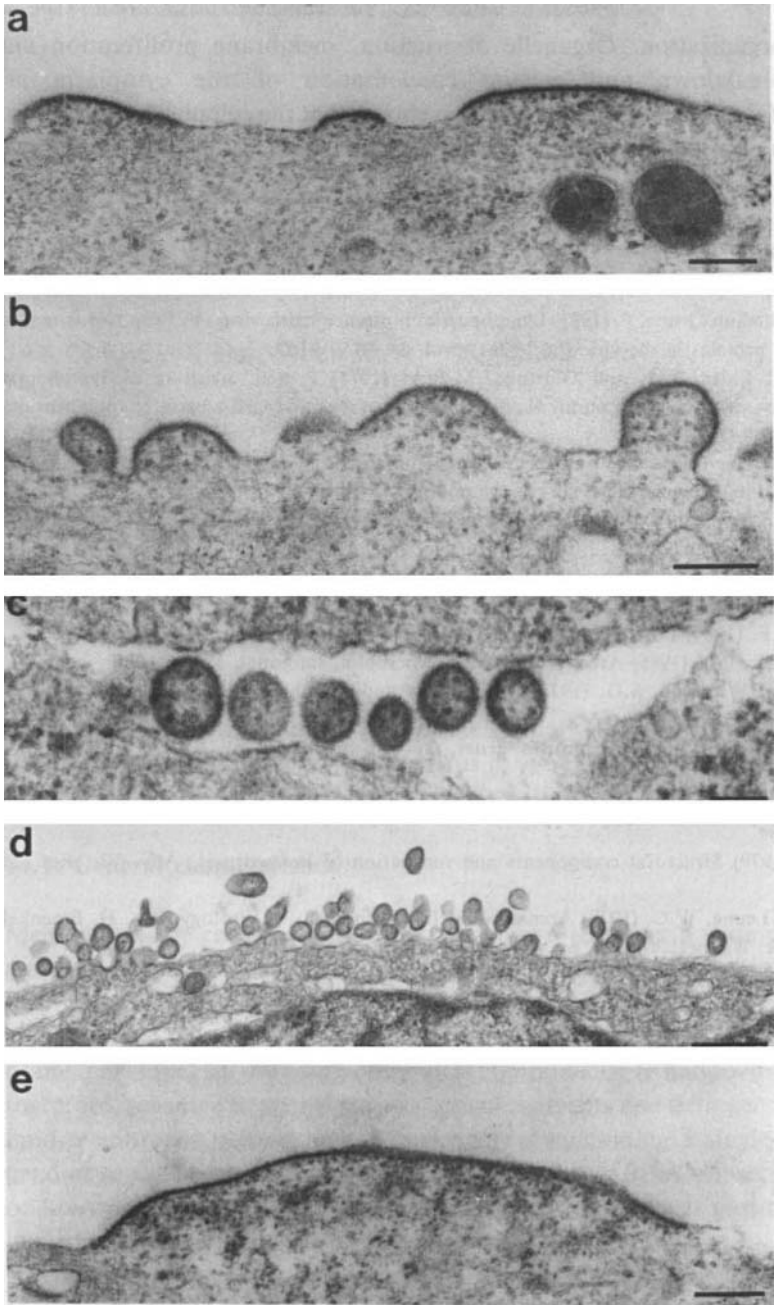

Fig. 13.10. Thin-section analyses of Pichinde virus in Vero cells showing budding and release of typical arenavirus particles. Note the characteristic presence within mature virions of electron-dense ribosome-like structures. Cultures were harvested at (a–d) 48 h and (e) 96 h post-infection; at this stage of infection extensive areas of modified membranes are observed. Bar markers represent 200 nm in a, b, c, e; 500 nm in d.

cytoplasmic organization. Organelle destruction, membrane proliferation and subsequent breakdown and general condensation of the cytoplasm are characteristic features. Although it has been shown that the cell nucleus is required for replication, no specific alteration in nuclear morphology has been observed.

Suggested reading

Bruns, M. and Lehmann-Grube, F. (1983) Lymphocytic choriomeningitis virus. V. Proposed structural arrangement of proteins in the virion. J. Gen. Virol. 64, 2157–2167.

Buchmeier, M.J., Elder, J.H. and Oldstone, M.B.A. (1978) Protein structure of lymphocytic choriomeningitis virus. Identification of the virus structural and cell-associated polypeptides. Virology 89, 133–145.

Casals, J. (1984) Arenaviruses. In Viral Infections of Humans. Epidemiology and Control, Ed. A.S. Evans; pp. 127–150. Plenum, New York and London.

Howard, C.R. and Simpson, D.I.H. (1980) The biology of arenaviruses. J. Gen. Virol. 51, 1–14.

Howard, C.R. (1986) Arenaviruses. Elsevier-North Holland, Amsterdam.

Lehmann-Grube, F. (1971) Lymphocytic choriomeningitis virus. Virology Monographs. Vol. 10, Springer-Verlag, New York.

Lehmann-Grube, F. (1984) Portraits of viruses: Arenaviruses. Intervirology 22, 121–145.

Lehmann-Grube, F. (Ed.) (1986) Arenaviruses. Med. Microbiol. Immunol. 175, 61–220.

Murphy, F.A. and Whitfield, S.G. (1975) Morphology and morphogenesis of arenaviruses. Bull. W.H.O. 52, 409–419.

Oldstone. M.B.A. (Ed.) (1987) Arenaviruses: genes, proteins and expression. Curr. Top. Microbiol. Immunol. Vol. 133.

Oldstone, M.B.A. (Ed.) (1987) Arenaviruses: biology and immunotherapy. Curr. Top. Microbiol. Immunol., Vol. 134.

Pedersen, I.R. (1979) Structural components and replication of arenaviruses. Adv. Vir. Res. 24, 277–330.

Rawls, W.E. and Leung, W.C. (1979) Arenaviruses. In Comprehensive Virology, Eds. H. Fraenkel-Conrat and R.R. Wagner; Vol. 14, pp. 157–192. Plenum, New York.

Nermut/Steven (eds) Animal Virus Structure

CHAPTER 14

Rhabdoviridae

JAY C. BROWN and WILLIAM W. NEWCOMB

Department of Microbiology, University of Virginia Medical School, Charlottesville, VA 22908, U.S.A.

Family: Rhabdoviridae
Genera: Vesiculovirus: species, vesicular stomatitis virus
Lyssavirus: species, rabies virus

14.1. General characteristics

Members of the rhabdovirus family are known to infect a wide variety of plant and animal species. Rhabdoviruses are ordinarily recognized initially by their unique bullet shape. No other virus type has the same morphology. Other properties characteristic of rhabdoviruses include: (a) the presence of a lipoprotein membrane (envelope) surrounding other viral components; (Rhabdovirus infectivity is, therefore, sensitive to agents such as organic solvents and detergents which disrupt lipid membranes.); (b) a helical nucleocapsid containing a single-stranded RNA genome of the negative (complementary to messenger RNA) sense; (c) the presence of RNA-dependent RNA polymerase activity inside the virus particle. Many rhabdoviruses are transmitted by insect vectors.

Animal rhabdoviruses are separated on the basis of serological relationships into two genera, Vesiculovirus and Lyssavirus. Ten of the thirty or more known animal rhabdovirus species have been classified in this way; the remaining species have not been studied thoroughly enough to permit their classification. The Vesiculo genus includes five serotypes (Indiana, New Jersey, Cocal, Argentina and Brazil) of vesicular stomatitis virus plus Piry, Chandipura and Isfahan viruses. The Lyssa

genus includes rabies virus, the most medically important rhabdovirus, plus Lagos bat, Duvenhage, Kotonkan, Mokola and Obodhiang viruses. Since the structure of all rhabdoviruses is thought to be fundamentally the same, this review will focus on the structure of vesicular stomatitis virus (VSV), the most thoroughly studied rhabdovirus. Overlapping material has been treated in a series of monographs edited by Bishop (1979) and in recent reviews by Wagner (1975) and by Dubois-Dalcq et al. (1984).

14.2. Physical and chemical properties of VSV

14.2.1. Morphology

Native VS virions are domed cylinders with a length of 180 nm and an outside diameter of approximately 80 nm. The overall shape is clearly visualized in electron micrographs of either negatively stained or embedded and sectioned material, as shown in Fig. 14.1. Electron micrographs also reveal two significant substructural features: (a) a series of regularly spaced cross-striations along the entire length of the virus particle, and (b) surface projections (spikes) which extend 10 nm or more out from the membrane. Complete virus particles contain 30–35 cross-striations which have a spacing (pitch) of 4.5–5.0 nm and a pitch angle of 4°. They almost certainly correspond to individual turns of the nucleocapsid helix as described below. The surface spikes (approximately 10 nm long) consist of a proximal stalk and a distinct thickening or bulb at the distal end (Fig. 14.1b).

14.2.2. Chemical properties

VSV has a total mass of 266×10^6 daltons and a buoyant density of 1.21 g/cm^3. It contains protein, lipid, carbohydrate and RNA in the proportions (by weight) shown in Table 14.1.

TABLE 14.1.

Chemical composition of VSV[a]

Component	Mass in MDa	% of total mass
Protein	198.0	74.5%
Lipid	56.0	21.1%
Carbohydrate	7.9	3.0%
RNA	3.7	1.4%
Total	265.6	100.0%

[a] Thomas et al. (1985).

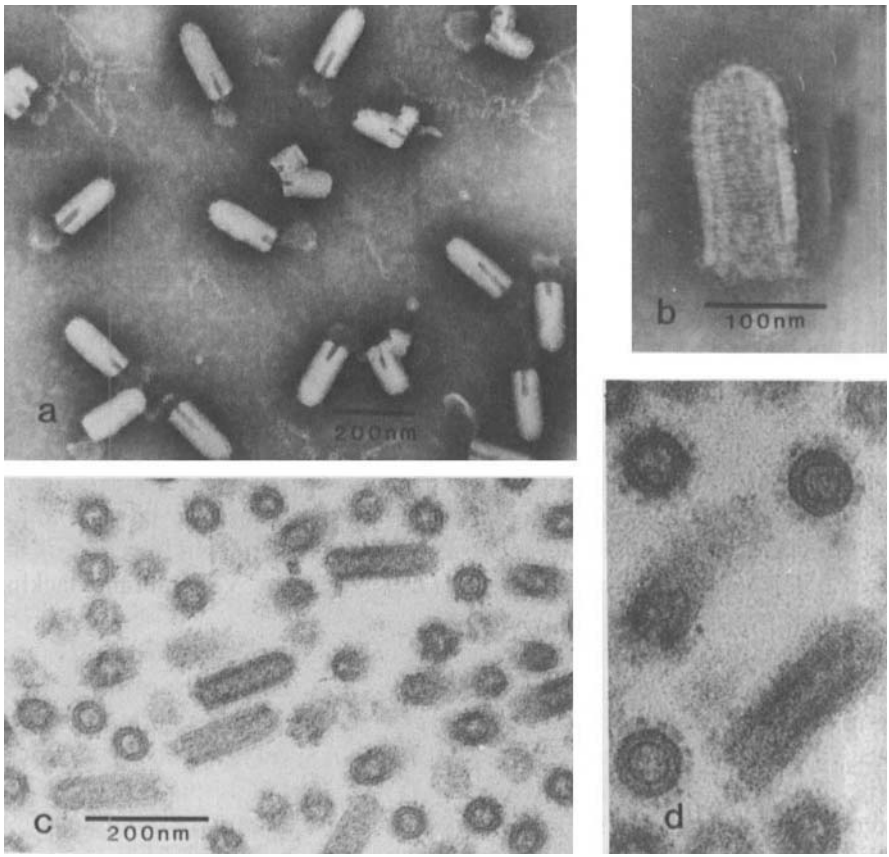

Fig. 14.1. Electron microscopy of native VSV. (a) and (b) show negatively stained preparations. Thin sections are shown in (c) and (d). (a) × 55 000; (c) × 80 000; (b) and (d) × 160 000.

The content of RNA (1.4%) corresponds to one copy per virion of the single-stranded RNA genome. VSV RNA has a sedimentation coefficient of 42 S and a molecular weight of 3.7×10^6 and is negative in sense. Recently the RNA of VSV Indiana has been sequenced (Rose and Gallione, 1981; Gallione et al., 1981; Schubert et al., 1984). The RNA is 11 162 nucleotides in length and it codes for the five VSV proteins, N, NS, M, G and L, all of which are found in the native virus. The order of the genes along the RNA is shown in Fig. 14.2. In infected cells, the five VSV genes are transcribed into separate mRNA molecules by the virion-associated RNA-dependent RNA polymerase. Most of the nucleotides in the genome (93.4%, i.e., all but the leader, trailer and four small intergene regions) code directly for the five proteins. All but the 5′-terminal 59 nucleotides (the trailer region, t) are transcribed. VSV genes do not contain introns.

The five virus-coded *polypeptides* (N, NS, M, G and L) account for nearly three-

fourths of the VSV mass. Of the five, G, N and M are present in significantly greater quantities than the other two (L and NS; see Table 14.2.).

The G protein (glycoprotein) forms spikes that protrude from the surface of the virion. It is the only VSV protein containing covalently bound carbohydrate and the only one exposed on the outside of the virus membrane. The mature G protein consists of a polypeptide chain 495 amino acids long with two identical, asparagine-linked carbohydrate groups (total M_r 6528) and a single covalently bound palmitate. The G protein is a trans-membrane protein. The overall molecule consists of three domains, a large (90.5% of the total G protein mass) external domain, a 20 amino acid trans-membrane domain and a C-terminal domain (cytoplasmic domain) 29 amino acids in length found inside the virus membrane. The external domain has a net negative charge and contains both carbohydrate groups. The internal domain has a net positive charge.

Spikes on the VSV surface almost certainly consist of oligomers of G protein, but the exact stoichiometry is not known. Dimers, trimers and tetramers are all viable possibilities. The G protein spikes are involved in attaching the virus to the host cell surface and in the membrane fusion event that results in injection of the nucleocapsid from endosomes into the host cell cytoplasm. VSV mutants lacking the G protein are non-infectious.

The N protein is the major structural component of the VSV nucleocapsid (also called the 'ribonucleoprotein' or 'template'). Nucleocapsids consist of the genome RNA to which approximately 1250 N protein molecules are tightly, but non-covalently, bound in a linear array. The morphological subunits observed in negatively stained nucleocapsid preparations (Fig. 14.3b) correspond to N protein monomers (Thomas et al., 1985). Monomers are approximately 9.0 nm long, 5.0 nm high and 3.3 nm wide. In nucleocapsids they are arranged with a center-to-center spacing of 3.3 nm to yield an overall structure with a measured length of 3.7 μm (Nakai and Howatson, 1968). Individual N protein molecules span approximately 9 nucleotides along the VSV RNA chain. In infected cells, N protein is also associated with VSV leader RNA and with full-length positive RNA strands.

The function of the N protein appears to be to protect VSV RNA from mechanical damage and from damage by ribonucleases. In nucleocapsids, the

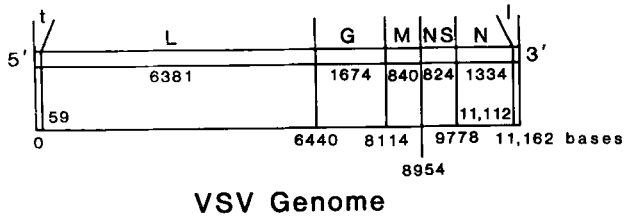

Fig. 14.2. Map of the VSV-Indiana genome. The map shows the positions of the five VSV genes (L, G, M, NS and N) plus the leader (l) and trailer (t) regions.

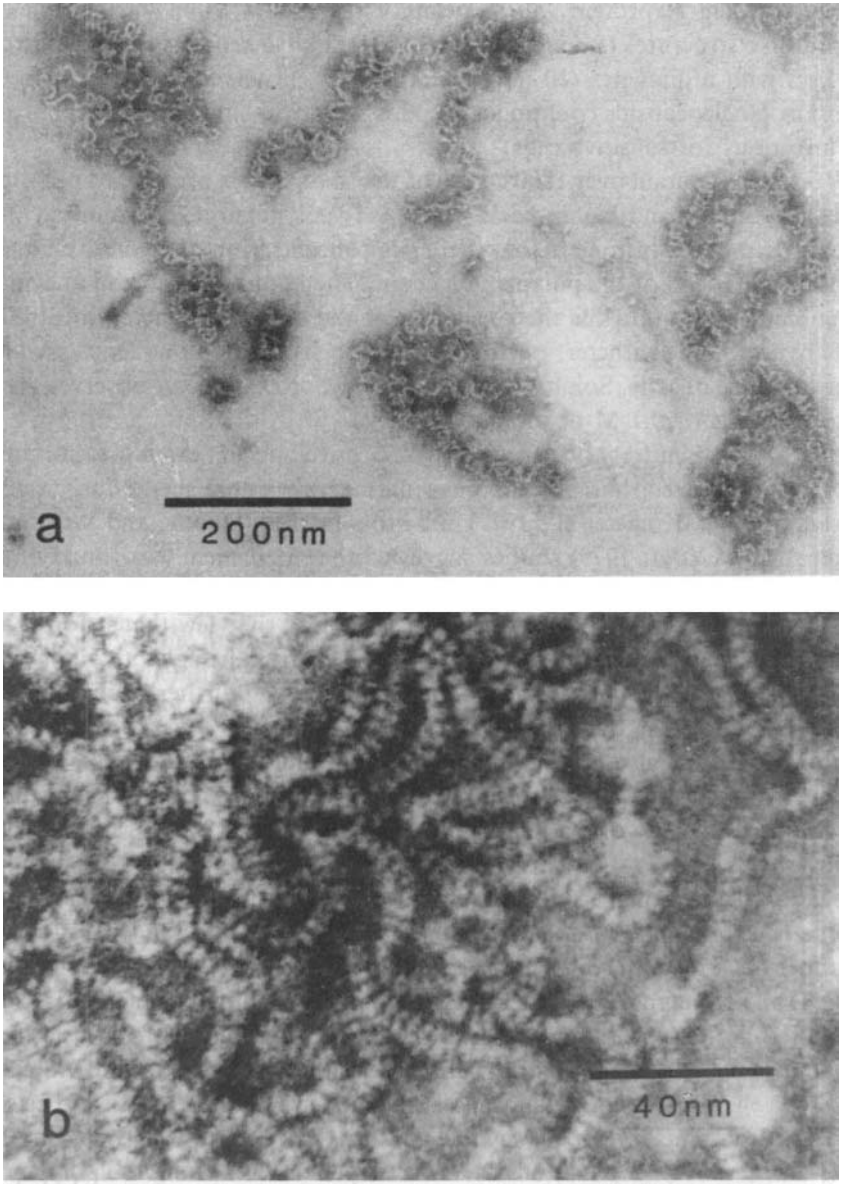

Fig. 14.3. Negatively stained VSV-nucleocapsids in (a) transmission electron microscope (× 125 000) and (b) STEM (× 613 000). Individual protein subunits are clearly visible in (b).

genome RNA is completely resistant to ribonuclease digestion in vitro. Both positive and negative VSV RNA strands must contain bound N protein in order to serve as templates for RNA synthesis by the virion RNA-dependent RNA

polymerase. Purified N protein will associate with VSV RNA in vitro to yield nucleocapsid-like structures (Blumberg et al., 1983). It also self-associates in vitro to form discs with a diameter (20 nm) similar to that observed for coils in free nucleocapsids. Nucleocapsids containing L and NS proteins, in addition to N protein, are infectious for sensitive cells.

Intact VS virions contain over 1800 copies of the M or matrix protein. M protein is a small, hydrophilic and highly basic (pI = 9.1) polypeptide 229 amino acids in length. It resembles a histone in that there is a concentration of positive charge near the N-terminal end of the polypeptide chain. The N-terminal 19 amino acids carry a net charge of +9, while the remainder of the molecule is nearly neutral. Despite its hydrophilic character, purified M protein is soluble in aqueous media only in the presence of salts. Solubility at neutral pH, for example, is observed only at ionic strengths of 0.1 M or more.

M protein is found entirely interior to the VSV envelope. Its exact location inside the virion, however, has not yet been definitively established. Early subcellular fractionation (Knipe et al., 1977) and cross-linking (Dubovi and Wagner, 1977; Pepinsky and Vogt, 1979) studies suggested that M protein was found in a thin layer between the membrane and the helical nucleocapsid. More recent reassembly (Newcomb et al., 1982) studies have supported the view that it forms a core which fills the axial channel created by the nucleocapsid helix. Both views (as well as hybrids of the two) are viable at the present time. Further experimental work is required to define the location of M protein.

In vitro and probably also in infected cells the M protein functions to condense the VSV nucleocapsid into the compact, helical form (the skeleton) which buds from the cell surface. M is often identified as an 'assembly' or 'maturation' protein to suggest this function. In vitro it also inhibits RNA synthesis by the virion RNA-dependent RNA polymerase (Carroll and Wagner, 1979), and this may be a part of its in vivo function, as well.

The L and NS proteins are components of the VS virion-associated RNA-dependent RNA polymerase; specific RNA synthesis requires both proteins. L and NS are minor components of the virus particle, accounting together for only 12% of the viral protein, as shown in Table 14.2. In native virions both L and NS are associated with the nucleocapsid which serves as the template for RNA synthesis. Free RNA is not used as a template by the VSV RNA polymerase. NS protein is heat-stable and can be phosphorylated at several specific sites along the polypeptide chain. Only the most highly phosphorylated form(s) is active in RNA synthesis. In vitro reconstitution experiments have shown that NS protein is required for binding of L to the nucleocapsid.

All the VSV *lipids* are a part of the virus envelope which is derived from the host cell plasma membrane. The virus lipid composition, therefore, bears a close resemblance to that of the host cell membrane and it varies depending on the host cell employed for virus growth (Lenard and Compans, 1974). Representative

TABLE 14.2.

Properties of the five VSV proteins

Protein	M_r	Copies per virion[a]	% viral protein (by wt.)	Location in virion	Function
G	62354	1205	36%	Spikes on envelope	Binds virus to cell surface; involved in entry of nucleocapsid into cytoplasm
N	47355	1258	29%	Main structural component of nucleocapsid	Protects RNA from RNase and mechanical damage
M	26064	1826	23%	Central core and/or inner side of membrane	Condenses nucleocapsid; inhibits transcription
L	241102	50	6%	Bound to nucleocapsid	Components of RNA-dependent RNA polymerase
NS	25110	466	6%	Bound to nucleocapsid	

[a] Thomas et al. (1985).

results for VSV-Indiana grown on BHK-21 cells are shown in Table 14.3. As with VSV grown on many vertebrate cell types, the major phospholipid species are phosphatidylcholine, phosphatidylethanolamine and sphingomyelin. The predominant fatty acyl chains correspond to palmitic (16:0), stearic (18:0) and oleic (18:1) acids. Like many mammalian cell plasma membranes, the VSV membrane has a high (0.6 or greater) molar ratio of cholesterol:phospholipid and its amino-

TABLE 14.3.

Lipid composition of VSV[a]

	% of VSV mass
Total lipid	21.1%
Cholesterol	5.9%
Phospholipid	15.2%
	% of VSV phospholipid
Phospholipid	
Phosphatidylcholine	29.3%
Phosphatidylethanolamine	36.5%
Sphingomyelin	20.9%
Phosphatidylserine plus phosphatidylinositol	10.2%
Other phospholipid	3.1%
Total	100.0%
Cholesterol:phospholipid molar ratio = 0.75	

[a] VSV-Indiana grown on BHK-21 cells (Fong, 1978).

phospholipid components, phosphatidylethanolamine and phosphatidylserine, are found preferentially in the inner phospholipid monolayer (Fong et al., 1976). The VSV membrane is consistently found to have a higher microviscosity than the host cell plasma membrane from which it is derived. In the case of VSV-Indiana grown on L-929 cells, for instance, the virus membrane microviscosity is found to be 4.90 poise at 37°C, while that of the cell surface membrane is 2.29 poise (Barenholz et al., 1976).

14.3. VSV architecture

The nucleocapsid can be considered to be the basic structural component of the VS virion. It is arranged as a helix of approximately 35 turns which together form the overall domed cylinder shape. Approximately 30 turns are of constant diameter (40–45 nm outside diameter) and form the cylindrical part of the virion. The remainder have decreasing diameters to create the dome at one end. The overall helix is approximately 160 nm long. Individual turns of the helix in the cylindrical portion of the structure contain 30–35 N protein monomers which are arranged with their long dimensions (approximately 9.0 nm) pointing radially out from the helix axis, as shown in Fig. 14.4. The nucleocapsid helix, therefore, has an axial channel 22–27 nm in diameter. The properties of the nucleocapsid helix are most compatible with the view that one end of the nucleocapsid is found at the blunt end and the other at the domed end of the overall helix. It is not known, however, which corresponds to the 3′ and which to the 5′ end of the viral RNA.

In intact VSV particles the nucleocapsid helix is tightly associated with M protein and surrounded by the lipoprotein envelope. As described above, the position of M protein inside the virion has not yet been definitively established. It is most likely to lie either between the membrane and the nucleocapsid or in the axial channel created by the nucleocapsid helix. Thin-section electron micrographs such as those shown in Fig. 14.1c indicate that the axial channel is not empty, but they give no clues about the identity of the material filling it. Recent quantitative, scanning-transmission electron microscopic (STEM) studies have indicated that the axial channel contains 10–15% of the total viral mass (D. Thomas, W. Newcomb, J. Brown, J. Hainfeld, B. Trus, J. Wall and A. Steven, unpublished observation). This could correspond to the M protein or perhaps to the L and NS proteins.

The virus envelope consists of lipids and G protein. Together, these two components account for approximately 49% of the total VSV mass. Host cell-coded proteins do not occur in significant quantities in the VSV membrane or in the virion as a whole. The lipid components of the membrane are organized as a bilayer. The external domain of the G protein molecule forms the 'spikes' which

extend approximately 10 nm out from the membrane surface. The spikes are closely packed on the virus surface (with center-to-center spacing of about 5 nm), forming a dense, external glycoprotein layer (Fig. 14.1b). The spikes are removed when intact VS virions are treated with proteolytic enzymes (see Emerson (1976) for references).

Fig. 14.4 shows a schematic representation of VSV which includes the structural features described above.

VSV defective interfering (DI) particles have the same overall structure as the standard virus except that they are shorter. This results from the fact that DI particle RNAs are shorter (because they carry deletions) than the standard virus RNA (Lazzarini et al., 1981). In intact DI particles, the shorter (by 50–75% depending on the particular DI particle) nucleocapsids are helically arranged with the same

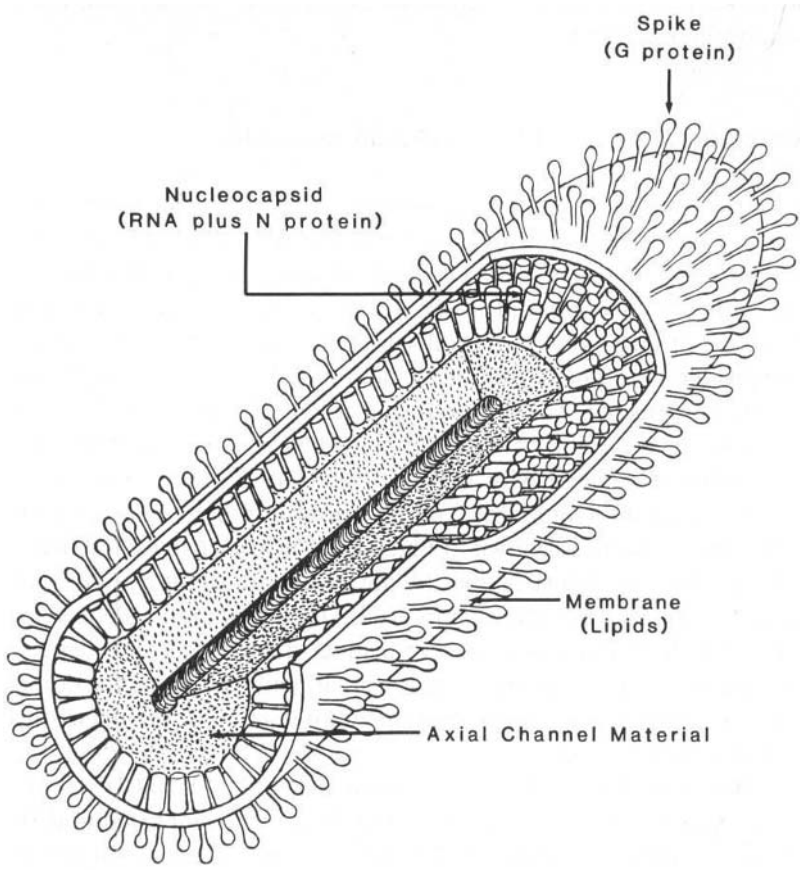

Fig. 14.4. Schematic representation of VSV. The drawing shows the coiled nucleocapsid made up of N protein subunits (represented as short cylinders). It also shows the lipoprotein envelope with G protein spikes and the filled (probably with M protein) axial channel. In the virion L and NS proteins are associated with the nucleocapsid.

helical parameters, including the same diameter, found in standard VSV. The domed and blunt ends of DI particles have the same structure as those found in standard virions. The overall length of DI particles is simply less due to the shorter RNA and, therefore, the shorter nucleocapsid.

14.4. Antigenic properties

Neutralizing antibodies to rhabdoviruses are directed to the glycoprotein, the only viral polypeptide exposed on the virion surface. Studies with monoclonal antibodies to the VSV G protein have demonstrated that there exist several different epitopes to which neutralizing antibodies may be directed. For classification purposes, rhabdoviruses are divided into serotypes based on immunological cross-reactions among the glycoproteins.

14.5. Detergent-mediated disassembly of VSV and reassembly

Controlled disruption of VSV by non-ionic detergents such as Triton X-100 or octylglucoside has provided important information about the virion structure. The extent of disassembly is found to depend critically on ionic strength. When native VSV is treated with effective concentrations (0.2% or greater) of a non-ionic detergent at low ionic strength (below a total salt concentration of approximately 0.02 M) the lipoprotein envelope is completely solubilized, but the internal components are not greatly affected. The G protein and membrane lipids are dissolved, but the nucleocapsid remains tightly condensed in the helical form found in native virions, and it remains associated with the M, L and NS proteins. The overall structure, called the 'skeleton' (comparable to the 'cores' of other viruses), has the same shape as the intact virion, as shown in Fig. 14.5. The dimensions and helical parameters of the nucleocapsid in skeletons are not greatly different from the corresponding values for intact VSV (Newcomb et al., 1982). In favorable electron micrographs (Fig. 14.5b–d) one can recognize distinct domed and blunt ends in skeletons as one can in intact virions. This suggests that maintenance of the domed end of the nucleocapsid helix does not depend on an interaction of the nucleocapsid with the lipoprotein envelope.

Detergent-induced disruption at high ionic strength ($\geqslant$0.1 M NaCl) is much more drastic. The viral G protein, M protein and lipids are solubilized and the nucleocapsid helix is completely disrupted. The nucleocapsid takes on a highly extended, more or less random coil form, as suggested by electron micrographs such as those shown in Fig. 14.3a. A significant amount (more than half) of the L and NS proteins is removed from the nucleocapsid. Solubilization of the M protein and disruption of the nucleocapsid helix at high ionic strength provide support for

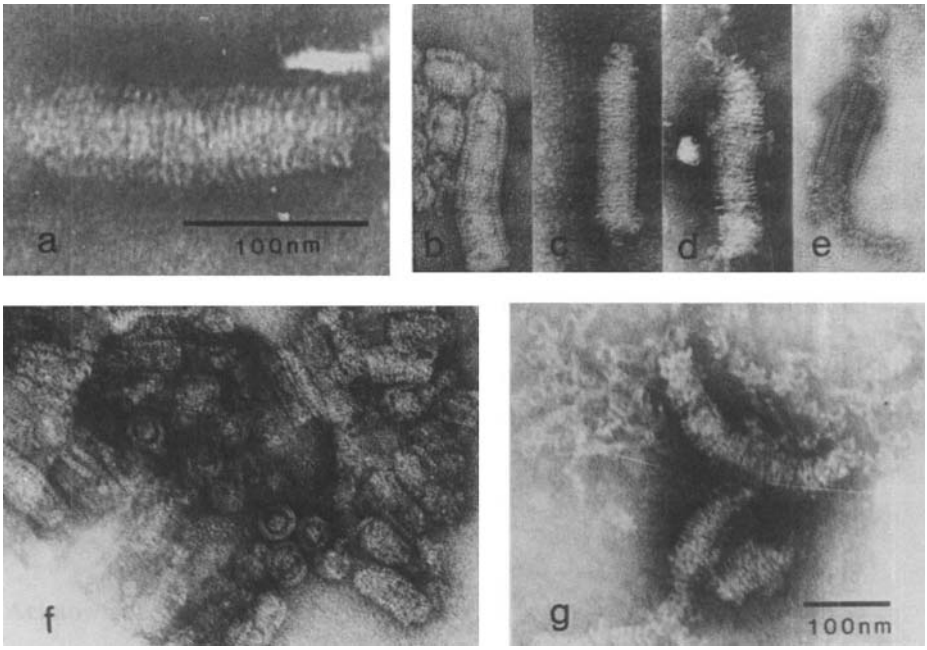

Fig. 14.5. VSV skeletons prepared using non-ionic detergent (a–f). Panel (g) shows reassembled skeletons. Negative staining. (a) × 310 000; (b–g) × 195 000.

the view that M protein is involved in maintaining the nucleocapsid in the condensed form found in native virions.

When native VSV is solubilized in non-ionic detergent at high ionic strength and then dialysed to remove salt, the M protein rapidly re-condenses with nucleocapsids to form structures nearly identical to 'native' skeletons (Fig. 14.5g). For example, the nucleocapsid forms a helix in 'reassembled' skeletons, and the helix has the same diameter and pitch found in native skeletons. These results suggest that M protein may function in vivo to condense the nucleocapsid prior to packaging into mature virions.

14.6. Virus–cell interactions

VSV is taken up into sensitive cells by endocytosis at coated pits. There probably exists a specific cell surface receptor recognized by the G protein, but so far it has not been unambiguously identified. Current evidence suggests that lipids may be involved as receptors for both VSV (Schlegel et al., 1983) and rabies virus (Wunner et al., 1984). Shortly after uptake into sensitive cells, VS virions are found in cytoplasmic vesicles which are rapidly acidified (probably by fusion with endosomes).

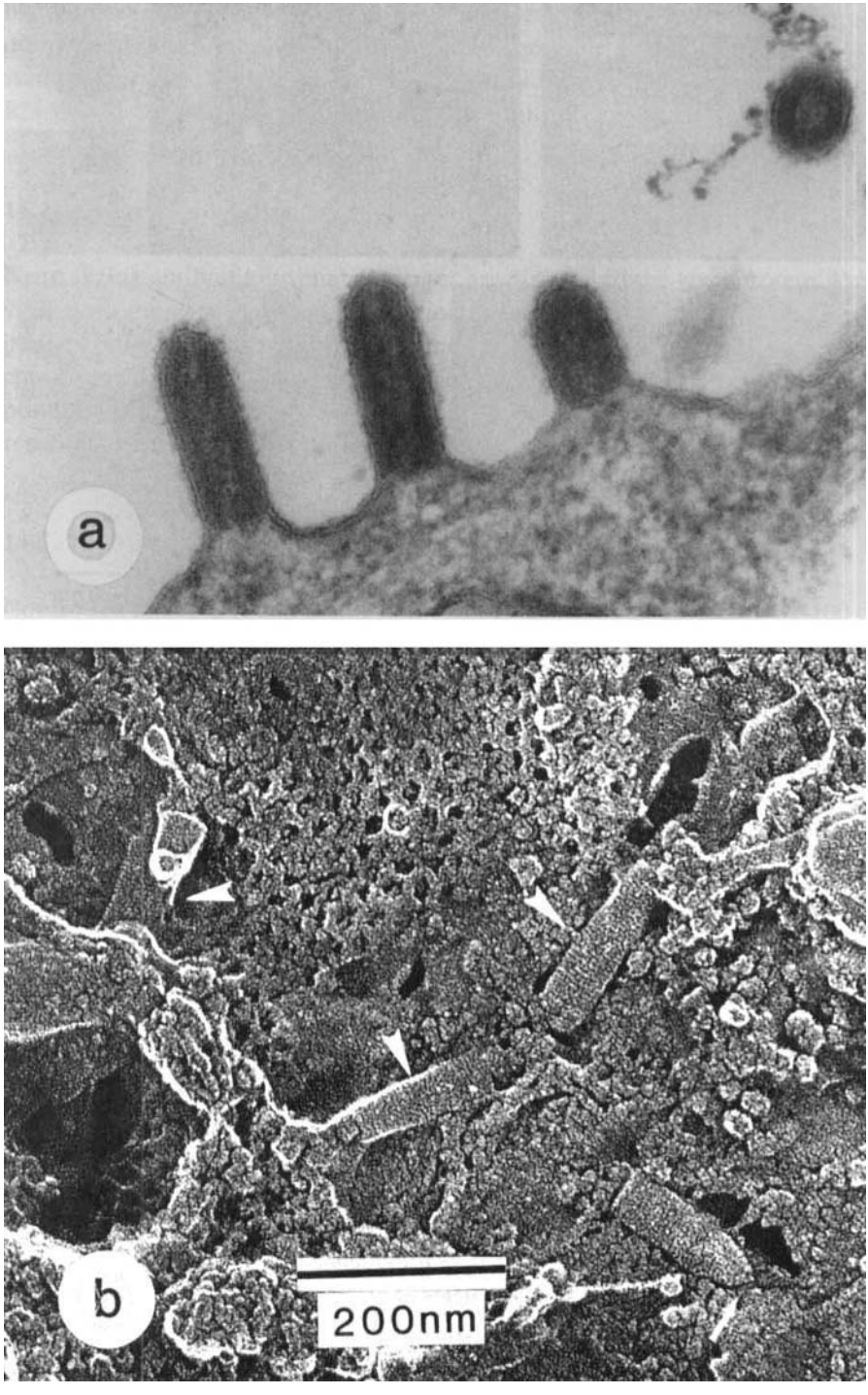
a
b
200nm

Acidification promotes fusion of the virus and vesicle membranes, which results in transfer of the VSV nucleocapsid to the cell cytoplasm. A low-pH-induced conformational change in the G protein (converting in into a membrane 'fusogen') is thought to be involved in initiation of the membrane fusion process.

Progeny virions leave the host cell cytoplasm when they mature by budding at the plasma membrane. In a complicated, but remarkably rapid, process the nucleocapsid condenses as it associates with the inner surface of the plasma membrane and buds out, domed end first, acquiring its lipoprotein envelope in the process (Fig. 14.6a). The presence of the G protein specifies the membrane site at which budding can take place, and interaction of the nucleocapsid (or skeleton) with the glycoprotein spikes is thought to provide the motive force. Depending on the host cell type and the conditions of infection, VSV may mature by budding through intracellular membranes rather than the plasma membrane. Other rhabdoviruses, including rabies virus, are frequently found to mature at intracellular membranes.

Acknowledgements

We thank Ms. N. Salomonsky for help with the electron microscopy, Drs. J. Wall and A. Steven for Fig. 14.3b and Drs. W. Odenwald and M. Dubois-Dalcq for Fig. 14.6b. Work in our laboratory is supported by NIH grant GM-34036.

References

Barenholz, Y., Moore, N. and Wagner, R. (1976) Enveloped viruses as model membrane systems: microviscosity of vesicular stomatitis virus and host cell membranes. Biochemistry 15, 3563–3570.

Bishop, D. (1979) Rhabdoviruses, Volumes I–III. CRC Press, Boca Raton, FL.

Blumberg, B., Giorgi, C. and Kolafsky, D. (1983) N-protein of vesicular stomatitis virus selectively encapsidates leader RNA in vitro. Cell 32, 559–567.

Carroll, A. and Wagner, R. (1979) Role of the membrane (M) protein in endogenous inhibition of in vitro transcription by vesicular stomatitis virus. J. Virol. 29, 134–142.

Dubois-Dalcq, M., Rentier, B. and Holmes, K. (1984) Assembly of rhabdoviruses. In Assembly of Enveloped RNA Viruses, Eds. M. Dubois-Dalcq. B. Rentier and K. Holmes; pp. 21–43. Springer-Verlag, New York.

Fig. 14.6. Maturation of VSV by budding at the cell surface. Panel (a) is a conventional thin section showing VSV budding beginning at the domed end. Panel (b) is a platinum replica showing the cytoplasmic face of the plasma membrane in BHK cells infected with VSV. Apposed to the membrane are four assembled nucleocapsids (skeletons) showing the characteristic 5 nm periodicity (arrowheads). The domed end of one skeleton is indicated by the arrow. A clathrin sheet (c) is found between the viral skeletons. (× 120000).

Dubovi, E. and Wagner, R. (1977) Spatial relationships of the proteins of vesicular stomatitis virus. J. Virol. 22, 500–509.

Emerson, S.U. (1976) Vesicular stomatitis virus: Structure and function of virion components. Curr. Top. Microbiol. Immunol. 73, 1–34.

Fong, B. (1978) Asymmetric distribution of phosphatidylethanolamine in the membrane of vesicular stomatitis virus. Ph.D. thesis, University of Virginia.

Fong, B., Hunt, R. and Brown, J. (1976) Asymmetric distribution of phosphatidylethanolamine in the membrane of vesicular stomatitis virus. J. Virol. 20, 658–663.

Gallione, C., Greene, J., Iverson, L. and Rose, J. (1981) Nucleotide sequences encoding the vesicular stomatitis virus N and NS proteins. J. Virol. 39, 529–535.

Knipe, D., Baltimore, D. and Lodish, H. (1977) Separate pathways of maturation of the major structural proteins of vesicular stomatitis virus. J. Virol. 21, 1128–1139.

Lazzarini, R., Keene, J. and Schubert, M. (1981) The origins of defective interfering particles of the negative-strand RNA viruses. Cell 26, 145–154.

Lenard, J. and Compans, R. (1974) The membrane structure of lipid-containing viruses. Biochim. Biophys. Acta 344, 51–94.

Nakai, T. and Howatson, A. (1968) The fine structure of vesicular stomatitis virus. Virology 35, 268–281.

Newcomb, W., Tobin, G., McGowan, J. and Brown, J. (1982) In vitro reassembly of vesicular stomatitis virus skeletons. J. Virol. 41, 1055–1062.

Pepinsky, R. and Vogt, V. (1979) Identification of retrovirus matrix proteins by lipid-protein cross-linking. J. Mol. Biol. 131, 819–837.

Rose, J. and Gallione, C. (1981) Nucleotide sequences of the mRNAs encoding the vesicular stomatitis virus G and M proteins determined from cDNA clones containing the complete coding regions. J. Virol. 39, 519–528.

Schlegel, R., Tralka, T., Willingham, M. and Pastan, I. (1983) Inhibition of VSV binding and infectivity by phosphatidylserine: is phosphatidylserine a VSV-binding site? Cell 32, 639–646.

Schubert, M., Harmison, G. and Meier, E. (1984) Primary structure of the vesicular stomatitis virus polymerase (L) gene: evidence for a high frequency of mutations. J. Virol. 51, 505–514.

Thomas, D., Newcomb, W., Brown, J., Wall, J., Hainfeld, J., Trus, B. and Steven, A. (1985) Mass and molecular composition of vesicular stomatitis virus: a scanning transmission electron microscopic study. J. Virol. 54, 598–607.

Wagner, R. (1975) Reproduction of rhabdoviruses. In Comprehensive Virology, Eds. H. Frankel-Conrat and R. Wagner; Vol. 4, pp. 1–93. Plenum, New York.

Wunner, W., Reagan, K. and Koprowski, H. (1984) Characterization of saturable binding sites for rabies virus. J. Virol. 50, 691–697.

Nermut/Steven (eds) Animal Virus Structure

CHAPTER 15

Orthomyxoviridae

J.S. OXFORD and D.J. HOCKLEY

National Institute for Biological Standards and Control, Blanche Lane, South Mimms, Potters Bar, Herts EN6 3QG, U.K.

Family: Orthomyxoviridae
Genus: Influenza Virus A. Species: Human, avian, equine, etc.
Genus: Influenza virus B. Species: human.
Genus: Influenza virus C. Species: human, swine.

15.1. General characteristics

In general the influenza viruses are spherical, enveloped particles with two types of surface glycoprotein spikes and with a genome in the form of eight segments of single-stranded RNA. They infect epithelial cells of the nose, pharynx, trachea and bronchi, and damage to the respiratory epithelium results in the familiar symptoms of influenza disease. Influenza A virus is the classic pandemic virus infection of humans, affecting persons in all areas of the world. Influenza B viruses cause more limited epidemics, whilst influenza C virus is even more benign clinically, although many persons have antibody, suggesting widespread infection. Influenza A virus has an extended host range that includes horses, pigs and aquatic mammals such as seals and whales and also birds, which are infected in the gut. Influenza C virus can also infect pigs but the host range of influenza B virus appears to be restricted to humans. Several genes control the virulence of influenza A viruses, and gene 4 coding for haemagglutinin is considered to be the most important.

15.2. Chemical and physical characteristics

Most biochemical work has been carried out with influenza A virus, but it is assumed that influenza B virus shares many of the same characteristics. The mass of the influenza virus has been estimated as 178–200 $(\pm 22) \times 10^6$ daltons. The lipids of the viral envelope are derived from the host cell in which the virus has replicated; they constitute up to 25% of the mass of the virion. The RNA genome amounts to 2% of the total virus mass. Nucleotide sequencing of A/PR/8/34 (H1N1) virus RNA established an ssRNA genome of 13 600 nucleotides length. Eight pieces of RNA are present, or seven segments in the case of influenza C virus, and these code for at least ten viral polypeptides which are either incorporated into progeny virus (= structural proteins) or are produced in infected cells but not found in virus particles (= non-structural proteins): see Table 15.1 for

TABLE 15.1.
Influenza A virus genome RNA and protein coding assignments

Segment	Encoded polypeptide	Length (nucleotides)	Nascent polypeptide length (amino acids)	Experimentally determined molecular weight ($\times 10^{-3}$)	Carbohydrate	Approx. No. copies per virion	% of virion protein	Remarks
1	PB2, basic polymerase protein	2341	759	87	0	50	3%	Component of RNA transcriptase. mRNA synthesis. Host cell capped RNA recognition and binding.
2	PB1, basic polymerase protein	2341	757	96	0	40	2%	Component of RNA transcriptase. mRNA synthesis. Initiation of RNA transcription: possibly has endonuclease activity
3	PA, acidic polymerase protein	2233	716	85	0	40	1.5%	Component of RNA transcriptase. vRNA synthesis. Elongation of mRNA chains?
4	HA, haemagglutinin	1778	566	225	+	400	40	Surface glycoprotein, trimer. Cleaved into HA_1 and HA_2. Major antigenic determinant. Multiple functions in virus adsorption and fusion.

Table 15.1

Segment	Encoded polypeptide	Length (nucleotides)	Nascent polypeptide length (amino acids)	Experimentally determined molecular weight ($\times 10^{-3}$)	Carbohydrate	Approx. No. copies per virion	% of virion protein	Remarks
5	NP, nucleoprotein	1565	498	56	0	620	25	Associated with RNA segments to form ribonucleoprotein: structural component of RNA transcriptase.
6	NA, neuraminidase	1413	454	240	+	100	11	Surface glycoprotein, tetramer: neuraminidase activity. Functions in virus release.
7	M1, matrix	1027	252	27	0	1200	18	Important structural component of virus: underlies lipid bilayer. May interact with HA and NA.
	M2		96		?	–	–	Spliced mRNA, non-structural protein present on surface of infected cells.
	M3		?9		?	–	–	Spliced mRNA, peptide predicted by nucleotide sequence only.
8	NS1, non-structural protein	890	230	23	0	–	–	Non-structural protein: may be involved in shut-off of host cell protein synthesis and virus RNA synthesis.
	NS2		121		0	–	–	Spliced mRNA, non-structural protein, function unknown.

See also Lamb (1983), McCauley and Mahy (1983).

coding assignments of influenza A virus. Virus RNA transcription and replication occur predominantly in the cell nucleus. Two types of RNA transcripts are detected, namely polyadenylated messenger RNAs (mRNA) and full length complementary

RNAs (cRNA), the latter to be used as templates for subsequent transcription to new virus RNA by a replicase enzyme. Replication of the virus requires host cell nuclear RNA polymerase II for production of host-derived and newly synthesized capped cellular RNAs which serve as primers to initiate viral mRNA synthesis.

15.3. Structural characteristics

Influenza A and B virions visualized by negative-staining techniques are approximately spherical and have a diameter of 100–120 nm (Fig. 15.1A). More regular spherical morphology is found in virus particles stained with uranyl acetate or examined after mild fixation with glutaraldehyde (Fig. 15.1B). Freeze-dried or frozen-hydrated virus particles are typically spherical (Fig. 15.1C and D). Scanning electron microscopy of budding virus on cells shows spherical or slightly elongated particles and occasionally long filamentous particles (Fig. 15.2A,B,C). Thus the true shape of the virus appears to be either spherical or cylindrical with rounded ends, and pleomorphism (Fig. 15.1E) is mainly an artefact of preparation procedures.

15.4. Architecture of the virion

Myxoviridae can be described as 'enveloped cores'. The lipid envelope is derived from the host cell membrane but it also contains viral proteins. Enclosed within the envelope is the core, which consists of a shell of viral protein (= core shell) containing the viral genome in the form of a nucleoprotein complex.

15.4.1. Virus envelope

Lipid accounts for approximately 25% of the dry weight of influenza virus and it is entirely located in the viral envelope or membrane, which is a typical lipid bilayer. The lipid composition of the envelope closely reflects the lipid pattern of the host cell plasma membrane although within narrow limits selective rearrangement of membrane lipids may occur.

The lipid envelope of influenza A and B virus (Fig. 15.3A) is covered with approximately 400 haemagglutinin (HA) and 100 neuraminidase (NA) glycoprotein spikes. Both types of spike extend approximately 12 nm from the lipid membrane. The HA spikes are rod-shaped structures approximately 5 nm in width but broadest at their outer end (Fig. 15.3B and D) and triangular in 'cross-section' (Fig. 15.3C). The NA molecule has a box-shaped head approximately $9 \times 9 \times 5$ nm in size which is connected to the virus membrane by a narrow stalk (Fig. 15.3E and F). The spikes on A and B viruses do not seem to have a particularly ordered

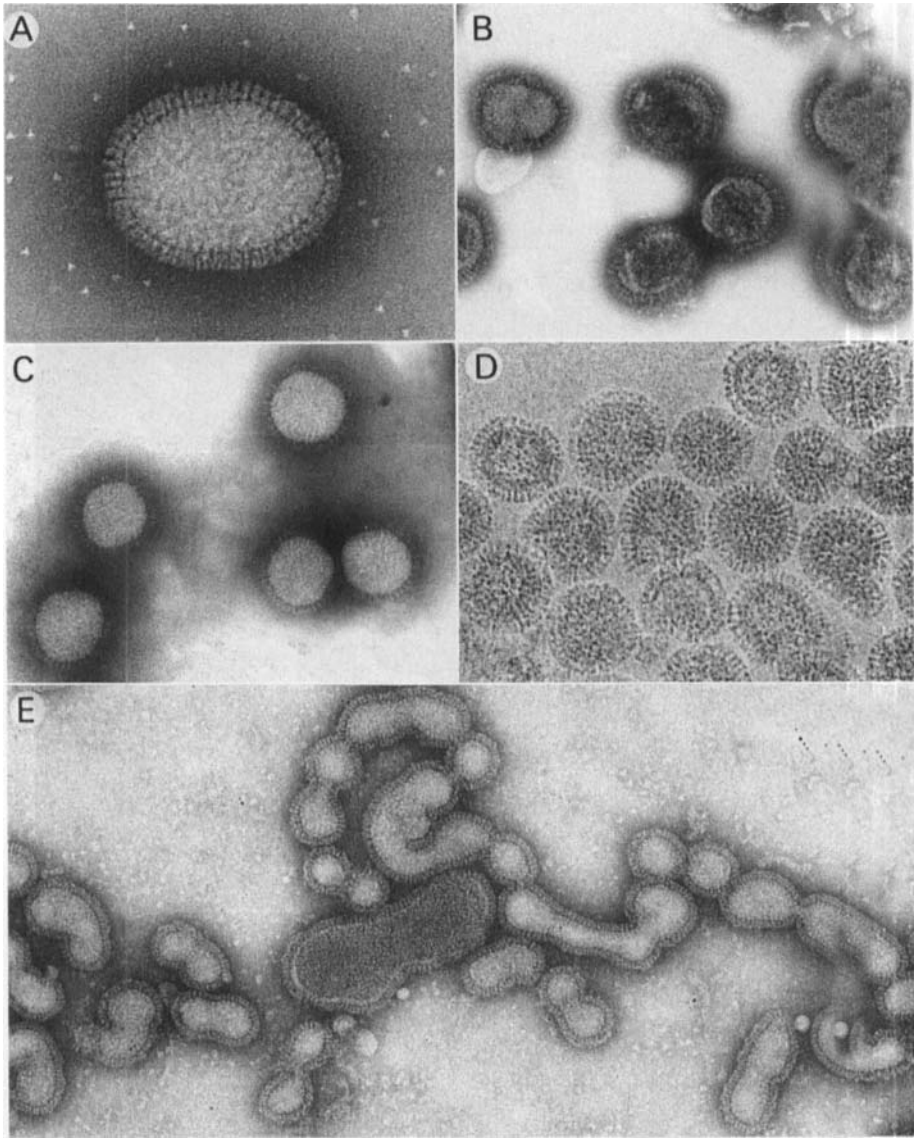

Fig. 15.1. Morphology of influenza A virus. Negative staining and transmission electron microscopy of undamaged specimens typically shows spherical particles approximately 100 nm in diameter. A. Unfixed virus, negative staining with 4% sodium silicotungstate. ×200 000. B. Virus fixed with 1.25% glutaraldehyde before negative staining. ×100 000. C. Virus freeze-dried after negative staining. ×100 000 (micrograph courtesy of Dr. M.V. Nermut). D. Frozen-hydrated, ice-embedded virus, no staining. ×100 000 (micrograph courtesy of Dr. F.P. Booy). E. Typical pleomorphic appearance of unfixed virus after negative staining with salts of tungstic acid. Variable morphology may be attributable to preparative procedures. ×75 000.

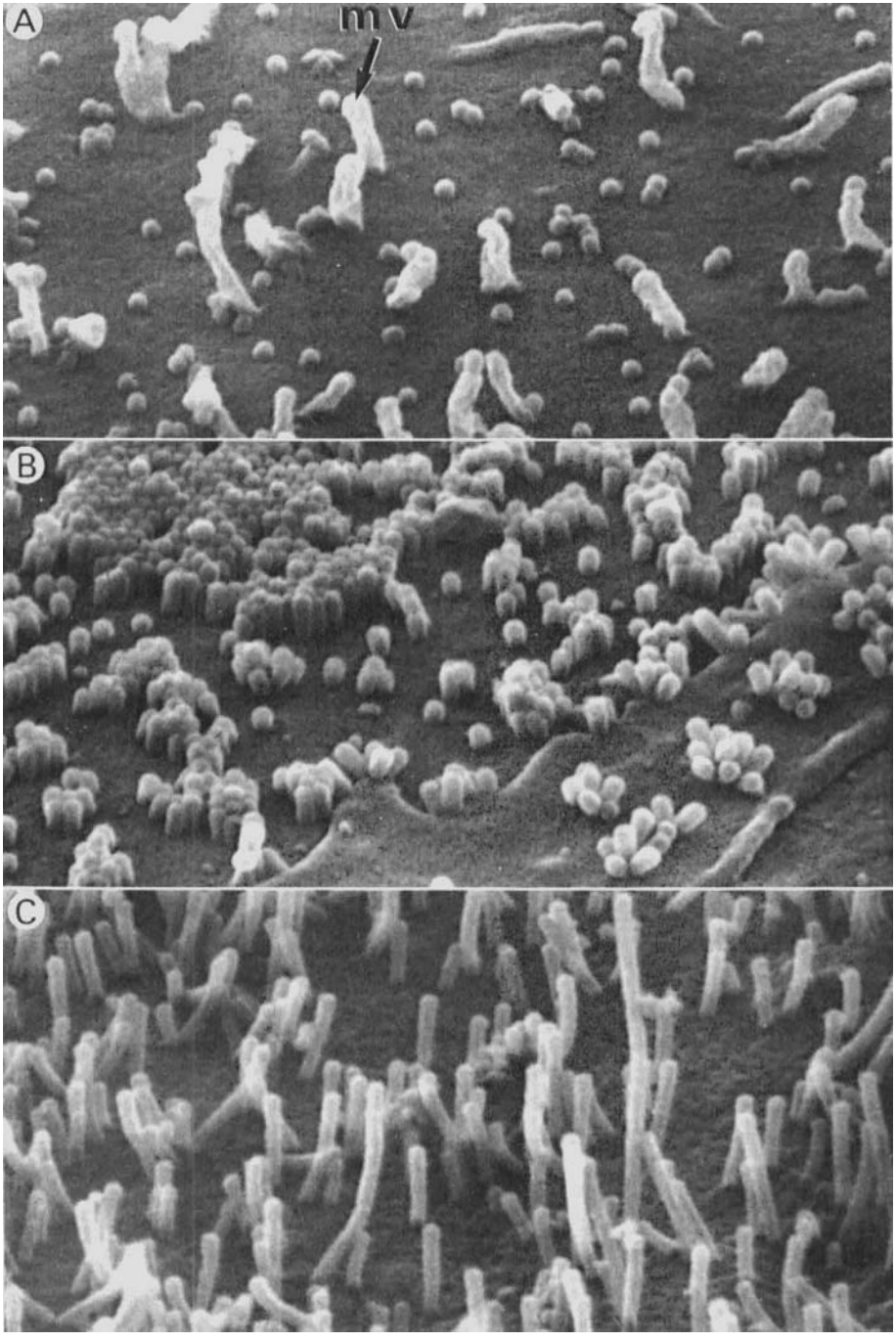
A
mv
B
C

arrangement (Fig. 15.3G) probably because of the presence of the square-shaped NA, which prevents an otherwise ordered arrangement of HA spikes. Influenza C virus has only one type of spike which may have receptor-destroying enzymatic functions as well as receptor-binding properties. This single glycoprotein of the influenza C virus is present in a regular hexagonal array on the surface of the particle (Fig. 15.3H). Both HA and NA spikes when freed from the lipid bilayer by the action of detergents tend to aggregate by their hydrophobic ends to form characteristic rosettes (Fig. 15.3D and F). Influenza HA and NA are the first two viral glycoproteins whose high-resolution structure has been determined by X-ray crystallography (Fig. 15.4).

(a) Haemagglutinin (HA)

The HA of influenza A virus was originally named because of the ability of the virus to agglutinate erythrocytes, but it is now apparent that the HA is a multifunctional protein with important roles in virus adsorption, fusion and virulence. Hydrolytic cleavage of the HA into HA1 and HA2 subunits is required before the HA can perform the latter two functions. The protein is a trimer of M_r 224 640 and comprises up to 40% of the protein of the virion. The two polypeptides HA1 and HA2 constituting each monomer are linked by disulphide bonds and the three monomers are linked together by non-covalent bonds.

The HA is a typical integral membrane glycoprotein: it has a three-domain structure with a large hydrophilic, carbohydrate-containing domain on the external surface of the membrane, an uncharged hydrophobic 'anchor' peptide of 25–28 amino acids spanning the virus membrane, and a small, hydrophilic domain of approximately 10 amino acids on the internal side of the membrane which possibly makes contact with the underlying M protein (Fig. 15.4). Typical of membrane glycoproteins, the haemagglutinin chain is initially synthesized to include an N-terminal hydrophobic 'signal' peptide, which is subsequently removed enzymatically as part of the process by which the protein is transported across the membrane.

The HA2 polypeptides form the main stem of the HA 'spike' and they contain long α-helices which terminate near the membrane in a compact five-stranded antiparallel β-sheet structure. The broad outer end of the 'spike' is composed entirely

Fig. 15.2. Scanning electron micrographs of influenza virus budding at the surface of infected cells. Note that three morphological types of particles are found. (All ×27 000). A. MDCK cells infected with A/NWS (H1N1) virus; single scattered spherical particles budding between cell microvilli (MV). Some budding particles also occur on microvilli. B. Vero cells infected with A/NWS virus; aggregates of slightly elongated viruses sometimes forming closely packed arrays. C. Vero cells infected with reassortant X-31 virus; long filamentous particles are observed which are not aggregated. The filaments can be up to 10 μm in length.

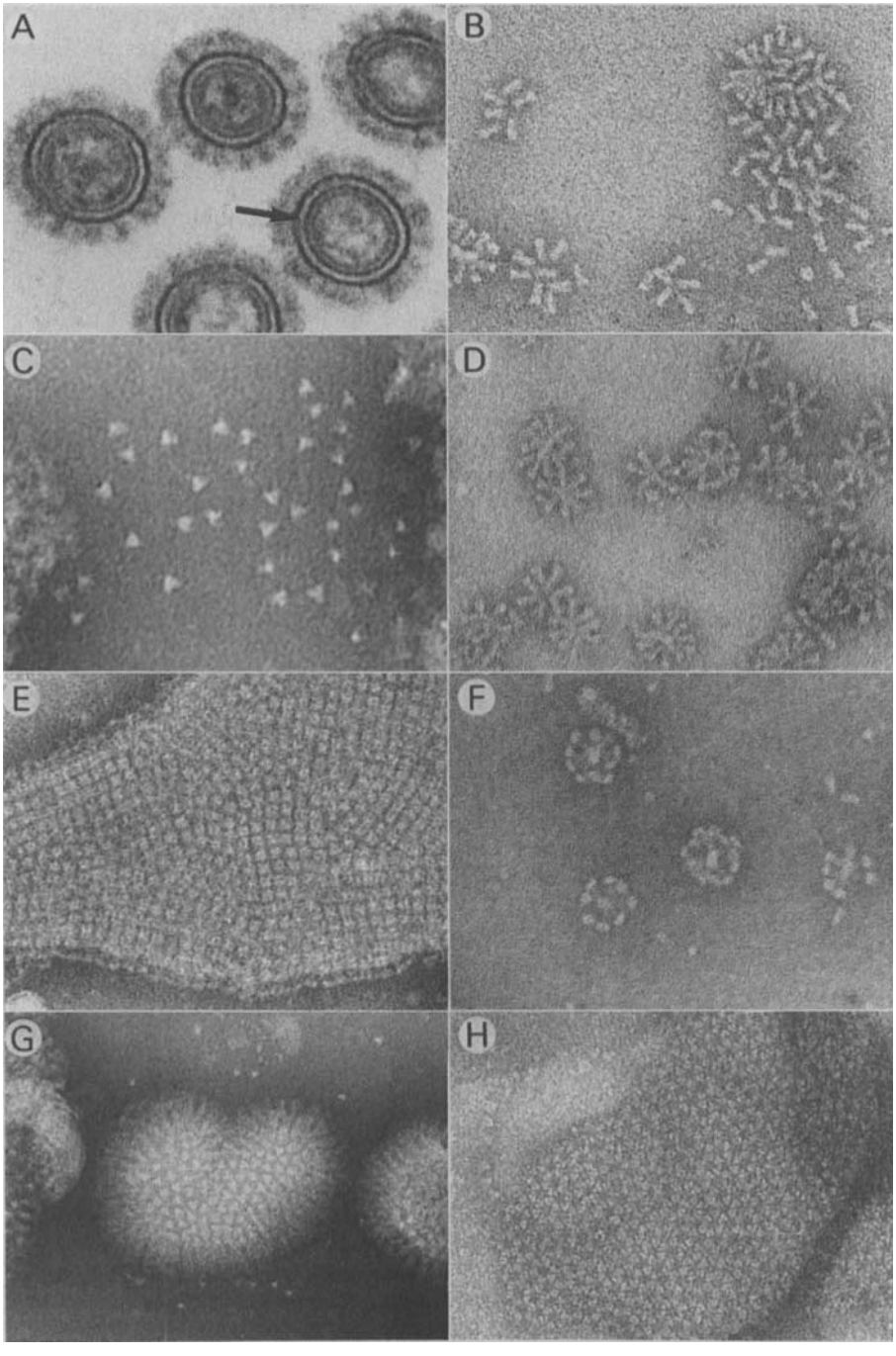
A
B
C
D
E
F
G
H

of HA1 sequences and the four (or perhaps five) variable antigenic determinants are located on the surface of this globular region (Fig. 15.4). Antibody to certain of these epitopes has virus-neutralizing activity and hence the HA is a vital component of influenza vaccines. A highly conserved region in a surface pocket on the distal end of the molecule appears to be the host cell receptor binding site. The most highly conserved sequence in the haemagglutinin molecule is the amino terminus of HA2. This sequence is associated with the fusion activity by which the virus is thought to penetrate a host-cell membrane to initiate infection (see below); it is exposed by a conformational change in the 'spike' which occurs at low pH. Several carbohydrate chains are located on HA1 and one or two on HA2 (dependent upon the subtype), all of which are linked via *N*-glycosidic linkages to asparagine residues. The carbohydrate chains are distributed along the length of the HA trimer and are located mainly on the surface of the molecule; they comprise approximately 19% by weight of the molecule. Fatty acids are covalently linked to the intramembranous portion of the HA 'spike'; they probably increase the hydrophobicity of this portion of the spike and thus have an anchoring function. There are six disulphide bonds in the HA molecule, four within the HA1 domain, one in the HA2 polypeptide and one linking HA1 and HA2.

(b) Neuraminidase (NA)

The NA glycoprotein of the influenza A and B virus surface is less abundant than HA and constitutes some 7–11% of the protein of the virion. The NA is thought to mediate virus release from infected cells but may also have a role in virus entry. It presumably prevents virus self-aggregation by removing sialic acid from the HA spike. NA subunits are tetramers of total molecular weight 240 000. The four individual polypeptide chains are held together by disulphide bonds. Unlike the HA and most membrane proteins, a hydrophobic N-terminal region in the stalk serves

---

Fig. 15.3. Morphology of influenza virus haemagglutinin (HA) and neuraminidase (NA) spikes. A. Sectioned virus showing viral membrane (arrow) with outer fuzzy covering of spikes. ×300 000. B. Negative staining of HA spikes removed from virus after breakdown of lipid membrane with detergent and separation from other components by centrifugation in sucrose gradients. The single spikes are rod-shaped and slightly broader at their outer end. ×200 000. C. HA spikes viewed end-on, showing their triangular shape in cross-section. ×400 000. D. HA spikes aggregated into rosettes by their hydrophobic ends. ×200 000. E. Aberrant virus particle covered only with NA spikes. The square-shaped end of the NA spikes can be clearly seen; they have a centre-to-centre spacing of approx 9 nm. ×200 000 (micrograph courtesy of Dr. H. Frank). F. NA spikes removed from virus and aggregated into rosettes. The box-shaped end of the spike is visible but the narrow stalk can only be seen in the centre of the rosette where the hydrophobic ends are aggregated. ×200 000. G. Whole influenza A virus showing triangular ends of HA spikes which are irregularly arranged. ×200 000. H. Influenza C virus showing hexagonal arrangement of glycoprotein spikes. ×200 000 (micrograph courtesy of Dr. R.W.H. Ruigrok).

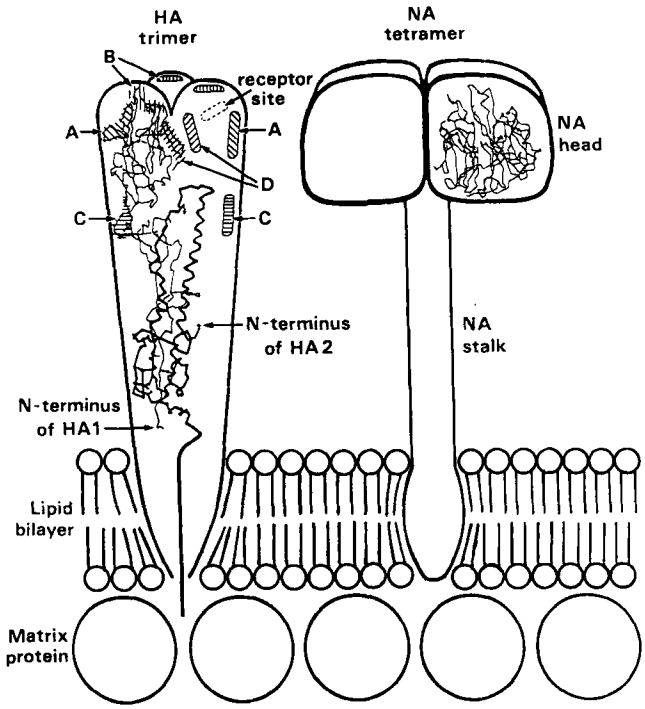

Fig. 15.4. Diagram summarizing features of the three-dimensional structure of HA and NA spikes and their possible relationship with the lipid bilayer (= membrane) and matrix protein. The HA1 polypeptide chain is shown as a thin line and HA2 as a thick line. The diagram indicates the extension of the C-terminus of HA2 through the lipid bilayer with a known hydrophobic portion spanning the membrane and a short hydrophilic region existing on the internal side of the membrane; the folding pattern of this portion of the polypeptide chain is not known. It might be expected that physical contact with matrix protein would be achieved but definitive evidence for this is lacking at present. Three long helices in the HA2 chains, one from each monomer, pack together as a triple-stranded coiled-coil to form the stem of the trimer. The N-terminus of HA2 (fusion-activation site) is deeply embedded in the spike at neutral pH but may be exposed at pH 5.0. HA1 forms a globular outer region of each monomer and contains the host-receptor binding sites and the antigenic sites A, B, C and D (site C may be subdivided to give a fifth epitope). The polypeptide chain then loops back again, with the N-terminus of HA1 adjacent to the viral membrane (Wilson et al., 1981; Wiley et al., 1981). The polypeptide chain of the NA monomer is composed of six identical folding units arranged in a propeller formation when viewed from above, down the axis of the spike. The 4-fold molecular symmetry of the tetramer is stabilized in part by metal ions bound on the symmetry axis. The catalytic sites are located on the upper corners of the box-shaped tetramer. Antigenic determinants form a nearly continuous surface across the top of the monomer and encircle the catalytic site. A hydrophobic region in the NA stalk spans the lipid bilayer and a short sequence may be present on the cytoplasmic side (Varghese et al., 1983; Coleman et al., 1983). As noted above with HA, it is possible that the NA stalk makes contact with the matrix protein, although there is no evidence of this at present.

to anchor the neuraminidase in the virus membrane and it is long enough to span the lipid bilayer of the virus (Fig. 15.4). The slender stalk is also unexpectedly rich in carbohydrate, with approximately half of the oligosaccharides of the NA. The remaining carbohydrate chains are found on the top and bottom of the box-shaped NA head, and one oligosaccharide is found at a subunit interface. The folding of the NA polypeptide chain is considered to be unique. Each monomer contains six β-sheets; each sheet contains four strands with the topology of a 'w'. Viewed from above the head, each monomer consists of six of the four-stranded sheets arrayed like the petals of a flower, but twisted like the blades of a pinwheel.

The enzymatic and catalytic site of the NA protein is surrounded by 14 conserved and charged amino acid residues and contains three hydrophobic residues also found in the sialic acid recognition sites of influenza HA. Important antigenic determinants cluster around the enzyme active site on the NA and hence are more disperse in their location than are the epitopes on HA.

15.4.2. Virus core

The core of myxoviridae is a delicate structure difficult to isolate from the lipid envelope and thus it has not often been considered as a distinct morphological structure. It consists of a core shell (thought to be formed from M protein) which encloses the nucleoprotein complex of the virus (often referred to as the nucleocapsid).

(a) Core shell and M protein (M1, M2, M3)

M1 (also called M, major, membrane or matrix) is one of the more abundant proteins in the virion and is considered to function as a stabilizer of virus structure, and possibly as a critical component during virus assembly. There is evidence that M1 interacts with the viral membrane and possibly also with HA, NA and nucleoprotein. In electron micrographs of sectioned viruses M protein seems to be present as an electron-dense layer 3–4 nm in thickness which is located beneath the lipid bilayer (Fig. 15.5C–D). Negative staining of disrupted virions reveals a continuous layer of closely packed parallel strands 3–4 nm in diameter (Fig. 15.5E–H) which sometimes appear to be beaded and helically arranged.

At present less information is available on the structure and functional significance of M2, although it is known that the protein is present in abundance in infected cells and also on the cell surface and is coded by gene 7 in a second reading frame. The M2 protein is most likely a non-structural protein (M_r 15 000) and thus resides only in infected cells and not in virus particles. In addition to HA and NA, it is a third membrane protein associating with the same cell membrane fractions as HA and NA. A third short peptide (M3) may also be synthesized in influenza virus infected cells.

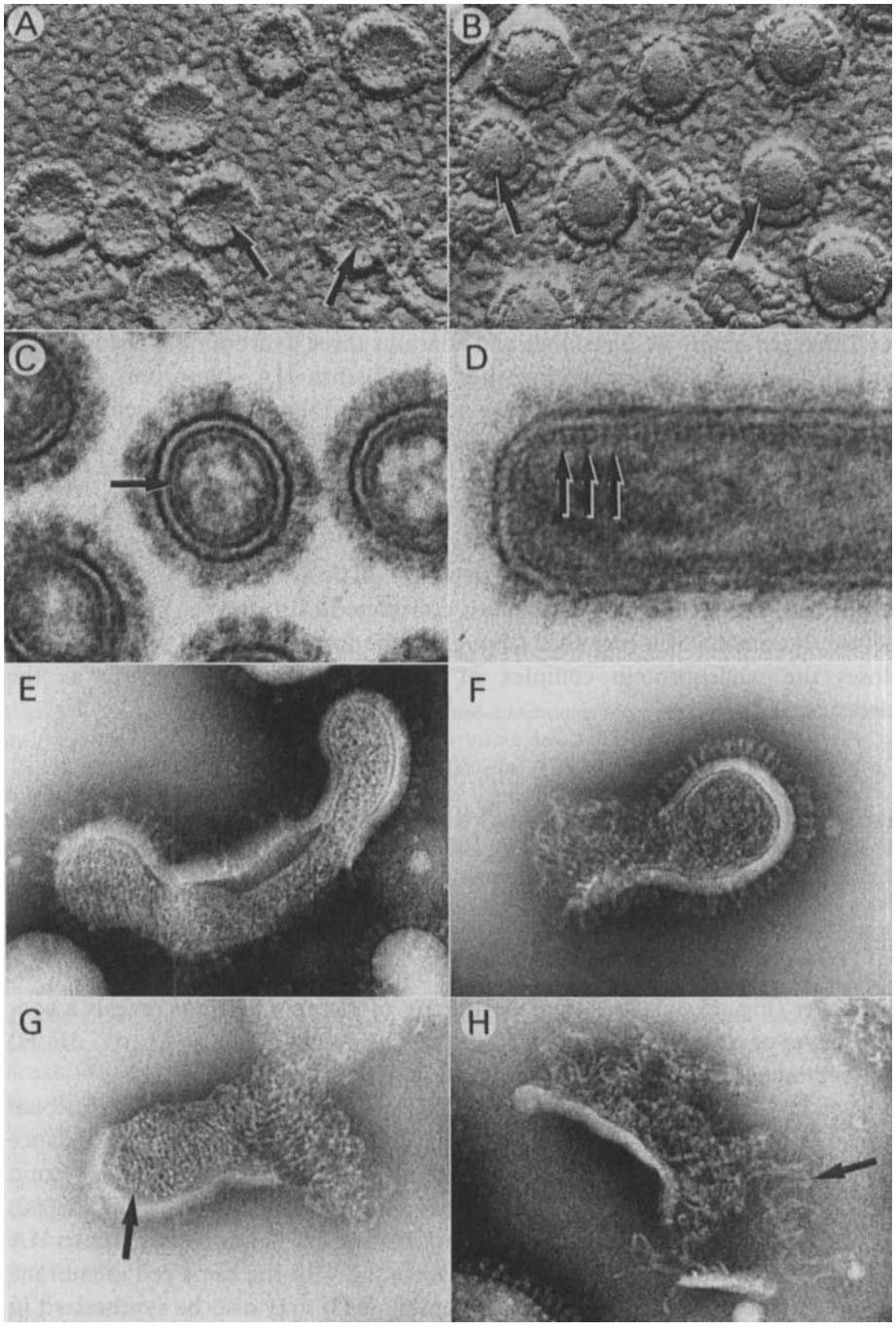
A
B
C
D
E
F
G
H

(b) Nucleoprotein complex

The nucleoprotein complex consists of nucleoprotein (NP) and polymerase proteins (basic proteins PB1 and PB2 and the acidic protein PA) together with the single-stranded RNA of the virus. The three polymerase proteins are thought to constitute an RNA transcriptase enzyme responsible for initiating RNA transcription in the infected cell. The virus RNA genome is closely associated with NP producing ribonucleoprotein (RNP) structures. Electron microscopy of sectioned viruses has revealed little about RNP morphology except that a 7 + 1 configuration of electron-dense material is often seen in filamentous virus particles (Fig. 15.6A and B). The RNP, however, seems to be restricted to the distal end of filamentous particles and most of the filament appears to be empty (Fig. 15.6C,D,E). Sections of small spherical virions simply show central granular dense contents. Negative staining of partly disrupted virions indicates that the RNP is present as a continuous strand approximately 8 nm in diameter arranged in the form of a coil or helix (Fig. 15.7A,B,C). During the preparation of purified RNP the large helix appears to re-organize into linear structures 50–100 nm in length and 10 nm in width (Fig. 15.7D,E,F) which are composed of NP subunits arranged like beads on a string that has been doubled back on itself and again twisted into a helix, which in this case is known to be right-handed. These portions of RNP become less tightly coiled in high salt concentrations and can finally break down into ring-shaped structures 5 nm in thickness and 7 nm in diameter (Fig. 15.7F). Each NP molecule is associated with some 20 nucleotides of RNA that are partly exposed, since they are accessible to RNAase activity. Furthermore, it appears that the RNA is an integral part of the total structure, since RNAase digestion destroys the RNP. NP is phosphorylated but the role of the phosphate is unclear. There is experimental evidence that two forms of NP of different molecular weight are produced in virus-infected cells by post-translational modification.

The relationship of the nucleoprotein complex, core shell and viral envelope is summarized in Fig. 15.8.

Fig. 15.5. Morphology of influenza virus core shell (M protein) and its relationship to the viral membrane and spikes. A and B. Freeze-fracture replicas of whole virus showing inner surfaces of lipid bilayer. Small particles are present (arrows), mainly on concave fracture faces (A) and less frequently on convex fracture faces (B), indicating the presence of protein molecules in the lipid bilayer. Possibly the HA and NA spikes penetrate through the bilayer to make contact with the underlying M protein (see also Fig. 15.4). × 100 000 (micrographs courtesy of Dr. M.V. Nermut). C. Sectioned virus showing core shell layer or M protein (arrow) beneath the lipid bilayer envelope. × 400 000. D. Longitudinally sectioned filamentous virus showing periodic structure in M protein layer and possible connections to lipid bilayer. × 400 000. E, F, G and H. Negative staining of virions in which lipid envelope has been disrupted so that core shell is revealed. All × 200 000. E. M protein appears to form a complete sac-like structure inside the lipid envelope. F. Ruptured core shell showing disintegration into fine strands of M protein. G. parallel striations or possibly helical arrangement of M protein strands. H. Severely disrupted virus showing long strands of M protein 3–4 nm in width.

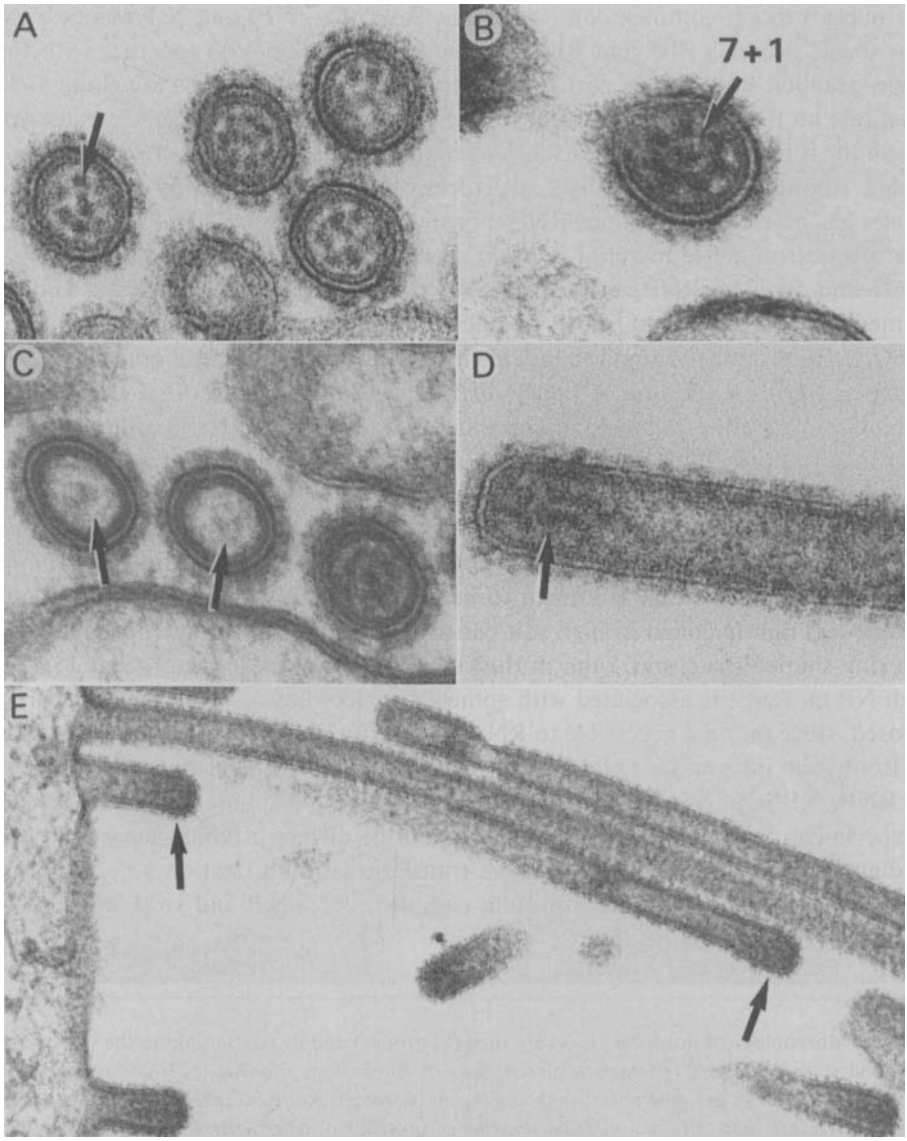

Fig. 15.6. Structure of viral ribonucleoprotein complex (RNP) demonstrated by sectioning of intact virus. A. Transversely sectioned elongated particles contain a variable number of central dense RNP structures. ×200 000. B. The most common arrangement of the RNP in the elongated particles consists of a 7 + 1 configuration. ×300 000. C. Many transversely sectioned filamentous particles appear empty (arrows). ×200 000. D and E. Longitudinal sections of budding filamentous particles indicate that RNP is present only at the distal end of the particle. D, ×200 000; E, ×75 000.

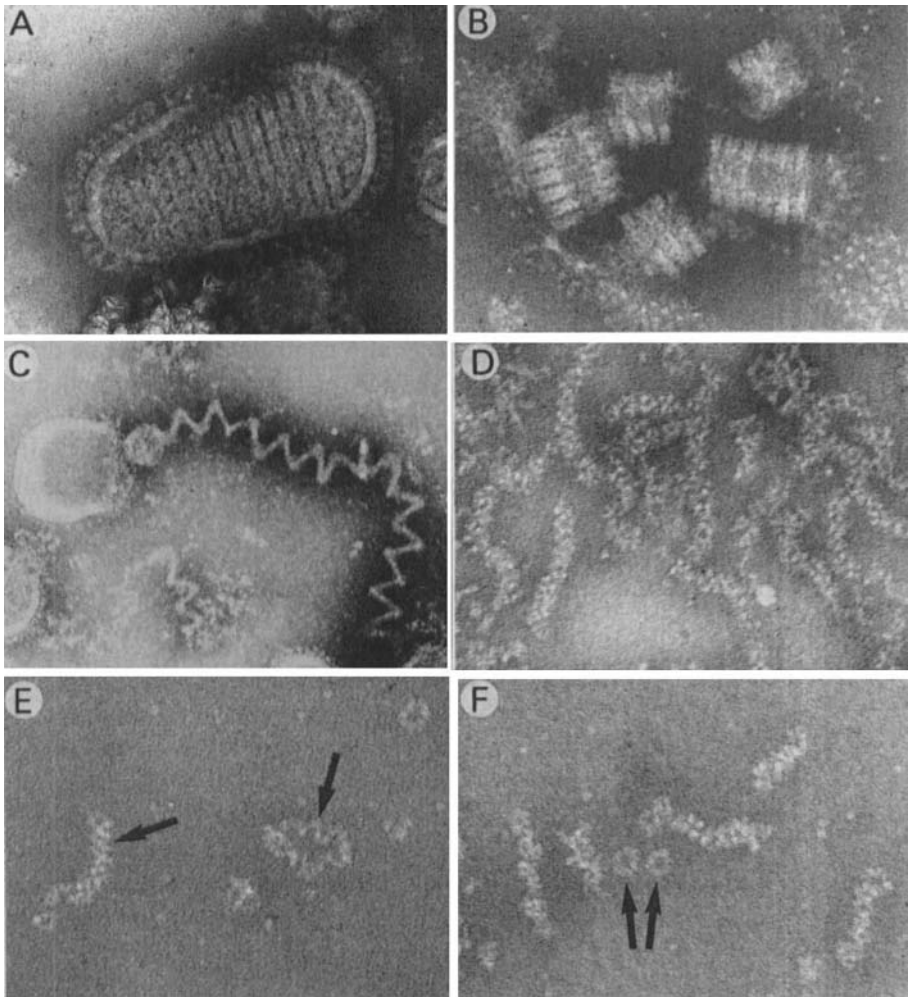

Fig. 15.7. Structure of RNP demonstrated by negative staining of disrupted virions. A. Minor disruption of lipid bilayer allowing entry of stain shows virion completely filled with parallel strands of RNP 8 nm in width. ×200 000. B. RNP released from disrupted virions shows evidence of helical coil structure. ×200 000. C. Long uncoiled strand of RNP (8 nm in width) released from detergent-treated virion ×100 000 (micrograph courtesy of Dr. K. Murti, and with permission of Academic Press). D. Purified preparation of RNP consists of short strands of various lengths and 10 nm in width. ×200 000. E. RNP preparations showing coiled or helical structure in the strands of RNP. ×200 000. F. Ring-shaped structures in RNP preparation probably represent short uncoiled fragments of RNP. ×200 000.

15.5. Antigenic properties of influenza viruses

The earliest serological studies with the HA of influenza A viruses in the 1930s and 1940s provided documentation of almost yearly antigenic change or 'drift'. It is now considered that antigenic drift (confined mainly to the HA or NA glycoproteins) occurs by accumulation of single amino acid substitutions, resulting in a change in one or more of the antigenic determinants of HA or NA. These new and epidemiologically significant antigenic variants are selected mainly by immunological pressure exerted via antibody in the general population, although more recently it has been appreciated that non-immune pressures exerted via receptor sites on the HA and varying host cells may also contribute to antigenic drift.

In contrast, the term antigenic 'shift' in the HA or NA antigens is applied to the emergence or re-emergence of a 'new' influenza A virus possessing a completely different HA or NA, both antigenically and also in amino acid sequence. 'Shift' has not been described for influenza B or C viruses. Thirteen antigenically distinguishable HA subtypes of influenza A virus are known to exist, of which three (H1, H2 and H3) have been shown to be associated with human disease. Also nine NA subtypes are extant, of which only two (N1 and N2) are known to be

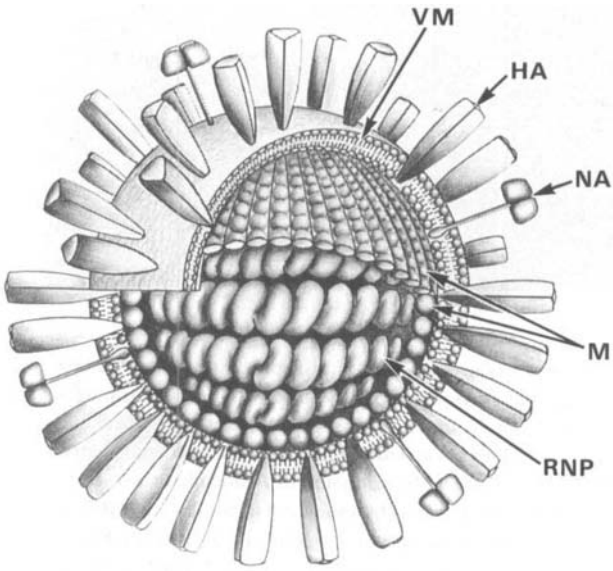

Fig. 15.8. Composite diagram of influenza virus showing three-dimensional relationships of viral membrane (VM) and HA and NA spikes (= envelope) together with M protein and RNP (= core). Note that the various structural components are drawn to scale but the diagram represents a particle 50 nm in diameter, which is about half the normal size of the virus.

associated with infection of humans. The system of nomenclature for antigenic subtypes of influenza viruses has been described in a WHO memorandum (1980).

The subtypes of HA and/or NAs are sufficiently different in nucleotide sequence to allow the conclusion that they have not arisen by mutation from the preceding virus subtype. Rather, such new HA and NAs may result from genetic reassortment occurring between influenza A viruses of human or non-human hosts ('animal or bird reservoir' theory) or from a reappearance of a virus after an apparent prolonged absence in humans ('recycling' theory) or after a persistent or latent infection. Thus the origin of such viruses is necessarily speculative at present.

Influenza A, B and C viruses are differentiated serologically by the possession of antigenically unique NP and M antigens. Minor degrees of antigenic variation are detectable among the NP and M antigens of influenza A viruses using monoclonal and polyclonal antibodies, but the NS1 proteins induced in infected cells by influenza A viruses appear to be antigenically similar. The antigenic properties and relationships of PB1, PB2 and PA proteins have not been clearly established to date.

15.6. Virus–cell interactions

Receptor-mediated uptake of influenza virus is thought to occur at 'coated pits' in the cell plasma membrane (Fig. 15.9A). Receptor-bound viruses are taken into the cell in coated vesicles and then transported to endosomes and possibly lysosomes. In the low-pH environment of these vesicles a configurational change is thought to occur in the HA, which brings together the HA 'fusion sequence' (the N-terminus of the HA2 polypeptide) and the lipid bilayer of the vesicle. After fusion of viral and vesicle lipid bilayers, virion RNA is released into the cytoplasm and rapidly transported to the nucleus as an RNP + M + polymerase protein (80 S) 'core complex'. A 50 S complex (composed of RNP + polymerase proteins) has been found in the nucleus and, presumably, M protein dissociates from the complex at the nuclear membrane. Virus mRNA and cRNAs are synthesized within minutes of infection of the cell and approximately 2 h later non-structural protein (NS1), nucleoprotein and polymerase polypeptides may be detected intracellularly by pulse-labelling techniques. NS1 in particular is made in large amounts in infected cells; it is phosphorylated and accumulates in the nucleus as well as being found associated with polysomes (Fig. 15.9B). Late in infection NS1 has been demonstrated to form electron-dense crystalline arrays (Fig. 15.9C), again emphasizing the abundance and importance of this protein in infected cells. The virus structural proteins HA and NA are presumably synthesized by membrane-associated polysomes, carbohydrate is added and the proteins are transported to the cell membrane where budding occurs by approximately 5 h post-infection,

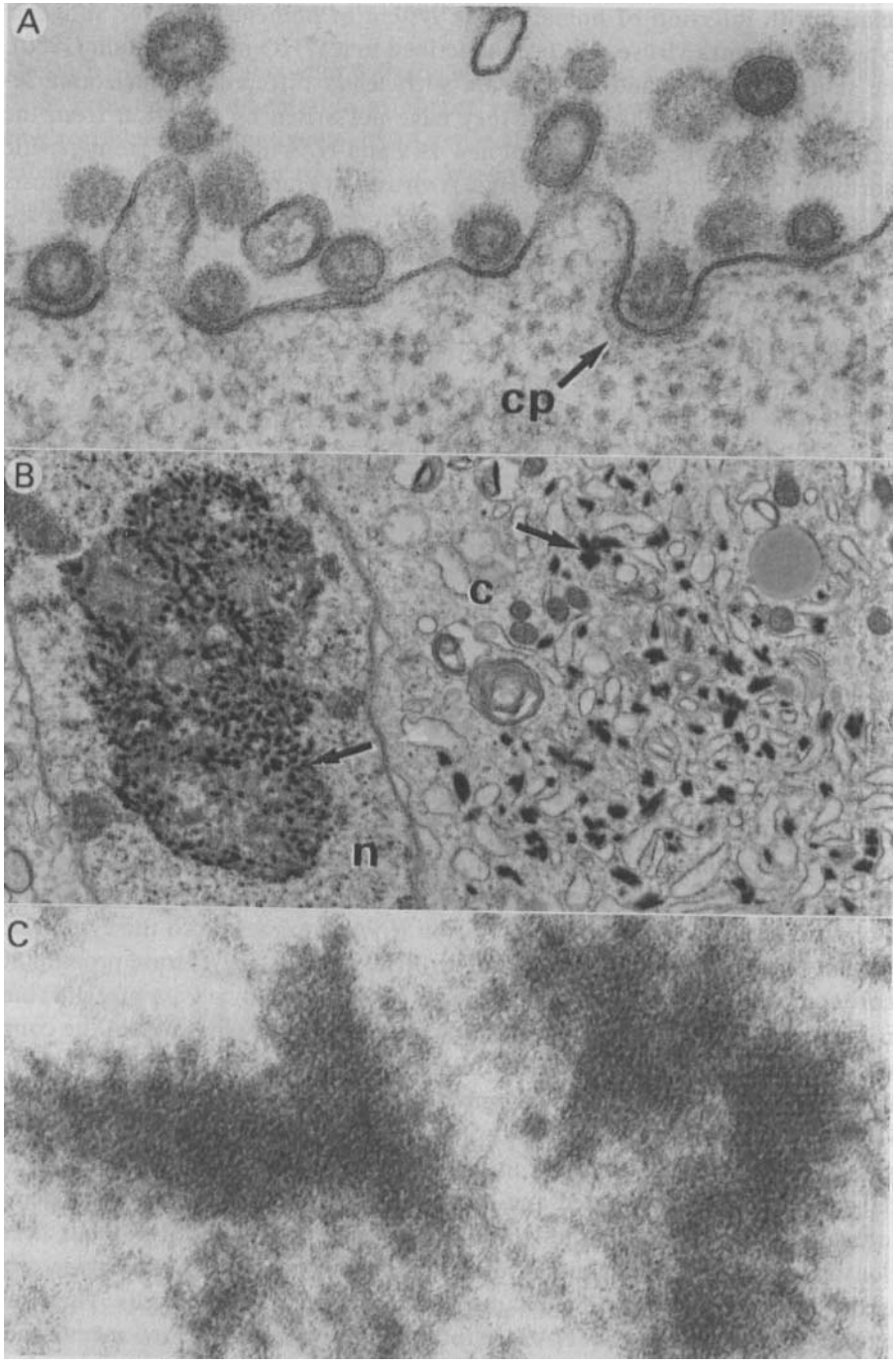
A
cp
B
c
n
C

often in the absence of marked morphological change in the cells. In reality little is known about the details of budding except that NA activity is necessary to ensure virus release from the cell. Proteolytic cleavage of the HA into HA1 and HA2 polypeptides occurs either on smooth internal membranes or at the plasma membrane by an unknown host enzyme with a similar specificity to trypsin. There is evidence that 'tails' of the HA and NA proteins protrude through the plasma membrane where they may interact with patches of M protein (see also Fig. 15.4). In turn, M protein could be recognized by the RNP complex (presumably containing the correct complement of RNAs) and thus all the components of the new virus would be in physical contact and prepared for budding and release from the cell. At the final stage, portions of the cell membrane with the associated viral proteins bud from the cell surface and are cut off, thus releasing the new virion.

Acknowledgements

We are grateful to C.L. Baigent for help with SEM; R.D. Wood for TEM of sections; L.J. Kelly and J. Pipkin for the drawings.

References

Colman, P.M., Varghese, J.N. and Laver, W.G. (1983) Structure of the catalytic and antigenic sites in influenza virus neuraminidase. Nature 303, 41–44.

Compans, R.W. and Klenk, H.-D. (1979) Viral envelopes. In Comprehensive Virology, Eds. H. Fraenkel-Conrat and R. Wagner; Vol. 13, pp. 293–407. Plenum, New York.

Dimmock, N.J. (1982) Initial stages of infection with animal viruses. J. Gen. Virol. 59, 1–22.

Dubois-Dalcq, M., Holmes, K.V. and Rentier, B. (1984) Assembly of Enveloped RNA Viruses. Springer-Verlag, New York.

Lamb, R.A. (1983) The influenza virus RNA segments and their encoded proteins. In Genetics of Influenza Virus, Eds. P. Palese and D.W. Kingsbury. Springer-Verlag, Vienna.

Lamb, R.A., Zebedee, S.L. and Richardson, C.D. (1985) Influenza virus M2 protein is an integral membrane protein expressed on the infected cell surface. Cell 40, 627–633.

Laver, W.G. and Valentine, R.C. (1969) Morphology of the isolated haemagglutinin and neuraminidase subunits of influenza virus. Virology 38, 105–119.

Lenard, J. and Compans, R.W. (1974) The membrane structure of lipid-containing viruses. Biochim. Biophys. Acta 344, 51–94.

Fig. 15.9. Morphology of virus–cell interactions: transmission electron micrographs of sectioned Vero and MRC-5 cells infected with A/NWS virus in vitro. A. Surface of Vero cell showing virus particles on the outer membrane and initial stages of infection by uptake in coated pit (cp). ×98 000. B. MRC-5 cell 24 hours post-infection showing electron-dense inclusions of non-structural protein (arrows) in the nucleus (n) and cytoplasm (c). ×13 000. C. Crystalline structure of non-structural protein (NS1) in cytoplasm of MRC-5 cell 24 hours post-infection. ×195 000.

Marsh, M. (1984) The entry of enveloped viruses into cells. Biochem. J. 218, 1–10.

McCauley, J.W. and Mahy, B.W.J. (1983) Structure and function of the influenza virus genome. Biochem. J. 211, 281–294.

Nermut, M.V. (1972) Further investigation on the fine structure of influenza virus. J. Gen. Virol. 17, 317–331.

Oxford, J.S., Hockley, D.J., Heath, T.D. and Patterson, S. (1981) The interaction of influenza virus haemagglutinin with phospholipid vesicles; morphological and immunological studies. J. Gen. Virol. 52, 329–343.

Patterson, S., Oxford, J.S. and Dourmashkin (1979) Studies on the mechanism of action of influenza virus entry into cells. J. Gen. Virol. 43, 223–229.

Reginster, M. and Nermut, M.V. (1976) Preparation and characterization of influenza virus cores. J. Gen. Virol. 31, 211–220.

Schulze, I.T. (1973) Structure of influenza virion. In Advances in Virus Research, Eds. M.A. Lauffer, F.B. Bang, K. Maramorosch and K.M. Smith; Vol. 18, pp. 1–55. Academic Press, New York and London.

Stuart-Harris, C.H., Schild, G.C. and Oxford, J.S. (1985) Influenza, the Virus and the Disease, 2nd edition. Edward Arnold, London.

Schild, G.C., Oxford, J.S., de Jong, J.C. and Webster, R.G. (1983) Evidence for host cell selection of influenza virus antigenic variants. Nature 303, 706–709.

Varghese, J.N., Laver, W.G. and Colman, P.M. (1983) Structure of the influenza virus glycoprotein antigen neuraminidase at 2.9 Å resolution. Nature 303, 35–41.

Webster, R.G., Laver, W.G., Air, G.M. and Schild, G.C. (1982) Molecular mechanisms of variation in influenza viruses. Nature 296, 115–121.

WHO Memorandum (1980) A revision of the system of nomenclature for influenza viruses. Bull. WHO 58, 585–591.

Wiley, D.C., Wilson, I.A. and Skehel, J.J. (1981) Structural identification of the antibody-binding sites of Hong Kong influenza haemagglutinin and their involvement in antigenic variation. Nature 289, 373–378.

Wilson, I.A., Skehel, J.J. and Wiley, D.C. (1981) The structure of the haemagglutinin membrane glycoprotein of influenza virus at 3 Å resolution. Nature 289, 366–373.

Wrigley, N.G., Brown, E.B. and Skehel, J.J. (1986) Electron microscopy of influenza virus. In Electron Microscopy of Proteins, Eds. J.R. harris and R.W. Horne; Vol. 5, pp. 103–164. Academic Press, London.

Nermut/Steven (eds) Animal Virus Structure

CHAPTER 16

Paramyxoviridae

A. SCHEID

Institut für Medizinische Mikrobiologie und Virologie der Universität Düsseldorf, Universitätsstr. 1, 4000-Düsseldorf, F.R.G.

Family: Paramyxoviridae

Genus: Paramyxovirus. Species: Human parainfluenza virus types 1–4, mumps virus, Sendai virus, Newcastle disease virus, Simian virus 5 (SV5), and others

Genus: Morbillivirus (measles-rinderpest-distemper group). Species: Measles virus, Canine distemper virus, Rinderpest

Genus: Pneumovirus (respiratory syncytial virus group). Species: Respiratory syncytial virus, Pneumonia virus of mice

16.1. General characteristics

Paramyxoviridae are enveloped viruses with a helical nucleocapsid containing an unsegmented single-stranded RNA genome of negative polarity. They replicate in the cytoplasm of infected cells. Cytopathic effects differ with members of the group and host cell, ranging from extensive cell-cell fusion in some systems, cell rounding and stelliform appearance in others, to a total lack of overt cytopathic effect in spite of massive and continued virus production. Paramyxoviruses contain a hemagglutinin and neuraminidase activity. They share this feature with myxoviruses; however, they differ from myxoviruses in many respects, including genome structure and mode of replication. Paramyxoviridae are pathogens that cause respiratory diseases in man (parainfluenza virus types 1 to 4, mumps virus), other mammals, e.g. the mouse (Sendai virus), and birds (e.g. Newcastle disease virus), but also infections of the nervous system and gastroenteritis (in cattle).

Most of our knowledge regarding the paramyxovirus virion is based on studies of a few members of this large group of viruses, i.e., parainfluenza virus type 1 (Sendai virus), simian virus type 5 (SV5) and Newcastle disease virus (NDV). Recently, specific information on virus structure and replication has also emerged from work with parainfluenza virus type 3 and mumps virus. The members of the group differ with regard to antigenic properties, size of polypeptides, host range and pathogenic potential. However, they share common features of virion structure as well as of mode of replication and assembly, as summarized below for parainfluenza virus type 1 (Sendai virus), together with findings made with related viruses.

16.2. Parainfluenza virus type 1 (Sendai virus): chemical and physical characteristics

Purified virions contain approximately 74% protein, 19% lipid, 6% carbohydrate and 1% RNA. The total mass of virions has been estimated as $6–7 \times 10^8$ daltons, and the sedimentation coefficient as 1000–1100 S. In view of pleomorphism of virions, these values must be viewed as representing the average particle.

The genome consists of one single-stranded, linear, negative-sense RNA molecule of M_r $5–6 \times 10^6$ and a sedimentation coefficient of 50 S.

Buoyant density of the virus particles in sucrose is 1.18–1.20 g/cm^3. Nucleocapsids band at a density of 1.27–1.31 in caesium chloride. The polypeptide composition of virions and the properties of the polypeptides are summarized in Table 16.1.

16.3. Structural characteristics

Shape and size: by negative-contrast electron microscopy, virions are heterogeneous in size and shape (Fig. 16.1). Most are roughly spherical and measure approximately 200 nm in diameter, although larger particles with diameters of 500–600 nm are occasionally observed. In thin sections of infected cells, filamentous particles of approximately 150 nm in diameter and up to 1000 nm in length can be seen. It is not clear whether filamentous particles appear among released virions. It has been observed that virions harvested early after release from infected cells are rather uniform in size and shape (bacilliform) and are more stable than virions harvested late in infection or purified virions, which are usually rather pleomorphic (Fig. 16.1a–d; Shimizu et al., 1976; Kim et al., 1979).

TABLE 16.1.

Paramyxovirus polypeptides

	Molecular weight ($\times 10^{-3}$)	No. of copies per virion	Location	Function
HN	72	(gp) 1000	Spike	Hemagglutinin, neuraminidase
F_1	50	(gp) 1000[a]	Subunit of F spike	Membrane fusion
F_2	15	(gp) 1000[a]	Subunit of F spike	Membrane fusion
NP	60	2600	Nucleocapsid	Major structural component of nucleocapsid
P	79	300	Nucleocapsid	Part of RNA-polymerase
L	160	40	Nucleocapsid	Part of RNA-polymerase
M	34	3000	Inner side of envelope	Virus assembly; structural component of virion
C	22	0	Infected cell	Non-structural; function unknown

Molecular weights and copy numbers are from Lamb and Choppin (1978) and Scheid and Choppin (1977) and refer to Sendai virus. Polypeptides of different molecular weights that are analogous to the Sendai virus structural proteins in location and function have been identified in other paramyxoviruses, e.g., SV5, NDV, mumps virus and parainfluenza virus type 3.

[a] Virions contain the same number of copies of the precursor polypeptide F_0 if proteolytic cleavage to F_1 and F_2 has not taken place.

16.4. Architecture of the virion

Paramyxoviruses consist of a helical nucleocapsid enclosed in a lipid-containing envelope which is covered on the outer surface with spikes. Fig. 16.2 shows a simplified diagram of the virion architecture.

The virus envelope is a lipid bilayer containing two types of transmembrane glycoproteins. The relative content of individual lipid classes and fatty acid constituents reflects the lipid composition of the plasma membrane of the host-cell from which the virus membrane is derived during virus assembly (Klenk and Choppin, 1970). Two glycoproteins constitute two morphologically distinct spikes on the outer surface of the envelope (Fig. 16.3): the HN glycoprotein (so named because it carries *h*emagglutinating and *n*euraminidase activities) and the F glycoprotein (membrane *f*using protein) (Scheid and Choppin, 1972, 1974a). The glycoproteins can be conveniently isolated because they are soluble in non-ionic detergents at low ionic strength, whereas other virus components are not. The glycoproteins can be separated from each other by rate-zonal centrifugation (Scheid and Choppin, 1972, 1973) and by affinity chromatography (Scheid and Choppin, 1974b). The spikes are anchored in the envelope by hydrophobic interaction between a region at the base of the spike and the lipid of the membrane. This hydrophobic region of the spike is responsible for detergent binding (Hsu et al., 1981), rosette forma-

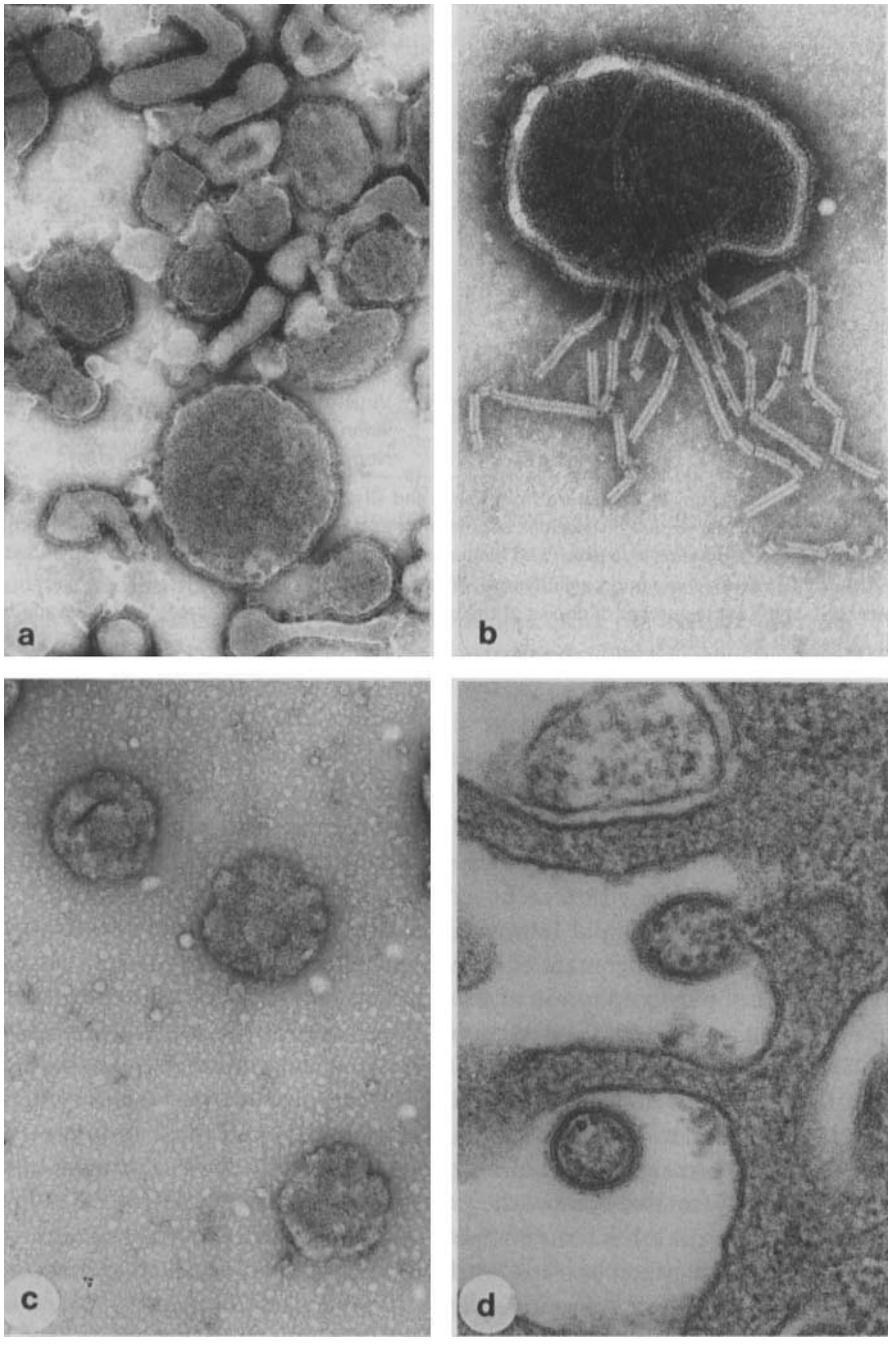
a
b
c
d

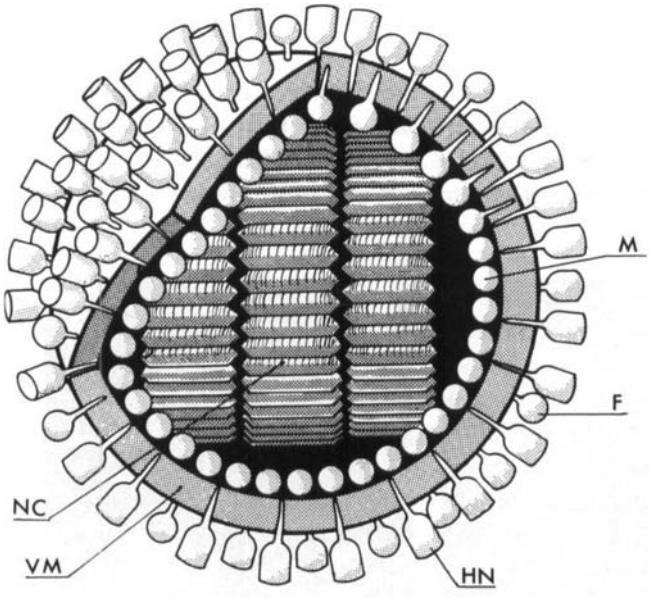

Fig. 16.2. Diagrammatic representation of paramyxovirus architecture. Part of the envelope has been removed to reveal virus interior. NC = nucleocapsid, VM = viral membrane, HN = haemagglutinin and neuraminidase spike, F = fusion spike, M = M protein (shown with transmembrane side-chain in upper part). Approximately in scale, except overall diameter. Drawing by Mr. Joe Brock.

tion of spikes in detergent-free aqueous media (Fig. 16.3a–c; Scheid et al., 1972), and insertion of glycoproteins in artificial lipid vesicles or 'filamentous liposomes' (Fig. 16.3d; Hsu et al., 1979).

The HN spike projects 12–15 nm from the outer surface of the lipid bilayer. It has a slim shaft which is barely resolved in negatively stained preparations, and a terminal knob (Fir. 16.3a). The spike contains four copies of the HN polypeptide. Pairs of the HN polypeptide are covalently linked by interchain disulfide bonds. The primary structure deduced from the nucleotide sequence of the HN gene shows only one hydrophobic domain, which is located close to the N-terminus and is likely to represent the region of the molecule that anchors the HN spike in the lipid bilayer (Hiebert et al., 1984; Blumberg et al., 1985b). This is in

---

Fig. 16.1. Sendai virions. (a) Negatively stained pleomorphic population of purified virus particles. × 55000. (b) Negatively stained virus particle partly disrupted with release of nucleocapsid. × 110000. (Both micrographs by courtesy of Dr. T. Bächi.) (c) Negatively stained virus particles harvested early after infection. × 50000. (d) Thin section of cell periphery with budding virus particles. Note round profiles of nucleocapsids and dense track below virus membrane. × 130000. (By courtesy of Dr. H. Hockley.)

accord with the finding that the C-terminus of HN is exposed at the surface of the virus envelope (Schuy et al., 1984).

The F spike projects 10–13 nm from the outer surface of the membrane. In negative staining, the shaft appears thicker than that of the HN spike, and the knob at the end is more pronounced (Fig. 16.3b,c,d). The deduced amino acid sequence suggests hydrophobic attachment through a transmembrane sequence close

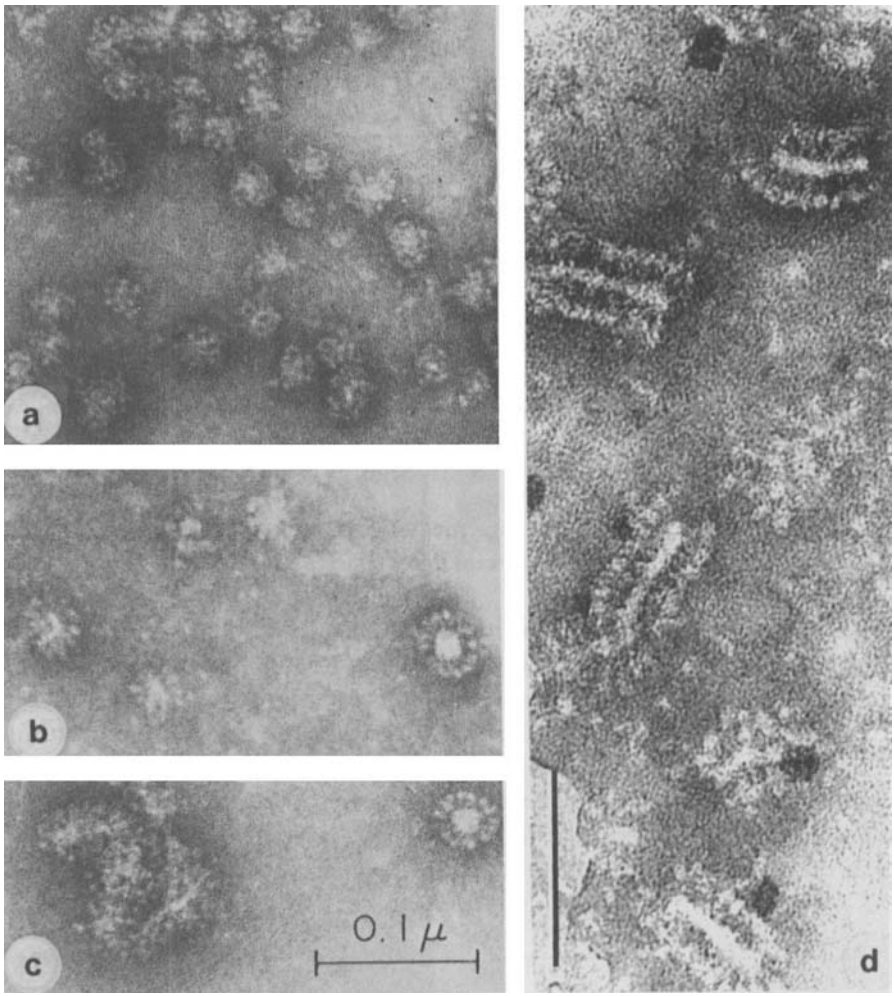

Fig. 16.3. Paramyxovirus spikes. (a) Negatively stained rosettes of HN protein isolated from SV5. (b,c) Negatively stained rosettes of F protein isolated from SV5. a–c: Glycoproteins were isolated in the presence of Triton X-100. Rosettes have formed after the removal of detergent (from Scheid et al., 1972 with permission). (d) 'Filamentous liposomes' reconstituted from lipid and F protein isolated from Sendai virus (from Hsu et al., 1979; with permission). Magnification: × 250000.

to the C-terminus which extends to the inner side of the envelope (Paterson et al., 1984; Blumberg et al., 1985a). The F protein is composed of two disulfide-bonded polypeptide chains, F_1 and F_2, that are derived by proteolytic cleavage from a precursor glycoprotein, F_0 (Scheid and Choppin, 1977). Cleavage is required for biological activity of the F spike in membrane fusion, i.e. in virus-induced hemolysis, cell-cell fusion and in virus penetration (Homma et al., 1973; Scheid and Choppin, 1974a). Spikes containing the cleaved F protein differ in structure (as determined by circular dichroism) from spikes composed of the uncleaved precursor (Hsu et al., 1979). In addition to the membrane-anchoring hydrophobic region, the cleaved F protein possesses another major hydrophobic domain which is not present on the uncleaved F_0 spike (Hsu et al., 1981). The primary structure of the F protein contains a hydrophobic stretch of amino acids at the N-terminus of F_1 which is generated by cleavage of the precursor. This hydrophobic region is highly conserved among paramyxoviruses and homologous with the cleavage-generated N-termini of the influenza A virus protein HA and the F protein of morbilliviruses (Gething et al., 1978; Scheid et al., 1978; Choppin and Scheid, 1980; Varsanyi et al., 1985). Recently obtained nucleotide sequences of F genes have extended the homology among F proteins of paramyxoviridae (Hsu and Choppin, 1984; Paterson et al., 1984; Blumberg et al., 1985a; Richardson et al., 1986). Studies with oligopeptides which are homologous to this region and which are inhibitory for the activity of F (Richardson et al., 1980; Richardson and Choppin, 1983) support the idea that this region of the molecule is of functional significance in the membrane-fusing activity of the F protein.

The M protein (*m*embrane or *m*atrix protein) is localized within the virus particle. The M protein can be solubilized by treatment of virus particles with non-ionic detergents in the presence of high salt concentration (0.5–1.0 M), and it precipitates from such extracts upon dialysis against buffer with low salt concentration (Scheid and Choppin, 1972, 1973). Ultrathin sections of young virions (Fig. 16.1d) indicate that, as in influenza virus, the paramyxovirus M protein lines the inner surface of the membrane. Isolated M protein can be visualized as subunits of 6 nm diameter, which aggregate into filaments, and such filaments associate into helical tubes or sheets in vitro (Fig. 16.4a,b; Hewitt and Nermut, 1977; Heggeness et al., 1982). On the inner fracture face of virus envelopes and of plasma membranes of infected cells, a rectangular pattern with a periodicity of approximately 9 nm has been visualized by freeze-fracture electron microscopy (Fig. 16.4; Bächi, 1980). These arrays may be attributable to a planar arrangement of the M protein on the inner surface of the plasma membrane (Fig. 16.4e; Büechi and Bächi, 1982). The primary structure of the M protein has been deduced from the nucleotide sequence (Blumberg et al., 1984), and this may help the eventual elucidation of the secondary structure and the nature of the interaction of M protein with both the plasma membrane and the nucleocapsid.

Isolated *nucleocapsids* appear in negative-staining electron microscopy as some-

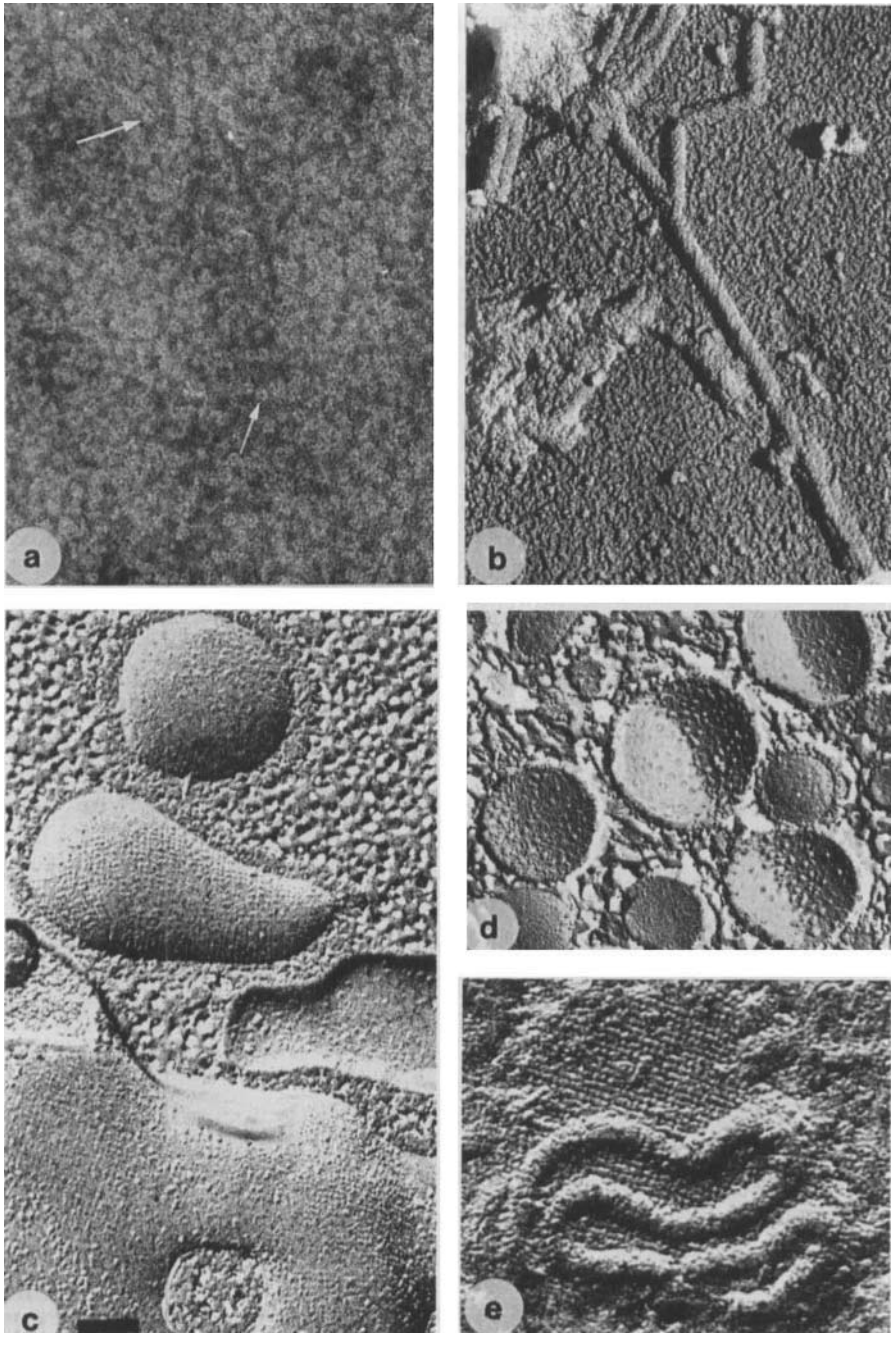
a
b
c
d
e

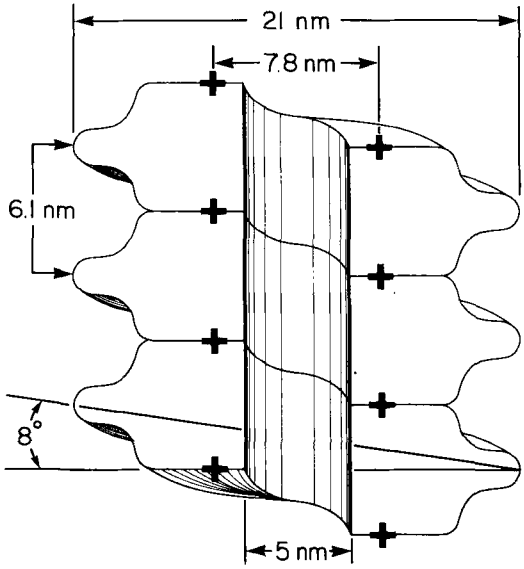

Fig. 16.5. Schematic representation of a segment of a paramyxovirus nucleocapsid. The calculated position of the RNA is indicated by crosses. Measurements were obtained from measles virus nucleocapsid and are not identical for all other paramyxoviruses (from Lund et al., 1984; with permission).

what flexible extended structures with a diameter of about 18 nm and a central channel 5 nm in diameter (Figs. 16.5 and 16.6). The nucleocapsid is a helical structure with an overall length of about 1 μm and a left-handed sense of the helix (see Choppin and Compans, 1974, for references). The helix has a pitch of 5 nm and contains 11–13 protein subunits per turn (Finch and Gibbs, 1970; Hosaka and Hosoi, 1983). The major structural protein subunit is the virus protein NP (*n*ucleocapsid *p*rotein) with a molecular weight of approx. 60 000. One nucleocapsid contains one molecule of single-stranded RNA and the number of NP protein subunits has been calculated as 2200–2600 (Compans and Choppin, 1975).

Fig. 16.4. Paramyxovirus M protein. (a) Isolated M protein of Sendai virus in high salt, negatively stained. × 250 000. (b) Helical assemblies of M protein from low-salt solution. Freeze-dried and shadowed. × 100 000. (Both pictures by courtesy of Drs. J.A. Hewitt and M.V. Nermut.) (c) Freeze-etch replica of EL-4 cell 48 h after infection with Sendai virus. Note periodic pattern of particles on protoplasmic fracture face of both the plasma membrane and the released virus particle. × 70 000. (From Bächi, 1980; with permission). (d) Freeze-fracture replica of purified Sendai virus. Intramembranous particles are confined mainly to external fracture face and are randomly organized. No periodic pattern can be seen × 50 000. (By courtesy of Dr. M.V. Nermut.) (e) Inner face of plasma membrane of MDBK cell 48 h after infection with Sendai virus, showing nucleocapsids attached to patch of orthogonal pattern most likely formed by M protein particles. × 150 000. (From Büechi and Bächi, 1982; with permission.)

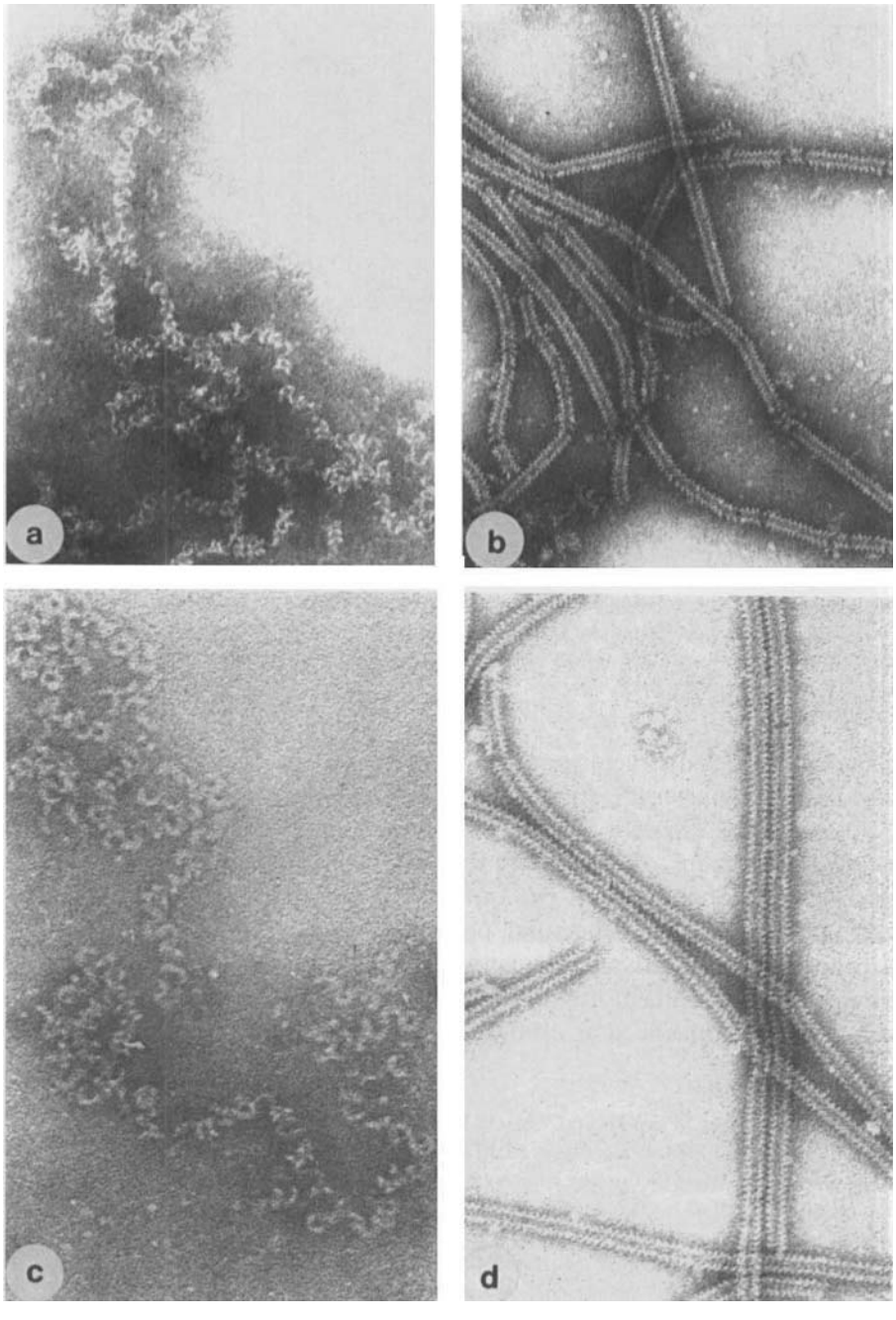
a
b
c
d

The molecular interactions between NP subunits are heavily influenced by ionic strength. The tightly coiled structures that are observed after routine negative staining in the presence of high salt concentrations (Fig. 16.6a) dissociate into loosely coiled helices at low ionic strength (Fig. 16.6b; Heggeness et al., 1980). About one-quarter of the molecule can be readily removed by a variety of proteases, without severely affecting the overall structure (Fig. 16.6c,d; Heggeness et al., 1981).

In addition to the major structural NP subunit, isolated nucleocapsids contain a smaller number of copies of the P protein (designation for *p*olymerase) and the L protein (*l*arge protein). For Sendai virus, the numbers of copies of P and L per nucleocapsid have been calculated as 300 and 40 (Lamb et al., 1976). The P protein is closely associated with the template RNA (Raghow and Kingsbury, 1979). Both the L and the P protein are involved in the RNA polymerase activities required for the transcription of mRNA and replication of genomic RNA (Hamaguchi et al., 1983). Nucleocapsids from infected cells containing RNA, NP, P and L are active in mRNA transcription in vitro; however, RNA replication in vitro requires additional soluble protein from the cytosol of infected cells (Carlsen et al., 1985). In nucleocapsids from virions, the P protein is evenly distributed over the entire length of the structure, whereas the P protein in nucleocapsids from infected cells is found in four to ten discrete clusters (Fig. 16.7; Portner and Murti, 1986), which may represent regions of transcriptase activity. Nucleocapsids from infected cells also contain attached M protein (cf. Büechi and Bächi, 1982; Portner and Murti, 1986), a finding that is consistent with the role of M protein in the recognition of nucleocapsid and the viral envelope during virus assembly (see below).

16.5. Antigenic properties

Type-specific antisera for each paramyxovirus can be obtained from guinea pigs; however, cross-reacting antibodies develop upon infection with related viruses (Chanock, R.M., 1979; Örvell et al., 1986). All virus proteins are immunogenic. Antibodies with neutralizing activity and with significance for protection are those

Fig. 16.6. Paramyxovirus nucleocapsid. (a) Sendai virus nucleocapsids, dialysed against 10 mM sodium phosphate, pH 7.2 (PB), fixed with formaldehyde, and negatively stained with phosphotungstate (PTA). (b) Sendai virus nucleocapsids, dialysed against PB, with 0.5 M NaCl added, fixed with formaldehyde, and negatively stained with PTA. Magnification for a and b: × 161 000. (c,d) Sendai virus nucleocapsids after treatment with trypsin. Though the M_r (60 000) of the NP protein was reduced to 48 000 the nucleocapsid morphology was not affected. Nucleocapsids were formaldehyde-fixed in PBS (c) or PBS with 0.4 M NaCl added (d). Magnification c and d: × 190 000. (Panels a–d are from Heggeness et al., 1980; with permission.)

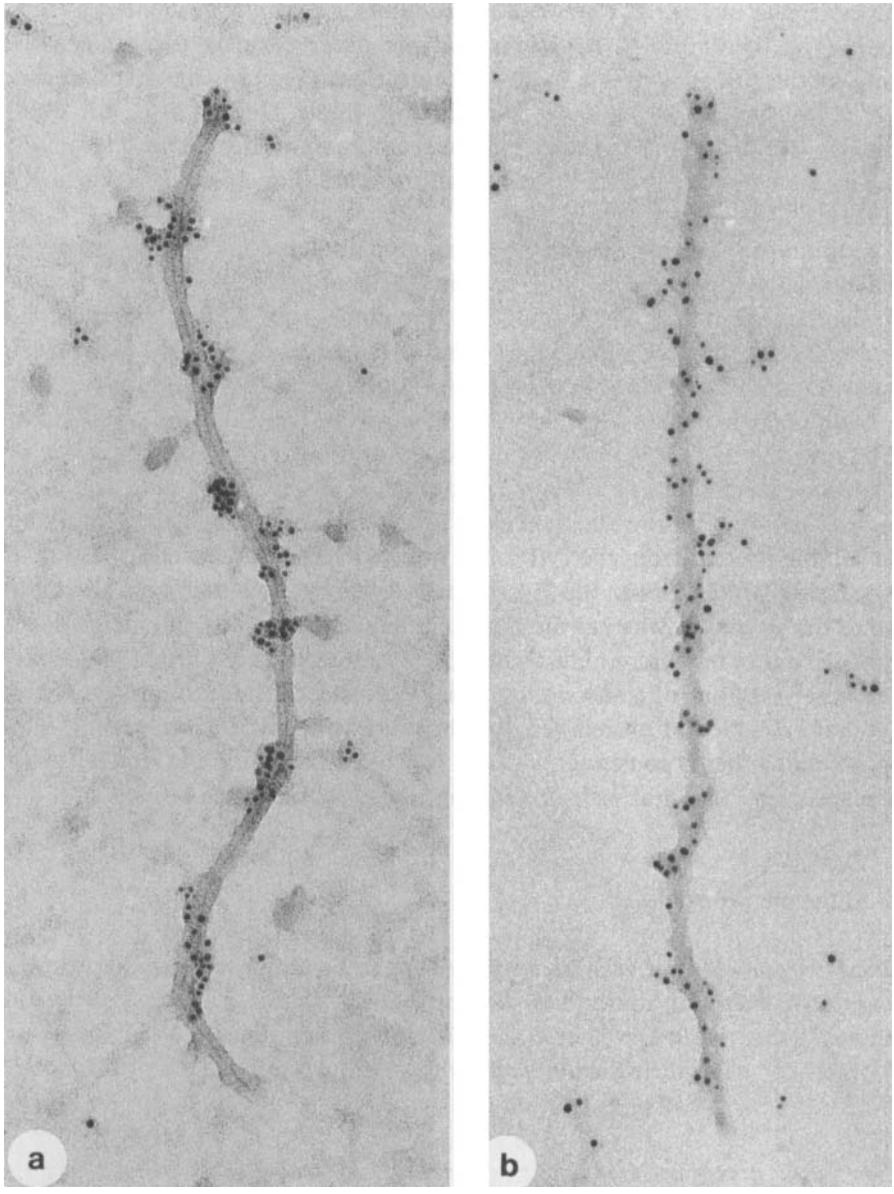

Fig. 16.7. Distribution of P protein on Sendai virus nucleocapsids. Nucleocapsids were isolated from (a) infected cells and (b) virions, reacted with a monoclonal anti-P antibody, treated with goat anti-mouse antibody conjugated with 5-nm gold particles, and positively stained with uranyl acetate. Magnification: (a) × 162 000; (b) × 171 000 (from Portner and Murti, 1986; with permission).

that are directed against the glycoproteins. Antibodies against HN inhibit the hemagglutinating and neuraminidase activities of the HN protein, and antibodies against F can interfere with the activity of the F protein in membrane fusion and virus penetration. Although antibodies to either glycoprotein can be shown to neutralize infectivity in in vitro tests, antibody against F is necessary for preventing spreading of virus in vivo (Merz et al., 1970; Choppin and Scheid, 1980).

16.6. Virus-cell interactions

Paramyxoviruses attach to cells by an interaction between the HN protein and neuraminic acid-containing receptors on the cell surface. Neuraminic acid residues of glycoproteins as well as glycolipids can serve as receptors for attachment. Virus penetration is due to a fusion between the virus membrane and the plasma membrane of the target cell, resulting in delivery of the inner contents of the virus particle into the cytoplasm of the cell (reviewed in Choppin and Scheid, 1980). Membrane fusion is dependent on the proteolytic cleavage of the F protein. Virions with the uncleaved protein (F_0) are unable to penetrate or to cause cell fusion or hemolysis; cleavage of F_0 by a cellular protease or by a suitable protease in vitro renders virions biologically active in penetration, hemolysis and cell-cell fusion. The membrane fusion activity requires the F protein to be present as an integral membrane protein, e.g., in the plasma membrane or in the lipid bilayer of liposomes, and no other virus-specific function is required for the membrane fusion reaction (Hsu et al., 1979). The optimum pH for fusion is neutral or slightly alkaline (Hsu et al., 1982), in contrast to the acidic conditions required for myxovirus fusion.

RNA replication, transcription, and synthesis of viral proteins are carried out in the cytoplasm. Translation, glycosylation and transport of viral glycoproteins proceed by the synthetic pathways of cellular glycoproteins. Assembly of nucleocapsids takes place in synchrony with RNA replication and in association with the cytoskeletal framework (Hamaguchi et al., 1986). Large accumulations of nucleocapsids can be found in cytoplasmic inclusions; however, it is not known whether they are pools for virus assembly or deposits of excess nucleocapsid.

Virus assembly takes place at the plasma membrane (Fig. 16.8; reviewed in Choppin and Compans, 1975; Dubois-Dalcq et al., 1983). Viral glycoproteins are inserted in the plasma membrane and gather into patches, from which cellular proteins are excluded. On the cytoplasmic side of the plasma membrane such regions appear as crystalline patches with an orthogonal pattern, which is thought to represent the M protein (Fig. 16.4c and d; Büechi and Bächi, 1982). Such a regular association of M protein molecules would suggest that the M protein is the scaffold for formation of the prospective virus envelope and that the glycoproteins are concentrated into the patches by an interaction between their cytoplasmic portion and

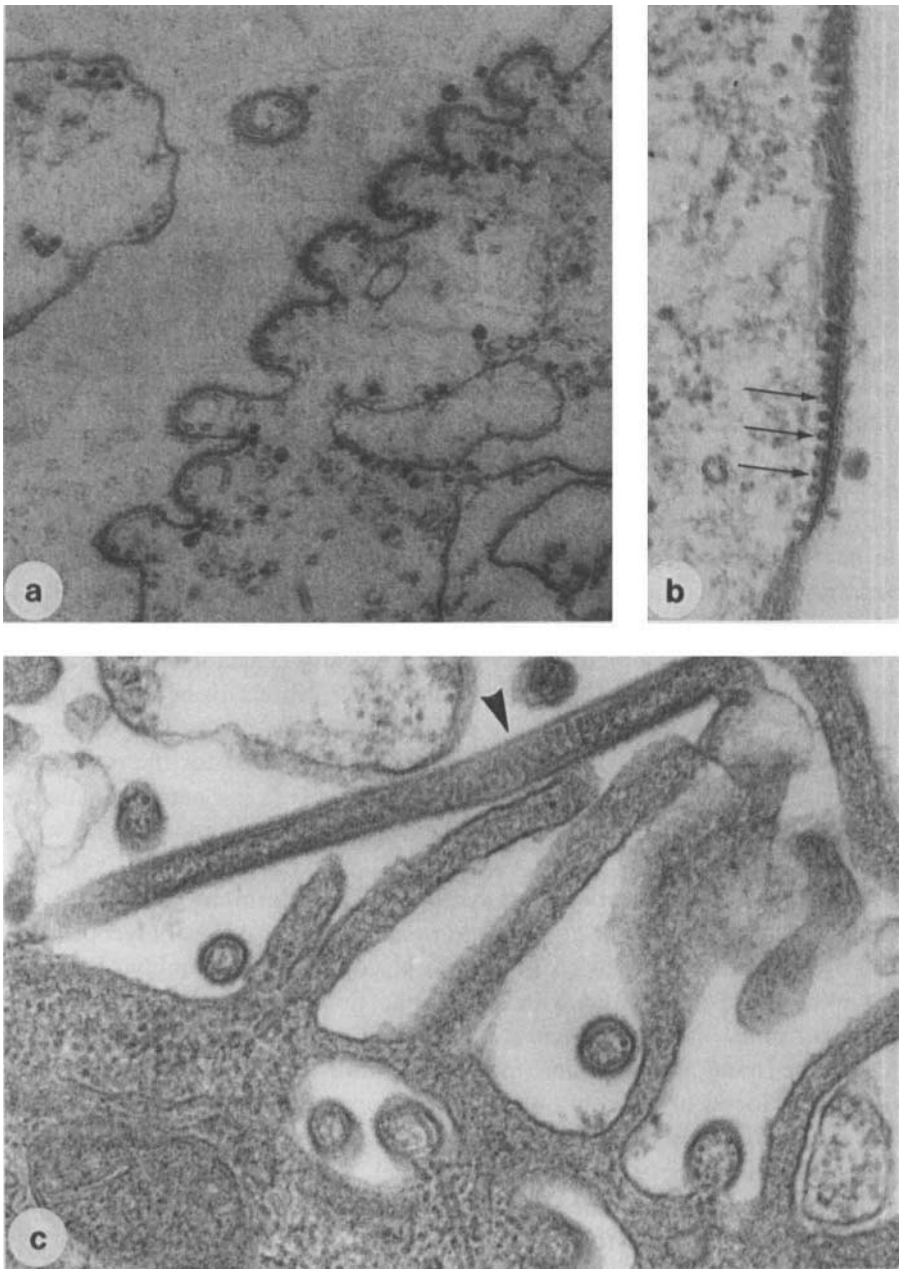

Fig. 16.8. Assembly of paramyxoviruses. (a) SV5 virions budding from the surface of monkey kidney cells. × 56 000. (b) Alignment of nucleocapsids beneath the area of plasma membrane with a patch of spikes in SV5-infected BHK-21F cells. × 77 000. (Both pictures from Choppin and Compans, 1975; with permission.) (c) Budding Sendai virus particles, both spherical and filamentous (arrowhead). × 85 000. All ultrathin sections. (By courtesy of Dr. D. Hockley.)

the M protein. The nucleocapsid aligns underneath such modified regions of the plasma membrane, and virus assembly is concluded by the budding of this region and release of the virus particle. Released virions contain actin (Wang et al., 1976) and actin filaments have been shown to protrude into budding virions (Fig. 16.9; Bohn et al., 1986), suggesting that the budding process may involve the vectorial growth of actin. Virus assembly and release are possible without overt damage to the cell, and persistent virus infection with continued virus production can be observed in vitro in many paramyxovirus-cell systems. The importance of the M protein for virus assembly is underscored by the finding that in patients suffering from subacute sclerosing panencephalitis (SSPE), a disease of the central nervous system caused by a persistent infection with measles virus, synthesis of the M protein is selectively suppressed and no mature virions are produced (Hall and Choppin, 1979; Cattaneo et al., 1986).

16.7. Pathogenicity

Parainfluenza viruses are respiratory pathogens. Mumps virus causes parotitis, orchitis and meningitis in man; Newcastle disease virus causes pneumonia and encephalitis in birds. With paramyxoviruses a mechanism has been established that accounts for virus- and host-dependent variation in pathogenicity. Thus, proteolytic cleavage and activation of the F protein, which is required for infectivity of the virus and for spread of virus and pathogenicity in the host, depends on the availability of host protease as well as susceptibility of the precursor protein to cleavage (Scheid and Choppin, 1976; Nagai et al., 1976).

Among the other paramyxoviridae, measles virus is the causative agent of measles in man, which may be complicated by encephalitis and, rarely, followed by subacute sclerosing panencephalitis (SSPE). Canine distemper virus causes respiratory disease and infection of the central nervous system in dogs, Rinderpest virus severe gastroenteritis in cattle. The pneumoviruses are respiratory agents. Respiratory syncytial virus causes severe respiratory disease in young infants.

The key features described above for Sendai virus and other paramoxyviruses apply to these viruses in a qualitative sense, even though the molecular weights of virus constituents and their physical parameters are not the same. One notable difference is the mode of virus attachment, which is not mediated by binding to neuraminic acid receptors. Furthermore, the protein responsible for hemagglutination and virus binding (H protein) does not in this case carry neuraminidase activity. There are antigenic relationships among viruses of the same genus, but not among different genera (Hall et al., 1980). Analysis of the primary structure of the polypeptides of morbillivirus M and F proteins shows extensive homology with the paramyxovirus proteins (Collins et al., 1984; Varsanyi et al., 1985; Bellini et al., 1986; Richardson et al., 1986).

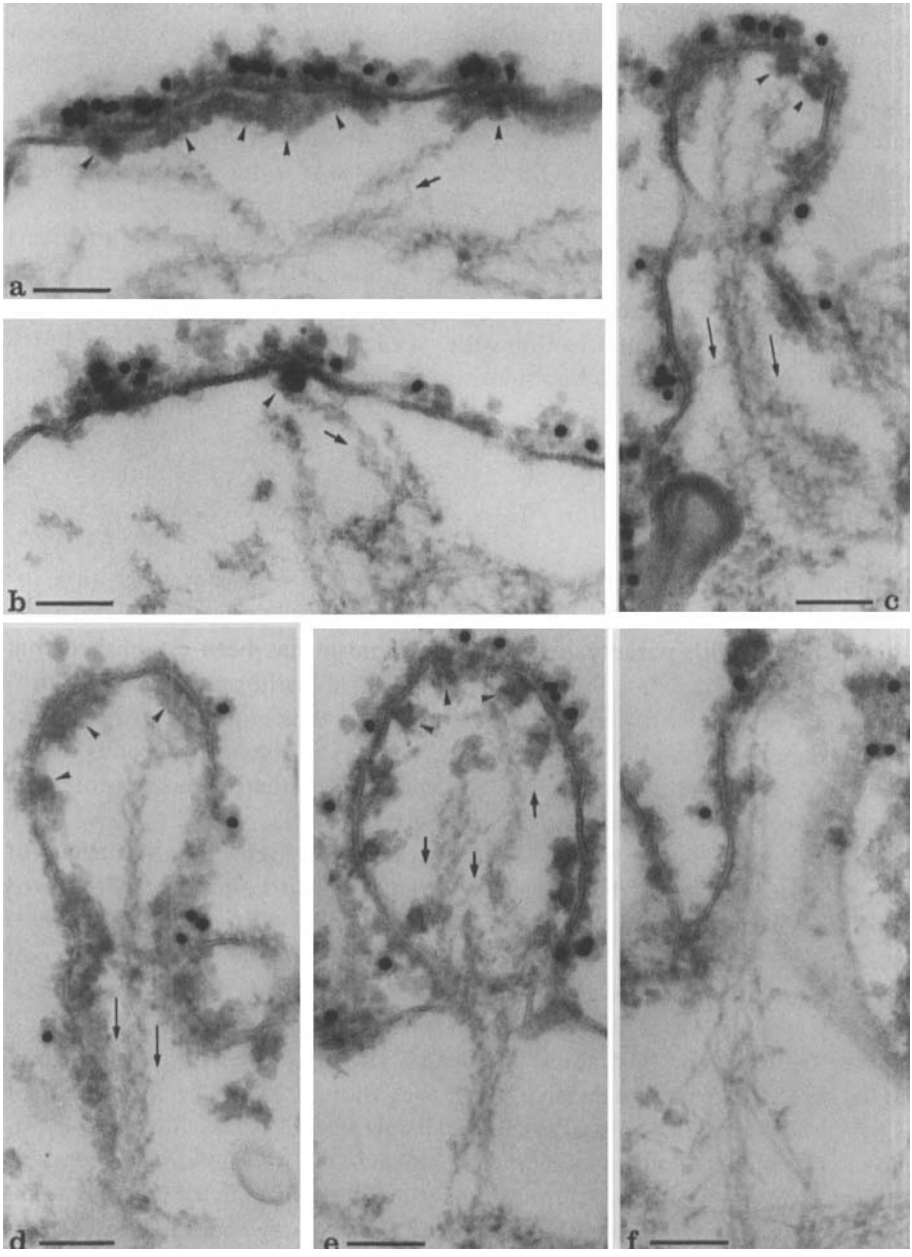
a
b
c
d
e
f

Acknowledgement

The author wishes to thank Dr. W. Bohn for valuable suggestions and comments on the manuscript.

References

Bächi, T. (1980) Intramembrane structural differentiation in Sendai virus maturation. Virology 106, 41–49.

Bellini, W.J., Englund, G., Richardson, C.D., Rozenblatt, S. and Lazzarini, R.A. (1986) Matrix genes of measles virus and canine distemper virus: Cloning, nucleotide sequences, and deduced amino acid sequences. J. Virol. 58, 408–416.

Blumberg, B.M., Rose, K., Simona, M.G., Roux, L., Giorgi, C. and Kolakofsky, D. (1984) Analysis of the Sendai virus M gene and protein. J. Virol. 52, 656–663.

Blumberg, B.M., Giorgi, C., Rose, K. and Kolakofsky, D. (1985a) Sequence determination of the Sendai virus fusion protein gene. J. Gen. Virol. 66, 317–331.

Blumberg, B., Giorgi, C., Roux, L., Raju, R., Dowling, P., Chollet, A. and Kolakofsky, D. (1985b) Sequence determination of the Sendai virus HN gene and its comparison to the influenza virus glycoproteins. Cell 41, 269–278.

Bohn, W., Rutter, G., Hohenberg, H., Mannweiler, K. and Nobis, P. (1986) Involvement of actin filaments in budding of measles virus: Studies on cytoskeletons of infected cells. Virology 149, 91–106.

Büechi, M. and Bächi, T. (1982) Microscopy of internal structures of Sendai virus associated with the cytoplasmic surface of host membranes. Virology 120, 349–359.

Carlsen, S.R., Peluso, R.W. and Moyer, S. (1985) In vitro replication of Sendai virus wild-type and defective interfering particle genome RNAs. J. Virol. 54, 493–500.

Cattaneo, R., Schmid, A., Rebmann, G., Backo, K., ter Meulen, V., Bellini, W.J., Rozenblatt, S. and Billeter, M.A. (1986) Accumulated measles virus mutations in a case of subacute sclerosing panencephalitis: Interrupted matrix protein reading frame and transcription alteration. Virology 154, 97–107.

Chanock, R.M. (1979) Parainfluenza viruses. In Diagnostic Procedures for Viral, Rickettsial and Chlamydial Infections, Eds. E.H. Lennette and N.J. Schmidt; pp. 611–632. American Public Health Association, Washington.

Choppin, P.W. and Compans, R.W. (1975) Reproduction of paramyxoviruses. In Comprehensive Virology, Eds. H. Fraenkel-Conrat and R.R. Wagner; Vol. 5, pp. 95–178. Plenum, New York, London.

Fig. 16.9. Actin filaments associated with viral structures at the plasma membrane of measles virus-infected cells. Extracted cytoskeletons were labelled with rabbit anti-measles antibody and protein-A-conjugated colloidal gold, and treated with heavy meromysin to decorate actin filaments (a–e; in panel f actin decoration is prevented by the presence of pyrophosphate). Arrowheads point to nucleocapsid-like structures. Arrows indicate the direction of arrowheads in actin filaments. Panels c–f show skeletal structures of budding viruses. Evaluation of many such images indicates that the majority of actin filaments protrude into the bud with the barbed end and only a few with the pointed end. The length of the bar is 0.1 μm. (From Bohn et al., 1986; with permission.)

Choppin, P.W. and Scheid, A. (1980) The role of viral glycoproteins in adsorption, penetration and pathogenicity of viruses. Rev. Inf. Dis. 2, 40–61.

Collins, P.L., Huang, Y.T. and Wertz, G. (1984) Nucleotide sequence of the gene encoding the fusion (F) glycoprotein of human respiratory syncytial virus. Proc. Natl. Acad. Sci. USA 81, 7683–7687.

Dubois-Dalcq, M., Holmes, K. and Rentier, B. (1984) Assembly of paramyxoviridae. Assembly of Enveloped RNA Viruses. Springer Verlag, New York, Vienna.

Finch, J.T. and Gibbs, A.J. (1970) Observations of the structure of the nucleocapsids of some paramyxoviruses. J. Gen. Virol. 6, 141–150.

Gething, M.J., White, J.M. and Waterfield, M.D. (1978) Purification of the fusion protein of Sendai virus: Analysis of the N-terminal sequence generated during precursor activation. Proc. Natl. Acad. Sci. USA 75, 2737–2740.

Hall, W.W. and Choppin, P.W. (1979) Evidence for lack of synthesis of the M-polypeptide of measles virus in brain cells in subacute sclerosing encephalitis. Virology 99, 443–447.

Hall, W.W., Lamb, R.A. and Choppin, P.W. (1980) The polypeptides of canine distemper virus. Synthesis in infected cells and relatedness to the peptides of other morbilliviruses. Virology 100, 433–449.

Hamaguchi, M., Yoshida, T., Nishikawa, K., Naruse, H. and Nagai, Y. (1983) Transcriptive complex of Newcastle disease virus. I. Both L and P proteins are required to constitute an active complex. Virology 128, 105–117.

Heggeness, M.H., Scheid, A. and Choppin, P.W. (1980) Conformation of the helical nucleocapsid of paramyxoviruses and vesicular stomatitis virus: Reversible coiling and uncoiling induced by changes in salt concentration. Proc. Natl. Acad. Sci. USA 77, 2631–2635.

Heggeness, M.H., Scheid, A. and Choppin, P.W. (1981) The relationship of conformational changes in the Sendai virus nucleocapsid to proteolytic cleavage of the NP polypeptide. Virology 114, 555–562.

Heggeness, M.H., Smith, P.R. and Choppin, P.W. (1982) In vitro assembly of the nonglycosylated membrane protein (M) of Sendai virus. Proc. Natl. Acad. Sci. USA 79, 6232–6236.

Hewitt, J.A. and Nermut, M.V. (1977) A morphological study of the M-protein of Sendai virus. J. Gen. Virol. 34, 127–136.

Hiebert, S.W., Paterson, R.G. and Lamb, R.A. (1985) Hemagglutinin-neuraminidase protein of the paramyxovirus simian virus 5: Nucleotide sequence of the m-RNA predicts an N-terminal membrane anchor. J. Virol. 54, 1–6.

Homma, M. and Ohuchi, M. (1973) Trypsin action on the growth of Sendai virus in tissue culture cells. III. Structural differences of Sendai viruses grown in eggs and in tissue culture cells. J. Virol. 12, 1457–1465.

Hosaka, Y. and Hosoi, J. (1983) Study of negatively stained images of Sendai virus nucleocapsids using minimum-dose system. J. Ultrastruct. Res. 84. 140–150.

Hsu, M.-c. and Choppin, P.W. (1984) Analysis of Sendai virus mRNAs with cDNA clones of viral genes and sequences of biologically important regions of the fusion protein. Proc. Natl. Acad. Sci. USA 81, 7732–7736.

Hsu, M.-c., Scheid, A. and Choppin, P.W. (1979) Reconstitution of membranes with individual paramyxovirus glycoproteins in phospholipid and cholate solution. Virology 95, 476–491.

Hsu, M.-c., Scheid, A. and Choppin, P.W. (1981) Activation of the Sendai virus fusion protein (F) involves a conformational change with exposure of a new hydrophobic region. J. Biol. Chem. 256, 3557–3563.

Hsu, M.-c., Scheid, A. and Choppin, P.W. (1982) Enhancement of membrane fusing activity of Sendai virus by exposure of the virus to basic pH is correlated with a conformational change in the fusion protein. Proc. Natl. Acad. Sci. USA 79, 5862–5866.

Kim, J., Hama, K., Miyake, Y. and Okada, Y. (1979) Transformation of intramembrane particles of HVJ (Sendai virus) envelopes from an invisible to visible form on aging of virions. Virology 95, 523–535.

Klenk, H.-D. and Choppin, P.W. (1970) Plasma membrane lipids and parainfluenza virus assembly. Virology 40, 939–947.

Lamb, R.A. and Choppin, P.W. (1978) Determination by peptide mapping of the unique polypeptides in Sendai virions and in infected cells. Virology 84, 469–478.

Lamb, R.A., Mahy, B.W.J. and Choppin, P.W. (1976) The synthesis of Sendai virus polypeptides in infected cells. Virology 69, 116–131.

Lund, G.A., Tyrrell, D.L.J., Bradley, R.D. and Scraba, D.G. (1984) The molecular length of measles virus RNA and the structural organization of measles nucleocapsids. J. Gen. Virol. 65, 1535–1542.

Merz, D.C., Scheid, A. and Choppin, P.W. (1980) The importance of antibodies to the fusion glycoprotein (F) of paramyxoviruses in the prevention of spread of infection. J. Exp. Med. 151, 275–288.

Nagai, Y., Klenk, H.-D. and Rott, R. (1976) Proteolytic cleavage of viral glycoproteins and its significance for the virulence of Newcastle disease virus. Virology 72, 494–508.

Örvell, C., Rydbek, R. and Löve, A. (1986) Immunological relationships between mumps virus and parainfluenza viruses studied with monoclonal antibodies. J. Gen. Virol. 67, 1929–1939.

Paterson, R.G., Harris, T.J.R. and Lamb, R.A. (1984) Fusion protein of the simian virus 5: Nucleotide sequence of mRNA predicts a highly hydrophobic glycoprotein. Proc. Natl. Acad. Sci. USA 81, 6706–6710.

Portner, A. and Murti, K.G. (1986) Localization of P, NP and M proteins on Sendai virus nucleocapsid using immunogold labeling. Virology 150, 469–478.

Raghow, R. and Kingsbury, D.W. (1979) Protein-RNA contacts in Sendai virus nucleocapsids revealed by photo-crosslinking. Virology 98, 267–271.

Richardson, C.D. and Choppin, P.W. (1983) Oligopeptides that specifically inhibit membrane fusion by paramyxoviruses: Studies on the site of action. Virology 131, 518–532.

Richardson, C.D., Scheid, A. and Choppin, P.W. (1980) Specific inhibition of paramyxovirus and myxovirus replication by oligopeptides with amino acid sequences similar to those at the N-termini of the F_1 or HA_2 viral polypeptides. Virology 105, 205–222.

Richardson, C.D., Hull, D., Greer, P., Hasel, K., Berkovich, A., Englund, G., Bellini, W., Rima, B. and Lazzarini, R. (1986) The nucleotide sequence of the mRNA encoding the fusion protein of measles virus (Edmonston strain). A comparison of fusion proteins from several different paramyxoviruses. Virology, in press.

Scheid, A., Caliguiri, L.A., Compans, R.W. and Choppin, P.W. (1972) Isolation of paramyxovirus glycoproteins. Association of both hemagglutinating and neuraminidase activities with the larger SV5 glycoprotein. Virology 50, 640–652.

Scheid, A. and Choppin, P.W. (1973) Isolation and purification of the envelope proteins of Newcastle disease virus. J. Virol. 11, 263–271.

Scheid, A. and Choppin, P.W. (1974) Identification of biological activities of paramyxovirus glycoproteins. Activation of cell-fusion, hemolysis and infectivity by proteolytic cleavage of an inactive precursor protein of Sendai virus. Virology 57, 475–490.

Scheid, A. and Choppin, P.W. (1974b) The hemagglutinating and neuraminidase (HN) protein of a paramyxovirus: Interaction with neuraminic acid in affinity chromatography. Virology 62, 125–133.

Scheid, A. and Choppin, P.W. (1976) Protease activation mutants of Sendai virus: Activation of biological properties by specific proteases. Virology 69, 265–277.

Scheid, A. and Choppin, P.W. (1977) Two disulfide-linked polypeptide chains constitute the active F protein of paramyxoviruses. Virology 80, 54–66.

Scheid, A., Graves, M.C., Silver, S.M. and Choppin, P.W. (1978) Studies on the structure and functions of paramyxovirus glycoproteins. In Negative Strand Viruses and the Host Cell, Eds. B.W.J. Mahy and R.D. Barry; pp. 181–193. Academic Press, London.

Schuy, W., Garten, W., Linder, D. and Klenk, H.-D. (1984) The carboxyterminus of the hemagglutinin-neuraminidase protein of Newcastle disease virus is exposed at the surface of the viral envelope. Virus Res. 1, 415–426.

Shimizu, Y.K., Shimizu, K., Ishida, N. and Homma, M. (1976) On the study of Sendai virus hemolysis. II. Morphological study of envelope fusion and hemolysis. Virology 71, 48–60.

Varsanyi, T.M., Jornvall, H. and Norrby, E. (1985) Isolation and characterization of the measles virus F_1 polypeptide. Comparison with other paramyxovirus fusion proteins. Virology 147, 110–117.

Wang, E., Wolf, B.A., Lamb, R.A., Choppin, P.W. and Goldberg, A.R. (1985) The presence of actin in enveloped viruses. In Cell Motility, Eds. R. Goldman, T. Pollard and J. Rosenbaum; pp. 589–599. Cold Spring Harbor Laboratory, Cold Spring Harbor, NY.

Nermut/Steven (eds) Animal Virus Structure

CHAPTER 17A

Retroviridae

H. FRANK

Max-Planck-Institut für Entwicklungsbiologie, Spemannstrasse 35, D-7400 Tübingen, F.R.G.

Family: Retroviridae (syn. Retraviridae, Oncoviridae, Leucoviridae, Oncornaviruses)

Subfamily: Oncovirinae. Genus, oncovirus B; Species, mouse mammary tumor viruses. Genus, oncovirus C; Species, murine leukemia and sarcoma viruses, avian leukemia and sarcoma viruses, etc. Genus, oncovirus D; Species, Mason Pfizer monkey virus, etc.

Subfamily: Lentivirinae. Genus, Lentivirus; Species, maedi-visna viruses, etc.

Subfamily: Spumavirinae. Genus, Spumavirus; Species, human foamy virus, simian foamy virus, etc.

17A.1. General characteristics

Retroviruses are enveloped particles most of which are about 100–120 nm in diameter with a core comprising a protein shell, a ribonucleoprotein complex and some (20–70) molecules of the enzyme reverse transcriptase. Utilizing both RNA- and DNA-dependent polymerase activities together with an RNase H activity, retroviruses replicate in a unique way: the linear, single-stranded positive-sense viral RNA is transcribed to a double-stranded DNA intermediate which is inserted as a provirus into the genome of the host. The production of RNA-containing virus progeny is started by regular transcription of the provirus. Retroviruses can be transmitted horizontally, i.e. by regular infection of other members of the host species (exogenous virus) or vertically by genetic transmission through the germ line (endogenous virus). The production of endogenous viruses in cell cultures can

start spontaneously or can be induced by chemical agents or radiation. Endogenous proviruses are common in the genome of many animal species.

Criteria for classification of retroviruses are predominantly morphological features as seen in ultrathin sections, schematically presented in Fig. 17A.1: site of core assembly (preformed in the cytoplasm or formed during the budding process at the plasma membrane); shape and size of surface protrusions (spike- or knob-like); presence or absence of electron-lucent space between envelope and core in immature particles, and shape and position of cores in mature particles. Classification of retroviruses into types A, B and C was introduced by Bernhard (1958).

17A.2. Oncovirinae

This main group of retroviruses contains all oncogenic members. Other members are of low oncogenicity or are non-oncogenic.

(a) *Intracisternal particles of type A* (syn. Cisternavirus A) (Fig. 17A.1a) are very similar in structure to cores of retroviruses: a double-layered structure with an electron-lucent center. These particles are often found in cells producing particles of types B and D. Biological effects of these particles are unknown.

(b) *Intracytoplasmic particles of type A* (Fig. 17A.1b) are complete cores of particles of type B, D, assembled in the cytoplasm before budding.

(c) *Oncovirus B* (syn. particles of type B) (Fig. 17A.1b). Cores assemble in the cytoplasm (as A-type particles) and acquire their envelope at the plasma membrane. Cores of mature viruses are located eccentrically within the envelope. Surface projections (knobs on stalks) are easily recognizable in thin sections.

(d) *Oncovirus C* (syn. particles of type C) (Fig. 17A.1c). Cores of this main group of Oncovirinae are assembled during the budding process at the plasma membrane. Cores of released viruses always remain centrically located within their envelope even in the collapsed mature form. Surface projections are knob-like and often hardly recognizable in thin sections.

(e) *Oncovirus D* (syn. particles of type D) (Fig. 17A.1d). Assembly of cores takes place in the cytoplasm. In contrast to type B cores, they reveal regular projections on their surface. The surface projections of the envelope, however, resemble the knobs of C-type particles. Mature particles frequently show a tubular core similar to the aberrant cores of type C.

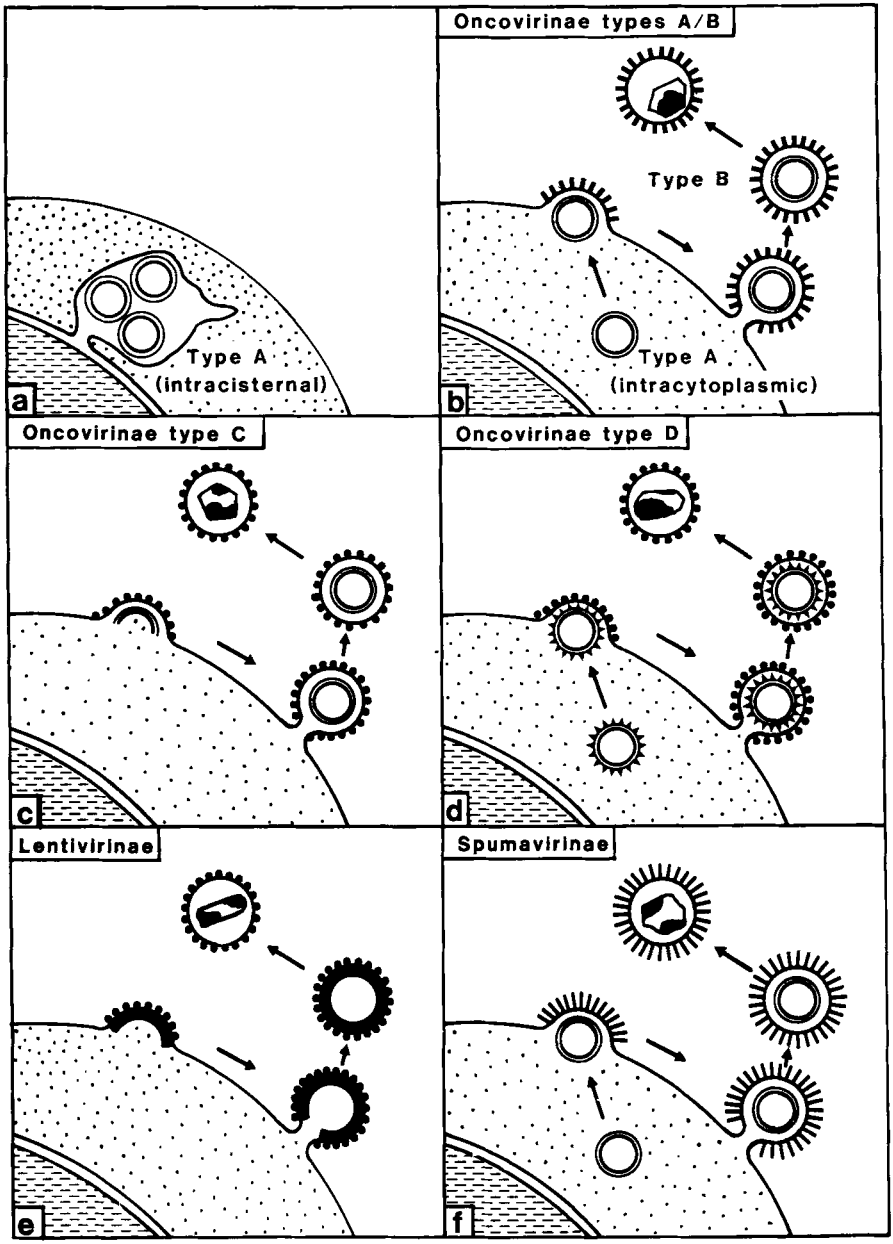

Fig. 17A.1. Illustration for classification of retroviruses according to morphological criteria.

17A.3. Lentivirinae (syn. slow viruses) (Fig. 17A.1e)

This subfamily contains pathogenic viruses causing 'slow virus infections'. As with oncoviruses of type C, core assembly takes place synchronously with the budding process at the plasma membrane. In contrast to particles of types B, C and D, the envelope and the core of budding and immature particles appear to be always in close contact in ultrathin sections. Surface projections are knob-like, similar to those of types C and D. Cores of mature particles are located centrically and are often tubular in shape.

17A.4. Spumavirinae (syn. foamy viruses) (Fig. 17A.1f)

No members of this subfamily are known to be pathogenic. Cores assemble in the cytoplasm in the same way as those of type B. Surface spikes are easily recognizable and clearly longer than those of type B.

Reference

Bernhard, W. (1958) Electron microscopy of tumor cells and tumor viruses. A review. Cancer Res. 18, 491-509.

Nermut/Steven (eds) Animal Virus Structure

CHAPTER 17B(i)

Oncovirinae: type B oncovirus

NURUL H. SARKAR

Memorial Sloan-Kettering Cancer Center, 1275 York Avenue, New York, NY 10021, U.S.A.

Genus: Oncovirus B
Species: murine mammary tumor virus (MuMTV)

17B(i).1. General characteristics

The murine mammary tumor virus (MuMTV), a complex enveloped RNA virus, is the only virus known to be the etiological agent of spontaneous mammary tumors in mice (Bentvelzen and Hilgers, 1980). MuMTV can be transmitted by two principal routes: (1) congenital infection of suckling mice by milk-borne exogenous virus and (2) genetically as an endogenous provirus. Exogenous MuMTV causes mammary adenocarcinomas in infected females at a high incidence (90–100%) between 7 and 9 months of age, and large quantities of MuMTV produced early (second and third parity) in the mammary glands of these mice are expressed in their milk. Their mammary tumor cells also produce large quantities of MuMTV. If the progeny of strains of mice that have a high incidence of cancer (except for the GR strains) are foster-nursed at birth on a mouse whose milk does not contain MuMTV, the resulting substrain of mice develop mammary tumors at a lower frequency (10–50%) and with a longer latent period (12–14 months), indicating the presence of genetically transmitted MuMTV proviruses.

Although MuMTV has been the subject of intense investigation for about half a century and historically was the first retrovirus to be isolated from mammalian sources, our knowledge about its structural organization and morphogenesis and its biology is still far from complete. Perhaps the most striking feature that

distinguishes MuMTV from other retroviruses is the presence of prominent projections on the viral surface. Furthermore, glucocorticoid hormone enhances the expression of the MuMTV genome at the level of transcription, resulting in increased production of MuMTV particles.

17B(i).2. Morphology of MuMTV

The first electron microscopic observation of a putative virus associated with the mammary tumors of mice was made by L. Dmochowski, C. Haagenson and Dan Moore in 1955 using thin sections of tumor cells. Three types of particles, classified in 1958 by W. Bernhard as Type A, budding B, and B particles, were observed (Fig. 17B(i).1). The intracytoplasmic A particles, which are believed to be synthesized and assembled near the Golgi area, are double-shelled spherical particles (Fig. 17B(i).1a), the diameters of the inner and outer shells being about 55 and 75 nm, respectively. The inner shell of the particles is more electron-dense than the outer. Clusters of A particles are always found inside the cytoplasm, often in close association with cytoplasmic vacuoles and near the cell membrane. The budding B particles at the cell membrane contain as their internal constituents doughnut-shaped structures which are morphologically indistinguishable from the intracytoplasmic A particles. The B particles (Fig. 17B(i).1b), often abbreviated as MTV, MMTV or MuMTV, are found outside the cell and occasionally inside cell vacuoles. MuMTV consists of an electron-dense nucleoid (viral core) of about 40–60 nm in diameter contained within an envelope 90–120 nm in diameter, which is acquired from the plasma membrane during budding. Usually the viral core is eccentrically located and is surrounded by a core shell. The viral membrane is covered with distinct projections consisting of knobs on stalks.

17B(i).3. Physical and chemical characteristics

MuMTV is composed of 1% RNA, 70% protein and 30% lipid. It has a sedimentation coefficient of about 1000 S and a buoyant density of 1.18 g/cm^3 in sucrose gradients. The viral core contains a 60–70 S RNA comprised of two identical

---

Fig. 17B(i).1. Electron micrographs of thin sections of cultured (panel b) and freshly obtained (panel a) mouse mammary tumor cells showing MuMTV particles. The intracytoplasmic A particles (panel a) consist of two concentric layers. The core of the budding B particles (bB) is spherical and has a morphology similar to that of A particles, whereas the core of the extracellular mature virus particles (mB) is condensed and eccentrically located (panel b). Both budding and mature particles exhibit projections (P) on their envelope surface. Panel (a), × 30000; panel (b), × 155000.

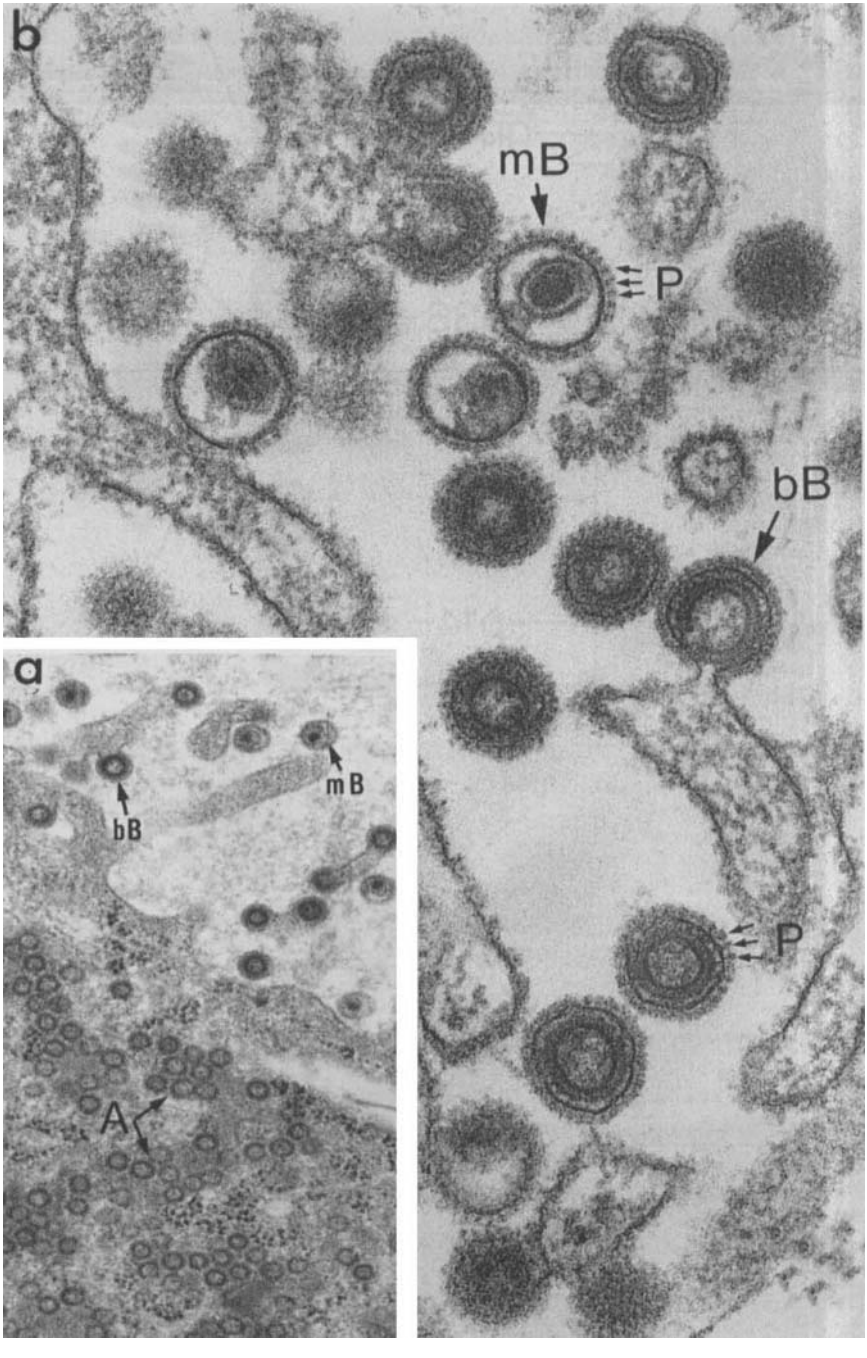
b
mB
P
bB
a
mB
bB
A
P

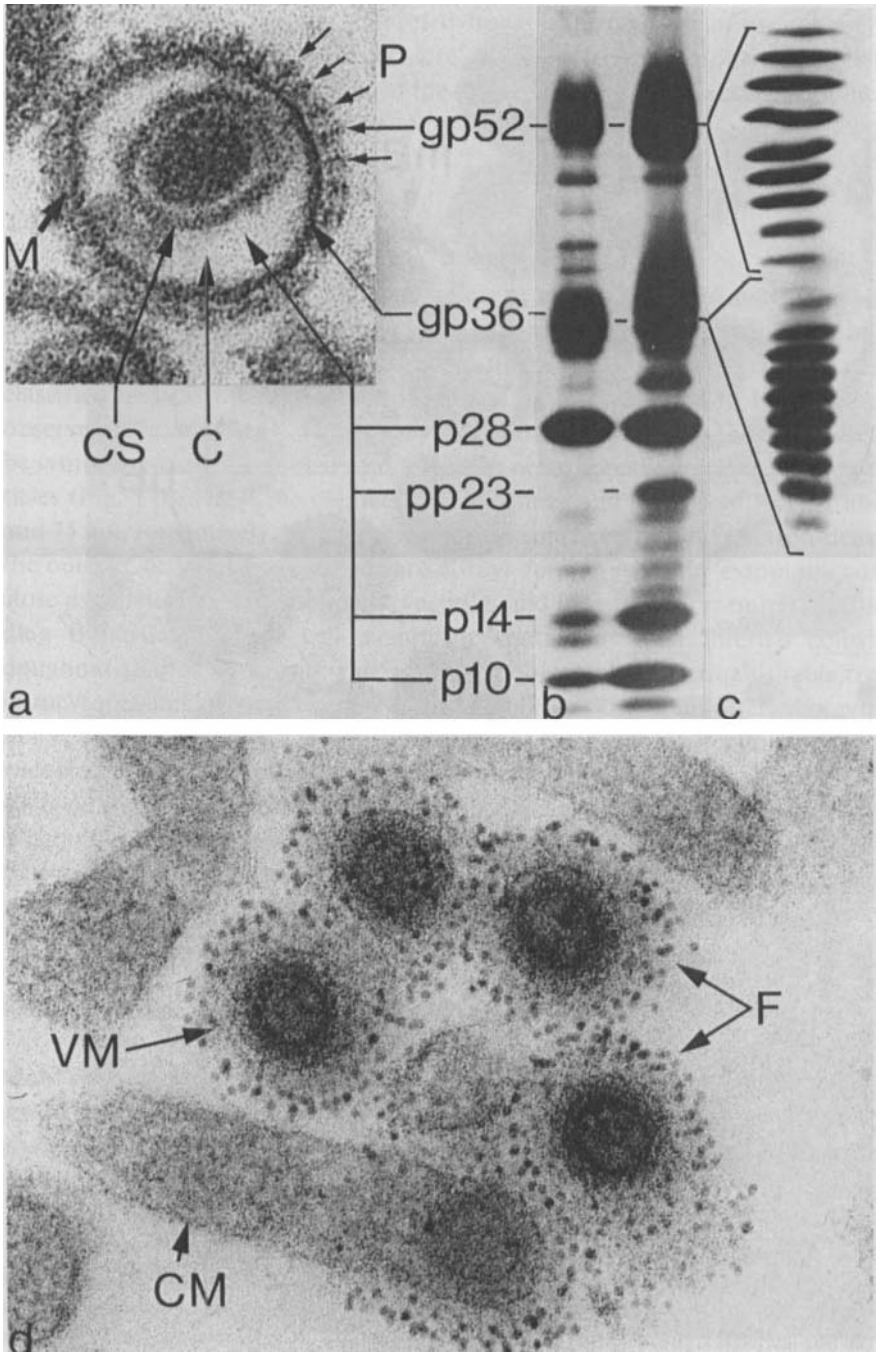
P
M
CS
C
gp52
gp36
p28
pp23
p14
p10
a
b
c
VM
F
CM
d

TABLE 17B(i).1.

Characteristics of the structural polypeptides of MuMTV

Protein (M_r)	Precursor^{gene}	Percentage of total virion protein	Location	Isoelectric point (hydrophobicity)	Properties
gp52 (52 000)	Pr70^{env}	30	Viral membrane, knob structure of the projections	5.5–7.0 (moderate)	Glycoprotein, 10% carbohydrate by weight; plays an important role in virus infection.
gp36 (36 000)	Pr70^{env}	20	Viral membrane, within lipid bilayer	4.5–5.0 (very strong)	Glycoprotein, 20% carbohydrate; transmembrane; anchors gp52 on the virus surface.
p28 (28 000)	Pr73^{gag}	24	Viral core	6.5–6.8 (strong)	Partially phosphorylated, postulated to be a component of the core shell; precise location within the viral core and function is unknown.
pp23 (23 000)	Pr73^{gag}	4	Viral core	4.5–5.0 (weak)	Phosphorylated; deficient in methionine; function unknown.
p14 (14 000)	Pr73^{gag}	10	Viral core	8.8 (weak)	Basic protein; considered as ribonucleoprotein; binds to single-stranded DNA; assumed to be complexed with viral RNA and thus may aid in RNA packaging.
p10 (10 000)	Pr73^{gag}	12	Viral core	7.5 (strong)	Most hydrophobic of the *gag* gene products; may function in interactions between viral core and membrane that leads to the budding of the virus.

Fig. 17B(i).2. Identification of the major polypeptides of MuMTV with the structural components of the virus. Panel (a) is a thin-section electron micrograph of a virion showing surface projections (P), membrane (M), core (C) and core shell (CS). Panel (b) shows the polypeptide composition of purified MuMTV, as resolved by polyacrylamide gel electrophoresis, radiolabeled in tissue culture with either [^{35}S]methionine (left lane) or with ^{14}C-labeled amino acids (right lane). The molecular weights of the proteins (p), phosphoprotein (pp) and glycoproteins (gp) are expressed in units of 1000. Panel (c) shows the heterogeneity of gp52 and gp36; [^{3}H]glucosamine-labeled MuMTV was subjected to isoelectric focusing. Panel (d) exhibits ferritin labeling of the MuMTV surface that demonstrates the association of gp52 with the distal end (i.e., the knob) of the viral projections. Mammary tumor cells were sequentially treated with goat anti-pg52 serum, hybrid antibody anti-goat γG/anti-ferritin, and ferritin (F) and then processed for electron microscopy. Note that, unlike the viral membrane (VM), the cell membrane (CM) is not labeled with ferritin. (a), × 365 000; (d), × 160 000.

copies of 35 S single-stranded RNA, each about 7.8 kb long. The genomic RNA is complexed with a number of associated cellular tRNAs. MuMTV is composed of 6 major polypeptides and a few molecules of RNA-dependent DNA polymerase (reverse transcriptase, RT, M_r 80–100). The genomic origin, viral location and properties of these polypeptides are summarized in Table 17B(i).1 and Fig. 17B(i).2. MuMTV appears to have a protease activity inside the virion which cleaves the MuMTV gag precursor polyprotein with high specificity (Sen and Sarkar, 1980). All the MuMTV-specific polypeptides are encoded by three distinct genes in the viral RNA. In a 5′ to 3′ order these are arranged into *gag, pol* and *env* genes. The *gag* gene codes for p28, pp23, p14 and p10, the *pol* gene for RT, and the *env* gene for gp52 and gp36.

MuMTV-gp52 is exposed at the viral surface. The most direct and convincing evidence is the finding that, unlike monospecific anti-MuMTV-gp36 antibody, anti-MuMTV-gp52 reacts with the viral surface, specifically with the knobs of the MuMTV projections (Fig. 17B(i).2d). It has been shown that gp36 and gp52 interact with each other hydrophobically to form triplet complexes that comprise the viral projections observed by electron microscopy (Marcus et al., 1978; Dion et al., 1979; Racevskis and Sarkar, 1980). It is assumed, therefore, that gp36 acts as a transmembrane protein which anchors gp52 on the viral surface.

17B(i).4. Organization of the virus surface

The architecture of the MuMTV surface is complex, exhibiting characteristic surface projections (Sarkar et al., 1973; Hageman et al., 1981). The projections, as observed after negative staining, are found to be composed of two distinct components, spherical/ellipsoidal knob-like structures approximately 5.5 nm in diameter, and thin stalks about 4.0 nm in length and 2.0 nm in diameter, which

Fig. 17B(i).3. High-power micrographs of MuMTV particles negatively stained with phosphotungstic acid (pH 7.0). The particles in panels (a) and (c) are intact; spherical or pear-shaped projection (P) knobs can be clearly seen to be attached to their membranes by thin stalks. The particle in panel (c) exhibits regularly arranged projections on its surface. Examples of the six- and five-fold clustering of the projections are circled; note that many of the projections are triangular in appearance and seem to be composed of three subunits. Panel (b) shows the membrane of a virus particle in which the surface projections are viewed end-on. The projections are distributed in a six-coordinate array, i.e., each projection is surrounded by six others. The projections associated with a detached MuMTV membrane in panel (d) have a triangular appearance and form a sort of reticular (R) network. Panels (e–i) show images of the projections produced by a three-fold ($n = 3$) rotation about the central part of five selected knobs in which the three subunits are either very tightly or loosely bound together. (a), × 502 000; (b), × 302 000; (c), × 440 000; (d), × 280 000; (e–i), × 2 900 000.

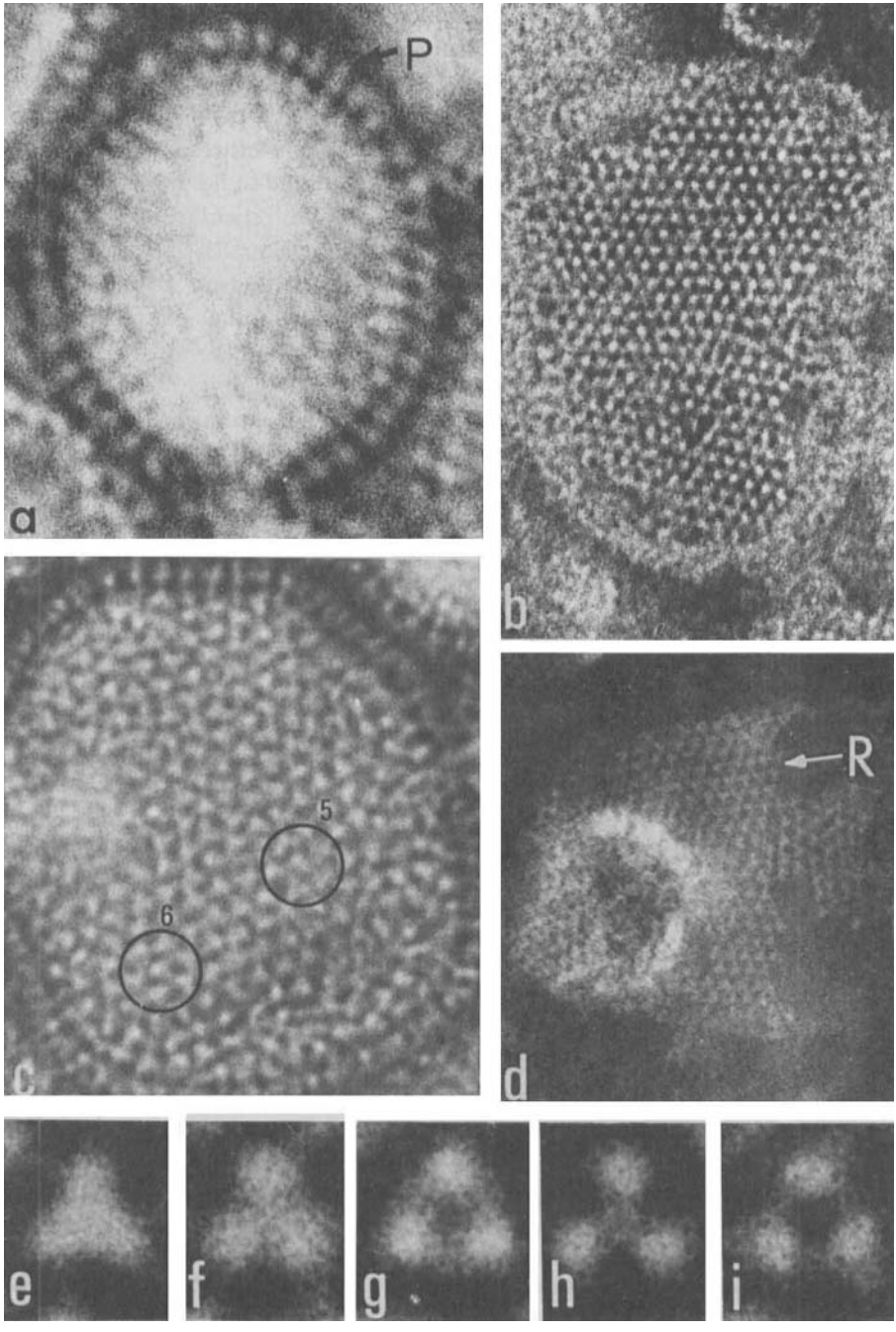
P
a
b
5
6
c
R
d
e
f
g
h
i

connect the knobs to the viral membrane (Fig. 17B(i).3). The length of the projections is about 9.5 nm and they are spaced about 7.4 nm apart. Both morphological and biochemical studies have provided strong evidence that the knobs of the viral projections are composed of at least three subunits 1.5–2.5 nm in diameter. Most of the viral projections are distributed in a six-coordinated array (Fig. 17B(i).3b,c), i.e., each projection is surrounded symmetrically by six others (Nermut, 1973; Sarkar and Moore, 1974). Some projections are also found to have five immediate neighbors (Fig. 17B(i).3c). The viral surface appears as a 'reticular' structure (Fig. 17B(i).3d) exhibiting a regular hexagonal array and occasionally pentavalent units (Sarkar and Moore, 1974). The spacing between the nearest corners of the 'reticular' structure is about 7.4 nm, which is the same as that of the center-to-center spacing of the projections. Under certain circumstances rings formed by 6 (rarely 5) projections have been observed. These are either contiguous and measure about 16–18 nm from center-to-center or appear as two complete rings in close contact with a center-to-center spacing of 18–20 nm (Nermut, 1973; Calberg-Bacq et al., 1976).

However, when purified or budding MuMT virions are examined after freeze-drying and shadowing a regular array of pits arranged with a hexagonal symmetry (with occasional five-coordinated pits) is observed (Fig. 17B(i).4). The approximate distance between the pits is about 18 nm, which is close to the center-to-center spacing of rings seen in negatively stained preparations. A plausible explanation would be that the pits are depressions in the rings of projections which are too close to be resolved by shadowing. Considering these observations it has been proposed that the organization of the envelope is quasi-icosahedral, that is, like a geodesic dome (Sarkar and Moore, 1974).

17B(i).5. The internal structure of MuMTV

The structural organization of the core of type B particles is not yet understood because it has been difficult to isolate intact cores from purified MuMTV. Isolated cores in negatively stained preparations usually appear as collapsed structures with tangled threads 3–5 nm in diameter. Occasionally cores with filamentous, possibly helical, structures 7–9 nm in diameter are observed (Fig. 17B(i).5). Similar struc-

Fig. 17B(i).4. The appearance of freeze-dried and shadowed MuMTV particles. Panel (a) shows purified MuMTV prepared from the milk of strain RIII mice. The particles exhibit highly regular pits on their surface and most of the pits are six-coordinated. Pits with five neighbors are also seen occasionally. The area enclosed by a pentagon contains 9 pits distributed in a six-fold and five-fold arrangement. The area enclosed by the circle outlines 7 pits – a central pit surrounded by six immediate neighbors. Panel (b) shows the appearance of MuMTV particles (mostly budding) on the surface of cultured mammary tumor cells. The virions have pits on their surface which are arranged in a six-coordinated array. The arrows point to the direction of shadows. (a), × 180 000; (b), × 185 000.

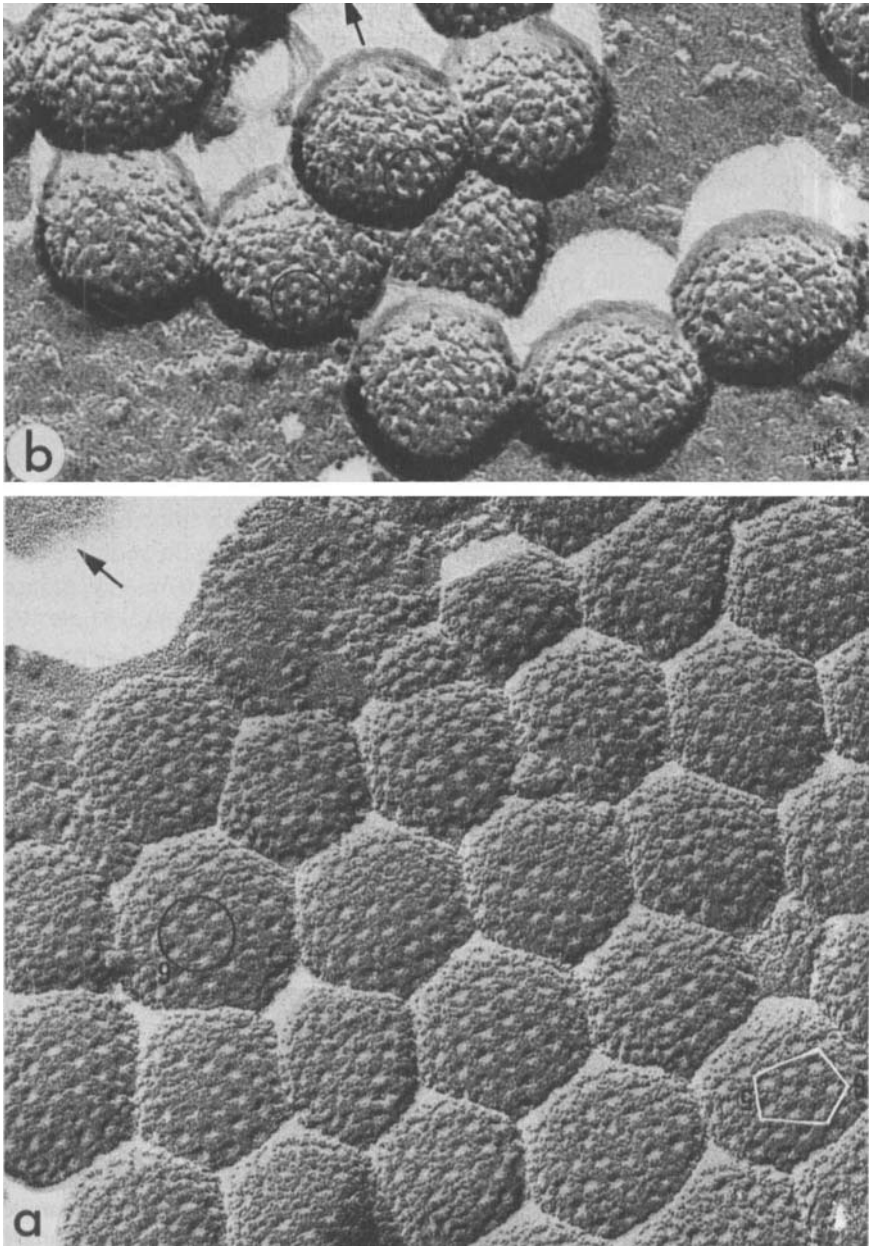
b
a

tures are also seen in the cores of budding B particles that have been prepared for electron microscopy by whole cell mount negative staining as well as in purified negatively stained B particles in which the electron stain has penetrated. The application of the techniques of freeze-drying and shadowing to isolated cores has not resolved the question of whether or not regularly arranged subunit structures are present on the surface. Thus, the possibility that the MuMTV core is icosahedral remains to be established.

Fig. 17B(i).6 shows a tentative model of MuMTV with the main structural complexes. Some of them are still hypothetical (the architecture of the core and the RNP complex) or not generally accepted, such as the inner coat apposed to the membrane as in oncovirus C (see Chapter 17B(ii) and Fig. 17B(i).5e).

17B(i).6. Biological properties of MuMTV

There are at least 5 strains of MuMTV, which are classified on the basis of their biological properties, i.e., their potency for tumor induction, and the mouse strain from which they originated. For example, MuMTVs isolated from the mouse strains C3H, GR, RIII, A and DBA are highly oncogenic, whereas those MuMTVs derived from C3Hf, RIIIf, Af and DBAf are weakly oncogenic. In general, the biophysical and biochemical properties of the various MuMTVs that have been studied appear to be similar. However, unlike gp36 and p14, the peptide maps of the other polypeptides of MuMTV, gp52, p28 and p10 of GR-, RIII- and C3H-MuMTVs exhibit strain-specific differences (Gautsch et al., 1978). In addition, different MuMTV strains exhibit differences in their antigenic determinants. For example, monoclonal antibodies directed to gp52 recognize type-specific determinants of C3H-MuMTV, class-specific determinants shared by C3H- and GR-MuMTV and group-specific determinants shared by C3H-, RIII-, GR- and C3Hf-MuMTV (Massey et al., 1980). The presence of type- and group-specific antigenic determinants has been reported in gp36 and p28; gp36 also shows interspecies-

---

Fig. 17B(i).5. Panel (a) shows whole cell mount negative staining of part of a mouse mammary tumor cell grown in tissue culture. The projections (P), the membrane (VM) and the core (C) of the budding virus particle can be clearly distinguished. Note the smooth appearance of the surface of the cell membrane (CM) as compared to the projection-covered surface of the budding virus particle. The A particle in panel (b) was purified from a mammary tumor of the mouse. Panel (c) shows a mature B particle with the same structural features as in panel (a). The MuMTV core shown in panel (d) was obtained by means of Tween-ether treatment. The core shows two concentric rings with beaded appearance (outer ring = core shell, inner ring is probably the RNP complex). Panel (e) shows an intact MuMTV particle after negative staining with uranyl acetate. The core and a thin spherical shell (inner coat) underneath the envelope have been visualized. (Courtesy of Dr. H. Frank.) Magnification: (a) × 320000; (b), × 560000; (c), × 410000; (d), × 660000; (e), × 220000.

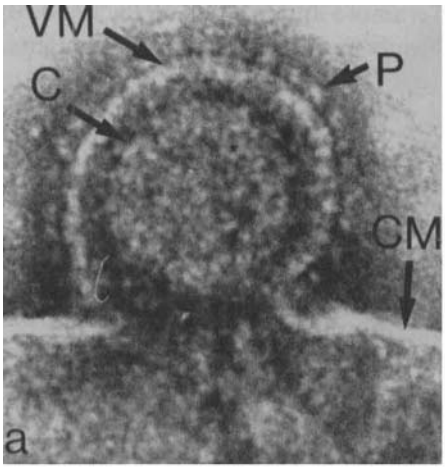
VM
C
P
CM
a

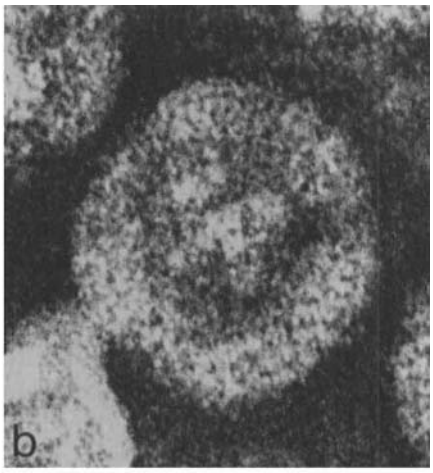
b

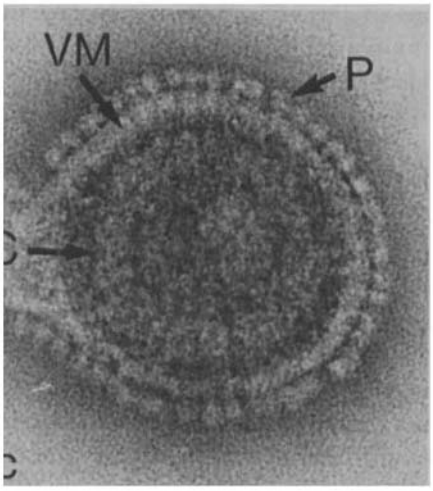
VM
P
c

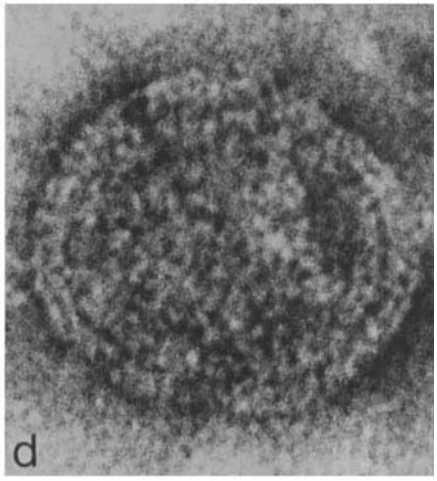
d

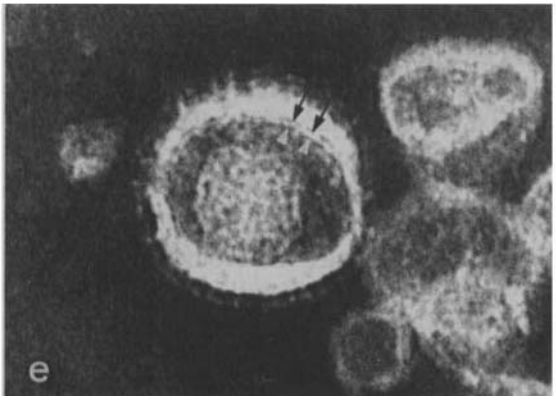
e

specific determinants (Marcus et al., 1979; Teramoto and Schlom, 1978, 1979). By contrast, p14 and p10 appear to show only group-specific antigenic determinants.

17B(i).7. MuMTV replication

The life-cycle of MuMTV, like other retroviruses, begins with the infection of a susceptible host cell, in which intact virus penetrates the cell membrane (Fig. 17B(i).7), probably via 'coated pits' (Sarkar et al., 1970). Once inside the cell the various structural components of the virus are dissociated and the genetic information in the viral RNA is reverse-transcribed into double-stranded DNA, which then becomes integrated into the chromosomal DNA of the host cell. The integrated viral DNA (proviral DNA) is transcribed into the 35 S genomic RNA and two messenger RNAs (mRNAs) 35 S and 24 S in size. From the 35 S mRNA a polyprotein ($Pr73^{gag}$) precursor of the core proteins of the virus is translated and then undergoes post-translational modification by phosphorylation (Dickson and Atterwill, 1979; Nusse et al., 1978; Racevskis and Sarkar, 1979; for review, see Dickson and Peters, 1983). Reverse transcriptase is also translated from the 35 S mRNA as a fusion protein, $Pr160^{gag\text{-}pol}$.

Reconstruction of the sequence of morphogenetic events from electron micrographs, together with the observations that A particles are related immunologically and biochemically to the core component of B particles, suggests that the intracytoplasmic A particles are the precursor of B particles (Tanaka, 1977; Cardiff et al., 1978). Thus it appears that viral RNA, $Pr73^{gag}$, reverse transcriptase, and possibly a specific protease are assembled together intracellularly into A particles which then migrate to the cell membrane, often to the tips of the microvilli, and adhere to the inner surface of the plasma membrane, initiating the process of viral budding; meanwhile, the envelope glycoproteins of MuMTV are synthesized from a 24 S mRNA initially as a precursor with a molecular weight of 60 000 (Dickson and Atterwill, 1980). During glycoprotein synthesis at least five core oligosaccharide units composed of glucosamine and mannose are added to the growing polypeptide chain. The molecular weight of the glycosylated precursor ($Pr70^{env}$) is about 70 000. After primary glycosylation, $Pr70^{env}$ is cleaved into gp52 and gp36 (Arthur et al., 1982; Sarkar and Racevskis, 1983). The sequence of gp52 and gp36 within $Pr70^{env}$ is NH_2-gp52-gp36-COOH. Both gp52 and gp36 are then modified by secondary glycosylation and interact to form intracellular complexes, which then migrate to the cell surface to become the projections on the budding A particles. The A particles are then enveloped by the plasma membrane and released from the cell by budding. Consequently the core of the freshly budded B particles, which are known as immature B particles, resembles the intracytoplasmic A particle. As soon as a budding virus is released from the cell membrane, the *gag* precursor ($Pr73^{gag}$) contained within the particle is cleaved by a protease

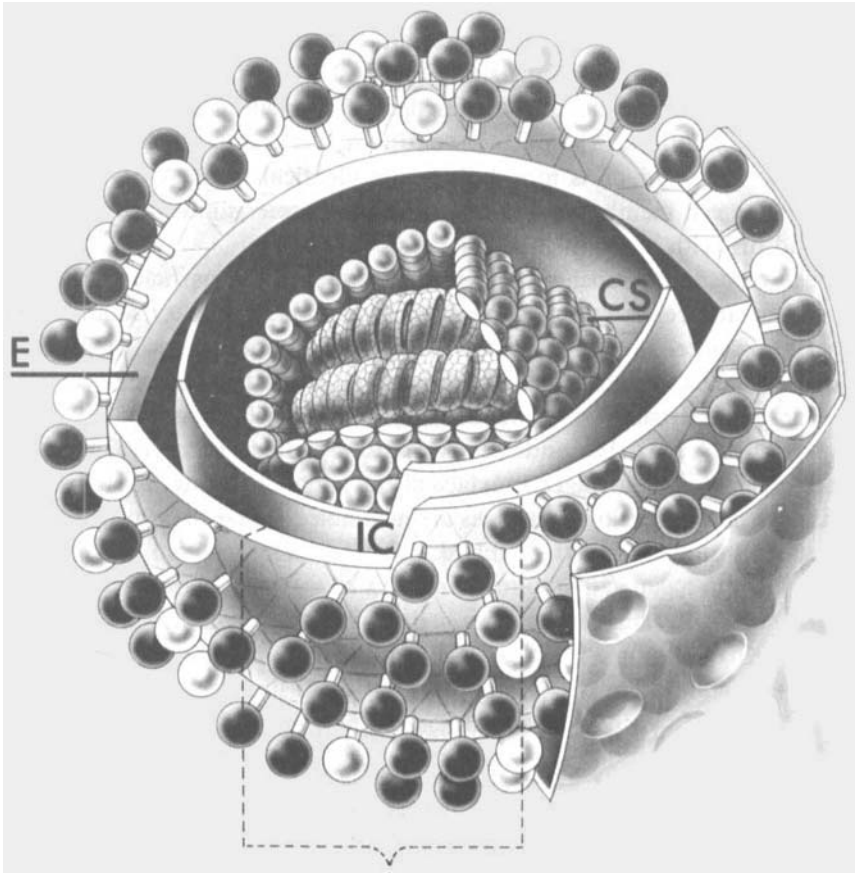

Fig. 17B(i).6. A three-dimensional model of MuMTV showing the following structural features. At the center of the virion is the core comprising an RNA/protein complex (here shown as a 'nucleohelix') and a core shell (SC) with possible icosahedral symmetry. The surface of the viral membrane (E) is covered with glycoprotein projections in regular hexagonal array. Both closely packed projections and rings of six projections (bracket) are shown here. The lower right corner shows the position of pits as observed after freeze-dry shadowing. Below the envelope is a thin spherical shell – the inner coat (IC). Approximately in scale. Drawing by Mrs. Cynthia Clarke (biomedical illustrator).

into the mature core proteins p28, pp23, p14 and p10, whose sequence in the precursor is NH_2-p10-pp23-p28-p14-COOH. Concomitant to this precursor polyprotein processing, the hollow double-shelled spherical core of the immature B particle undergoes a rapid structural transition, possibly due to a change in the spatial arrangement of the core proteins, to yield a condensed nucleoid without any noticeable change in the structure of the viral envelope.

There appears to be another mode of morphogenesis of the MuMTV core in

which the budding of MuMTV, like other retroviruses, is initiated by the formation of a viral core underneath the cell membrane at the site of viral budding, resulting in the protrusion of the cell membrane and the formation of a crescent consisting of two electron-dense layers (Sarkar et al., 1977). The cell membrane involved in virus budding shows the presence of projections characteristic of MuMTV. As the budding of the particle continues, the crescent enlarges until it forms a hollow sphere which is morphologically identical to an A particle. The virus buds off the cell membrane and matures in a manner similar to those particles that bud off with preformed A particles.

There seems to be a relationship between the synthesis of A particles, the mode of virus budding and cellular environment. First, normal mammary cells, as well as mammary tumor cells in vivo, are always found to contain more A particles than budding particles, and the clusters of A particles around cytoplasmic vacuoles do not appear to participate in virus budding. By contrast, cultured mammary tumor cells show very few A particles inside the cytoplasm, giving the impression that A particles are assembled near the cell surface at the site of budding. It is possible, however, that in cultured cells A particles are assembled inside the cytoplasm and

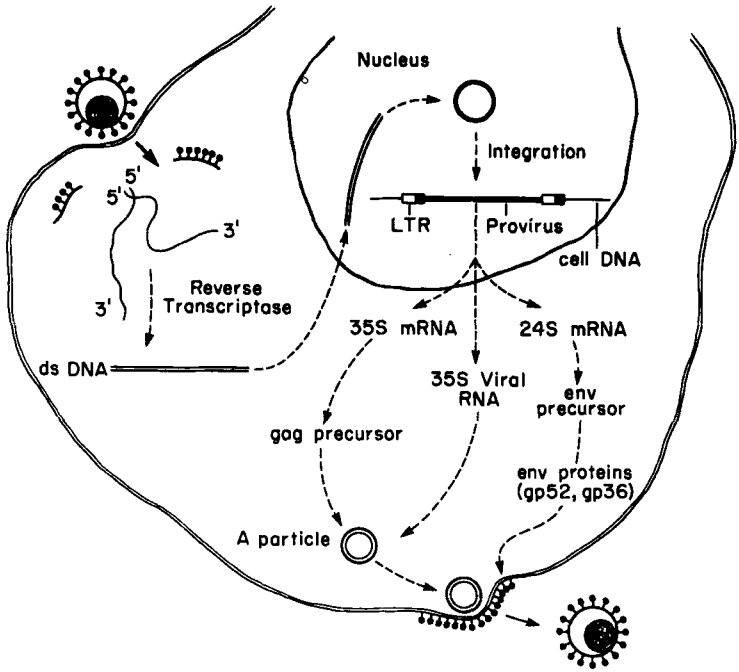

Replicative cycle of MuMTV

Fig. 17B(i).7. Replicative cycle of MuMTV. See text for details.

that they migrate to the cell membrane as soon as they are synthesized. Thus, unlike in vivo, A particles are not found to accumulate in the cytoplasm of cultured cells. Secondly, budding particles consisting of incomplete A particles are found more often in cultured cells than in the freshly excised mammary cells of the mouse.

17B(i).8. Concluding remarks

Our understanding of the synthesis and processing of the structural polypeptides of MuMTV is fairly comprehensive, but our knowledge about the assembly of MuMTV is limited. Some of the questions that remain to be answered are, for example, the nature of the interaction between $Pr73^{gag}$ and viral RNA, and why $Pr73^{gag}$ interacts with the viral RNA to form A particles before being processed intracellularly. An equally important question concerns the role the host cell must play in this process. We know that the MuMTV-*gag* and the -*env* polypeptides are synthesized independently of each other, yet they must interact at the cell surface in a precise manner to initiate viral budding. It is now important to determine whether or not A particles or *gag* polypeptides first make contact with discrete areas of the cell membrane which then serve as the nucleation sites for the subsequent assembly of the viral glycoproteins. Finally, studies on the existence of pits on the viral surface and the organization of the viral core may lead to a greater understanding of the intriguing structural features of MuMTV.

Acknowledgements

The author's laboratory is supported by NIH grants CA-17129-10 and CA-25679-05.

References

Arthur, L.O., Copeland, T.D., Oroszlan, S. and Schochetman, G. (1982) Processing and amino acid sequence analysis of the mouse mammary tumor virus *env* gene product. J. Virol. 41, 414–422.

Bentvelzen, P. and Hilgers, M. (1980) Murine mammary tumor virus. In Viral Oncology, Ed. G. Klein; pp. 311–355. Raven Press, New York.

Calberg-Bacq, C.M., François, C., Kozma, S., Gosselin, L., Osterrieth, P.M. and Rentier-Delrue, F. (1976) On the organization of the mouse mammary tumour virus envelope. Proc. VIth Eur. Congr. Electron Microsc., Vol. B, pp. 564–566, Jerusalem.

Cardiff, R.D., Puentes, M.J., Young, L.J.T., Smith, G.H., Teramoto, Y.A., Altrock, B.W. and Pratt, T.S. (1978) Serological and biochemical characterization of the mouse mammary tumor virus with localization of p10. Virology 85, 157–167.

Dickson, C. and Atterwill, M. (1979) Composition, arrangement and cleavage of the mouse mammary tumor virus polyprotein precursor $Pr77^{gag}$ and $P110^{gag}$. Cell 17, 1003–1012.

Dickson, C. and Atterwill, M. (1980) Structure and processing of the mouse mammary tumor virus glycoprotein precursor $Pr73^{env}$. J. Virol. 35, 349–361.

Dickson, C. and Peters, G. (1983) Proteins encoded by mouse mammary tumor virus. In Mouse Mammary Tumor Virus, Eds. P.K. Vogt and H. Koprowski; pp. 1–34. Springer-Verlag, New York.

Dion, A.S., Pomenti, A.A. and Farwell, D.C. (1979) Vicinal relationships between the major structural proteins of murine mammary tumor virus. Virology 96, 249–257.

Gautsch, J.W., Lerner, R., Howard, D., Teramoto, Y.A. and Schlom, J. (1978) Strain-specific markers for the major structural proteins of highly oncogenic murine mammary tumor viruses by tryptic peptide analyses. J. Virol. 27, 688–699.

Hageman, P.C., Calafat, J. and Hilgers, J. (1981) The biology of the mouse mammary tumor virus. In Mammary Tumors in the Mouse, Eds. J. Hilgers and M. Sluyser; pp. 392–463. Elsevier/North-Holland, New York.

Marcus, S.L., Smith, S.W., Racevskis, J. and Sarkar, N.H. (1978) The relative hydrophobicity of oncornaviral structural proteins. Virology 86, 398–412.

Marcus, S.L., Kopelman, R. and Sarkar, N.H. (1979) Simultaneous purification of murine mammary tumor virus structural proteins: analysis of antigenic reactivities of native gp34 by radioimmunoprecipitation assays. J. Virol. 31, 341–349.

Massey, R.J., Arthur, L.O., Nowinski, R.C. and Schochetman, G. (1980) Monoclonal antibodies identify individual determinants on mouse mammary tumor virus glycoprotein gp52 with group, class or type specificity. J. Virol. 34, 635–643.

Nermut, M.V. (1973) Size, shape and surface structure of mouse mammary tumour virus (MTV). Arch. Gesamte Virusforsch. 41, 284–289.

Nusse, R., Janssen, H., deVries, L. and Michalides, R. (1980) Analysis of secondary modifications of mouse mammary tumor virus proteins by two-dimensional gel electrophoresis. J. Virol. 35, 340–348.

Racevskis, J. and Sarkar, N.H. (1980) Murine mammary tumor virus structural protein interactions: Formation of oligomeric complexes with cleavable cross-linking agents. J. Virol. 35, 937–948.

Sarkar, N.H., Lasfargues, E.Y. and Moore, D.H. (1970) Attachment and penetration of mouse mammary tumor virus in mouse embryo cells. J. Microsc. 9, 477–484.

Sarkar, N.H., Moore, D.H., Kramarsky, B. and Chopra, H.C. (1973) The mammary tumor virus. In Ultrastructure of Animal Viruses and Bacteriophages, Eds. A.J. Dalton and F. Haguenau; pp. 307–321. Academic Press, New York.

Sarkar, N.H. and Moore, D.H. (1974) Surface structure of mouse mammary tumor virus. Virology 61, 38–55.

Sarkar, N.H., Pomenti, A.A. and Dion, A.S. (1977) Replication of mouse mammary tumor virus in tissue culture: I. Establishment of a mouse mammary tumor cell line, virus characterization and quantitation of virus production. Virology 77, 31–44.

Sarkar, N.H. and Racevskis, J. (1983) Expression and disposition of the murine mammary virus envelope gene products by murine mammary tumor cells. Virology 126, 279–300.

Sen, G.C., Haspel, H. and Sarkar, N.H. (1980) Presence of a proteolytic activity in murine mammary tumor virus. J. Biol. Chem. 255, 7098–7101.

Tanaka, H. (1977) Precursor-product relationship between nonglycosylated polypeptides of A and B particles of mouse mammary tumor virus. Virology 85, 211–221.

Teramoto, Y.A. and Schlom, J. (1978) Radioimmunoassays demonstrating type-specific and group-specific antigenic reactivities for the major internal structural protein of murine mammary tumor viruses. Cancer Res. 28, 1990–1995.

Teramoto, Y.A. and Schlom, J. (1979) Radioimmunoassays for the 36000-dalton glycoprotein of murine mammary tumor viruses demonstrate type, group, and interspecies determinants. J. Virol. 31, 334–340.

Nermut/Steven (eds) Animal Virus Structure

CHAPTER 17B(ii)

Oncovirinae: type C oncovirus

H. FRANK

Max-Planck-Institut für Entwicklungsbiologie, Spemannstrasse 35, D-7400 Tübingen, F.R.G.

17B(ii).1. General characteristics

The overwhelming majority of oncovirinae are of type C. They can induce leukemias, lymphomas and sarcomas but some strains are of low oncogenicity or not oncogenic at all. The frequency of recombination is very high due to the diploidy of the viral genome and the complex mode of replication, which can also include interactions with endogenous proviruses or the cellular genome. There are two main groups of genetically different particles of type C.

(1) *Viruses of low oncogenicity which are competent for replication.* They can transform only a small portion of specific target cells. The ordering of their three genes is: 5′, *gag, pol, env,* 3′. Gross and Moloney strains of murine leukemia virus are members of this group.

(2) *Viruses of high oncogenicity* which are:
(a) *Defective for replication.* In most cases sections of the viral genome essential for replication are replaced by an oncogene derived from the host genome. The genome structure of these particles may, somewhat simplified, be: 5′, *gag, onc,* 3′. They can be reproduced only in the presence of a helper virus which is competent for replication. The strains Rauscher and Friend of murine leukemia viruses and some strains of avian leukosis viruses are associated with helper viruses.
(b) *Competent for replication.* Rous sarcoma viruses contain the oncogene *src* in addition to the regular viral genome. Their genome structure is: 5′, *gag, pol, env. src,* 3′. (For comprehensive reviews see Stephenson, 1980; Weiss et al., 1982.)

Particles of type C have been found in tapeworms, insects, fishes, reptiles, birds and mammals. Avian and murine C-type particles as well as those of primates have been the most intensively investigated. A series of C-type particles of human origin have been described. Recently, human T-cell leukemia virus I and II (HTLV-I, HTLV-II) and adult T-cell leukemia/lymphoma virus (ATLV) have been shown to be the etiological agents of human T-cell leukemia/lymphoma. However, lymphadenopathy-associated virus/human T-cell leukemia virus III (LAV/HTLV-III), causing acquired immune deficiency syndrome (AIDS), is related to lentivirinae (see also Section 17B(ii).8. C-type viruses of human origin).

17B(ii).2. Chemical and physical characteristics

Retroviruses of type C contain 30–40% lipid originating from the plasma membrane of the host cell, 60–70% protein, 2–4% carbohydrate and about 1% RNA. The RNA genome (50–70 S, M_r 5–8 × 10^6) comprises two identical molecules containing at least three genes, enumerated from the 5′ end: the *gag* gene codes for the structural proteins of the core, the *pol* gene for reverse transcriptase, and the *env* gene for the proteins of the envelope. This sequence of genes has been found without exception in all retroviruses. With oncogenic C-type viruses, the *env* gene can be followed by the *onc* gene, coding for the cell-transforming protein(s). The structural gene products are termed by the molecular weight ($\times 10^{-3}$) prefixed by p for protein, gp for glycoprotein, pp for phosphoprotein and Pr for polyprotein precursors (August et al., 1974; Table 17B(ii).1). The density of type C retroviruses is 1.16–1.18 g/cm³ in sucrose and 1.16–1.21 g/cm³ in caesium chloride. They are

TABLE 17B(ii).1.

Correlation of structural proteins, morphological elements and antigenic specificities of MuLV (data from Bolognesi et al., 1978; Stephenson, 1982; and Dubois-Dalcq et al., 1984)

Polyprotein precursor[gene]	Structural protein	Structural component		Antigenic specificity		
				type	group	interspecies
Pr80-90[*env*]	gp70-S(env1)	Knobs	Envelope	+	+	+
	p15e-S(env2)	Transmembrane protein		−	+	+
	p12e[a]	"				
Pr65[*gag*]	p15c(gag1)	Inner coat		−	+	+
	pp12c(gag2)	Core shell associated	Core	+	+	−
	p30(gag3)	Core shell		+	+	+
	p10(gag4)	Nucleoprotein		−	+	+
Pr180[*gag-pol*]	p80	Reverse transcriptase		−	+	+

[a] Probably degradation product of p15e.

sensitive to lipid solvents and detergents, are inactivated by heating at 56°C for 30 min, but are highly resistant to UV light and X-rays.

17B(ii).3. Architecture of the virion

As a morphological prototype for C-type particles, Friend leukemia virus (FLV) is presented. This is one of the murine viruses and has been thoroughly studied in the electron microscope (Nermut et al., 1972; Frank et al., 1978). The FLV strain is a mixture of transforming particles defective for replication and leukemogenic helper viruses (Dawson et al., 1968).

Shape

Virus particles appear approximately spherical in thin sections (Fig. 17B(ii).2a) and, under appropriate conditions, also in negatively stained preparations (Figs. 17B(ii)1a–c, 2c and e), as well as after shadowing (Fig. 17B(ii).1e and f). 'Tailed' forms (Fig. 17B(ii).1d), often described in early publications, have been demonstrated to be preparation artefacts (Nermut et al., 1972; see also Chapter 2A).

Size

The diameters of virus particles obtained from thin sections range from 100 to 120 nm (Fig. 17B(ii).2a). In negatively stained preparations only the diameters of particles fully infiltrated by, and well embedded in, stain agree with those found in thin sections (Fig. 17B(ii).2). Particles that are not penetrated by stain are flattened during the drying process, and their diameter increases substantially (Fig. 17B(ii).1a–c). Some particles with a still larger diameter (Fig. 17B(ii).1a) contain two or more cores or a core which is aberrant in shape (Fig. 17B(ii).4).

Envelope

The viral envelope is composed of three morphologically distinct elements: knob-like surface projections, viral membrane and inner coat.

(a) *Surface projections.* The projections are knob-like, about 10 nm in diameter and contain the glycoprotein gp70. The knobs are recognizable after freeze-drying and shadowing of virus particles (Fig. 17B(ii).1f), after negative staining with uranyl acetate (Fig. 17B(ii).1a–d), and also in thin sections (Figs. 17B(ii).2a, 5a and 6b–e).

Knobs of C-type particles are easily lost during preparation for EM (Fig. 17B(ii).1a) but also during the purification procedures, e.g. density gradient centrifugation. The lability of the knobs has been used with advantage in isolating the glycoprotein component of FLV (Moennig et al., 1974). However, in some species (e.g. pig leukemia virus), knobs are found to be anchored more firmly, whereas

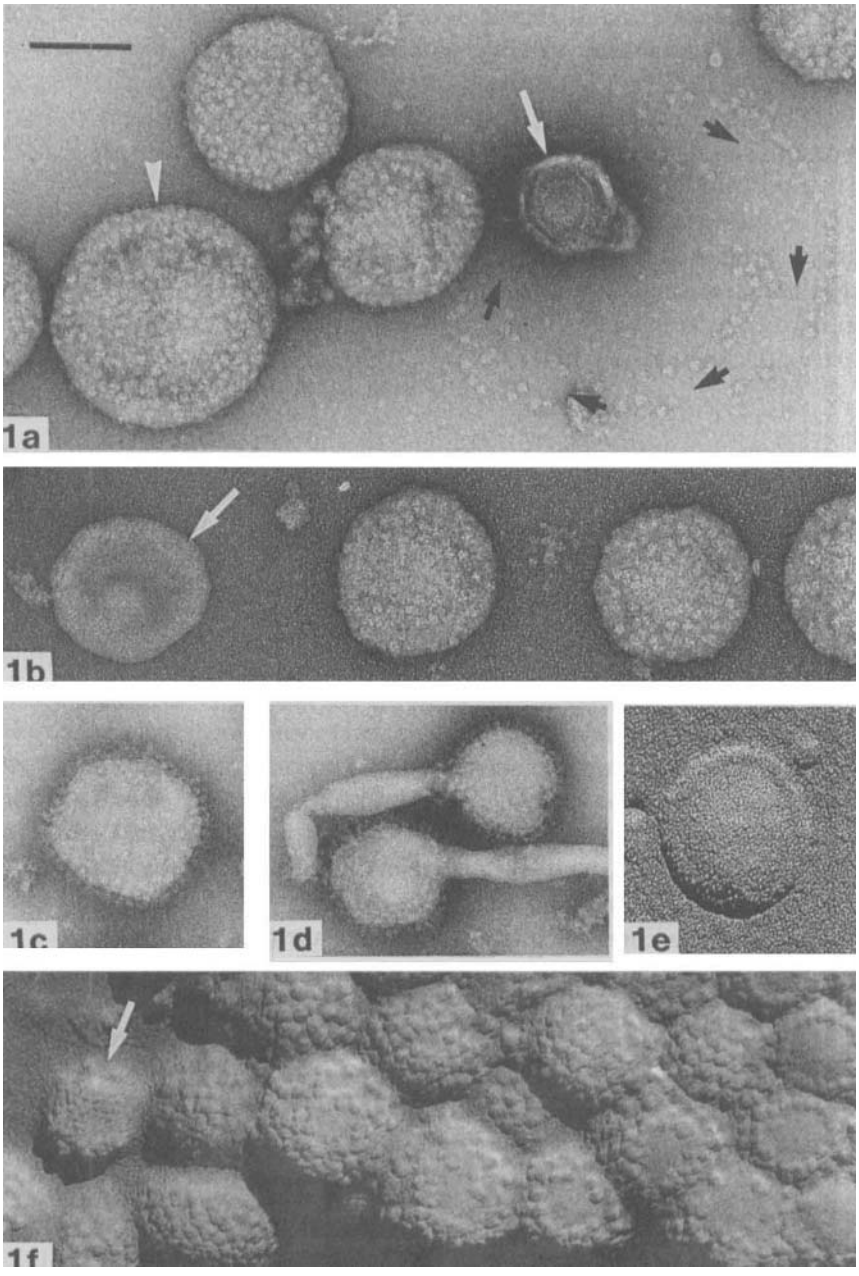
1a
1b
1c
1d
1e
1f

in other species (e.g. woolly monkey virus SSV-1/SSAV-1) they are even more loosely attached than in FLV.

(b) *Viral membrane.* The membrane derives from the plasma membrane of the host cell. In thin sections the membrane has a typical 'triple track' appearance (Fig. 17B(ii).2a).

(c) *Inner coat.* This refers to the thin protein layer, adjacent to the inner side of the viral membrane. This morphological element becomes visible in negatively stained preparations with particles completely penetrated by the stain, especially after brief pretreatment of viruses with dilute detergent (Fig. 17B(ii).2f). In thin sections, the inner coat is not clearly visible as a distinct layer, but the inner line of the unit membrane structure often appears thicker than the outer one, suggesting that it is covered inside with additional material (Fig. 17B(ii).2a and b). The possible candidates for the inner coat constituents are the proteins pp12c and p15c (Bolognesi et al., 1978; Dubois-Dalcq et al., 1984).

(d) *Transmembrane protein.* The existence of a connection between surface knobs and the inner coat was postulated from experiments which showed that the removal of lipids by detergent treatment does not result in the loss of knobs (Fig. 17B(ii).6n and o). A candidate for such a connection is the protein p15e, which is inserted into the membrane and remains connected with the glycoprotein gp70 by disulfide bonds even after cleavage of their common precursor, the *env* gene product gp90 (Bolognesi et al., 1978).

Core

Depending on the plane of section, cores appear as two-layered ring- or horseshoe-like structures. Usually, cores are separated from the envelope by an electron-lucent space (Figs. 17B(ii).2a and 5a). In negatively stained preparations, however, all structural layers appear to be in close contact with each other (Fig. 17B(ii).2c and e). In thin sections the inner layer of the core is stained more heavily than the outer one, indicating the position of the viral RNP-complex (Figs. 17B(ii).2a and 5a). In contrast to the RNP, which appears homogeneous in negatively stained preparations, the core shell reveals two parallel lines periodically interrupted and

---

Fig. 17B(ii).1. Murine leukemia virus, strain Friend (FLV). (a,b) Negatively stained with uranyl acetate (UA) for a few seconds to reveal surface projections. White arrowhead points to an abnormally large particle, white arrow to a stain-penetrated average-size virus particle. Black arrows indicate rows of surface knobs left behind as 'footprints' of virus particles removed during preparation. Virus particle devoid of surface knobs is arrowed in (b). In (c) and (d) are FLV negatively stained with sodium phosphotungstate. Surface projections as shown here are rarely observed and most virus particles have 'tails'. (e) Air-dried and shadowed FLV are collapsed and knobs are not visualized. Compare with freeze-dried FLV in (f). Arrow points to a free virus core. Bar represents 100 nm. (Panel e is from Nermut et al. (1972) with the permission of Academic Press.)

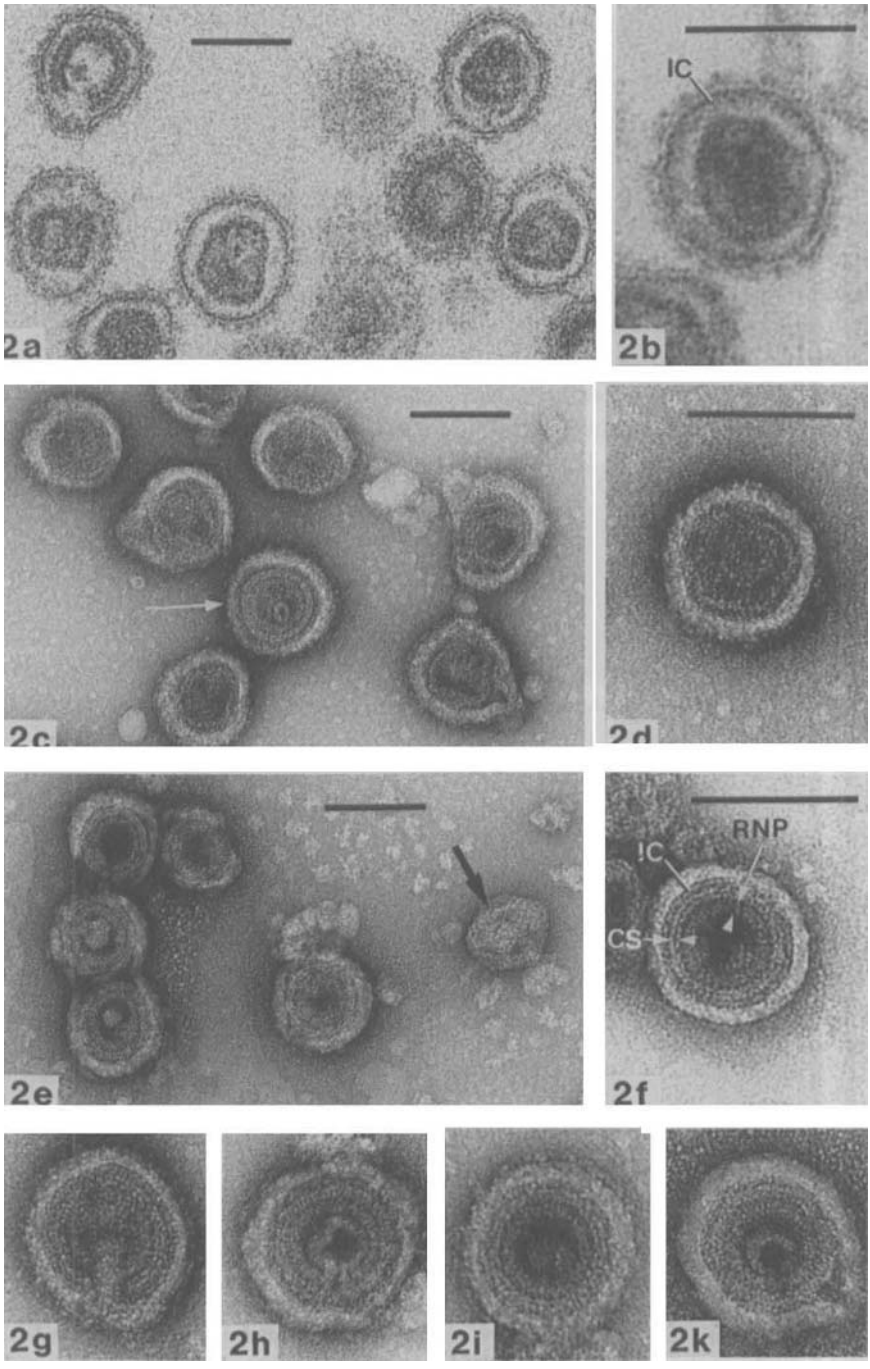
2a
IC
2b
2c
2d
2e
RNP
IC
CS
2f
2g
2h
2i
2k

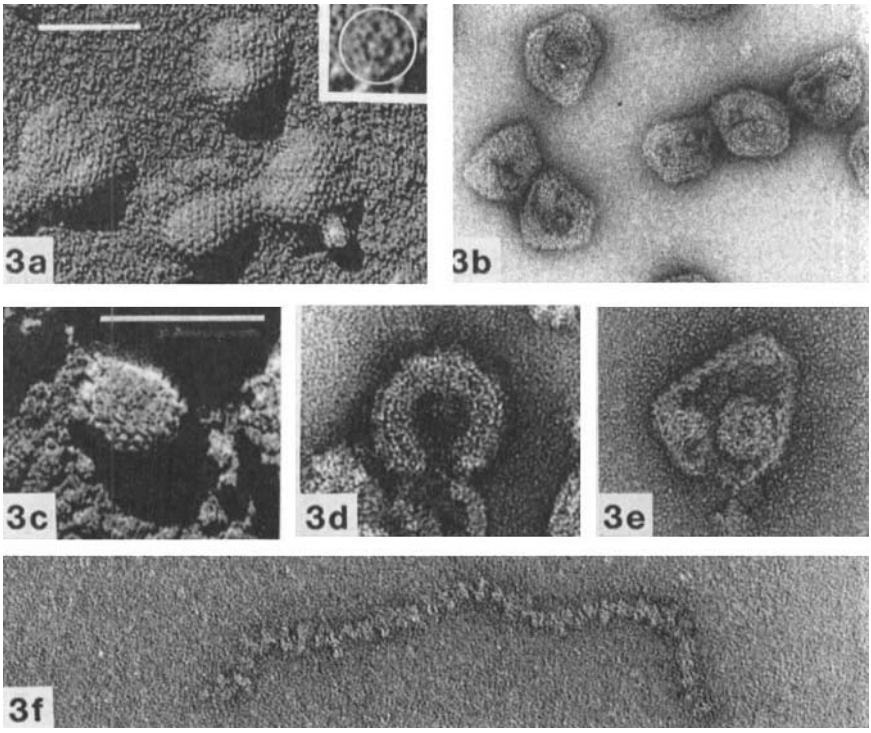

Fig. 17B(ii).3. (a–e) Cores of FLV released by ether treatment of viruses; (f) filamentous structure (probably RNP) observed after degradation of cores at pH 3.0. (a and c) Freeze-dried and shadowed; (b), (d) and (e) negatively stained with UA. Inset in (a) shows five-coordinated subunit. Cores shown in (c) and (d) are immature and these are very rarely found in preparations of released cores. Core particle in (e) reveals disorganized RNP material after collapse of the native 'immature' structure. Bars represent 100 nm. (Inset in panel a is from Nermut et al. (1972) with the permission of Academic Press.)

sometimes striated (Figs. 17B(ii).2f and 5b). So far, this has been observed only for particles of type C.

(a) *Core shell.* The core shell contains protein p30, a portion of the *gag* gene product, and is built up of hexagonally arranged subunits (8–9 nm in diameter),

---

Fig. 17B(ii).2. (a,b) Thin sections of FLV showing 'mature' and 'immature' forms (upper left corner in a). (c,d) Fresh virus particles after prolonged staining (3–5 min) with UA to reveal internal structure. Most particles are 'mature'; arrow points to an 'immature' particle. (e–k) Virus particles after treatment with dilute Nonidet P40 for a few seconds followed by brief negative staining with UA. Most virus particles display 'immature' morphology. Arrow indicates a released 'mature' core. IC = inner coat, CS = core shell, RNP = ribonucleoprotein. Invaginations of viral membrane into the core can be seen in (e) and (g) to (k). Bars represent 100 nm. (Panels c, e and g to k are from Frank et al. (1978) with the permission of Z. Naturforsch.)

recognizable in freeze-dried and shadowed preparations (Figs. 17B(ii).1f, 3a and c) but hardly ever in negatively stained preparations of released cores (Fig. 17B(ii).3b). The presence of five-coordinated subunits indicates that the core shell has icosahedral symmetry (Fig. 17B(ii).3a, inset), but its triangulation number (probably $T = 25$, or thereabouts) has not yet been determined. As a unique feature, the core shell contains an opening (Figs. 17B(ii).2a,g–k and 3d,e) representing the site of the virus particle which was synthesized last during the budding process (Fig. 17B(ii).6b–d).

(b) *Ribonucleoprotein (RNP) complex.* The basic protein p10 is associated with the viral RNA. The filamentous nature of this complex has been demonstrated by gentle dissociation of the released cores by treatment with dilute acetic acid (Fig. 17B(ii).3f) or by negative staining with phosphotungstic acid. This filament, probably of helical symmetry, is suggested to be arranged in a spiral to form a beehive-like structure. The openings of the core shell and the beehive structure are always in register (Figs. 17B(ii).2a, 3d and 5b).

Frequently, with negatively stained particles, an invagination of envelope material into the opening of the core is observed. Depending on how far the stain has penetrated and from which side the virus is viewed, the invaginated material appears (Fig. 17B(ii).2) as a solid stalked knob (panel g), as a stalked vesicle (panel h), as a solid knob (panel i), or as a vesicle (panel k). This characteristic prepara-

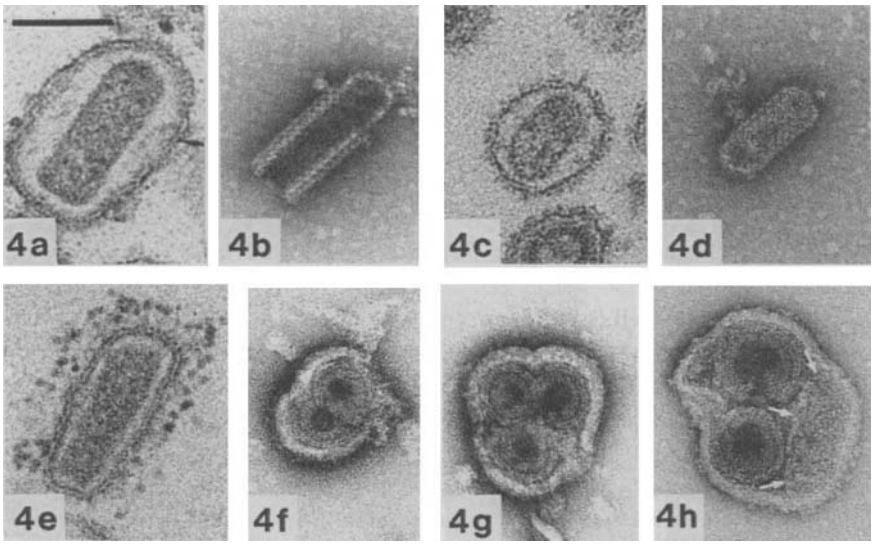

Fig. 17B(ii).4. Aberrant forms of FLV. (a, c and e) Thin sections; (b and f–h) negatively stained with UA. Particle in (e) was labelled with ferritin-coupled antibody to gp70. Arrows in (h) indicate a tubular core. Bar represents 100 nm. (Panels a, b and e are from Frank et al. (1978) with the permission of Z. Naturforsch.)

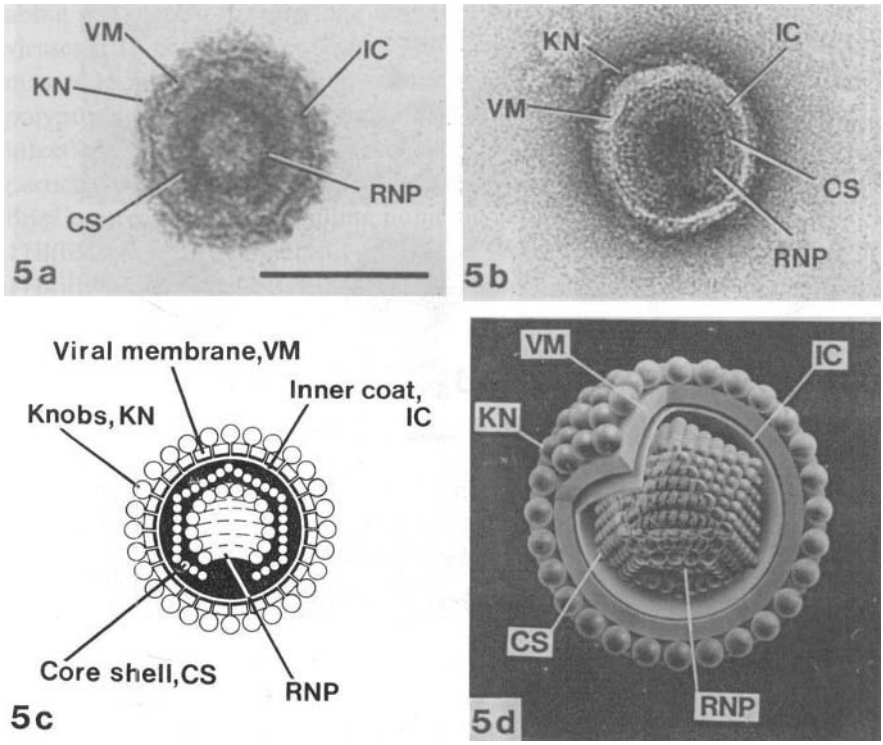

Fig. 17B(ii).5. Model of a C-type virion. (a) Thin-sectioned and (b) negatively stained virus particle, both revealing all structural features. (c) Diagram of the virion in cross-section and (d) three-dimensional model. The front triangle of the icosahedron was removed for better visualization of the hypothetical organization of the RNP coil. The connections between knobs and inner coat were omitted. KN = knobs, VM = viral membrane, IC = inner coat, CS = core shell, RNP = ribonucleoprotein. Bar in (a) represents 100 nm. (Panels c and d are from Frank et al. (1978) with the permission of Z. Naturforsch. The three-dimensional model was drawn by H. Engler.)

tion artefact is not only an indicator of the existence of the opening of the core, but above all provides a marker for the presence of C-type particles in samples containing only small quantities of virus particles relative to vesicles of cellular origin (Fig. 17B(ii).7b).

17B(ii).4. 'Immature' and 'mature' cores

Two distinct morphological patterns are usually observed in thin sections and negatively stained preparations of C-type retroviruses. Most cores appear as dense angular bodies, slightly retracted from the envelope ('mature' viruses with collapsed cores) (Fig. 17B(ii).2a–d). A small proportion of cores (with FLV constantly

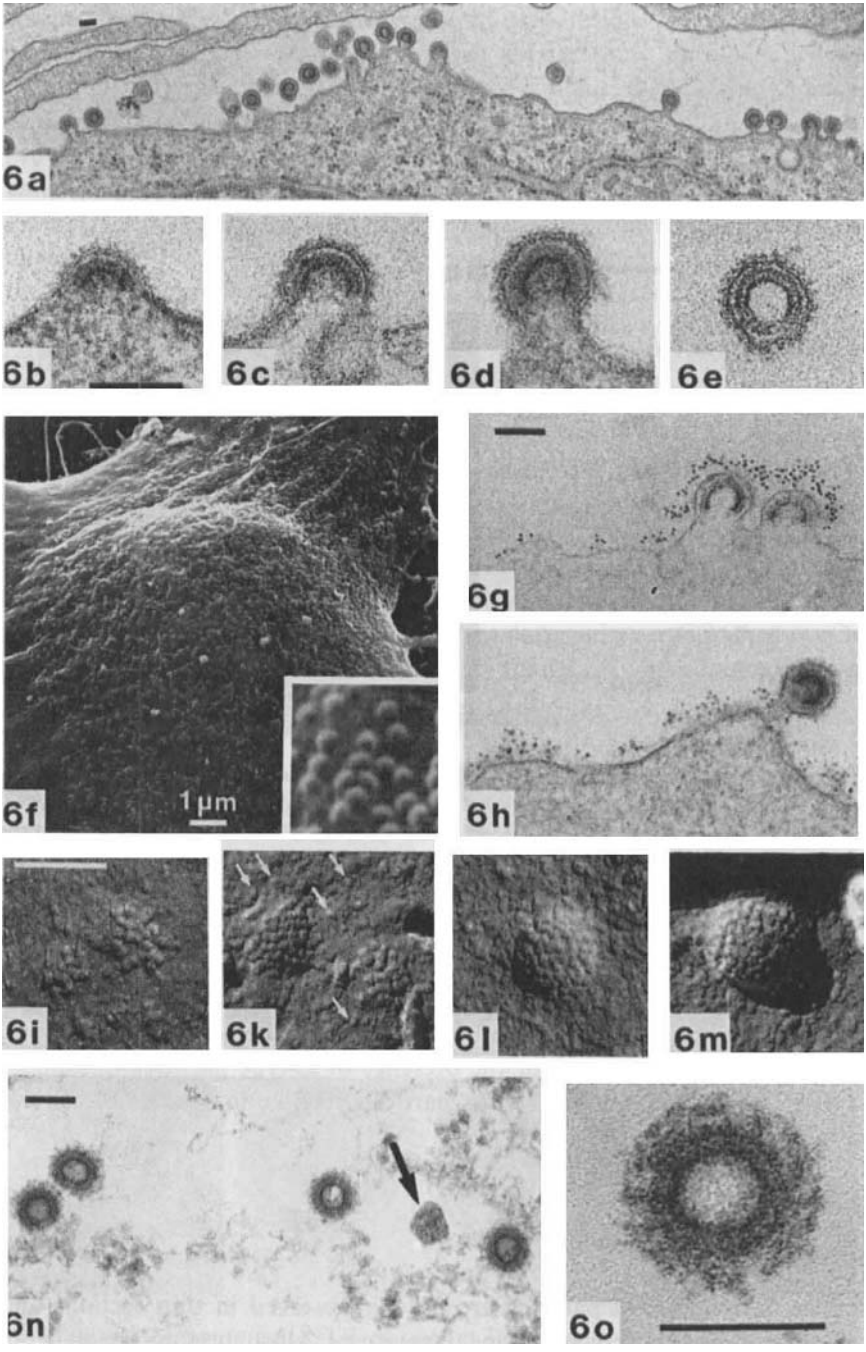
6a
6b
6c
6d
6e
6f
1 µm
6g
6h
6i
6k
6l
6m
6n
6o

about 5%) retain the ring-like structure as seen in budding viruses ('immature' viruses with native cores) (Figs. 17B(ii).2a,c, 5a and b). The transition from immature to mature morphology coincides with the cleavage of the *gag* gene-coded polyprotein precursor Pr65 (Table 17B(ii).1), which makes the immature particles infectious. However, it has been shown that in the case of FLV the proportion of particles with the 'immature' morphology can be increased from 5% to 50% by brief pretreatment with a dilute nonionic detergent before negative staining (Fig. 17B(ii).2e-k) (Frank et al., 1978) or embedding for thin sectioning (Fig. 17B(ii).6n). This indicates that the cleavage of Pr65 and the morphology of virus particles are two separate phenomena.

17B(ii).5. Morphological aberrations

In a population of FLV a few particles are found with tubular cores (Fig. 17B(ii).4a-d). That these particles are related to murine leukemia viruses is suggested by the observation that they are labelled with ferritin-coupled antibodies to the gp70 envelope antigen of FLV (Fig. 17B(ii).4e).

A second type of aberrant particle is formed if budding sites are located close to each other. Thereby two or more cores may share a common envelope (Fig. 17B(ii).4f and g). Particles containing up to 6 cores have been observed. In some cases regular cores together with a tubular one have been found (Fig. 17B(ii).4h).

17B(ii).6. The model of a C-type virion

A schematic representation of the architecture of C-type particles is shown in Fig. 17B(ii).5c, together with a particle thin-sectioned (Fig. 17B(ii).5a) and a particle negatively stained (Fig. 17B(ii).5b), both being examples of the rarely found particles revealing all structural elements at once. A three-dimensional model is presented in Fig. 17B(ii).5d. The correlation of structural elements with structural proteins together with their antigenic properties is given in Table 17B(ii).1.

Fig. 17B(ii).6. Budding of FLV from surface of FEM (Friend-Evelyne-Monolayer) cells shown in sections (a-e, g, h, n, o), scanning electron microscopy (f) and surface replica (i-m). Note high density of virus particles in (f) and well-resolved knobs (arrows) in replicas. Panel g shows budding virus particles labelled with ferritin-tagged antibody to gp70, whereas (h) shows distribution of pp12c on cell surface. Note absence of label on virus particle. Panels (n) and (o) show virus particles in cells treated with 0.1% NP40 for 15 min before fixation and embedding in Epon. Most viruses are well preserved and the presence of surface projections indicates that they interact with inner coat in the native state. Arrow in (n) points to a free 'mature' core. Bars, with the exception of (f), represent 100 nm. (Panel f courtesy of Dr. M. Claviez; panels g and h courtesy of Dr. H. Schwarz.)

17B(ii).7. Virus-cell interaction

Adsorption of viruses takes place through their surface glycoproteins to specific receptors of the host cell. The mode of penetration, however, is not clear in all details. Both endocytosis (viropexis) via coated pits and direct entry through the plasma membrane have been described in different C-type viruses (for review see Howe et al., 1980). Infection with murine retroviruses can be inhibited by lysosomotropic agents, indicating that the infection route leads through an acidic compartment (lysosomes, endosomes) of the cell (Andersen and Nexo, 1983).

In contrast to particles of types B, D and Spumavirinae, assembly of cores of type C takes place at the cell membrane simultaneously with the budding process. Budding of FLV is presented in Fig. 17B(ii).6b–e in thin sections and in Fig. 17B(ii)6i–m in replicas of freeze-dried virus-producing cells. In these replicas, early budding sites are indicated by the moving together of knob-like particles which were formerly irregularly distributed over the surface of the producing cell. Correspondingly, budding viruses in thin sections are heavily labelled with ferritin-coupled gp70 antibody, in contrast to the randomly labelled residual surface of the virus-producing cell (Fig. 17B(ii).6g). A similar distribution of label on the surface of virus-producing cells, but never on budding sites, was observed with pp12c antibody (Fig. 17B(ii).6h) (Schwarz et al., 1976). This is also an indication of the presence of at least one section of the *gag* gene product in the cell membrane of virus-producing cells. Besides budding from the plasma membrane, virus particles are frequently released into cisternae and vacuoles of the cell.

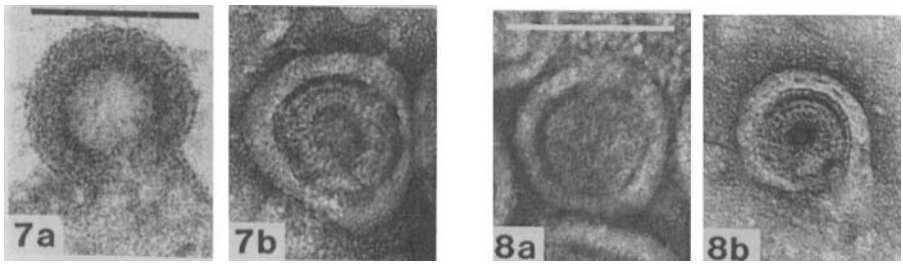

Fig. 17B(ii).7. HTDV (human teratocarcinoma-derived virus particle). (a) Thin section, (b) pretreated with NP40 and negatively stained with uranyl acetate. Bar represents 100 nm. (Panel a courtesy of Dr. K. Boller; panel b from Boller et al. (1983) with the permission of the Society for General Microbiology.)

Fig. 17B(ii).8. ATLV (adult T-cell leukemia virus) negatively stained with uranyl acetate. (b) Pretreated with NP40, revealing immature core structure. Bar represents 100 nm. (ATL viruses were kindly provided by Dr. G. Hunsmann.)

The production of retroviruses does not normally destroy the cell. Particles are released continuously and, with cell cultures adapted to grow in suspension, the production of large quantities of viruses is possible (Fig. 17B(ii).6a and f) (Seifert et al., 1975).

17B(ii).8. C-type viruses of human origin

The search for human retroviruses has been long and often disappointing. First retrovirus-like particles were found in thin sections of normal human placenta (Kalter et al., 1972). However, these particles could not be propagated in cell cultures.

Similar particles have been found in thin sections of human teratocarcinomas (Bronson et al., 1978). Tissue cultures of teratocarcinomas were induced to produce these HTD (human teratocarcinoma-derived) particles (Fig. 17B(ii).7) (Löwer et al., 1981; Boller et al., 1983), but their infectivity could not be demonstrated. The lack of mature forms indicates that they are at least defective for proteolytic processing of the *gag* polyprotein.

The first human retrovirus demonstrated to be an infectious agent was human T-cell leukemia virus I (HTLV-I) (Poiesz et al., 1980), followed by adult T-cell leukemia/lymphoma virus (ATLV), the Japanese isolate of the same virus (Hinuma et al., 1981), HTLV-II, and lymphadenopathy-associated virus/human T-cell leukemia virus III (LAV/HTLV-III), the latter of which is associated with acquired immune deficiency syndrome (AIDS) (Barré-Sinoussi et al., 1983; Gallo et al., 1984). The members of the human T-cell leukemia/lymphoma group are now named human T-cell lymphotropic viruses or human T-lymphotropic viruses. LAV/HTLV-III and the other AIDS-related isolates have recently been uniformly termed human immunodeficiency viruses (HIV) (Coffin et al., 1986).

All retroviruses of human origin, together with bovine leukemia virus (BLV) and Lentivirinae, possess a common morphological feature which is different from all other retroviruses: in thin sections, the envelope and core are always in close contact, lacking the typical electron-lucent space in between (Figs. 17B(ii).7 and 8; Figs. 17C.3a–d, 8, 9 of Lentivirinae (Chapter 17C)). However, more recently HIV (HTLV-III/LAV) was shown by molecular hybridization and heteroduplex analysis to be more related to Visna virus, a member of the subfamily of Lentivirinae, than to any other retrovirus (Gonda et al., 1985). Both viruses also have an additional morphological peculiarity. In thin sections of released viruses, tubular cores are observed much more frequently than in other type-C viruses.

The classification of human retroviruses as members of the type-C oncovirus group is therefore only provisional. HTLV-I/ATLV and HTLV-II may represent a new type of oncovirinae, although, prepared under appropriate conditions, they are morphologically very similar to C-type viruses (compare Figs. 17B(ii).2e, 2f

and 5b with Figs. 17B(ii).7b and 8b). HIV (LAV/HTLV-III), however, should be classified as a member of Lentivirinae (Gonda et al., 1985; Alizon and Montagnier, 1985) and will be dealt with in Chapter 17C, on Lentivirinae.

References

Alizon, M. and Montagnier, L. (1985) Relationship of AIDS to other retroviruses. Nature 313, 743.

Andersen, K.B. and Nexo, B.A. (1983) Entry of murine retrovirus into mouse fibroblasts. Virology 125, 85–98.

August, J.T., Bolognesi, D.P., Fleissner, E., Gilden, R.V. and Nowinski, R.C. (1974) A proposed nomenclature for the virion proteins of oncogenic RNA viruses. Virology 60, 595–601.

Barré-Sinoussi, F., Chermann, J.C., Rey, F., Nugeyre, M.T., Chamaret, S., Gruest, J., Dauguet, C., Axler-Blin, A., Vezinet-Brun, F., Rouzioux, C., Rozenbaum, W. and Montagnier, L. (1983) Isolation of a T-lymphotropic retrovirus from a patient at risk for acquired immune deficiency syndrome (AIDS). Science 220, 868–871.

Bolognesi, D.P., Montelaro, R.C., Frank, H. and Schäfer, W. (1978) Assembly of type C oncornaviruses: A model. Science 199, 183–186.

Boller, K., Frank, H., Löwer, J., Löwer, R. and Kurth, R. (1983) Structural organisation of unique retrovirus-like particles budding from human teratocarcinoma cell lines. J. Gen. Virol. 64, 2549–2559.

Bronson, D.L., Ritzi, D.M., Fraley, E.E. and Dalton, A.J. (1978) Morphologic evidence for retrovirus production by epithelial cells derived from human testicular tumor metastasis. J. Natl. Cancer Inst. 60, 1305–1308.

Coffin, J., Haase, A., Levy, J.A., Montagnier, L., Oroszlan, S., Teich, N., Temin, H., Toyoshima, K., Varmus, H., Vogt, P. and Weiss, R. (1986) What to call the AIDS virus? Nature 321, 10.

Dawson, P.J., Tacke, R.B. and Fieldsteel, A.H. (1968) Relationship between Friend virus and an associated lymphatic leukaemia virus. Br. J. Cancer 22, 569–576.

Dubois-Dalcq, M., Holmes, K.V. and Rentier, B. (1984) Assembly of enveloped RNA viruses. Springer Verlag, Wien, New York.

Frank, H., Schwarz, H., Graf, T. and Schäfer, W. (1978) Properties of mouse leukemia viruses. XV. Electron microscopic studies on the organisation of Friend leukemia virus and other mammalian C-type viruses. Z. Naturforsch. 33c, 124–138.

Gallo, R.C., Salahuddin, S.Z., Popovic, M., Shearer, G.M., Kaplan, M., Haynes, B.F., Palker, T.J., Redfield, R., Oleske, J., Safai, B., White, G., Foster, P. and Markham, P.D. (1984) Frequent detection and isolation of cytopathic retroviruses (HTLV-III) from patients with AIDS and at risk for AIDS. Science 224, 500–503.

Gonda, M.A., Wong-Staal, F., Gallo, R.C., Clements, J.E., Narayan, O. and Gilden, R.V. (1985) Sequence homology and morphologic similarity of HTLV-III and Visna virus, a pathogenic Lentivirus. Science 227, 173–177.

Hinuma, Y., Nagata, K., Hanaoka, M., Nakai, M., Matsumoto, T., Kinoshita, K.-I., Shirakawa, S. and Miyoshi, I. (1981) Adult T-cell leukemia: antigen in an ATL cell line and detection of antibodies to the antigen in human sera. Proc. Natl. Acad. Sci. USA 78, 6476–6480.

Howe, C., Coward, J.E. and Fenger, T.W. (1980) Viral invasion: Morphological, biochemical and biophysical aspects. In Comprehensive Virology, Eds. H. Fraenkel-Conrat and R. Wagner; Vol. 16, pp. 1–72. Plenum Press, New York.

Kalter, S.S., Helmke, R.J., Heberling, R.L., Panigel, M., Fowler, A.K., Strickland, J.E. and Hellmann, A. (1973) C-type particles in normal human placentas. J. Natl. Cancer Inst. 50, 1081–1084.

Löwer, R., Löwer, J., Frank, H., Harzmann, R. and Kurth, R. (1984) Human teratocarcinoma cultured in vitro produce unique retrovirus-like viruses. J. Gen. Virol. 65, 887–898.

Moennig, V., Frank, H., Hunsmann, G., Schneider, I. and Schäfer, W. (1974) Properties of mouse leukemia viruses. VII. The major viral glycoprotein of Friend leukemia virus. Isolation and physicochemical properties. Virology 61, 100–111.

Nermut, M.V., Frank, H. and Schäfer, W. (1972) Properties of mouse leukemia viruses. III. Electron microscopic appearance as revealed after conventional preparation techniques as well as freeze-drying and freeze-etching. Virology 49, 345–358.

Poiesz, B.J., Ruscetti, F.W., Reitz, M.S., Kalyanaraman, V.S. and Gallo, R.C. (1981) Isolation of a new type C retrovirus (HTLV) in primary uncultured cells of a patient with Sézary T-cell leukaemia. Nature 294, 268–271.

Schwarz, H., Hunsmann, G., Moennig, V. and Schäfer, W. (1976) Properties of mouse leukemia viruses. XI. Immunelectron microscopic studies on viral structural antigens on the cell surface. Virology 69, 169–178.

Seifert, E., Claviez, M., Frank, H., Hunsmann, G., Schwarz, H. and Schäfer, W. (1975) Properties of mouse leukemia viruses. XII. Produktion größerer Mengen von Friend-Virus durch eine permanente Zell-Suspensions-Kultur (Eveline-Suspensions-Zellen). Z. Naturforsch. 30c, 698–700.

Stephenson, J.R. (Ed.) (1980) Molecular biology of RNA tumor viruses. Academic Press, New York.

Weiss, R., Teich, N., Varmus, H. and Coffin, J. (Eds.) (1982) RNA Tumor Viruses. Cold Spring Harbor Laboratory, NY.

This Page Intentionally Left Blank

Nermut/Steven (eds) Animal Virus Structure

CHAPTER 17B(iii)

Oncovirinae: type D oncovirus

HANS GELDERBLOM

Robert Koch-Institut des Bundesgesundheitsamtes, Nordufer 20, D-1000 Berlin 65, Germany

Subfamily: Oncovirinae
Genus: Type D oncovirus
Species: Mason-Pfizer monkey virus (MPMV), Squirrel monkey retrovirus (SMRV), Langur type D retrovirus (PQ-1-Lu)

17B(iii).1. General characteristics

Type D oncoviruses are indigenous to primates, where they occasionally cause protracted non-malignant diseases closely resembling human AIDS. They are, however, unrelated to simian or human T cell lymphotropic viruses, which are classified as Lentivirinae. Some members of the type D genus are transmitted vertically as endogenous viruses (interpreted as provirus in the host genome), while others, like MPMV, apparently are horizontally transmitted, as is characteristic for exogenous retroviruses.

MPMV, the prototype of type D Oncovirus, was isolated from a spontaneous breast carcinoma of a female rhesus monkey. In addition to several subsequent isolates from macaques, a morphologically indistinguishable endogenous virus has also been recovered from an Old World monkey, from the tissue of a langur (PQ-1-Lu). SMRV isolates, endogenous type D viruses, have been recovered from the lung of a squirrel monkey, a member of the New World monkeys. SMRV lacks nucleic acid homology and a close immunological relationship to MPMV and PQ-1-Lu of Old World monkeys. In addition, several isolates morphologically and immunologically similar to MPMV have been isolated from human tissues and cells (Graffi et al., 1974; Gelderblom et al., 1974).

17B(iii).2. Chemical and physical characteristics

Purified virus particles have a buoyant density of 1.17 g/cm^3 in sucrose and 1.21 g/cm^3 in caesium chloride. They contain 60% protein, 35% lipid, 3% carbohydrate and about 2% genomic RNA. The genome sequences of several type-D oncoviruses have been determined (Sonigo et al., 1986). The integrated provirus of MPMV containing two LTRs of 349 bp is transcribed into genomic RNA of 7943 nucleotides. There are 4 consecutive open reading frames coding for (1) the internal virion proteins (*gag*), (2) a viral protease (*pro*), (3) the reverse transcriptase/RNase H and endonuclease/integrase complex (*pol*), and (4) the envelope glycoproteins (*env*; Sonigo et al., 1986). Six structural proteins have been purified from MPMV (p4, p10, p12, the nucleic acid binding protein p14, the major core protein p27, and a phosphoprotein pp18) (Henderson et al., 1985). The envelope contains two glycoproteins; gp20, a poorly glycosylated transmembrane protein, and gp70, a highly glycosylated external spike protein (Sonigo et al., 1986).

The reverse transcriptase of type-D retroviruses (M_r about 80 000) prefers Mg^{2+} as its divalent cation (Colcher and Schlom, 1980).

17B(iii).3. Architecture of the virion

Shape and size. Type-D virus particles show two characteristic morphological features. (1) Intracytoplasmically preformed virus cores with a diameter of 76 nm which, except for regular surface protrusions, are reminiscent of the type-A precursor particles of mouse mammary tumour viruses. Only preformed cores can be observed during budding; they can be clearly separated from the protruding cell

---

Fig. 17B(iii).1. Ultrathin sections of D type retrovirus (MPMV)-producing HeLa cells. (a) A cluster of preformed viral cores is occasionally seen in the cytoplasm. These A-type-like particles show a fringe of tiny spikes at their outer periphery and, depending on the section plane, an electron-lucent center. (b) 'Mature', i.e. cell-released HeLa virus particles exhibit different projections of the viral core. Bar represents 100 nm.

Fig. 17B(iii).2. Ultrathin sections of MPMV-producing HeLa cells. (a–e). Sequence of D-type virus budding; usually preformed cores become enveloped but, in contrast to murine A-type particles, intracellular D-type cores show defined surface protrusions; (e–h) after release from the cell 'immature' D-type particles (e) are rarely seen; the majority contain tubular cores with a central electron-dense ribonucleoprotein portion surrounded by a core shell of centro-symmetric (f), triangular (g) or tubular (h) outline. Bar represents 100 nm.

Fig. 17B(iii).3. (a–c) D-type virus particles from HeLa cells negatively contrasted with PTA after gradient purification. A loose envelope surrounds a spherical core with a defined surface structure. Bar represents 100 nm.

membrane (Gelderblom et al., 1974; Fine and Schochetman, 1978). (2) After budding this spherical precursor structure becomes a tubular or conical core and a relatively small, very condensed RNP complex ('maturation', Figs. 17B(iii).1 and 2). In this respect 'mature' D-type particles differ from the human and simian T lymphotropic lentiviruses, which show a more homogeneous RNP distribution.

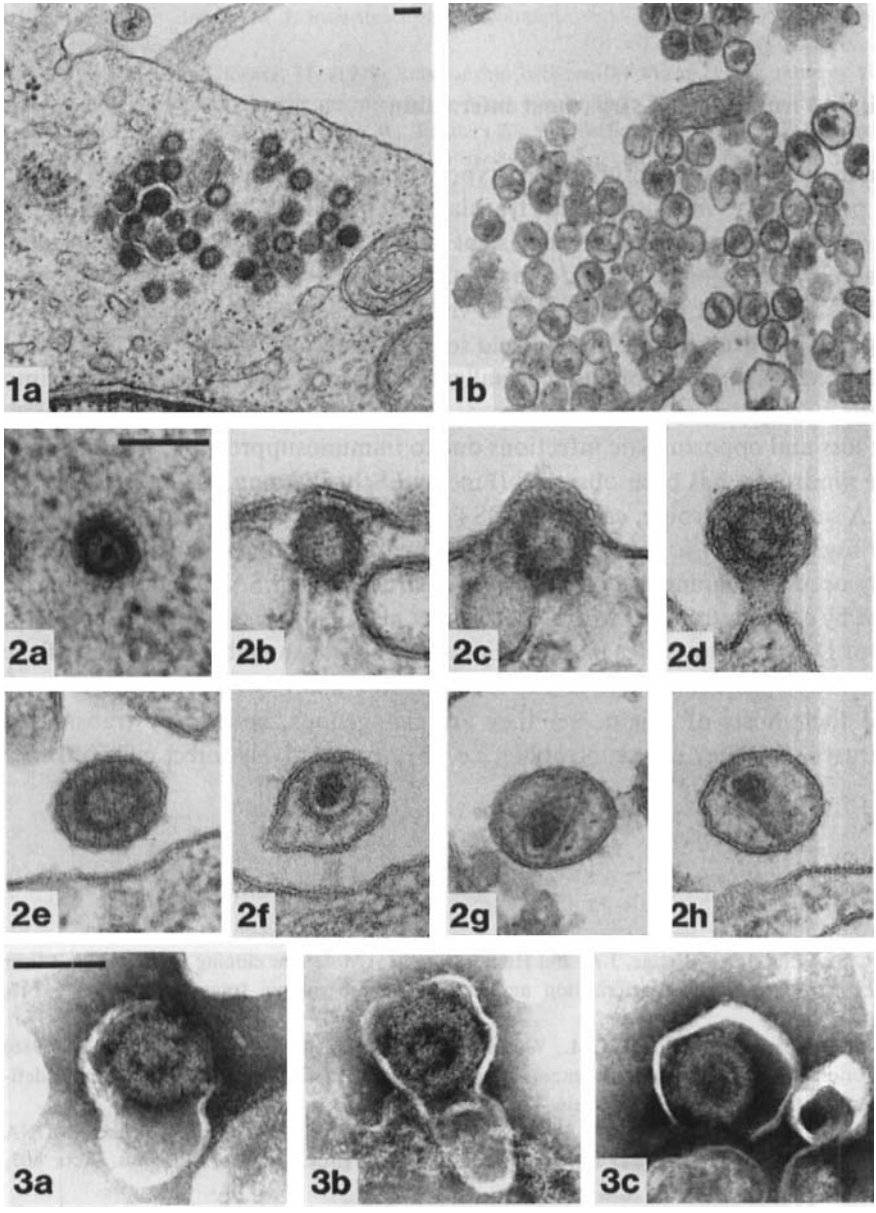

In thin sections, 'mature' cell-released particles measure 110–130 nm in diameter. The tubular core, 75 nm in length, spans the internal cavity of the virion and contains the electron-dense ribonucleoprotein (RNP) complex, which is about 40 nm in diameter.

The envelope of type D oncoviruses is studded with tiny surface projections 5 nm in length, which are revealed best by negative staining (Gelderblom et al., 1974).

17B(iii).4. Virus–cell and virus–host interaction

In human and nonhuman primate cells type D oncoviruses induce syncytia, i.e. cell fusion presumably via a virus-coded translational product (Chatterjee and Hunter, 1980). The infection in culture is persistent and non-lytic, i.e. not accompanied by detectable cytolysis or cell transformation.

MPMV and similar exogenous type D viruses are spread as infectious agents in macaques (i.e. virus-specific nucleic acid sequences are detectable only in infected animals). MPMV does not induce malignant tumors, but after injection into newborn macaques a spectrum of diseases, such as lymphadenopathy, diarrhoea, weight loss and opportunistic infections due to immunosuppression, i.e. a wasting disease syndrome, has been observed (Fine and Schochetman, 1978; Weiss et al., 1984). A similar syndrome, called SAIDS (simian acquired immunodeficiency syndrome together with a unique form of retroperitoneal fibromatosis, RF) occasionally occurs spontaneously in primate research centers. SAIDS and RF can be induced by certain strains of MPMV (Bryant et al., 1986). The immunosuppressive action of D-type oncoviruses has been linked to the transmembrane portion of the gp20 envelope protein (Sonigo et al., 1986). SMRV and PQ-1-Lu are found in all cells of their hosts of origin, i.e. they are endogenous, genetically transmitted retroviruses, and they are xenotrophic, i.e. they productively infect cells of other species.

References

Barker, C.S., Wills, J.W., Bradac, J.A. and Hunter, E. (1985) Molecular cloning of the Mason-Pfizer monkey virus genome: characterization and cloning of subgenomic fragments. Virology 142, 223–240.

Bryant, M.L., Marx, P.A., Shiigi, S.M., Wilson, B.J., McNulty, W.P. and Gardner, M.B. (1986) Distribution of type D retrovirus sequences in tissues of macaques with simian acquired immune deficiency and retroperitoneal fibromatosis. Virology 150, 149–160.

Colcher, D. and Schlom, J. (1980) Purification and characterization of RNA-directed DNA polymerase of a primate type-D retrovirus: Mason-Pfizer virus. Biochim. Biophys. Acta 607, 445–456.

Chatterjee, S. and Hunter, E. (1980) Fusion of normal primate cells: a common biological property of the D-type retroviruses. Virology 107, 100–108.

Fine, D. and Schochetman, G. (1978) Type D primate retroviruses: a review. Cancer Res. 38, 3123–3139.

Henderson, L.E., Sowder, R., Smythers, G., Benveniste, R.E. and Oroszlan, S. (1985) Purification and N-terminal amino acid sequence comparisons of structural proteins from retrovirus-D/Washington and Mason-Pfizer monkey virus. J. Virol. 55, 778–787.

Gelderblom, H., Bauer, H., Ogura, H., Wigand, R. and Fischer, A. (1974) Detection of oncornavirus-like particles in HeLa cells. I. Fine structure and comparative morphological classification. Int. J. Cancer 13, 246–253.

Gelderblom, H. and Schwarz, H. (1979) Relationship between the Mason-Pfizer monkey virus and HeLa virus in immunoelectron microscopy. J. Natl. Cancer Inst. 56, 635–637.

Graffi, V.A., Bierwolf, D., Widmaier, R., Bender, E., Wunderlich, V., Rudolph, M., Mothes, E., Niezabitowski, A. and Pabsdorf, G. (1974) In der Gewebekultur zuchtbares Oncornavirus in malignen permanenten menschlichen Zelllinien vom Embryo einer krebskranken Frau. Deutsch. Gesundheitsw. 29, 1489–1498.

Sonigo, P., Barker, C., Hunter, E. and Wain-Hobson, S. (1986) Nucleotide sequence of Mason-Pfizer monkey virus: an immunosuppressive D-type retrovirus. Cell 45, 375–385.

Weiss, R.A., Teich, N., Varmus, H. and Coffin, J. (Eds.) (1982) RNA Tumor Viruses, Second edition. Cold Spring Harbor Laboratory, NY.

This Page Intentionally Left Blank

Nermut/Steven (eds) Animal Virus Structure

CHAPTER 17C

Lentivirinae

H. FRANK

Max-Planck-Institut für Entwicklungsbiologie, Tübingen, F.R.G.

Subfamily: Lentivirinae
Genus: Lentivirus (Latin lentus = slow)
Species: Maedi/Visna virus (MVV), Progressive pneumonia virus (PPV), Zwoegerziekte virus, Caprine arthritis-encephalitis virus (CAEV), Equine infectious anemia virus (EIAV), Human immunodeficiency virus (HIV), Simian T-lymphotropic virus-III (STLV-III), etc.

17C. General characteristics

Lentiviruses are retroviruses which cause nonmalignant diseases of animals characterized by an incubation time of several months to many years, followed by a protracted course of the disease; hence the term 'slow virus infection' (Sigurdson, 1954).

The prototype of this subfamily is MVV (Figs. 17C.1–3), affecting the lung and nervous system of sheep. Other isolates from sheep (PPV and Zwoegerziekte virus) and CAEV, an isolate from goat, are related to each other (Weiss et al., 1982). EIAV (Figs. 17C.4–7) has only recently been classified as a member of this subfamily (Bouillant and Becker, 1984). There are some indications that HIV, the virus causing acquired immune deficiency syndrome (AIDS) (Figs. 17C.8–13), is closer to lentivirinae than to oncovirinae of type C (see Chapter 17B(ii)). In addition to morphological similarities (compare Figs. 17C.1, 3 and 8, 9 and 12) and sequence homologies (Gonda et al., 1985), there are also similarities in pathological characteristics: MVV is the causative agent of a degenerative

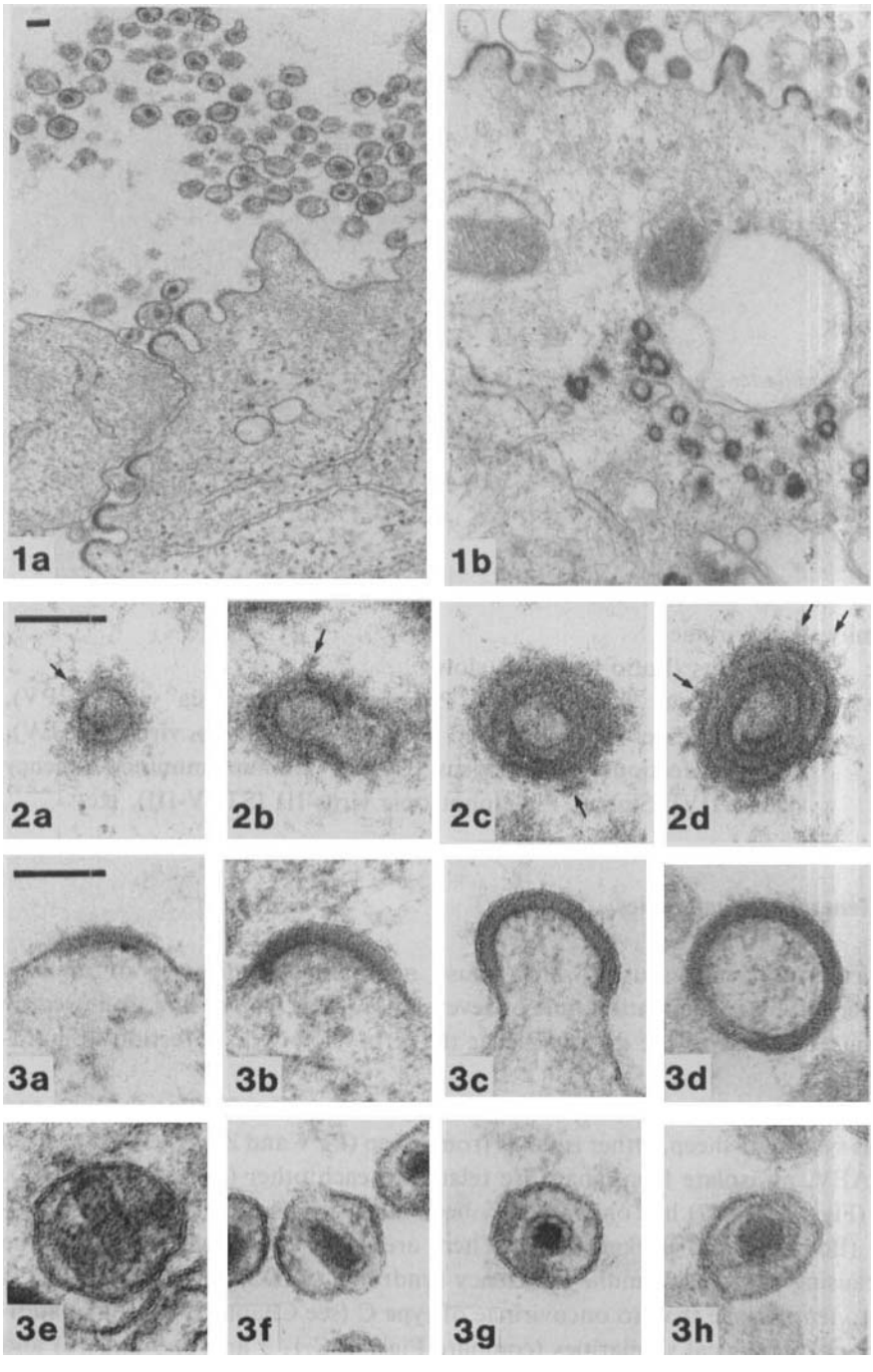
1a
1b
2a
2b
2c
2d
3a
3b
3c
3d
3e
3f
3g
3h

neurological disease in sheep, and HIV is probably the cause of AIDS-related encephalopathy in man (Shaw et al., 1985). However, the most striking finding is the detection of a novel and unique central region Q (also named SOR) in the nucleic acid between the *pol* and *env* gene of both MVV and HIV. The common genome structure of MVV and HIV is, therefore, 5′, *gag, pol, Q (SOR), env*, 3′. Furthermore, a cross-immunoreactivity has been found between the major core proteins of EIAV and HIV (Sonigo et al., 1985).

Recently a new type of human immunodeficiency virus was isolated from West African patients with AIDS (Clavel et al., 1986) which is now termed HIV 2 (originally LAV-2). This virus is morphologically very similar to HIV (now numbered HIV 1) (compare Figs. 17C.8, 9, 10 and 12, 13) but seems to be closer to STLV-III, a SAIDS (simian AIDS) related virus, than to HIV 1: there is a cross-reactivity between glycoproteins of HIV 2 and STLV-III but not with glycoproteins of HIV 1. The cross-reaction between HIV 1 and HIV 2 is restricted to core proteins (Brun-Vézinet et al., 1987). This means that at this time HIV 2 infections are not recorded by the HIV tests.

17C.2. Chemical and physical characteristics

MVV contains about 2% RNA, 60% protein, 35% lipid and 3% carbohydrate. The 60–70 S ssRNA is composed of subunits of 35 S (M_r 3.0–3.5 × 10^6 each). The genome contains *gag, pol, Q(SOR)*, and *env* genes. *gag* codes for the structural proteins of the core (precursor polyprotein Pr55, structural proteins p30, p16 and p14), *pol* for reverse transcriptase (precursor polyprotein Pr150, 2 subunits of p70) and *env* for the glycoproteins of the envelope (precursor polyprotein GPr150, a major structural glycoprotein gp135 and a glycoprotein gp70). The significance of the region *Q* (*SOR*) situated between *pol* and *env* genes is not yet known. It has

---

Fig. 17C.1. Ultrathin sections of maedi-visna virus (MVV) infected cells. a, sheep choroid plexus cells (SCP) with budding and released virus particles; b, sheep testes cell with budding viruses and laminar bodies in the cytoplasm. Bar represents 100 nm.

Fig. 17C.2. Higher magnification of laminar bodies. a and b, single-layered; c and d, multi-layered; d, spiral-like. Laminar bodies are often surrounded by ribosomes (arrows). Bar represents 100 nm.

Fig. 17C.3. MVV at various budding stages (a–d) and released virus particles with tubular (e and f), spherical (g) and conical (h) core profiles depending on the plane of section. Bar represents 100 nm.

(Figs. 17C.1, 2, 3a, b and e–h courtesy of Dr. F. Weiland; Fig. 3c and d from Weiland and Bruns (1980) with permission of Springer Verlag.)

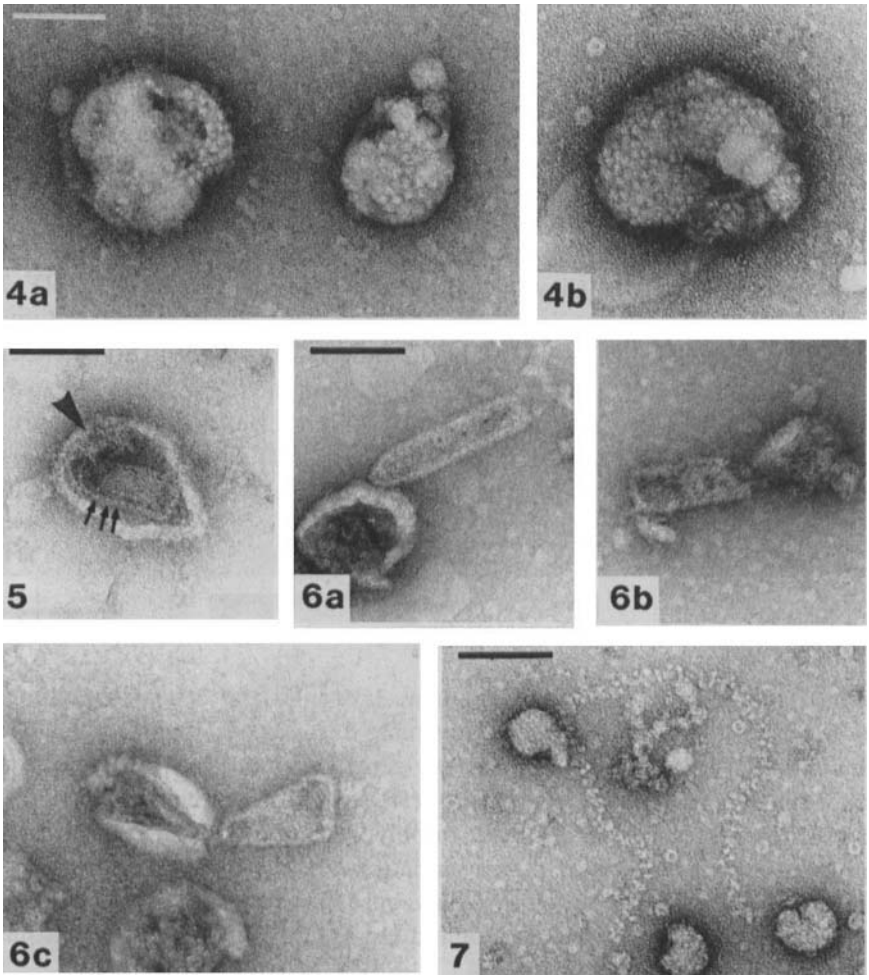

Figs. 17C.4–7. Equine infectious anemia virus (EIAV), negatively stained with uranyl acetate. Bar represents 100 nm. (Reproduced courtesy of Dr. F. Weiland.)

Fig. 17C.4. The surface of particles is covered with knob-like projections.

Fig. 17C.5. Particle with a tubular core revealing subunits of the core shell (small arrows). Arrowhead indicates additional amorphous material (see also Fig. 17C.9f and h).

Fig. 17C.6. Cores released by detergent treatment of virus particles reveal various sizes and shapes.

Fig. 17C.7. Filament with helical structure occasionally found in negatively stained preparations and similar to those described as RNP filaments of Friend leukemia virus.

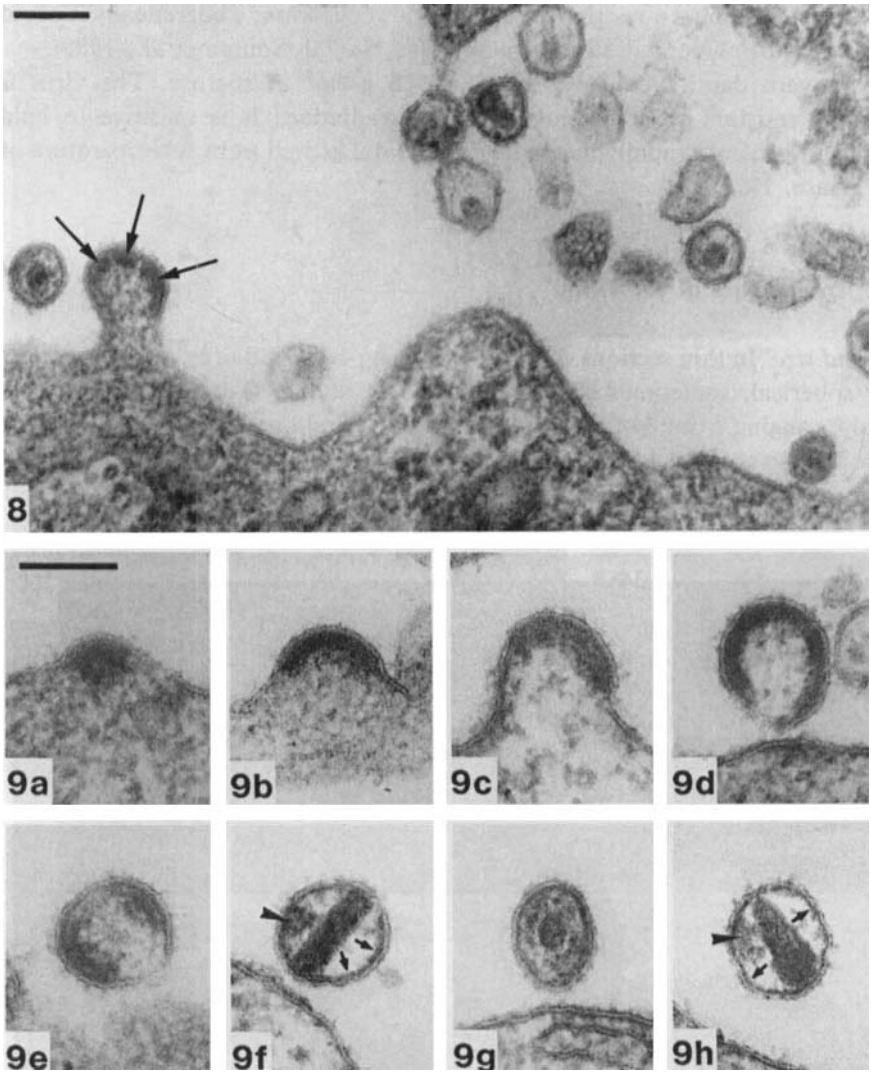

Fig. 17C.8 Ultrathin section of a HIV 1-producing H9 cell. The budding particle contains three incomplete cores indicated by arrows. Bar represents 100 nm.

Fig. 17C.9 Budding (a–e) and released (f–h) HIV 1 particles. Budding viruses in (d) and (e) reveal two cores each. Small arrows in (f) and (h) indicate the inner coat of the envelope; the clumped material (arrowheads), however, may derive from incomplete cores which originate if budding sites are located close together but start budding at different times. The profile of complete cylindrical cores varies with the section plane (f–h). Bar represents 100 nm.

(Figs. 17C.8 and 9 courtesy of Dr. H. Gelderblom.)

been postulated to play a restrictive role in viral replication. Theoretically it could code for a hydrophilic and basic protein of M_r 28 000 (Sonigo et al., 1985).

The buoyant density of MVV is 1.15–1.16 g/cm^3 in sucrose. The virus is remarkably resistant to sonication and UV irradiation. It is sensitive to lipid solvents and becomes rapidly inactivated at pH 4.2 as well as by a temperature of 56°C (Haase, 1975).

17C.3. Architecture of the virion

Shape and size. In thin sections of virus-producing cells lentivirus particles appear mostly spherical, sometimes elliptic (Figs. 17C.1 and 3). Their size varies considerably, ranging from 64 to 140 nm. Pictures of budding viruses show the core in close contact with the envelope; the electron-lucent space which is typical of most retroviruses is missing (Figs. 17C.1, 3, 8, 9 and 12).

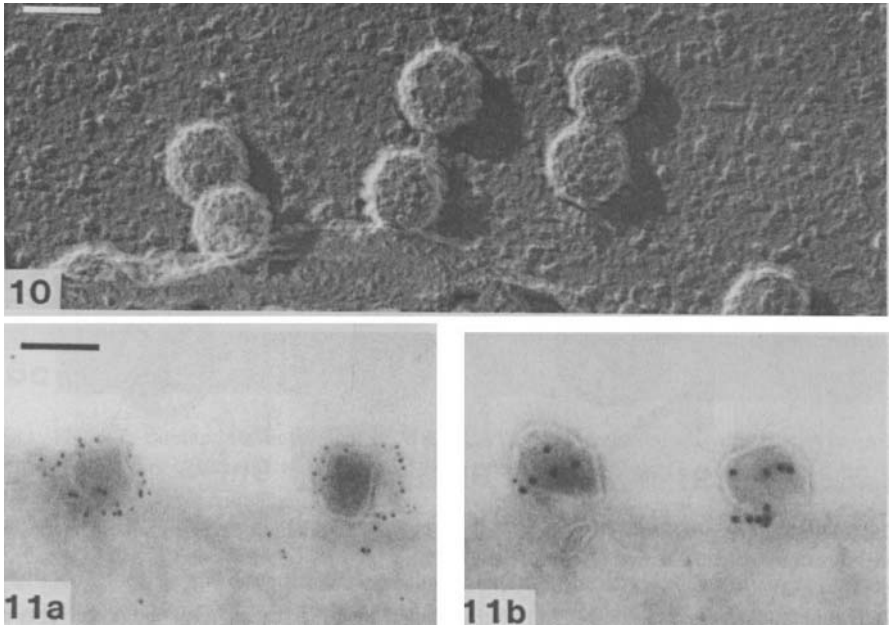

Fig. 17C.10. Replica of a HIV 1-producing H9 cell after critical-point drying. Knobs on the surface of the virus particles are clearly recognizable. Bar represents 100 nm.

Fig. 17C.11. Ultrathin cryo-section of HIV 1-producing H9 cells immuno-gold-labeled with (a) anti-gp120 and (b) with anti-p24 antibody. Bar represents 100 nm.

(Fig. 17C.10 courtesy of Dr. M. Özel; Fig. 17C.11 courtesy of Dr. H. Gelderblom.)

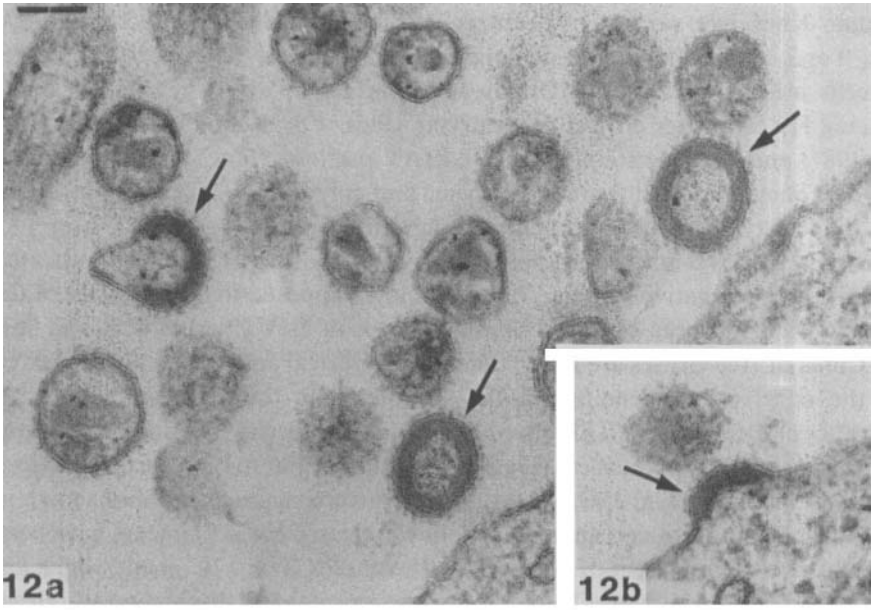

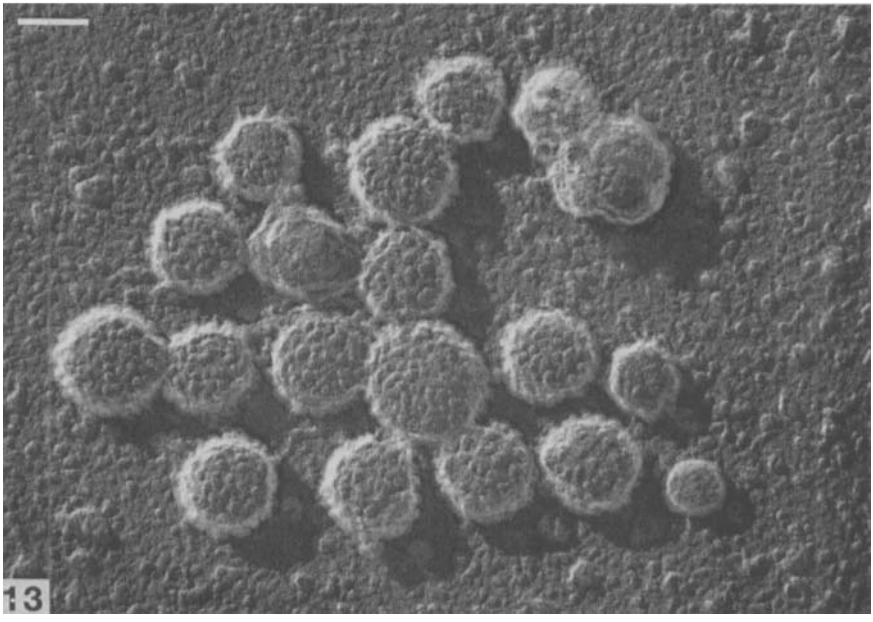

Fig. 17C.12. Ultrathin section of a HIV 2-producing H9 cell. (a) General view; (b) budding virus particle. Arrows indicate particles with immature structure and clearly visible surface knobs. Bar represents 100 nm.

Fig. 17C.13. Surface replica of a HIV 2-producing H9 cell after critical-point drying. Knobs on the surface of the viruses are clearly recognizable. Bar represents 100 nm.

(Fig. 17C.12 courtesy of Dr. H. Gelderblom; Fig. 17C.13 courtesy of Dr. M. Özel.)

Envelope. Knob-like surface projections become visible in thin sections (Figs. 17C.3, 9 and 12) but have been demonstrated more clearly in replicas of freeze-dried cells infected with MVV (Dubois-Dalcq et al., 1976), in replicas of HIV-producing H9 cells after critical-point drying (Figs. 17C.10 and 13) (Gelderblom et al., 1987) and negative staining of free EIAV particles (Fig. 17C.4 (Weiland et al., 1977). They are about 8 nm in diameter and contain the major glycoprotein, which induces type-specific and neutralizing antibody.

The inner coat as described in type C oncovirus has not yet been demonstrated in lentiviruses by negative staining, but a thin layer apposed to the inner side of the viral membrane has been observed in thin sections of HIV (Figs. 17C.9f and 9h).

Core. Cores of free viruses are approximately cylindrical and are always separated from the envelope. Depending on the section plane they appear cylindrical, spherical or conical (Figs. 17C.3e–h, 9f–h and 12a). In negatively stained preparations cores are mostly cylindrical (Figs. 17C.5 and 6b) but may differ in size (Fig. 17C.6a; compare also Fig. 17C.3e and f). Aberrant forms such as those shown in Fig. 17C.6c are not frequent. In preparations of released cores filaments have been found which are reminiscent of a helical RNP complex (Fig. 17C.7) and which are similar to those found in type C oncovirus preparations after dissolution of released cores (p. 279). The core shell of MVV contains the structural protein p30 which is of group-specific antigenicity. The minor basic protein p14 of MVV is associated with the viral RNA.

A diagram of the virion is shown in Fig. 17C.14. A correlation between structural elements and structural proteins of MVV, HIV 1, HIV 2 and STLV-III is given in Table 17.1.

17C.4. Virus–cell interactions

Lentiviruses spread horizontally. There are as yet no indications for endogenous lentiviruses. The expression of MVV in vivo is restricted by a blockage at the level

TABLE 17C.1

Correlation of morphological elements and structural proteins of MVV, HIV 1, HIV 2 and STLV-III (data from Clavel et al., 1986; Gelderblom et al., 1987; Quinn et al., 1987; Weiss et al., 1982)

Structural component	Structural protein of:			
	MVV	HIV 1	HIV 2	STLV-III
Knobs	gp135	gp120	gp140	gp120
Transmembrane protein	(gp70?)	gp41	gp36	gp32
Inner coat	p16?	p17	?	?
Core shell	p30	p24	p26	p26
Nucleoprotein	p14	p15?	p16	p15

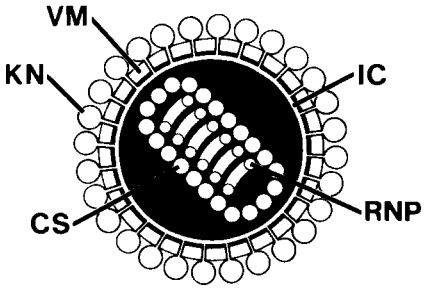

Fig. 17C.14. Diagram of the architecture of lentivirinae. Kn, knobs; VM, viral membrane; IC, inner coat; CS, core shell; RNP, ribonucleoprotein complex.

of transcription. The infection is persistent for years despite a specific immune response of the host.

However, propagation of MVV in cell culture reveals a lytic cycle. Penetration of cells take place after adsorption of the viral surface glycoproteins to specific receptors of the host cell. The mode of entry of the viruses has not yet been investigated in detail. The core is probably released into the cytoplasm after fusion of viral membrane and cell membrane. After reverse transcription of viral RNA a linear viral DNA is found in the nucleus consisting of a full-length minus strand and two plus strands separated by a gap in the middle of the molecule. A minor proportion of DNA is found in two circular forms differing in size. Only a small and variable proportion of viral DNA is associated with cellular DNA. It is assumed that the insertion of viral DNA into the host genome is not necessary for transcription of MVV RNA in vitro (Blum et al., 1985).

As demonstrated with oncoviruses of type C, assembly of cores of lentivirinae takes place at the cell membrane simultaneously with the budding process (Figs. 17C.3a–d, 9a–d and 12b). However, in some types of virus-producing cells, e.g. in testes cells of sheep, intracytoplasmic structures are observed reminiscent of particles of type A oncovirinae (Figs. 17C.1b, 2a and 2b). These 'laminar' bodies (Bouillant and Becker, 1984) are mostly multilayered (Fig. 17C.2c and 2d), sometimes in the form of a spiral (Fig. 17C.2d). The similarity of each layer to the crescent of cores in the budding process indicates their viral origin (compare Figs. 17C.2 and 3). Similar structures (test tube and ring-shaped forms, tubuloreticular inclusions and vesicular rosettes) have been also found in thin section of lymphocytes of AIDS patients (for review see Reichert et al., 1985).

References

Blum, H.E., Harris, J.D., Ventura, P., Walker, D., Staskus, K., Retzel, E. and Haase, A.T. (1985) Synthesis in cell culture of the gapped linear duplex DNA of the slow virus visna. Virology 142, 270–277.

Bouillant, A.M.P. and Becker, S.A.W.E. (1984) Ultrastructural comparison of oncovirinae (type C), spumavirinae and lentivirinae: three subfamilies of retroviridae found in farm animals. J. Natl. Cancer Inst. 72, 1075–1084.

Brun-Vézinet, F., Katlama, C., Roulot, D., Lenoble, L., Alizon, M., Madjar, J.J., Rey, M.A., Girard, P.M., Yeni, P., Clavel, F., Gadelle, S. and Harzic, M. (1987) Lymphadenopathy-associated virus type 2 in AIDS and AIDS-related complex. Lancet i, 128–132.

Clavel, F., Guétard, D., Brun-Vézinet, F., Chamaret, S., Rey, M. A., Santos-Ferreira, M.O., Laurent, A.G., Dauguet, C., Katlama, C., Rouzioux, C., Klatzmann, D., Champalimaud, J.L. and Montagnier, L. (1986) Isolation of a new human retrovirus from West African patients with AIDS. Science 233, 343–346.

Dubois-Dalcq, M., Reese, T.S. and Narayan, O. (1976) Membrane changes associated with assembly of visna virus. Virology 74, 520–530.

Gelderblom, H.R., Hausmann, E.H.S. Özel, M., Pauli, G. and Koch, M. (1987) Fine structure of human immunodeficiency virus (HIV) and immunolocalization of structural proteins. Virology 156, 171–176.

Gonda, M.A., Wong-Staal, F., Gallo, R.C., Clements, J.E., Narayan, O. and Gilden, R. (1985) Sequence homology and morphological similarity of HTLV-III and visna virus, a pathogenic lentivirus. Science 227, 173–177.

Haase, A.T. (1975) The slow infection caused by visna virus. Curr. Top. Microbiol. Immunol. 72, 101–156.

Shaw, G.M., Harper, M.E., Hahn, B.H., Epstein, L.G., Gajdusek, D.C., Price, R.W., Navia, B.A., Petito, C.K., O'Hara, C.J., Groopman, J.E., Cho, E.-S., Oleske, J.M., Wong-Staal, F. and Gallo, R.C. (1985) HTLV-III infection in brains of children and adults with AIDS encephalopathy. Science 227, 177–182.

Sigurdson, B. (1954) Maedi, a slow progressive pneumonia of sheep: An epizoological and pathological study. Br. Vet. J. 110, 255–270.

Sonigo, P., Alizon, M., Staskus, K., Klatzmann, D., Cole, St., Danos, O., Retzel, E., Tiollais, P., Haase, A. and Wain-Hobson, S. (1985) Nucleotide sequence of the visna lentivirus: relationship to the AIDS virus. Cell 42, 369–382.

Quinn, T.C., Mann J.M., Curran, J.W. and Piot, P. (1986) AIDS in Africa: an epidemiologic paradigm. Science 234, 955–963.

Reichert, M., Kelly, V.L. and Macher, A.M. (1985) Pathologic features of AIDS. In: AIDS, Etiology, Diagnosis, Treatment and Prevention, Eds. V.T. De Vita, S. Hellman and St.A. Rosenberg; pp. 111–160. J.B. Lippincott, Philadelphia, New York.

Weiland, F., Matheka, H.D., Coggins, L. and Härtner, D. (1977) Electron microscopic studies on equine infectious anemia virus (EIAV). Arch. Virol. 55, 335–340.

Weiland, F. and Bruns, M. (1980) Ultrastructural studies on maedi-visna virus. Arch. Virol. 64, 277–285.

Weiss, R., Teich, N., Varmus, H. and Coffin, J. (Eds.) (1982) RNA Tumor Viruses. Cold Spring Harbor Laboratory, NY.

Nermut/Steven (eds) Animal Virus Structure

CHAPTER 17D

Spumavirinae

HANS GELDERBLOM[1] and HERMANN FRANK[2]

[1]*Robert Koch-Institut des Bundesgesundheitsamtes, Nordufer 20, D-1000 Berlin (West) 65, and*
[2]*Max-Planck-Institut für Entwicklungsbiologie, Spemannstr. 35, D-7400 Tübingen, F.R.G.*

Subfamily: Spumavirinae
Genus: Spumavirus
Species: Simian foamy virus (SFoV), bovine syncytial virus (BSV), human syncytium-forming virus (HSFoV)

17D.1. Introduction

Spumavirinae, commonly called foamy viruses, are enveloped viruses with characteristic RNA-containing cores. They have been isolated from a number of mammalian species, e.g. from hamsters, rabbits, cats, cattle, monkeys and man (Weiss et al., 1982). They are spread as exogenous agents mainly horizontally, but also vertically from mother to offspring, leading to lifelong persisting infections without apparent pathogenic potential. In susceptible cell cultures, however, they induce pathognomonic syncytial formation, i.e. multinucleated polycaryons followed by a vacuolating, 'foamy' degeneration. This effect was first observed in a 'spontaneously' degenerating primary kidney cell culture from a macaque, and this led to designations such as simian foamy or bovine syncytial virus (SFoV, BSV).

Foamy viruses as a separate subfamily of the retroviridae differ from onco- and lentivirinae in the following biological and biophysical properties. Firstly, they do not induce malignancies or other diseases in their natural hosts, but lead to persistent infections in spite of the production of antiviral antibody. In vitro

spumavirinae are able to infect productively a broad range of mammalian species. As a common feature, they do not induce cell transformation, but rather a lytic, cytopathic effect which is characterized initially by multi-nucleated, vacuolated cells, which eventually die after the formation of large syncytia. Secondly, during early virus replication, viral antigens can be demonstrated in the cell nuclei. At later stages they disappear from the nuclei and instead virus antigens appear in the cytoplasm. Thirdly, foamy viruses do not share group-specific antigens. Finally, spumavirinae may be readily differentiated from the other two retrovirus subfamilies by the length of their envelope projections and by the characteristic electron-lucent centers of the viral core before and after release from the cell, i.e. after maturation (for comprehensive reviews see Hooks and Gibbs, 1975; Schidlovsky et al., 1973; Weiss et al., 1982).

17D.2. Physical and chemical characterization

Only a few foamy viruses have been characterized in detail. Their genome is a single- stranded RNA of 60–70 S with additional smaller RNA species (8 S, 5 S and 4 S) (Cavalieri et al., 1981; Loh and Matsuura, 1981). The genome is transcribed into an infectious DNA intermediate, which can be isolated from infected cells. Also, as regards the properties of the RNA-dependent DNA polymerase (RDDP, reverse transcriptase) the foamy viruses reflect the characteristics of the retrovirus family. The monomeric enzyme of SFoV 1 has an M_r of 81 000 and exhibits two distinct activities: (1) the RDPP (Parks et al., 1971; Benzair et al., 1982), and (2) an RNase H, which degrades RNA-DNA hybrids that are formed in early retrovirus replication. Both activities have a divalent cation requirement, with Mn^{2+} preferred over Mg^{2+} (Benzair et al., 1982, 1983). The buoyant density of complete virus particles in sucrose is 1.16 g/cm^3.

Structural proteins

Five structural proteins have been found in complete virions, but only those

---

Figs. 17D.1–3. Ultrathin sections of HSFV (human syncytial forming virus), assembly and 'maturation' in human embryonic lung cells. 1, most HSFV particles are seen budding from the cell surface, often forming multiple buds. 2, only occasionally are cells with abundant cellular virus precursors observed. 3a–c, virus particles at various budding stages, showing preformed cores and prominent surface projections. 3d, typical morphology of a released 'mature' HSFV particle with a fringe of prominent spikes and the pathognomonic electron-lucent spherical core. 3e–h, HSFV showing different signs of degradation and/or abnormalities, e.g. loss of spikes and/or particles with double or elongated cores. Bars represent 100 nm.

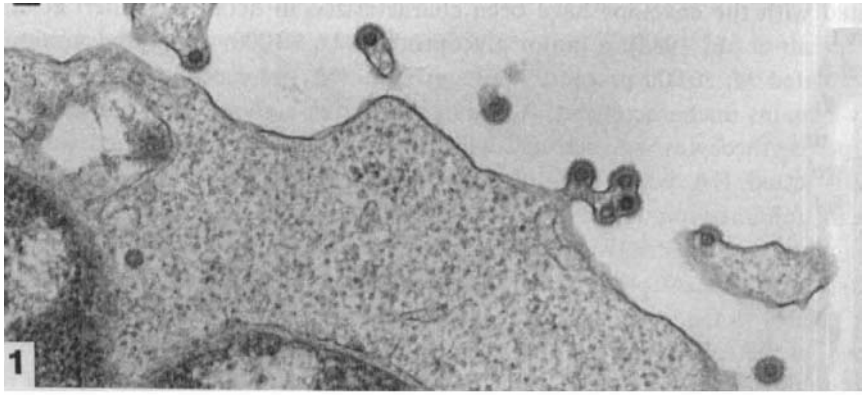
1


2

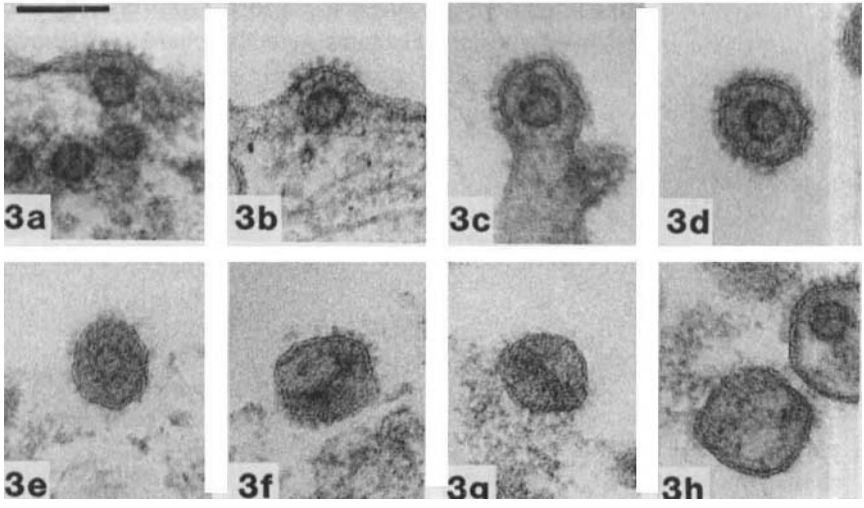
3a
3b
3c
3d
3e
3f
3g
3h

associated with the envelope have been characterized in detail (Cavalieri et al., 1981; Benzair et al., 1985): a major glycoprotein (M_r 70000; gp70) and a minor unglycosylated M_r 30000 protein. While gp70 shows type-specific reactivity, the p30 env remains uncharacterized. A hemagglutinating activity (HA) restricted to guinea pig erythrocytes was detected with SFoV 1 when highly purified suspensions were tested. HA, which certainly reflects properties of the viral envelope, was specifically inhibited not only by type-specific neutralizing antisera, but also by antisera against other strains of SFoV, which are unable to neutralize the heterologous strains. At present it is unknown how this cross-reactivity in HA inhibition relates to the strictly type-specific pattern of foamy virus neutralization. It seems that the envelope structures responsible for both functions reside on different domains of the viral envelope (Peries and Todaro, 1977). This is similar to the occurrence and function of different HA and neutralization domains described earlier on murine retroviruses (Witter et al., 1973).

17D.3. Fine structure and morphogenesis

Size of the virion = 100–130 nm from thin sections.
Envelope = studded with glycoprotein projections 15 nm in length.
Core = polygonal; can be isolated after controlled detergent degradation; buoyant density 1.22 g/cm^3 in sucrose; 50 nm in diameter.

No direct observation of foamy viruses in normal or pathological tissues has been described. Passage of tissues in cell culture often leads to the expression of the virus and many of the inadvertently observed isolates were also characterized morphologically. Irrespective of their species of origin, foamy viruses resemble each other in morphology so closely that no distinctive criterion for a particular foamy virus can be given.

The mode of entry of simian foamy virus as studied in HEp-2 cell cultures is either by fusion of the viral and cell surface membranes (direct entry) or by endocytosis (Dermott and Samuels, 1973a).

Fig. 17D.4. Ultrathin sections of an SFoV (simian foamy virus) -producing rhesus monkey kidney cell. a, perinuclear regions contain many SFoV cores, often in close association with enlarged cisternae of smooth endoplasmic reticulum (ER). Some bare cores are found in the cytoplasm, near the nucleus, but most have envelopes (b), which are contiguous with the ER. Viral cores differ in contrast, presumably because of the different amounts of nucleic acid in the RNP complex, and show electron-opaque surface projections and an electron-lucent center. The envelopes of budding SFoV are studded with surface projections (arrow). Bars represent 100 nm.

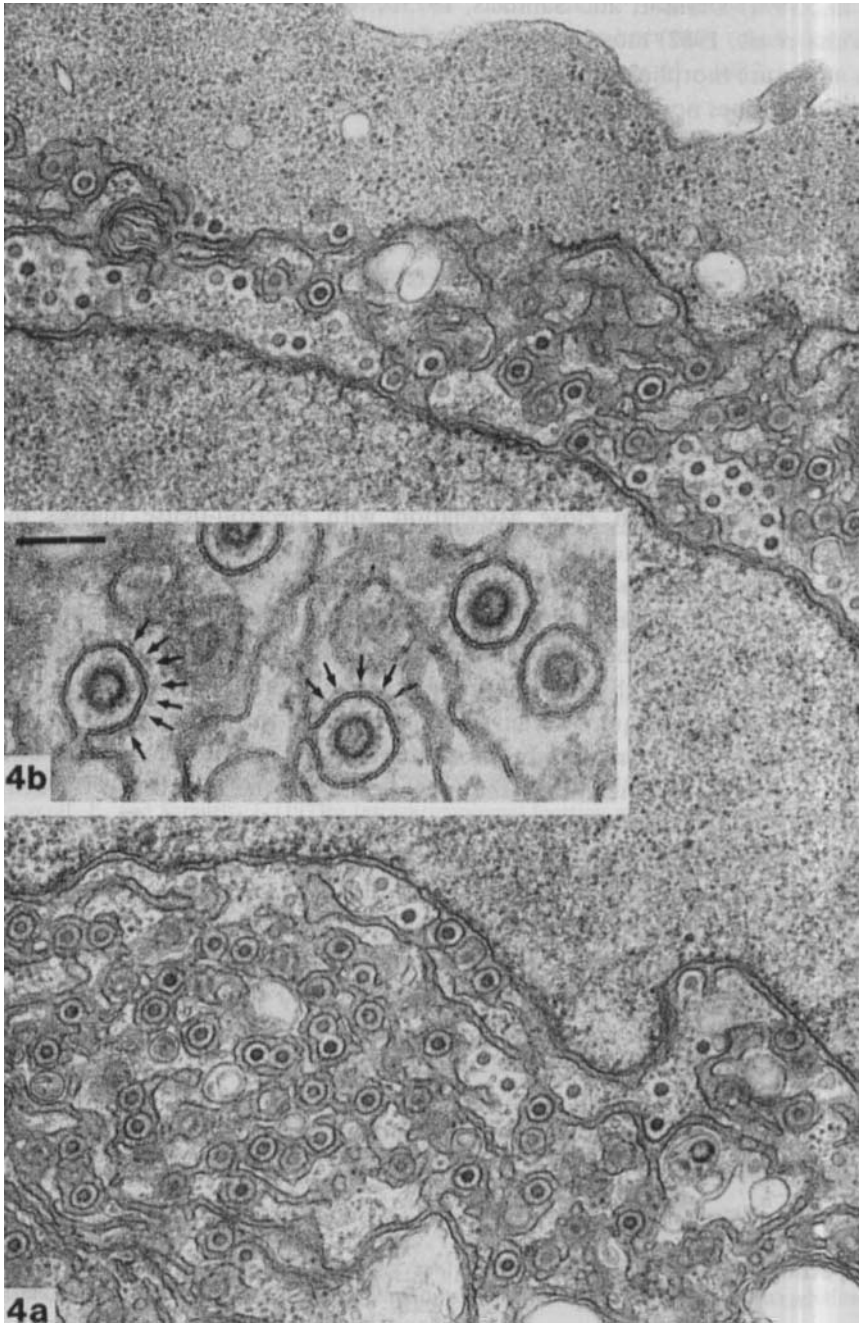
4b
4a

In thin sections of infected cells (Clarke et al., 1969; Boothe et al., 1970; Dermott et al., 1971; Dermott and Samuels, 1973b; reviewed by Schidlovsky et al., 1973; Weiss et al., 1982) most foamy virus particles, both budding and released, have an immature morphology, i.e. the spherical ribonucleoprotein core observed during budding does not condense after release of the virion, which is a distinctive criterion of most 'mature' retroviruses. Depending on the host cell type, budding is observed either preferentially at the cell surface (Fig. 17D.1) or at the channel system of the endoplasmic reticulum (Fig. 17D.4). Only complete cores are observed at both sites of budding, and in this respect foamy viruses resemble B- and D-type oncovirinae. Cores are assembled in the cytoplasm apparently by a fast process, since incomplete cores are seen very rarely. In addition, inclusions of virus core-specific material are occasionally formed in the cytoplasm; in longitudinal sections they appear as parallel rows of electron-dense tubules (Clarke et al., 1969).

In specific virus host cell combinations (Dermott et al., 1971; Dermott and Samuels, 1973b) incomplete as well as complete cores were also detected in the nuclei of infected cells in close association with electron-dense masses indistinguishable from condensed chromatin. This intra-nuclear appearance of virus-specific structures was to be expected on the basis of earlier observations by immunofluorescence of foamy virus antigens in the nucleus.

Usually, cores appear to be dispersed randomly throughout the cytoplasm (Figs. 17D.1,2,4a), sometimes with a concentration at the membrane stacks of the Golgi apparatus. These cores acquire an envelope by budding through the membranes of the Golgi and/or the endoplasmic reticulum (Fig. 17D.4). When cores bud through the cytoplasmic membrane the inner leaflet of the membrane thickens somewhat and spiky projections appear on the surface of the bud. These spikes measure about 15 nm in length, show a regular spacing of 15 nm and are a prominent and distinctive feature of the foamy virus subfamily. As the membrane bud grows, the number of associated spikes increases, and finally, after release from the particular membrane system, the spherical virion is completely studded with a fringe of spikes (Fig. 17D.3d). After budding, the viral core, initially spherical, becomes slightly distorted. Upon release, virus particles often increase in diameter and lose part of their corona of spikes (Fig. 17D.3 e–h).

The few morphological studies carried out on isolated virus particles, using negative staining, generally corroborate the findings obtained from thin sections (Clarke and McFerran, 1970; Schidlovsky et al., 1973; Benzair et al., 1985).

17D.4. Pathogenicity

Though foamy viruses have, on occasion, been isolated from diseased animals and men, they have not yet been linked to malignancies or other diseases. In natural

hosts, infections generally lead to the induction of high titers of antiviral antibodies and to virus persistence. The virus can be recovered from numerous tissues, and experimental infection of a heterologous host may result again in persistent infections (for a detailed discussion see Weiss et al., 1982).

Suggested reading

Benzair, A.-B., Rhodes-Feuillette, A., Emanoil-Ravicovitch, R. and Peries, J. (1982) Reverse transcriptase from simian foamy virus serotype 1: purification and characterization. J. Virol. 44, 720–724.

Benzair, A.-B., Rhodes-Feuillette, A., Emanoil-Ravicovitch, R. and Peries, J. (1983) Characterization of RNase H activity associated with reverse transcriptase in simian foamy virus type 1. J. Virol. 47, 249–252.

Benzair, A.-B., Rhodes-Feuillette, A., Lasneret, J., Emanoil-Ravier, R. and Peries, J. (1985) Purification and characterization of the major envelope glycoprotein of simian foamy virus type 1. J. Gen. Virol. 66, 1449–1455.

Boothe, A.D., Van der Maaten, M.J. and Malmquist, W.A. (1970) Morphological variation of a syncytial virus from lymphosarcomatous and apparently normal cattle. Arch. Ges. Virusforsch. 31, 373–384.

Cavalieri, F., Rhodes-Feuillette, A., Benzair, A.-B., Emanoil-Ravicovitch, R. and Peries, J. (1981) Biochemical characterization of simian foamy virus type 1. Arch. Virol. 68, 197–202.

Clarke, J.K., Attridge, J.T. and Gay, F.W. (1969) The morphogenesis of simian foamy viruses. J. Gen. Virol. 4, 183–188.

Clarke, J.K. and McFerran, J.B. (1970) The morphology of bovine syncytial virus. J. Gen. Virol. 9, 155–157.

Dermott, E. and Samuels, J. (1973a) Electron microscopic observations on the mechanisms of entry of simian foamy virus in HEp-2 cells. J. Gen. Virol. 19, 135–139.

Dermott, E. and Samuels, J. (1973b) Intrachromosomal location of MK 5, a foamy type 1 virus. J. Gen. Virol. 19, 141–143.

Hooks, J.J. and Gibbs, C.J. (1975) The foamy viruses. Bacteriol. Rev. 39, 169–185.

Loh, P.C. and Matsuura, F.S. (1981) The RNA of human syncytium-forming (foamy) virus. Arch. Virol. 68, 53–58.

Matthews, R.E.F. (1982) Classification and nomenclature of viruses. Fourth report of the international committee on taxonomy of viruses. Intervirology 17, 234–238.

Parks, W.P., Todaro, G.J., Scolnick, E.M. and Aaronson, M.A. (1971) RNA dependant DNA polymerase in primate syncytium forming (foamy) viruses. Nature 229, 258–360.

Peries, J. and Todaro, G.J. (1971) A haemagglutination assay for the primate syncytium-forming (foamy) viruses. J. Gen. Virol. 34, 195–199.

Schidlovsky, G., Ahmed, M. and Dalton, A. (1973) Syncytial (foamy) viruses. In: Ultrastructure of Animal Viruses: An Atlas, Eds. A.J. Dalton and F. Haguenau; pp. 369–373. Academic Press, New York and London.

Weiss, R.A., Teich, N., Varmus, H. and Coffin, J. (eds.) (1982) RNA tumor viruses. Cold Spring Harbor Laboratory, NY.

Witter, R., Frank, H., Moennig, V., Hunsmann, G., Lange, J. and Schäfer, W. (1973) Properties of mouse leukemia virus. IV. Haemagglutination assay and characterization of haemagglutinating surface components. Virology 54, 330–345.

This Page Intentionally Left Blank

Nermut/Steven (eds) Animal Virus Structure

CHAPTER 18

The filoviridae

D.S. ELLIS

London School of Hygiene and Tropical Medicine, Keppel Street, London WC1E 7HT, U.K.

Family: Filoviridae
Genus: Filovirus, containing two species, Marburg virus and Ebola virus. There are two known strains of Ebola virus, one isolated from the Sudan and the other from Zaire, which have several distinguishing characteristics.

18.1. Origin and general features

The few isolates of this genus have each come from central Africa, and have been responsible for outbreaks of a severe and often fatal form of haemorrhagic fever, spread by close personal contact or as a result of contamination from infected body fluids or tissues. A natural reservoir in Africa has yet to be found and no vector has been identified in spite of an intensive search.

Mature particles are enveloped, negative sense, single-stranded RNA viruses existing in a variety of shapes unique to this genus: these include 'torus', 'filamentous' and 'branched' forms, some up to 20 μm in length, and many of them, obtained from patients, exhibit a variety of aberrant forms. The viral envelope is covered with 'spikes'.

18.2. Some chemical and physical characteristics

The lipid and carbohydrate content of these viruses has yet to be determined, but five proteins (VP0, VP1, VP2, VP3 and VP4) have been identified with respective

molecular masses of 190, 125, 104, 40 and 26 kDa in the Ebola strains and 190, 140, 98, 38 and 22 kDa in Marburg virus. Viral RNA has a molecular weight of 4.2×10^6 and a sedimentation coefficient of 46 S (in 0.15 M NaCl at pH 7.4).

18.3. Antigenic properties

The Filoviridae do not cross-react with other RNA viruses. There appear to be no antigens common to both Marburg and Ebola viruses. There are, however, many shared antigens between the two Ebola strains, and some degree of cross-protection can be achieved, although often this has proved difficult to assess owing to the very high virulence of the Zaire strain, which may kill before adequate antibodies have had time to appear.

18.4. Structural characteristics

The mature particles have varying tubular shapes, which nevertheless have a uniform cross-sectional diameter of 80 nm. They are covered with a lipid-bilayer envelope (containing the VP1 and VP4 proteins) from which regular spikes 7–10 nm in length project approximately 12 nm apart. (Figs. 18.1 and 13). Beneath the envelope lies a nucleoprotein complex consisting of a hollow tube, internal diameter 20 nm, external diameter 45 nm, which contains the viral RNA plus VP2 and VP3. The striated outer surface of this tube is made up of a coil with a pitch of approximately 7.5 nm (Fig. 18.3). Aberrant forms of this arrangement are very common (Fig. 18.15), and can contain up to 5 or 6 nucleoprotein tubes within a single envelope, which is itself sometimes absent in other particles. The frequency of these aberrant forms and of the various normal mature shapes as found in cultures of these viruses is shown in Table 18.1. Fig. 18.2 combines some of these forms into one single model particle.

Fig. 18.1. Marburg virus; negatively stained, with surface spikes clearly visualized. ×315 000.

Fig. 18.2. A composite model of a single Ebola virus embodying representations of the various types of particles found. T = 'torus', F = 'figure 6' formation, B = branch, A^1 = aberrant filament without envelope, A^2 = part of filament without 'core', S = spikes.

Fig. 18.3. A Marburg virus 'torus', negatively stained, showing the spikes, and striations, 7.5 nm apart, (arrowed) on the internal RNP tube. ×126 000.

Fig. 18.4. Negatively stained Marburg 'figure 6' formation. The arrow marks the parts of the envelope that have already fused, as a step in 'torus' formation. ×140 000.

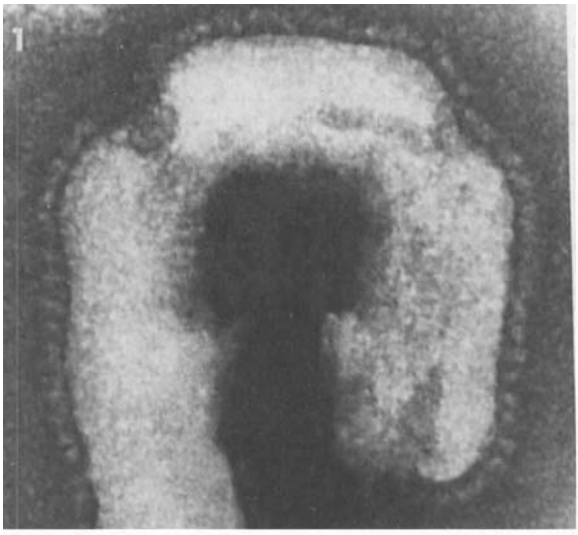
1

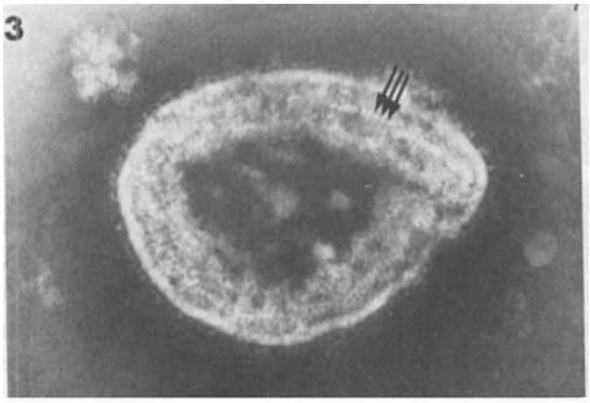
3

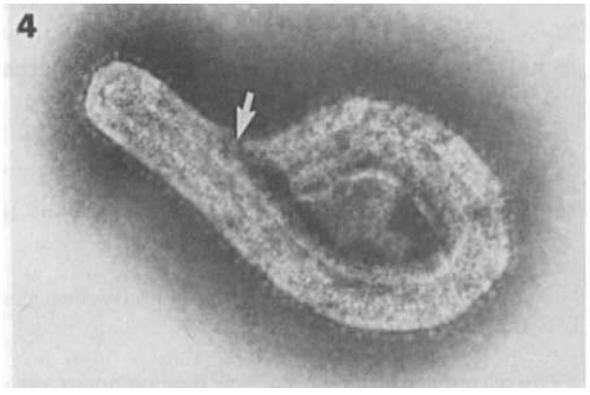
4

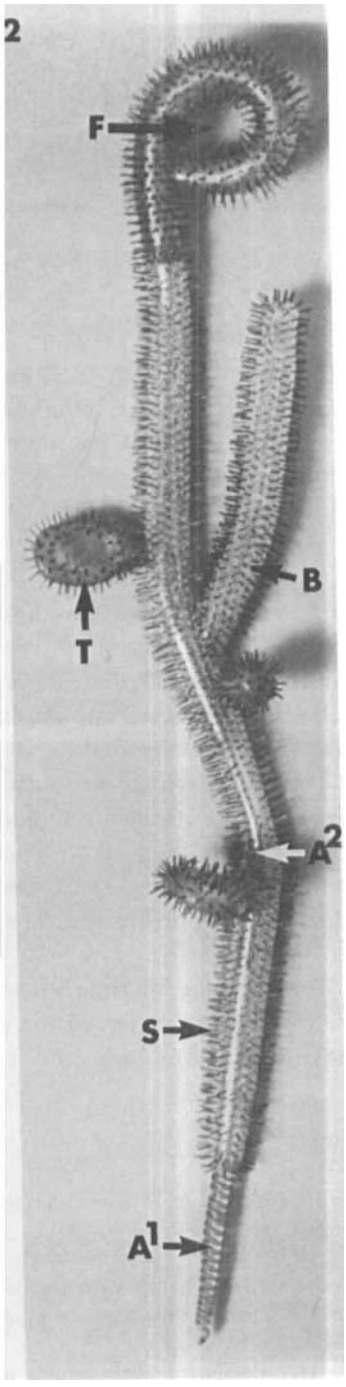
2
F
B
T
A2
S
A1

TABLE 18.1.

	Marburg virus	Ebola virus	
		Zaire strain	Sudan strain
Most common forms found	Mostly 'torus' and short forms	Very long and branched forms	Long forms
Degree of branching	Frequent	Very frequent	Some branching
Presence of aberrant forms	Very few	Few	Very many

'Torus' forms (Fig. 18.3) are usually about 300 nm in outer diameter, as are the heads of the 'figure 6' configuration (Fig. 18.4). These latter are precursors of the 'torus', which itself has been proposed as the infective form (see below). The 'filamentous' forms (Fig. 18.5) are often several micrometers long, while branching forms (Figs. 18.5, 11, 14) may be extremely complex and variable.

18.5. Virus-cell and virus-host interaction

(a) *Replication.* This occurs in the cytoplasm of infected cells, the completed particles being liberated into the extracellular spaces by a process of budding from the host cell plasmalemma.

The nucleoprotein tubes (sometimes referred to elsewhere as 'cores') form in large cytoplasmic inclusion bodies (readily seen by light microscopy), beginning as coils of RNP (Fig. 18.6). Their final forms are 30–40 nm in diameter and of a uniform length (Fig. 18.7). Those grown in Vero cells were approximately 700 nm long, though purification via sucrose gradient has suggested a slightly longer core for Ebola viruses.

These 'tubes' migrate to proliferating areas of host cell plasmalemma where budding and insertion of the surface spikes occur (Fig. 18.8). At this stage they may often follow each other continuously, 'head to tail', through the same area

Fig. 18.5. A part of an Ebola virus particle (Zaire strain) with many branches. A forming 'torus' is arrowed. ×12 000.

Fig. 18.6. RNP coils, an early stage in the formation of the internal nucleoprotein tube developing in a cell infected with the Zaire strain of Ebola virus. ×63 000.

Fig. 18.7. Completed 'nucleocapsids' in a Vero cell infected as in Fig. 18.6. Note their uniformity, each one being approximately 700 nm in length and 30–40 nm in diameter. ×20 000.

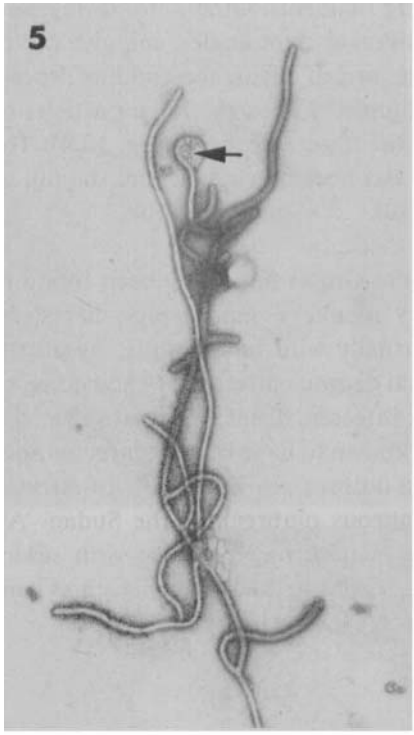
5

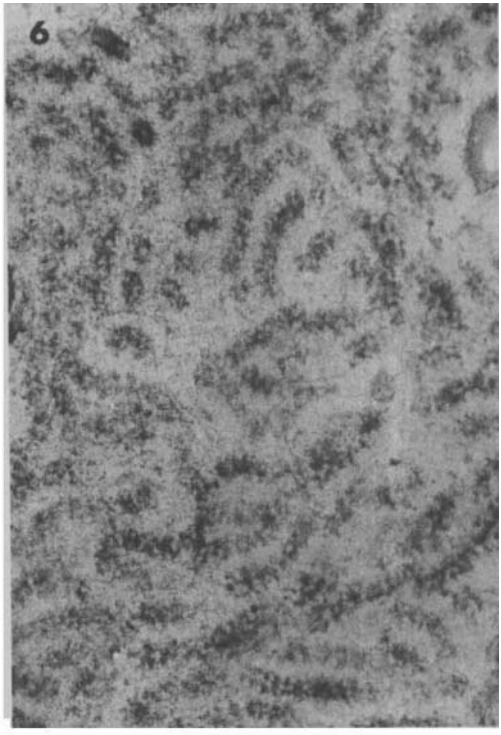
6

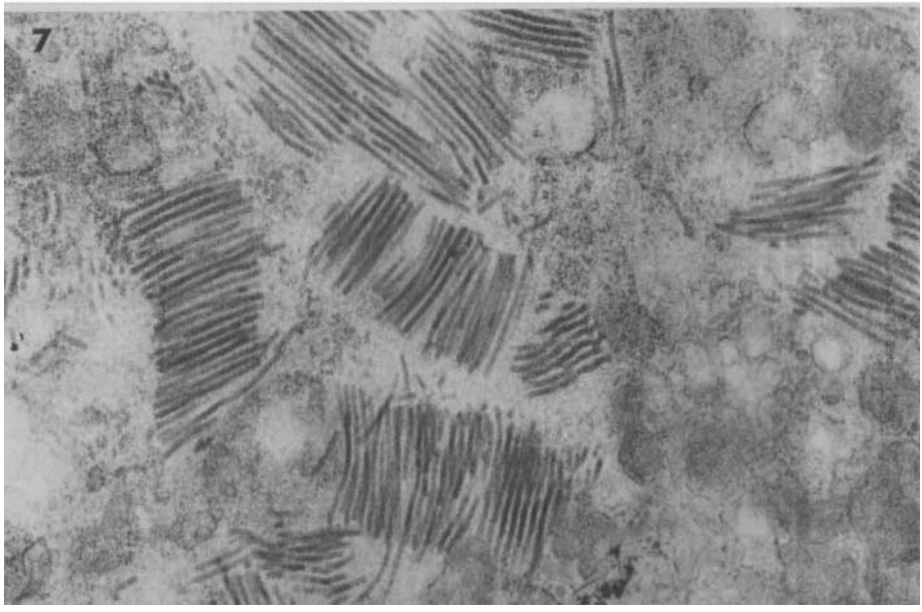
7

of plasmalemma to produce the distinctive long filaments. Others, following each other in the same fashion, but oriented sometimes at right angles, can give rise to the branched forms. The 'torus' is occasionally formed during the budding process (Fig. 18.9) but seems more commonly to be completed in extracellular particles by the rounding up of a free end. This produces the 'figure 6' shape (Fig. 18.4). The rounding process continues until the particle has become circular and the tail of the 'figure 6' has been pinched off (Fig. 18.10).

(b) *Pathogenicity.* Outside the laboratory, these viruses have only been found in man and cercopithecus monkeys. Laboratory monkeys, guinea pigs, hamsters, suckling mice and rabbits can be infected, usually with fatal results, by all the filoviridae. In laboratory animals the individual disease patterns vary according to which of the two different Ebola strains is the infecting agent. Incubation periods vary from 4 to 9 days. Of the 36 non-Africans known to have become infected with Marburg virus, 9 died. During the 1977 Ebola outbreak in Zaire 88% of African patients died, while 53% died in the simultaneous outbreak in the Sudan. All members of the genus cause a similar acute haemorrhagic disease with severe bleeding from mucous surfaces and prominent lesions in the liver, spleen and lymphoid tissues.

Acknowledgements

The author is grateful for permission to reproduce micrographs from the Journal of Medical Virology, and to the Wellcome Institute for the History of Medicine for the photograph of the Ebola virus model.

Fig. 18.8. Completed Marburg tubular 'nucleocapsids' budding through a host cell plasmalemma. A forming 'torus' is arrowed. ×42 000.

Fig. 18.9. A 'torus' forming while still attached to the host cell plasmalemma (Marburg virus). ×80 000.

Fig. 18.10. Negatively stained preparation of an extracellular particle in the process of 'pinching-off' a completed 'torus' from a long 'filamentous form' (Zaire strain of Ebola virus). ×190 000.

Fig. 18.11. Branched forms of Ebola virus (Zaire strain). The negative stain has penetrated the envelopes to show the ends of the 'nucleocapsids' (arrows). ×32 000.

Fig. 18.12. An enlarged area similar to those in Fig. 18.11. The termination of one 'nucleocapsid' is arrowed. ×126 000.

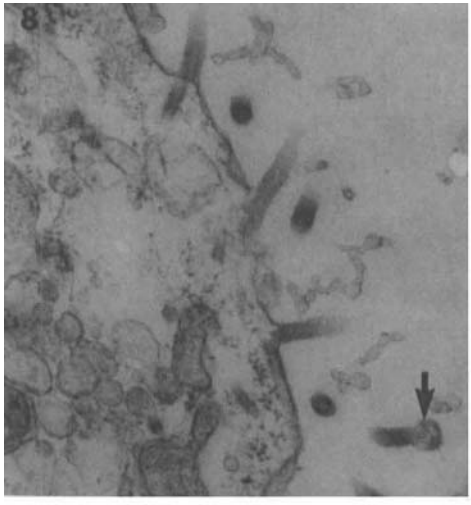
8

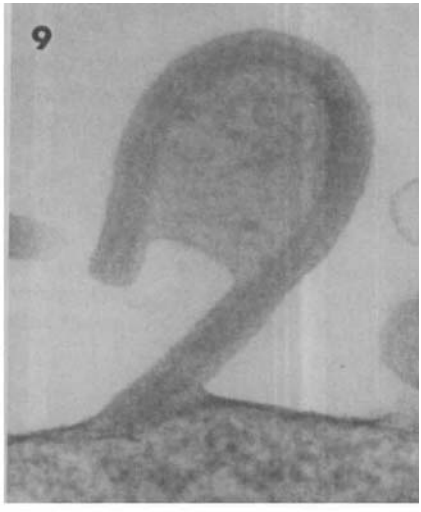
9

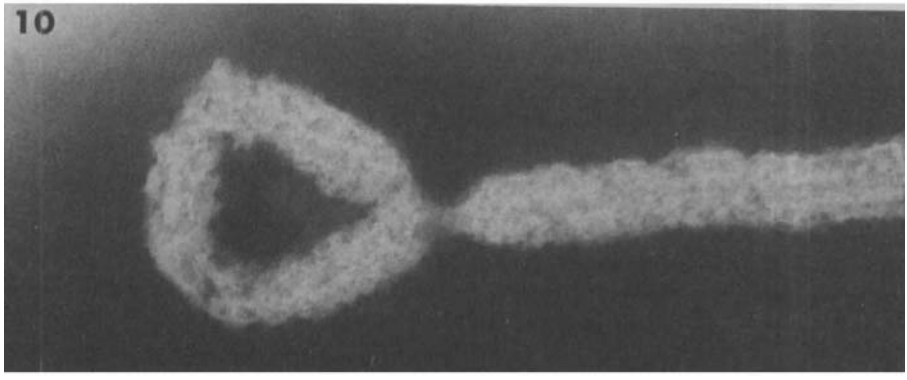
10

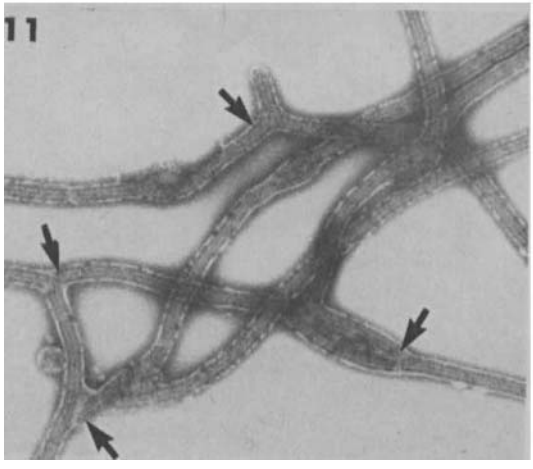
11

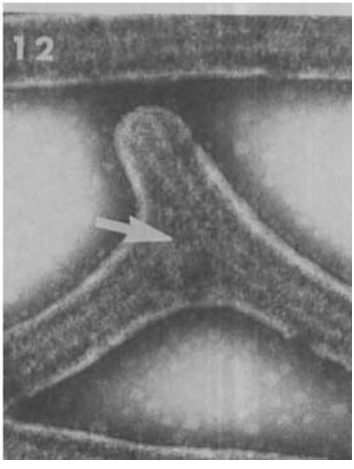
12

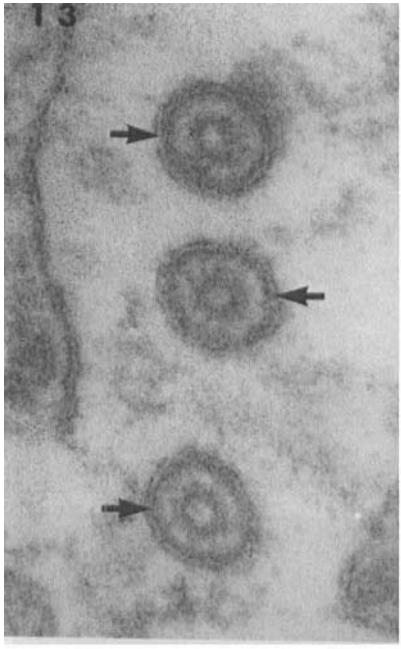
13

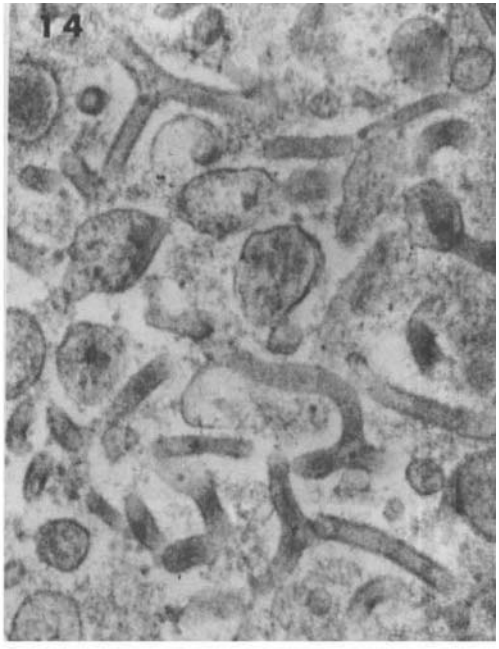
14

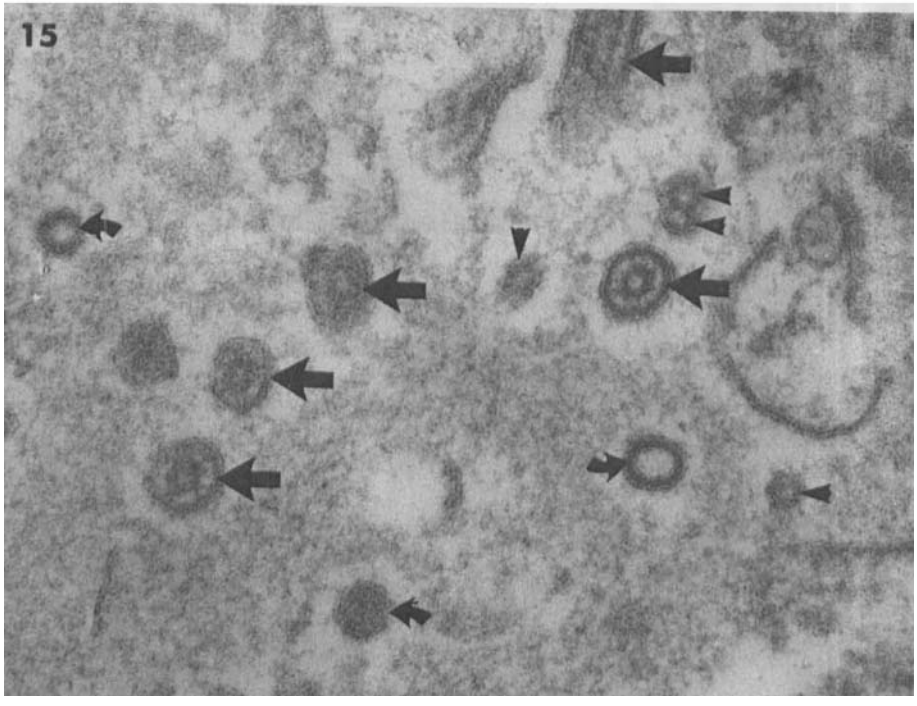
15

Suggested reading

Ellis, D.S., Stamford, S., Tovey, D.G., Lloyd, G., Bowen, E.T.W., Platt, G.S., Way, H. and Simpson, D.I.H. (1979) Ebola and Marburg viruses: II. Their developement within Vero cells and the extra-cellular formation of branched and torus forms. J. Med. Virol. 4, 213–225.

Kiley, M.P., Bowen, E.T.W., Eddy, G.A., Isaacson, M., Johnson, K.M., McCormack, J.B., Murphy, F.A., Pattyn, S.R., Peters, D., Prozesky, O.W., Regnery, R.L., Simpson, D.I.H., Slenczka, W., Sureau, P., van der Groen, G., Webb, P.A. and Wulff, H. (1982) Filoviridae: a taxonomic home for Marburg and Ebola viruses? Intervirology 18, 24–32.

Murphy, F.A., van der Groen, G., Whitfield, S.G. and Lange, J.V. (1978) Ebola and Marburg virus morphology and taxonomy. In Ebola Virus Haemorrhagic Fever, Ed. S.R. Pattyn; pp. 61–85 (and other papers in this collection). Elsevier/North-Holland Biomedical Press, Amsterdam, New York.

Fig. 18.13. Cross-sections of Ebola virus (Sudan strain) in human liver. The envelope surrounding the hollow 'nucleocapsid' is arrowed. The internal channel of the latter here measures 15 nm. ×200 000.

Fig. 18.14. Ebola virus particles (Zaire strain) in monkey liver with many branched forms, lying in the extracellular spaces. ×50 000.

Fig. 18.15. Cross-sections of some Ebola virus particles (Sudan strain) in human liver, many of which are aberrant forms: unenveloped 'cores' are marked by arrowheads, envelopes by curved arrows and complete virions by thick arrows. ×126 000.

This Page Intentionally Left Blank

PART V

DNA-containing virus families

This Page Intentionally Left Blank

Nermut/Steven (eds) Animal Virus Structure

CHAPTER 19

Parvoviridae

BARRIE J. CARTER[1] and PETER J. TATTERSALL[2]

[1]Laboratory of Molecular and Cellular Biology, National Institute for Arthritis, Diabetes, and Digestive and Kidney Diseases, Building 8, Room 304, National Institutes of Health, Bethesda, MD 20892, U.S.A., and [2]Department of Human Genetics, Yale University School of Medicine, 333 Cedar Street, New Haven, CT 06510, U.S.A.

Family: Parvoviridae

Genus: Parvovirus. Species: RV and H-1 (rat viruses), MVM (minute virus of mice), MVC (minute virus of canines), BPV (bovine parvovirus), ADV (Aleutian desease virus of mink), PPV (porcine parvovirus), FPV (feline parvovirus), LPV (lapine parvovirus), GPV (goose parvovirus), B19 (human serum parvovirus), LuIII and TVX (isolated from human cell lines), and RTV (isolated from rat cell line)

Genus: Dependovirus. Species: adeno-associated virus (AAV). AAV2, AAV3, AAV5 (human); AAV1, AAV4 (simian); AAAV (avian); CAAV (canine); OAAV (ovine); BAAV (bovine)

Genus: Densovirus. Species: densonucleosis virus (DNV). Densonucleosis viruses of Galleria, Junonia, Agraulis and Bombyx insect species

19.1. General characteristics

The sigla 'parvo' comes from *parvus* (L. small). Parvoviridae are nonenveloped isometric particles approximately 20–25 nm in diameter consisting of an exterior protein shell (capsid) and an internal DNA genome. The capsid has icosahedral symmetry (Fig. 19.1). Parvoviruses contain no essential lipid or carbohydrate, and particle infectivity is resistant to organic solvents (e.g. ether, chloroform), heat (60°C for 15 min), dehydration, chaotropic agents and detergents. Parvoviruses

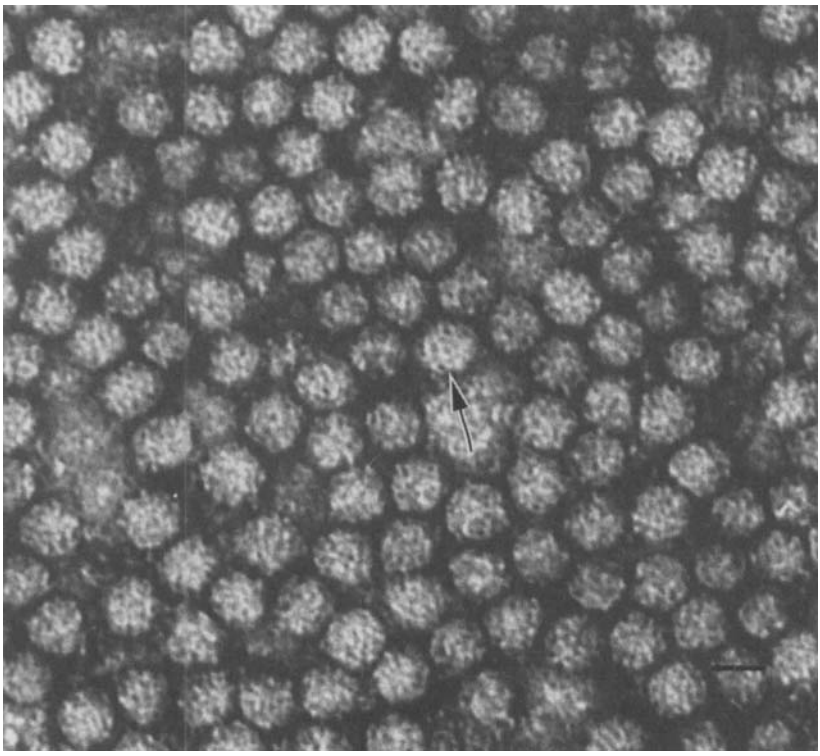

Fig. 19.1. Electron micrographs of mature H-1 virus particles purified from infected hamster embryo fibroblasts and negatively stained with 0.1% uranyl acetate. The particle diameter is 25 nm and the virion indicated by the arrow exhibits well-defined capsomers. The bar shows 25 nm. (The photograph was provided per courtesy of I. I. Singer.)

replicate and assemble in the nucleus of infected cells and form dense aggregates and polycrystalline arrays of virus particles (Fig. 19.2). Members of the parvovirus genus are pathogenic in many animals though usually confined to one species in natural infections. However, feline parvovirus has, on separate occasions, segregated host range variants specific for mink (MEV, mink enteritis virus) and dog (CPV, canine parvovirus). Most members of the parvovirus genus depend for their growth upon host cell functions present only in S-phase of the cell cycle. Members of the dependovirus genus are defective and grow in host cells only in the presence of a helper virus, either an adenovirus or a herpesvirus. Members of the densovirus genus grow only in larvae of various insects. Each genus is discussed separately below.

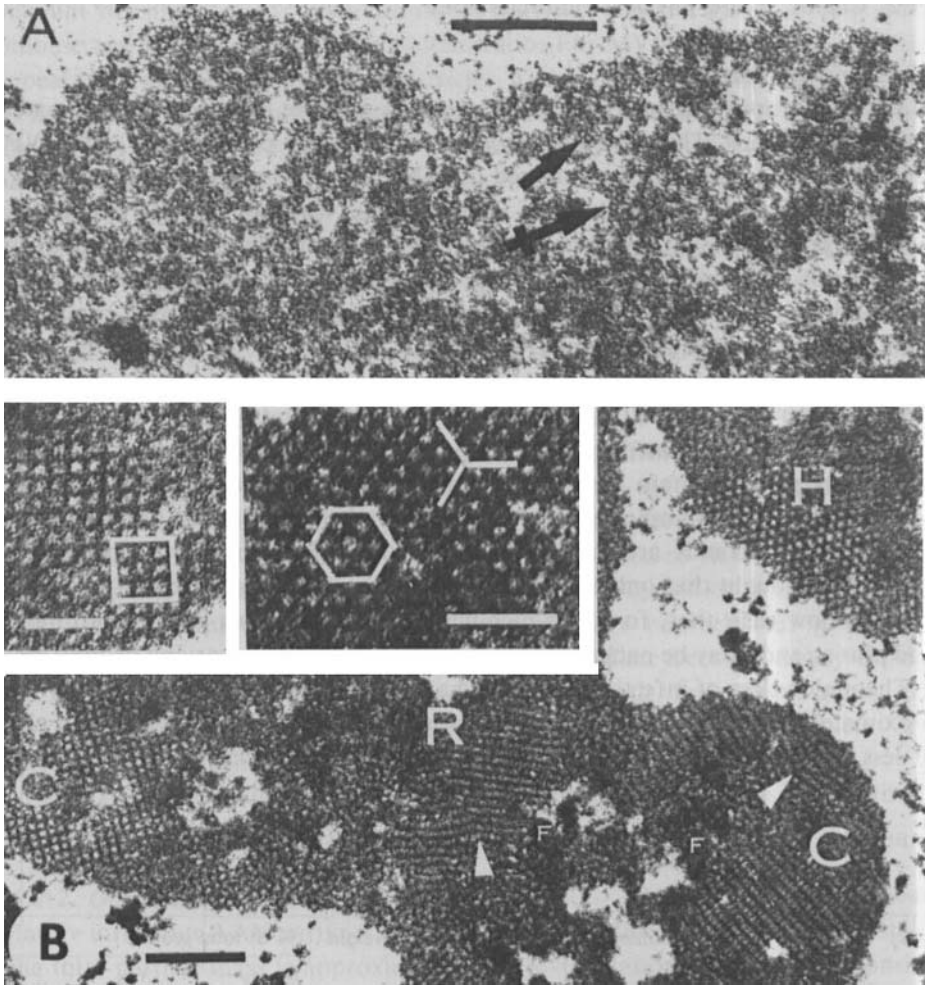

Fig. 19.2. Structure of aggregates and polycrystals of the *ts*1 mutant of H-1 virus grown in SV40-transformed newborn human kidney (NB) cells at the non-permissive temperature of 39.5°C. Ultrathin sections were prepared at 16 h after infection. (Panel A) Dense aggregates of *ts*1 H-1 capsids in the cell nucleus. Various degrees of interparticle clustering are exhibited (arrows). Bar = 0.5 μm. (Panel B) Portion of a single H-1 polycrystalline aggregate with rodlike (R), hexagonal (H) and cuboidal (C) arrays. Dislocations of the lattice planes are apparent (arrow heads) and dense floccules (F) are found adjacent to internal cavities. The H-1 crystals are cubic with a unit cell thought to contain 16 particles (Singer and Rhode, 1977). Bar = 0.2 μm. (Left inset) View approximately perpendicular to a four-fold axis showing tetragonal arrays. Bar = 0.2 μm. (Right inset) Image plane is about normal to a three-fold axis exhibiting hexagonal patterns. White lines at upper right indicate the positions of the three lattice planes which intersect at approximately 120° angles in this view. Bar = 0.1 μm. (Reprinted with permission from Ward and Tattersall, 1978.)

19.2. Chemical and physical characteristics

19.2.1. Genus Parvovirus

Mature infectious parvovirus particles have a particle mass of approximately 5.6×10^6 daltons. The protein moiety consists of three polypeptides, VP1, VP2 and VP3, respectively, as summarized in Table 19.1. Polypeptides VP1 and VP2 are primary translation products of viral mRNAs, whereas VP3 is a maturation cleavage product of VP2. VP1 and VP2 overlap in amino acid sequence, all of the sequence of VP2 being contained within VP1. The VP1-specific region of VP1 is very basic and may be located internally in the capsid, and perhaps is complexed with viral DNA in intact virions (Fig. 19.4).

The genome is a single linear strand with a molecular weight of approximately $1.6–1.8 \times 10^6$. The MVM and H-1 genomes are 5081 and 5176 nucleotides long, respectively, as determined by nucleotide sequencing. The DNA genomes of the parvovirus genus contain both a 3′ and a 5′ terminal palindromic sequence. However, there is no homology between the palindromes at the respective termini and the DNA strands are linear when viewed by electron microscopy. It was previously thought that only strands of minus sense were packaged into particles but it is now clear that, for some members of the parvovirus genus, both minus and plus strands may be packaged into individual particles in varying proportions.

The major class of infectious particles has a buoyant density (ϱ) in CsCl of approximately 1.41 g/cm^3 and a sedimentation coefficient of 110 S. A second class of less infectious particles, also with a sedimentation coefficient of 110 S, has a

TABLE 19.1.

Parvovirus proteins

Virus	Protein	Molecular weight ($\times 10^{-3}$)	% of total protein	
			empty	full
MVM (genus parvovirus)	VP1	83	17	14
	VP2	64	83	15–76
	VP3	61	0	70
AAV2 (genus dependovirus)	VP1	87	8	8
	VP2	73	5	5
	VP3	62	86	86
DNV1 (genus densovirus)	VP1	107	12	13
	VP2	71	29	29
	VP3	61	22	21
	VP4	43	37	37

The proteins for one example of a virus from each genus are listed. The proportion of each individual protein as a percentage of the total protein of empty or full virus particles is also shown.

buoyant density of 1.45. Both classes of particles contain the same size DNA genome and have the same DNA:protein ratio. For MVM, the $\varrho \approx 1.45$ particles appear to be precursors of $\varrho \approx 1.41$ particles. The $\varrho \approx 1.45$ particles usually contain VP2 as their major capsid protein, in addition to VP1, with little VP3. In contrast, the $\varrho \approx 1.41$ particles usually contain VP3 as the predominant polypeptide in addition to VP1 and VP2. The VP2, but not the VP1, molecules present in DNA-containing 'full' virions can be cleaved in vitro by trypsin or cell-conditioned medium to yield a polypeptide comigrating with VP3, apparently mimicking an in vivo maturation step. However, this in vitro cleavage does not appear to change the density of 1.45 particles in CsCl. Empty capsids of this genus contain only VP1 and VP2, and have a buoyant density in CsCl of 1.32 g/cm^3 and a sedimentation coefficient of 70 S. These intact capsids appear to be precursors of full virions. The VP2 of empty capsids cannot be cleaved in vitro, indicating that the introduction of the DNA into the capsid induces a conformational change involving the majority of the VP2 molecules and exposing the maturational cleavage site. Assembly apparently occurs by association of a preformed empty capsid with a DNA genome in an extended or unstable conformation to yield a nucleoprotein complex which sediments between 70 S and 110 S (Fig. 19.3). A heterogeneous density class of mature virions which band in CsCl between 1.35 g/cm^3 and 1.40 g/cm^3 have sedimentation coefficients intermediate between empty capsids and full virions, contain shorter than full genome length viral chromosomes, and are defective for lytic growth without a virion containing the complete viral genome acting as a helper.

No enzymatic activities necessary for infectivity have been consistently found associated with purified particles.

19.2.2. Genus Dependovirus

Mature infectious AAV particles contain, by weight, 26% DNA and 74% protein. The total particle mass is approximately 5.6×10^6 daltons. The protein consists of three polypeptides, VP1, VP2, and VP3, as summarized in Table 19.1.

The genome is a single linear strand having a molecular weight of approximately 1.5×10^6 and for AAV2 the genome is 4675 nucleotides long as determined by nucleotide sequencing. AAV DNA strands viewed by electron microscopy appear as circular single strands held by a small (3% of strand length) panhandle formed by hydrogen bonding between the identical 3′ and 5′ palindrome sequences present as terminal repeats. Strands of plus or minus complementarity are packaged into individual particles. Equal numbers of plus or minus strand DNA-containing particles are generated.

The major class of infectious AAV particles has a buoyant density in CsCl of 1.41 g/cm^3, a sedimentation coefficient of 111 S and a particle/infectivity ratio of 50–100. A second (minor) class of AAV particles (having a 16–200-fold lower particle/infectivity ratio) has a buoyant density in CsCl of 1.45 and a sedimentation

coefficient of 109 S. A precursor-product relationship between these particles has not been established for AAV. Since both classes of particles contain the same size DNA genome, the same relative amounts of VP1, VP2 and VP3 and have the same DNA/protein ratio, they appear to be conformational variants. Empty capsids of AAV contain the same ratio of the three capsid proteins but have a density in CsCl of 1.32 and a sedimentation coefficient of 66 S. An assembly intermediate comprising a capsid and a DNA genome associated in an extended conformation having a CsCl buoyant density of 1.40–1.45 and a sedimentation coefficient of 60 S has been described. Finally, variant or defective-interfering particles comprising a normal capsid but containing a deleted genome have intermediate buoyant densities (1.32–1.41) and sedimentation coefficients of 60–110 S.

19.2.3. Genus Densovirus

DNV1 and DNV2 have particle masses of 5.7×10^6 daltons and comprise a single-stranded, linear DNA genome (1.9×10^6 daltons), a protein capsid (3.55×10^6 daltons) and polyamines (totalling $\approx 80\,000$ daltons). The capsid consists of VP1 ($M_r \approx 100\,000$), VP2 ($M_r \approx 70\,000$), VP3 ($M_r \approx 58\,000$) and VP4 ($M_r \approx 42\,000$). VP1, VP2, VP3 and VP4 represent about 12%, 29%, 22% and 37%, respectively, of the total protein mass. Both empty and full particles contain similar amounts of each of the four polypeptides. Sedimentation coefficients of full and empty particles are 112 S and 60 S, respectively. The viral DNA genome is similar to AAV in that strands of either complementarity are packaged into individual particles in approximately equal numbers and contain the same terminal palindrome sequence at both 3′ and 5′ termini.

19.3. Antigenic properties

Monoclonal antibody studies have revealed that the capsid surface of CPV contains two or more determinants involved in neutralization, each of which comprises several different but overlapping epitopes (Parrish and Carmichael, 1983). There is also evidence for minor determinants on the capsid surface, not involved in neutralization, which cross-react between parvoviruses of different neutralization serotypes. Antibodies raised against SDS-disrupted MVM particles detect buried antigenic determinants common to most parvoviruses.

19.4. Architecture of the virion

Unlike most other animal viruses, parvoviruses appear to have no distinctive internal core structure as determined by electron microscopy or mild disruption methods. All of the protein appears to be present in the capsid. The only known

internal component is the DNA genome, although densonucleosis virus contains sufficient polyamines to titrate about 26% of the charge on the DNA phosphates. It is not known whether parvovirus or dependovirus particles contain polyamines. For the genus parvovirus, as well as dependovirus, all three proteins, VP1, VP2 and VP3, are accessible to external iodination with lactoperoxidase or chloramine-T procedures. For DNV1 and DNV2 the two proteins VP3 and VP4 were not labeled by external iodination but this may simply reflect the absence of accessible tyrosine on the surface.

There is no definitive evidence regarding the precise structure of the protein shell or even the number of capsomers, although the particles appear spherical, and presumably icosahedral, by electron microscopy. The mature viral particles are generally 18–25 nm in diameter but little surface detail is apparent and there are no spikes. Based on the particle mass, each capsid must comprise about 60

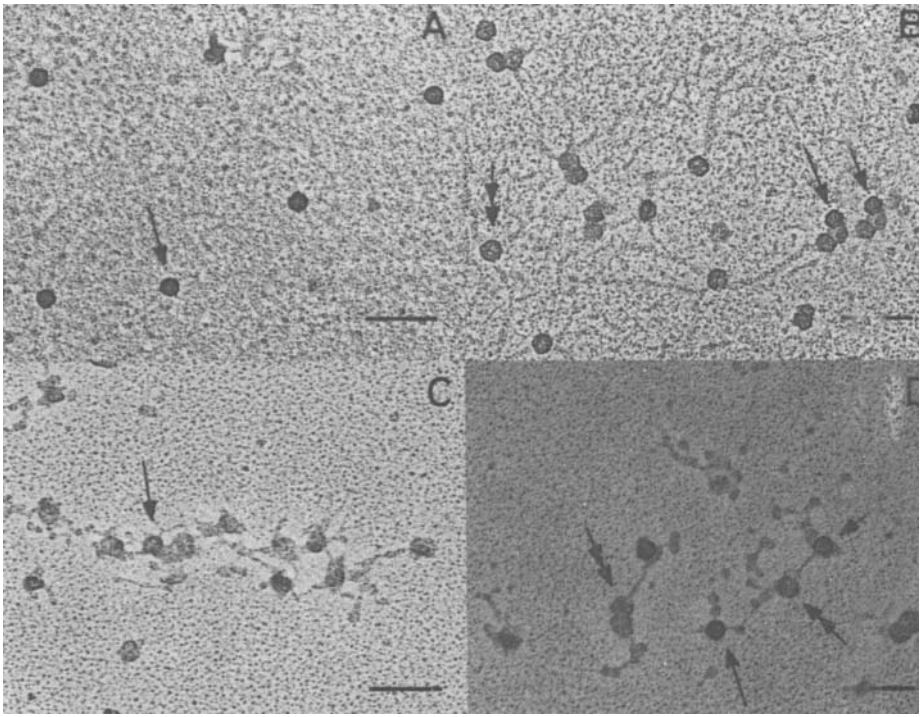

Fig. 19.3. Electron microscopy of nucleoprotein complexes of LuIII virus extracted from lysates of NB cells (15 h after infection) by velocity sedimentation in sucrose gradients. The complexes were prepared for electron microscopy by low-angle rotary shadowing with platinum either in the native state or after fixation with glutaraldehyde. (A) Native 110 S LuIII virions. (B) Native 70 S to 100 S complexes (assembly intermediates). (C and D) 70 S to 100 S complexes after fixation. The arrows indicate mature, compact 110 S virions (←) or ballooned, immature particles (◄—). All bar markers represent 0.1 μm. (Reprinted from Müller and Siegl (1983) with permission.)

polypeptides which is consistent with its being a $T = 1$ icosahedron (Fig. 19.4a). Since VP1 and VP2 each comprise only 7–8% of the total protein mass in mature particles it is unclear how these proteins can be arranged symmetrically within the capsid. Recent evidence indicates that for MVM, H-1 and AAV2 the proteins VP1, VP2 and VP3 differ from one another by the presence of additional amino-terminal sequences and have common carboxy-terminal sequences (Paradiso et al., 1984; Tattersall et al., unpublished data; Janik et al., 1984).

The VP1 components of empty, but not of full (i.e. DNA-containing), H-1 capsids could be irreversibly aggregated by treatment with high-molecular-weight polyethylene glycols into pentameric or hexameric structures. Also, dimethyl-suberimidate cross-linking of empty capsids resulted in heterologous dimers of VP1 and VP2. Paradiso (1983) suggested that VP1 proteins may be clustered in the empty capsids. Alternatively, such VP1 interactions may be internal rather than on the exterior of the capsid. A variety of other evidence indicates that the capsid undergoes a conformational alteration during encapsidation of DNA and maturation of the viral particle (Fig. 19.3).

One model consistent with these observations (Fig. 19.4b) is that the additional amino-terminal region of VP1 may be located internally in the capsid. Thus, the outer surface of the capsid may indeed comprise a symmetrical arrangement of protein sequences. The internal location of the amino termini of VP1 might possibly be important for interaction with viral DNA and particle stability. This possibility is consistent with recent evidence which shows that deletion of the region of the AAV2 genome that specifies the amino terminal sequence of VP1

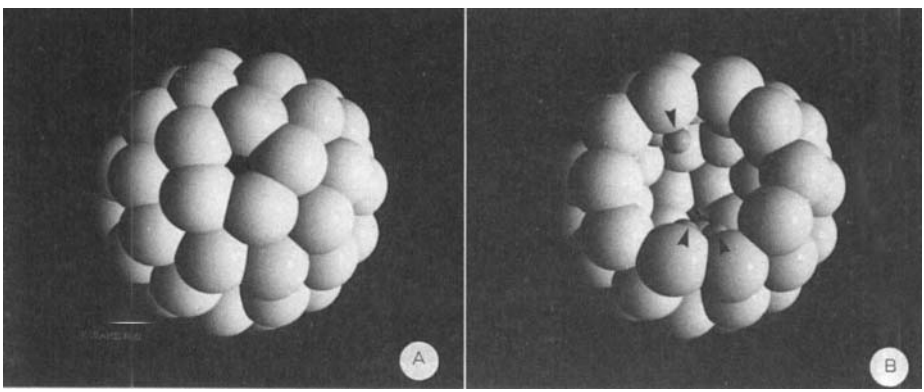

Fig. 19.4. A three-dimensional model of a parvovirus capsid. (A) A complete particle showing icosahedral symmetry and a pentavalent subunit. (B) A view of the same particle with the pentavalent subunit removed to show the interior of the particle. Arrows indicate the possible internal location of the amino-terminal moieties of the VP1 protein (small spheres) as discussed in the text. The DNA genome is not shown, since there is no available information on its orientation in the particle. The schematic model was constructed using computer graphics generated by R.J. Feldmann, NIH.

(Janik et al., 1984) results in viral mutants which replicate DNA and produce abundant amounts of VP3 protein but fail to assemble stable particles (Tratschin et al., 1984; Hermonat et al., 1984).

19.5. Virus–cell interaction

Little is known about the mechanism of uptake of viral particles into the cell. However, there appears to be a saturable number of receptors (between 10^5 and 10^6) on cells for both AAV and MVM. The MVM receptor appears to involve a glycoprotein. Virus particles are assembled in the cell nucleus. The maturation cleavage of VP2 to VP3 in MVM can occur as a late step in infection after assembly of the full virion in the nucleus, or as an early step following the adsorption and penetration of the predominantly VP2-containing virions (i.e. $\varrho \approx 1.45$ particles).

Although widespread in humans and other mammals as well as in avian species, members of the genus dependovirus appear not to be pathogenic. A new serotype of AAV (AAV5) was recently isolated from human penile chondylomatous lesions but has not been definitively associated with any disease (Georg-Fries et al., 1984). All serotypes of AAV appear to be defective and grow only in cells in which certain helper functions are expressed by either an adenovirus or a herpesvirus. The helper functions have not been completely defined. For AAV2 the helper functions provided by adenovirus appear to comprise a subset of adenovirus early gene functions and also the small adenovirus VA_I RNA.

Members of the genus parvovirus are pathogenic to fetal and newborn animals and produce a number of clinical symptoms, including fetal mummification, abortion, panleukopenia, enteritis, central nervous system lesions, osteolytic degeneration and immune-complex diseases. The recently isolated human parvovirus, B19, appears to be the aetiologic agent for aplastic crisis in patients with chronic hemolytic anemia and is apparently also the infectious agent of the pediatric disease erythema infectiosum (Fifth disease). This virus has recently been shown to be most closely related to the autonomously replicating parvoviruses of rodents and thus presumably belongs to the genus parvovirus.

Acknowledgements

We thank Irwin Singer (Merck and Co., New Jersey) and Günter Siegl (Bern) for generously providing electron micrographs, and Richard J. Feldmann (Division of Computer Research and Technology, NIH) for generating the computer graphics in Fig. 19.4.

Suggested reading

Berns, K.I. (Ed.) (1984) The Parvoviruses. Plenum Press, New York.

Cotmore, S.F. and Tattersall, P. (1984) Characterization and molecular cloning of a human parvovirus. Science 226, 1161–1165.

Georg-Fries, B., Biederlack, S., Wolf, J. and Zur Hausen, H. (1984) Analysis of proteins, helper dependence and seroepidemiology of a new human parvovirus. Virology 134, 64–71.

Hermonat, P.L., Labow, M.A., Wright, R., Berns, K.I. and Muzyczka, N. (1984) The genetics of adeno-associated virus: isolation and preliminary characterization of mutants in AAV-2. J. Virol. 51, 329–339.

Janik, J.E., Huston, M.M. and Rose, J.A. (1984) Adeno-associated virus proteins: origin of the capsid components. J. Virol. 52, 591–597.

Muller, D.E. and Siegl, G. (1983) Maturation of parvovirus LuIII in a subcellular system. II. Isolation and characterization of nucleoprotein intermediates. J. Gen. Virol. 64, 1055–1067.

Paradiso, P.R. (1983) Analysis of the protein-protein interactions in the parvovirus H-1 capsid. J. Virol. 46, 94–102.

Paradiso, P.R., Williams, K.R. and Constantino, R.L. (1984) Mapping of the amino terminus of the H-1 parvovirus major capsid protein. J. Virol. 52, 77–81.

Parrish, C.R. and Carmichael, L.E. (1983) Antigenic structure and variation of canine parvovirus type-2, feline panleukopenia virus, and Mink enteritis virus. Virology 129, 401–414.

Tratschin, J.D., Miller, I.L. and Carter, B.J. (1984) Genetic analysis of adeno-associated virus: properties of deletion mutants constructed in vitro and evidence for an adeno-associated virus replication function. J. Virol. 51, 611–619.

Siegl, G., Bates, R.C., Berns, K.I., Carter, B.J., Kelly, D.C., Kurstak, E. and Tattersall, P. (1985) Characteristics and taxonomy of parvoviridae. Intervirology, 23, 61–73.

Siegl, G. (1976) The Parvoviruses. Springer-Verlag, Vienna.

Singer, I.I. and Rhode, S.L. (1977) Ultrastructural studies of H-1 parvovirus replication IV. Crystal development and structure with the temperature sensitive mutant *ts*1. J. Virol. 24, 343–352.

Ward, D.C. and Tattersall, P. (Eds.) (1978) Replication of Mammalian Parvoviruses, Cold Spring Harbor Laboratory. NY.

Nermut/Steven (eds) Animal Virus Structure

CHAPTER 20

Papovaviridae

TIMOTHY S. BAKER[1] and IVAN RAYMENT[2]

[1] *Department of Biological Sciences, Purdue University, West Lafayette, IN 47907, U.S.A. and*
[2] *Department of Biochemistry, University of Arizona, Tucson, AZ 85721, U.S.A.*

Family: Papovaviridae
Genus: Papillomavirus. Species: rabbit (Shope) papilloma virus; also cow, deer, dog, goat, hamster, human and sheep papilloma virus
Genus: Polyomavirus. Species: polyoma virus (mouse); also BKV and JCV (human), HD (stump-tailed macaque), K (mouse), RKV (rabbit) and SV40 (monkey)
The prefix 'papova' derives from pa(pilloma), po(lyoma) and va(cuolating agent), the original name for Simian Virus 40.

20.1. General characteristics

Papovaviruses are non-enveloped isometric particles ranging in size from ≈45 nm (polyomaviruses) to 55 nm diameter (papillomaviruses). They have a protein shell (capsid) composed of 72 capsomers in a skew icosahedral arrangement which encapsulates a 'minichromosome' composed of a single molecule of closed circular double-stranded DNA associated with cellular histones: there are no lipids present. Non-infectious polymorphic forms, including empty capsids, small isometric particles and hollow cylindrical aggregates of capsomers, are usually present in virus preparations. Their role in viral replication is unclear; they may be assembly intermediates, although they most likely represent either byproducts of abortive assembly pathways or artifacts of isolation procedures.

Papovaviruses replicate and assemble in the nuclei of infected cells, are resistant

to treatment with acid, heat or ether, and most species are potentially oncogenic. Papillomaviruses cause tumors in natural hosts, whereas polyomaviruses cause tumors in species different from the species of origin. Of all transforming viruses known, polyomaviruses contain the smallest amount of genetic information. Several species haemagglutinate by reacting with neuraminidase-sensitive receptors.

Polyoma and SV40 are the most extensively characterized papovaviruses, in part due to the absence of a reproducible cell culture system permissive for replication of the papillomaviruses. Polyoma virus is described in detail, since it is the first animal virus whose capsid structure was solved at low-resolution by X-ray crystallography. Its structure is of particular interest because the arrangement of subunits in the polyoma capsid violates a fundamental prediction of the widely accepted dogma concerning the construction of icosahedral virus shells (Caspar and Klug, 1962).

The papovaviruses show remarkable similarities in their structural and genetic organization, so that polyoma virus can be considered to be representative of the entire class. Fig. 20.1 illustrates the distinctive surface morphologies of polyoma and SV40 viruses revealed by electron microscopy.

20.2. Polyoma virus (Py): physical and chemical characteristics

Mature virions are isometric particles (Fig. 20.1) with a diameter of 49.5 nm (interparticle distance in crystals) and a mass of about 25×10^6 daltons. They sediment at 250 S and have a buoyant density of 1.34 g/cm^3 in CsCl. Each particle contains a nucleohistone complex contained within a shelf of protein subunits (the capsid). Table 20.1 compares several chemical and physical properties of Py, SV40 and the papilloma viruses.

The genome consists of a single molecule of closed circular double-stranded DNA (M_r 3.5×10^6; 5292 basepairs; 47.3% GC content). Isolated DNA contains approx. 25 right-handed superhelical turns, is infectious, and codes for three structural (VP1, VP2, VP3) and three nonstructural proteins (small, middle and large T antigens). In the virion, the genome is associated with an approximately equal mass of cellular histones (H2A, H2B, H3 and H4) forming a 'minichromosome' with $\approx$25 nucleosomes (Fig. 20.2). During the lytic cycle the 'minichromosomes' are used as templates for DNA replication or for the transcription of 'early' and 'late' genes.

20.3. Architecture of the virion

Icosahedral capsid

The structure of the virus capsid has been extensively studied by electron microscopy (Finch and Crawford, 1975; and Fig. 20.1) and by X-ray crystallography

TABLE 20.1.

Chemical and physical properties of Papovaviruses

	Py	SV40	Papilloma
Diameter (nm)	45 (EM) 49.5 (XR)	45 (EM)	50–55 (EM)
Symmetry	Icosahedral	Icosahedral	Icosahedral
Triangulation number	7d	7d	7d (human) 7 I (rabbit)
Number of capsomers	72	72	72
Number of VP1 molecules	360	360 (?)	360 (?)
Number of VP2 and VP3 molecules	≈60	≈60	>60[a]
Virion mass (daltons)	24.6×10^6	27×10^6	40×10^6
Sedimentation coefficient (S)			
virion	240	240	296–300
capsid	180	180	168–172
Density in CsCl (g/cm³)			
virion	1.34	1.34	1.34
capsid	1.29	1.29	1.29
Protein composition (M_r)			
VP1 (structural viral proteins)	42404	40168	57000 (human)
VP2	34761	38351	(≈10 minor proteins)
VP3	22866	26965	
H3 (cellular histones)	15300	15300	15300
H2A	14000	14000	14000
H2B	13800	13800	13800
H4	11300	11300	11300
DNA molecular weight	3.5×10^6	3.5×10^6	$4.5\text{–}5.5 \times 10^6$
Number of basepairs	5292 (A2)	5243	≈7500
% GC	47.3	40.7	41–50
DNA content (%w/w)	14	13	12.5
Number of superhelical twists	20–30	22–26	?
Non-structural viral proteins			
Large T antigen	87991	81632	?
Middle T antigen	49710	not found	?
Small T antigen	22785	20451	?

Abbreviations: EM, electron microscopy; XR, X-ray diffraction; GC, guanine-cytosine content; CsCl, cesium chloride; VP, viral protein; A2, large plaque, A2 strain.

The molecular weights for Py and SV40 viral proteins are calculated from the DNA sequences.

Data compiled from the suggested reading list.

[a] Including other minor proteins.

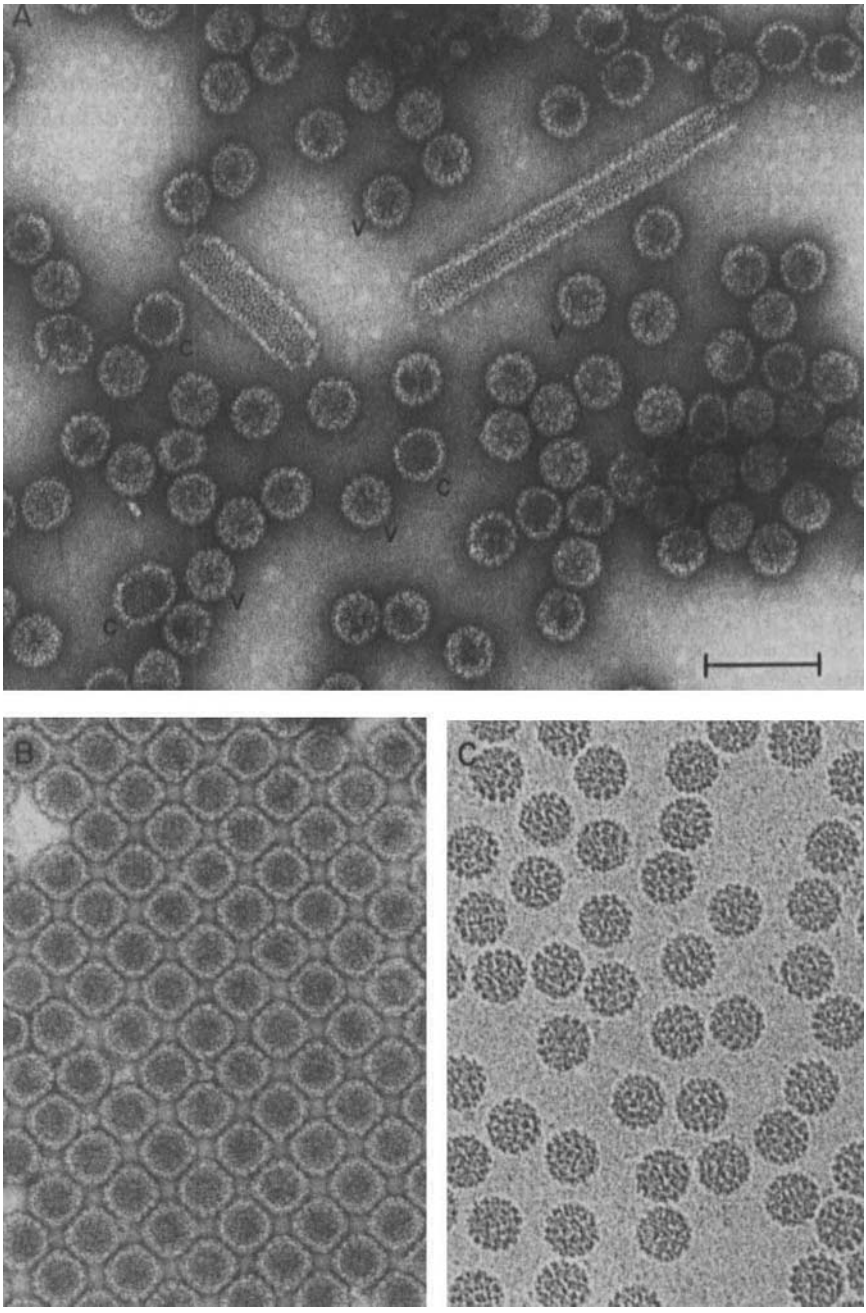

Fig. 20.1. (A) Negatively stained Py virions (V), capsids (C) and wide tubes. (B) Negatively stained SV40 array prepared by the method of Horne and Pasquali-Ronchetti (1974). (C) SV40 suspended in vitreous ice ($\approx -170°C$) over a hole in the carbon substrate. The unstained virus appears black because it is denser than ice. All images are at the same magnification (scale marker in (A) = 0.1 μm). (B) and (C), which illustrate the morphological comparison between SV40 and Py, were obtained as part of a collaborative study (Baker, Drak and Bina (1985) Biophys. J. 47, 50a).

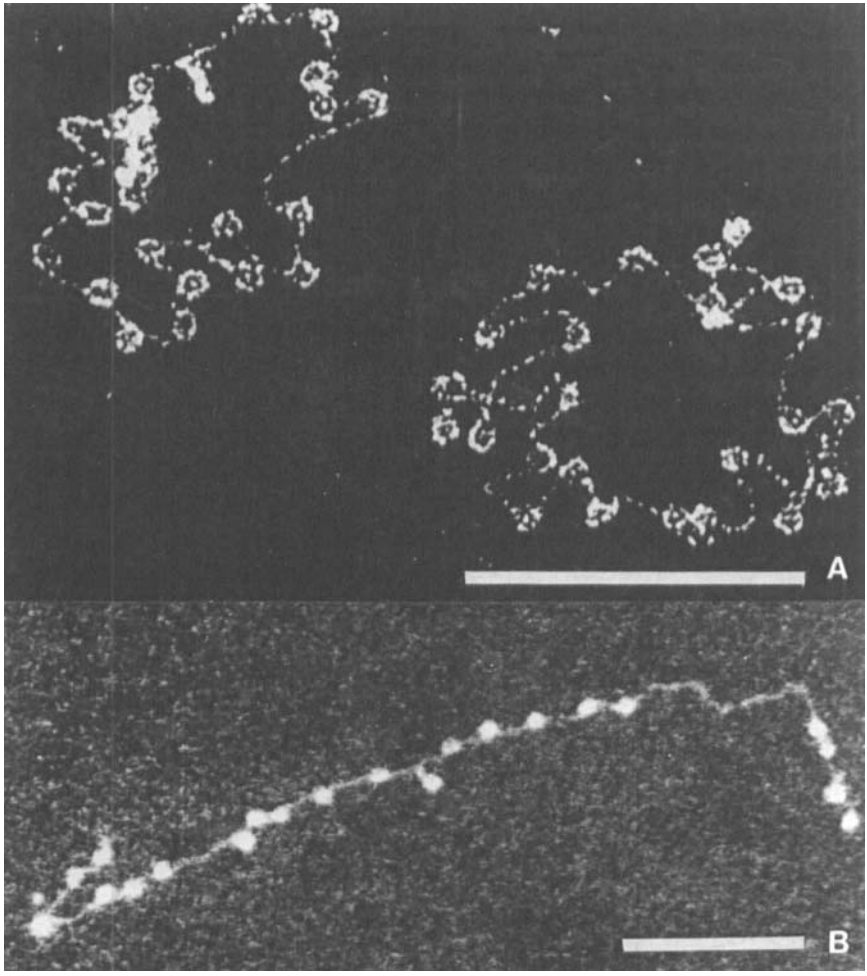

Fig. 20.2. (A) Dark-field electron micrograph of SV40 'minichromosomes' displaying the organization of nucleosomes on the circular, double stranded DNA molecule (reproduced by permission of S. Saragosti, G. Moyne and M. Yaniv). Bar = 100 nm. (B) Dark-field, scanning transmission electron micrograph of an unstained, freeze-dried SV40 'minichromosome' which has opened and spread out on the grid, displaying the characteristic 'beads-on-a-string' appearance of the nucleosomes on the DNA (kindly provided by J. Wall, J. Wooley and A. Varshavsky). Bar = 100 nm.

(Rayment et al., 1982). The capsid is composed of 72 morphological units (capsomers) arranged on the vertices of a $T = 7$d (right-handed) icosahedral surface lattice. There are 12 pentavalent capsomers (each adjacent to five hexavalent capsomers) located at the twelve icosahedral vertices, and 60 hexavalent capsomers (each adjacent to one pentavalent and five hexavalent neighboring capsomers) located in groups of three on each of the 20 icosahedral faces (Fig. 20.3).

Figs. 20.4 and 5 summarize the X-ray crystallographic studies of the empty capsid structure. All 72 capsomers are pentamers of VP1. This arrangement of subunits violates the theory of quasi-equivalence set forward by Caspar and Klug (1962) to explain how a virus shell could be constructed from a large number of identical subunits in such a way as to conserve subunit–subunit interactions. This theory predicts that a $T = 7$ capsid should contain 420 ($= 7 \times 60$) structural subunits in 72 capsomers, of which 12 are pentamers and 60 are hexamers.

There are six subunits (seven were predicted) in each icosahedral asymmetric unit, five from the hexavalent and one from the pentavalent pentamer, and they each occupy a symmetrically distinct environment. These six units can be put into three different classes according to their bonding relations inferred from the electron-density map (schematically illustrated in Fig. 20.5e,f).

The electron-density map may be divided into two regions: the protruding pentagonal caps (Fig. 20.5a,b) and the basal parts connecting capsomers (Fig. 20.5c,d). The contacts between capsomers extend inward from $\approx$21 nm radius of the capsid. The protruding caps are $\approx$8.5 nm in diameter and extend out $\approx$4 nm. The central hole in each capsomer has a diameter of 4 nm at a radius of 21 nm and tapers shut 1.5 nm from the surface, leaving a dimple on the top of the cap. The basal parts of the capsomers extend inwards $\approx$4 nm. The map suggests a two-

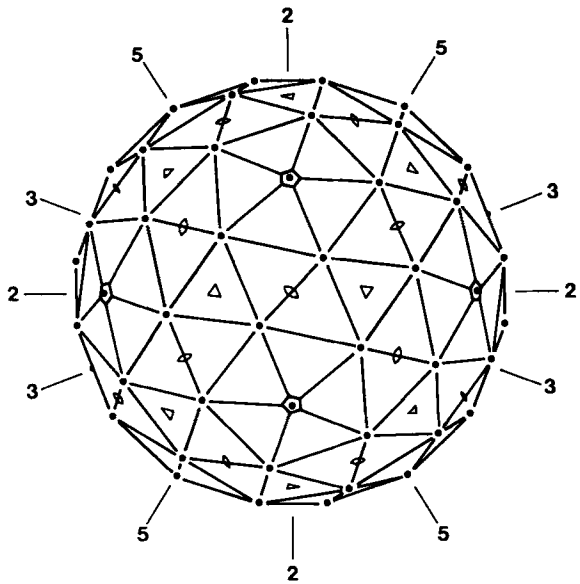

Fig. 20.3. $T = 7$d icosahedral surface lattice with five-, three- and two-fold axes marked ⬠, △ and ⬭ respectively. The drawing shows one side of the polyhedral surface, which consists of 60 six-coordinated and 12 five-coordinated lattice points at the same radius. The location of the six-coordinated point is that determined for the hexavalent morphological unit in the polyoma capsid.

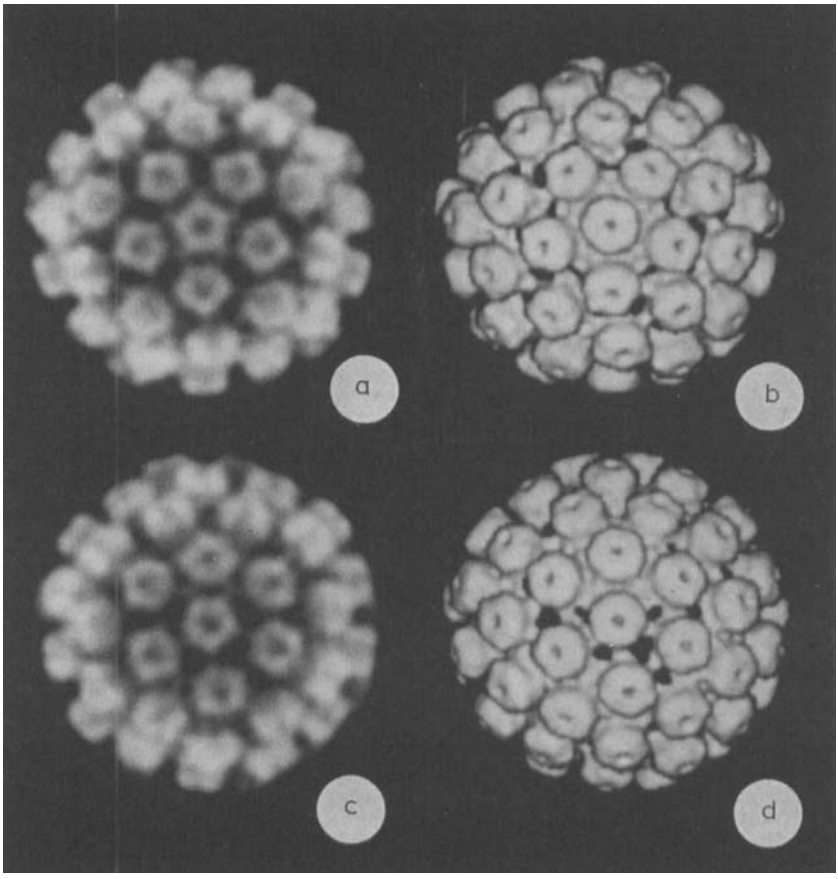

Fig. 20.4. Views of half the capsid down the five-fold symmetry axis (a,b) and down the axis of the hexavalent unit (c,d). (a) and (c) are projections of the electron-density map at 2.25 nm resolution and (b) and (d) are computer graphics representations of the surface at a contour level, which includes density in the basal parts of the structure where capsomers contact.

domain model for the subunit structure, with one domain contributing to the protruding part of the morphological unit while the other participates in the interactions at lower radii in the shell. It also suggests that the interactions in the protruding part of the capsomer are conserved in both hexavalent and pentavalent units.

VP1, the major coat protein, constitutes about 80% of the virus protein. The protruding morphological units must be composed entirely of VP1, since purified capsid preparations containing only VP1 have been isolated and the surface morphology of the capsid is the same as that observed in complete virions. The role of the minor proteins VP2 and VP3 in the structure of the mature virion is unclear.

Crystallographic analysis of virions shows the same surface features as observed in the empty capsid but does not reveal details of the nucleohistone complex structure, since the analysis imposes icosahedral symmetry on the entire virus particle and the core may not be organized with this symmetry.

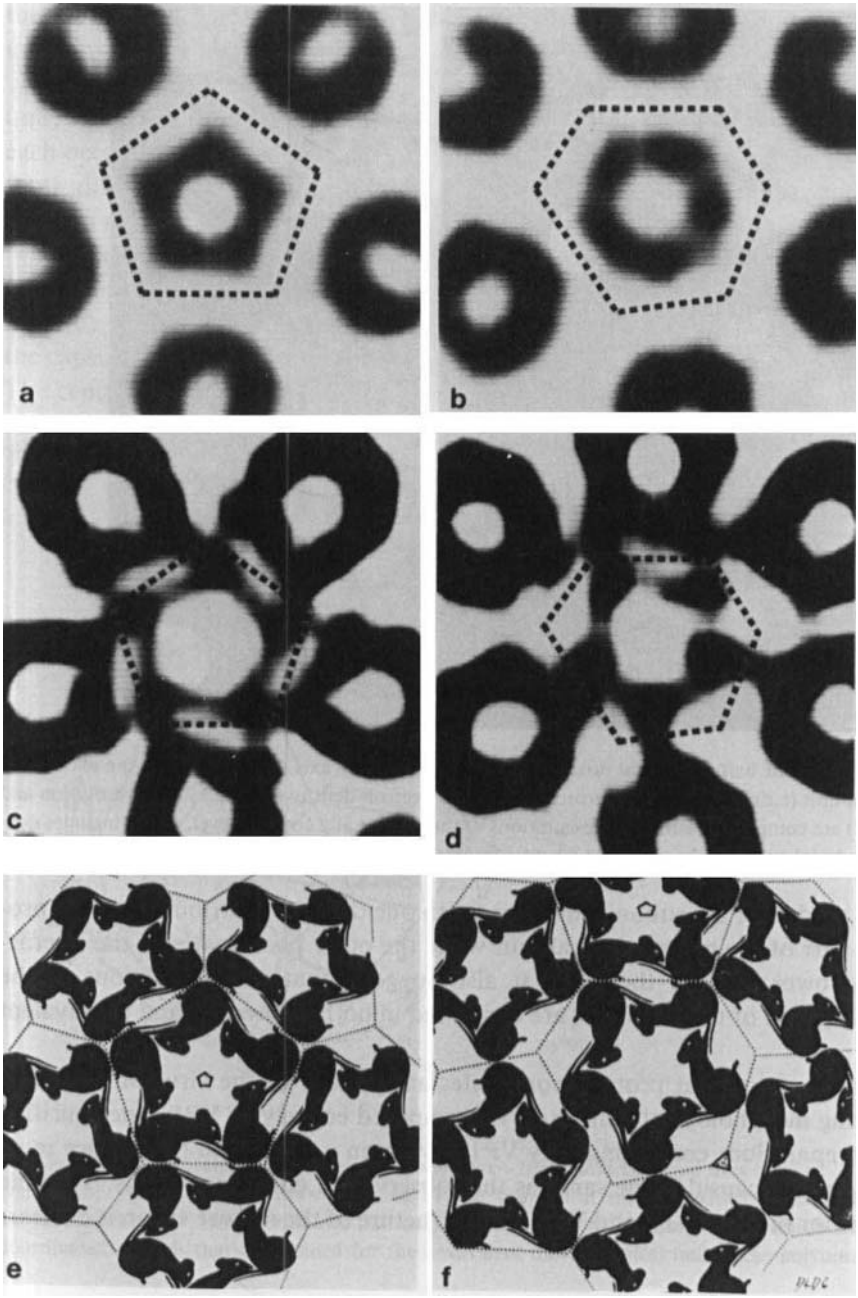

The tubular forms of Py (and Shope papilloma and human wart) have been studied by electron microscopy and image analysis. Two general classes of tubes are observed: narrow (≈ 30 nm diameter) built of pentamers and wide (≈ 45–50 nm) originally thought to contain hexameric morphological units. A reexamination of the wide tubes using minimal-irradiation electron microscopy and image analysis (Baker et al., 1983; and Fig. 20.6) revealed that all tubes are assemblies of paired capsomers with a simple relationship between the packing arrangements of pentamers in the different tubes.

Gentle dissociation of the virions and capsids with EGTA ([ethylenebis(oxyethylenenitrile)]tetraacetic acid) or DTT (dithiothreitol) produces isolated morphological units. There is no evidence for monomers or hexamers of VP1 in solution, implying that the pentamer may represent a stable functional form of VP1.

Nucleoprotein complex

The DNA/protein complex in Py and SV40 – also called a minichromosome – contains a duplex DNA molecule (M_r 3.5×10^6) associated with about 25 octameric aggregates of cellular histones (two copies each of H3, H4, H2A and H2B). The primary repeating unit of both viral and cellular chromatin is the nucleosome, which contains a fairly well-defined length of DNA (≈ 200 basepairs) associated with the histone octamer (Kornberg, 1977). Viral chromatin lacks histone H1, which presumably helps form more compact, higher-ordered states of cellular chromatin (Thoma et al., 1979).

A well-characterized nucleosome core particle, produced by limited digestion of cellular chromatin with micrococcal nuclease, has been studied extensively by electron microscopy and X-ray and neutron diffraction techniques (e.g. Richmond et al., 1984). The nucleosome core particle (M_r 206 000) contains 146 (± 2) basepairs of duplex DNA and the histone octamer (M_r 110 000), and is a flat, somewhat wedge-shaped cylinder (5.7 nm high and 11 nm in diameter) with a bipartite character and a two-fold axis of symmetry. The DNA is wound around the outside

Fig. 20.5. Sections of the electron-density map showing substructure of the capsomers (a–d) and drawings on a polyhedral surface (e,f) illustrating an inferred packing relationship of structure units. Left column: views down the five-fold axis through a pentavalent capsomer (same orientation as Fig. 20.4a,b). Right column: views through a hexavalent capsomer (same orientation as Fig. 20.4c,d). Panels (a) and (b) are sections 21.5 nm above the center of the capsid at a level where there is little contact between neighboring capsomers. Panels (c) and (d) are 19.5 nm above the center. At this level and below, the five subunits of each capsomer splay out and contact the basal parts of the neighboring subunits. The section planes are perpendicular to the axis of the central capsomer and slice through the neighboring capsomers obliquely. The polygons delineating the domain of the central capsomer are marked by dotted lines in a–d. In (e) and (f), the drawings illustrate that the interactions between subunits (mice) are not conserved.

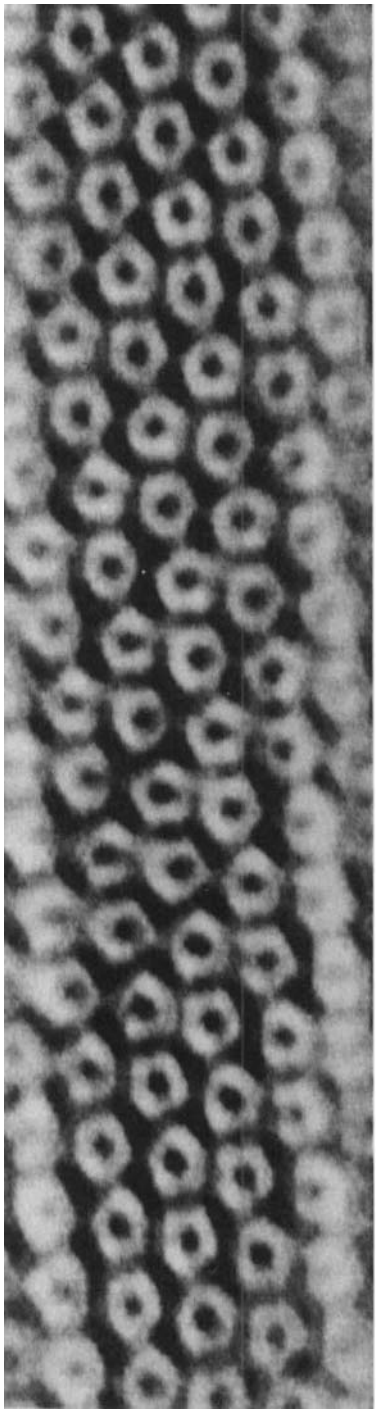

a

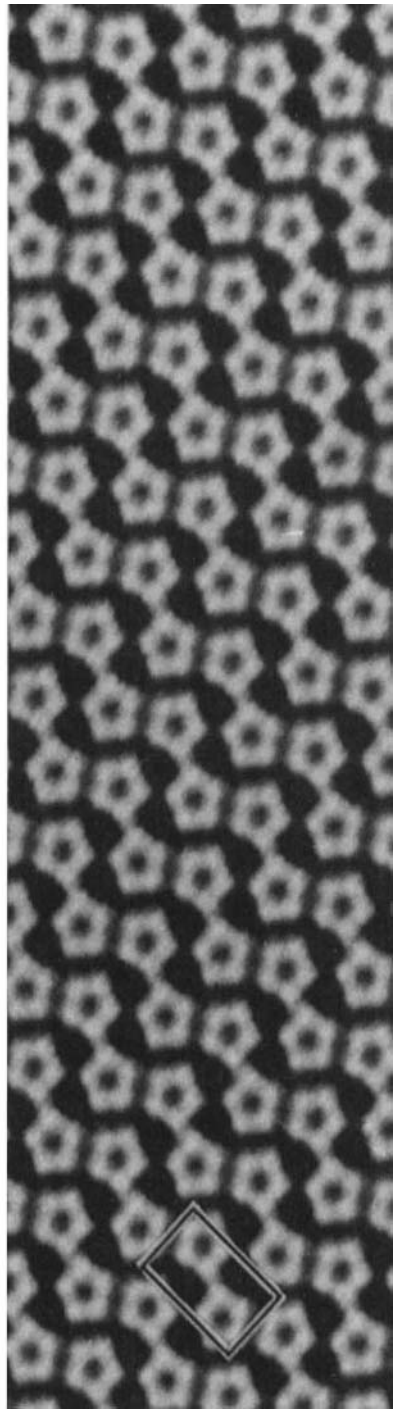

b

of the histone octamer in 1.8 turns of a flat superhelix with a pitch of 2.8 nm. The histone octamer, either associated with DNA in nucleosome core particles (Richmond et al., 1984) or in tubular aggregates free of DNA (Klug et al., 1980), is wedge-shaped with a roughly circular outline ($\approx$7 nm diameter) at its broadest aspect and, at right angles to this, is $\approx$5.6 nm at its thickest point.

The specific organization of the minichromosome inside the virus is not known, although it must be in a condensed state, since it is confined to an approximately spherical space of diameter 30–32 nm defined by the capsid. It is not known whether the viral chromatin adopts a higher-order structure such as the solenoid of cellular chromatin (Finch and Klug, 1976), nor is it known what specific interactions between the nucleohistone and viral proteins (VP1, VP2 and VP3) are important for assembling stable, infectious particles. A hypothetical model for the structure of the nucleohistone core of SV40 virus was proposed (Martin, 1977) in which 21 nucleosomes could be packed, with little or no perturbation of their structure, inside the capsid. In the model, a single nucleosome at the center of the virus is surrounded by 20 others, each beneath one of the 20 faces of the icosahedral protein shell.

20.4. Antigenic properties

Py and SV40 each occur in a single antigenic type immunologically unrelated to each other. There is a certain level of cross-reactivity between Py and SV40 VP1 (slightly less with BKV and JCV). T (tumor) antigens (see following section) do not cross-react with capsid protein. The T antigens of BKV, JCV and SV40 unexpectedly all cross-react, with the cross-reaction generally much stronger than that detected between their V antigens (Tooze, 1981).

20.5. Biological properties

Lytic infection of permissive cells

The infection cycle of Py is initiated by adsorption and pinocytosis of virions into permissive cells such as mouse embryo or kidney. Virions lose capsid protein and the DNA may associate with host proteins and enter the nucleus. The limited DNA coding potential means that the cell supplies the enzymes and factors required for

---

Fig. 20.6. (a) Computer-filtered image of the front layer of a flattened wide tube similar to the tube at the left in Fig. 20.1A. (b) Computed model of a single layer of regular pentamers arranged with the same lattice parameters observed in (a). One choice of unit cell is boxed.

viral replication, transcription and translation. Infection alters normal cellular functions: resting cells reenter the cell cycle and the entire complement of host DNA is replicated and cellular protein synthesis is enhanced.

Early expression of the viral genome leads to production of non-structural viral proteins (T antigens). The large T antigen is required for induction of host-cell functions and initiation of viral DNA replication; the expression of late genes results in the appearance primarily of the structural proteins (VP1, VP2, VP3). All of the viral mRNAs are products of splicing. The VP1 amino-terminal region is encoded by the same DNA that codes for the carboxyl ends of VP2 and VP3. The different amino acid sequences between VP1 and VP2/VP3 in these overlapping regions result from translation of the mRNAs in different reading frames. The coding regions of VP2 and VP3 overlap and are translated in the same reading frame; VP3 is identical to the carboxy-terminal half of VP2. The three Py T antigens all share identical amino-terminal sequences.

The relationship between the early and late phases of viral replication are still unclear. However, it appears that the middle T antigen which functions as an ATPase is indirectly necessary to enhance the phosphorylation of VP1. This modification is required for assembly, since mutants which are defective in the large T antigen still synthesize appropriate levels of the viral DNA and viral coat proteins but do not produce normal levels of mature virion (Garcea and Benjamin, 1983).

The pathway for assembly of mature virions has been studied in detail for SV40 and is similar for Py. Viral proteins are synthesized in the cytoplasm and then transported through the nuclear membrane into the nucleus, where assembly occurs. A 75 S nucleoprotein complex, consisting of a single molecule of the closed circular viral DNA with cellular histones and a small amount of capsid proteins, is the first assembly intermediate observed. VP1 and VP3 are added to this nucleoprotein complex to form a 200 S previrion intermediate. Further addition of VP1, VP2 and VP3 leads to a 250 S intermediate which is unstable in high salt. The final steps involved in the maturation of the 250 S particle are unknown but may include the formation of intersubunit disulfide cross-links.

Virions remain in the nucleus or move to the cytoplasm after rupture of the nuclear membrane and accumulate in cytoplasmic vacuoles awaiting cell lysis for release.

Non-lytic infection and transformation of non-permissive cells

Py is widespread in mouse populations both in the wild and in laboratories. The virus is normally transmitted through animal excretions or secretions. It has a broader range of oncogenicity than SV40, transforming not only mouse cells but also cultured cells of rat, rabbit, guinea pig, dog, cow, monkey and man. Innoculation into animals results, after a latent period of several months, in tumors in virtually all organs and tissues except the brain.

Viral DNA integrates into cellular DNA, generally at several sites ($\approx$ 1–10 genome equivalents/diploid quantity of cellular DNA), with no specificity for the site of integration and no preferred site at which the circular viral genome is opened to promote integration. The entire viral genome is not required for integration or transformation. Cells often contain both integrated and non-integrated viral genomes. Integration does not appear to be a requirement for transformation: expression of the viral genome is.

20.6. Other Papovaviruses

Py and SV40 are morphologically indistinguishable (Fig. 20.1) and share marked similarities in most other physical, chemical, genetic and biological properties. Nevertheless, there are distinct differences between the two viruses. The DNA sequences differ except for remarkable conservation at the viral origin of DNA replication (including BKV). SV40, BKV and JCV lack the middle T antigen. SV40 grows well only in primary cells of African green monkey kidneys, certain other monkey cells and cell lines derived therefrom. It does not grow well in its persistently infected host (rhesus monkey kidney cells). The human viruses, BK and JC, have the most limited host range of the polyomaviruses. JC was the first human virus which could be shown to induce a tumor in a primate.

Papillomaviruses cause benign skin tumors (warts) in a variety of mammalian species which serve as natural hosts. In rabbits the tumors regularly become malignant if they persist for a sufficiently long time; occasionally separate warts regress spontaneously, suggesting an immunological mechanism. The structure of papillomaviruses has been extensively studied by electron microscopy. At the limits of resolution of the technique, these viruses appear to have a morphology similar to that of the smaller polyomaviruses. Recent evidence suggests that SV40 has a 72-pentamer capsid structure similar to Py (Baker et al., 1985). Thus the capsid structure of all papovaviruses, including other members of the polyoma and papilloma genera, may be a highly conserved phenotype.

Acknowledgements

This chapter is dedicated to D.L.D. Caspar and W.T. Murakami for years of encouragement and support. We thank M. Bina for valuable suggestions, P. Flicker and P.N.T. Unwin for expert assistance in the photography of frozen-hydrated SV40 samples, W. Boyle, J. Black and N. Olson for photography and M. Radermacher for programs. This manuscript was funded in part by NIH grant GM33050 to T.S.B. Fig. 20.2B was imaged with the Brookhaven STEM with funds from NIH Biotechnology Resource Grant RR 01777.

Suggested reading

Baker, T.S., Caspar, D.L.D. and Murakami, W.T. (1983) Polyoma virus 'hexamer' tubes consist of paired pentamers. Nature 303, 446–448.

Baker, T.S., Drak, J. and Bina, M. (1985) Cryo-electron microscopy and image analysis of SV40. Proc. 43rd Annu. Meet. Electron Microsc. Soc. Am. 43, 316–317.

Caspar, D.L.D. and Klug, A. (1962) Physical principles in the construction of regular viruses. Cold Spring Harb. Symp. Quant. Biol. 27, 1–24.

Finch, J.T. and Klug, A. (1976) Solenoidal model for superstructure in chromatin. Proc. Natl. Acad. Sci. USA 73, 1897–1901.

Finch, J.T. and Crawford, L.V. (1975) Structure of small DNA-containing animal viruses. In Comprehensive Virology, Eds. H. Fraenkel-Conrat and R.R. Wagner; Vol. 5, pp. 119–154. Plenum Press, New York.

Garcea, R.C. and Benjamin, T.C. (1983) Host range transforming gene of polyoma virus plays a role in virus assembly. Proc. Natl. Acad. Sci. USA 80, 3613–3617.

Horne, R.W. and Pasquali-Ronchetti, I. (1974) A negative staining–carbon film technique for studying viruses in the electron microscope. I. Preparative procedures for examining icosahedral and filamentous viruses. J. Ultrastruct. Res. 47, 361–383.

Klug, A., Rhodes, D., Smith, J., Finch, J.T. and Thomas, J.O. (1980) A low resolution structure for the histone core of the nucleosome. Nature 287, 509–516.

Kornberg, A. (1977) Structure of chromatin. Annu. Rev. Biochem. 46, 931–954.

Lancaster, W.D. and Olson, C. (1982) Animal papillomaviruses. Microbiol. Rev. 46, 191–207.

Martin, R.G. (1977) On the nucleoprotein core of simian virus 40. Virology 83, 433–437.

Perbal, B.V., Linke, H.K. and Fareed, G.C. (1983) Polyomaviruses. In Molecular Biology of Polyomaviruses and Herpesviruses, pp. 1–59. Wiley-Interscience, New York.

Richmond, T.J., Finch, J.T., Rushton, B., Rhodes, D. and Klug, A. (1984) Structure of the nucleosome core particle at 7 Å resolution. Nature 311, 532–537.

Rayment, I. (1984) Animal Virus Structure. In Biological Macromolecules and Assemblies, Eds. F.A. Jurnak and A. McPherson; Virus Structures, Vol. 1, pp. 255–298. Wiley-Interscience, New York.

Rayment, I., Baker, T.S., Caspar, D.L.D. and Murakami, W.T. (1982) Polyoma virus capsid structure at 22.5 Å resolution. Nature 295, 110–115.

Thoma, F., Koller, Th. and Klug, A. (1979) Involvement of histone H1 in the organization of the nucleosome and of the salt-dependent superstructures of chromatin. J. Cell Biol. 83, 403–427.

Tooze, J. (1981) DNA Tumor Viruses, Molecular Biology of Tumor Viruses, 2nd Edn., Part 2/Revised. Cold Spring Harbor Laboratory, NY.

Nermut/Steven (eds) Animal Virus Structure

CHAPTER 21

Baculoviridae

D.C. KELLY

Institute of Virology, Mansfield Road, Oxford OX1 3SR, U.K.

Family: Baculoviridae
Genera: three subgroups recognized: A, nuclear polyhedrosis viruses; B, granulosis viruses; C, non-occluded baculoviruses
Species: *Autographa californica* nuclear polyhedrosis virus, *Trichoplusia* ni granulosis virus, *Oryctes rhinoceros* non-occluded baculovirus

21.1. General characteristics

Baculoviruses are complex viruses which cause diseases in invertebrates, notably insects. The virus particles are enveloped rod-shaped entities. The envelope surrounds a nucleocapsid containing a deoxyribonucleoprotein complex. In the case of nuclear polyhedrosis virus (NPV) or granulosis virus (GV) the virus particles may be 'occluded' within a large proteinaceous crystal. The packaging of virus particles within this crystal is characteristic for the subgroups. NPVs typically contain many virus particles within a crystal, whereas GVs contain one virus particle, rarely more, per crystal. Non-occluded baculoviruses (NOBVs) characteristically are never packaged in such crystals.

NPVs are classified into two types depending on the envelopment of nucleocapsids within an envelope of the occluded form of the virus. Some virus particles contain many nucleocapsids within an envelope and are designated multiple NPVs (hence MNPV), whereas others contain a single nucleocapsid (hence SNPV). This appears to be a genetically determined trait. GV and NOBV virus particles very rarely contain more than one nucleocapsid per envelope.

Baculoviruses replicate in the cell nucleus, undergoing a morphologically complicated cycle resulting in two forms of virus particles, one acquiring an envelope 'de novo' within the nucleus and the other acquiring an envelope at the plasma membrane. The two forms of the virus are quite different biochemically and serologically, and reflect their different functions in the pathogenesis of baculovirus disease. The occluded form of the virus, the form packaged into crystals in the nucleus, is destined to infect another animal, whereas plasma membrane-released virus infects additional cells within that organism. The enveloped virus particles of NOBVs are infectious in both circumstances.

21.2. Chemical and physical characteristics

Baculovirus particles contain 13% DNA, 87% protein plus carbohydrate, lipid and polyamines in amounts which have not been accurately determined. The nucleocapsids comprise just DNA (36%) and protein (64%). The total mass of virus particle containing a single nucleocapsid is approximately 460×10 Da[6] and that of the nucleocapsid approximately 240×10^6 Da. The polyhedron or granule, i.e. the complete virus of NPV or GV, comprises about 95% protein plus the virus particle components and the carbohydrates contained by the outer layer of mature polyhedra.

The genome is a single covalently closed double-stranded DNA molecule of molecular weight $70–110 \times 10^6$, most commonly about 80×10^6. Occasionally concatenated molecules are observed. The intact molecule has a low superhelical density in physiological conditions. The molecule is about 40 μm long.

The buoyant density of occlusion bodies is about 1.21 g/cm^3, virus particles 1.32 g/cm^3, and nucleocapsids 1.40 g/cm^3, in CsCl.

The sedimentation coefficient of virus particles is 1200–1600 S.

21.3. Structural characteristics

The most conspicuous characteristic of NPVs and GVs is the massive size of the occlusion body. Polyhedra are 1–4 μm in size and are cubic or quasispherical in shape, although the atypical *Tipula paludosa* is crescent-shaped. A polyhedron may contain as many as 100 virus particles. Granules are smaller, ovocylindrical in shape, some 0.3–0.5 μm in length and 0.1–0.4 μm in width, although cuboidal granules have been described. Granules typically contain a single virus particle. The structure of granules and polyhedra in fine detail is similar.

The surface of polyhedra may appear 'pitted' or 'smooth' (Fig. 21.1). The smooth polyhedra are mature and possess a distinct outer layer – the polyhedron envelope which is not a conventional lipid bilayer but a layer of ill-defined carbo-

hydrate. The pitted polyhedra lack this structure and the pits represent holes in which virus particles were once placed. Granules always appear smooth and most granules possess an outer 'envelope' similar to that of polyhedra.

The virus particles are rod-shaped due to the cylindrical nucleocapsids within and are about 350 nm long. The width is variable, ranging from about 50 nm for virus particles containing 1 nucleocapsid to 150 nm for virus particles containing 3 nucleocapsids. NOBVs appear more compact, with dimensions of 100 × 220 nm, and may have an irregular shape. Nucleocapsids are rod-shaped, and appear flexible within virus particles, and do not represent rigid structures. They are about 350–400 nm long; isolated nucleocapsids frequently appear longer than the virus

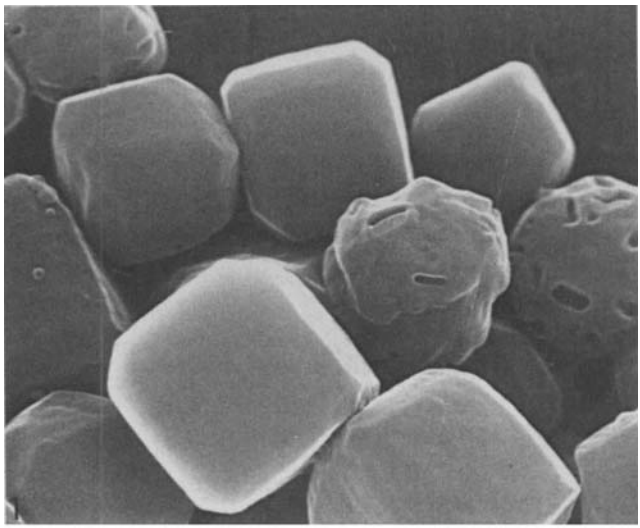

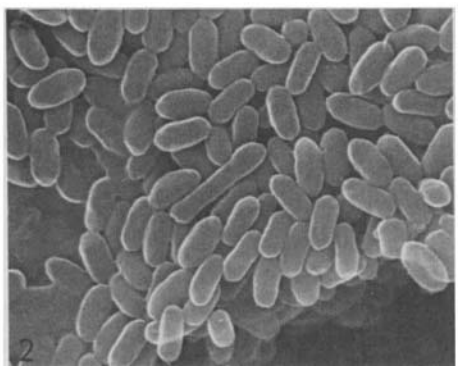

Fig. 21.1. Scanning electron micrograph depicting mature and immature polyhedra of *Trichoplusia* ni MNPV. The 'pitted' polyhedra are immature forms lacking an outer envelope (× 18 000).

Fig. 21.2. Scanning electron micrograph depicting granules of *Trichoplusia* ni GV (× 18 000).

particles from which they are derived, and are 40 nm in width. Some nucleocapsids possess tailed structures, especially NOBVs.

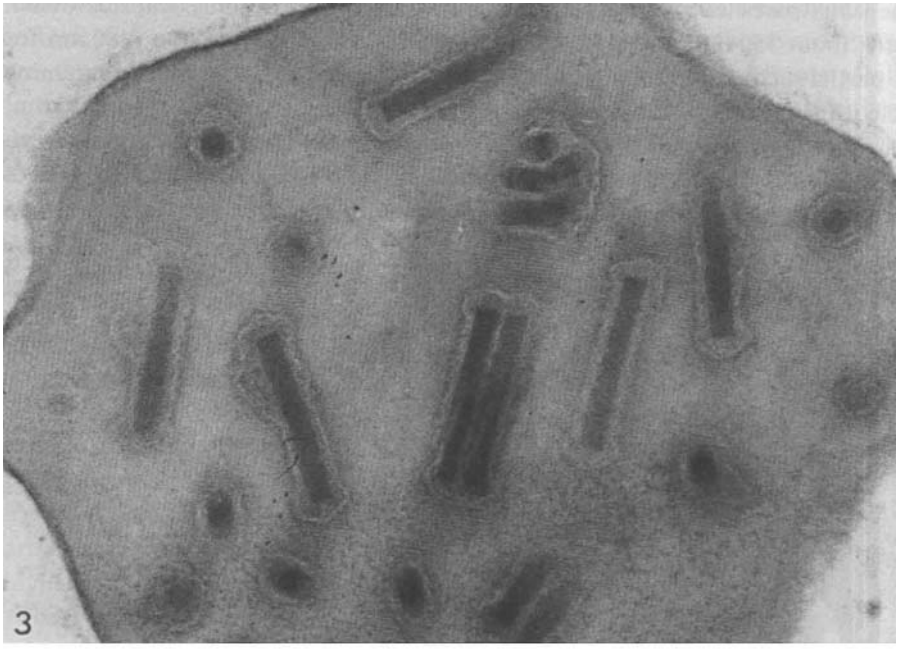

3

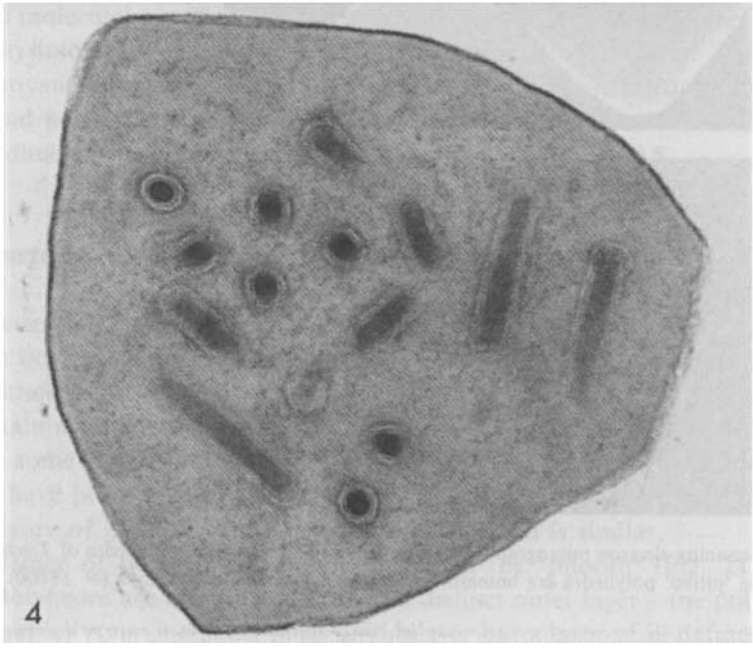

4

21.4. Architecture of virus particles

The polyhedra and granules are crystalline structures comprising a face-centred cubic lattice with a 4 nm repeat. The lattice is not distorted by the virus particles contained within it. Virus particles (and not nucleocapsids) are occluded and they lie at random within the lattice (Figs. 21.3 and 4). The lattice protein is in intimate contact with the virus particle envelope and the outer polyhedron 'envelope' where it occurs. Fig. 21.5 shows a negatively stained preparation of granules showing a single virus particle within. The protein associated with the crystalline lattice is a non-phosphorylated glycoprotein of molecular weight about 34 000.

Virus particles, whether derived from polyhedra or from the plasma membrane, have no obvious structural features (Figs. 21.6–8) although peplomer structures at the termini of the particles have been recorded. The virus particles contain approximately 20 polypeptides, ranging in size from 120 000 to 5000 daltons, commonly between 85 000 and 8000 (Table 21.1).

Nucleocapsids have a well-defined architecture. They have a capsid and an inner deoxyribonucleoprotein complex. The capsid is built up from 4.5-nm subunits arranged in a 12-start helix system of monomer units along the main cylinder of the capsid (Figs. 21.9 and 11). This results in an open stacked ring structure running parallel to the cylinder axis and repeating every third ring at a distance of 13.2 nm. Double- and triple-length nucleocapsids are sometimes observed and the integrity of the structure is retained along the full length of the capsid; such capsids may well contain concatenated DNA. The nucleocapsids contain about 7–10 polypeptides.

At the nucleocapsid ends structures different from the main body are observed. Three main features have been described and they are referred to as claws, nipples or tails. The claw may be found at both ends of the nucleocapsid, whereas the nipple is found at just one end and so may be derived from the claw (Fig. 21.9). Their function is unknown, although DNA or deoxyribonucleoprotein is extruded preferentially from the capsid ends. Tails have been observed mainly with NOBVs. The baculovirus from *Oryctes rhinoceros* has a tail structure about 10 nm wide and up to 300 nm long (Fig. 21.10). The tails have been observed coiled between the capsid and envelope and undoubtedly contribute to the irregular appearance of the

---

Fig. 21.3. Transmission electron micrograph of a section through a polyhedron of *Spodoptera exempta* MNPV showing virus particles (containing one or more nucleocapsids) orientated at random within the polyhedron lattice (× 100 000).

Fig. 21.4. Transmission electron micrograph of a section through a polyhedron of *Trichoplusia orichalcea* SNPV showing the protein lattice occluding virus particles which contain single nucleocapsids (× 100 000).

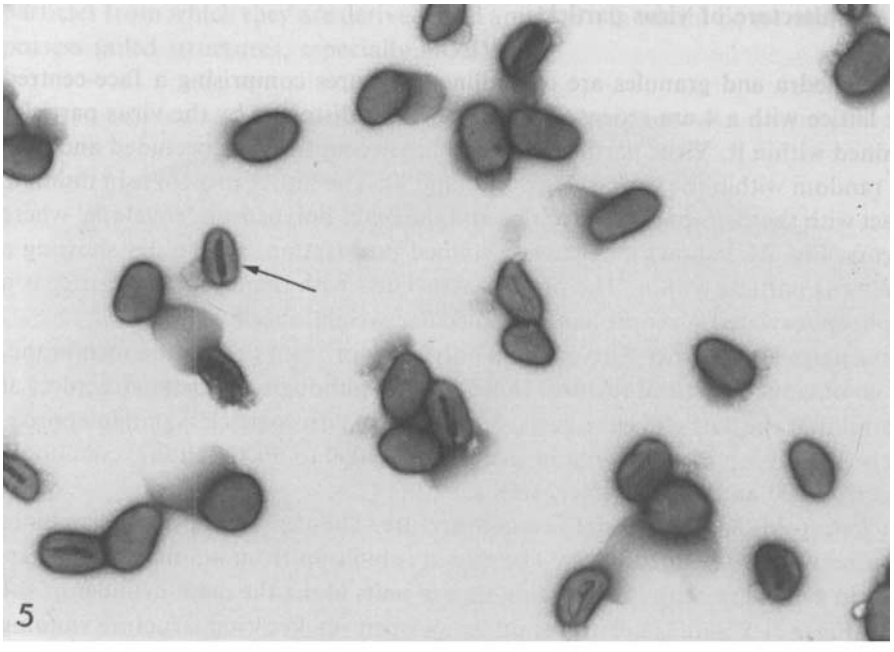
5

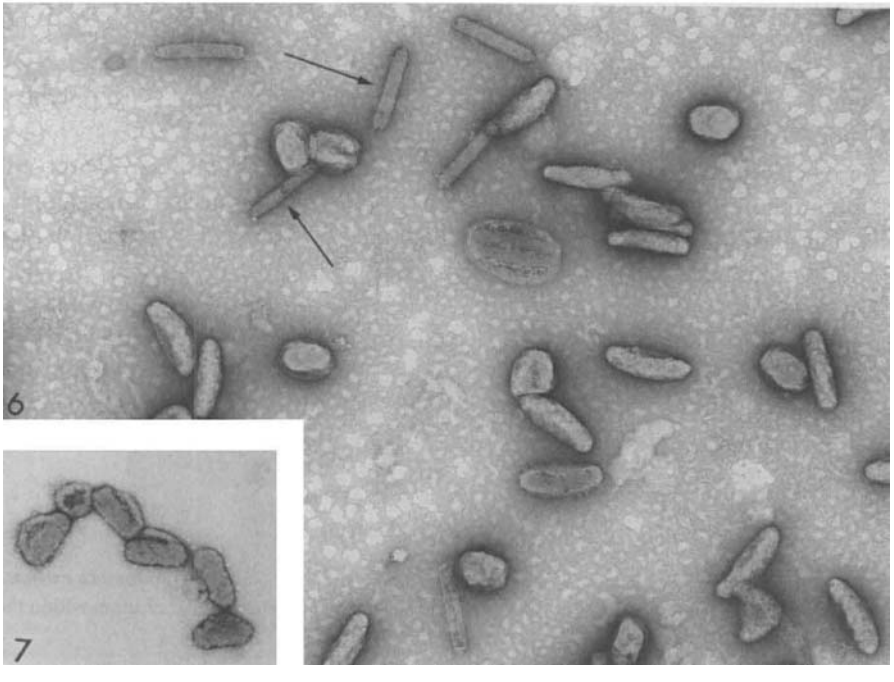
6

7

TABLE 21.1.

Baculovirus structural polypeptides[a]

M_r ($\times 10^{-3}$)	Function	Modification
82	Unknown	
75	Envelope protein	Glycosylated
72	Unknown	
67	"	
64	"	
61	"	
48	"	Glycosylated
42	"	
37	"	
34	Polyhedron protein	Glycosylated
25	Unknown	
21	"	
20	"	
18	"	
12	"	
11	"	
10	Basic DNA binding	
8	Unknown	

[a] Based on *Trichoplusia* ni MNPV.

virus particles. The structure is assumed to be a deoxyribonucleoprotein. The unusual NPV from *Tipula paludosa* possess a similar structure.

The capsid, the outer sheath of the nucleocapsid, is about 4 nm thick and encloses a complex of DNA and protein which is 32 nm in diameter (Fig. 21.11). The capsid comprises predominantly one polypeptide (Table 21.1). The 40-μm-long DNA molecule is integrated into a structure 350 × 32 nm and the low superhelical density facilitates condensation of the molecule. DNA extrusion from the nucleocapsids occurs preferentially at the termini of the nucleocapsid, as shown in Fig. 21.12. The extruded DNA lacks nucleosomal structure (no histones are pre-

Fig. 21.5. Granules of *Pieris brassicae* GV negatively stained with uranyl acetate to show single virus particles within (arrow) (× 20000).

Fig. 21.6. Virus particles of *Trichoplusia* ni MNPV stained with uranyl acetate which appear relatively structureless when compared with contaminating nucleocapsids (arrows) (× 66000).

Fig. 21.7. Virus particles of *Oryctes monoceros* NOBV stained with uranyl acetate (× 33000).

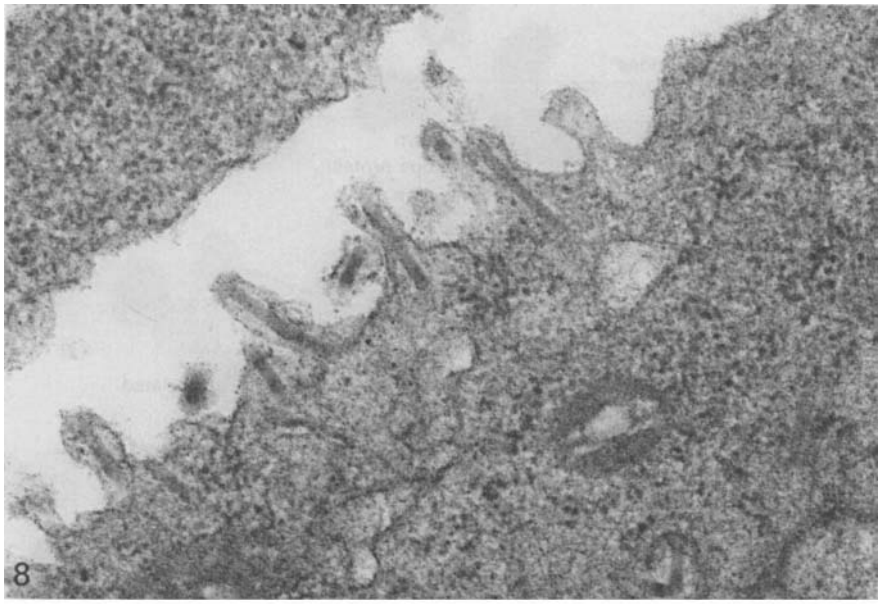

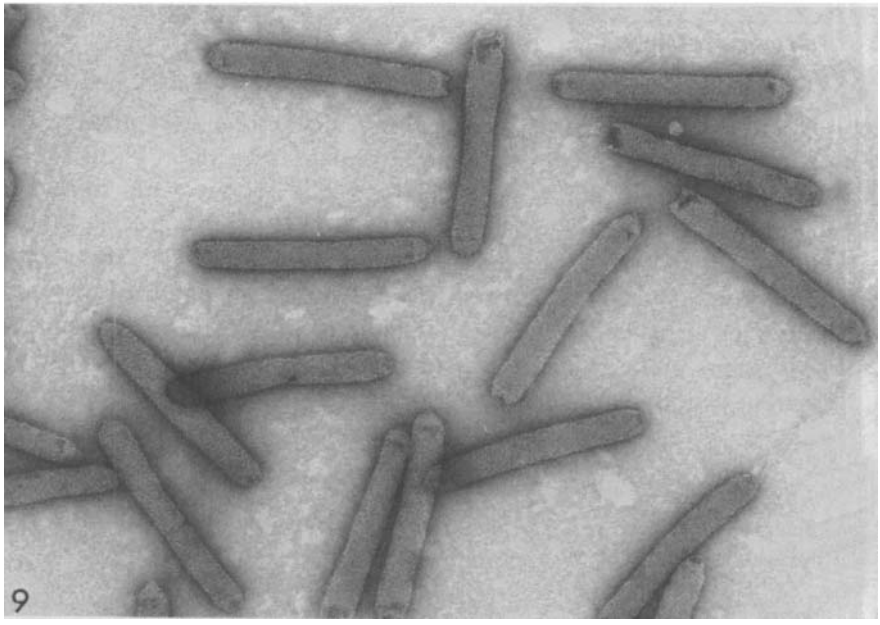

Fig. 21.8. Virus particles of *Trichoplusia* ni MNPV acquiring an envelope at the plasma membrane. The envelope contains predominantly single nucleocapsids. The observation is made on *Trichoplusia* ni cells in culture (× 52 000).

Fig. 21.9. Nucleocapsids of *Heliothis armigera* SNPV stained with uranyl acetate. Note the structures at both ends of the nucleocapsids. DNA can be seen exuding from the ends of the nucleocapsids (× 100 000).

sent in nucleocapsid preparations), and loops rather than free ends are observed, which is consistent with the packaging of a circular molecule (Fig. 21.12 shows DNA so released). The deoxyribonucleoprotein comprises the viral genome plus multiple copies (about 7500) of a single very basic, arginine-rich, protamine-like molecule of molecular weight about 12000.

The purified viral genome exists as a circular molecule with a low number of supertwists (Fig. 21.13).

21.5. Antigenic properties

The major components of the baculovirus particles are antigenically distinct. The polyhedron or granule protein is antigenically unrelated to virus particle components. Antigenic cross-reactivity between different isolates appears to reside in the nucleocapsids, which are serologically cross-related. Specificity in isolates resides in the envelope proteins. Interestingly, there are two phenotypic variants for the virus particles of NPVs and GVs. The two forms (polyhedron-derived virus and cell-released virus) share no common envelope antigens and indeed appear to be quite distinct viruses by conventional virological standards.

The antigenic interrelationships between various isolates have not been adequately defined. Briefly, it appears that the polyhedron protein appears to be the most extensively cross-reacting antigen although it appears not to cross-react with isolates derived from insects from different orders. Granule protein shares few common antigens with the polyhedron protein. Virus particle components share fewer common antigens.

21.6. Biological properties

Two forms of the virus exist – polyhedron-derived virus or cell-released virus. Virus particles released from the alkaline-labile polyhedron or granule, at the alkaline pH of the insect gut juices, infect mid-gut cells by fusion of the envelope with the plasma membrane of microvilli of columnar cells. Later in infection progeny virus released from cells infect at around neutral pH by cell fusion. The nucleocapsids are then rapidly uncoated to release the deoxyribonucleoprotein, which gains entry to the nucleus to subvert the cell and produce progeny virus particles and occlusion bodies containing virus particles. A complex sequence of genome expression, in at least 5 cascade steps, permits the assembly of a nuclear site of replication (the virogenic stroma), the assembly of nucleocapsids, envelopment of nucleocapsids either within the nucleus or at the plasma membrane, and the subsequent occlusion of some of the virus particles in the nucleus within polyhedra or granules. This last step does not occur with NOBVs.

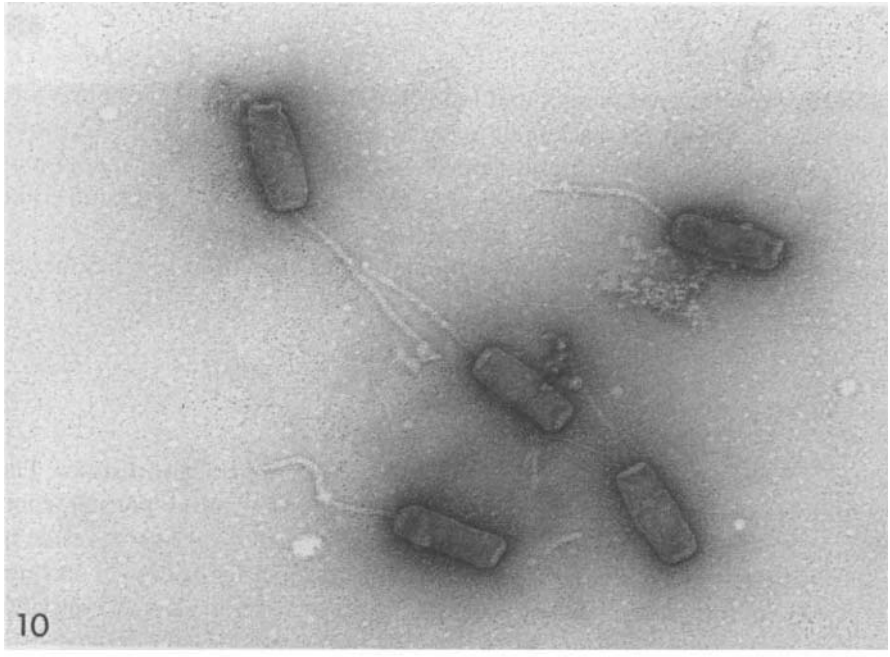

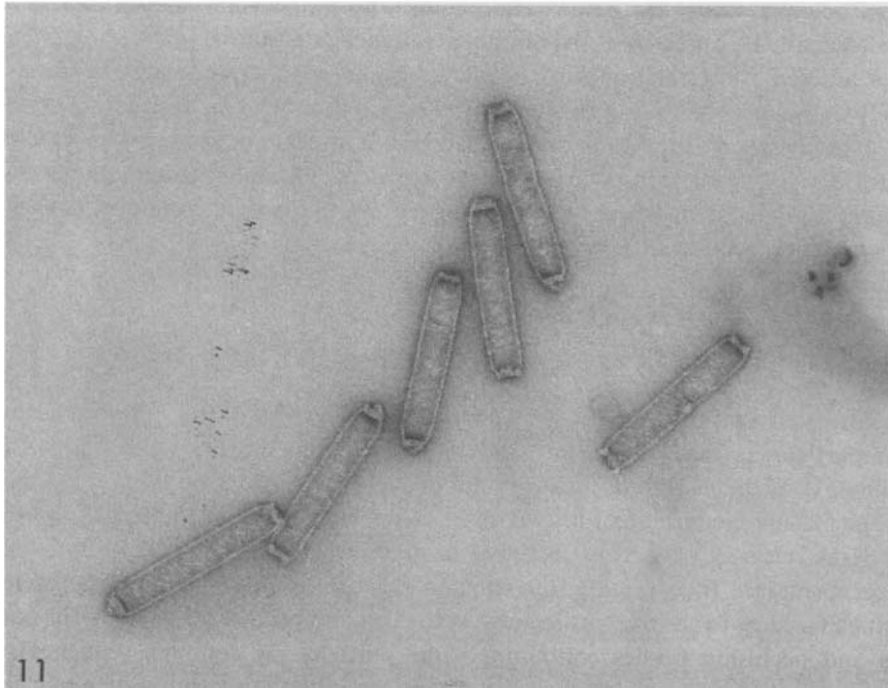

Fig. 21.10. Nucleocapsids of *Oryctes monoceros* NOBV stained with uranyl acetate showing tails at one end of the structure (× 66 000).

Fig. 21.11. Capsids of *Heliothis zea* SNPV showing the stacked disc arrangement of the capsid subunits (× 66 000).

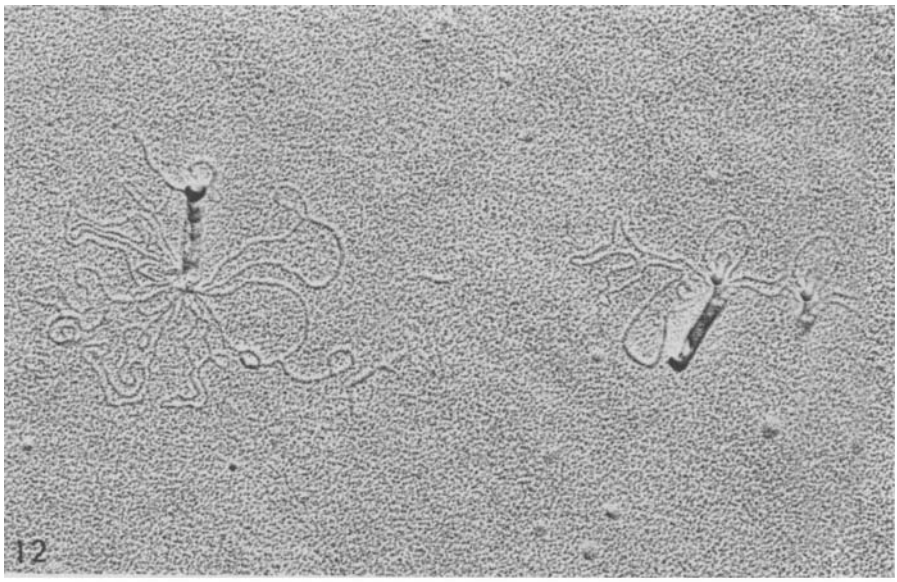

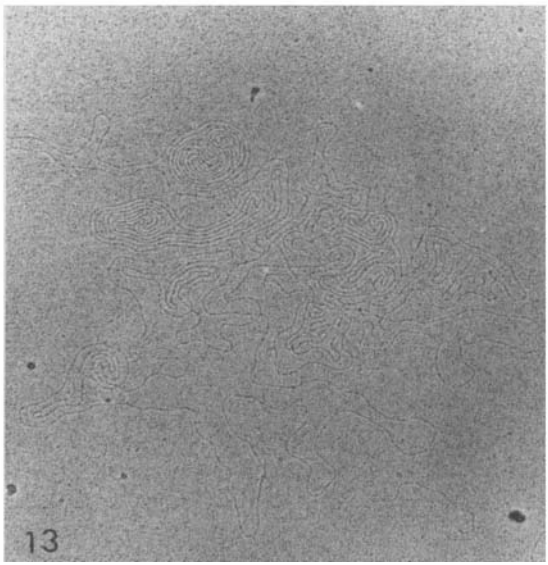

Fig. 21.12. Nucleocapsids of *Heliothis zea* SNPV, spread by the Kleinschmidt technique, showing DNA exuding from the capsid. Note the loops of DNA and the lack of nucleosomal structure (× 32 000).

Fig. 21.13. The genome of *Trichoplusia* ni MNPV, spread by the Kleinschmidt technique, showing its circular form. The genome is in its relaxed form (× 30 000).

21.7. Pathogenicity

Baculoviruses cause systemic disease in larval forms of Diptera and Lepidoptera. Infections in Hymenoptera are restricted to the gut, as some infections in Coleoptera may be.

The unusual NPV infecting *Tipula paludosa* infects haemocytes, causing a huge increase in the numbers of haemocytes present in the haemolymph.

Suggested reading

Bud, H.M. and Kelly, D.C. (1980) An electron microscope study of partially lysed baculovirus nucleocapsids: the intranucleocapsid packaging of viral DNA. J. Ultrastruct. Res. 73, 361–380.

Burley, S.K., Miller, A., Harrap, K.A. and Kelly, D.C. (1982) Structure of the baculovirus nucleocapsid. Virology 120, 433–440.

Crawford, A.M. and Sheenan, C. (1985) Replication of Oryctes baculovirus in cell culture: Viral pathogenesis, infectivity and protein synthesis. J. Gen. Virol. 66, 529–539.

Doefler, W. and Böhm, P. (1986) The molecular biology of baculoviruses. Curr. Top. Microbiol. Immunol. 131, 1–168.

Granados, R.R. (1980) Infectivity and mode of action of baculoviruses. Biotechnol. Bioeng. 22, 1377–1407.

Kelly, D.C. (1982) Baculovirus replication. J. Gen. Virol. 63, 1–13.

Kelly, D.C. (1985) The structure and physical characteristics of baculoviruses. In Viral Insecticides for Biological Control, Eds. K. Maramorosch and K.E. Sherman; pp. 469–498. Academic Press, New York, London.

Summers, M.D. and Smith, G.E. (1978) Baculovirus structural polypeptides. Virology 84, 390–402.

Nermut/Steven (eds) Animal Virus Structure

CHAPTER 22

Hepadnaviridae

LINDA M. STANNARD

Department of Medical Microbiology, U.C.T. Medical School, Observatory, Cape Town, Republic of South Africa

Family: Hepadnaviridae
Genus: No genera established
Species: Human hepatitis B virus (HBV), Woodchuck hepatitis virus (WHV), Ground Squirrel hepatitis virus (GSHV), Duck hepatitis virus (DHV)

22.1. General characteristics

Hepatitis B virus (HBV) causes both acute and chronic liver infections in man. HBV particles contain a circular DNA genome and an endogenous DNA polymerase which are enclosed within an isometric capsid, commonly termed a core particle. Both core particles and DNA are replicated within the nuclei of hepatocytes. Mature virions have an outer coat of virus-coded protein termed surface antigen (HBsAg). The surface antigen is generally produced in vast excess and is found in the blood of infected individuals in the form of filamentous and spherical particles (Fig. 22.1). An unusual feature of HBV infections is the prolonged viraemia, lasting for up to several months in acute infections and for many years (even for life) in chronic infections. There is a strong correlation between HBV infections and hepatocellular carcinoma. HBV-DNA can become integrated into the host cell genome, and cell lines established from hepatoma tissue from chronic HBV carriers persistently release hepatitis B surface antigen into the culture medium. As yet, no in vitro system for the culture of HBV has been established, but cell cultures have been successfully transfected with HBV-DNA to allow expression of the viral gene products, and chimpanzees have been used as experimen-

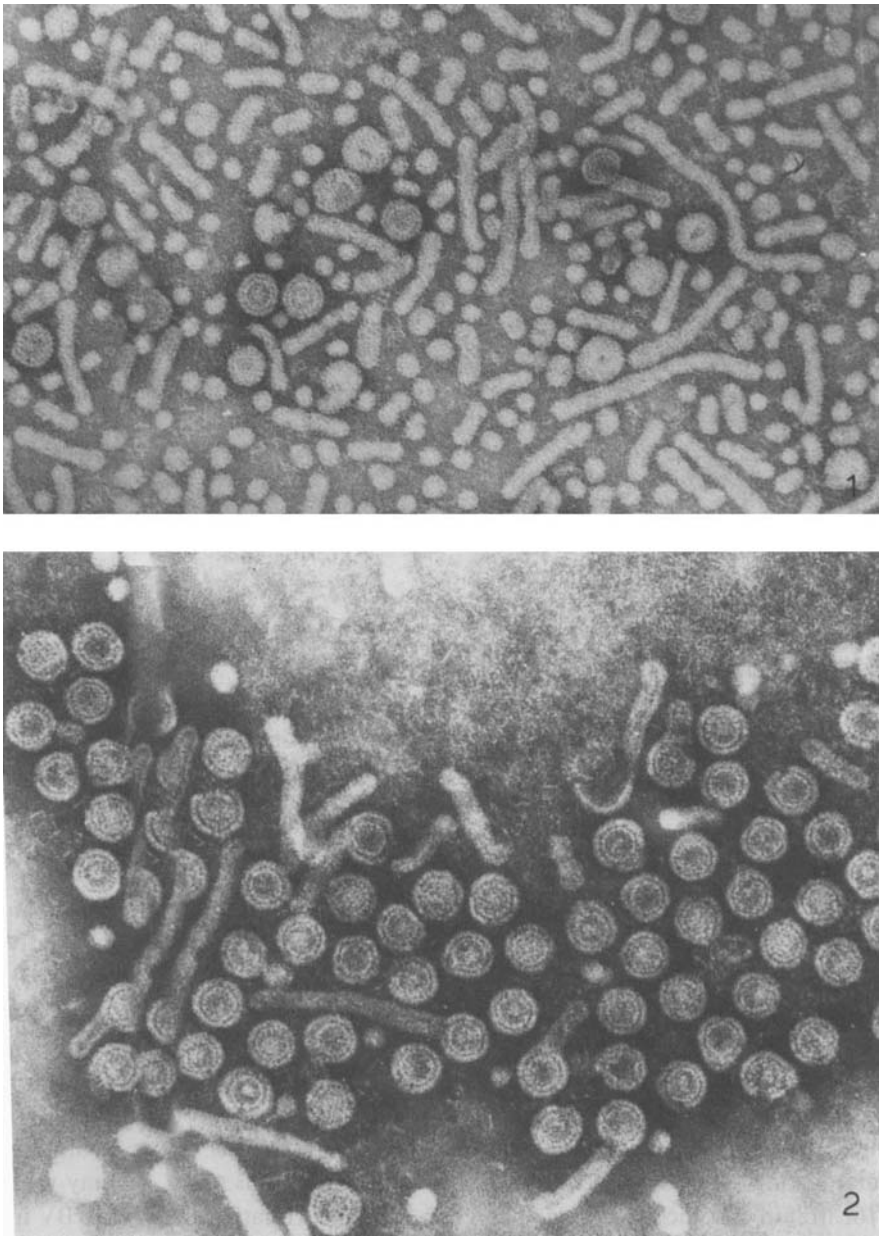

Fig. 22.1. Human hepatitis B virions and filamentous and spherical forms of HBsAg as found in the serum of an HBV carrier. × 120 000.

Fig. 22.2. A cluster of hepatitis B virions. Note tadpole-like forms. × 150 000.

All micrographs are of negatively stained preparations using 2% phospho-tungstic acid, pH 6.0.

tal animal models for the study of HBV pathogenesis. Animals from a diverse range of species, including woodchucks, ground squirrels and ducks, are naturally infected with viruses which, although antigenically distinct, share common morphology and genome structure with HBV. This family of viruses has been termed hepadna viruses (from *hepa*totrophic *DNA* viruses).

22.2. Human hepatitis B virus: structural characteristics

Virions (sometimes known as Dane particles, after the man who first described them) are seen in the blood as spherical particles 42 nm in diameter (Figs. 22.2 and 3). These possess a nucleocapsid or 'core' particle, 27 nm in diameter, surrounded by an outer coat, approximately 4 nm thick, of surface antigen (HBsAg). The coat apparently contains some lipid (Gavilanes et al., 1982) and has at times been termed an envelope although there is no direct evidence of a lipid bilayer. Rather, it appears to be assembled as a regular array of repeating protein subunits each approximately 3 nm in diameter. It may be better to equate the coat of HBV with an extra outer capsid (such as is seen in many double-stranded RNA viruses). Occasional virions have a tadpole-like appearance, where the coat is extended in the form of a 'tail' about 20–22 nm in diameter (Fig. 22.4). These tails are identical to the filamentous forms of HBsAg described below.

Filamentous and spherical forms of HBsAG

Excess viral coat protein or surface antigen (HBsAg) is found in the blood in the form of particles with distinctive morphology. These particles are either roughly spherical, with diameters ranging from 17 to 25 nm (mean 22 nm), or filamentous particles of similar diameter and varying in length from less than 40 nm to over 500 nm (see Fig. 22.1). The diameter of the filaments is not always constant over their entire length. The surface structure of the spherical and filamentous forms of HBsAg is identical to that of the virion coats. Filamentous forms of HBsAg frequently display regular non-helical, transverse striations approximately 4 nm apart (Fig. 22.5). Penetration of the small spheres and filaments by negative stain reveals that they have hollow centres and walls about the same thickness as the virion coats. They contain no nucleic acid. Identical morphological forms have been seen in the culture fluids of an HBsAg-producing hepatoma-cell line which does not produce intact infectious virus.

A diagrammatic representation of the hepatitis B virion and the surface antigen components is given in Fig. 22.6. Dimensions are proportional, but the actual arrangement of the structural units is only schematic.

Occasional virions found in the blood contain defective or incomplete cores (Fig. 22.7) and, rarely, two core particles have been observed to be enclosed within a single coat (Fig. 22.8).

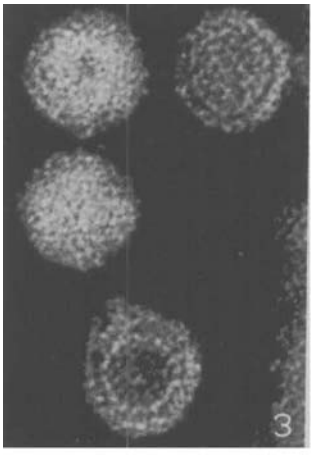
3

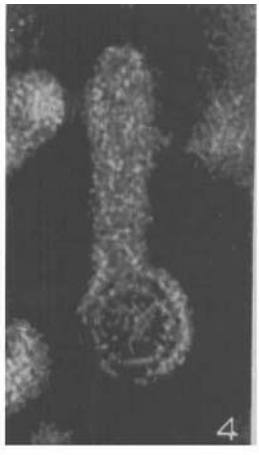
4


5

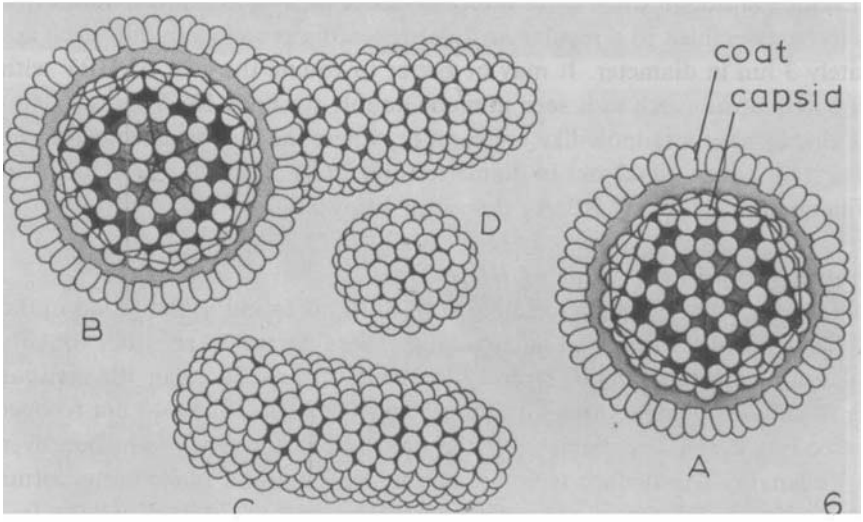
coat
capsid
B
D
C
A
6


7

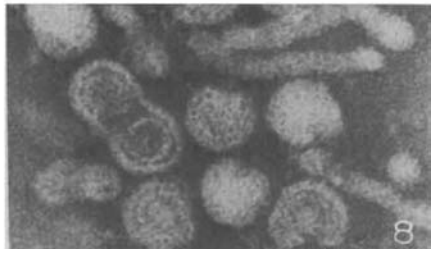
8

Core particles

The DNA-containing nucleocapsids of HBV are termed cores. The majority of core particles seen in the nuclei of hepatocytes, or in the centre of virions isolated from blood, are isometric, 27 nm in diameter and sometimes with an angular profile suggestive of icosahedral symmetry. The actual number and arrangement of capsomers have so far proved difficult to establish with certainty, although the semi-translucent appearance of negatively stained core particles (Figs. 22.9 and 10) is suggestive of capsomers arranged in a lattice formation (cf. Fig. 22.6). Smaller core particles, diameter 21 nm, are produced at low frequency (Fig. 22.11).

An additional distinct HBV specific antigen, designated 'e' (HBeAg), is present in sera which contain numeous virus particles. The role of HBeAg is as yet poorly defined, but claims that HBeAg may be released from disrupted core particles (Takahashi et al., 1979), together with evidence which indicates that loss of HBeAg results in a considerable increase in the number of virions with aberrant cores, suggest that HBeAg may perform an essential role in the structural assembly of HBV cores. The e-antigen is too small (M_r 30 000) to be resolved by current conventional electron microscopy techniques, although circulating immune complexes of e-antigen have been identified using anti-HBe tagged with colloidal gold (Stannard et al., 1982).

22.3. **Physico-chemical properties** (see Table 22.1)

The HBsAg of the virion coat and small spherical and filamentous particles contains protein, lipid and a small amount of carbohydrate. HBsAg comprises two major polypeptides: P1 (M_r 23 000–25 000) and P2 (M_r 29 000–30 000), which is

---

Fig. 22.3. Four HBV virions: two are not penetrated by stain and show surface structure of the outer coat. × 320 000.

Fig. 22.4. A tadpole-like form of HBV. × 320 000.

Fig. 22.5. Filamentous forms of HBsAg show striations. × 320 000.

Fig. 22.6. Diagrammatic representation of HBV. (A) A regular spherical virion showing an isometric nucleocapsid (DNA + HBcAg), commonly termed a core, surrounded by a coat of HBsAg which is made up of repeating subunits. The lattice-like arrangement of capsomers on the nucleocapsid is purely speculative. (B) A tadpole-like virion where the coat is extended in the form of a tail (cf. Fig. 22.4); and (C) filamentous and (D) spherical forms of the excess coat protein of HBsAg.

Fig. 22.7. Some HBV virions contain defective, bean-shaped cores. × 200 000.

Fig. 22.8. Two core particles can be seen enclosed within a single coat. × 200 000.

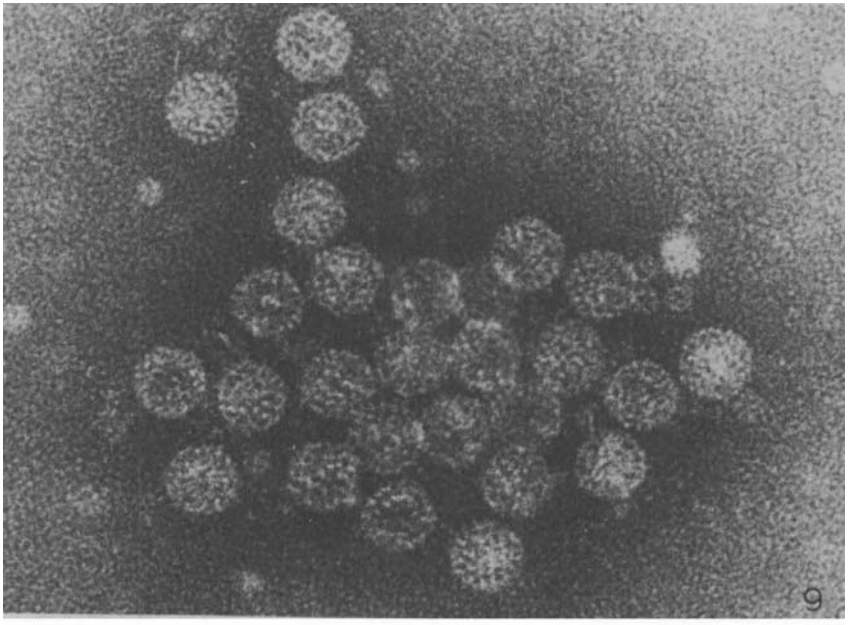
9


10

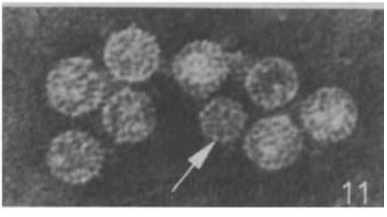
11

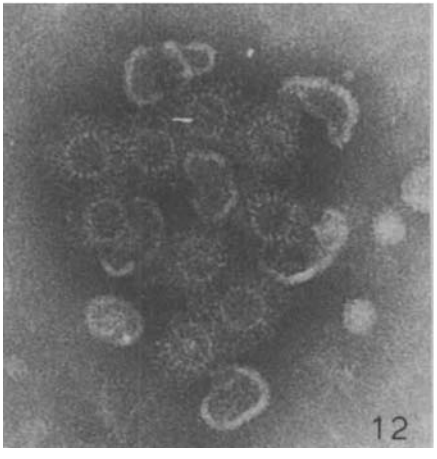
12


13

TABLE 22.1.

Physical and chemical properties of hepatitis B virus components

Morphological form	Common terminology	Mean diameter (nm)	Density in CsCl (g/cm^3)	Major polypeptide	M_r ($\times 10^{-3}$)
Virion	Dane particle	42	1.24–1.30	P1, P2, P19	see below
Nucleocapsid	Core (HBcAg)	27	1.32–1.38	P19	19
Filamentous and spherical forms (excess virus coat protein)	Surface antigen (HBsAg)	22	1.19–1.20	P1 P2	23 –25 29 –30
	e antigen		1.30		14.5–15.5
ds circular DNA					2000

glycosolated. In addition at least five minor polypeptides have been identified. Buoyant density in CsCl of the 22-nm spheres is 1.19–1.20 g/cm^3, whereas buoyant density of the complete virions is in the range 1.24–1.30 g/cm^3, probably dependent upon the content of DNA. For the same reason the core particles have also been detected at a wide density range of 1.32–1.38 g/cm^3. The major HBcAg polypeptide (P19) has an M_r of 19 000 and an isoelectric point (p*I*) of 4.5. Minor polypeptides of M_r 45 000, 70 000 and 80 000 have also been detected.

The HBeAg is difficult to purify because of its tendency to associate with other serum components, especially IgG and lipid. However, HBeAg freed in the presence of chaotropic ions has been shown to have an M_r of 30 000, density of 1.30 g/cm^3 and p*I* of 4.5–5.0 (Tedder and Bull, 1979). This probably represents a dimer of the basic polypeptide of HBeAg which, isolated from serum under reducing conditions by SDS-PAGE, has been shown to have an M_r of approximately 15 500 (Takahashi et al., 1980). HBeAg released into the culture fluids of cells transfected with HBV-DNA has been shown to have a basic polypeptide of M_r 14 500 and an apparent proclivity to form multimers. Protein kinase activity has been associated with the isolated HBeAg (Serrano and Hirschman, 1984).

Figs. 22.9–11. HBV cores purified from a liver homogenate. Fig. 22.9, × 360 000; Fig. 22.10, × 450 000; Fig. 22.11, × 240 000 (arrow indicates smaller core).

Fig. 22.12. HBV cores released from virus particles in serum by detergent treatment. Core particles are surrounded by haloes of attached molecules of specific antibody. × 200 000.

Fig. 22.13. Woodchuck hepatitis virus – morphologically identical to HBV. × 124 000.

The HBV genome (Tiollais et al., 1984; and Fig. 22.14) is a small, circular, partially double-stranded DNA molecule (M_r 2×10^6) with a full-length minus strand and a short plus strand of variable length. A DNA polymerase activity in the core repairs the single-stranded region to make fully double-stranded molecules of about 3200 basepairs (bp). The long DNA strand contains a nick at a specific site situated approximately 300 bp from the 5′ end of the short strand. A cohesive overlap of the two strands exists at the 5′ termini which maintains the circular configuration. A protein is covalently linked to the 5′ end of the minus strand. Full nucleotide sequences have been determined and four large, overlapping reading frames identified. Coding regions C and S, which code respectively for the major polypeptides of HBcAg (P19) and HBsAg (P1), have been located. Region S is subdivided into gene S and the strongly conserved pre-S region. The two additional reading frames, regions X and P, may code for polypeptides of 154 and 832 amino acids respectively. The P-region polypeptide might well represent the virus-coded DNA polymerase. It is probable that HBV-DNA synthesis involves the initial reverse transcription of an RNA template (Summers and Mason, 1982).

22.4. Antigenic properties

The HBsAg of the virion coat and the 17–25 nm spherical or filamentous particles is virus-coded, and specific antibody (anti-HBs) can agglutinate all three morphological forms. Antibody to HBsAg provides immunity to HBV infections. Genetic subtypes of HBsAg consist of a group-specific determinant, *a*, and two mutually exclusive type-specific determinants (*d,y* or *w,r*) which behave as alleles. Thus four major phenotypes (*adw, ayw, adr* or *ayr*) may be found and a number of subtypes of each of these phenotypes have been identified. Mixed subtypes (*adyw* and *adyr*) have also been reported. No differences between these subtypes with regard to their morphology, physico-chemical properties or biological activity have been found. Antigens contributed by the host may also be closely associated with the HBsAg (Burrell, 1975; Stannard and Moodie, 1976).

HBcAg is a single antigenic type, quite distinct from HBsAg, and found only in the core particle (capsid). Antibody to the core antigen (anti-HBc) is found in high titre in the serum of individuals exposed to hepatitis B infections. This antibody will aggregate core particles released by disruption of the virion coat with detergents or lipid solvents (Fig. 22.12), or cores obtained from liver cell homogenates.

HBeAg can be found in early acute-phase sera as well as in the serum of some chronic carriers of HBV. At least two determinants of e-antigen, HBe_1Ag and HBe_2Ag, have been detected. The presence of HBeAg in serum correlates well with the simultaneous presence of numerous virus particles and high DNA polymerase activity and is therefore indicative of high infectivity of that serum. Because of the

frequent observation of naturally occurring immune complexes of virions alone in the absence of anti-HBs (Fig. 22.2), it has been postulated that the virion coats contain an additional antigen which is distinct from HBsAg and is not present on the smaller spherical and filamentous structures of surface antigen (Moodie et al., 1974).

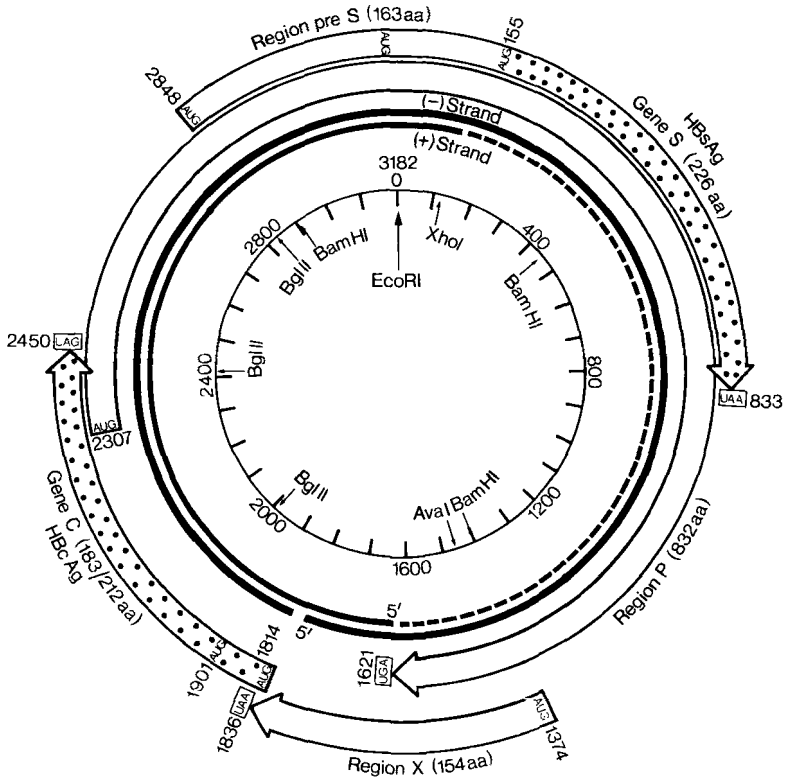

Fig. 22.14. HBV DNA consists of two linear unequal strands, the (−) and the (+) strands. The circular structure is maintained by 5′ cohesive ends. The dashed line corresponds to the single-stranded region of variable length. A single *Eco*RI site is used as the origin of the physical map, and nucleotide numbering follows the polarity (5′ to 3′) of the (+) strand. The broad arrows surrounding the genome represent the four large open reading frames of the (−) strand transcript. These four potential coding regions are termed region S (gene S + region pre-S), gene C, region P and region X. The number of amino acids in brackets corresponds to the length of the hypothetical polypeptides. The two regions corresponding to the defined genes S and C are represented by stippling. (Reproduced with kind permission of Professor P. Tiollais, and Grune & Stratton, Inc.; from Viral Hepatitis and Liver Disease (1984) Grune and Stratton, Orlando, FL.)

22.5. Biological properties

Hepatitis B virus infections are initiated predominantly by the parenteral route. The liver is the main target organ, although it is possible that alternative sites of primary replication exist. In the infected hepatocytes, HBcAg is replicated and core capsids are assembled in the nuclei. Free extrachromosomal viral DNA has generally been found in the liver cells of HBeAg-positive individuals, while integrated forms are present predominantly in HBeAg-negative persons and in hepatocellular carcinoma. In addition to hepatocytes, HBV-DNA has been detected in non-hepatocytes, such as bile duct epithelium, endothelial and smooth muscle cells, lymphoblastoid cells from the bone marrow and in peripheral leukocytes of patients with HBV infections. Immunohistochemical techniques have demonstrated HBsAg on the surface of infected hepatocytes, but the manner and site of acquisition of the virion outer coat has not been conclusively established. HBV infection in the liver appears to be non-cytopathic, with hepatitis resulting instead from the immunological response of the host to virus-specific determinants on the hepatocyte cell surface.

22.6. Other hepadna viruses

To date, apparent counterparts to human hepatitis B virus have been found in woodchucks (WHV), ground squirrels (GSHV) and Pekin ducks (DHV). All these viruses are ultrastructurally very similar (see WHV in Fig. 22.13), although the virions of the non-human species are sometimes slightly larger in size than HBV, and filamentous or spherical surface antigen components are not generally seen in the sera of infected ducks. The DNAs of all 4 hepadna viruses have similar sizes and basic structures, and studies of DNA homology have shown limited cross-hybridization between HBV-DNA and the DNA of each of the other species. All possess virus-coded DNA polymerase. The surface antigens of the three mammalian hepadna viruses cross-react to a small but significant extent, but stronger cross-reactivity occurs between the core antigens of the same three species. All hepadna viruses may cause persistent infection, with high concentrations of virus and viral forms continuously in the blood. WHV infection in woodchucks has been associated with both acute and chronic hepatitis, as well as a high frequency of liver carcinoma in that species. It may certainly be anticipated that many more hepatitis B-like viruses will be detected in a diverse range of animal species. Of note is the recent preliminary report of a hepatitis B-like agent in Taiwan Stink snakes (Yang et al., 1984).

References

Burrell, C.J. (1975) Host components in hepatitis B antigen. J. Gen. Virol. 27, 117–126.

Gavilanes, F., Gonzales-Ros, J.M. and Peterson, D.L. (1982) Structure of hepatitis B surface antigen. J. Biol. Chem. 257, 7770–7777.

Howard, C.R. and Burrell, C.J. (1976) Structure and nature of hepatitis B antigen. In Progress in Medical Virology, Vol. 22; pp. 36–103. Karger, Basel.

Moodie, J., Stannard, L.M. and Kipps, A. (1974) Dane complexes in hepatitis B antigen. J. Gen. Virol. 24, 375–379.

Stannard, L.M. and Moodie, J.W. (1976) Hepatitis B antigen: IgG components shown by immune electron microscopy. J. Gen. Virol. 30, 269–272.

Stannard, L.M., Lennon, M., Hodgkiss, M. and Smuts, H. (1982) An electron microscopic demonstration of immune complexes of hepatitis B e-antigen using colloidal gold as a marker. J. Med. Virol. 9, 165–175.

Serrano, M.A. and Hirschman, S.Z. (1984) Properties of hepatitis B e antigen synthesized by rat cells transfected with circular viral DNA. J. Gen. Virol. 65, 1373–1383.

Summers, J. and Mason, W.S. (1982) Properties of the hepatitis B-like viruses related to their taxonomic classification. Hepatology 2, 61–66 S.

Takahashi, K., Akahane, Y., Gotanda, T., Mishiro, T., Imai, M., Miyakawa, Y. and Mayumi, M. (1979) Demonstration of hepatitis B e antigen in the core of Dane particles. J. Immunol. 122, 275–279.

Takahashi, K., Imai, M., Gotanda, T., Sano, T., Oinuma, A., Mishiro, S., Miyakawa, Y. and Mayumi, M. (1980) Hepatitis B e antigen polypeptides isolated from sera of individuals infected with hepatitis B virus: comparision with HBeAg polypeptide derived from Dane particles. J. Gen. Virol. 50, 49–57.

Tedder, R.S. and Bull, F.G. (1979) Characterization of 'e' antigen associated with hepatitis B. Clin. Exp. Immunol. 35, 380–389.

Tiollais, P., Dejean, A., Brechot, C., Michel, M.-L., Sonigo, P. and Wain-Hobson, S. (1984) Structure of hepatitis B DNA. In Viral Hepatitis and Liver Disease, Eds. G.N. Vyas, J.L. Dienstag, J.H. Hoofnagle; pp. 49–65. Grune and Stratton, Orlando, FL.

Viral Hepatitis and Liver Disease. Proceedings of the 1984 International Symposium on Viral Hepatitis (1984) Eds. G.N. Vyas, J.L. Dienstag and J.H. Hoofnagle. Grune and Stratton, Orlando, FL.

Yang, C.S., Wang, S.C., Hsu, L.C., Chan, T.C. and Lee, S.C. (1984) Transmission of snake hepatitis B-like agent to Taiwan Stink snakes, *Elaphe carinata* (Guenther). Sixth International Congress of Virology, Sendai, Japan.

Zuckerman, A.J. and Howard, C.R. (1979) Hepatitis viruses of man, pp. 1–269. Academic Press, London.

This Page Intentionally Left Blank

Nermut/Steven (eds) Animal Virus Structure

CHAPTER 23

Adenoviridae

M.V. NERMUT

National Institute for Medical Research, Mill Hill, London NW7 1AA, U.K.

Family: Adenoviridae

Genus: Mastadenovirus (mammalian). Subgenera (groups): A, B, C, D, E, F, G. Species* (serotypes): Human adenovirus (A–E), simian, bovine, canine, murine, ovine, caprine, equine, porcine

Genus: Aviadenovirus (avian). Species* (serotypes): Adenovirus of fowl, turkey, goose, duck, pheasant

23.1. General characteristics

Adenoviruses are non-enveloped isometric particles with an icosahedral surface shell (capsid) and a DNA-containing core. They replicate and assemble in nuclei of infected cells and cause typical cytopathic effects. Many subgenera agglutinate red blood cells of various animal species. Adenoviruses are mild pathogens whose host ranges are usually confined to single species of animals or birds. No vectors are known. Some human strains can transform cells in tissue culture and many virus species are oncogenic in experimental animals.

23.2. Human adenovirus: chemical and physical characteristics

Adenovirus particles contain 87% protein (including a small amount of glycoproteins) and 13% dsDNA. The virion mass is approximately 170×10^6 daltons

* The definition of adenovirus species based on serology has been discontinued (ICTV meeting in Sendai, 1984).

TABLE 23.1.
Total mass of human adenoviruses

Method	Species	Mean ± S.D. (10^6 daltons)	Reference
Analytical chemistry	average of several species	175 ± 17	Green et al. (1967) Virology 31, 562.
Sum of protein mass + DNA	Ad5	162	Based on data in Table 23.2 and M_r of DNA = 23.25 × 10^6.
From DNA M_r and proportion[a]	Ad2	167	B. Jacrot (personal communication)
Neutron diffraction	Ad2	155 ± 8	B. Jacrot (personal communication)
Quantitative TEM	Ad12	189 ± 9	Lampert (1969) Naturwissenschaft 11, 537.
Scanning TEM	Ad5	157 ± 10	Ruigrok et al. (1984) J. Virol. Methods 9, 69.

[a] Based on M_r of DNA = 22.188 × 10^6 and 13.3% of virion mass.

(Table 23.1). No lipids appear to be present. The polypeptides and their location in the virion are summarized in Table 23.2.

The genome is a single linear molecule of dsDNA of M_r 20–25 × 10^6 and 11–12 μm long. This corresponds to 35 000–40 000 basepairs. DNA of adenovirus type 2 (Ad2) has been sequenced: it contains 35 937 basepairs, corresponding to M_r 23.25 × 10^6. DNA preparations obtained without protease treatment consist of circular molecules closed by association of the terminal protein (M_r 55 000) covalently attached at each end of the DNA molecule.

The buoyant density of virus particles (in CsCl) is 1.33–1.34 g/cm^3; virus cores have a density of 1.42 g/cm^3. The sedimentation coefficient of the virus particle is 560 S, and that of the DNA is 29–32 S (mammalian) or 35 S (avian viruses).

23.3. Structural characteristics

Shape and size. Adenoviruses are icosahedral in shape, i.e., they have 20 triangular facets, 12 vertices and 30 edges. They possess 5×, 3× and 2× rotational symmetry. The dimensions of an icosahedron are derived from the length of the edge (E) and are given as the distance between opposite vertices ($P = E \times 1.9$), or facets ($F = E \times 1.539$) or edges ($E_d = E \times 1.618$), or as the diameter of the virion along the five-fold symmetry axis ($D = E \times 1.7$). The following values for the edge have been reported: 42.5 nm (from freeze-drying), 44 nm (from freeze-etching), 44.5 nm (from hexon dimensions), 52 nm (from neutron diffraction), 50.5 nm (from frozen hydrated electron microscopy). The average from the three middle values is about 46 nm, giving the following values: $P = 87.4$ nm; $F = 70.8$ nm; $E_d = 73.6$ nm and $D = 78.2$ nm.

TABLE 23.2.

Adenovirus structural proteins

Viral protein	M_r ($\times 10^{-3}$)	No. of copies per virion	Structural element or location (No. of molecules/virion)	Sediment coefficient (S)	p/	Remarks
II	108	720	Hexon (240 trimers)	12.9	5.4 –6.1	
III	85	36(?)	Penton base (12 trimers)	9.5	5.85	
IIIa	66	60(?)	Penton assoc. (5 per penton)	6.0	5.95–6.08	Phosphorylated
IV	62	24	Fibre (12 dimers)	6.0	5.3 –6.6	Glycosylated
IVa	50	(?)	Internal			DNA-binding
	55	2	DNA-terminal (2)			DNA-binding to 5' end of DNA
V	48	180	Core protein 1 (180)	3.5	6.7	Basic, weakly phosphorylated DNA-binding
VI	24	450	Hexon-associated (?)	3.8	5.81	Phosphorylated, DNA-binding
VII	18.5	1070	Core protein 2 (1070)	2.3	7.5	Basic, DNA-associated
VIII	13	(?)	Hexon-associated	1.6	5.2	
IX	14.3	280(?)	Associated with GONs	2.3	5.9	
X			μ-protein (?), internal			μ is basic, XI and XII are probably cleavage fragments from higher M_r proteins
XI	3–7		Internal			
XII			Internal			

Compiled from various sources (see Nermut, 1980; Philipson, 1983; Pettersson, 1984) and based mainly on Ad2 and Ad5.

23.4. Architecture of the virion

The adenovirion consists of two 'structural complexes': the capsid (outer icosahedral shell) and the core (internal body comprising the nucleocapsid and the core shell).

The capsid is built up from 252 capsomers ($T=25$), i.e. 240 six-coordinated (called hexons) and 12 five-coordinated (called pentons). However, other polypeptides are also associated with the capsid, including VP-IIIa, VI and IX. It can be dissociated by means of various treatments into 'groups of nine hexons' (GONs) originating from the triangular facets of the icosahedron (Fig. 23.1c). Free pentons (from dissociated capsids) can form associations called dodecons (= 12 pentons).

The hexon is a trimer of VP-II, which in the case of Ad2 is of M_r 109 058 (= 967 amino acid residues). The primary structure of this polypeptide suggests that the conformation of the middle portion is different from that of the two ends.

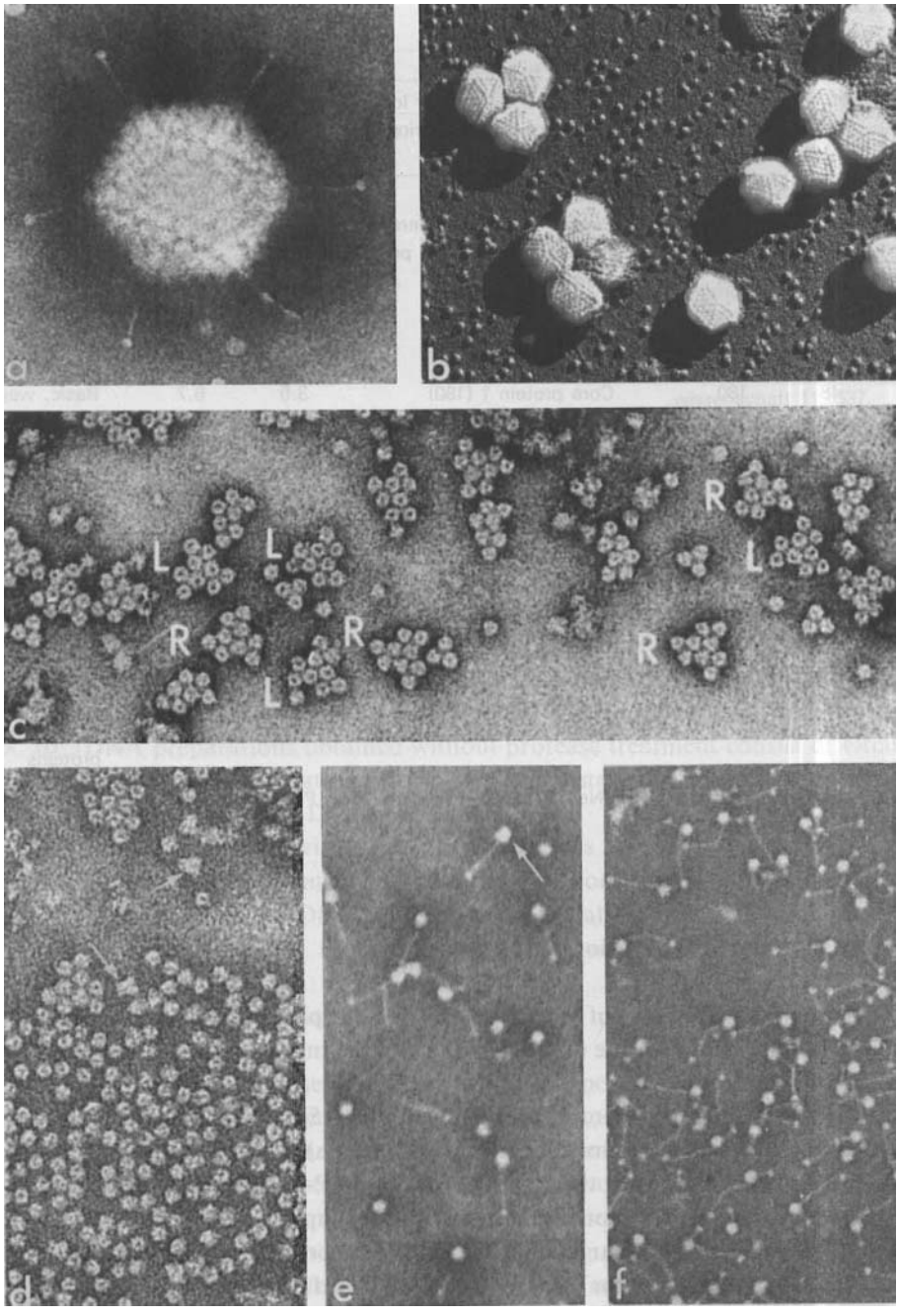
a
b
L
L
R
R
L
R
R
L
c
d
e
f

Clusters of hydrophobic residues are rare, but a very acidic region is probably exposed on the surface of the hexon.

The structure and dimensions of the hexon obtained by electron microscopy (Fig. 23.1d) and X-ray crystallography are summarized in Fig. 23.2. The remarkable feature of the hexon is that the three subunits form a tripartite body with a round base, a hexagonal waist and a triangular top. The individual subunits undergo a twist between the base and the top by less than 60° so that the apices of the triangles are offset by 10–15° anticlockwise relative to the midpoints of the hexagonal edges. The pseudohexagonal portion of the hexon allows it to interact with its six neighbours in such a way that the capsid interior is completely sealed off, as shown in Fig. 23.3c). This packing arrangement also explains the orientation of the right-handed GONs and the azimuth of their triangular tops within the face of the icosahedron (see Fig. 23.3a,b).

The high-resolution (2.9Å) three-dimensional structure (including chain tracing) has recently been published (Roberts et al., 1986).

The structural 'polarity' of the hexon is accompanied by differences in surface properties of the hexon: the top of the hexon appears negatively charged, whereas the base is rather hydrophobic. The net charge of the hexon is highly negative at alkaline pH.

The penton consists of the penton base (VP-III) and fibre (VP-IV). The molecular weight of the base of Ad2 is 246 000, while that of the polypeptide itself (as estimated from gel electrophoresis) is about 85 000. This suggests that the base is made of three subunits instead of the expected five. However, a pentagonal shape has been observed by electron microscopy and also a conical shape when viewed from the side (Fig. 23.1e,f).

The fibre consists of a shaft about 2 nm thick and 10–37 nm long (depending on serotype) which terminates in a knob about 4 nm in diameter bearing a positive charge. The fibre is generally considered to mediate early contacts between virus particles and specific cell surface receptors (42 kDa glycoprotein in HeLa cells, 65 kDa in KB cells). Ad2 fibre has been proposed to be a dimer of VP-IV (M_r 62 000; Green et al., 1983), but recent evidence speaks in favour of a trimer (van Oostrum

---

Fig. 23.1.(a) Adenovirus (serotype 5) after negative staining. Six fibres with terminal knobs are clearly visible. ×320 000. From Valentine and Pereira (1969) with permission. (b) Same virus prepared by freeze-drying and shadowing revealing the icosahedral shape and surface structure. ×62 500. (c) Groups of nine hexons in left-handed (L) and right-handed (R) orientations. ×250 000. From Nermut (Virology, 1975) with permission. (d) Adenovirus hexons mostly in upright orientation; only a few are oriented lengthwise (arrows). Negative staining, ×250 000. (e) Pentons of Ad5, negatively stained. Some penton bases exhibit conical profiles (arrow). ×200 000. (f) Pentons of an avian adenovirus (CELO) with two fibres of different lengths. ×200 000. Micrographs (a), (e) and (f) were kindly supplied by Dr. N.G. Wrigley.

and Burnett, 1985). Avian adenoviruses have two fibres on each penton base, sometimes of different lengths (Fig. 23.1f).

Organization of the capsid. The adenovirus capsid belongs to the $P=1$ class and has a triangulation number $T=25$. However, it embodies two examples of structural unorthodoxy. The six-coordinated capsomer (the hexon) is a trimer (not a hexamer) of VP-II; the penton complex consists of a pentameric base and a

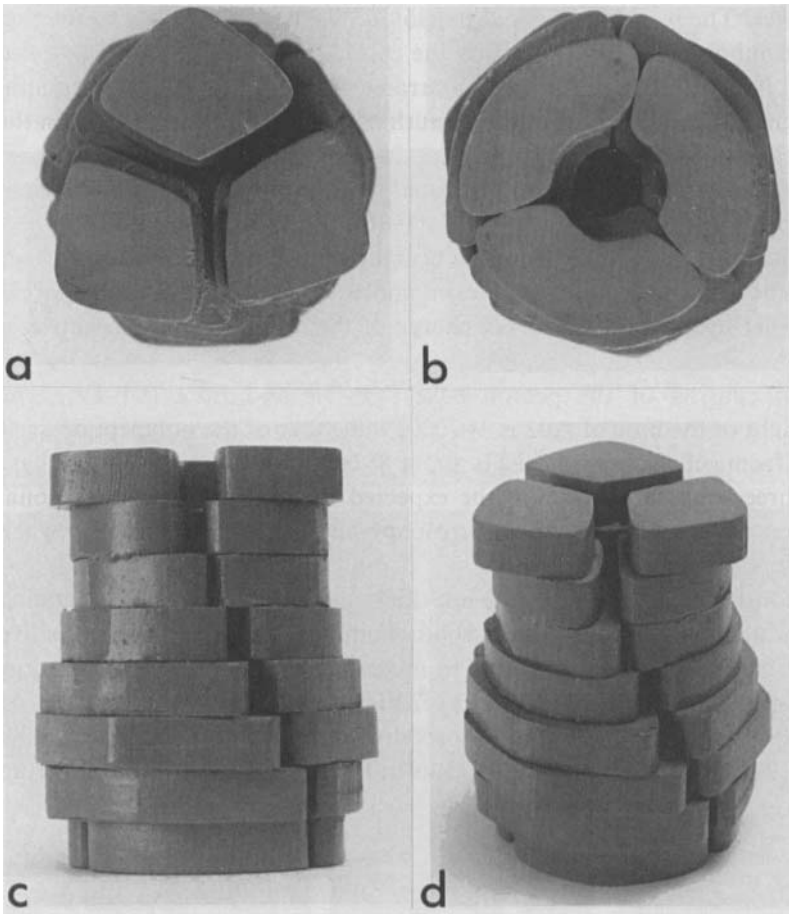

Fig.23.2. Model of adenovirus hexon developed from electron microscopy and computer modelling. The three polypeptide subunits form a tripartite body with a triangular top (a), a pseudo-hexagonal lower waist (3rd and 4th layer in (c), and a round bottom (b). Dimensions (mainly from X-ray crystallography - see Burnett, 1984): height = 11.6 nm; edge of the triangular top = 9.5 nm (corner-to-edge distance = 9 nm); edge-to-edge distance of the 'pseudohexagon' = 8.9 nm and corner-to-corner distance = 10.5 nm; diameter of the round bottom = 7.5–8 nm, the axial hole = 2.5–3 nm in diameter. The central channel (about 1.5 nm in the middle) widens in both directions, but considerably more towards the base.

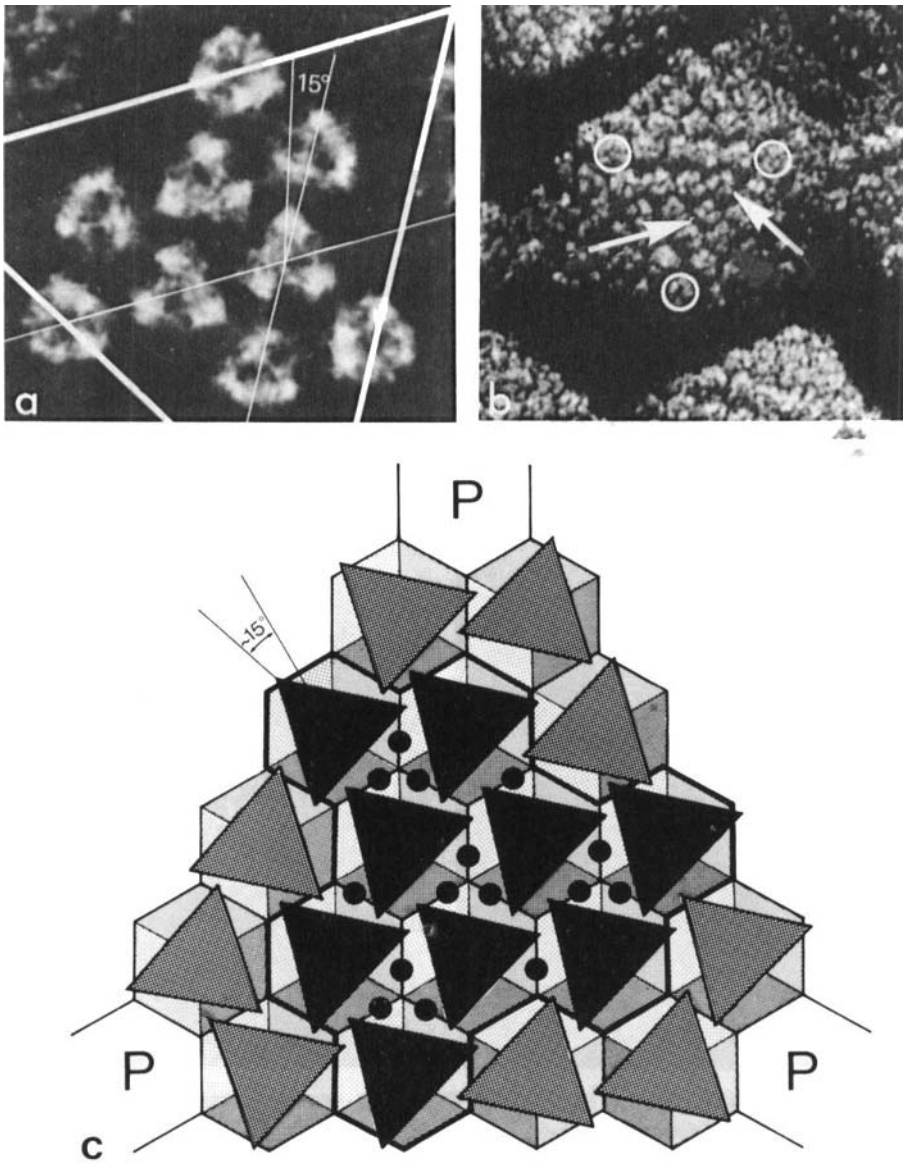

Fig. 23.3.(a) Right-handed group of nine hexons (GON) after rotational averaging and photographic reversal to conform with their left-handed orientation in the capsid. Thick lines represent edges of the triangular facet. The azimuth of the top triangles is offset by about 15° anticlockwise in this particular case as shown, but 10° has been reported by Burnett (1984). (c) Diagram of hexon packing within one of the triangular facets of the capsid. Hexagons represent the pseudo-hexagonal portions of the hexons, triangles the top portions. The three polypeptide subunits are shown in three different shades. The thick contours delineate one GON. Black dots show the possible location of VP-IX. They are placed between non-identical parts of the subunits. The four 'trimers' would lend strength to GONs. Trimers of VP-IX in the same places have been suggested by Burnett (1984, 1985). (b) Freeze-dried and shadowed virus particle showing the triangular tops of some hexons and their orientation as seen in (a) and (c). Pentons are encircled. × 500 000.

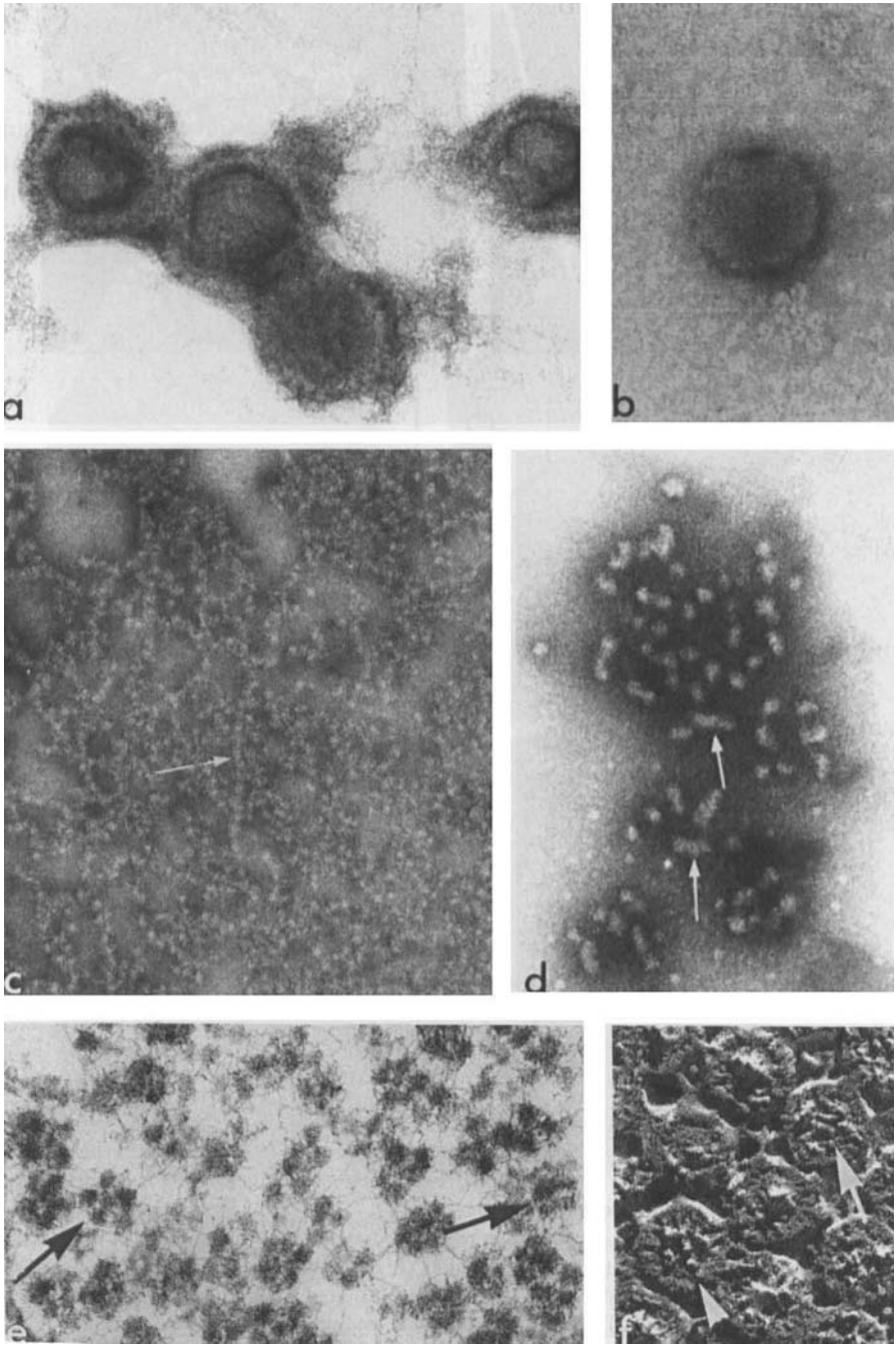
a
b
c
d
e
f

trimeric fibre. The interaction of the hexon with its six neighbours is accomplished through the pseudohexagonal waist. Little is known about the penton base except that five copies of VP-IIIa form a complex with the base pentamer and that the peripentonal hexons face the penton as shown in Fig. 23.3c. VP-IX appears to be associated with GONs (see Burnett, 1984, and Nermut, 1984, for references). The close contact between adjacent hexons means that the capsid interior is completely sealed off and thus together with the core shell may fulfil the role of a permeability barrier.

The core consists of DNA and VP-V, VP-VII and VP-X, but some uncertainty exists about the presence of VP-VI. Cores prepared by means of detergents or pyridine are usually rather 'relaxed'; only freeze-fracturing followed by replication or negative staining reveals their native shape (Fig. 23.4a,b). The cores are assumed to be icosahedral, because they are closely apposed to the inner surface of the capsid. Their 'diameter' in 5-fold symmetry orientation is about 58 nm. The core shell is most probably made from VP-V or VP-VI and if icosahedral should contain 180 or 240 copies of either of them (see Table 23.1). The shell is only 4–5 nm thick and rather fragile.

Two models have been proposed regarding the architecture of the virus interior. (a) Brown et al. (1975) proposed that there are 12 large beads (20 nm in diameter) in the virus interior, one in each corner of the icosahedron. Some support for this model has been provided by ion-beam-etching (Newcomb et al., 1984; and Fig. 23.5). (b) A nucleosome-like model based on morphological evidence of nucleosome-like particles (about 10 nm in diameter) and biochemical data (e.g. micrococcal nuclease digestion pattern) has been proposed recently (see Nermut, 1984, for references). It suggests that the 'beads-on-a-string' condense into a solenoid forming six rod-like elements as observed in the electron microscope (Fig. 23.4). Biochemical studies suggest that VP-VII and VP-X ($=\mu$) are closely associated with DNA, but it is VP-VII that forms the core of a 'nucleosome' with DNA wound around it. VP-V and VP-X are easily removed from the core, e.g. by high salt concentrations. Cores can be relaxed into linear structures by withdrawing calcium (EGTA, high salt or high pH). This model is further sup-

Fig. 23.4.(a) Adenovirus cores visualized within the capsid by freeze-fracturing followed by negative staining. ×300 000. (b) Virus core liberated from the capsid by 0.5% deoxycholate. Negative staining with uranyl acetate. Note fine structure of the core surface. ×300 000. (c) Beaded filaments observed after treating virus cores (prepared by treatment with deoxycholate) and EGTA (Nermut, 1980). Negative staining. ×100 000. (d) Same cores as in (c) but exposed to 1 M NaCl. Note the rod-like elements (arrow). ×100 000. (e) Ultrathin section of cores prepared by deoxycholate followed immediately by fixation and processing. Note cores with six round profiles and the rod-like elements (arrows). ×100 000. (f) Cross-fractured virus particles, one showing a similar configuration of six round 'bodies' (arrowheads) or 3–4 rods (arrows). ×100 000.

ported by freeze-etching of adenovirus particles, ultrathin sections of virus cores (see Nermut, 1984) and by magnetic birefringence experiments showing that the virus interior does not follow the icosahedral organization of the capsid (Torbet, 1983).

However, the protein/DNA interactions in adenovirus cores are probably not strictly analogous to those in cellular nucleosomes, since the ultraviolet cross-linking experiments (Chatterjee et al., 1986) showed that VP-VII is a dimer (lying in the major groove) and that VP-V too can be cross-linked with DNA. The finding of VP-VIII molecules not covalently atached to DNA after UV irradiation suggests that viral DNA might be wrapped about clusters of VP-VII, as in the nucleosome-like model.

The basic structural features of the virion are summarized in the model shown in Fig. 23.6 representing an overall view of the virus approximately in three-fold symmetry orientation (a). One 'group of nine hexons' is shown dark. Note mutual orientation of the hexons at the edge where two GONs meet. Fig. 23.6b represents a view of the virus interior. The capsid is lined up with the 'core shell' and the nucleocapsid is shown in a hypothetical 'superhelical' organization.

The complex structure of the adenovirion is maintained by the energy of the bonds between structural elements (macromolecules) and structural complexes.

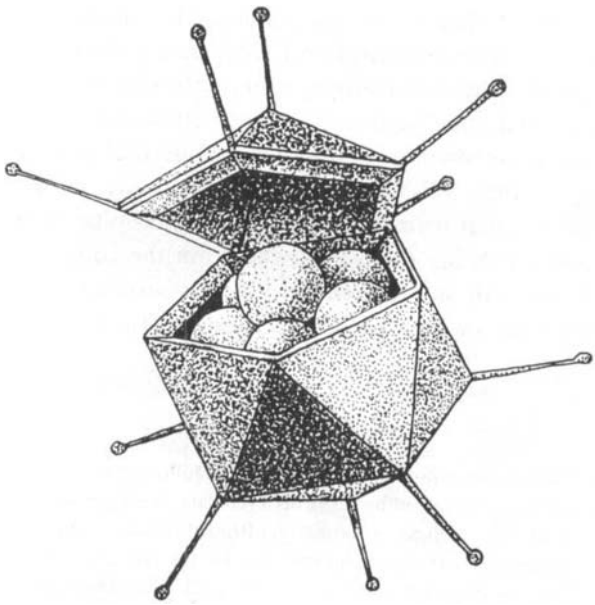

Fig. 23.5. Model of adenovirus interior as proposed by Newcomb et al. (19847. Virus DNA-protein(s) complex is shown as composed of 12 globular bodies located at the vertices. By courtesy of Dr. J.C. Brown and with permission of J. Virology. Drawing by Mr. Rex Slack.

TABLE 23.3.

Antigens associated with major structural proteins of mammalian adenoviruses

Protein	Designation	Specificity	Remarks
Hexon (VP-II)	α	Group (= genus)	Bottom of hexon
	ε	Type (= species)	Top of hexon
Penton base (VP-III)	β	Group	Carries toxin activity
Fibre (VP-IV)	γ	Type	
	δ	Intrasubgroup	Located at the proximal part of fibre (in subgenera A, C, D, E)
VP-VII	-	Group and type	Ad2 and Ad3 examined only
VP-IIIa	-	Group	
VP-IX	-	Group and type	Ad2 and Ad5 examined only

Adapted from Pettersson (1984).

The nature of these interactions determines the degree of cohesion within the virus particle. In the capsid there are predominantly hydrophobic interactions between GONs, since the capsid disintegrates to yield them when treated with heat or detergents. The hexon-hexon interactions within the GON remain unclear; they might be reinforced by the presence of a low molecular weight protein (VP-IX; see Fig. 23.3c).

TABLE 23.4.

Classification and some properties of human adenoviruses

Subgenus (group)	Serotype	Haemagglutination	% G+C in DNA	Oncogenicity
A	h 12, 18, 31	Rat RBC-incomplete	47–49	High
B	h 3, 7, 11, 14, 16, 21, 34, 35	Monkey RBC	50–52	Weak
C	h 1, 2, 5, 6	Rat RBC-incomplete pattern	57–59	None, but could transform rodent cells in vitro
D	h 8, 9, 10, 13, 15, 17, 19, 20, 22–30, 32, 33, 36, 37	Rat RBC	57–60	As C
E	h 4	RBC Rat-incomplete (atypical) Pattern	57	None

RBC = red blood cell.

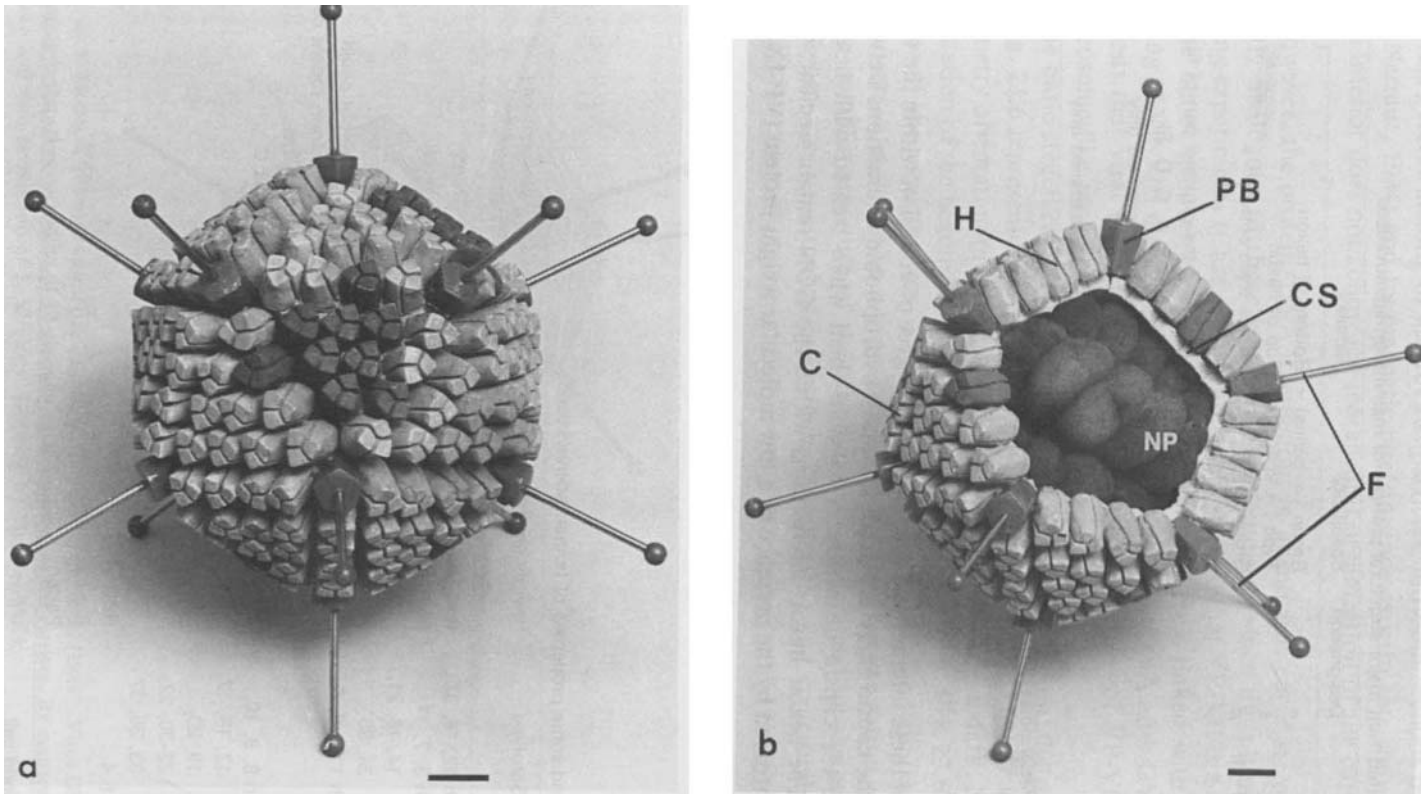

Fig. 23.6. Three-dimensional model of adenovirus in a three-fold (approximately) symmetry orientation (a) with GONs and pentons in dark tone. (b) Insight into the virion showing core shell (CS) and superhelical rod-like element of the DNA-protein complex (NP). H = hexon, C = capsid, PB = penton base, F = fibres. From Nermut (1984) with permission. Bar represents 10 nm.

The interactions of pentons with the surrounding hexons are primarily electrostatic in nature, since the pentons can be removed from the capsid by dialysis at pH 6.3. The hexon base has been found to be hydrophobic and this suggests a similar means of interaction between it and the 'core shell', which is made of VP-V or VP-VI. POlypeptide V has a large proportion of arginine residues, which in turn could neutralize some of the negative charges on the surface of the DNA-protein(s) complex. The relaxation experiments (see above and Fig. 23.4) suggest that the 'superhelical' structure of the DNA-protein(s) complex is maintained by calcium ions binding to DNA phosphates. The arginine-rich VP-VII presumably forms the 'core' of a 'nucleosome' by interacting directly with the DNA.

23.5. Biological properties

The antigenic properties of mammalian adenoviruses are summarized in Tables 23.3 and 23.4. Some of the capsid proteins are produced in excess during the infectious process and are called 'soluble antigens'.

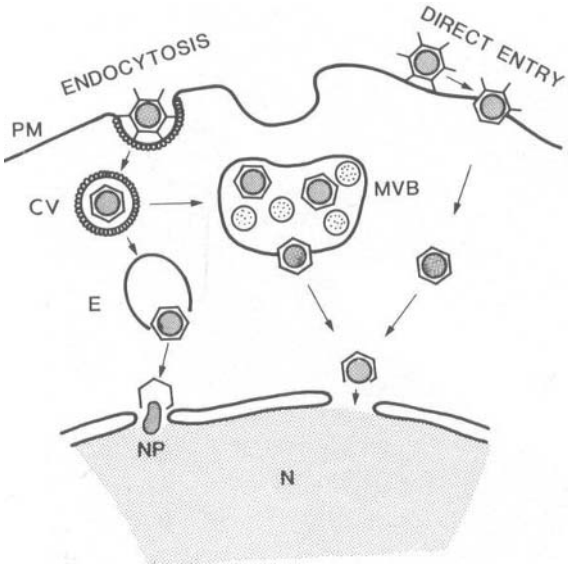

Fig. 23.7. Diagrammatic representation of the two modes of entry of adenovirus into cells: receptor-mediated endocytosis and direct entry. PM = plasma membrane; CV = coated vesicle with adenovirus; E = endosome; MVB = multivesicular body; N = nucleus; NP = nuclear pore. Viruses penetrate endosomal membrane by an unknown mechanism, migrate towards nucleus and are uncoated close to nuclear pores. In some adenovirus species virus particles appear in lysosomes, but this is not typical.

Virus–cell interactions. Most virus particles are taken up via receptor-mediated endocytosis but some can penetrate the plasma membrane by 'direct entry' (Figs. 23.7 and 23.8). Typically, after 10–20 min virus particles are found close to the nuclear membrane, where they are uncoated and the cores pass into the nucleus through the nuclear pores (Fig. 23.9d). However, a certain destabilization of virus particles (e.g. rendering them sensitive to DNase I) takes place before 'physical' uncoating. The replication of adenovirus DNA takes place within the nucleoplasm and is not associated with the nuclear membrane. Virus-coded proteins (DNA polymerase, 72 KDa DNA-binding protein, 55 kDa terminal protein) as well as cellular factors (including a topoisomerase) are required. Replicating viral DNA is usually first detected at about 6–8 h p.i. DNA synthesis proceeds by a semiconservative strand-displacement mechanism and reaches its maximum level about 19 h p.i. Approximately 10^5–10^6 progeny viral genomes are produced by 24 h, but only about 20% are packaged into virus particles. Replication of cellular DNA is heavily reduced during adenovirus infection (Kelly, 1984).

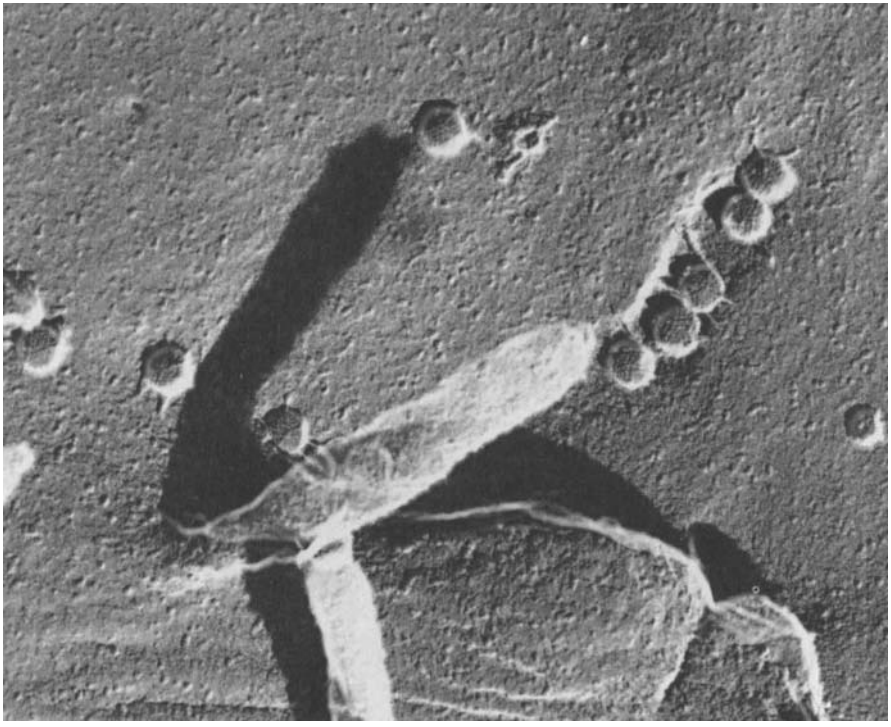

Fig. 23.8. Surface replica of HeLa cell with Ad5 particles attached (4 min at 37°C). Fibres are visible in several cases. Critical-point-dried. ×65 000.

Adenovirus structural proteins are synthesized in the cytoplasm and rapidly transported to the nucleus. Empty capsids are formed from 'groups of nine hexons' by a process of self-assembly. The core proteins and viral DNA are inserted into the preformed capsid (assembly intermediates). The next stage in the maturation process yields the so-called 'young' virions, with a structure morphologically identical to that of mature virions but with precursor proteins IIIa, VI, VII, VIII. Proteolytic cleavage of these proteins completes the assembly process (see Philipson, 1983, 1984, for details). DNA replication and assembly of virus-coded proteins are carried out in the nucleus. Surplus capsomer proteins are often found in paracrystalline arrays in the cell (Fig. 23.9e). Virions are released slowly after the death of the cell.

Pathogenicity. Adenoviruses cause mainly respiratory or enteric diseases, but they also cause eye infections in man, hepatitis in dogs and fowl, a drop in egg production in fowl, etc. There are at least 33 human pathogenic strains, 24 pathogenic strains in primates, and more than 10 pathogenic strains in birds (Wigand et al., 1982). Several adenovirus species have a capacity to transform cell cultures (Table 23.4).

23.6. Aviadenovirus

Avian adenoviruses differ in the following features from mammalian adenoviruses. The buoyant density of virus particles is 1.35 g/cm^3 (in CsCl). The virion contains 17% DNA (M_r 30 × 10^6) and the penton has two fibres (about 10 nm and 40 nm long) attached to each penton base (Fig. 23.1). In CELO (chick embryo lethal orphan) virus 14 structural proteins have been reported whose molecular weights are rather different from those of human adenoviruses.

CELO virus capsid only rarely dissociates into GONs, and antibodies against avian adenoviruses do not react with the hexon group- (genus) specific antigen of mastadenoviruses. An alternative proposal for the avian adenovirus core organization has been proposed by Li et al. (1984).

Acknowledgements

The author's thanks are due to Drs. W.C. Russell and K. Quade for comments on the manuscript and to Drs. J.S. Flint and B. Jacrot for providing experimental data before publication.

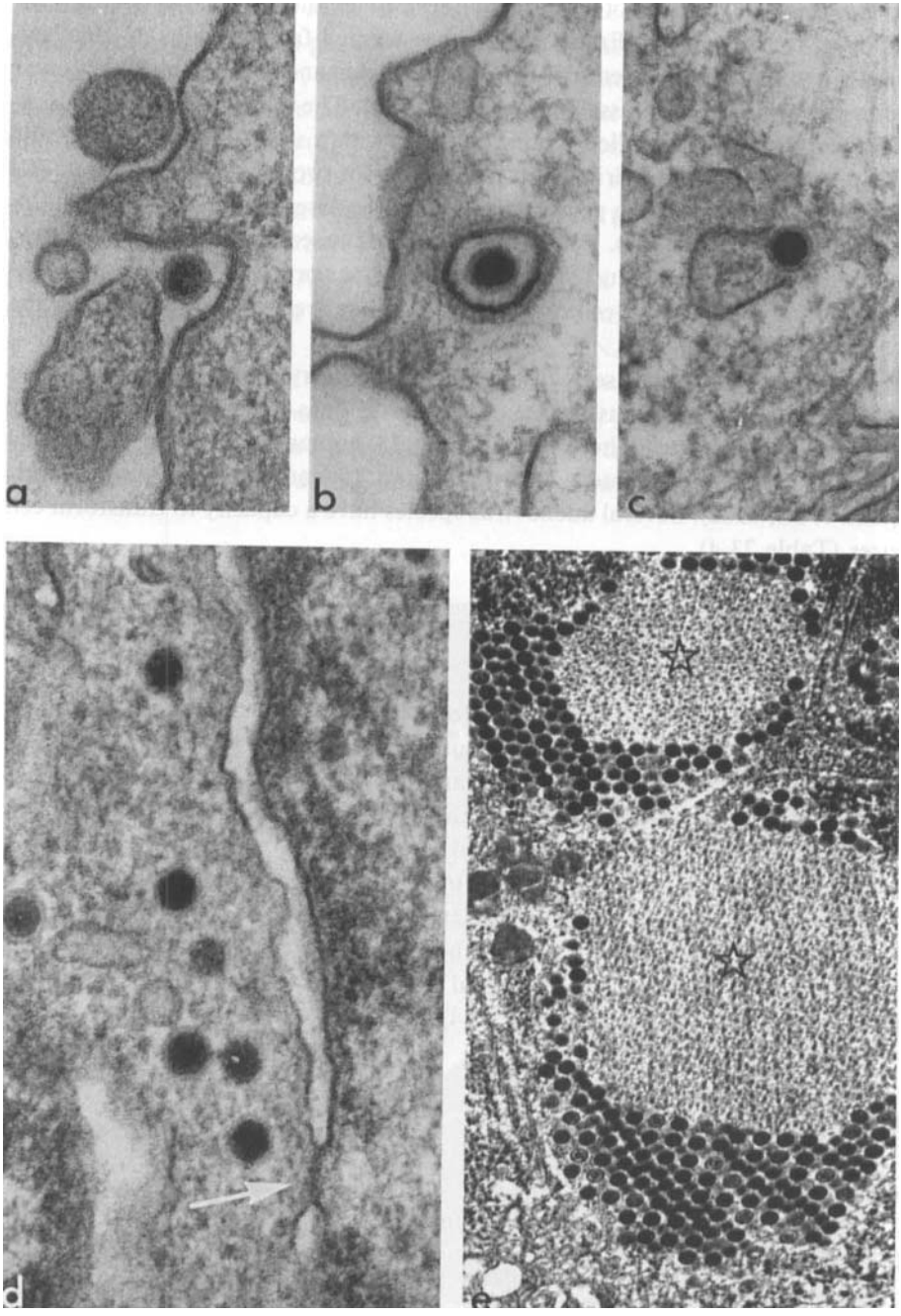
a
b
c
d
e

Suggested reading

Akusjärvi, G., Aleström, P., Petterson, M., Lager, M., Jörnvall, H. and Pettersson, U. (1984) The gene for the adenovirus 2 hexon polypeptide. J. Biol. Chem. 259, 13976–13979.

Brown, D.T., Westphal, M., Burlingham, B.T., Winterhof, U. and Doerfler, W. (1975) Structure and composition of adenovirus type 2 core. J. Virol. 16, 366–387.

Burnett, R.M. (1984) Structural investigations of hexon, the major coat protein of adenovirus. In Biological Macromolecules and Assemblies, Eds. F.A. Jurnak and A. McPherson; Vol. 1, pp. 337–385. John Wiley & Sons, New York.

Burnett, R.M. (1985) The structure of the adenovirus capsid. II. The packing symmetry of hexon and its implications for viral architecture. J. Mol. Biol. 185, 125–143.

Chatterjee, P.K., Vayda, M.E. and Flint, S.J. (1986) Identification of proteins and protein domains that contact DNA within adenovirus nucleoprotein cores by ultraviolet light crosslinking of oligonucleotides ^{32}P labelled in vivo. J. Mol. Biol. 188, 23–37.

Flint, S.J. (1980) Structure and genomic organisation of adenoviruses. In DNA Tumor Viruses, Molecular Biology of Tumor Viruses, Ed. J. Tooze; 2nd Edn., Part 2., pp. 383–442.

Ginsberg, H.S. (1979) Adenovirus structural proteins. In Comprehensive Virology, Eds. H. Fraenkel-Conrat and R.R. Wagner; Vol. 13, pp. 409–457. Plenum, New York and London.

Green, N.M., Wrigley, N.G., Russell, W.C., Martin, S.R. and McLachlan, A.D. (1983) Evidence for a repeating cross-beta sheet structure in the adenovirus fibre. EMBO J. 2, 1357–1363.

Howe, C., Coward, J.E. and Fenger, T.W. (1981) Viral Invasion. In Comprehensive Virology, Eds. H. Fraenkel-Conrat and R. Wagner; Vol. 16, pp. 1–72. Plenum Press, New York and London.

Kelly, T.J. (1984) Adenovirus DNA replication. In The Adenovirus Ed. H.S. Ginsberg; pp. 271–308. Plenum Press, New York and London.

Li, P., Bellett, A.J.D. and Parish, C.R. (1984) Structural organization and polypeptide composition of the avian adenovirus core. J. Virol. 52, 638–649.

Nermut, M.V. (1975) Fine structure of adenovirus type 5. Virology 65, 480–495.

Nermut, M.V. (1980) The architecture of adenoviruses: recent views and problems. Arch. Virol. 64, 175–196.

Nermut, M.V. (1984) The architecture of adenoviruses. In The Adenoviruses, pp. 5–34. Ed. H.S. Ginsberg; Plenum Press, New York and London.

Newcomb, W.W., Boring, J.W. and Brown, J.C. (1984) Ion etching of human adenovirus 2. Structure of the core. J. Virol. 51, 52–56.

Van Oostrum, J. and Burnett, R.M. (1985) Molecular composition of the adenovirus type 2 virion. J. Virol. 56, 439–448.

Pettersson, U. (1984) Structural and nonstructural adenovirus proteins. In The Adenoviruses, pp. 205–270. Ed. H.S. Ginsberg; Plenum Press, New York and London.

Philipson, L. (1983) Structure and assembly of adenoviruses. In The Molecular Biology of Adenoviruses 1, Ed. W. Doerfler; Curr. Topics Microbiol. Immunol. Vol. 109, pp. 1–52. Springer Verlag, Berlin, Heidelberg.

Fig. 23.9. Ultrathin sections of cells at different stages of infection with Ad5. (a) Virus particle attached to a coated pit (8 min p.i.) $\times$ 100 000. (b) Virus particle within a coated vesicle (8 min p.i.), $\times$ 100 000. (c) Virus particle leaving endosome (10 min p.i.) $\times$ 100 000. (d) 30 min p.i. most virus particles are found close to nucleus. They look morphologically intact even when close to nuclear pore (arrow). $\times$ 100 000. (e) 42 h p.i. cells are normally packed with 'crystals' of virus particles or excess capsid antigens (*) $\times$ 25 000.

Philipson, L. (1984) Adenovirus assembly. In The Adenoviruses, Ed. H.S. Ginsberg; pp. 309-337. Plenum Press, New York and London.

Roberts, M.M., White, J.L., Grütter, M.G. and Burnett, R.M. (1986) Three-dimensional structure of the adenovirus major coat protein hexon. Science 232, 1148-1151.

Svensson, U. and Persson, R. (1984) Entry of adenovirus 2 into HeLa cells. J. Virol. 51, 687-694.

Torbet, J. (1983) Internal structural anisotropy of spherical viruses studied with magnetic birefringence. EMBO J. 2, 63-66.

Valentine, R.C. and Pereira, H.G. (1965) Antigens and structure of the adenovirus. J. Mol. Biol. 13, 13-20.

Vayda, M.E., Leong, K. and Flint, S.J. (1983) The structure of nucleoprotein cores released from adenoviruses. Nucleic Acids Res. 11, 441

Wigand, R., et al. (1982) Adenoviridae: Second report. Intervirology 18, 169-176.

Nermut/Steven (eds) Animal Virus Structure

CHAPTER 24

Herpesviridae

JOHN HAY[1], CHESTER R. ROBERTS[1], WILLIAM T. RUYECHAN[1] and ALASDAIR C. STEVEN[2]

[1]Departments of Microbiology and Biochemistry, F. Edward Hébert School of Medicine, Uniformed Services University of the Health Sciences, Bethesda, MD 20814, U.S.A., and [2]Laboratory of Physical Biology, National Institute of Arthritis, Musculoskeletal and Skin Diseases, National Institutes of Health, Bethesda, MD 20892, U.S.A.

Family: Herpesviridae
Subfamilies:
Alphaherpesvirinae: genera: simplexvirus: example - HSV of man
poikilovirus: example - PRV of pig
varicellavirus: example - VZV of man
Betaherpesvirinae: genera: cytomegalovirus: example - CMV of man
muromegalovirus: example - CMV of mouse
Gammaherpesvirinae: genera: lymphocryptovirus: example - EBV of man
thetalymphocryptovirus: example - MDV of chicken
rhadinovirus: example - HVS of primates

24.1. General characteristics

Genetically amongst the most complex of all viruses, herpesviruses have an envelope surrounding an icosahedral capsid approximately 100 nm in diameter,

Abbreviations: HSV, herpes simplex virus; EBV, Epstein Barr virus; VZV, varicella zoster virus; PRV, pseudorabies virus; HVS, herpesvirus saimiri; CCV, channel catfish virus; CMV, cytomegalovirus; MDV, Marek's Disease virus; LHV, Lucké herpesvirus of frogs; EHV-1, equine herpesvirus type 1.

which contains the dsDNA genome. The family herpesviridae contains about 50 members covering a wide range of host systems. The family has been divided into three sub-families, the alphaherpesvirinae (rapidly growing, cytolytic), the betaherpesvirinae (slowly growing, cytomegalic) and the gammaherpesvirinae (lymphocyte-associated). The pathogenesis of herpesvirus infections covers a wide variety of phenomena, from lytic infection through persistent infection to latent infection (with recurrences). Several members of the family have been shown to cause or to be implicated in tumor formation in man and other animals.

24.2. Physical and chemical characteristics

The herpesviruses are large, DNA-containing viruses with an icosahedral nucleocapsid and a loosely-fitting envelope derived (uniquely amongst virus families) from the cell's nuclear membrane (Fig. 24.1A and B). Virions are usually 150–200 nm in diameter, but may appear even larger, depending on the virus and on its mode of preparation for electron microscopy. Some physical and chemical properties are listed in Table 24.1.

24.3. Architecture of the virion

The virion has four main structural components: envelope, capsid, DNA-protein complex (core) and tegument (Fig. 24.1A).

(a) Envelope

The structural appearance of the viral envelope seems to be quite variable in negatively stained preparations, as is its size, and it has the basic morphological features of a normal cell's nuclear membrane (Fig. 24.2). The envelope is typically triple-layered in sections and floppy and has small spikes about 10 nm long spaced 5 nm apart on its surface; it is also rather fragile and can easily be damaged by chemical action or physical stress.

(b) Capsid

The capsid structures of all herpesviruses appear to be morphologically similar, although there is significant variability among their major capsid proteins in such respects as molecular weight (in the range $140–160 \times 10^3$; see below). Accordingly, the following account of the HSV capsid structure will be assumed to be applicable to other members of the family in general terms. The herpes virus capsid (about 100 nm in diameter) is an icosahedron of triangulation number $T = 16$, with 150 hexavalent and 12 pentavalent capsomers. The distinctive configuration of capsomers to which this structure corresponds (Fig. 24.4c) is discernible in electron

TABLE 24.1.

Chemical and physical properties of herpesviruses

Diameter (nm)	120–250 (virion); 100–110 (capsid)			
Symmetry of capsid	Icosahedral			
Triangulation number	$T = 16$			
Number of capsomers	162			
DNA	Double-stranded, linear, 32–75% G + C, 80–150 MDa (120–225 kbp)			
Carbohydrate	Linked to envelope proteins; exact amount unknown			
Lipid	Located in envelope; amount probably variable			
Virion mass[a]	approximately 1450 MDa (HSV-1)			
Density in CsCl	1.20–1.29 g/cm^3 (virion)			
Proteins:	M_r ($\times 10^{-3}$)	Copies/Virion[d]		Function/Designation
Nucleocapsid:	155	790[b]	970[c]	Major capsid, VP5
	50– 55	780	860	DNA binding, VP19c
	42	–	260	?
	40	1430	2560	DNA encapsidation Virion maturation, VP22
	33– 34	1670	1420	?
	26	ND	ND	?
	12	ND	ND	?
Envelope:	129	572	ND	Syncytium formation? gC
	126	437	ND	Infectivity, syncytium formation, gB
	119	388	ND	gA, gB precursor
	86– 88	ND	ND	Fc receptor activity, gE
	60– 65	1649	1280	Major target of neutralizing antibody, gD
Tegument:	>260	184	204	Three distinct polypeptides
	162	62	58	?
	148–149	78	ND	Phosphoprotein
	130	ND	39	?
	100	ND	97	?
	91	ND	272	?
	82	689	ND	?
	80	922	ND	?
	73	446	563	?
	69	ND	ND	Phosphoprotein
	68	ND	ND	?
	65	ND	ND	Trans-activating protein[e]

These data, for HSV-1 and HSV-2, are compiled from the suggested reading list; the other herpesviruses appear to be rather similar.

ND, not done.

[a] The mass value is calculated from a genome mass of 97 MDa, a protein:DNA ratio of 10.7:1 and a lipid molar fraction of 22%.

[b,c] Calculated from autoradiography and Coomassie Blue staining, respectively.

[d] Data from Heine et al. (1974).

[e] Tentatively placed in the tegument; there may be more than one polypeptide at this apparent M_r.

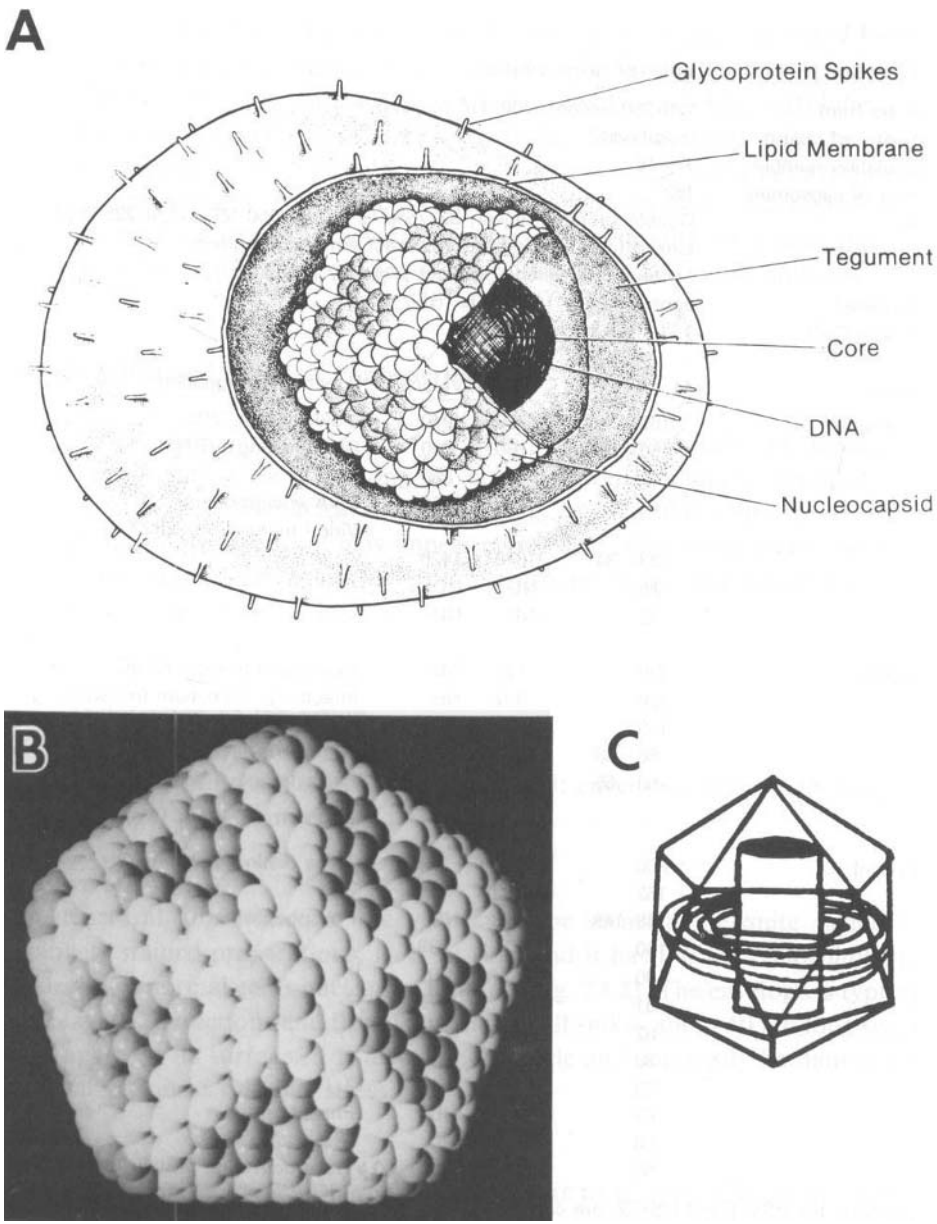

Fig. 24.1. Structural models of the herpesvirus virion and nucleocapsid. (A) A cutaway diagram of a virion showing the individual structural components. (B) A computer-constructed model of the herpes capsid showing capsomers with six-fold symmetry and with (assumed) five-fold symmetry at the vertices. (C) A drawing of the 'toroidal' core model for the herpes capsid. (We are grateful to Dr. R. Feldmann, N.I.H., for assistance with construction of models.)

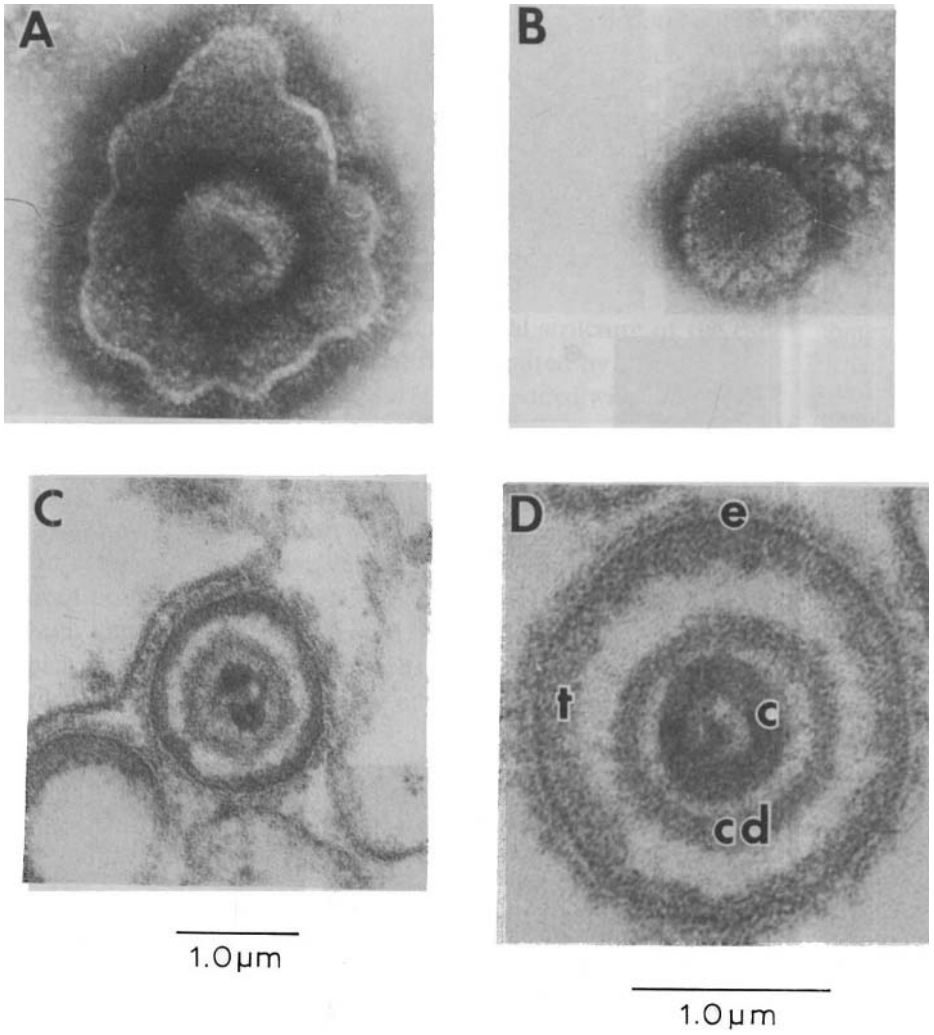

Fig. 24.2. Electron micrographs of a negatively stained VZV virion (A), a full capsid (B) and two examples of thin sections through virions (C and D). In C, the core has been sectioned so that its 'toroidal' appearance is evident. D reveals the four morphological features of the virus: envelope (e), tegument (t), capsid (cd) and core (c). Magnifications: × 160 000 (A, B and C) and × 300 000 (D). (We are grateful to Ms. Sally Hensen, Pediatrics Department, USUHS, for assistance with thin sections.)

micrographs of negatively stained capsids and, most clearly, in partially disrupted particles such as those in Fig. 24.3. However, there has been considerable discussion as to whether the hexavalent capsomers are indeed hexamers. Electron

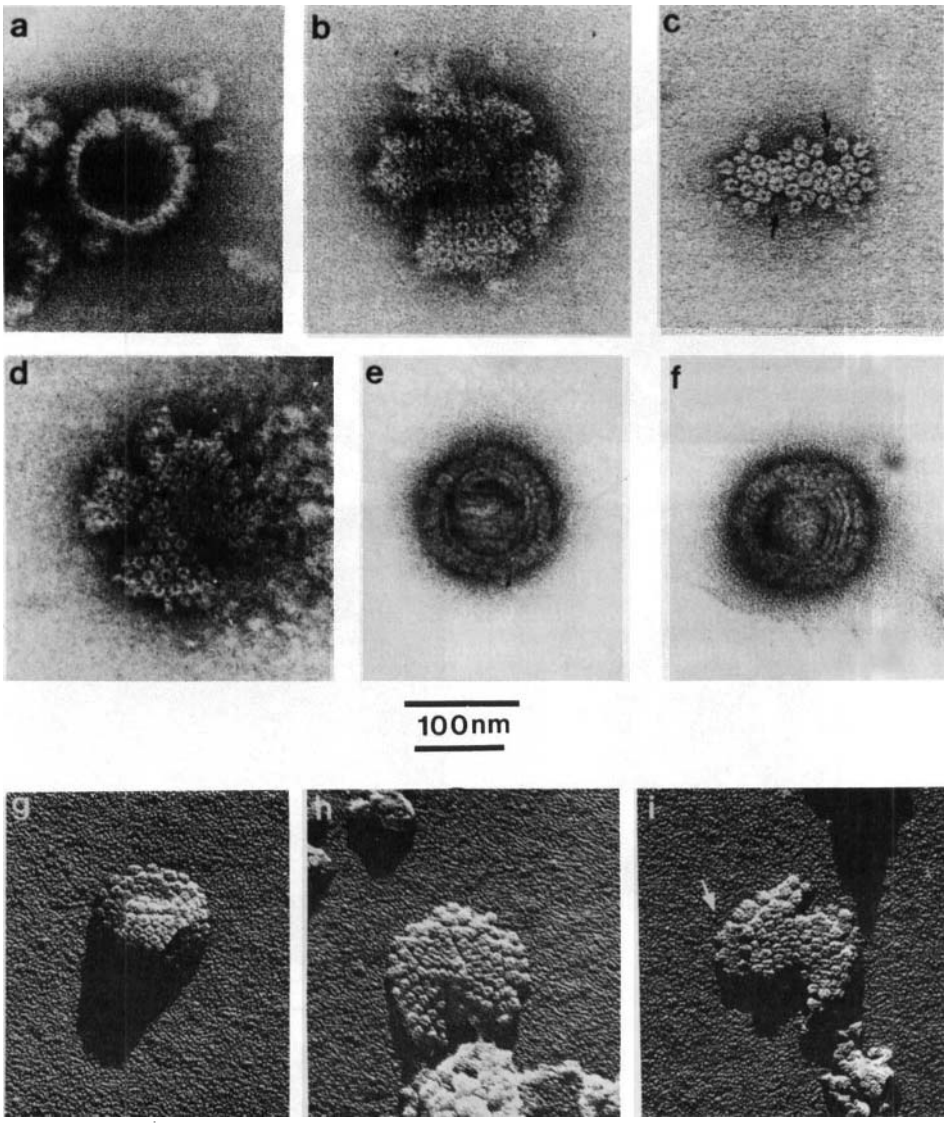

Fig. 24.3. Electron micrographs of HSV-2 (a to d, g to i) and VZV (e and f) nucleocapsids isolated from density gradients of infected cell extracts. In (a) is an intact empty capsid, while (b) and (d) show particles flattened with concomitant splitting along their icosahedral edges, resulting in a 'Maltese cross' morphology; (c) is a fragmented capsid, and arrows indicate probable sites of pentavalent capsomers. The VZV nucleocapsids in (e) and (f) appear to contain coiled core structures that are interpretable in terms of the 'toroidal' model of the HSC core (see text and Fig. 24.1C). Specimens (a) to (f) were negatively stained with uranyl acetate. Panels (g) to (i) show HSV-2 nucleocapsids prepared by freeze-drying and platinum shadowing. Particles in (g) and (h) are viewed along three-fold and five-fold symmetry axes respectively. In (i), the relatively smooth inner surface of the nucleocapsid shell is exposed (arrows) on the underside of this flattened particle. Magnifications: × 150 000 (a–f) and × 125 000 (g–i). (Unpublished data of C. Roberts, J. Hay, M. Bisher, B. Trus and A. Steven.)

microscopic evidence has been interpreted in this way and rotational power spectrum analysis seems to support this conclusion. On the other hand, three-fold symmetry has been inferred from rotational integration studies, implying a trimer, as is the case with adenovirus, another large icosahedral capsid with a non-skew triangulation number. Recent work in our laboratories using computer image averaging to synthesize an optimally averaged image from a number of electron micrographs of fragmented capsids (Fig. 24.4b,d) depicts the hexavalent capsomer as having pronounced six-fold symmetry. This observation strongly supports the proposition that this capsomer is indeed a hexamer, which is consistent with the biochemical data of Heine et al. (1974).

Further insight into the three-dimensional structure of the capsid comes from electron micrographs of nucleocapsids prepared by freeze-drying and shadowing (Fig. 24.3g,h and i). The outer surface is studded with indented protrusions (each a capsomer), whereas the inner surface appears much smoother (Fig. 24.3i). This representation is entirely consistent with the impression given in capsomer side-views seen at the edges of intact negatively stained nucleocapsids of the capsomer as a cylindrical and, at least partially, hollow cone (Fig. 24.3a).

In summary, the hexavalent capsomer is, most likely, a hexamer of the major capsid protein with the form of a cylindrical cone $\approx$ 12 nm in diameter and $\approx$ 14 nm long. It has a deep central indentation $\approx$ 4 nm wide at the outer surface which tapers progressively towards the base of the capsomer (Fig. 24.4c). The structure and molecular identity of the pentavalent capsomers remain obscure.

*(c) DNA-protein complex**

Early electron microscopic observations described the herpesvirus DNA-protein complex (or nucleoid) as a centrally located electron-dense spherical mass with a somewhat variable less-dense centre; the overall diameter was between 30 and 75 nm. Furlong et al. (1972) showed with HSV-1 that this complex could be visualized as a toroidal structure 50 nm high, with an outer diameter of 70 nm and an inner diameter of 18 nm. It contains a centrally located cylindrical structure (see Figs. 24.1C and 2C), which is probably proteinaceous and, in their model, the viral DNA is wound round it in coils of a 4–5-nm-thick strand. Its thickness implies that this strand is unlikely to represent naked DNA, and is most likely a nucleoprotein filament. This model has received experimental support from investigators working with other herpesviruses, and is widely accepted as a general description of the structure. The concentric coil structures have been observed on numerous occasions in negatively stained nucleocapsid preparations in which the stain has penetrated the capsids to reveal their contents (see, for example, the VZV images in Figs. 24.2D and 3e and f). Nevertheless, on the basis of other electron micro-

* Here we use 'DNA-protein complex' (often referred to as 'the core') to designate the structures contained within the capsid.

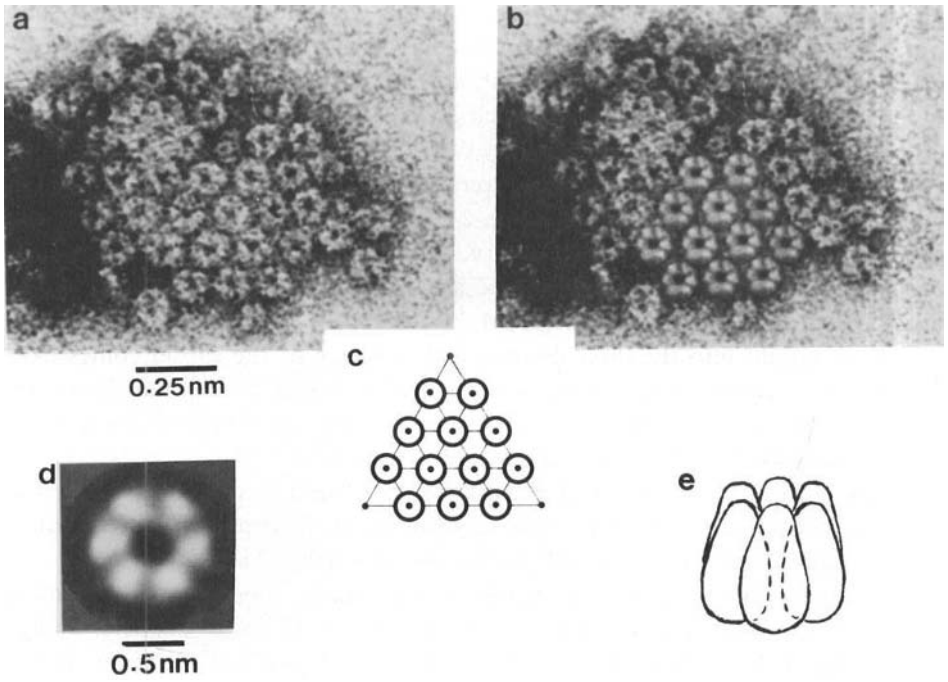

Fig. 24.4. Electron micrographs of a fragment of an HSV-2 nucleocapsid after limited trypsin treatment and negative staining. In (a) is the original micrograph, while in (b) the individual hexavalent capsomers that make up one facet of the disrupted icosahedron have been replaced by processed capsomer images obtained by computer averaging. Distinct six-fold symmetry is evident in the processed image of the hexavalent capsomer. In (c) is a diagrammatic representation of a single facet of the icosahedral ($T = 16$) herpes capsid showing the disposition of the twelve hexavalent capsomers. Magnification: × 400 000. Panel (d) shows a single hexavalent capsomer at higher magnification and (e) is a perspective drawing designed to convey the three-dimensional organization of the capsomer. (We are grateful to Dr. B. Trus, N.I.H., for assistance with computer averaging.)

scopic observations, alternative models have been proposed for herpesvirus DNA-protein complexes, including a 'crossed disc', a 'five sphere' and a 'four cylinder' model. Conceivably, some of the structures imaged may represent different stages in assembly, or they may be breakdown products or aberrant forms.

There is some, as yet inconclusive, evidence that the capsid is assembled first and subsequently filled with DNA. Several viral proteins are associated with the viral DNA (Table 24.1), as is a substantial amount of the polyamine spermidine, but the positioning and functions of these proteins have yet to be characterized.

The organization of the viral genome varies quite substantially among different herpesviruses. The types of DNA structure observed so far are shown in Fig. 24.5, and several general features can be discerned. The DNAs are all linear double-stranded molecules which are probably able to circularize upon infection of a cell. Several viral genomes (e.g. HSV-1 and HSV-2) contain inverted repeat regions

(TR_L, IR_L, IR_S, TR_S) which allow the unique regions of the DNA (U_L, U_S) to invert in orientation; this leads to the existence of four different HSV genome forms. In an analogous fashion, VZV DNA appears to have two principal isomeric forms, resulting from inversion of U_S, although a small repeat at the ends of U_L seems to allow a limited amount of inversion of that region. The function of these repeat regions, other than giving viral genes encoded by them a diploid status, is unknown. Other herpesviruses, such as EBV and HVS, have only one genome form, but may also contain internal complexities such as stretches of short reiterated sequences. The entire sequence of EBV DNA has recently been determined, and large regions of other DNAs have either been sequenced or are about to be.

(d) Tegument

The rather ill-defined structure lying between the capsid and the envelope in herpesviruses has been named the tegument. Specific structural features are difficult to define, but fibrous material is often observed, and the size of this structure varies very much from virus to virus. It is conceivable that the tegument may play the same general role in linking the herpes capsid to the envelope as has been imputed to the 'matrix' proteins of some RNA viruses.

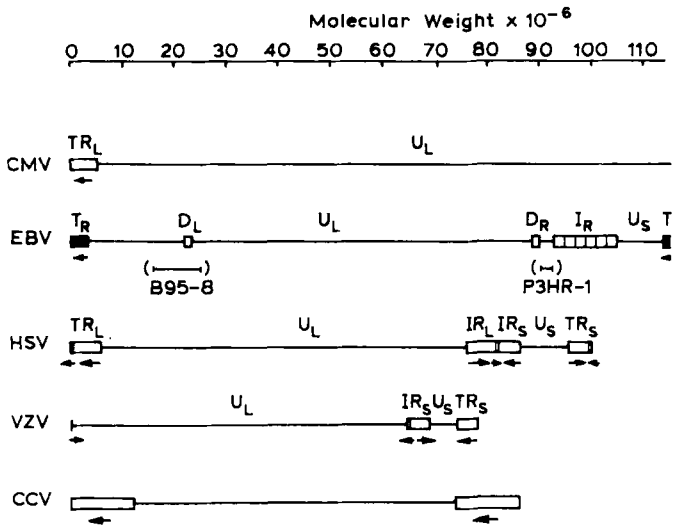

Fig. 24.5. The structures of herpesvirus DNAs. Lines represent unique DNA sequences, while boxes delimit regions of repetitive sequences. Arrows give the polarity of the DNA sequence in a specific region. The notation under the EBV structure shows strain differences; U_L and U_S are unique long and short regions respectively, while IR and TR are internal and terminal repeat regions. There are four HSV and CMV genome forms and two major forms for VZV (see text); all others have only one.

24.4. Locations and functions of proteins present in herpes virions

Analyses of 10 to 12 herpesviruses from both human and non-human sources indicate that 14 to 34 polypeptides are present in intact virus particles. This rather large range could be due to definite differences between individual viruses but it is more likely to be reflective of the sophistication and discriminatory power of the analytical techniques employed in the various studies. A reasonable working number for herpesvirus structural proteins is probably 30–35. The discussion of the proteins present in each of the virion's morphological elements will deal primarily with HSV-1 and HSV-2, as there exists a substantial and detailed body of knowledge concerning the structural polypeptides of these important human pathogens (see Table 24.1). Relevant data on the structural polypeptides of other herpesviruses will be cited when available and appropriate.

(a) Envelope proteins

The lipid components of the envelope of herpesviruses are derived from the host cell's nuclear membrane. In contrast, the protein components of the envelope consist of virus-coded glycoproteins which make up the short, densely packed spikes present on the surface of virions and which are the primary targets of neutralizing antibodies. Four major glycoproteins (gB, gC, gD and gE; see Table 24.1) have been identified and extensively characterized in the HSV-1 system. A previously reported glycoprotein designated gA has been shown to be a precursor of gB. These glycoproteins are unrelated at the polypeptide level, since their genetic loci have been mapped to unique sites on the HSV-1 genome. All, however, contain complex O- and N-linked carbohydrates and at least one (gE) is sulfated.

Extensive work with temperature-sensitive mutants has shown that gB is required for viral infectivity. gB appears to be involved in fusion of the virus envelope with the plasma membrane as well as in the fusion of infected cells to form giant, multinucleated syncytia.

In contrast to gB, glycoprotein gC does not seem to be required either for viral infectivity or for virion morphogenesis, but it is believed to be involved in fusion of infected cells, since some mutants which do not produce gC promote syncytium formation. This view is clouded, however, by the fact that syncytium-promoting strains which do produce gC have also been described; the true role of gC remains a mystery.

Recently, a gC-related protein (called gC-2 or gF) present in HSV-2-infected cells and virions has been characterized which has 75% DNA homology with HSV-1 gC (gC-1). A glycoprotein with a molecular weight similar to that of HSV-1 gC has been described in the HSV-2 system; it is not antigenically related to gC-1, has recently been mapped to the U_S region of HSV-2 and is designated gG. The function of this polypeptide is unknown.

The roles of the two remaining glycoproteins, gD and gE, are even less well

understood. gE contains an Fc binding activity and it has been speculated that this glycoprotein may bind to some cell surface protein whose structure is similar or related to that of IgG-Fc. Such an interaction would presumably enhance the efficiency of adsorption of the virus. No specific function or activity has been assigned to gD. However, a relatively large amount of neutralizing antibody to gD is produced during infection, suggesting that this polypeptide is accessible for interaction with polypeptides in the infected cell.

(b) Capsid and internal proteins

Particles consisting of capsids containing DNA-protein complexes (nucleocapsids)* can be obtained either by treatment of purified virions with detergents and/or lipid solvents, or direct detergent extraction from infected cells. SDS gel electrophoresis studies have shown that nucleocapsids of HSV-1 and HSV-2 contain 5–8 polypeptides ranging in molecular mass from 155 to 12 kDa. The 155 kDa species is the major capsid protein, and proteins of similar molecular mass have been identified as major capsid proteins in VZV, EBV, CMV and in a variety of non-human herpesvirus systems. The major capsid proteins of different herpesviruses also share wide-ranging antigenic relationships. Antisera against HSV-1 nucleocapsids react strongly with HSV-2 nucleocapsids and to some extent with EBV, VZV, CMV, MDV and LHV. Despite these similarities, the major capsid proteins examined thus far all appear to have unique protease fragmentation patterns. There have also been reports that the major capsid proteins of HSV-1, HSV-2 and VZV are capable of interacting with DNA. Whether this property is specific for viral DNA and is utilized in nucleocapsid assembly or whether it simply reflects non-specific charge–charge interactions is not yet clear.

The remaining HSV-1/HSV-2 nucleocapsid proteins are all much smaller, with molecular masses ranging from 50 to 12 kDa. Extensive tryptic and immunological analyses have shown that these polypeptides are unrelated to the major capsid protein. The specific locations and functions of most of these proteins are unknown. However, it has been found that the 50 kDa species (VP19c) is present in both full and empty nucleocapsids, may line the inner capsid surface, and has affinity for dsDNA. It has been suggested that VP19c may be involved in packaging and/or anchoring the viral DNA in the nucleocapsid. Capsid proteins of similar molecular weights have been identified in VZV, human CMV, EBV and EHV-1. It has recently been shown that a VZV 50 kDa nucleocapsid protein also binds to DNA.

The 40–46 kDa species has been designated VP22 and is found only in full capsids. Radioactive labelling studies have shown that VP22 coats the surface of the capsids and inhibits iodination of the major capsid protein (VP5) and VP19c.

* This usage of 'nucleocapsid' is traditional in the herpes literature but is somewhat different from that found in other chapters herein.

VP22 appears to be the mature form of a family of polypeptides present in infected cells, at least some of which are phosphorylated. 'Empty' capsids are rarely enveloped and may sometimes contain short stretches of DNA. This fact, coupled with the finding that viral mutants with temperature-sensitive lesions in the VP22 gene may not encapsidate viral DNA, suggests that VP22 has two functions: (1) it plays a role in encapsidation of viral DNA and (2) it permits the capsid to interact with other macromolecules, leading ultimately to mature, enveloped virions.

(c) Tegument proteins

The twenty or so virion proteins which have not been assigned either to the nucleocapsid or to the envelope are presumably contained in the proteinaceous tegument region physically located between these two structures. In direct contrast to the nucleocapsid and envelope proteins, there is considerable diversity amongst the tegument proteins of different herpesviruses.

One general statement that can be made about herpesvirus tegument proteins, however, is that basic phosphoproteins make up one of the subclasses. At least four basic phosphoproteins (149–68 kDa) have been identified as tegument proteins in the HSV-1/HSV-2 system. Higher molecular mass phosphoproteins (175, 150 and 118 kDa) have been identified in VZV, human and simian CMV virions respectively. The 175 kDa protein definitely binds DNA, while the CMV proteins have been described as basic and, hence, should be capable of interacting with the negatively charged sugar-phosphate backbone of DNA.

Two enzymatic activities have been associated with HSV-1 tegument/capsid structures. These are an Mg^{2+}-dependent protein kinase and an ATPase. Both activities are enhanced following detergent disruption of virions. The protein kinase specifically phosphorylates virion components even in the presence of exogenous proteins although it is not clear whether this specificity is due to substrate recognition or simply to limited accessibility of the kinase. It is also not clear whether these two activities are in fact specified by the virus. Recently, an Mg^{2+}-dependent protein kinase has been observed in detergent-disrupted VZV virions which has different biochemical properties from that of the HSV-1 activity.

In summary, the nucleocapsid and envelope proteins of a number of herpesviruses have been identified and catalogued. While there are striking superficial similarities between the proteins present in various herpesvirus systems, only the HSV-1/HSV-2 proteins have been extensively characterized with regard to location and function and, even in these cases, the ascertaining of the function of specific proteins has been difficult and, so far, incomplete.

24.5. Antigenic properties

Despite the common morphological features of herpesvirus particles, no herpesvirus common antigen has been identified so far. There is also considerable anti-

genic diversity even among viruses with quite similar biological properties. In the human herpesviruses, for example, HSV-1 and HSV-2 share many antigenic properties, but CMV, EBV and VZV seem much more distant from each other and from HSV. In HSV, infected individuals appear to produce neutralizing antibodies chiefly against gD, and, to some extent, against other glycoproteins. In addition, antibodies against gD, gC, gE and gB will all neutralize HSV infectivity. Anti-gD antisera contain both type-specific and type-common antibodies and neutralize in the presence and absence of complement. Antibodies to gC are mainly type-specific and also neutralize in the presence and absence of complement. Antibodies to gE (the Fc surface receptor) neutralize only in the presence of complement, while those against gB (both type-common and type-specific) do not require complement for neutralization. It seems likely that structural proteins other than these glycoproteins will also turn out to be involved in virus neutralization.

24.6. Virus–cell interactions

The envelope seems to be essential for normal herpesvirus infectivity, although purified, intact herpesvirus DNA molecules are infectious in various cell lines. The viral glycoproteins in the envelope appear to play a central role in successful recognition of a cell to be infected. Virus enters cells either by fusion of the viral envelope with the plasma membrane or by endocytosis. At present, the former mechanism seems likely to be the more relevant to successful infection, but both pathways have been reported. Virus in phagocytotic vesicles appears to be degraded. Capsids entering the cell via fusion seem to migrate rapidly across the cytoplasm to the nuclear membrane through which the nucleoprotein complex must be transported to initiate viral DNA transcription in the nucleus.

The process of envelopment of progeny capsids takes place either by budding through specific areas of the nuclear membrane (where viral glycoproteins have been inserted) or by association with invaginations of the membrane in the nucleoplasm. Envelopment may also take place via budding into cytoplasmic vacuoles. Involvement of all these processes can be inferred from electron microscopic observations but it is not yet clear which represent(s) the normal mechanism. Other cellular membranes (e.g. the plasma membrane) may also become associated with viral glycoproteins during infection.

Virus multiplication

Transcription from herpesvirus DNA takes place in three general phases (α, β and γ, or immediate early, early and late). This phased transcription is catalysed in the nucleus by host RNA polymerase activity and is self-controlled in an interlocking

cascade mechanism in which, for example, an α product switches on β transcription. Immediate early proteins are DNA-binding proteins which, among other things, play a role in the control of subsequent gene expression; early proteins probably have the same role at least in part, but also have functions necessary for viral DNA replication such as DNA polymerase activity, a major DNA-binding protein etc. In the main, late proteins seem to be structural but a few structural proteins seem to be made early (before DNA synthesis). Viral DNA is probably replicated by a 'rolling circle' type mechanism and two origins of DNA synthesis have been described. Because of the relatively independent (vis-à-vis the cell) mode of DNA replication, it has been possible to develop successful antiviral agents which inhibit viral but not cellular DNA synthesis.

Acknowledgements

This work was supported by grants No. AI 18449 from the National Institutes of Health (W.T.R. and J.H.) and No. CO7311 from the Uniformed Services University of the Health Sciences (J.H.). The opinions or assertions contained herein are the private ones of the authors and should not be construed as official or reflecting the views of the Department of Defense or of the Uniformed Services University of the Health Sciences.

Suggested reading

Virus structure

Furlong, D., Swift, H. and Roizman, B. (1972) Arrangement of herpesvirus DNA in the core. J. Virol. 10, 1071.

Honess, R.W. (1984) Herpes Simplex and 'The Herpes Complex': Diverse observations and a unifying hypothesis. J. Gen. Virol. 65, 2077.

Nii, S. and Yashuda, I. (1975) Detection of viral cores having toroid structures in eight herpesviruses. Biken J. 18, 41.

O'Callaghan, D.J. and Randall, C.C. (1976) Molecular anatomy of herpesviruses: recent studies. Prog. Med. Virol. 22, 152.

Roizman, B. (1982) The family herpesviridae: general description, taxonomy and classification. In The Herpesviruses, Vol. 1, Ed. B. Roizman; pp. 1–23. Plenum Press, New York.

Spear, P.G. (1980) Composition and organisation of herpesvirus virions and properties of some of the structural proteins. In Oncogenic Herpesviruses, Vol. 1, Ed. F. Rapp; pp. 54–78. CRC Press, Boca Raton.

Capsid structure

Almeida, J., Lang, D. and Talbot, P. (1978) Herpesvirus morphology: visualisation of a structural subunit. Intervirology 10, 318.

Furlong, D. (1978) Direct evidence for 6-fold symmetry of the herpesvirus hexon capsomer. Proc. Natl. Acad. Sci. USA 75, 2764.

Palmer, E.L., Martin, M. and Gary, G.W. (1975) The ultrastructure of disrupted herpesvirus nucleocapsids. Virology 65, 260.

Steven, A.C., Roberts, C.R., Hay, J., Bisher, M., Pun, T. and Trus, B. (1986) The hexavalent capsomers of herpes simplex virus type 2: symmetry, shape, dimensions and oligomeric status. J. Virol., in the press.

Vernon, S.K., Lawrence, W.C. and Cohen, G.H. (1974) Morphological components of herpesvirus. 1. Intercapsomeric fibrils and the geometry of the capsid. Intervirology 4, 237.

Envelope proteins

Dowbenko, D.J. and Lasky, L.A. (1984) Extensive homology between the herpes simplex virus type 2 glycoprotein F gene and the herpes simplex virus type 1 glycoprotein C gene. J. Virol. 52, 154.

Eberle, R. and Courtney, R.J. (1980) gA and gB glycoproteins of herpes simplex virus type 1: two forms of a single polypeptide. J. Virol. 36, 665.

Johnson, D.C. and Spear, P.G. (1984) O-linked oligosaccharides acquired by herpes simplex virus glycoproteins in the Golgi apparatus. Cell 36, 309.

Manservigi, R., Spear, P.G. and Buchan, A. (1977) Cell fusion by herpes simplex virus is promoted and suppressed by different viral glycoproteins. Proc. Natl. Acad. Sci. USA 74, 3913.

Pizer, L., Cohen, G.H. and Eisenberg, R.J. (1980) Effect of tunicamycin on herpes simplex virus glycoproteins and infectious virus production. J. Virol. 34, 142.

Ruyechan, W.T., Morse, L.S., Knipe, D.M. and Roizman, B. (1979) Molecular genetics of herpes simplex virus. II. Mapping of the major viral glycoproteins and the genetic loci specifying the social behavior of infected cells. J. Virol. 29, 677.

Sarmiento, M., Haffey, M. and Spear, P.G. (1979) Membrane proteins specified by herpes simplex viruses. III. Role of glycoprotein VP7(B2) in virion infectivity. J. Virol. 29, 1149.

Nucleocapsid proteins

Braun, D.K., Batterson, W. and Roizman, B. (1984) Identification and genetic mapping of a herpes simplex virus capsid protein that binds DNA. J. Virol. 50, 645.

Cohen, G.H., Ponce de Leon, M., Diggelman, H., Lawrence, W.C., Vernon, S.K. and Eisenberg, R.J. (1980) Structural analysis of the capsid polypeptides of herpes simplex virus types 1 and 2. J. Virol. 34, 521.

Gibson, W. and Roizman, B. (1974) Proteins specified by herpes simplex virus. X. Staining and radiolabelling properties of B capsid and virion proteins in polyacrylamide gels. J. Virol. 13, 155.

Heine, J.W., Honess, R.W., Cassai, E. and Roizman, B. (1974) Proteins specified by herpes simplex virus. XII. The virion polypeptides of type 1 strains. J. Virol. 14, 640.

Zweig, M., Heilman, C.J. and Hampar, B. (1979) Identification of disulfide linked protein complexes in the nucleocapsids of herpes simplex virus type 2. Virology 94, 442.

This Page Intentionally Left Blank

Nermut/Steven (eds) Animal Virus Structure

CHAPTER 25

Iridoviridae

FRANÇOISE DARCY[1,*] and GÉRARD DEVAUCHELLE[2]

[1] Laboratoire de Virologie et Groupe de Recherches INSERM U 74, Faculté de Médecine, 3 rue Koeberlé, 67000 Strasbourg, France, and [2] Laboratoire de Microbiologie, LA 203 du CNRS, 76130 Mont-Saint-Aignan, France

Family: Iridoviridae
Genus: Iridovirus; species, Chilo iridescent virus (C.I.V., insect iridescent virus type 6)
Genus: Chloriridovirus; species, Mosquito iridescent virus (M.I.V., iridescent virus type 3)
Genus: Ranavirus; species, Frog virus 3 (FV3)
Genus: unnamed; species, Lymphocystis disease virus, flounder isolate (LCDV1)
Genus: unnamed; species, African swine fever virus (ASFV)

25.1. General characteristics

The name 'Iridoviridae' comes from the fact that the purified pellets of some viruses produce a blue (Iridoviruses) or yellow-green (Chloriridoviruses) iridescence. However, this phenomenon is not a general feature throughout the family.

Iridoviridae are large isometric particles with an icosahedral surface shell, a lipid membrane underneath, and a DNA-protein(s) complex. Some members have an (outer) envelope derived from the plasma membrane (Fig. 25.1).

* Present address: Centre d'Immunologie et de Biologie Parasitaire, Unité Mixte INSERM U167 – CNRS 624, Institut Pasteur, 15, rue Camille Guérin, 59019 Lille Cédex, France.

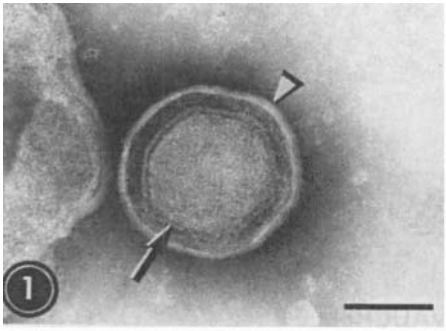

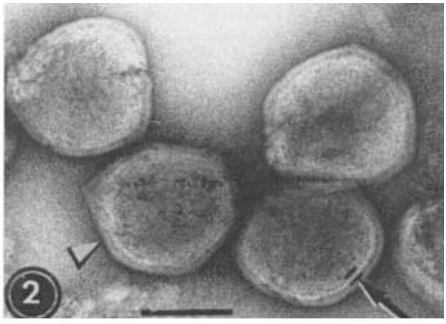

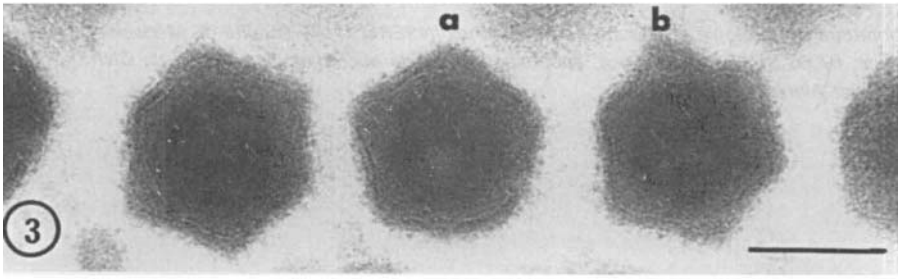
a
b

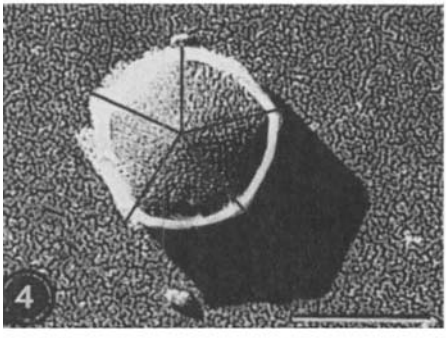

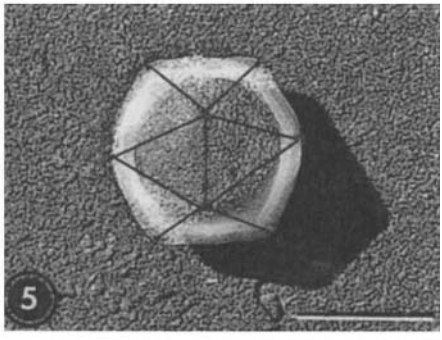

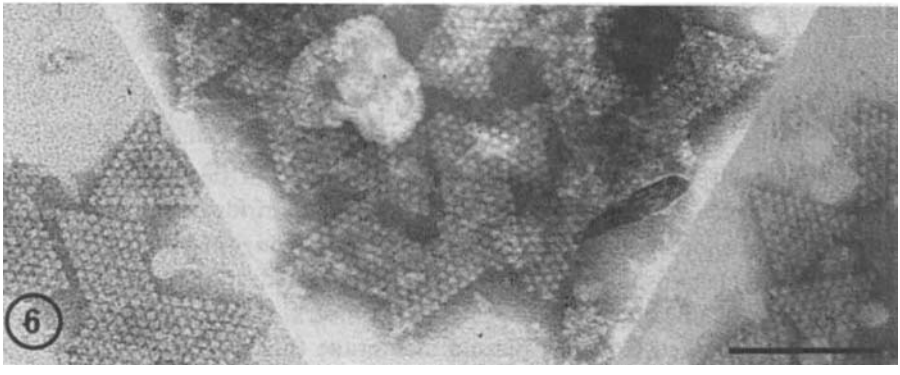

The multiplication cycle, which generally takes place between 26°C and 29°C, is complex, since a nuclear step (cf. virus–cell interactions) is required before virus assembly takes place in the cytoplasm. Iridoviridae do not agglutinate red blood cells and are not oncogenic.

Members of this family have been described in a wide range of vertebrate and invertebrate hosts (mammals, insects, molluscs, fishes, etc...).

Inclusion of ASFV among Iridoviridae raises a major problem. This virus shares some characteristic features (morphology, cytoplasmic assembly) with the other members of this family, but differs from Iridoviridae in biochemical aspects: its genome is not methylated, and has covalently closed ends and terminal repetitions (Ortin et al., 1979); the virion contains several enzymes related to DNA transcription (Kuznar et al., 1980): a DNA-dependent RNA polymerase (whereas other members require host cell RNA polymerase II), RNA capping enzymes, and a poly(A) polymerase which leads to the synthesis of poly(A)-containing mRNAs absent during the replication of other members.

Considering these basic differences between ASFV and the mainstream Iridoviridae we think that ASFV should be left out of this family.

25.2. Physical and chemical characteristics

The molecular masses of irido-virions range from 500×10^6 daltons (FV3) to 2000×10^6 daltons (MIV), their sedimentation coefficients from 1800 S (ASFV) to 4450 S (MIV) and the buoyant densities from 1.16 to 1.35 g/cm^3.

Fig. 25.1. Enveloped FV3 particle after fixation with formaldehyde and negative staining with sodium phosphotungstate. The icosahedral capsid (arrow) can be seen under the envelope (arrowhead). × 120 000. Bars represent 100 nm in all figures, unless otherwise stated.

Fig. 25.2. Naked FV3 particles after fixation with formaldehyde and negative staining with uranyl acetate. Side views of surface subunits can be observed in some areas (arrowhead); the white layer underneath the capsid corresponds to the inner lipid membrane (arrow). × 120 000.

Fig. 25.3. Thin section of Iridovirus type 27 in the cytoplasm of an infected cell of Nereis diversicolor. Pentagonal (a) and hexagonal (b) outlines are characteristic of the icosahedral shape of the capsid. × 180 000.

Figs. 25.4 and 25.5. FV3 prepared by freeze-etching (1 min) and replication after glutaraldehyde and osmium tetroxide fixation. The icosahedral shape is well preserved; viral particles presented here are in five-fold (Fig. 25.4) and two-fold (Fig. 25.5) symmetry orientation. × 180 000.

Fig. 25.6. Disruption of SIV capsids into 'trisymmetrons' after a few weeks storage in distilled water at +4°C. Negatively stained with sodium silicotungstate (courtesy of Dr. N.G. Wrigley). × 200 000.

Chemical composition. Iridoviridae contain 13 to 35 structural polypeptides with molecular weights ranging from 8×10^3 to 200×10^3 (Table 25.1 lists polypeptides of FV3). Most members possess several virion-associated enzymes, particularly a nucleotide triphosphohydrolase and a protein kinase.

Viral particles without (outer) envelopes contain 5–9% lipid, predominantly phospholipids (about 75%). Enveloped viruses have considerably more lipids. No carbohydrates have been detected.

Nucleic acid. The genome is a single molecule of linear dsDNA, M_r 93–250 $\times 10^6$ (FV3 DNA = 100×10^6, 52 μm long) representing 12–30% by weight of the virus particle. G/C content ranges from 20 to 58% (53% for FV3). The genomes of Ranavirus, Lymphocystis disease virus, and at least one Iridovirus species are circularly permuted and terminally redundant; the DNAs of Ranavirus and Lymphocystis disease virus are heavily methylated, whereas DNA of ASFV is not.

TABLE 25.1.

Frog Virus 3 structural polypeptides[a]

M_r	Location	Remarks
140 000	Internal	Phosphorylated[b]
113 000		
105 000		
94 000		
90 000	Internal	Phosphorylated, DNA binding
70 000	Internal	Weakly phosphorylated, DNA binding
63 000	Inner membrane	
58 000	Envelope	
56 000		
48 000	Capsid	Major polypeptide
< 48 000		Phosphorylated, DNA binding
44 000	Inner membrane + small amount in capsid(?)	
40 000	Internal	
31 000		
28 000		DNA binding
27 000		
26 000		DNA binding
24 000		
23 000		Phosphorylated
16 000		
15 000	Internal	DNA binding
12 000		
9 000		

[a]Polypeptide map from Aubertin, A.M., Tondre, L., Martin, J.P. and Kirn, A. (FEBS Lett. 112 (1980) 233–238).

[b]'Phosphorylated' means present as phosphoproteins in the virion.

Antigenic properties
Most major antigens of the Iridoviridae family are related to surface viral polypeptides. Antigenic relationships between some members of Iridovirus and Chloriridovirus genera have been established. Antibodies appear to be non-neutralizing.

Structural characteristics
Iridoviridae are icosahedral in shape: their dimensions vary considerably from one genus to another (Table 25.2).

25.3. Architecture

The Iridovirion consists of three or four 'structural complexes': the envelope (not reported in all Iridoviridae), the capsid (outer isocahedral shell), the inner membrane containing lipids and some proteins, and the DNA-protein(s) complex. In addition, some members of Iridovirus, Chloriridovirus and Lymphocystis disease virus genera possess an external fringe of fibrillar elements of various lengths.
The envelope of some viruses such as MIV, Tipula iridescent virus (TIV) and FV3 is much thicker (about 20 nm for FV3) than the cell membrane from which they have issued, due to the presence of a virus specific inner dense layer (Figs. 25.1 and 25.22). In contrast, the ASFV envelope has the same thickness as the plasma membrane.
The capsid (Figs. 25.2–5) is icosahedral with a skew class of symmetry. The triangulation number (T) of SIV and TIV is probably 147 (= 1472 capsomers), that of FV3 133 (= 1332 capsomers), and that of ASFV, 189 to 217 (= 1892 to 2172 capsomers).

TABLE 25.2.

Dimensions (in nm) of Iridoviridae

Genus	Face to face	Diameter[a]	Vertex to vertex
Iridovirus	130		145
Chloriridovirus	187–230		203–250
Ranavirus	138	165	162
		180–200[b]	
Lymphocystis disease virus group		198–227	
African swine fever virus group	191–203		210–228

[a]In five-fold symmetry orientation (see Darcy-Tripier et al., 1984, for details).
[b]Enveloped particles.

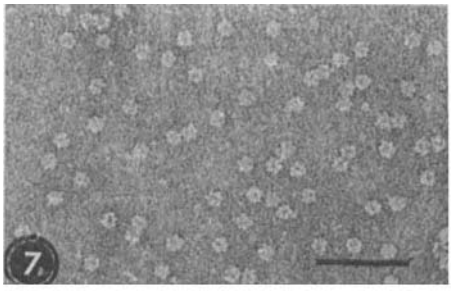
7

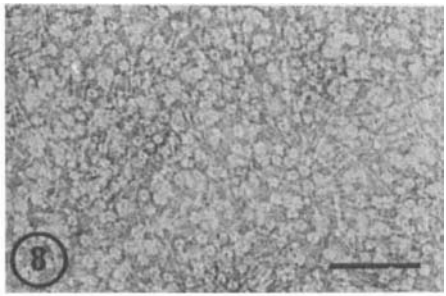
8

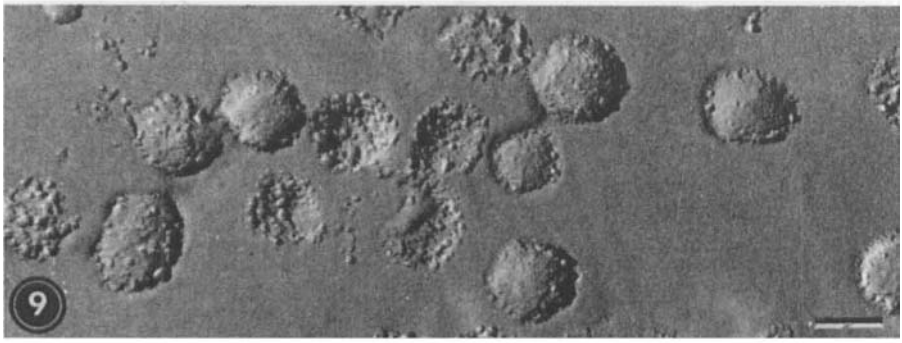
9

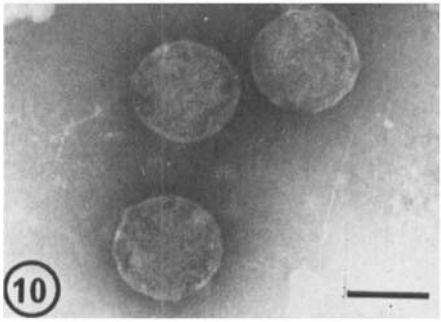
10

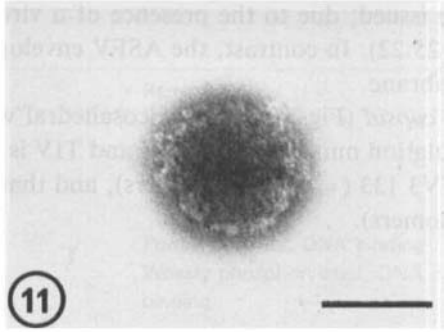
11


12

Several Iridovirus and Chloriridovirus isolates dissociate into triangular and in some cases pentagonal groups of capsomers named respectively tri- and pentasymmetrons (Stoltz, 1973). This kind of dissociation has not been observed in other genera.

Capsomers isolated from some Iridoviruses and FV3 are roughly cylindrical, about 7 nm in diameter and 7–10 nm high, possibly with a central channel (Figs. 25.7 and 25.8). In addition, preparations of capsomers isolated from Iridoviruses contain fibrillar elements (Fig. 25.8). ASFV capsomers are hexagonal prisms 7 nm in diameter and 11–13 nm in length, with a central hole (Carrascosa et al., 1984).

The oligomeric structure of the capsomers has only been studied in some Iridovirus and Ranavirus species. In both cases, the six-coordinated capsomers have been shown to be trimers of an M_r 50000 (CIV) or 48000 (FV3) polypeptide. In the case of CIV, but not FV3, some polypeptides are linked by disulphide bridges. The quaternary structure and number of polypeptides of the five-coordinated capsomers at the vertices of the icosahedron are not known in any Iridoviridae.

The inner membrane is composed of lipids (mainly phospholipids with a high phosphatidylinositol content in the case of CIV) and proteins; it is closely apposed to the inner side of the capsid. Replicas of FV3 and CIV freeze-fractured through this membrane (Fig. 25.9) show the presence of intramembrane particles associated with both leaflets of the lipid bilayer.

On removal of the capsids of FV3 and CIV by mild treatment with pronase, spherical particles bound by this membrane are obtained (Fig. 25.10).

Fig. 25.7. FV3 capsomers released by six cycles of freezing and thawing in the presence of 0.5 M urea. Negative staining with uranyl sulphate. × 250000 (bar represents 50 nm). (Courtesy of Ms. E. Brown.)

Fig. 25.8. CIV capsomers released by freezing and thawing. Negative staining with uranyl acetate. × 230000 (bar represents 50 nm).

Fig. 25.9. Freeze-etching of unfixed FV3. Virus particles are membrane-fractured, with intramembranous particles on both fracture faces (convex and concave). × 90000.

Fig. 25.10. Spherical subviral particles obtained after treatment of FV3 with pronase. Negatively stained with sodium phosphotungstate. × 105000.

Fig. 25.11. FV3 'core' obtained after treatment with Nonidet P40 (0.5%, 37°C, 1 h). Negatively stained with sodium phosphotungstate. × 140000.

Fig. 25.12. Freeze-etching replica of a paracrystalline array of virus particles in chick embryo fibroblasts 22 h after infection with FV3. Cells were fixed with glutaraldehyde and osmium tetroxide before freeze-etching. In cross-fractured virus particles, rod-like (arrows) and round profiles can be seen, presumably two different views of a filamentous structure 10 nm in diameter. × 120000.

The virus interior contains DNA and several proteins (6 DNA-binding proteins in FV3 and CIV). However, no 'core shell' has been demonstrated yet. Neutron scattering has shown that in FV3 the distribution of DNA and protein is approximately uniform without any discontinuity at the periphery indicative of a protein shell; the DNA-protein complex appears to be highly hydrated. 'Cores' prepared by means of detergents are usually rather 'relaxed' with no evidence of a shell (Fig. 25.11). The structures revealed in freeze-fractured virus particles (Fig. 25.12) suggest that the DNA-protein complex forms a convoluted filament. In the case of CIV, a thermodynamic approach suggests that the nucleoprotein complex could be organized in a nucleosome-like fashion (Klump et al., 1983).

A three-dimensional model of FV3 is shown in Fig. 25.13.

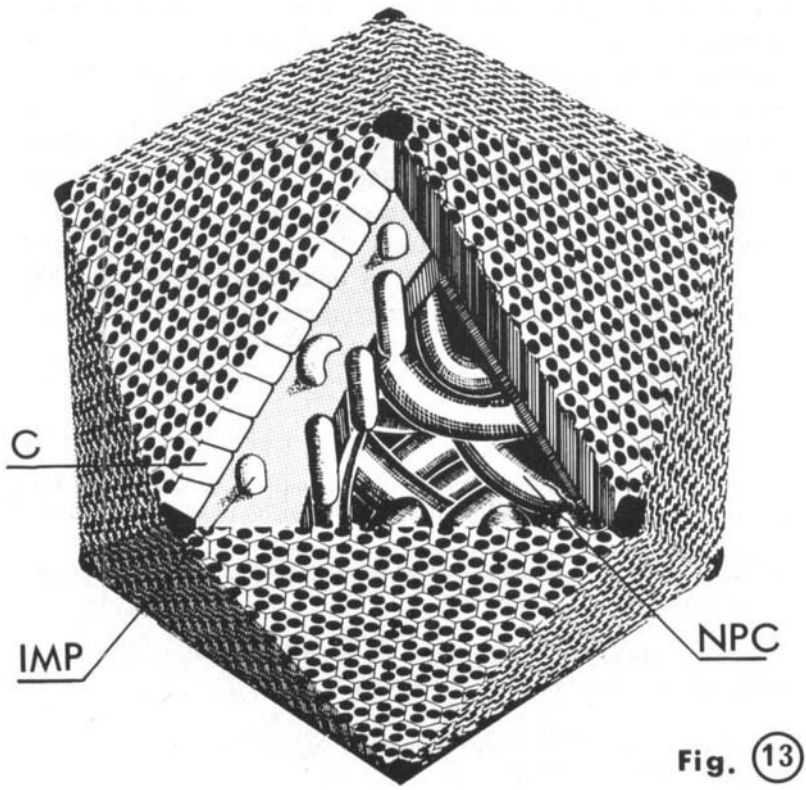

Fig. 25.13. Three-dimensional model of FV3 virion (approximately in scale; dimensions derived from electron micrographs). The capsomers (C) are schematized as trimers arranged on a hexagonal net (corresponding to $T = 133$ skew). One triangular facet of the icosahedron has been removed, revealing the inner membrane with intramembranous particles (IMP) and, underneath, the nucleoprotein complex (NPC) arranged in the form of a convoluted filamentous structure (although this is only one possible organization compatible with the limited structural data presently available). Approximately × 700 000.

25.4. Virus–cell interactions

The predominant mode of entry of Iridoviridae into the host cells is by endocytosis, but viral particles can be observed free in the cytoplasm shortly after infection. For FV3 it has been shown that enveloped viruses are preferentially taken up by adsorptive endocytosis via clathrin-coated pits and vesicles (Fig. 25.16), endosomes and finally lysosomes; only a few naked FV3 particles enter by the same mechanism; the majority of them enter the cell by fusion with the plasma membrane, allowing their nucleoproteic content to be released into the cytoplasm (Fig. 25.17).

DNA synthesis of FV3 occurs in two stages:

(1) During stage 1, which takes place in the nucleus (up to 2 h post-infection), the size of the replicating DNA ranges from genome size to twice genome size.

(2) At stage 2 (only at 3 h or more post-infection), DNA replication takes place in the cytoplasm and the replicating molecules are large concatemers which serve as precursors for the production of mature FV3 DNA.

Iridoviridae assemble in the cytoplasm; in the case of insect Iridoviridae, FLDV and ASFV, the sites of virus assembly are dense virogenic stroma (Fig. 25.18), whereas FV3 'viroplasms' appear as electron-translucent areas devoid of ribosomes and often surrounded by mitochondria (Fig. 25.19). The earliest recognizable viral structures are incomplete icosahedral profiles, then closed electron-lucent 'immature' particles, and finally 'mature' particles with an electron-dense core (Figs. 25.18 and 25.19). Cylindrical aberrant forms, often capped at one or both ends by icosahedral portions, have been reported as morphogenetic products of various Iridoviridae (Figs. 25.14 and 25.15).

Viral particles either migrate to the plasma membrane, where they acquire an envelope during the budding process, or form paracrystalline arrays in the cytoplasm (Figs. 25.20 and 25.21), from which they are released (naked) when cell lysis occurs. At later stages of morphogenesis, in the insects infected by some Iridoviridae, the originally transparent tissues display a blue, purple (Iridoviruses) or yellow-green (Chloriridoviruses) iridescence likely due to the presence of these viral microcrystals in the infected cells.

For most Iridoviridae the process of budding is similar to that reported for FV3, where the plasma membrane appears thickened due to the presence of a dense layer under the unit membrane, on the cytoplasmic side (Fig. 25.22). For other viruses, such as ASFV, budding it not accompanied by morphological modifications of the plasma membrane.

25.5. Pathogenicity

Most members of Iridoviridae family exhibit a severe and early cytotoxic effect by

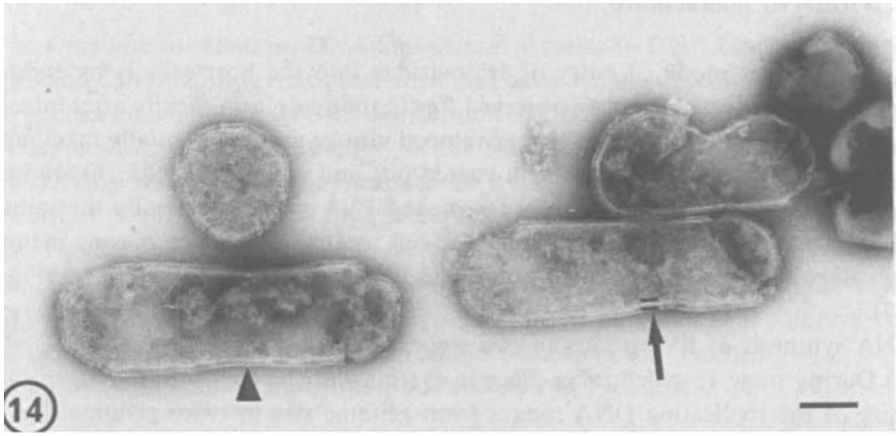

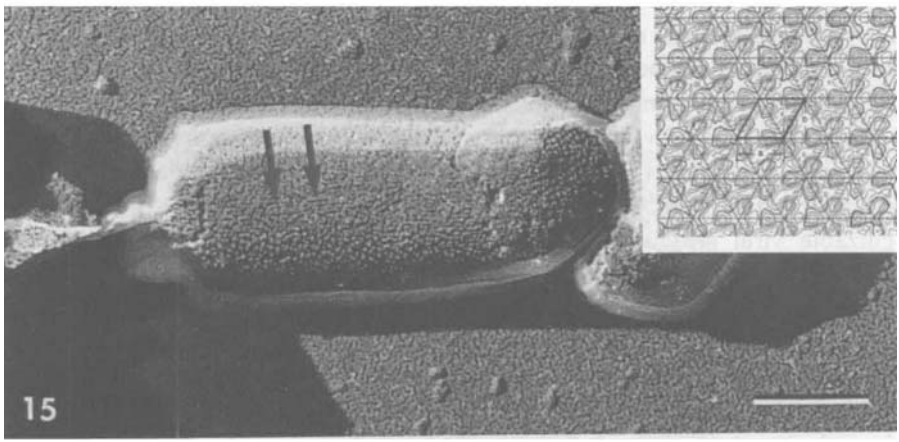

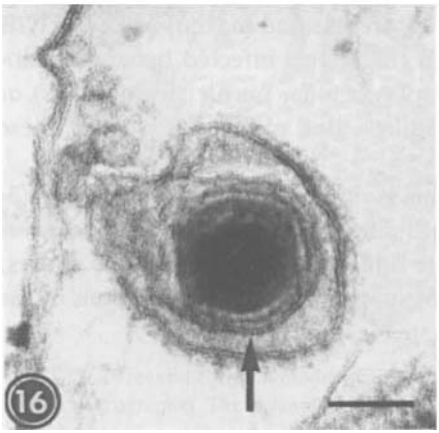

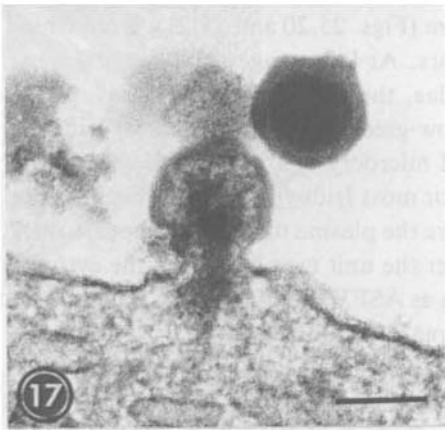

See p. 419 for legend.

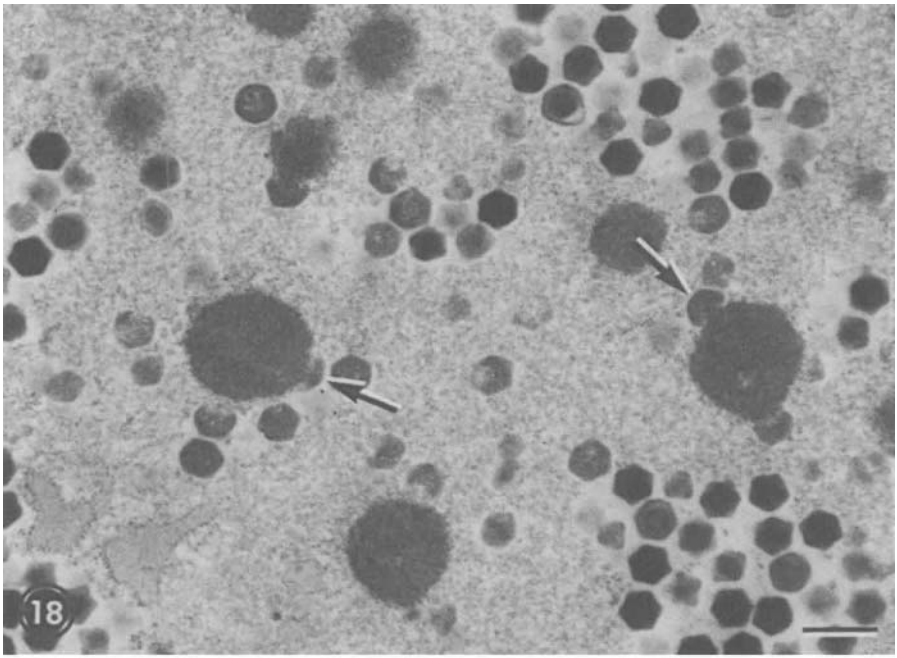

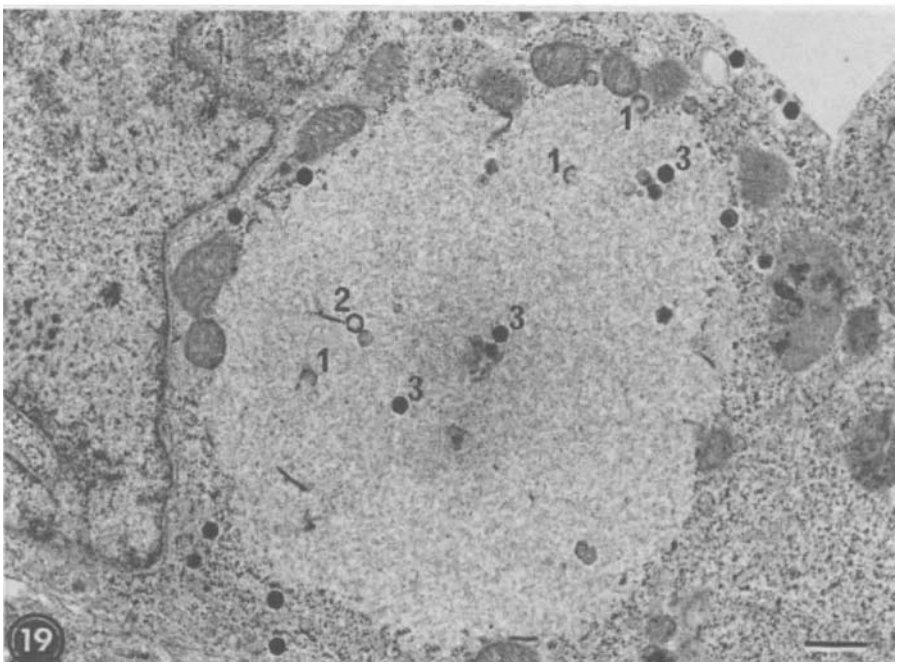

See p. 419 for legend.

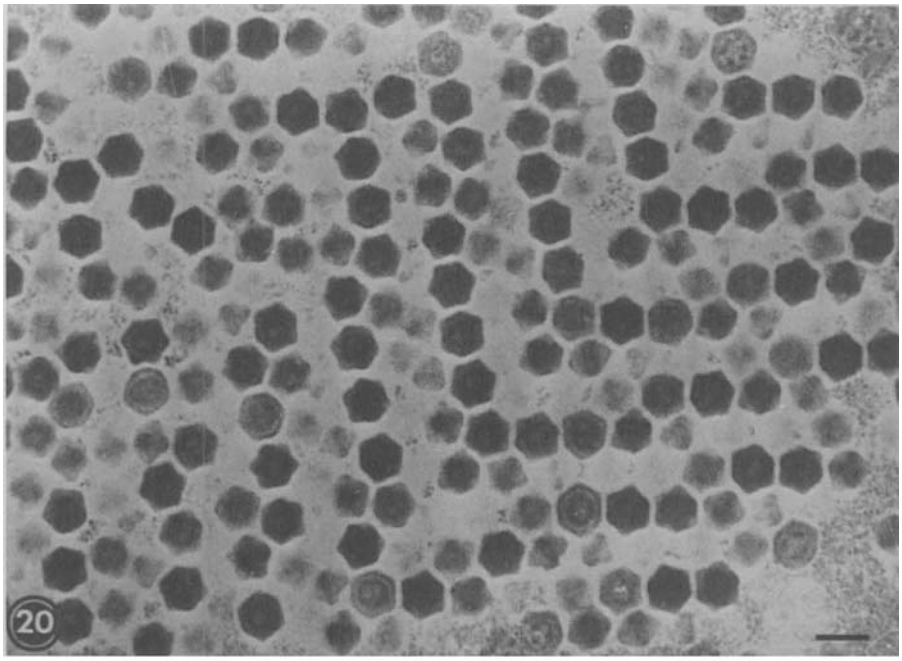
20

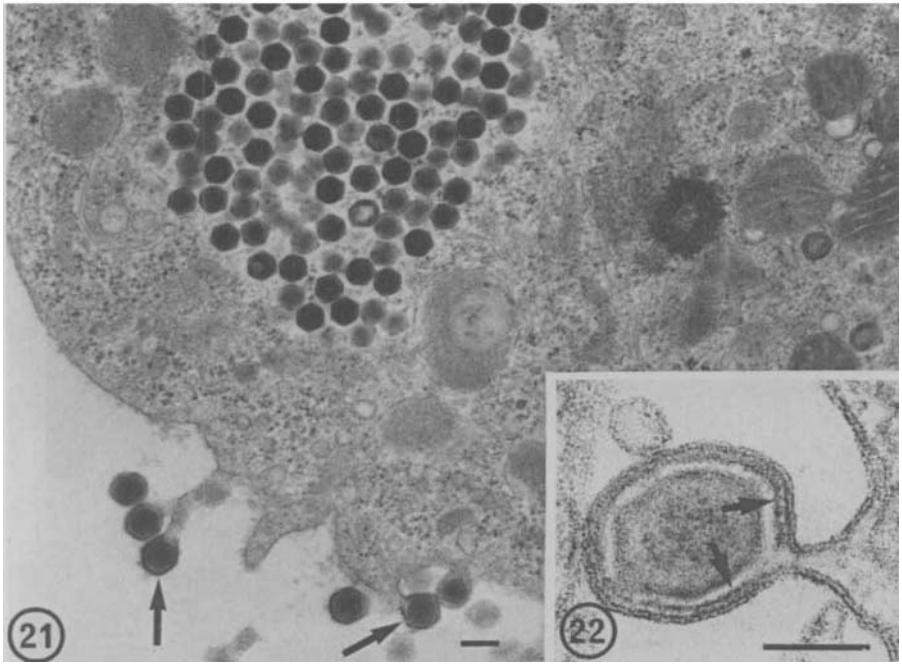
21
22

inhibiting host cell macromolecular syntheses at both the permissive (= 26–29°C) and the non-permissive (= 37°C) temperatures. In addition, CIV inoculation of vertebrate or invertebrate cells rapidly leads to a massive formation of syncytia.

When inoculated into mice, FV3 and CIV (or even viral proteins solubilized from these viruses) produce acute hepatitis which kills the animals within 24–48 hours.

Fig. 25.14. Cylindrical aberrant forms of FV3. Fixed with glutaraldehyde and negatively stained with sodium silicotungstate. Profiles of surface subunits (arrowhead) and of inner membrane (arrow) can be observed in some places. × 72 000.

Fig. 25.15. Freeze-etching of an aberrant form of FV3, displaying parallel 'rows of particles' (arrows). Same preparation as in Figs. 25.4 and 25.5. × 150 000. Inset: Density map of the virus surface showing the trimeric nature of the capsomers.

Fig. 25.16. Thin section through periphery of a BHK21 cell 10 min after infection with enveloped FV3 showing a virus particle in a coated vesicle. Arrow points to virus envelope. × 115 000.

Fig. 25.17. Thin section of a Kupffer cell soon after infection with naked FV3 showing a viral particle fusing with the plasma membrane and shedding its inner dense content into the cytoplasm (courtesy of Dr. J.L. Gendrault). × 115 000.

Fig. 25.18. Thin section of a *Nereis diversicolor* cell infected with Iridovirus type 27: virus particles at different stages of assembly and maturation. Fragments of virus capsids with angular outlines can be observed at the periphery of the virogenic stroma (arrows). × 45 000 (bar represents 200 nm).

Fig. 25.19. Thin section of chick embryo fibroblasts 15 h after infection with FV3. Inside a large viroplasm, less electron-dense than the surrounding cytoplasm, various stages of viral maturation can be observed: partial capsids (1), empty capsids (2) and dense mature viral particles (3). × 15 900 (bar represents 500 nm).

Fig. 25.20. Paracrystalline array of Chilo iridescent virus in the larva of *Galleria melonella*. × 36 000 (bar represents 200 nm).

Fig. 25.21. Thin section of chick embryo fibroblasts 22 h after infection with FV3. Virus particles are found in paracrystalline arrays, or are budding through the plasma membrane (arrows). × 25 000 (bar represents 200 nm).

Fig. 25.22. Detail of a budding FV3 particle demonstrating the continuity of the plasma membrane with the external part of the viral envelope and the presence of a virus-specific inner dense layer (arrows). × 140 000 (bar represents 100 nm).

ASFV infects various species of swine, in which it causes a chronic disease or a peracute febrile disease with mortality approaching 100%. This virus, which can multiply in and be transmitted by ticks, is the only known DNA-containing arthropod-borne virus.

LCDV infects fish, where it causes the formation of giant host connective tissue cells.

Acknowledgements

The authors thank A. Kirn and A.M. Aubertin for fruitful discussion, and M. Valle and G. Reinhardt for photographic work.

Suggested reading

Carrascosa, J.L., Carazo, J.M., Carrascosa, A.L., Garcia, N., Santisteban, A. and Vinuela, E. (1984) General morphology and capsid fine structure of African swine fever virus particles. Virology 132, 160–172.

Darai, G., Anders, E., Koch, H.G., Gelderblom, H., Samalecos, C. and Flügel, R.M. (1983) Analysis of the genome of fish lymphocystis disease virus isolated directly from epidermal tumours of Pleuronectes. Virology 126, 466–479.

Darcy-Tripier, F., Nermut, M.V., Braunwald, J. and Williams, L.D. (1984) The organization of Frog Virus 3 as revealed by freeze-etching. Virology 138, 287–299.

Darcy-Tripier, F., Nermut, M.V., Brown, E., Nonnenmacher, H. and Braunwald, J. (1986) Ultrastructural and biochemical evidence of the trimeric nature of Frog Virus 3 six-coordinated capsomers. Virology 149, 44–54.

Devauchelle, G., Stoltz, D.B. and Darcy-Tripier, F. (1984) Comparative ultrastructure of Iridoviridae. In Iridoviridae, Ed. D. Willis; Curr. Topics Microbiol. Immunol. Vol. 110, pp. 1–21. Springer Verlag, Berlin, Heidelberg, New York.

Goorha, R. and Granoff, A. (1979) Icosahedral cytoplasmic deoxyriboviruses. In Comprehensive Virology, Eds. H. Frankel-Conrat and R.R. Wagner; Vol. 14, pp. 347–399. Plenum Press, New York and London.

Kirn, A., Gut, J.P., Bingen, A. and Steffan, A.M. (1983) Murine hepatitis induced by Frog Virus 3: a model for studying the effect of sinusoidal cell damage on the liver. Hepatology 3, 105–111.

Klump, H., Baumais, J. and Devauchelle, G. (1983) Structural and thermodynamic investigations of the Chilo iridescent virus (Iridovirus type 6). Arch. Virol. 75, 269–276.

Kuznar, J., Salas, M.L. and Vinuela, E. (1980) DNA-dependent RNA polymerase in African swine fever virus. Virology 101, 169–175.

Ortin, J., Enjuanes, L. and Vinuela, E. (1979) Cross-links in African swine fever virus DNA. J. Virol. 31, 579–583.

Stoltz, D.B. (1973) The structure of icosahedral cytoplasmic deoxyriboviruses. II. An alternative model. J. Ultrastruct. Res. 43, 58–74.

Wardley, R.C., Andrade, C., Black, D.N., de Castro-Portugal, F.L., Enjuanes, L., Hess, W.R., Mebus, C., Ordas, A., Rutili, D., Sanchez, Vizcaino, J., Vigario, J.D. and Wilkinson, P.J. (1983) African swine fever virus. Arch. Virol. 76, 73–90.

Nermut/Steven (eds) Animal Virus Structure

CHAPTER 26

Poxviridae

G. MÜLLER[1] and J.D. WILLIAMSON[2]

[1]Bernhard-Nocht-Institut für Schiffs- und Tropenkrankheiten, Bernhard-Nocht-Strasse 74, 2000 Hamburg 4, F.R.G., and [2]Virology Division, Department of Medical Microbiology, St. Mary's Hospital Medical School, London W2 1PG, U.K.

Family: Poxviridae
Genera: Orthopoxvirus (vaccinia, smallpox, cowpox, rabbitpox, monkeypox, ectromelia)
Avipoxvirus (fowlpox, canary pox, pigeon pox)
Capripoxvirus (sheep pox, goat pox, lumpy skin disease)
Leporipoxvirus (myxoma, rabbit fibroma)
Suipoxvirus (swinepox virus)
Parapoxvirus (orf, bovine pustular dermatitis)
Entomopoxvirus (insect poxviruses)
Unclassified – molluscum contagiosum, Tanapox, Yaba virus

Orthopoxvirus species have been classified by immunological methods, polypeptide analysis, nucleic acid hybridization and restriction enzyme analysis. Vaccinia virus has been studied most intensively and will be discussed primarily in this chapter; important differences from other poxviruses will be mentioned where such information is available.

26.1. General characteristics

Poxviruses are widespread in various vertebrate and invertebrate hosts, although insect poxviruses do not appear to infect vertebrates. With the global eradication of smallpox from the human population, most poxvirus infections are now found

in other primates, mammals and avian species. The mature virions are sufficiently large to be visualized by light microscopy but detailed structure is discernible only by electron microscopy. This reveals an almost rectangular shape which is quite unlike the shapes of other animal virus particles. Although poxviruses contain DNA, both DNA replication and virus assembly take place in the cytoplasm of infected cells rather than in the nucleus. Enzymes associated with viral mRNA synthesis are contained in the virus cores and hence a non-genetic process can allow the reactivation of a heat- or urea-inactivated poxvirus by these constitutive enzymes in another co-infecting poxvirus. Other enzymes required for viral DNA synthesis are encoded in the virus genome. Purified orthopoxvirus DNA does not appear to be infectious but its expression can occur in cells which are infected with another poxvirus provided that the virus-specific mechanisms for DNA replication have been established.

26.2. Chemical and physical characteristics

Vaccinia virus was the first animal virus to be purified sufficiently for detailed characterization. The virion has a dry weight of about 5×10^{-15} g ($= 3 \times 10^3$ MDa), a bouyant density of 1.16 g/cm^3 and a sedimentation coefficient of 5000 S. Chemical analysis shows 3.2% DNA, 90% protein and 5% lipid. Similar information is lacking for other poxviruses, apart from fowlpox virus, which differs primarily in an unusually high lipid content of 34% comprised mainly of squalene and cholesterol esters.

The molecular weights of poxvirus genomes range from 85×10^6 for parapoxvirus to 200×10^6 for avipoxviruses. The vaccinia virus genome is a linear molecule of dsDNA with a molecular weight of 123×10^6, corresponding to 185 000 basepairs. Covalent linkages join the two DNA strands at their ends and inverted terminal repeats are also present which, in the vaccinia genome, comprise 10 000 basepairs. Restriction enzyme analysis shows sequence conservation in the central region of all orthopoxvirus genomes but considerable variation exists at the ends of these molecules. Parapoxvirus and avipoxvirus genomes give different restriction fragment patterns.

Virus structural proteins

Numerous studies have been made of the polypeptide profiles of whole poxvirus particles or core preparations obtained by controlled degradation of virions with detergents and 2-mercaptoethanol. The protein composition of the other structural elements of vaccinia virus has been described recently (Ichihashi et al., 1984). A total of 36 different proteins with molecular weights from 110 000 to 13 000 were

resolved by SDS-PAGE. However, some proteins existed as disulphide-linked unit complexes which were dissociated in SDS under reducing conditions only. The relative abundance of such proteins in the core and outer envelope suggests that self-assembly mechanisms, based on intramolecular or intermolecular disulphide bonds, are important in the morphogenesis of poxvirùses. Viral proteins with DNA-binding capacity are present in the core and in the lateral bodies: the locations of these and other protein components of vaccinia virus structural elements are shown in Table 26.1. Extracellular, enveloped virions are known to possess an additional eight proteins and all except one are glycoproteins. Some proteins present in intracellular virions are absent from the extracellular, enveloped virions or present in reduced amounts, although the relative proportion of one protein is increased in the extracellular virus.

Comparative studies on the structural proteins of other orthopoxviruses have shown polypeptides corresponding to those of vaccinia virus, but some differences permit the characterization of individual viruses on the basis of protein composition. Such differentiation is based on protein located near the virion's surface, since viral cores have similar polypeptide profiles. The synthesis of functional mRNA is carried out by a transcriptional system located in the core of all infectious poxvirus particles. Other enzymes such as protein kinase and alkaline protease are also present in vaccinia core preparations.

TABLE 26.1.

Protein components of vaccinia virus structural elements

Location	Protein constituents (VP)	Remarks
Virus envelope	54K; 37K; 34K; 32K; 29K; 25K; 21K; 18K; 17K; 16K; 14.2K; 13K	VP25K-VP17K form a complex under non-reducing conditions
Lateral bodies	70K; 69K; 66K; 64K; 13.8K	VP13.8K is a DNA-binding protein
Palisade layer and core envelope	61K; 57K; 22K	VP57K-VP22K form a unit complex; VP57K is a DNA-binding protein
Nucleoprotein	27K; 13K	VP27K-VP13K form a unit complex; both are DNA-binding proteins

Based on Ichihashi, Oie and Tsuruhara (1984).

Although the material obtained with non-ionic detergent and 2-mercaptoethanol had a density similar to that of surface tubules, this fraction had no tubular figures and contained VP54K, VP20K and VP16K.

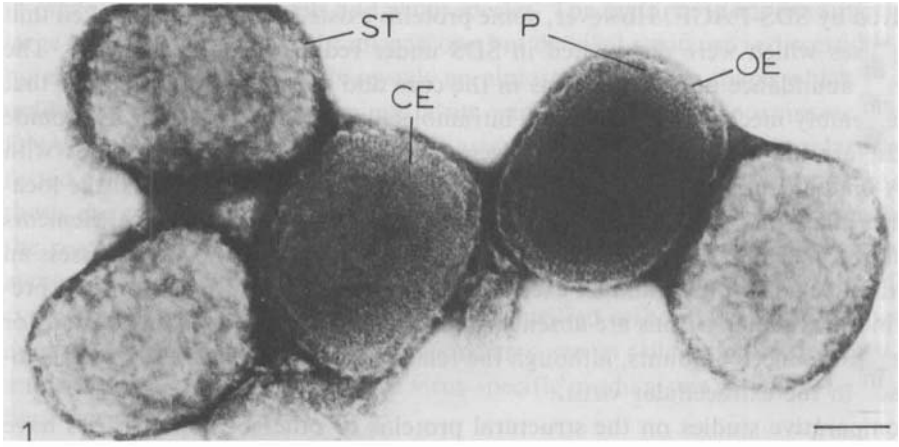
ST
P
OE
CE
1

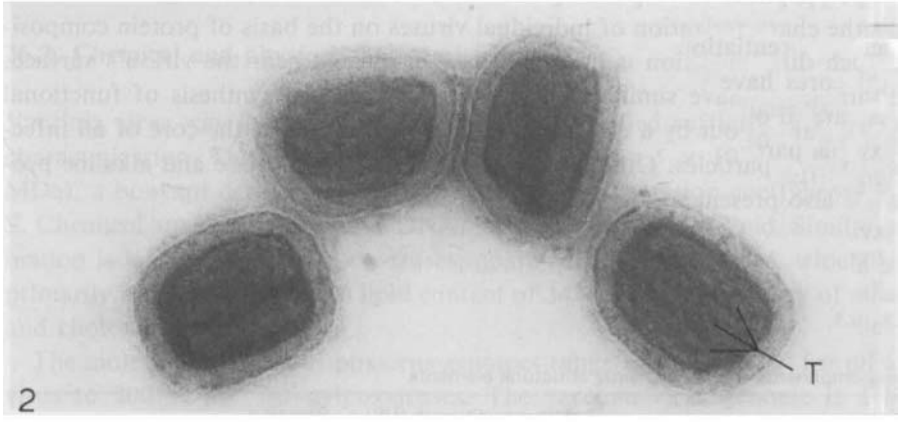
T
2

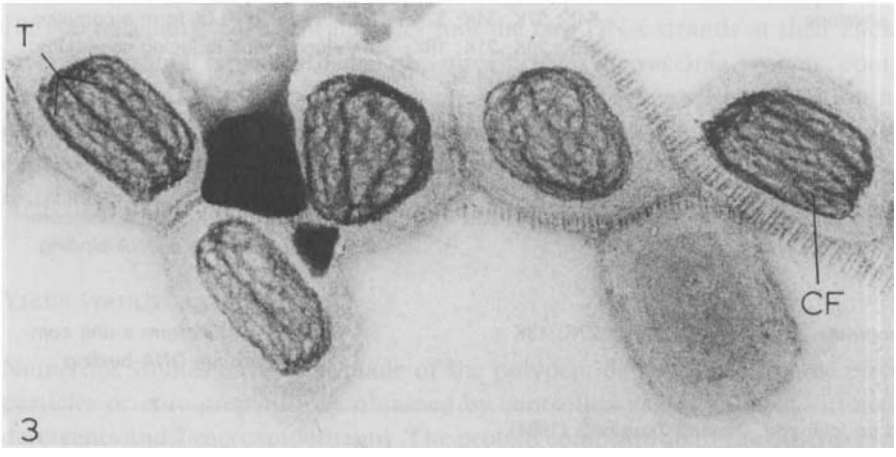
T
CF
3

26.3. Structural characteristics

Shape and size. Poxvirus particles are characteristically brick-shaped with rounded edges. Vaccinia virions released artificially by disruption of infected cells have dimensions of 300 × 230 × 180 nm, although the size of individual particles may vary. Extracellular virus particles released naturally have an additional lipoprotein envelope derived from the Golgi vesicle membranes but it is labile and readily lost during preparative procedures. Other orthopoxviruses, together with avipoxviruses and leporipoxviruses, have a similar size and shape but capripoxviruses are smaller and entomopoxviruses show considerable size variation.

26.4. Architecture of the virion

There are three principal structural components of the 'naked' vaccinia virion: a central core, lateral bodies associated with the virus core and an outer coat (Figs. 26.1–3 and 6). Extracellular virus also has an additional envelope (Fig. 26.4).

The coat consists of the limiting envelope, a 5 nm thick lipid bilayer, and the so-called surface tubules best visualized by negative staining procedures (Figs. 26.1 and 26.7). When examined by freeze-etching or drying these surface convolutions appear as 'paired ridges' with small subunits (Fig. 26.5), and the U-shaped profile (Fig. 26.7) indicates that they are grooves rather than tubes. The 'tubules' are arranged randomly over the virion's surface in lengths of about 50–100 nm. The observed periodicity is about 4 nm and they are about 8 nm in diameter. The inner 'cavity' is about 2.5 nm wide. The mode of interaction of the 'tubules' with the lipid bilayer is unknown. Purified preparations of vaccinia surface 'tubules' examined by SDS-PAGE consisted of a single 58 kDa polypeptide. Although the limiting envelope of naked vaccinia virions has a morphological appearance which is consistent with a lipid bilayer, its stability in SDS following the complete removal of phospholipids indicates that the structural integrity of the outer envelope is, in fact, dependent upon viral proteins (Ichihashi et al., 1984). Parapoxviruses appear to have a single continuous thread covering the outer sur-

---

Fig. 26.1. Different images of purified virions showing surface tubules (ST), core envelope (CE), outer envelope (OE) and palisade layer (P). Negative stain: sodium silicotungstate. × 100 000. Bar 100 nm.

Fig. 26.2. Virions revealing triplet elements (T) in the homogeneous core matrix. Negative stain: Reinecke salt in combination with sodium silicotungstate (Müller, G. (1972) J. Ultrastruct. Res. 39, 77–84). × 100 000.

Fig. 26.3. Virions with triplet elements (T) and core fibrils (CF) clearly seen. Negative stain: Reinecke salt in combination with sodium silicotungstate (see legend to Fig. 26.2). × 100 000. Figs. 26.1–3 are negatively stained preparations of whole vaccinia virus particles.

face of the virion and the typical criss-cross pattern of whole particle preparations is due to the superposition of images from the upper and lower planes.

Isolated vaccinia cores have a brick-shaped profile but in the mature virion the core is distorted by the presence of one or two lateral bodies (Fig. 26.6). The core is limited by a membrane (the core envelope), on the outer surface of which there is a 'palisade' layer comprising a radial arrangement of rod-shaped molecules 5 nm

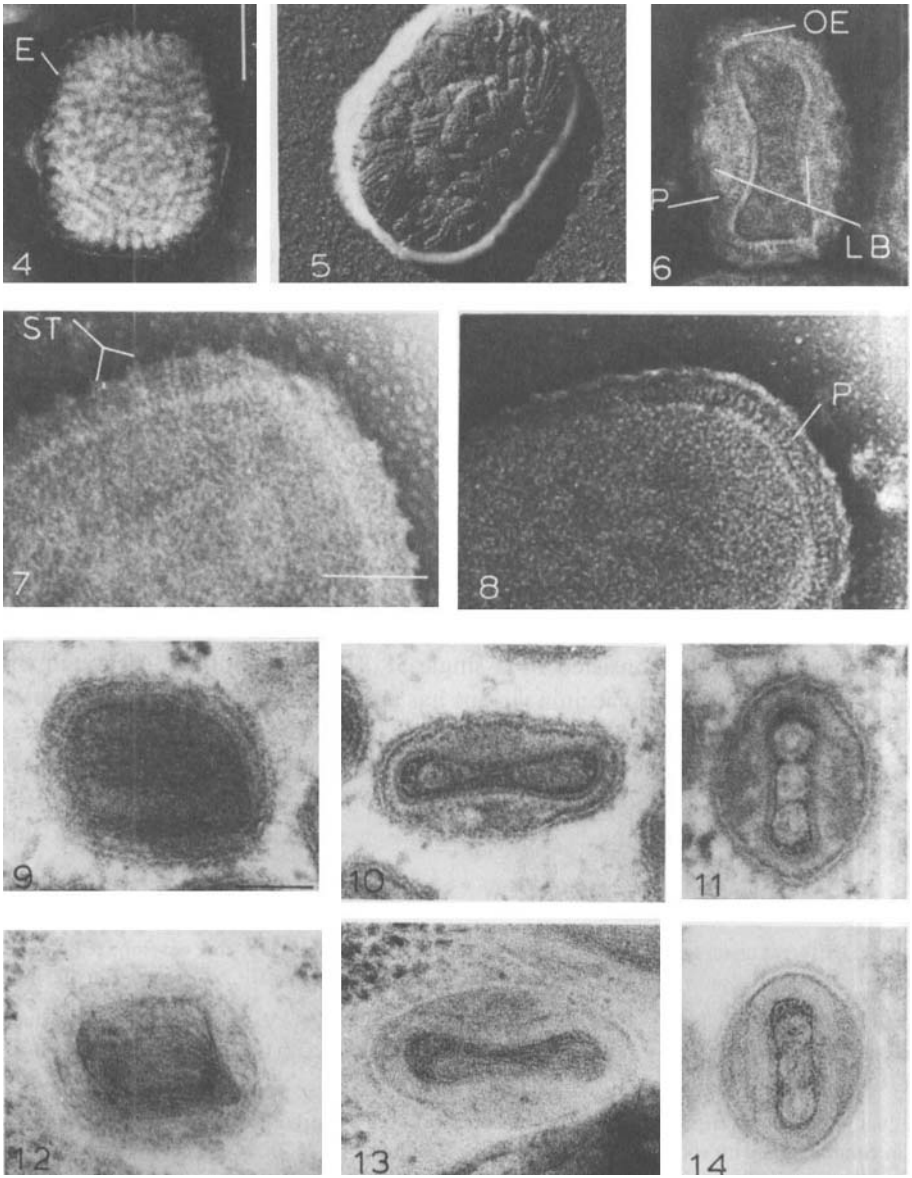

in diameter and 20 nm long (Fig. 26.8). Three coils, 250 nm in length and 50 nm in diameter, can be discerned inside the core of negatively stained preparations as well as in ultrathin sections (Figs. 26.2, 3 and 9–11). It is uncertain whether the coils are three separate entities or a single, folded cable. The remaining space in the core has a homogeneous texture as visualized in some preparations, although others appear to contain a loosely tangled, filamentous structure which must be considered to be DNA (Figs. 26.12–14). It remains to be determined whether the triplet element forms part of the virion's genetic material. A central core is a common morphological feature of all poxviruses but insect poxviruses have been described with unilaterally concave or cylindrical cores. The core infrastructure of different poxviruses also shows some variation in the number of coils or folds of the cable.

The two lateral bodies in vaccinia virus particles are ellipsoidal structures, shaped rather like rugby balls, which are embedded between the palisade layer of the core and the outer coat of the virion (Fig. 26.6). The functional significance of these structures is uncertain but they have been reported to be present in various poxviruses, although an entomopoxvirus has been shown to have a single lateral body.

A model of the vaccinia virion is shown in Fig. 26.15.

26.5. Antigenic properties

The orthopoxvirus, avipoxvirus and leporipoxvirus genera have been shown to be immunologically distinct from each other in serological tests based on the whole

---

Fig. 26.4. Extracellular virus particle with additional envelope (E). × 100000. Bar 100 nm. Negative staining.

Fig. 26.5. Surface replica of vaccinia virus after freeze-drying and shadowing showing 'paired ridges' with small particles. × 100000. Courtesy of Dr. M.V. Nermut.

Fig. 26.6. Lateral bodies (LB) located between palisade layer (P) and outer envelope (OE). Note the typical biconcave nature of the core in mature virus particles. × 100000.

Fig. 26.7. Surface tubules (ST) showing the 'saw-tooth' profile and small subunits. × 280000. Bar 50 nm.

Fig. 26.8. Palisade layer (P) on the outer surface of the core envelope becomes visible when stain penetrates outer envelope. × 280000. Figs. 26.6–8 are negatively stained preparations of whole vaccinia virus particles.

Figs. 26.9–14. Sections of vaccinia virus particles (in cells) cut along their long axis (Figs. 9, 10, 12, 13) or perpendicularly to the long axis (Figs. 11, 14). The triplet elements are particularly well visualized in Figs. 11 and 14. They are embedded in a dense 'matrix' probably of fibrillar nature as seen in Figs. 12 and 13. × 100000. Bar 100 nm.

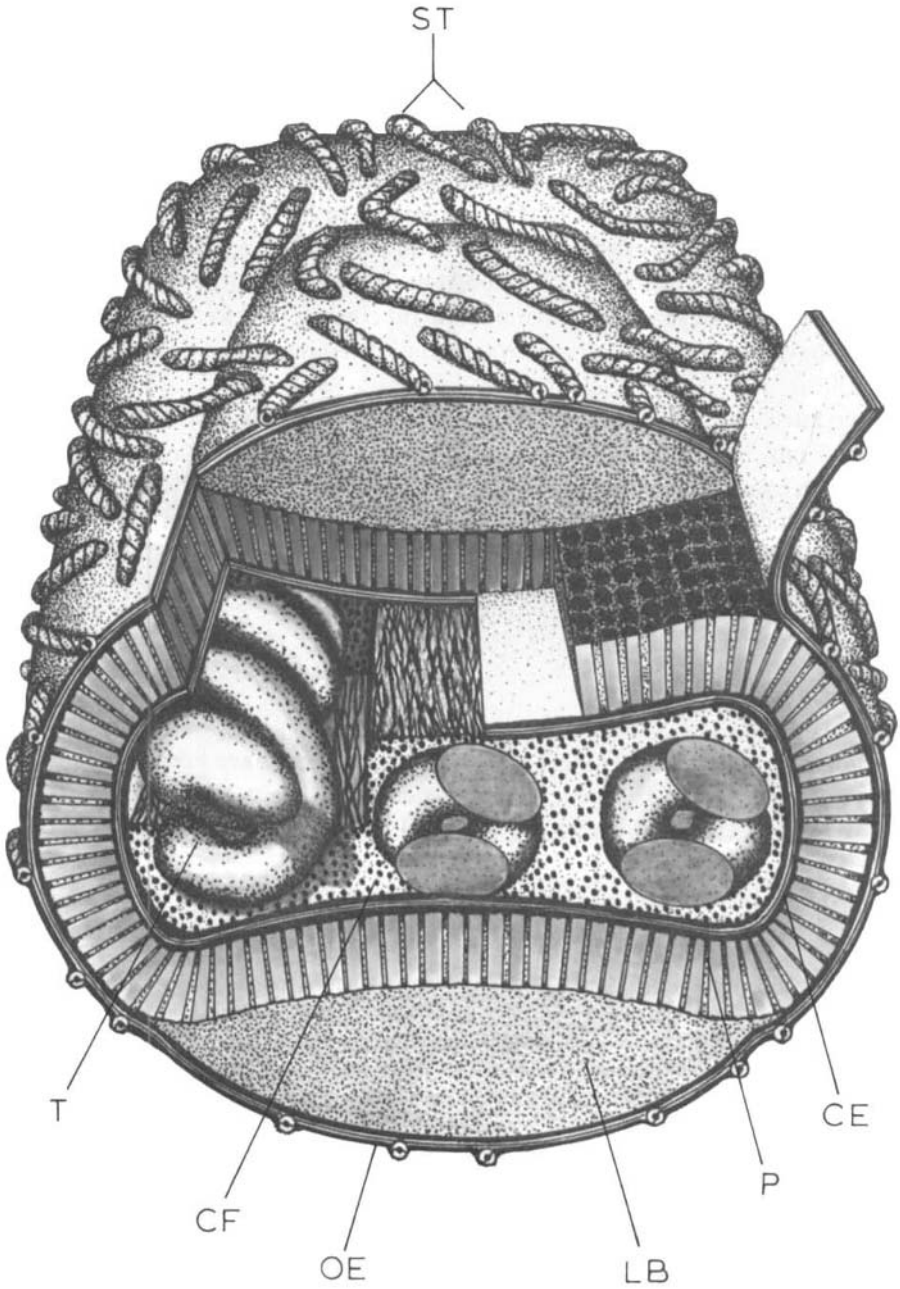

Fig. 26.15. Model of vaccinia virus in cross-section (by Heinz Hohenberg, Heinrich-Pette-Institut). CE, core envelope; CF, core fibrils; LB, lateral bodies; OE, outer envelope; P, palisade layer; ST, surface tubules; T, triplet elements. Bar 50 nm.

virus or soluble antigens. However, a nucleoprotein antigen with cross-reactivity between these genera (group specificity) has been reported to be present in alkaline extracts of purified vaccinia and myxoma virus particles. Although close antigenic relationships exist within each genus, individual members can be recognized by cross-absorbed antisera.

An appreciation of the potential antigenic complexity of individual virions can be gained from the resolution of more than 100 polypeptides after two-dimensional electrophoresis of disrupted vaccinia virions. At least five different antigenic determinants are associated with the production of neutralizing antibodies in orthopoxvirus infections. Antiserum prepared against the 58 kDa protein component of vaccinia surface tubules neutralizes virus infectivity and suppresses cell-to-cell fusion. Another antigen characteristic of extracellular rabbitpox virus induces antibody which controls the spread of virus in tissue culture and protects rabbits from rabbitpox infection, indicating its importance in natural immunity. The envelope of extracellular vaccinia virus also contains a haemagglutinin identified as an 85 kDa glycoprotein but similar activity is also present in virus-free extracts of tissues infected with vaccinia or other orthopoxviruses. Only some fowl red blood cells are susceptible to agglutination by the orthopoxvirus haemagglutinins: other fowls and most other animals possess red blood cells which are agglutinated to a much decreased titre or are completely insensitive.

26.6. Biological properties

Virus–cell interaction. Adsorption occurs rapidly, particularly with the extracellular form of the virus (with its additional envelope) but in this case the mechanism of penetration is not understood. With naked (= intracellular) virions penetration is known to occur by fusion of the virus envelope with the cell membrane, resulting in the release of the free core directly into the cytoplasm. Alternatively, an invagination of the cell membrane encloses the attached virions in a vacuole (viropexis) which moves into the cytoplasm before membrane fusion releases the cores (Fig. 26.21). A second uncoating step is required to release the genome from the core into the cytoplasm before viral DNA synthesis can begin.

Morphologically distinctive regions of fibrillar material appear in the cytoplasm soon after infection and they are the sites of virus replication. The next structures to become visible are crescent-shaped bilayer membranes located at the periphery of these viral 'factories' (Fig. 26.16). Prominent spicules on one surface force the membrane to curve as they increase in size until closed spherical particles filled with fibrillar material are formed: these structures are immature virions (Figs. 26.17 and 26.18). The next step involves condensation of the fibrillar material into an oval configuration characterized by parallel striations which has been shown to contain DNA (Figs. 26.19 and 26.20). Loss of spicules from the outer surface of

the envelope appears to be a prerequisite for further developments involving the formation of lateral bodies while the core gains its final biconcave shape and the overall dimensions of the particles diminish. During these last maturation stages the surface tubules are acquired at sites on the virus coat occupied formerly by the spicules.

Progeny virus is produced in vaccinia-infected cells from about 6 hours post-infection, although this eclipse phase lasts about 36 hours during fowlpox virus

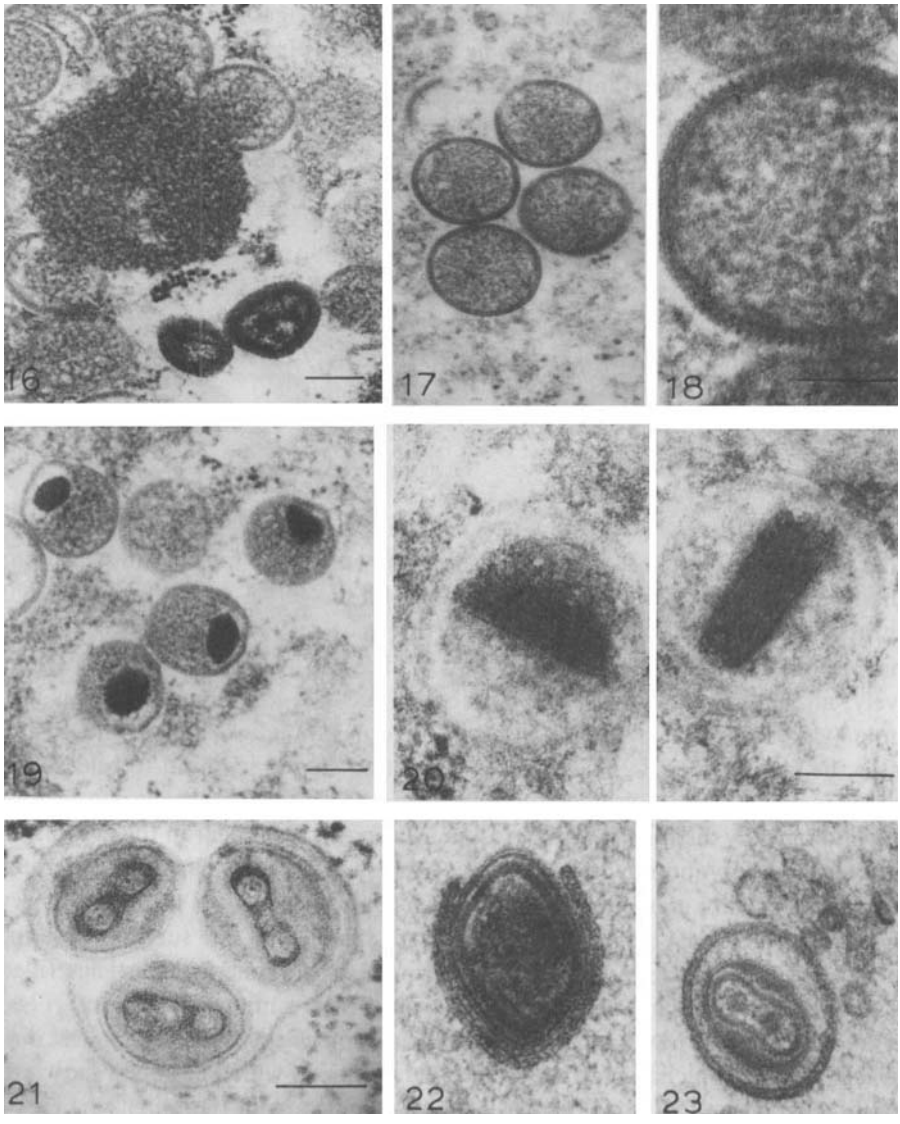

replication. Vaccinia virions may be released after the acquisition of a membrane-like sheath in the cytoplasm within which they move to penetrate the tips of many fine extrusions or microvilli developed by the cell membrane after infection. The virions are externalized at these sites within a single membrane envelope by fusion of the sheath membrane with the plasma membrane. Another release route involves individual virions wrapped in the coalescent membranes of several Golgi vesicles to form cisternae (Figs. 26.22 and 26.23) which migrate through the cytoplasm to fuse with the cell membrane and, again, externalize the virions within a single membrane envelope. Most virus, however, remains intracellular, and intercellular fusion of infected cells allows direct cell-to-cell spread of progeny virus. A diagrammatic representation of the vaccinia virus replication cycle is shown in Fig. 26.24.

Poxvirus replication is accompanied by the formation of intracytoplasmic inclusion bodies demonstrable by autoradiography, immunofluorescence and histochemical techniques. These viral 'factories' can be visualized soon after infection as basophilic (B-type) inclusions and they are present in the cytoplasm of all poxvirus-infected cells. Acidophilic (A-type) inclusions may appear at later times in cowpox, ectromelia and fowlpox-infected cells and they can contain virus particles enmeshed in a dense protein matrix depending on the strain of virus. Host cell macromolecular synthesis is inhibited in cell cultures infected with vaccinia or other orthopoxviruses leading eventually to cell death. Conversely, hyperplasia has been shown to occur in cell cultures and in animals infected with fowlpox virus, Shope papilloma virus, Yaba virus and molluscum contagiosum virus.

Figs. 26.16–23. Sections cut through the cytoplasmic areas of vaccinia-infected cells.

Fig. 26.16. Cytoplasmic 'factory' with crescent-shaped membranes at the periphery of the viroplasm. Note the two parental cores (lower right). × 40000. Bar 200 nm.

Fig. 26.17. Spherical envelopes at an early stage of virus maturation. × 40000.

Fig. 26.18. Spicules on the surface of the closed spherical envelope. × 130000.

Fig. 26.19. Immature subviral particles containing DNA in condensed form. × 40000. Bar 200 nm.

Fig. 26.20. Parallel striations can be seen in the condensed material at higher magnification. × 130000. Bar 100 nm.

Fig. 26.21. Endocytic vacuole containing three virus particles. × 60000. Bar 200 nm.

Fig. 26.22. Progeny virion wrapped in the membranes of the endoplasmic reticulum. × 100000.

Fig. 26.23. Progeny virion enclosed in the cisternae derived from the endoplasmic reticulum. × 100000.

Pathogenicity

Smallpox, the most notorious disease caused by poxvirus infection in man, has been eradicated. Man is also the only known host for molluscum contagiosum but zoonosal infections such as human monkeypox, Tanapox, cowpox and orf are

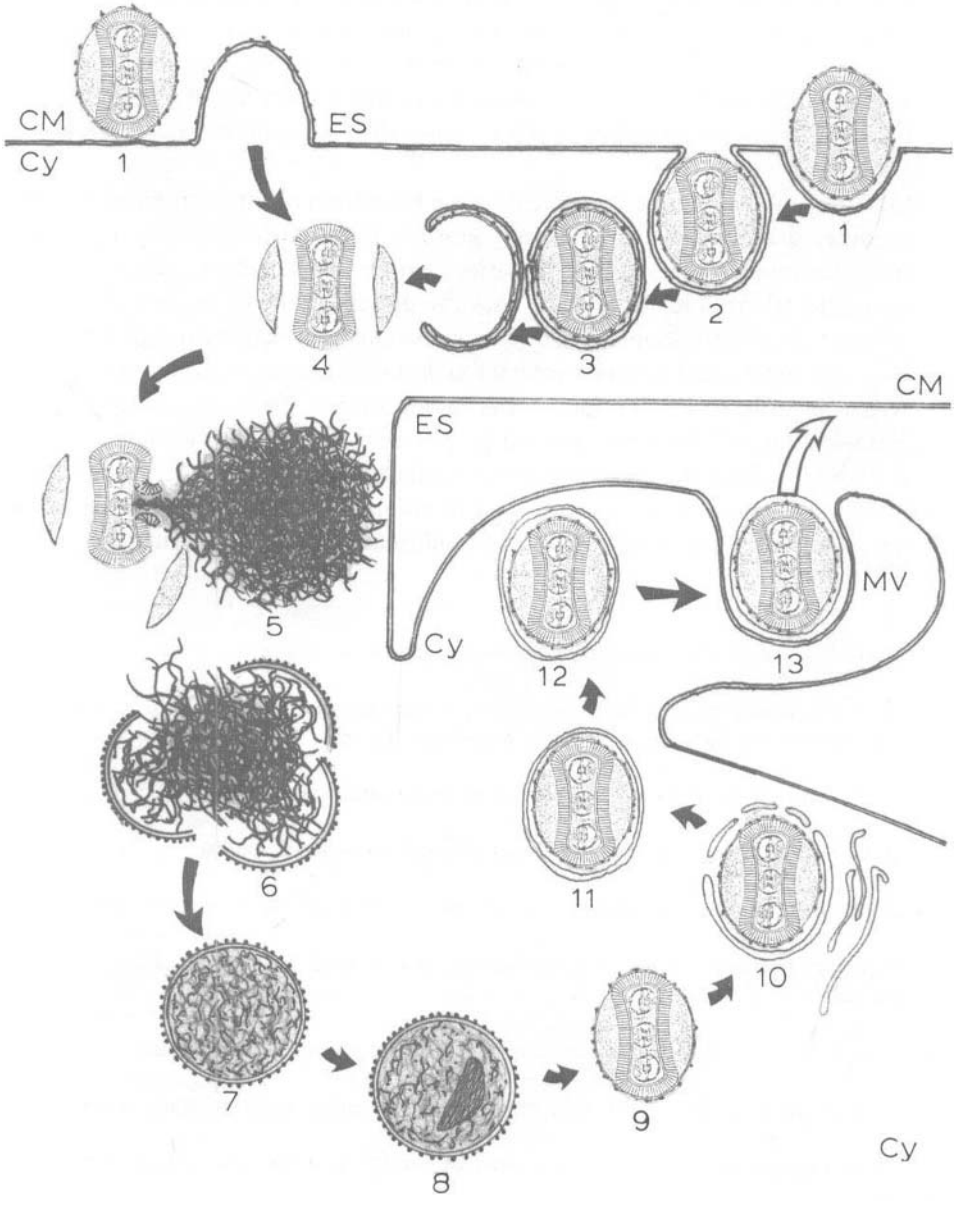

known to occur, although the primary animal reservoirs of these diseases are not known. Orf or contagious pustular dermatitis of sheep is an economically significant disease and the viruses of sheeppox, goatpox and camelpox are also important animal pathogens. Avian poxvirus infections have some veterinary importance and myxoma virus has been used for the biological control of wild rabbit populations. Most recently, infectious vaccinia virus recombinants containing foreign genes from important human pathogens have been shown to have considerable potential as new live vaccines.

Suggested reading and references

Bergoin, M. and Dales, S. (1971) Comparative observations on poxviruses of invertebrates and vertebrates. In Comparative Virology, Eds. K. Maramorosch and E. Kurstak; pp. 169–205. Academic Press, New York and London.

Dales, S. and Pogo, B.G. (1981) Biology of poxviruses. In Virology Monographs, Vol. 18, Eds. D.W. Kingsbury and H. zur Hausen; pp. 1–109. Springer Verlag, Vienna and New York.

Fenner, F. (1985) Poxviruses. In Virology, Ed. B.N. Fields; pp. 661–684. Raven Press, New York.

Ichihashi, Y., Oie, M. and Tsuruhara, T. (1984) Location of DNA-binding proteins and disulphide-linked proteins in vaccinia virus structural elements. J. Virol. 50, 929–938.

Moss, B. (1985) Replication of poxviruses. In Virology, Ed. B.N. Fields; pp. 685–703. Raven Press, New York.

Fig. 26.24. A diagrammatic representation of the vaccinia virus replication cycle (by Heinz Hohenberg, Heinrich-Pette-Institut) showing sequential stages of viral morphogenesis within the cytoplasm of an infected cell. ES, extracellular space, CM, cell membrane; CY, cytoplasm; MV, microvilli. 1. Naked, infective virion in contact with the cell membrane. 2. Invagination of the cell membrane together with the attached virion. 3. Fusion of the virus membrane with the membrane of the enclosing vesicle. 4. Release of the core and lateral bodies into the cytoplasm; this may also result directly from fusion of the virus envelope with the cell membrane. 5. 'Factory' established at the site of genome release after final uncoating of the virus core. 6. Assembly of the viral, bilayer membrane. 7. Immature virion. 8. Condensation of viral DNA. 9. Mature virion. 10. Virion surrounded by Golgi vesicles or cytoplasmic membrane-like sheath. 11. Virion in cisternae. 12. Migration of the enwrapped virion through the cytoplasm to the cell membrane or into microvilli. 13. Fusion of the cisternal membrane with the cell membrane and release of the progeny virion within a single membrane envelope.

This Page Intentionally Left Blank

Subject Index